Structure and activity-guided biotechnological engineering to produce improved anti-Gram-negative darobactins

Dissertation

zur Erlangung des Grades

des Doktors der Naturwissenschaften

der Naturwissenschaftlich-Technischen Fakultät

der Universität des Saarlandes

von

Carsten Eric Maximilian Seyfert

Saarbrücken

2023

Tag des Kolloquiums:	23. Februar 2024
Dekan:	Prof. Dr. Ludger Santen
Berichterstatter:	Prof. Dr. Rolf Müller Prof. Dr. Andriy Luzhetskyy Prof. Dr. Helge B. Bode
Akad. Mitglied:	Dr. Michael Kohlstedt
Vorsitz:	Prof. Dr. Anna K. H. Hirsch

Diese Arbeit entstand unter der Anleitung von Prof. Dr. Rolf Müller am Institut für Pharmazeutische Biotechnologie der Naturwissenschaftlich-Technischen Fakultät der Universität des Saarlandes am Helmholtz-Institut für pharmazeutische Forschung Saarland von Januar 2020 bis Dezember 2023.

„Der Schlüssel zum Erfolg ist Kameradschaft…“ Fritz Walter 1920-2002

Danksagung

Zu allererst möchte ich mich bei meinem Doktorvater Herrn Prof. Dr. Dr. Rolf Müller herzlich bedanken mir die Möglichkeit gegeben zu haben, in seiner Arbeitsgruppe, zu promovieren. Seine Unterstützung und die Freiheiten, die er mir gelassen hat, mich weiterzuentwickeln und vor allem das Darobactinprojekt voranzutreiben schätze ich sehr. Herrn Prof. Dr. Andriy Luzhetskyy möchte ich auch herzlich danken, in den letzten Jahren mein wissenschaftlicher Begleiter gewesen zu sein. Der Austausch war immer konstruktiv und hilfreich.

Als Zweites möchte ich mich bei Dr. Chantal Bader, Dr. Andreas Kany und Dr. Daniel Krug bedanken sowie auch bei Clemens Schumm für das Gegenlesen meiner Dissertationsschrift. Sie haben mir geholfen die Arbeit so zu gestalten, wie sie ist und dafür bedanke ich mich herzlich.

Chronologisch vorgehend möchte ich mich als nächstes bei Dr. Domen Pogorevc und Dr. Sebastian Groß bedanken, die trotz ihres Eingebundenseins in anderen Projekten für mich in meiner Anfangszeit greifbar waren. Das schnelle Vorankommen gerade im ersten Jahr meiner Promotion wäre nicht ohne Dr. Joachim Hug möglich gewesen, mit dem ich im Schichtsystem nach dem Coronalockdown kooperiert hatte, um unsere jeweiligen Experimente in der reduzierten Zeit zu erledigen.

Das Darobactinprojekt wäre initial nicht ohne Dr. Fabian Panter so erfolgreich verlaufen. Vor allem Fabian hat mich in die Analytik, die Aufreinigung mittels diverser Techniken sowie in unkonventionellen, aber effizienten Methodiken geschult. Ihm habe ich zu verdanken, dass ich nicht nur auf dem mir vertrauten molekularbiologischen Gebiet sicher bin, sondern auch die Reinigung und analytische Auswertung meiner Experimente selbstständig bewältigen konnte. Kein Abend war ihm zu lang, um mit mir an der Waters Prep zu reinigen. Allerdings wäre gerade die Aufreinigung nicht so vorangekommen, ohne Christoph Porten, der mit Dr. Kamal Teheranii und mir die Methodik adaptierte, um erst die Mengen an Darobactin, die wir benötigten zu reinigen. Zusammen mit Selina Deckarm haben wir so manche Produktions- und Reinigungsschlacht bestritten, gewonnen und keine Deadline gerissen. Neben dem Gegenlesen der Arbeit möchte ich mich auch nochmal bei Andreas sowie bei Dr. Jennifer Herrmann bedanken, die Teile der Projektadministration gemanagt haben.

Kollegen an der Seite zu haben ist nicht nur in meinen interdisziplinären Projekten, sondern auch generell während meiner gesamten Promotionszeit, wichtig gewesen. Der Zusammenhalt weiter Teile der MINS Gruppe ist außergewöhnlich und ohne die Gemeinschaft, wäre die Motivation und Freude an der Promotion bei Weitem nicht so groß für mich gewesen. Hier möchte ich besonders meine Büronachbarn, vor allem Dr. Jake Haeckl und Dr. Peter Sullivan nennen. Wir hatten in den gemeinsamen Jahren, nie Streit oder Disharmonie. Vielleicht lag das auch daran, dass die Bierkasse stets gefüllt wurde und folgend der Kühlschrank auch. Außerdem habe ich vor allem durch Jake, aber auch durch Peter viel dazulernen können. Erfahrene Postdocs direkt um sich zu haben, war viel wert. Gerade weil ich relativ schnell viel Verantwortung tragen dürfte.

Ohne die Unterstützung von neuen kompetenten Doktoranden, wäre vieles nicht möglich gewesen: Allen voran möchte ich mich bei meiner ehemaligen Masterandin und nun Kollegin Alison Müller bedanken. Vom ersten Tag an hat das Zusammenarbeiten mit ihr super harmoniert, wir hatten und haben viel Spass zusammen und die Erfahrung jemanden über ein Jahr zu betreuen möchte ich nicht missen. Ohne sie wäre vieles für mich schwerer gewesen. Ein weiterer besonderer Glücksfall war für mich Alexander Voltz, der nach dem Weggang der Analytiker Fabian, Nico und Chantal den Laden zusammenhält und eine wichtige Ansprechperson für mich wurde, auch im Privaten. Besonders möchte ich mich noch bei Philipp Donate, Fabienne Wittling, Kai Schließmann, und Dr. Jan Schlemmer sowie Simon van Nooy bedanken, mit denen ich vor allem außerhalb der Arbeitszeit viel Spass erleben dürfte. Die fast täglichen Mensagänge und Mittagspausen oder HopShop/Staden Events haben meine Promotionszeit bunt gestaltet. Weiterhin möchte ich mich namentlich bei Anna-Lena Huber, Joy

Birkelbach und Sebastian Walesch sowie Felix Deschner, Franzi Fries und Timo Risch bedanken, sowie allen weiteren aktuellen und ehemaligen MINSlern, die mir meine Promotion positiv gestaltet haben.

Hervorheben möchte ich noch unsere Officedamen Tina Decker und Ellen Merckel sowie Besnik Qallaku, die großartige TA-Abteilung, sowie unsere ITler Marc Caspari, Michael Roth und Patrick Bund, sowie unsere Hausmeister Frank Jakob, Marco Schmitt und Christian Zeuner.

Immer konnte ich mich auf meinen „Nicht-HIPS-Freundeskreis“ verlassen. Besonders zu nennen sind hier die Mitglieder der Betze BBG Gruppe: speziell Milena Kuhn (der ich fast immer mein Mittagessen verdanke), Florian Böhnlein, Marcel Jost, Marc Schmitt, Jonas Wolf, Fabian Krewer und Louis Beltz; meine Schul- und Studienfreunde Dr. Aline Lanzrath, Dennis Wendel, Elias Brugger und Patricia Marini; sowie meine ältesten Freunde Kay Wagner und Marcel Neukirch.

Ein besonderer Dank gilt abschließend auf jeden Fall meiner Familie ohne die vieles nicht möglich gewesen wäre: Meinen Geschwistern Birgit und Stefen und unseren Eltern.

Vorveröffentlichungen aus dieser Dissertation

Teile dieser Arbeit wurden vorab mit Genehmigung der Naturwissenschaftlich-Technischen Fakultäten, vertreten durch den Mentor der Arbeit, in folgenden Beiträgen veröffentlicht oder sind derzeit in Vorbereitung zur Veröffentlichung:

Publikationen

S. Groß[1], F. Panter[1], D. Pogorevc[1], **C. E. Seyfert**[1], S. Deckarm, C. D. Bader, J. Herrmann and R. Müller*: Improved broad-spectrum antibiotics against Gram-negative pathogens via darobactin biosynthetic pathway engineering ***Chem. Sci.*** 2021, 12, 11882.

C. E. Seyfert[1], C. Porten[1], B. Yuan[1], S. Deckarm[1], F. Panter, C. Bader, J. Coetzee, K. H. M. E. Tehrani, P. G. Higgins, H. Seifert, T. C. Marlovits*, J. Herrmann* and R. Müller*: Darobactins exhibiting superior antibiotic activity by cryo-EM guided biosynthetic engineering ***Angew. Chem. Int. Ed.*** 2023, 62, e202214094.

C. E. Seyfert, A. V. Müller, D. J. Walsh, J. Birkelbach, A. M. Kany, C. Porten, B. Yuan, D. Krug, J. Herrmann, T. C. Marlovits, A. K. H. Hirsch, R. Müller*: New genetically engineered derivatives of antibacterial darobactins underpin their potential for antibiotic development ***J. Med. Chem.*** 2023, https://doi.org/10.1021/acs.jmedchem.3c01660

---

[1] Die Autoren trugen gleichwertig zum Manuskript bei.

Publikationen die nicht Teil dieser Arbeit sind

C. E. Seyfert, C. Porten, B. Yuan, S. Deckarm, F. Panter, C. Bader, J. Coetzee, K. H. M. E. Tehrani, P. G. Higgins, H. Seifert, T. C. Marlovits*, J. Herrmann* and R. Müller*: Darobactine mit Überlegener Antibiotischer Aktivität Generiert durch Strukturgeleitetes Kryo-EM-Biosynthese-Design. ***Angew. Chem.*** 2023, 135, e202214094.

C. E. Seyfert, C. Porten, B. Yuan, S. Deckarm, F. Panter, C. Bader, J. Coetzee, K. H. M. E. Tehrani, P. G. Higgins, H. Seifert, T. C. Marlovits*, J. Herrmann* and R. Müller*: Innentitelbild: Darobactine mit Überlegener Antibiotischer Aktivität Generiert durch Strukturgeleitetes Kryo-EM-Biosynthese-Design (Angew. Chem. 2/2023). ***Angew. Chem.*** 2023, 135.

C. E. Seyfert, C. Porten and R. Müller*: Darobactin – ein neues Antibiotikum in Entwicklung **BIOspektrum** 2023, 05, 539.

Patentanmeldungen

C. E. Seyfert, F. T. Panter, R. Müller, S. Deckarm, S. Groß, D. Scherzer, C. Bader, J. Herrmann: Novel darobactin derivatives. International application under patent cooperation treaty, ***WIPO/PCT***. WO 2022/175443 A1.

Tagungsbeiträge

C. E. Seyfert (2021) Darobactin project presentation – Improved broad-spectrum antibiotics against Gram-negative patogens (Oral communication) **Leibniz Science Campus Living Therapeutic Materials - Status Meeting, Saarbrücken, Germany**

C. E. Seyfert (2022) Improved broad-spectrum antibiotics against Gram-negative pathogens via darobactin biosynthetic pathway engineering. (Poster) **Helmholtz Institut für Pharmazeutische Forschung Saarland (HIPS) Symposium 2022, Saarbrücken, Germany**

S. Dey, **C. E. Seyfert**, R. Mueller, S. Sankaran **(2022)** Thermoresponsive living therapeutic materials – Darobactin releasing bacterial hydrogels for treating chronic pathogen infections. (Poster) **3rd International Conference on Engineered Living Materials (ELMs), Saarbrücken, Germany**

C. E. Seyfert (2022) Implementation of activity and structure-guided darobactin biosynthetic pathway engineering to generate novel derivatives with superior antibacterial activity. (Oral communication) **HIPS Papers/HIPS projects 2022, Saarbrücken, Germany**

C. E. Seyfert, S. Dey and S. Basaran **(2022)** Infrared controlled Darobactin producing LTM. (Oral Communication), **LSC consortium meeting 2022, Saarbrücken, Germany**

C. E. Seyfert , C. Porten , B. Yuan, S. Deckarm , F. Panter, C. D. Bader, J. Coetzee, F. Deschner, K. Tehrani, P.G. Higgins , H. Seifert , T. Marlovits, J. Herrmann and R. Müller **(2022)** Implementation of activity and structure-guided darobactin biosynthetic pathway engineering to generate novel derivatives with improved antibacterial activity against Gram-negative pathogens. (Poster) **VAAM-International VAAM Workshop 2022-Biology of Microorganisms Producing Natural Products, Dortmund, Germany**

C. E. Seyfert (2022) Implementation of activity and structure-guided darobactin biosynthetic pathway engineering to generate novel derivatives with improved antibacterial activity against Gram-negative pathogens. (Oral Communication) **VAAM-International VAAM Workshop 2022-Biology of Microorganisms Producing Natural Products, Dortmund, Germany**

C. E. Seyfert (2023) Darobactins – A novel class of antibiotics against MDR Gram-negative pathogens. (Oral Communication) **PhD Assembly – Saarland University, Saarbrücken, Germany**

C. E. Seyfert (2023) Darobactins – A novel class of antibiotics against MDR Gram-negative pathogens. (Oral Communication) **Helmholtz Institut für Pharmazeutische Forschung Saarland (HIPS) Symposium 2023, Saarbrücken, Germany**

C. E. Seyfert and Rolf Müller **(2023)** Optimization of Darobactins Improving the Antibiotic Activity by Structure and Activity Guided Biosynthetic Engineering (Poster) **ASM/ESCMID Joint conference on**

drug development to meet the challenge of antimicrobial resistance, Boston, United States of America

C. E. Seyfert (2023) Optimization of Darobactins Improving the Antibiotic Activity by Structure and Activity Guided Biosynthetic Engineering (Oral communication) **ASM/ESCMID Joint conference on drug development to meet the challenge of antimicrobial resistance, Boston, United States of America**

Zusammenfassung

Die Antibiotikaklasse der Darobactine zeichnet sich durch antibakterielle Aktivität gegen ein breites Spektrum Gram-negativer Pathogene aus. Diese Doktorarbeit beschäftigt sich mit der Etablierung einer heterologen Expressionsplattform, um ribosomal produzierte und posttranslational modifizierte Peptide (RiPPs) dieser neuen Substanzklasse zu studieren und einer Weiterentwicklung zuzuführen. Das biosynthetische Darobactin-Gencluster wurde funktionell charakterisiert und natürliche sowie artifizielle Darobactinderivate produziert. Dabei fiel ein neuartiges Darobactin (**D9**) auf, das im Vergleich zum nativen Darobactin A (**DA**) eine bis zu 8-fach erhöhte antibakterielle Aktivität gegen kritisch eingestufte Pathogene aufweist. Zur Optimierung von **D9** wurde ein struktur– und aktivitätsgeleiteter Ansatz verfolgt, um verbesserte Derivate zu erzeugen. Von diesen ist **D22** hervorzuheben, das **D9** in seiner antibakteriellen Aktivität übertrifft. Basierend auf Strukturdaten des BamABCDE (BAM)-**D9-** und BAM-**D22**-Komplexes wurden weitere Modifikationen des Darobactin-Grundgerüsts modelliert und experimentell untersucht. Anhand der struktur- und aktivitätsgeleiteten Modifikationen des Darobactin-Heptapeptids an Position 2, 4, 5, 6 und 7 wurden anschließend die Auswirkungen auf die Bioaktivität charakterisiert. Somit stellt diese Arbeit auch eine Fallstudie für die Entwicklung von RiPPs hin zu neuen Antibiotika dar.

Abstract

The darobactins are a recently discovered class of antibiotic candidates showing antibacterial activity against Gram-negative pathogens. This thesis showcases the establishment of a versatile heterologous expression platform to overproduce these ribosomally produced and post-translationally modified peptides (RiPPs) to investigate this pharmaceutically promising compound class and to make darobactins available for further development. The biotechnological approach enabled the functional characterization of the biosynthetic gene cluster and the generation of novel analogues. Derivatives were profiled and Darobactin 9 (**D9**) was highlighted, a molecule with up to 8-fold enhanced antibacterial activity against hard-to-treat pathogens compared to its native counterpart. Optimization of **D9** using a structure–activity relationship (SAR) approach by structural elucidation of the molecule's binding mode with the target protein inspired a second series of analogues, with derivative **D22** surpassing the activity of **D9**. The generated SAR data facilitated a third derivatisation series, where modelled modifications at hitherto underexplored positions were applied, enabling comprehensive understanding of the influence of different substitutions at positions 2, 4, 5, 6 and 7 of the heptapeptide for bioactivity. Moreover, diverse models were utilized to profile darobactins, paving the way for *in vivo* studies. This thesis can serve as a blueprint for future efforts in RiPPs antibiotic development.

Table of contents

Chapter 1 - Introduction

1.1 Natural products and their historical use by mankind

Microbial natural products (NPs) are specialized metabolites biosynthesized by microorganisms to communicate with their environment and facilitate survival. Many of these NPs are small molecules that have been correlated to antibacterial, antifungal, or cytotoxic activities and are therefore suspected to provide the respective microorganisms with an advantage over other organisms living in their ecological niche[1]. Remarkably, humans, oblivious to the exact molecular mechanisms of these activities, have been using the power of NPs in particular for medical treatment of infectious diseases for thousands of years. Valuable examples have been preserved for posterity in libraries where, for example, written testimonies from ancient Egypt are kept. It is documented that the Egyptian healer Imhokep (2650 - 2600 BC) described the successful treatment of skin infections with moldy bread[2]. Today, it is proven that the anti-infective activity of the moldy bread bases on the production of antibiotic NPs through the respective fungi. Other known treatment methods for curing infections have been practiced in traditional medicine for more than 2000 years. Until now, traditional Chinese medicine in particular extensively practiced the usage of plant materials as extracts in well-described treatment methods to cure infections[3]. In view of the knowledge acquired in the last century on the treatment of bacterial infections, it is now possible to recognize and reconstruct many historical uses of NPs in ancient medical treatment methods. Nowadays we can elucidate the advantages of using e.g. plant extracts for bacterial infections to the presence of antibacterial compounds produced either by certain plants themselves or by symbiotic microorganisms residing on leaves, beneath tree bark or in the soil[4]. These symbionts, mostly bacterial strains or fungi, are exposed to attacks and require protection within their habitat from other competitors to survive[5]. As a side effect, the host is protected by the symbiotic microorganisms from the invaders. So, both profit from the production of the bioactive NPs. However, research has only begun in recent decades to understand the symbiotic relationships between microorganisms and their hosts. The capacity of symbiotic microorganisms to produce NPs that act selectively against certain invading pathogens and not kill the host is still understudied. However, the potential benefit for developing new drugs seems to be there.

1.2 Natural products and their development as drugs to cure bacterial infections

In the last century, the progress in science and the building of experimental laboratories led to the discovery and development of the first nature-derived and commercially available antibiotic, penicillin[6,7]. Alexander Fleming and his colleagues noticed in 1928, that no colonies of the Gram-

positive bacterium *Staphylococcus aureus*, streaked on an agar plate, were growing near contaminated spots of mold fungi of the species *Penicillium chrysogenum*[6]. In contrast to Imhokep, they could realize that the mold fungi potentially produced antibacterial compounds killing the bacteria on the plate because it had already been known to this date that microorganisms produce substances that exhibit bioactivity. However, the initiated research and development of penicillin and the market approval in 1942 was significantly expedited by the discovery of chemically synthesized sulfonamides by Gerhard Domagk in 1935[8,9]. Sulfonamides were shown to be highly active especially against *Escherichia coli* and *Staphylococcus* species and the fast market approval under the name Prontosil by Bayer in the same year, proved the general potency of small molecules to fight pathogenic bacteria[9]. Chemically engineered small molecules such as sulfonamides and the NP penicillin saved millions of peoples' lifes and initiated an inventive spirit to treat bacterial infections[9]. Particularly during World War II, the use of penicillin by the Allied forces and Prontosil by the German army significantly reduced the mortality risk associated with bacterial infections after injuries (Figure 1)[9,10].

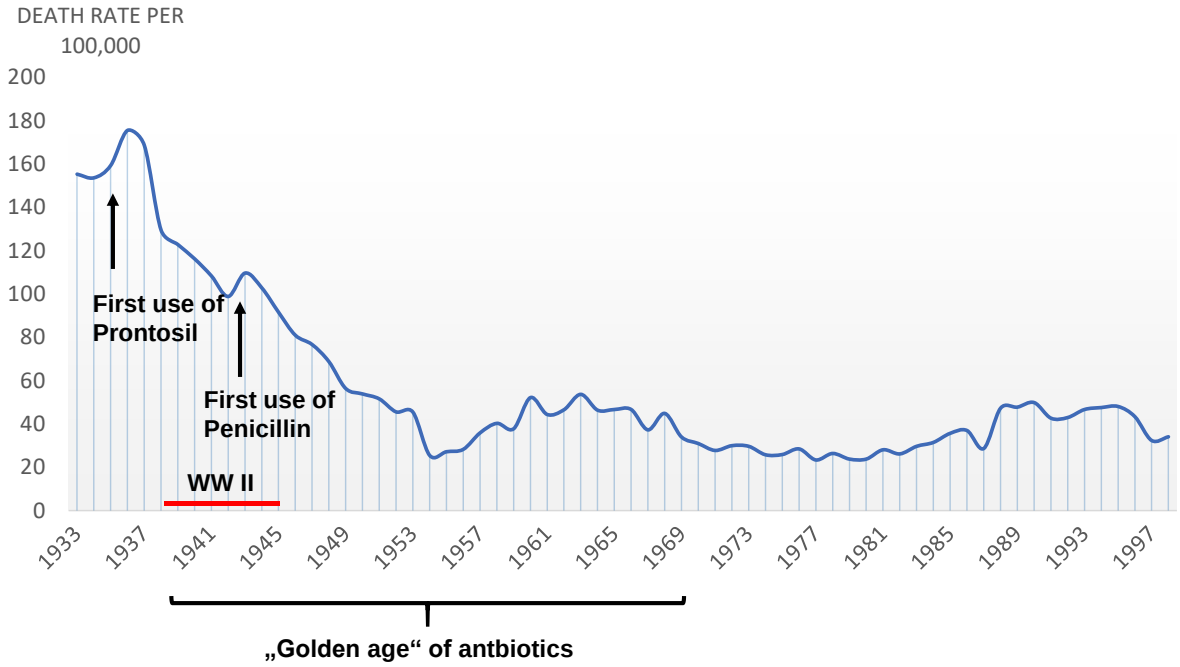

Figure 1: Infectious disease mortality rates from 1933 to 2000. The medical use of antibiotics significantly reduced the mortality rate from about 160 per 100,000 in 1933 to about 30 per 100,000 in 2000. Black arrows highlight the market entry of the first chemically synthesized antibiotic Prontosil in 1935 and the first natural product penicillin in 1942. The period between 1940 and 1970 is referred to as the "Golden Age of antibiotics". World War II (WW II). The raw data were taken from the OECD Health Policy Studies 2018[11].

The remarkable capacity of soil-dwelling bacteria and fungi to produce highly potent antibacterial compounds spurred the systematic screening of soil samples to isolate hitherto undiscovered producers of novel natural products, showing antibacterial activity[12]. A mentionable pioneering platform for antibiotic discovery, known as "Waksman platform"[13], was developed by Selman

Waksman and his colleagues Albert Schatz and Elizabeth Bugie[14]. They mainly investigated Gram-positive bacteria of the genus *Actinomyces*, producers of a diverse array of broad-spectrum antibacterial compounds, also termed as specialized or secondary metabolites. *Actinomyces* were a viable source for anti-infective compounds, and were able to produce these specialized metabolites in sufficient quantities to subsequently extract and isolate them for further studies[15]. Up to date, approximately 60–65 % of all, naturally–isolated antibiotics so far are derived from *Actinomycetota* and especially its genus *Streptomyces*[16]. Profoundly relevant antibiotic classes such as streptomycins[17], vancomycines[18], and tetracyclines[19] were isolated from *Streptomyces* and – among others such as the glycopeptides or the cephalosporins – completely revolutionized the treatment options for bacterial infectious diseases (Figure 2)[12]. The systematic screen of soil bacteria to identify new antibiotics was so successful in the upcoming years, that the time between 1940s – 1960s became known as the "Golden age of antibiotics"[20]. A majority of the antibiotic classes that are highly effective and still on–market were discovered during this periode[21,22] (Figure 2), ultimately leading to a rapid decrease of infant mortality alongside with patients suffering from infections with critical and clinically-relevant pathogens (Figure 1, Figure 2)[7,12,23].

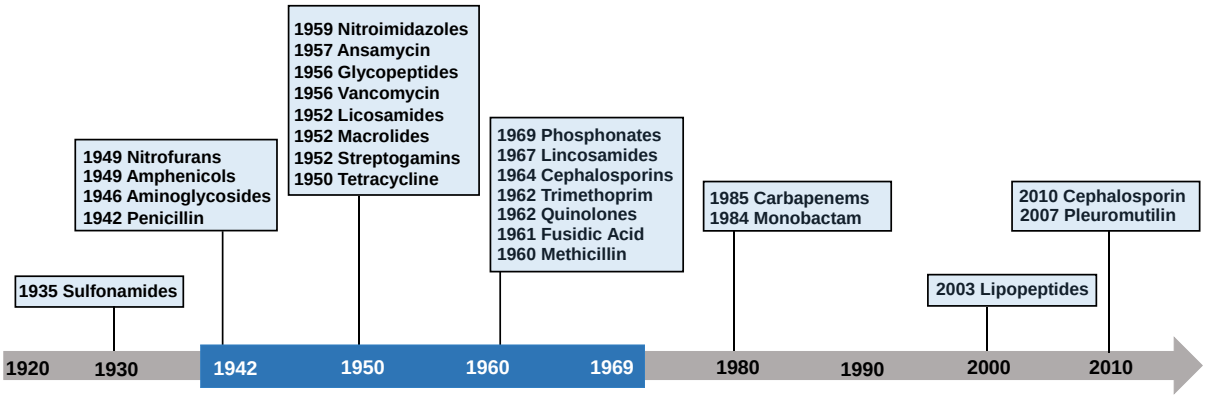

Figure 2: Timeline of market entry of the most relevant antibiotic classes from 1920 to 2010. Exemplified antibiotic classes that are still in market are summarized and exhibit the introduction of antibiotics especially from 1940 to 1970. The "Golden Age" of antibiotic discovery is highlighted by the blue front color. The timeline was adapted from Walesch *et al.*, 2023; Ventola, 2015 and Hutchings *et al.*,2019[7,22,24].

1.3 Challenges in the development of novel anti-infectives

The rapid development and market introduction of highly effective antibacterial agents effectively killing both Gram-negative and Gram-positive pathogens came with a major drawback: As the problem seemed solved, most of the large pharmaceutical companies stopped investing in antibiotics research and rather focused on evolving of the ones already on the market[12]. Consequently, the discovery of

active natural products decreased due to reduced interest and increasing development costs (Figure 2)[25–27]: Even for companies that still invested in the discovery of new antibiotics out of soil-living microorganisms presented more and more challenges[39]. The structural complexity of most newly discovered NPs, low fermentation yields unsuitable for industrial production, or heightened toxicity rates and non-selectivity of newly characterized NPs, led to abandonment of many potent antibiotics[22,28,29].

An alternative to NPs are completely chemically synthesized molecules. They have the advantage that their synthesis is generally scalable and therefore sufficient material is available. In addition, the possibility of combining different chemical reactions offers enormous potential for derivatization. Thus, a large number of often only slightly modified analogs can be produced to screen for the most optimal compound. Specialized high throughput screening (HTS) methods to assess the antibacterial efficacy of these large, predominantly chemically synthesized, compound libraries yielded many antibacterial molecules[40]. However, most of them failed as drug candidates due to adverse effects such as toxicity due to off-target binding, poor solubility, unfavorable *in vitro* ADME (absorption, distribution, metabolism, and excretion) data or limited *in vivo* efficacy e.g. from inefficient paths to reaching their sites of action[22,29,30]. One additional challenge in antibiotics development is identification of molecules with activity against Gram-negative bacteria, as many antibiotics discovered in target-based approaches were found inefficient in crossing the double membrane layer of these types of bacteria. To circumvent this issue, one recent approach focused on development of antibodies against special bacterial surface proteins but has faced challenges owing to the low conservation of outer membrane proteins (OMPs) across different bacterial species. The low conservation reduces the chance to identify antibodies against OM surface proteins, present in divers bacterial species. Moreover, OM surface proteins were often not mutation tolerant resulting in high frequency of resistance[31].

The decline in the introduction of novel antibiotics to the market coincided with the negligent and improper treatment with low-cost antibiotics by humans and in the husbandry[32,33]. These factors triggered an increasingly rapid spread of antibiotic-resistant bacteria. To decipher how bacteria develop resistance against certain antibiotics it is important to elucidate the exact mode of action (MoA) of an antibiotic. A comprehensive understanding of involved target proteins, including their significance within bacterial cells such as their involvement in essential metabolic pathways or cell renewal are crucial to prioritize the best antibiotic leads.

1.4 Mechanism of action and antimicrobial resistance

As of the present day, we can differentiate five distinct global mechanisms by which antibiotics on the market act on bacteria either by inhibiting the growth or causing cell death (Figure 3 A, B) [34]. Antibiotics can impede the cell wall synthesis as exemplified by penicillins, carbapenems, vancomycin and monobactams, or interfere with protein biosynthesis by binding to the 30 S Ribosomal Subunit (e.g. aminoglycosides and tetracycline) or to the 50S Ribosomal Subunit (e.g. chloramphenicol, macrolides, lincosamides or streptogramins). In addition, certain antibiotics were developed to interfere with DNA/RNA synthesis and replication (e.g. quinolones or ansamycins). The first commercially available antibiotic class -the sulfonamides- target the metabolic pathway of the folic acid synthesis. Other antibiotics such as polymyxins inhibit cell wall synthesis or induce the depolarization of the cell membrane as shown for lipopeptides. Notably, two novel MoAs are currently under investigation for antibiotics development: Cell division is inhibited by benzamide but they have not reached the clinical pipeline yet and bacterial fatty acid biosynthesis is selectively targeted by the FabI inhibitor afabicin, which reached clinical trials phase 2. All MoAs are characterized by the fact that essential, often highly complex cellular processes are inhibited by the interaction of the respective antibiotic[22].

In concert with additional factors as the native and acquired immune system, the attack of the antibiotics helps humans and animals to recover in the vast majority of cases[27,35]. However, some bacterial species exhibit less sensitivity or are even resistant to the effect of certain antibiotics (Figure 3 C).

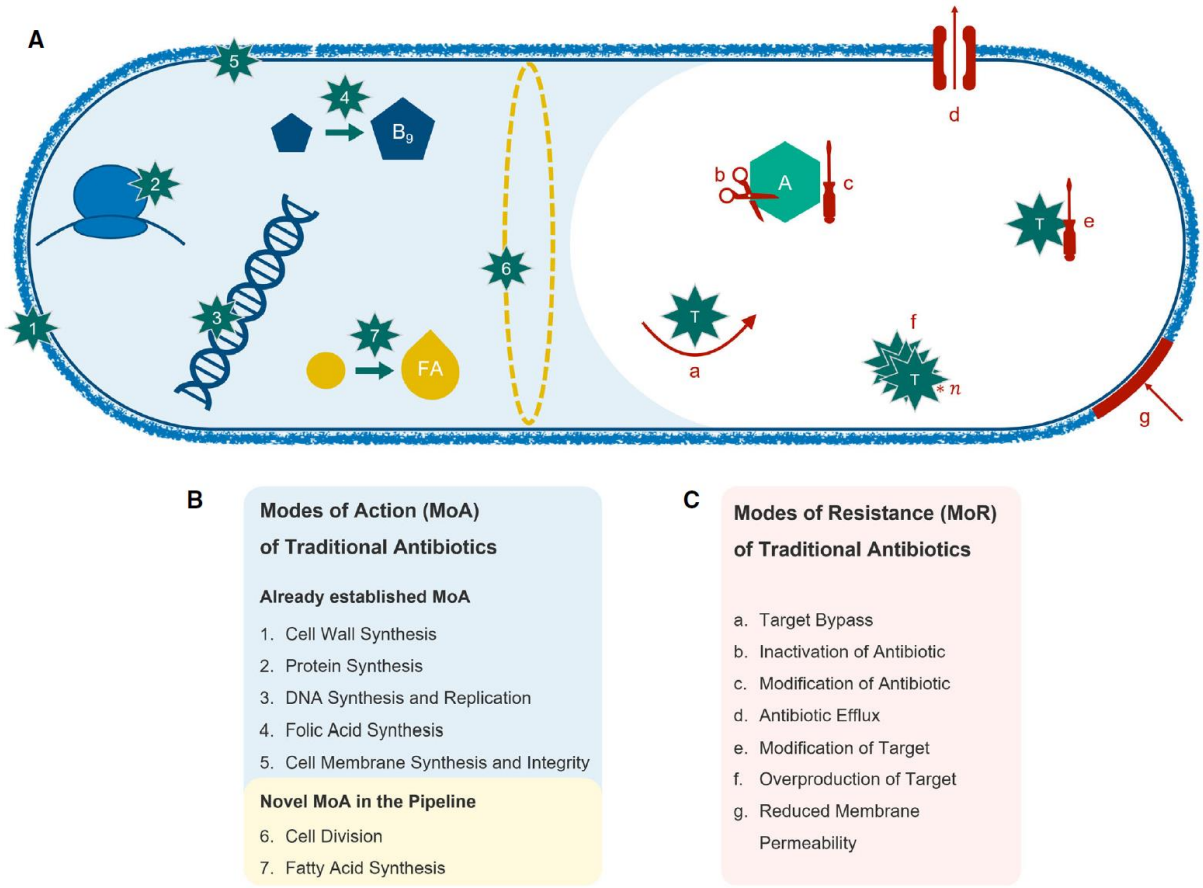

Figure 3: Modes of Action (MoA) of antibiotics and Modes of Resistance (MoR) in a schematic bacterial cell. A, B: Five different MoAs of traditional antibiotics that are in clinical use. Traditional antibiotics can attack bacterial cell wall synthesis (1), protein synthesis (2), DNA synthesis and replication (3), folic acid synthesis (4) and cell membrane synthesis and integrity (5). Two new MoA are in the pipeline but not market approved: the appropriate antibiotics are targeting cell division (6) or fatty acid synthesis (7). Each MoA is highlighted in **A** according to the numbering in green stars, correlating with the numbering in **B**. **C**: Bacteria developed or acquired resistance against antibiotics and seven general MoR can be defined, preventing the bacterial cells from the action of respective antibiotics. The MoR of traditional antibiotics are bypassing the target (a), inactivating of antibiotics (b), modifying of antibiotics (c), (antibiotic) efflux pump systems (d), modifying the target (e), overproducing of the target (f) and reducing the permeability of the bacterial membrane (g) to inhibit the entrance of antibiotics into the cell. The MoR are highlighted in red (**A**) and numbered according to the order depicted in **C**. The Figure is adapted from Walesch *et al.* 2022[22].

These bacterial stress responses can trigger gene mutations that permanently upregulate efflux pumps such as porins or can change the cell permeability of lipopolysaccharides to prevent antibiotic entry[36]. Additionally, mutations in the target site e.g. introduced by the mutated *rrs* gene in *Myxobacterium tuberculosis* result in change of the binding site on the 16 S rRNA in the A-site of the ribosome to prevent proper binding of e. g. aminoglycosides, kanamycin, amikacin and viomycin[37]. Besides mutations in the binding site, modification of the target through e.g. methylation of the 16 S subunit by rRNA methyltransferases can inhibit binding of aminoglycosides to the ribosome[38]. The methylation decreases binding efficiency of the respective antibiotic, which results in a reduced effect on the bacterial protein biosynthesis upon exposure to antibiotics acting on the methylated target site. Consequently, the bacterial cells expressing certain mutations are likely resistant against the appropriate antibiotic.

Next to point mutations or modifications of the target and upregulation of e.g. efflux pumps, many bacterial species have evolved antibacterial molecules and co-developed detoxification systems to inactivate the self-made antibiotic(s) in order to protect themselves from their bioactivity. Chromosomal gene mutations are known to be responsible for upregulating antibiotic-inactivating enzymes, such as β-lactamases in certain Gram-negative bacteria, among others in *Acinetobacter* or *Pseudomonas* species[39]. β-lactamases are in particular important for antibiotics in clinical use because they are hydrolysing and ultimatively opening the reactive β-lactam ring of β-lactam antibiotics to inhibit their function[40]. The underlying genes for inactivation enzymes are mostly co-located in the identical operon as the genes responsible for the expression of the machinery to perform the respective biosynthesis of an antibiotic. The clustered genes are located in a so-called biosynthetic gene cluster (BGC). Another example for inactivating enzymes are co-expressed acetyltransferases, as showcased in the odilorhabdin BGC, that blocks the pharmacophoric site of the broad-spectrum antibiotic odilorhabdin in the native producer *Xenorhabdus nematophila,* preventing the compound from acting on the producer itself[41,42] .

In general, bacteria that possess genes leading to increased or complete resistance to certain antibiotics have evolutionary advantages in survival. Thus, resistance mechanisms developed due to stress exposure in the past can result in increased fitness and selection of the bacteria cells carrying gene mutations responsible for higher expression rates of efflux pumps or of the target itself, among other adaptations.

Besides these specific adaptations of single bacteria to gain an advantage in survival, evolved machineries encoding for resistance can also be acquired from other bacteria in a process called horizontal gene transfer. This event, during which bacteria spread and exchange genetic information, can be divided into three mechanisms[43]: transformation, conjugation and transduction. The transformation of DNA from outside the cell represents a direct uptake of genetic information (commonly on plasmids) by the bacterial cell. Conjugation is defined by the transfer of genetic information from one cell directly to another. Transduction in contrast involves bacteriophages that serve as a vector to transfer the genetic information from cell to cell[43]. Horizontal gene transfer is more common between phylogenetically closely related bacteria but also occurs between Gram-negative and Gram-positive bacteria. For example, *Acinetobacter* species are naturally competent to take up any genetic information from the environment, frequently integrate these genes, and optionally can spread the acquired genes again on plasmids[44]. In general, the acquired genes can be expressed on transferred plasmids or be integrated into the genome of the bacterial cell where they can remain permanently.

To sum up, bacteria cannot only acquire gene clusters harboring antibiotic producing genes to gain the capacity to produce self-made weapons for combating against other bacteria. They can also acquire

genes e.g. encoding for antibiotic-inactivation enzymes or for mutated efflux pumps that are hindering antibiotics to act.

1.5 The antibiotic crisis and prospects for novel antibiotics

The intricate process of resistance development and the continuous spread of resistance among bacterial species have led to a surge in resistant pathogens. Consequently, the number of patients succumbing to infections caused by multi-drug resistant bacteria is on the rise[33,45,46]. This concerning trend is depicted in Gram-positive bacteria such as *Enterococcus*, *Staphylococcus*, and *Streptococcus* species. However, the challenge intensifies when dealing with Gram-negative bacteria due to their inherent double-membrane barrier. The World Health Organization (WHO) has emphasized the critical priority of addressing multiple Gram-negative strains, such as *E. coli*, *A. baumannii*, and *P. aeruginosa*, which significantly contribute to the alarming number of over 1.3 million deaths annually attributed to antibiotic resistance (Figure 4)[25,33,45]. The development of novel antibiotics that specifically target Gram-negative bacteria is a pressing need. Remarkably, since the introduction of monobactam (Figure 2), there has been a scarcity of new antibiotics on the market meeting this demand[22] with most novel anti-Gram-negative antibiotics being analogues of already existing antibiotic classes[26,47].

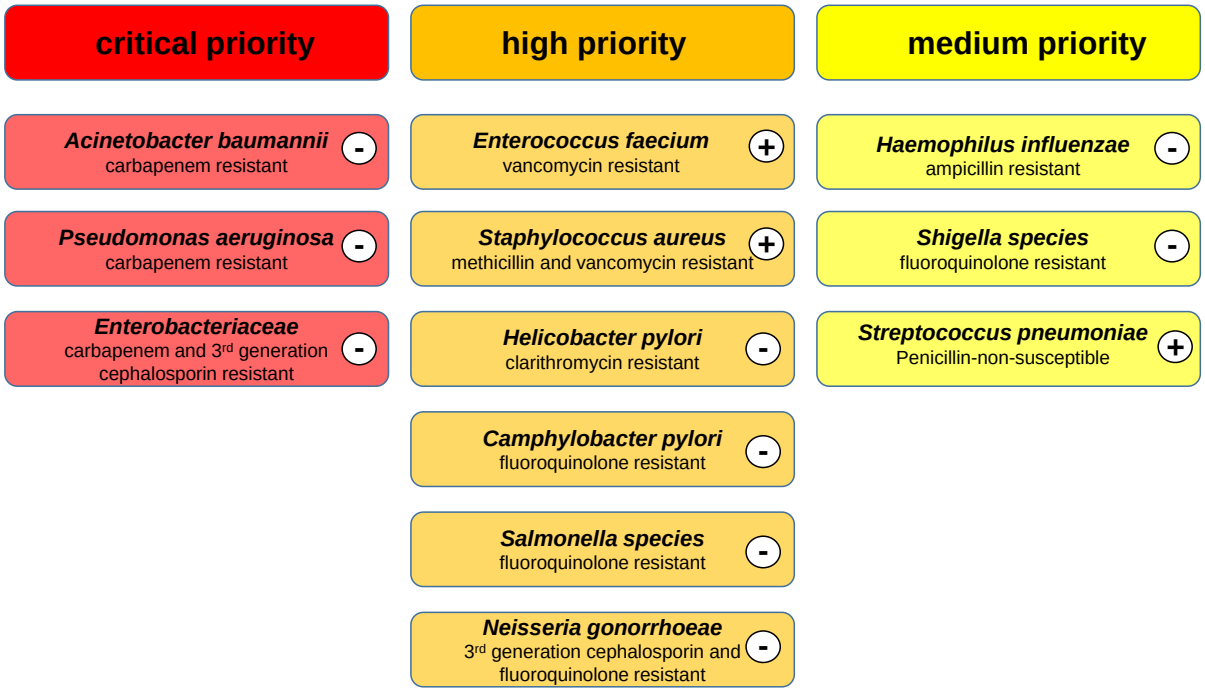

Figure 4: WHO prioritized critical and clinically relevant Gram-negative and Gram-positive pathogens. The WHO conducted a comprehensive analysis of national health reports from various countries, focusing on bacterial infections that presented limited treatment options due to antibiotic resistance against commonly used antibiotics. These hard-to-treat pathogens were classified by the WHO into three priority groups, namely critical, high, and medium. This categorization was based on the infection rates within each country and the associated mortality[48].

Despite this rather bleak picture, a few new antibiotic candidates are in development that exhibit promising antibacterial activity against Gram-negative and Gram-positive bacteria by targeting specific bacterial MoA's. The cystobactamids, for instance, originally discovered in myxobacterial isolates showed potent activity against Gram-negative and Gram-positive bacteria and no cross-resistance has been found with traditional antibiotics[49]. Furthermore, corramycin and odilorhabdin have the potency to be developed as novel rather broad-spectrum antibiotics against targets present in Gram-positive and Gram-negative bacteria[41,50]. It was possible to identify the respective antibiotic encoding BGCs responsible for the biosynthesis of these natural products. The highlighted new antibiotics were all originally isolated from their native producers and are synthesized by large and complex enzymatic machineries involving Polyketide Synthases (PKSs) and Non-Ribosomal Peptide Synthetases (NRPSs). Despite the structural difference in resulting products of these two machineries, they both follow a shared assembly scheme in which successive modules with specific domains are responsible for the assembly of individual building blocks. These building blocks are further modified by tailoring enzymes in the course of assembly, to be finally released as linear or cyclic product. The antibiotics described above combine properties such as promising antibacterial activity, little to no risk of cross-resistance and the accessibility via heterologous production or total synthesis[22]. However all three antibiotics are still in development and have to show their potency in further (pre-) clinical phases and ultimately will need to meet the demand of the pharmaceutical industry for cost-effectiveness. Heterologous production of the lead-optimized NPs is challenging due to partly low production titers, and total- or semi-synthesis often require too many expensive steps due to the high structural complexity of most NPs[21,22,25]. Their potential market approval is hard to predict with an additional risk of failure in clinical trials before even reaching to that state[38].

Thus, it is crucial to further proceed in the screening for bioactive substances to find new antibiotic classes to fight against the lack of antibiotics usable against hard-to-treat, multi-resistant pathogens[26,47]. The predicted number of deaths due to the reduced usability of antibiotics against multi-resistant pathogens might increase the number of deaths to over 10 million per year in 27 years and by then might surpass cancer in the number of deaths[51]. Consequently, research has to venture into novel paths and explore under-investigated naturally occurring antibiotic production platforms to fight against the antibiotic crisis, in order to reverse the current trend of increasing numbers of deaths[22,25,47,52].

1.6 Ribosomally synthesized and Post-translationally modified Peptides (RiPPs) in drug discovery

The majority of commonly used antibiotics are naturally synthesized via PKS and NRPS families, or from hybrid biosynthetic machineries, and their biogenesis is often used as grouping principle[53]. However,

the growing problem of antibiotic resistance has prompted the exploration of alternative sources for novel antibiotics, including the Ribosomally synthesized and Post-translationally modified Peptides (RiPPs) found with increasing rate over the past couple of years. Interestingly, bioactive NPs such as thiostrepton or bottromycin have been studied for decades without knowing that they were originally biosynthesized as RiPP[54]. The main reason for this is that the gene cluster organisation of RiPPs was less studied and unknown compared to PKS and NRPS. However, the investigation and research interest rapidly increased in the last 15 years, since it was identified how RiPPs are biosynthezised and concurrently they were named RiPPs. This emphasized the discovery of previously unknown RiPPs with intriguing antibacterial, antifungal or cytotoxic activity[55]. Tools developed in the current genomics-era include the search of RiPP-recognition elements (RRE), small ORFs and machine-learning programs to elucidate BGCs. However, RiPPs often face challenges related to poor solubility, limited bioavailability and fast enzymatic digestion within heterologous hosts that were likely also limiting factors to study newly identified RiPPs[56]. Nevertheless, they exhibit a huge biosynthetic diversity[57], which motivates ongoing research aimed at addressing physicochemical issues to harness the advantages of this family of secondary compounds that follow a relatively well-defined biosynthesis scheme (Figure 5)[57,58]. Typically, RiPPs consist of an N-terminal leader region and a C-terminal core region. The leader sequence carries a recognition sequence and is responsible for the structural orientation of the latter core region to be post-translationally modified by appropriate, mostly cluster-related enzymes. While the ribosomal synthesis directs much of the biosynthesis[57], the core sequences are often highly variable and amenable to mutations in the nucleotide sequence for broader amino acids substitution. In many cases, substrate tolerance allows for the generation of diverse analogues of mature peptides that are typically cleaved from the N-terminal leader/recognition sequence and optionally from a C-terminal tail for release. The release is catalyzed by cyclisation or by a specific or unspecific peptidase, which is often but not always associated with the BGC[57]. RiPPs can then be transported by specified transporter systems to certain cellular compartments or outside the cell.

RiPPs are classified into different families according to their specialized biosynthesis and modulation through PTMs[57]. The past years have yielded many new families and subclasses, although the majority remain incompletely characterized. Thus, the system of RiPP “taxonomy” might change in the coming years[57]. Importantly, multiple studies suggest promising antibacterial or antifungal activities of RiPPs allowing potential biotechnological and medical applications. A few of the currently best-described RiPPs are lassopeptides, lanthipeptides, thiopeptides, sactipeptides and Ras-RiPPs. All five groups comprise congeners with potent activities against diverse bacterial species[57]. Thus, these five RiPP families will be shortly summarized in the following paragraphs and selected examples of bioactive RiPPs from each family will be briefly described.

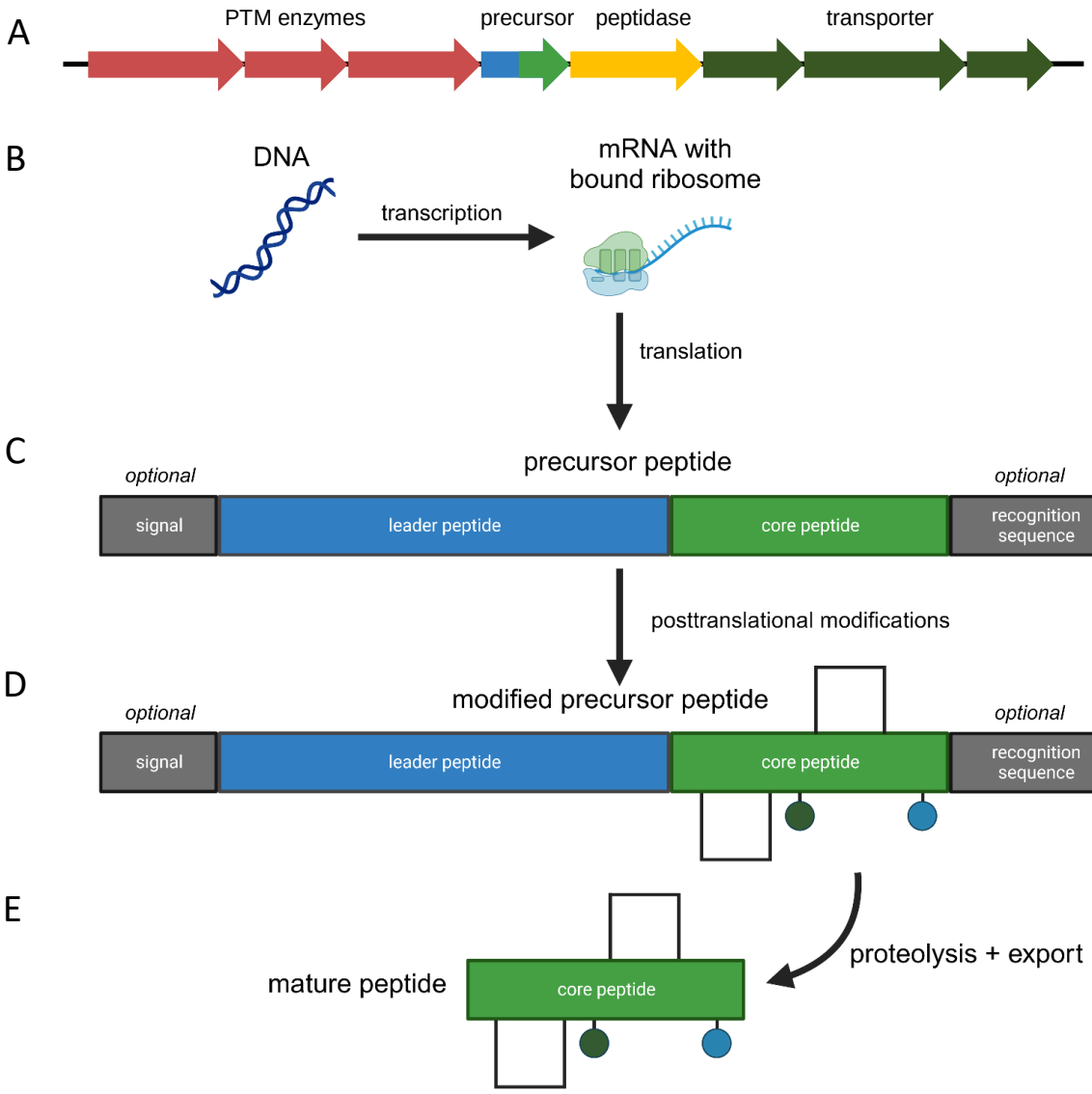

Figure 5: Scheme of Ribosomally produced and Post-translationally modified Peptide (RiPP) biosynthesis. A schematic illustration of a RiPP biosynthetic gene cluster (BGC). The BGC consists of genes encoding for posttranslational modifying (PTM) enzymes, the precursor peptide, and transporter systems and optionally for peptidase involved in proteolysis and export. **B-E** After successful transcription and translation of the precursor peptide, the leader peptide is usually crucial for the proper orientation and stabilization of the core peptide to PTM enzymes. PTM enzymes in RiPP biosynthesis recognize special parts of the leader peptide for binding and were found to e.g. catalyze cyclization, methylation or acetylation of the core peptide. Some RiPP BGC are known to carry a C-terminal recognition sequence, important for the PTM enzymes to correctly modify the RiPP but are also known to be an important sequence for peptidases to cleave and release the activated mature peptide. Certain precursor peptides carry an N-terminal signal sequence that is responsible for the secretion out of cells or for the transport into specialized cell types (e.g. in eukaryotic cells) to guide the RiPP to its destination.

1.6.1 Lassopeptides

Lassopeptides are isopeptide-linked macromolecules, often connecting the N-terminal core to a side chain containing an Asp/Glu residue (Figure 6 A). Most lassopeptides exhibit a catenane-like structure where the C-terminus interacts with the macrocycle, forming disulfide bonds and other sterically uncommon interactions, typically not seen in NRPS or PKS[59]. Lassopeptide biosynthesis involves only two main genes: a leader peptidase, typically a transglutaminase homolog, and a ring-forming

synthetase. Except in the leader cleavage site and on the isopeptide bonds, lassopeptides tolerate various modifications[57,86]. One instance of a lassopeptide with antibiotic activities is Microcin J25[60], which is originally produced by *E. coli* and showed activity against *Salmonella* species and various other *E. coli* strains[61](Figure 6 A). Similar to capistruin from *Burkholderia thailandensis*, Microcin J25 is a potent RNA polymerase inhibitor leading to cell lysis of *Bacillus* species[62] while another lassopeptide, lariatin, targets the ATPase in multiple *M. tuberculosis* species[63].

1.6.2 Lanthipeptides

Lanthipeptides, subgrouped into five classes, are known for thioether crosslinkages between cysteines[64,65]. Of the five known classes, only representatives of class one, two and three have shown to be bioactive, as the activity of the others remains yet elusive. Similar to lassopeptides, lanthipeptides undergo a two-step biosynthetic process. A dehydratase modifies serine or threonine to dehydroalanine or dehydrobutyrine, respectively, followed by glutamylation or phosphorylation of the dehydrated amino acids[64]. Subsequently, lanthionine or methyllanthionine is formed through a 1,4-nucleophilic addition of cysteine thiols to specific Dha/Dhb residues, resulting in the characteristic cyclic secondary structure of lanthipeptides (Figure 6 B). These peptides are of particular interest due to the high promiscuity of the acting dehydratases[58,64,66]. This feature enabled the fusion of artificial core regions to the leader sequence, generating novel antimicrobial peptides which find application as food preservatives, such as nisin[58,64](Figure 6 B). Notably, in randomized techniques such as phage or yeast display, recent studies described the successful identification of new lanthipeptides as binders to certain target proteins such as the HIV p6 protein with potentially enhanced activity compared to known inhibitors[67]. Lantibiotics[64], a subset of lanthipeptides, were found to exhibit antibacterial activity via multiple mechanisms, such initial lipid II sequestration resulting in pore formation (nisin), or binding to phosphatidylethanolamine, resulting in membrane depolarization (duramycin)[58].

1.6.3 Thiopeptides

Thiopeptides represent a structurally diverse class of RiPPs characterized by Dha/Dhb residues forming macrocyclic peptides, comparable with lanthipeptides[68] (Figure 6 C). However, contrary to lanthipeptides, they incorporate azoline heterocycles and carry a variable N-heterocycle out of six variable amino acids, allowing classification into subclasses[57]. The thiopeptide biosynthesis is relatively flexible and therefore not fully understood for all subclasses[68]. The initial steps typically involve multiple cyclization reactions on Cys residues and partial dehydrogenation, related to the biosynthesis of linear azoline-containing peptides[57,69]. Subsequent glutamylation and elimination reactions are often performed by a tRNA-dependent dehydrogenase[69], similar to lanthipeptides. The study of thiopeptides is hindered due to their often high hydrophobicity, leading to poor solubility[57]. However, some thiopeptides, such as GE2270A[70] (Figure 6 C), have demonstrated potent antibacterial activity against hard-to-treat *Clostridium difficile* strains. Development of semi-synthetic GE2270A derivatives

has yielded analogs with antibacterial activity comparable to the widely used broad-spectrum antibiotic vancomycin[71]. The intramolecular cyclization complicates structural predictions, but elucidation of some biosynthetic machineries already facilitates the generation of novel, *de novo* thiopeptides with enhanced bioactivity through mutations of core peptides[57].

1.6.4 Sactipeptides

An additional structurally interesting group of RiPPs are the Sactipeptides. They are characterized by "sulfur-to-alpha carbon linked"[57] thioesters that form a stable hairpin-like secondary structure (Figure 6 D). These cyclic thioesters have been successfully produced in heterologous hosts such as *E. coli* and exhibit substantial substrate tolerance[57]. Sactipeptides, such as subtilosin A or thuricin CD[72,73] (Figure 6 D), have been shown to effectively lyse *Bacillus subtilis* cells during co-cultivation experiments by disrupting their cell membrane[73].

1.6.5 Ras-RiPPs

Ras-modified RiPPs (Ras-RiPPs) were initially discovered using innovative genome mining approaches, revealing their unique biosynthesis that is distinct from other RiPPs[74]. The modular biosynthesis scheme of Ras-RiPPs comprises a precursor gene, grouped in a leader, core and optionally an N-terminal tail sub-sequence, additional PTM genes for the cleavage of the mature bioactive Ras-RiPP, comparable to other RiPP families[75]. In addition, Ras-RiPPs carry genes, which encode for Ras enzymes also termed rSAMs (to prevent confusion with the family of small Ras GTPases crucial in cell signaling, differentiation, and growth[76]). These rSAMs are (metallo-)enzymes that catalyze cyclization of the core peptide, thereby modulating the bioactive mature RiPP[77]. The cyclization process enabled by rSAMs is metal-dependent and can generate diverse linkages, predominantly but not exclusively between lysine and tryptophan, as observed in streptide[78], tryglysin A[79] and darobactin A[80] (Figure 6 E). However, rSAMs can also modulate ester linkages between two amino acids as demonstrated in darobactins[80] (Figure 6 E) or form cysteine bridges exemplified by streptosactin[77]. Numerous Ras-RiPPs exhibit antibacterial properties, serving as a defense mechanism to protect the native producer in its ecological niche[79]. Tryglysin A, produced by *S. thermophilus* for instance is effectively inhibiting the growth of other streptococci, which are co-residing in the mouth of humans and associated with infections of the mucous membrane[79]. Another Ras-RiPPs compound class, the darobactins, originally produced by *Photorhabdus khanii*, a nematodic symbiont, exhibit a remarkable broad-spectrum activity against anti-Gram negative bacteria[80].

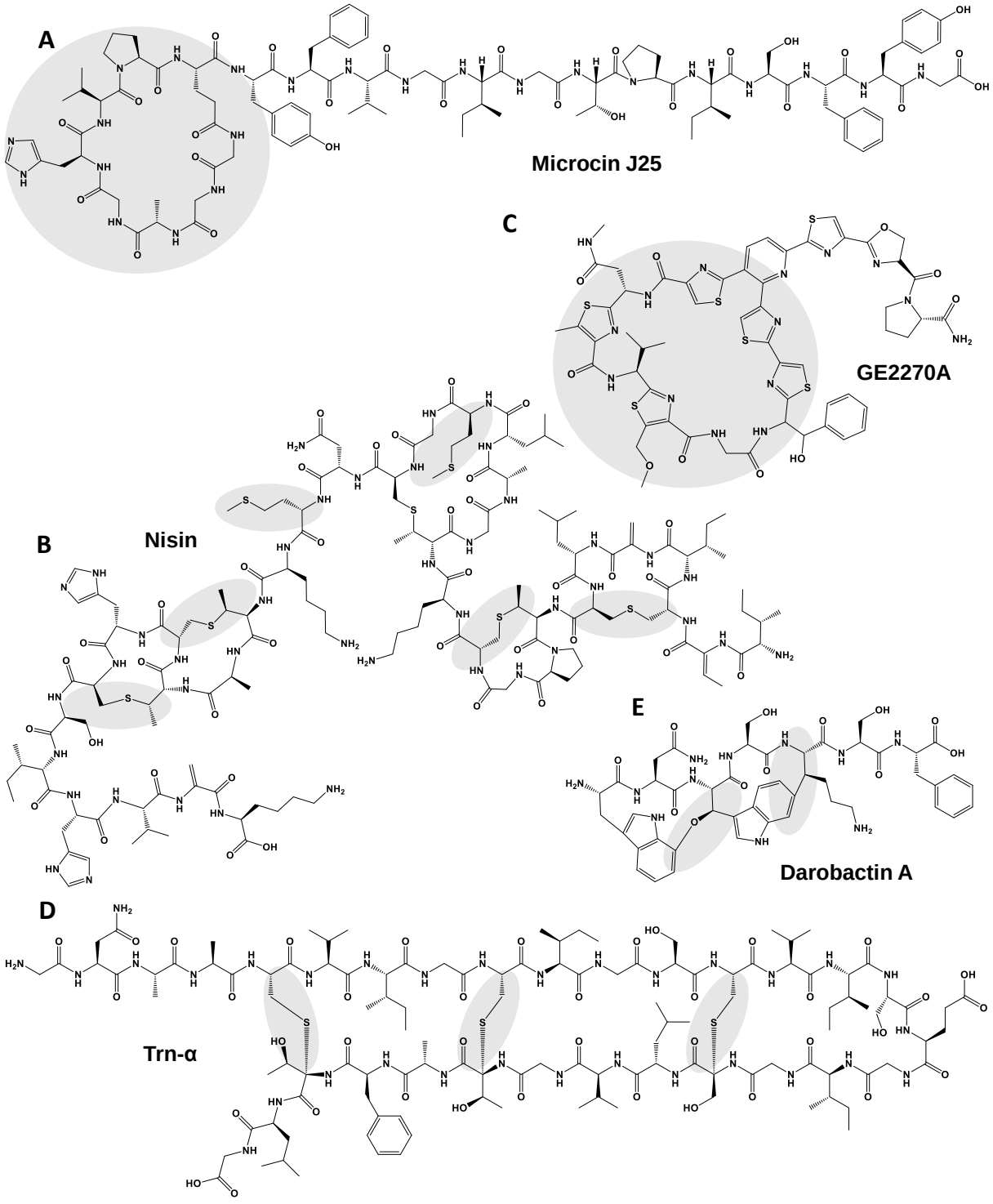

Figure 6: Representative RiPPs exhibiting antibacterial activity. A the lassopeptide Microcin J25[60] showing a characteristic N-terminal cyclization, **B** the lanthipeptide nisin exhibiting the thioether cross-links between cysteines[81], **C** the thiopeptide GE2270A froms a macrocycle[70], **D** the Trn-α part of the hairpin-forming thiopeptide Thuricin CD. In combination with Trn-β, Trn-α build the bacteriocin Thuricin CD [82], **E** the Ras-RiPP darobactin A showing the characteristic rSAM modulated bi-cyclication[80]. Characteristic structural features of each RiPP are highlighted in grey.

1.7 Darobactin – the discovery of a novel antibiotic class

In the quest for novel bioactive natural products, Kim Lewis and colleagues initiated the screen of various *Xenorhabdus* and *Photorhabdus* strains[80]. These bacteria species primarily inhabit the gut of soil-living nematodes, serving as entomopathogenic symbionts of their host[83]. They produce enzymes and secondary metabolites to digest the nutrients of nematodes or counteract diverse microorganisms and insects[84]. Numerous *Photorhabdus* strains have already been isolated, producing wide-ranging insecticides[85]. They were identified to be producers of a large variety of antifungal and antibacterial NPs[118–121]. This broad repertoire of bioactive secondary metabolites guarantees their survival in the gut microbiome of nematodes by defeating invaded bacteria, fungi, and insects. Consequently, the presence of symbiotic *Photorhabdus sp*. is an evolutionary advantage for both, the bacterium and the nematode and helps to keep the microbiome of nematodes intact[84,86]. The high number of BGCs in their 4 – 6 Mbp sized indicates substantial biosynthetic potential and also reflects the symbiotic lifestyle of the two closely related genera *Photorhabdus* and *Xenorhabdus*. With the limited number of genomes sequenced, it can be extrapolated that there are unexplored BGCs within these genera[80]. Thus, there is potential of finding and characterizing many novel secondary metabolites[86]. Due to their symbiotic lifestyle, it is to be expected that the secondary metabolites formed are selective against specific bacteria rather than acting broadly and therefore not against their symbiont or human target proteins, as they have not posed a respective evolutionary threat against which selection has occurred.

1.7.1 Discovery, identification and characterization of darobactin A

To investigate the production of bioactive NPs, Imai *et al.* initially spotted 67 isolates from 28 different X*enorhabdus* and *Photorhabdus* strains onto agar plates, overgrown with the target microorganism *E. coli* without any sign for bacterial growth inhibition. They concluded that potential bioactive natural products might be encoded by cryptic BGCs, prompting the need for extract generation from the bacterial cultures to increase the concentration of the bioactive NPs to see an effect. This effort led to a small inhibition zone of *E. coli* growth after spotting the agar plate with concentrated *P. khanii* HGB1456 extract. Further investigations involved large-scale fermentation of this strain, proceeding with analyzing the presence of novel compounds through high-performance liquid chromatography and high-resolution electrospray ionization mass spectrometry. This revealed a potential new molecule with the mass of 966.4104 and the molecular formula of $C_{47}H_{56}O_{12}N_{11}^{+}$. No matches were found in public databases, leading to the conclusion that this mass represented an unknown antibacterial metabolite. Consequently, the researchers purified the corresponding NP after large-scale fermentation of the native producer strain and elucidated its structure using mass spectrometry fragmentation and Nuclear Magnetic Resonance (NMR) techniques. The structural elucidation combined with an analysis of the mass-spectrometry fragmentation indicated a bi-cyclic heptapeptide

with the amino acid sequence of $W_1N_2W_3S_4K_5S_6F_7$. The first cyclization links the N-terminal tryptophan W_1 with the third amino acid–an additional tryptophan (W_3)–via an ester linkage. The second ring is formed through a carbon-carbon connection of W_3 and the lysine at position 5 (K_5) (Figure 7).

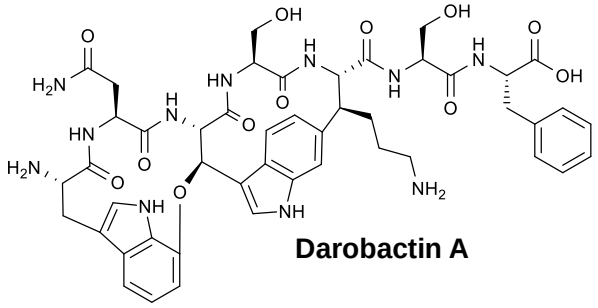

Figure 7: Chemical structure of darobactin A, the first isolated native darobactin[80].

The novel compound, named darobactin A (**DA**) (Figure 7, Figure 10 A), was tested for its bioactivity in MIC assays against clinically relevant pathogens, intestinal gut bacteria and human cell lines. **DA** had a remarkably low micromolar Gram-negative activity against the tested pathogens and –as hypothesized based on its biosynthesis by a symbiotic bacterium– no activity against human cell lines and notably not against phylogenetically distinct intestinal gut bacteria. Additionally, sequencing and analyzing the whole genome of *P. khanii* HGB1456 resulted in identification of the nucleotide sequence of the darobactin heptapeptide. They detected a characteristic RiPP-like BGC that could be differentiated into five genes: *darA* encodes the propeptide with the nucleotide sequence of **DA** and *darB*, *darC* and *darD* encode an ABC-like trans-envelope exporter. DarB and DarD are predicted to be the transporter domains of the trans-envelope exporter, and *darC* is predicted to be a membrane spanning protein. The terminal gene in the *dar* operon was found to encode a potential Ras-RiPP enzyme, also known as rSAM and termed *darE*. The workflow to discover and characterize **DA** is summarized in Figure 8 A – D.

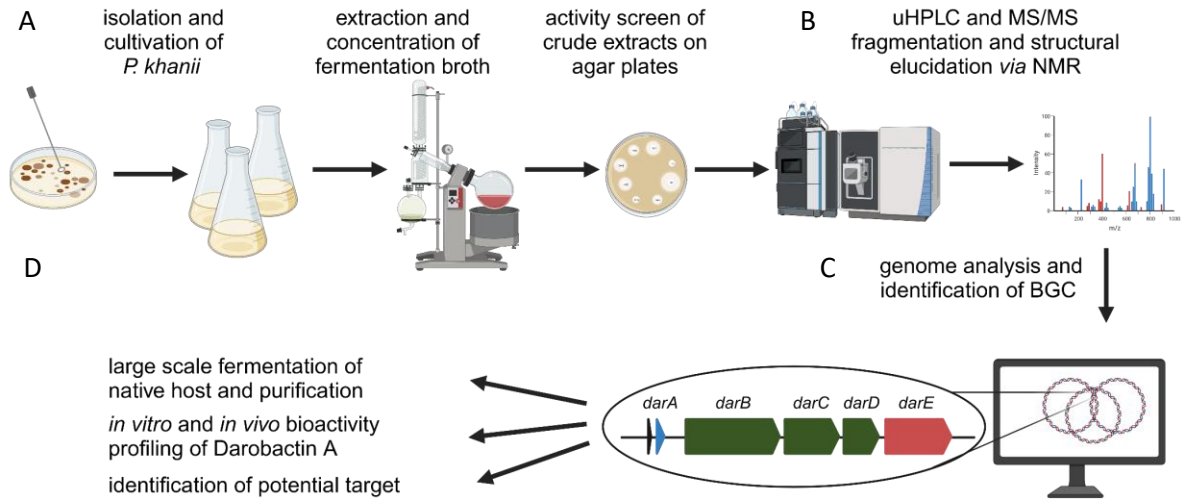

Figure 8: Discovery and characterization of the novel antibiotic candidate darobactin A (DA). 67 isolates of various *Xenorhabdus* and *Photorhabdus* species were cultivated for 8 days. Supernatants were concentrated to generate crude extracts for investigating antibacterial activity against *E. coli*. **B** The extracts displaying a zone of inhibition were subjected to various very spectrometric analysis methods. These analyses identified a potential unknown compound with the molecular formula of $C_{47}H_{56}O_{12}N_{11}^+$ and a calculated $[M + H]^+$ mass of 966.4104. **C** The genome of *P. khanii* HGB1456 was fully sequenced and assembled. Manual screening of all biosynthetic gene clusters (BGCs) in the genome led to the identification of a RiPP cluster. The core peptide sequence, WNWSKSF, matched the calculated molecular formula of the predicted novel compound. This RiPP gene operon was named *darABCDE* operon, and the compound was designated as **DA**. **D** The molecule was purified from the native producer strain to determine its exact structure *via* NMR. Subsequent *in vitro* and *in vivo* bioactivity profiling against a wide range of Gram-positive, Gram-negative bacterial strains, and eukaryotic cell lines was conducted. Furthermore, Imai *et al.* conducted *in vivo* pharmacokinetic/pharmacodynamics (PK/PD) studies and infection experiments. Mutated genes were analyzed, and the predicted target protein was purified based on the results obtained from FoR assays to study the potential effect of **DA** on its predicted target protein[80].

1.7.2 Target identification and mode of action of darobactin A

Inspired by **DA**'s promising selective anti-Gram-negative antibacterial activity, Lewis and colleagues aimed to identify **DA**'s MoA. They conducted a frequency of resistance (FoR) screening to get an idea of the likelihood of resistance development. Subsequently, the appearing mutants were sequenced to ideally find potential target proteins that carry mutations leading to the corresponding resistance against **DA**. The FoR led to three mutants with mutations in the gene encoding BamA. BamA is an outer membrane protein (OMP) spanning the bacterial outer membrane in Gram-negative bacteria and the key domain of the multi-domain Bam complex consisting of BamABCDE (BAM). BAM is crucial for the incorporation and proper folding of OMPs and consequently essential for the integrity of Gram-negative bacterial cells. In brief, BamA recruits OMPs in the periplasm, transfers and refolds them through the lateral gate on BamA into the membrane spanning β-barrel for integration into the membrane (Figure 9). Fortunately, mutants were characterized by a significant reduction in fitness and virulence. Thus, the risk of mutations is rather low due to the essential role of BAM for Gram-negative bacteria. *In vitro* refolding assays demonstrated the misfolding of tested OMP OmpT in the presence of darobactin, underpinning darobactin's crucial role in protein modeling (Figure 9). Further NMR

studies led Imai *et al.* to suggest that **DA** stabilizes a closed conformation of BamA, resulting in blockage of the entrance of the lateral gate of the BAM complex[80]. The predicted target BamA made darobactin a promising antibiotic candidate as it attacks a novel target site selectively present in Gram-negative bacteria.

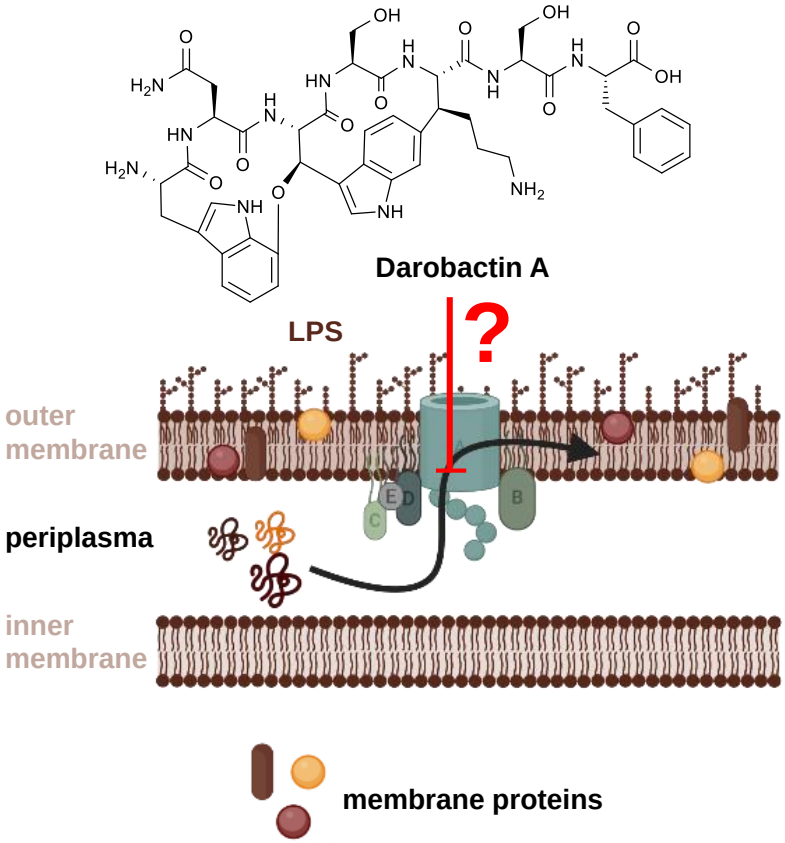

Figure 9: Identification of the target protein BamA and potential mode of action (MoA) of darobactin A (DA). Through a series of *in vitro* assays using purified BamA (a subdomain of the BamABCDE complex), it was determined that **DA** inhibits the proper folding of outer membrane proteins (OMPs) and prevents their incorporation into the outer membrane of Gram-negative bacteria. This mechanism likely underlies the bacteriolytic activity observed against Gram-negative bacteria. While the exact mode of binding of darobactin A remains unclear, it has been established that **DA** interacts with BamA. This interaction has led to the conclusion that darobactins target a novel protein, not targeted by currently available antibiotics on the market with the outer membrane as MoA. The figure is adapted from Seyfert et al. 2023[87].

1.7.3 *In vivo* activity of darobactin A

The promising *in vitro* MIC data of **DA** specifically against clinically relevant Gram-negative pathogens such as *E. coli*, *A. baumannii*, *P. aeruginosa* and *K. pneumonia* were substantiated by corresponding *in vivo* activity against *P. aeruginosa*, *K. pneumoniae* and *E. coli* in mouse infection models. The activity against *E. coli* is evident even at low concentrations of 2.5 mg/kg, comparable to gentamycin and prevents death of the experimental mice in all cases. However, its activity against tested *P. aeruginosa* and *K. pneumoniae* strains was diminished, requiring a 20-fold higher dosing for complete (for *K. pneumoniae*) or only partial rescue (for *P. aeruginosa*) of the mice[80].

1.7.4 Novel darobactin derivatives darobactin B–E

Further exploration in public sequence databases led to the discovery of homologous BGCs with partly artificial nucleotide core sequences in the propeptide-encoding *darA*. Imai *et al.* found sequences encoding potential native analogues named as darobactin B, C, D and E, which all occur in other *Photorhabdus* or *Yersinia* species (Figure 10 B – E). However, the four native analogues have not yet been isolated from the corresponding hosts, so no conclusions can be drawn as to whether they have similar or different bioactivities against the tested panel of microorganisms[80]. Since **DA** already showed a promising *in vivo* activity against *E. coli* and *P. aeruginosa* and *K. pneumoniae*, further investigations of the native derivatives would be of great interest. In general, the finding of variable core sequences in different darobactin BGCs hints at the possibility of generating large-scale amino acid substitutions in the core peptide to generate new non-native darobactins and test them for bioactivity.

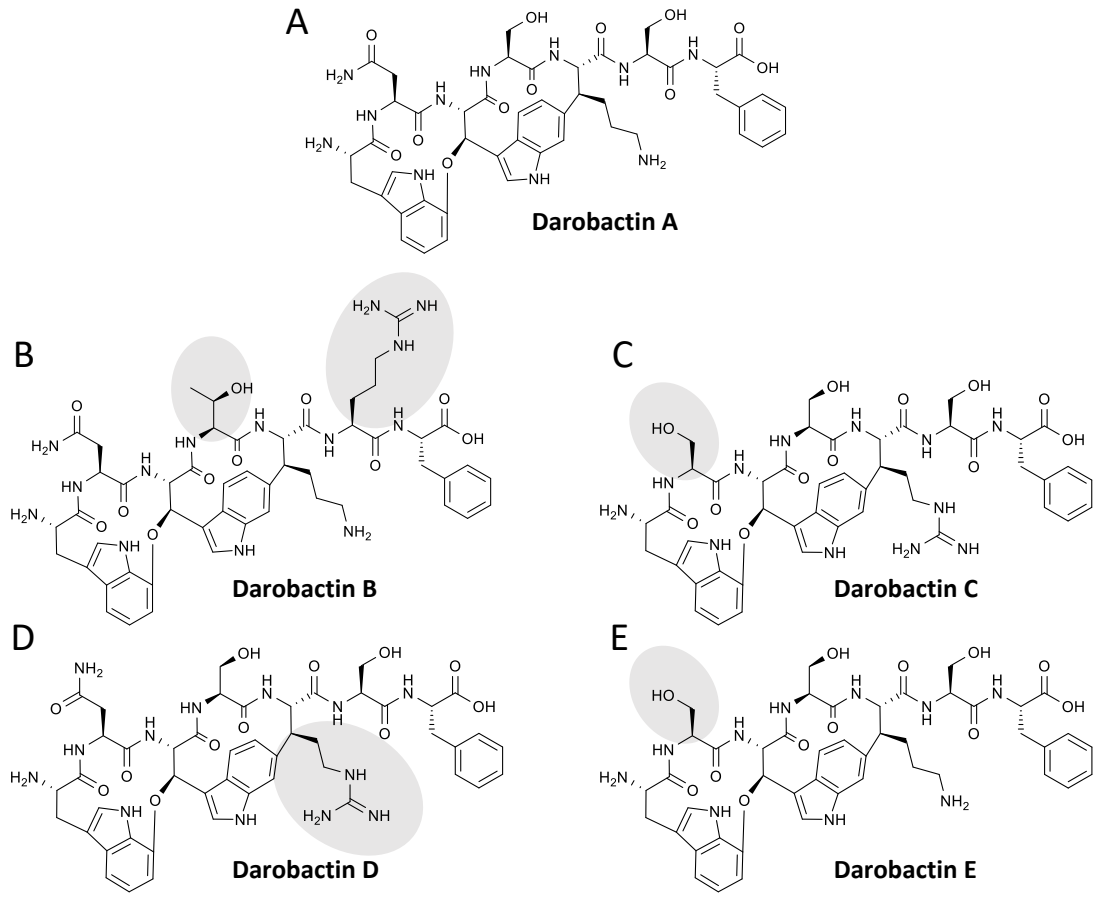

Figure 10: Native darobactin derivatives. Besides darobactin A, isolated from *P. khanii* HGB1456, four additional nucleotide core sequences similar to the darobactin BGC were found in the genome of phylogenetically closely related *Photorhabdus* and *Yersinia* species. They were named as darobactin B (*Photorhabdus symbioticus* and *Photorhabdus australis*), darobactin C (*Yersinia pseudotuberculosis* and *Yersinia pestis*), darobactin D (diverse *Yersinia* species) and darobactin E (*Yersinia bercovieri*)[80].

In summary, **DA** exhibits potent bacteriolytic activity against critical and clinically relevant pathogens, priorized by the WHO, against which many antibiotics on market are not active anymore or limited in their usability. The target site and the mechanism of action of **DA** is new: No antibiotic on the market

targets BamA or other domains of the BAM complex. Furthermore, BamA is an exceptionally interesting novel target, as it represents an essential protein for all Gram-negative bacteria and mutations come with reduced virulence and fitness.

1.8 Outline of this thesis

The thesis centers around the study of a recently discovered new antibiotic class, the darobactins. The promising selective antibacterial activity against Gram-negative pathogens of native **DA** recently described for the first time has already been demonstrated *in vitro* and *in vivo*. Additionally, the BGC responsible for the biosynthesis of the secondary metabolite has been decoded in the genome of the native producer *Photorhabdus khanii*. However, the low production titer in the native producer strains is the current bottleneck for further investigation and profiling of **DA** and the predicted additional native analogues such as **DB**, **DC**, **DD,** and **DE**. Along these lines, this work investigates possibilities to improve the production in a heterologous host, to elucidate biosynthesis in order to define the minimal cluster size, and to explore the efficacy of compound derivatisation for the production of additional antibacterial native and non-natural derivatives. The exact MoA had not been known yet, hindering targeted optimization of the molecule. To overcome this limitation, the work also addresses this issue through the development of a structure- and activity-driven approach to further increase the antibacterial activity of darobactins, and to eventually profile the best hits in advanced assays. The linkage between individual chapters of this thesis are illustrated in Figure 11.

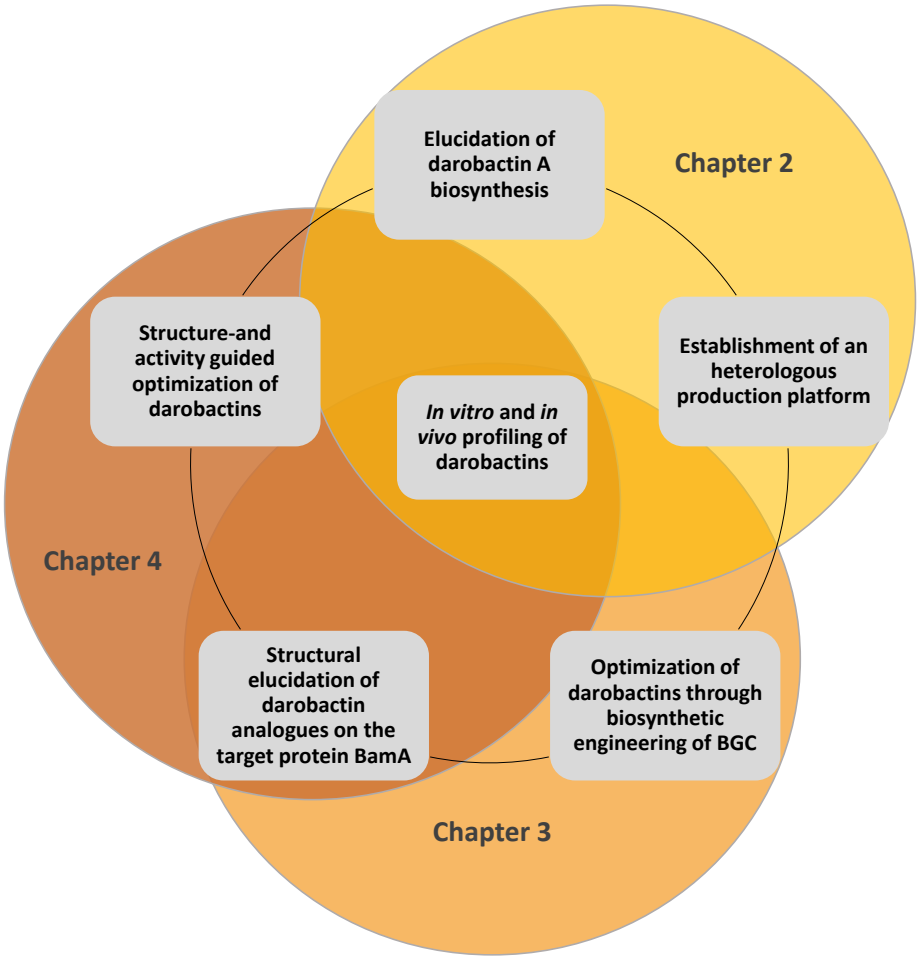

Figure 11: Illustration of the different chapters of this doctoral thesis and their interplay with each other.

Chapter 2 of this work addresses the *in silico* design of the darobactin BGC to heterologously express and overproduce **DA** and native analogues as well as non-native artificial derivatives**,** in the well–described host *E. coli.* Additonally, the chapter describes the characterization of the darobactin BGC, versatile cluster modifications expandable for future engineering of the BGC and the optimization of fermentation conditions. Subsequent analysis of the antibacterial activity and profiling of the derivatives resulted in the identification of **D9**, which exhibits an higher antibacterial activity compared to **DA**.

Since the heterologous production platform implemented in chapter 2 yielded derivatives with significantly increased activity compared to the native **DA**, the next step was more targeted optimization of **D9**. For this purpose, through elucidation of the BAM-**D9** Cryo-EM complex-structure, Chapter 3 describes 1) the analysis of the binding mode of **D9** in comparison to **DA** to explain its rise in antibacterial activity and 2) the design of new derivatives using the BAM-**D9** co-structure as a blueprint to increase the potential formation of hydrogen bonding interactions with its target protein to enhance the activity. This structure- and activity-guided approach results in darobactin 22 (**D22)**, exhibiting an up to 32-fold increased activity against clinical CRAB isolates compared to **D9**. In addition to further profiling of **D22**, chapter 3 also analyses for the first time which changes at certain positions of the heptapetide lead to increased or reduced antibacterial activity. This formed the basis for further specific derivatization of the new frontrunner **D22**, as discussed in chapter 4.

Consequently, starting from the complex-structure of BAM-**D22,** chapter 4 deals with so far underinvestigated positions of the darobactin heptapeptide. It describes the generation of derivatives **D58** to **D74** through investigation of previously less exposed positions 2, 4 and 5 by mutagenesis. Chapter 4 underpins the succesrate of our newly established workflow in generating highly active non-native darobactin analogues by yielding a further optimized derivative **D69**. In addition, its expansion by the establishment of a MST assay to subsequently analyze the binding constant K_D on its target protein for all purified derivatives is demonstrated. Moreover, the *in vitro* ADMET profiles of the frontrunner molecules **D22** and **D69** are summarized and paves the way for *in vivo* studies of these new darobactins.

Finally, in the discussion chapter perspectives for future development opportunities of the darobactin class are discussed, including the evaluation of **D22** and its chances as well as risks of being further developed as a new antibiotic candidate.

References

1 G. M. Cragg and D. J. Newman, *Biochim. Biophys. Acta*, 2013, **1830**, 3670.

2 M. Wainwright, *Mycologist*, 1989, **3**, 21.

3 a) D. Normile, *Science (New York, N.Y.)*, 2003, **299**, 188; b) A. K. Pandey and S. Kumar, *Pharmacologia*, 2013, **4**, 469;

4 a) P. D. Gupta and T. J. Birdi, *Journal of Ayurveda and integrative medicine*, 2017, **8**, 266; b) I. Ahmad and A. Z. Beg, *J. Ethnopharmacol.*, 2001, **74**, 113; c) M. Graf and I. Stappen, *Molecules (Basel, Switzerland)*, 2022, **27**, 7295; d) A. Abedini, M. Colin, J. Hubert, E. Charpentier, A. Angelis, H. Bounasri, B. Bertaux, A. Kotland, F. Reffuveille, J.-M. Nuzillard, J.-H. Renault and S. C. Gangloff, *Antibiotics*, 2020, **9**, 111; e) Dallas Rohraff and Roderick Morgan, *The FASEB Journal*, 2016, **30**, lb124-lb124;

5 a) N. Adnani, S. R. Rajski and T. S. Bugni, *Nat. Prod. Rep.*, 2017, **34**, 784; b) V. M. de Siqueira, R. Conti, J. M. d. Araújo and C. M. Souza-Motta, *Symbiosis*, 2011, **53**, 89;

6 A Fleming, *Br. J. Exp. Pathol.*, 1929, **10**, 226.

7 M. I. Hutchings, A. W. Truman and B. Wilkinson, *Curr. Opin. Microbiol.*, 2019, **51**, 72.

8 G. Domagk, *Angew. Chem.*, 1935, **46**, 657.

9 H. Otten, *J Antimicrob Chemother*, 1986, **17**, 689.

10 R. Bentley, *Journal of Industrial Microbiology & Biotechnology*, 2009, **36**, 775.

11 *Stemming the superbug tide. Just a few dollars more / OECD*, OECD Publishing, Paris, 2018.

12 M. A. Cook and G. D. Wright, *Sci. Transl. Med.*, 2022, **14**, eabo7793.

13 a) Waksman, S. A., Horning, E. S., Welsch, M., & Woodruff, H. B., 1942, 281; b) K. Lewis, *Nature*, 2012, **485**, 439; c) E. D. Brown and G. D. Wright, *Nature*, 2016, **529**, 336;

14 S. A. Waksman, A. Schatz and D. M. Reynolds, *Annals of the New York Academy of Sciences*, 2010, **1213**, 112.

15 S. A. Waksman and H. B. Woodruff, *J. Bacteriol.*, 1941, **42**, 231.

16 S. A. Waksman and A. Schatz, *Journal of the American Pharmaceutical Association (Scientific ed.)*, 1945, **34**, 273.

17 A. Schatz, E. Bugle and S. A. Waksman, *Experimental Biology and Medicine*, 1944, **55**, 66.

18 L. Katz and R. H. Baltz, *J. Ind. Microbiol. Biotechnol.*, 2016, **43**, 155.

19 D. J. Newman and G. M. Cragg, *J. Nat. Prod.*, 2016, **79**, 629.

20 B. Shen, *Cell*, 2015, **163**, 1297.

21 J. D. Hegemann, J. Birkelbach, S. Walesch and R. Müller, *EMBO Rep.*, 2022, **published concurrently**.

22 S. Walesch, J. Birkelbach, G. Jézéquel, F. P. J. Haeckl, J. D. Hegemann, T. Hesterkamp, A. K. H. Hirsch, P. Hammann and R. Müller, *EMBO Rep.*, 2022, e56033.

23 a) S. Kenyon, M. Boulvain and J. Neilson, *Obstet Gynecol*, 2004, **104**, 1051; b) T. S. P. Tiwari, A. L. Baughman and T. A. Clark, *Pediatrics*, 2015, **135**, 990;

24 C. L. Ventola, *Pharmacy and Therapeutics*, 2015, **40**, 277.

25 E. Tacconelli, E. Carrara, A. Savoldi, S. Harbarth, M. Mendelson, D. L. Monnet, C. Pulcini, G. Kahlmeter, J. Kluytmans, Y. Carmeli, M. Ouellette, K. Outterson, J. Patel, M. Cavaleri, E. M. Cox, C. R. Houchens, M. L. Grayson, P. Hansen, N. Singh, U. Theuretzbacher, N. Magrini, A. O. Aboderin, S. S. Al-Abri, N. Awang Jalil, N. Benzonana, S. Bhattacharya, A. J. Brink, F. R. Burkert, O. Cars, G. Cornaglia, O. J. Dyar, A. W. Friedrich, A. C. Gales, S. Gandra, C. G. Giske, D. A. Goff, H. Goossens, T. Gottlieb, M. Guzman Blanco, W. Hryniewicz, D. Kattula, T. Jinks, S. S. Kanj, L. Kerr, M.-P. Kieny, Y. S. Kim, R. S. Kozlov, J. Labarca, R. Laxminarayan, K. Leder, L. Leibovici, G. Levy-Hara, J. Littman, S. Malhotra-Kumar, V. Manchanda, L. Moja, B. Ndoye, A. Pan, D. L. Paterson, M. Paul, H. Qiu, P. Ramon-Pardo, J. Rodríguez-Baño, M. Sanguinetti, S. Sengupta, M. Sharland, M. Si-Mehand, L. L.

Silver, W. Song, M. Steinbakk, J. Thomsen, G. E. Thwaites, J. W. M. van der Meer, N. van Kinh, S. Vega, M. V. Villegas, A. Wechsler-Fördös, H. F. L. Wertheim, E. Wesangula, N. Woodford, F. O. Yilmaz and A. Zorzet, *Lancet Infect. Dis.*, 2018, **18**, 318.
26 K. Lewis, *Cell*, 2020, **181**, 29.
27 M. Miethke, M. Pieroni, T. Weber, M. Brönstrup, P. Hammann, L. Halby, P. B. Arimondo, P. Glaser, B. Aigle, H. B. Bode, R. Moreira, Y. Li, A. Luzhetskyy, M. H. Medema, J.-L. Pernodet, M. Stadler, J. R. Tormo, O. Genilloud, A. W. Truman, K. J. Weissman, E. Takano, S. Sabatini, E. Stegmann, H. Brötz-Oesterhelt, W. Wohlleben, M. Seemann, M. Empting, A. K. H. Hirsch, B. Loretz, C.-M. Lehr, A. Titz, J. Herrmann, T. Jaeger, S. Alt, T. Hesterkamp, M. Winterhalter, A. Schiefer, K. Pfarr, A. Hoerauf, H. Graz, M. Graz, M. Lindvall, S. Ramurthy, A. Karlén, M. van Dongen, H. Petkovic, A. Keller, F. Peyrane, S. Donadio, L. Fraisse, L. J. V. Piddock, I. H. Gilbert, H. E. Moser and R. Müller, *Nat. Rev. Chem.*, 2021, **5**, 726.
28 D. J. Payne, M. N. Gwynn, D. J. Holmes and D. L. Pompliano, *Nat. Rev. Drug Discov.*, 2007, **6**, 29.
29 F. A. Bernal, P. Hammann and F. Kloss, *Current opinion in biotechnology*, 2022, **78**, 102783.
30 Tommasi, R., Brown, D. G., Walkup, G. K., Manchester, J. I., & Miller, A. A., 2015, 529.
31 a) K. M. Storek, M. R. Auerbach, H. Shi, N. K. Garcia, D. Sun, N. N. Nickerson, R. Vij, Z. Lin, N. Chiang, K. Schneider, A. T. Wecksler, E. Skippington, G. Nakamura, D. Seshasayee, J. T. Koerber, J. Payandeh, P. A. Smith and S. T. Rutherford, *PNAS*, 2018, **115**, 3692; b) H. Kaur, J.-B. Hartmann, R. P. Jakob, M. Zahn, I. Zimmermann, T. Maier, M. A. Seeger and S. Hiller, *J. Biomol. NMR*, 2019, **73**, 375; c) P. White, S. F. Haysom, M. G. Iadanza, A. J. Higgins, J. M. Machin, J. M. Whitehouse, J. E. Horne, B. Schiffrin, C. Carpenter-Platt, A. N. Calabrese, K. M. Storek, S. T. Rutherford, D. J. Brockwell, N. A. Ranson and S. E. Radford, *Nat Commun*, 2021, **12**, 4174; d) J.-B. Hartmann, M. Zahn, I. M. Burmann, S. Bibow and S. Hiller, *J. Am. Chem. Soc.*, 2018, **140**, 11252;
32 a) H. C. Neu, *Science*, 1992, **257**, 1064; b) C. L. Ventola, *Pharmacy and Therapeutics*, 2015, **40**, 277;
33 Global Antimicrobial Surveillance System (GLASS) Report 2016-2017, https://apps.who.int/iris/bitstream/handle/10665/279656/9789241515061-eng.pdf?ua=1, (accessed 27 November 2020).
34 Z. Breijyeh, B. Jubeh and R. Karaman, *Molecules (Basel, Switzerland)*, 2020, **25**.
35 R. Anderson, G. Tintinger, R. Cockeran, M. Potjo and C. Feldman, *Pharmaceuticals (Basel, Switzerland)*, 2010, **3**, 1694.
36 P. A. Lambert, *J. Appl. Microbiol.*, 2002, **92 Suppl**, 46S-54S.
37 a) M. A. Abushaheen, Muzaheed, A. J. Fatani, M. Alosaimi, W. Mansy, M. George, S. Acharya, S. Rathod, D. D. Divakar, C. Jhugroo, S. Vellappally, A. A. Khan, J. Shaik and P. Jhugroo, *Dis. Mon.*, 2020, **66**, 100971; b) C. E. Maus, B. B. Plikaytis and T. M. Shinnick, *Antimicrob. Agents Chemother.*, 2005, **49**, 3192;
38 S. Garneau-Tsodikova and K. J. Labby, *Med. Chem. Commun.*, 2016, **7**, 11.
39 a) C. Ayoub Moubareck and D. Hammoudi Halat, *Antibiotics*, 2020, **9**; b) K. Poole, *Curr. Pharm. Biotechnol.*, 2002, **3**, 77;
40 a) K. Bush and G. A. Jacoby, *Antimicrobial agents and chemotherapy*, 2010, **54**, 969; b) K. Bush, *Antimicrobial agents and chemotherapy*, 2018, **62**;
41 L. Pantel, T. Florin, M. Dobosz-Bartoszek, E. Racine, M. Sarciaux, M. Serri, J. Houard, J.-M. Campagne, R. M. de Figueiredo, C. Midrier, S. Gaudriault, A. Givaudan, A. Lanois, S. Forst, A. Aumelas, C. Cotteaux-Lautard, J.-M. Bolla, C. Vingsbo Lundberg, D. L. Huseby, D. Hughes, P. Villain-Guillot, A. S. Mankin, Y. S. Polikanov and M. Gualtieri, *Mol. Cell*, 2018, **70**, 83.
42 A. Lanois-Nouri, L. Pantel, J. Fu, J. Houard, J.-C. Ogier, Y. S. Polikanov, E. Racine, H. Wang, S. Gaudriault, A. Givaudan and M. Gualtieri, *mBio*, 2022, e0282621.
43 A. R. Burmeister, *Evolution, medicine, and public health*, 2015, **2015**, 193.

44 S. N. Abdi, R. Ghotaslou, K. Ganbarov, A. Mobed, A. Tanomand, M. Yousefi, M. Asgharzadeh and H. S. Kafil, *Infect. Drug. Resist.*, 2020, **13**, 423.
45 C. J. L. Murray, K. S. Ikuta, F. Sharara, L. Swetschinski, G. Robles Aguilar, A. Gray, C. Han, C. Bisignano, P. Rao, E. Wool, S. C. Johnson, A. J. Browne, M. G. Chipeta, F. Fell, S. Hackett, G. Haines-Woodhouse, B. H. Kashef Hamadani, E. A. P. Kumaran, B. McManigal, R. Agarwal, S. Akech, S. Albertson, J. Amuasi, J. Andrews, A. Aravkin, E. Ashley, F. Bailey, S. Baker, B. Basnyat, A. Bekker, R. Bender, A. Bethou, J. Bielicki, S. Boonkasidecha, J. Bukosia, C. Carvalheiro, C. Castañeda-Orjuela, V. Chansamouth, S. Chaurasia, S. Chiurchiù, F. Chowdhury, A. J. Cook, B. Cooper, T. R. Cressey, E. Criollo-Mora, M. Cunningham, S. Darboe, N. P. J. Day, M. de Luca, K. Dokova, A. Dramowski, S. J. Dunachie, T. Eckmanns, D. Eibach, A. Emami, N. Feasey, N. Fisher-Pearson, K. Forrest, D. Garrett, P. Gastmeier, A. Z. Giref, R. C. Greer, V. Gupta, S. Haller, A. Haselbeck, S. I. Hay, M. Holm, S. Hopkins, K. C. Iregbu, J. Jacobs, D. Jarovsky, F. Javanmardi, M. Khorana, N. Kissoon, E. Kobeissi, T. Kostyanev, F. Krapp, R. Krumkamp, A. Kumar, H. H. Kyu, C. Lim, D. Limmathurotsakul, M. J. Loftus, M. Lunn, J. Ma, N. Mturi, T. Munera-Huertas, P. Musicha, M. M. Mussi-Pinhata, T. Nakamura, R. Nanavati, S. Nangia, P. Newton, C. Ngoun, A. Novotney, D. Nwakanma, C. W. Obiero, A. Olivas-Martinez, P. Olliaro, E. Ooko, E. Ortiz-Brizuela, A. Y. Peleg, C. Perrone, N. Plakkal, A. Ponce-de-Leon, M. Raad, T. Ramdin, A. Riddell, T. Roberts, J. V. Robotham, A. Roca, K. E. Rudd, N. Russell, J. Schnall, J. A. G. Scott, M. Shivamallappa, J. Sifuentes-Osornio, N. Steenkeste, A. J. Stewardson, T. Stoeva, N. Tasak, A. Thaiprakong, G. Thwaites, C. Turner, P. Turner, H. R. van Doorn, S. Velaphi, A. Vongpradith, H. Vu, T. Walsh, S. Waner, T. Wangrangsimakul, T. Wozniak, P. Zheng, B. Sartorius, A. D. Lopez, A. Stergachis, C. Moore, C. Dolecek and M. Naghavi, *Lancet*, 2022, **399**, 629.
46 World Health Organization (WHO), *Global tuberculosis report 2021*, Geneva, Switzerland, 2021.
47 K. Lewis, *Biochem Pharmacol*, 2017, **134**, 87.
48 World Health Organization, *Global priority list of antibiotic-resistant bacteria to guide research, discovery, and development of new antibiotics - 2017*, 2017.
49 a) S. Baumann, J. Herrmann, R. Raju, H. Steinmetz, K. I. Mohr, S. Hüttel, K. Harmrolfs, M. Stadler and R. Müller, *Angew. Chem.*, 2014, **126**, 14835; b) S. Groß, B. Schnell, P. A. Haack, D. Auerbach and R. Müller, *Nat. Commun.*, 2021, **12**, 1696; c) S. Hüttel, G. Testolin, J. Herrmann, T. Planke, F. Gille, M. Moreno, M. Stadler, M. Brönstrup, A. Kirschning and R. Müller, *Angewandte Chemie (International ed. in English)*, 2017, **56**, 12760;
50 a) C. Couturier, S. Groß, A. von Tesmar, J. Hoffmann, S. Deckarm, A. Fievet, N. Dubarry, T. Taillier, C. Pöverlein, H. Stump, M. Kurz, L. Toti, S. Haag Richter, D. Schummer, P. Sizun, M. Hoffmann, R. Prasad Awal, N. Zaburannyi, K. Harmrolfs, J. Wink, E. Lessoud, T. Vermat, V. Cazals, S. Silve, A. Bauer, M. Mourez, L. Fraisse, C. Leroi-Geissler, A. Rey, S. Versluys, E. Bacqué, R. Müller and S. Renard, *Angewandte Chemie (International ed. in English)*, 2022, **61**, e202210747; b) S. Renard, S. Versluys, T. Taillier, N. Dubarry, C. Leroi-Geissler, A. Rey, J.-C. Carry, O. Angouillant, S. Monget, T. Gouyon, I. Terrié-Vacher, K. Vilet, F. Thompson, G. Lebourg, A. Louboutin, C. Muller, J. Leroux, V. Certal, N. Lebreton, E. Arranz, G. Doerflinger, F. Bretin, V. R. Bacot-Davis and C. Couturier, eds., *Corramycin: Enlarging the Antibacterial Spectrum and Optimizing the Developability Profile of Corramycin, a Novel Class Natural Product Antibacterial. ASM Microbe 2022*, 2022; c) E. Bacqué, C. Leroi-Geissler, A. Fievet, N. Dubarry, S. Silve, V. Cazals, A. Rey, S. Sordello, E. Sentausa, T. Vermat, P. Nordmann, M. Attwood, A. Noel, A. McGowan, S. Das, A. von Tesmar, R. Müller, S. Renard and C. Couturier, eds., *Corramycin2, a new class potent antibacterial candidate with a novel mode of penetration into bacteria, a novel mechanism of action and compelling activities in animal models of infection. ASM Microbe 2022*, 2022; d) E. Racine, P. Nordmann, L. Pantel, M. Sarciaux, M. Serri, J. Houard, P. Villain-Guillot, A. Demords, C. Vingsbo Lundberg and M. Gualtieri, *Antimicrob. Agents Chemother.*, 2018, **62**, e01016; e) M. Sarciaux, L. Pantel, C. Midrier, M. Serri,

C. Gerber, R. Marcia de Figueiredo, J.-M. Campagne, P. Villain-Guillot, M. Gualtieri and E. Racine, *J Med Pharm Chem*, 2018, **61**, 7814;
51 a) J. O'Neil, *Antimicrobial Resistance: Tackling a crisis for the health and wealth of nations*, 2014; b) Tackling drug-resistant infections globally: final report and recommendations, https://apo.org.au/node/63983, (accessed 7 September 2023);
52 J. Davies and D. Davies, *Microbiol. Mol. Biol. Rev.*, 2010, **74**, 417.
53 M. Winn, J. K. Fyans, Y. Zhuo and J. Micklefield, *Nat. Prod. Rep.*, 2016, **33**, 317.
54 a) J. M. Waisvisz, van der Hoeven,M. G., J. F. Hölscher and B. te Nijnhius, *J. Am. Chem. Soc.*, 1957, **79**, 4522; b) U. Kazmaier, *Isr. J. Chem.*, 2021, **61**, 308; c) W. L. Kelly, L. Pan and C. Li, *J. Am. Chem. Soc.*, 2009; d) W. H. Trejo, L. D. Dean, J. Pluscec, E. Meyers and W. E. Brown, *J Antibiot*, 1977, **30**, 639;
55 K. J. Hetrick and Donk, Wilfred A. van der, *Curr. Opin. Chem. Biol.*, 2017, **38**, 36.
56 P. G. Arnison, M. J. Bibb, G. Bierbaum, A. A. Bowers, T. S. Bugni, G. Bulaj, J. A. Camarero, D. J. Campopiano, G. L. Challis, J. Clardy, P. D. Cotter, D. J. Craik, M. Dawson, E. Dittmann, S. Donadio, P. C. Dorrestein, K.-D. D. Entian, M. A. Fischbach, J. S. Garavelli, U. Göransson, C. W. Gruber, D. H. Haft, T. K. Hemscheidt, C. Hertweck, C. Hill, A. R. Horswill, M. Jaspars, W. L. Kelly, J. P. Klinman, O. P. Kuipers, A. J. Link, W. Liu, M. A. Marahiel, D. A. Mitchell, G. N. Moll, B. S. Moore, R. Müller, S. K. Nair, I. F. Nes, G. E. Norris, B. M. Olivera, H. Onaka, M. L. Patchett, J. Piel, M. J. T. Reaney, S. Rebuffat, R. P. Ross, H.-G. G. Sahl, E. W. Schmidt, M. E. Selsted, K. Severinov, B. Shen, K. Sivonen, L. Smith, T. Stein, R. E. Süssmuth, J. R. Tagg, G. L. Tang, A. W. Truman, J. C. Vederas, C. T. Walsh, J. D. Walton, S. C. Wenzel, J. M. Willey and W. van der Donk, *Nat. Prod. Rep.*, 2013, **30**, 108.
57 G. A. Hudson and D. A. Mitchell, *Curr. Opin. Microbiol.*, 2018, **45**, 61.
58 P. G. Arnison, M. J. Bibb, G. Bierbaum, A. A. Bowers, T. S. Bugni, G. Bulaj, J. A. Camarero, D. J. Campopiano, G. L. Challis, J. Clardy, P. D. Cotter, D. J. Craik, M. Dawson, E. Dittmann, S. Donadio, P. C. Dorrestein, K.-D. Entian, M. A. Fischbach, J. S. Garavelli, U. Göransson, C. W. Gruber, D. H. Haft, T. K. Hemscheidt, C. Hertweck, C. Hill, A. R. Horswill, M. Jaspars, W. L. Kelly, J. P. Klinman, O. P. Kuipers, A. J. Link, W. Liu, M. A. Marahiel, D. A. Mitchell, G. N. Moll, B. S. Moore, R. Müller, S. K. Nair, I. F. Nes, G. E. Norris, B. M. Olivera, H. Onaka, M. L. Patchett, J. Piel, M. J. T. Reaney, S. Rebuffat, R. P. Ross, H.-G. Sahl, E. W. Schmidt, M. E. Selsted, K. Severinov, B. Shen, K. Sivonen, L. Smith, T. Stein, R. D. Süssmuth, J. R. Tagg, G.-L. Tang, A. W. Truman, J. C. Vederas, C. T. Walsh, J. D. Walton, S. C. Wenzel, J. M. Willey and van der Donk, Wilfred A., *Natural product reports*, 2013, **30**, 108.
59 J. D. Hegemann, M. Zimmermann, X. Xie and M. A. Marahiel, *Acc. Chem. Res.*, 2015, **48**, 1909.
60 N. R. Braffman, F. J. Piscotta, J. Hauver, E. A. Campbell, A. J. Link and S. A. Darst, *PNAS*, 2019, **116**, 1273.
61 a) M. A. Delgado, M. R. Rintoul, R. N. Farías and R. A. Salomón, *Journal of bacteriology*, 2001, **183**, 4543; b) P. A. Vincent, M. A. Delgado, R. N. FarÃ-as and R. A. SalomÃ³n, *FEMS microbiology letters*, 2004, **236**, 103;
62 E. Semenova, Y. Yuzenkova, J. Peduzzi, S. Rebuffat and K. Severinov, *Journal of bacteriology*, 2005, **187**, 3859.
63 M. Iwatsuki, H. Tomoda, R. Uchida, H. Gouda, S. Hirono and S. Omura, *Adv. Ceram. Mater.*, 2006, **128**, 7486.
64 L. M. Repka, J. R. Chekan, S. K. Nair and van der Donk, Wilfred A, *Chem. Rev.*, 2017.
65 J. Lu, Y. Wu, Y. Li and H. Wang, *Angewandte Chemie (International ed. in English)*, 2020.
66 Q. Zhang, X. Yang, H. Wang and van der Donk, Wilfred A, *ACS Chem. Biol.*, 2014, **9**, 2686.
67 X. Yang, K. R. Lennard, C. He, M. C. Walker, A. T. Ball, C. Doigneaux, A. Tavassoli and van der Donk, Wilfred A, *Nat. Chem. Biol.*, 2018, **14**, 375.
68 X. Just-Baringo, F. Albericio and M. Alvarez, *Current topics in medicinal chemistry*, 2014, **14**, 1244.

69 G. A. Hudson, Z. Zhang, J. I. Tietz, D. A. Mitchell and van der Donk, Wilfred A., *J. Am. Chem. Soc.*, 2015, **137**, 16012.
70 A. Fabbretti, C.-G. He, E. Gaspari, S. Maffioli, L. Brandi, R. Spurio, M. Sosio, D. Jabes and S. Donadio, *Antimicrobial agents and chemotherapy*, 2015, **59**, 4560.
71 B. P. Goldstein, M. Berti, F. Ripamonti, A. Resconi, R. Scotti and M. Denaro, *Antimicrob. Agents Chemother.*, 1993, **37**, 741.
72 H. Mathur, M. C. Rea, P. D. Cotter, C. Hill and R. P. Ross, *Curr. Protein Pept. Sci.*, 2015, **16**, 549.
73 H. Mathur, V. Fallico, P. M. O'Connor, M. C. Rea, P. D. Cotter, C. Hill and R. P. Ross, *Front. Microbiol.*, 2017, **8**, 696.
74 K. Blin, S. Shaw, K. Steinke, R. Villebro, N. Ziemert, S. Y. Lee, M. H. Medema and T. Weber, *Nucleic Acids Res.*, 2019, W81-W87.
75 a) S. Luo and S.-H. Dong, *Molecules (Basel, Switzerland)*, 2019, **24**; b) S. Tan, G. Moore and J. Nodwell, *Antibiotics*, 2019, **8**;
76 I. G. Macara, K. M. Lounsbury, S. A. Richards, C. McKiernan and D. Bar-Sagi, *FASEB J.*, 1996, **10**, 625.
77 L. B. Bushin, B. C. Covington, K. A. Clark, A. Caruso and M. R. Seyedsayamdost, *Nat Chem Biol*, 2022, **18**, 1135.
78 a) K. R. Schramma, L. B. Bushin and M. R. Seyedsayamdost, *Nature chemistry*, 2015, **7**, 431; b) N. A. Isley, Y. Endo, Z.-C. Wu, B. C. Covington, L. B. Bushin, M. R. Seyedsayamdost and D. L. Boger, *J. Am. Chem. Soc.*, 2019, **141**, 17361;
79 B. E. Rued, B. C. Covington, L. B. Bushin, G. Szewczyk, I. Laczkovich, M. R. Seyedsayamdost and M. J. Federle, *mBio*, 2021, **12**.
80 Y. Imai, K. J. Meyer, A. Iinishi, Q. Favre-Godal, R. Green, S. Manuse, M. Caboni, M. Mori, S. Niles, M. Ghiglieri, C. Honrao, X. Ma, J. Guo, A. Makriyannis, L. Linares-Otoya, N. Böhringer, Z. G. Wuisan, H. Kaur, R. Wu, A. Mateus, A. Typas, M. M. Savitski, J. L. Espinoza, A. O'Rourke, K. E. Nelson, S. Hiller, N. Noinaj, T. F. Schäberle, A. D'Onofrio and K. Lewis, *Nature*, 2019, **576**, 459.
81 a) I. Mierau, K. Olieman, J. Mond and E. J. Smid, *Microb Cell Fact*, 2005, **4**, 16; b) D. Des Field, P. M. O. Connor, P. D. Cotter, C. Hill and R. P. Ross, *Mol. Microbiol.*, 2008, **69**, 218;
82 M. C. Rea, C. S. Sit, E. Clayton, P. M. O'Connor, R. M. Whittal, J. Zheng, J. C. Vederas, R. P. Ross and C. Hill, *Proceedings of the National Academy of Sciences of the United States of America*, 2010, **107**, 9352.
83 a) J. Dreyer, A. P. Malan and L. M. T. Dicks, *Front. Microbiol.*, 2018, **9**, 3177; b) E. Duchaud, C. Rusniok, L. Frangeul, C. Buchrieser, A. Givaudan, S. Taourit, S. Bocs, C. Boursaux-Eude, M. Chandler, J. F. Charles, E. Dassa, R. Derose, S. Derzelle, G. Freyssinet, S. Gaudriault, C. Medigue, A. Lanois, K. Powell, P. Siguier, R. Vincent, V. Wingate, M. Zouine, P. Glaser, N. Boemare, A. Danchin and F. Kunst, *Nat. Biotechnol.*, 2003, **21**, 1307;
84 M. M. M. Abd-Elgawad, *Plants (Basel, Switzerland)*, 2021, **10**.
85 a) D. Bowen, T. A. Rocheleau, M. Blackburn, O. Andreev, E. Golubeva, R. Bhartia and R. H. ffrench-Constant, *Science*, 1998, **280**, 2129; b) G. Yang, A. J. Dowling, U. Gerike, R. H. ffrench-Constant and N. R. Waterfield, *J. Bacteriol.*, 2006, **188**, 2254;
86 N. J. Tobias, B. Mishra, D. K. Gupta, R. Sharma, M. Thines, T. P. Stinear and H. B. Bode, *BMC Gen.*, 2016, **17**, 537.
87 Carsten E. Seyfert, Christoph Porten and Rolf Müller, 2023, **29**, 539.

Chapter 2

2.1 Improved broad-spectrum antibiotics against Gram-negative pathogens via darobactin biosynthetic pathway engineering

Previously published in:

Sebastian Groß,[abce] Fabian Panter,[abcde] Domen Pogorevc,[abce] Carsten E. Seyfert,[abce]

Selina Deckarm,[abc] Chantal D. Bader,[abc] Jennifer Herrmann,[abc] Rolf Müller*[abcd]

Chem. Sci., 2021 August 12; **12:** 11882-11893

DOI: 10.1039/D1SC02725E

Affilitation:

[a] Helmholtz Institute for Pharmaceutical Research Saarland (HIPS), Helmholtz Centre for Infection Research, Saarland University Campus, 66123 Saarbrücken, Germany

[b] Department of Pharmacy, Saarland University, 66123 Saarbrücken, Germany

[c] DZIF - German Centre for Infection Research, Partnersite Hannover-Braunschweig

[d]Helmholtz International Lab for Anti-Infectives, Campus E8 1, 66123 Saarbrücken, Germany

[e] These authors contributed equally

* Corresponding author

Contributions

Carsten E. Seyfert

The author significantly contributed to the investigations of this research article by conducting experiments and interpreting the results. He generated the heterologous expression constructs of darobactin 5, 6, 7, 8, 9, 17, 18, 19, 20 and 21, performed the cultivation and extractions of all generated derivatives and evaluated the antibacterial activity data. He produced and purified darobactin 9 and established the production and purification of DarF. He observed and analyzed the darobactin-degrading properties of DarF. Moreover, the author contributed to the writing and reviewing of the manuscript.

Contributions by Others

Sebastian Groß contributed to the conceptualization, project administration, visualization, writing, editing and reviewing of this research article. He supported the experimental investigations and the engineering of the biosynthetic gene cluster (BGC). Fabian Panter significantly contributed to the experimental investigations by establishing a purification method for darobactin A and 9. He led the formal analysis of this study and contributed to the visualization, writing, editing and reviewing of this manuscript. Domen Pogorevc contributed to the conceptualization, the methodology by engineering the BGC for heterologous expression of darobactins, the project administration and supported in the formal analysis of the experimental results. Selina Deckarm generated the remaining darobactin analogues, produced, and extracted the darobactins for further evaluation and determined the minimal cluster size. Chantal Bader supported the methology and the investigations by *de novo* structural elucidation and analysis of darobactin A and 9. Jennifer Herrmann supported in analyzing the experimental results and in writing of the original draft. Rolf Müller contributed to the conceptualization, the writing, including reviewing and editing. Moreover, he supervised the project and was responsible for the funding acquisition.

Abstract

The development of new antibiotics is imperative to fight increasing mortality rates connected to infections caused by multidrug-resistant (MDR) bacteria. In this context, Gram-negative pathogens listed in the WHO priority list are particularly problematic. Darobactin is a ribosomally produced and post-translationally modified bicyclic heptapeptide antibiotic selectively killing Gram-negative bacteria by targeting the outer membrane protein BamA. The native darobactin A producer *Photorhabdus khanii* HGB1456 shows very limited production under laboratory cultivation conditions. Herein, we present the design and heterologous expression of a synthetically engineered darobactin biosynthetic gene cluster (BGC) in *Escherichia coli* to reach an average darobactin A production titre of 13.4 mg/L. Rational design of *darA* variants, encoding the darobactin precursor peptide with altered core sequences, resulted in the production of 13 new 'non-natural' darobactin derivatives and 4 previously hypothetical natural darobactins. One of the non-natural compounds, darobactin 9, was more potent than darobactin A, and showed significantly improved activity especially against *Pseudomonas aeruginosa* (0.125 µg/mL) and *Acinetobacter baumannii* (1-2 µg/mL). Importantly, it also displayed superior activity against MDR clinical isolates of *E. coli* (1-2 µg/mL) and *Klebsiella pneumoniae* (1-4 µg/mL). Independent deletions of genes from the darobactin BGC showed that only *darA* and *darE*, encoding a radical forming *S*-adenosyl-L-methionine-dependent enzyme, are required for darobactin formation. Co-expression of two additional genes associated with the BGCs in hypothetical producer strains identified a proteolytic detoxification mechanism as a potential self-resistance strategy in native producers. Taken together, we describe a versatile heterologous darobactin platform allowing the production of unprecedented active derivatives in good yields, and we provide first experimental evidence for darobactin biosynthesis processes.

Introduction

Increasing levels of antimicrobial resistance (AMR) is a threat for health care systems globally and it leads to increasing morbidity and mortality rates. Notably, multidrug-resistant (MDR) Gram-negative pathogens such as *Klebsiella pneumoniae*, *Acinetobacter baumannii*, *Pseudomonas aeruginosa* and also *Enterobacter* species cause difficult-to-treat nosocomial infections and were consequently ranked with critical priority by the WHO.[1] Some MDR strains developed resistance towards almost all clinically approved antibiotics.[2] This exemplifies the need for the discovery and clinical development of new antibiotics to fight AMR-related infections in the future. Most of the recently FDA-approved antibiotics derive from well-known antibiotics classes such as the β-lactam/β-lactamase inhibitor combinations ceftolozane/tazobactam, ceftazidime/avibactam,[3] meropenem/vaborbactam,[4] imipenem-cilastatin (dipeptidase inhibitor)/relebactam,[5] the aminoglycoside plazomicin,[6] the tetracycline

derivative eravacycline,[7] and the siderophore cephalosporin cefiderocol,[8] which make rapid resistance development likely because resistance mechanisms against congeners of these antibiotics classes already exist among pathogens.

As a result of this challenge, future antibiotics discovery campaigns should focus on antibiotics with novel scaffolds, molecular targets and modes of action,[9] such as the cyclic peptidomimetic murepavidin, which targets the outer membrane (OM) biogenesis in Gram-negative bacteria by inhibiting the lipopolysaccharide transport protein D (LptD). Murepavidin is currently in preclinical development as precision antibiotic against *P. aeruginosa* to treat patients with cystic fibrosis.[10] Another example is the benzamide compound TXA709, which is active against *Staphylococcus aureus* by affecting septum formation during cell division through the inhibition of FtsZ, a protein without homolog in eukaryotic cells.[11] Moreover, the *streptomyces*-derived griselimycins are highly active against *Mycobacterium tuberculosis* by inhibiting the new antimicrobial target DnaN, the DNA polymerase sliding clamp.[12] Other examples are the spiropyrimidintrione zoliflodacin and the linear polyaromatic peptide cystobactamid, which show broad-spectrum antibacterial activity, e.g. against *Neisseria gonorrhoeae* and MDR *Escherichia coli*, respectively, by inhibiting DNA gyrase at distinct binding sites compared to other gyrase-targeting antibiotics like the quinolones.[13] However, the number of promising antibiotic lead structures with activity against Gram-negative pathogens currently in clinical development is limited. One key reason why it is so difficult to find novel antibiotics active against Gram-negative bacteria is their OM, which constitutes a major additional permeation barrier for most of the candidate compounds under development. Several new antibiotic classes currently under investigation avoid the issue of cell penetration since their molecular target is located in the OM itself. Among these antibiotics classes are the small molecule MRL-494,[14] the ribosomally produced and post-translationally modified peptide (RiPP) darobactin,[15] and a chimeric peptidomimetic combining the pharmacophores of murepavadin and polymyxin B_1.[16]

The antibiotic darobactin A was isolated from the bacterial nematode symbiont *Photorhabdus khanii* HGB1456 and it selectively kills Gram-negative bacteria such as *P. aeruginosa*, *K. pneumoniae*, *E. coli*, and *A. baumannii*.[15] In addition, it showed no cytotoxic activity against a variety of human cell lines or symbiotic gut bacteria, including Gram-negative members belonging to the genus *Bacteroides*. Darobactin targets the ß-barrel assembly machinery A protein (BamA)[17] located in the OM. It was recently shown that darobactin A binds to the open form BamA lateral gate with high affinity by mimicking a ß-strand in its BamA-bound binding pose.[18] Consequently, the ß-signal binding site of BamA is blocked, cognate substrate binding is inhibited and nascent OM proteins are not inserted into the OM. Darobactin A is a bicyclic

heptapeptide and part of the RiPP secondary metabolite class characterized by the precursor peptide amino acid sequence $W_1N_2W_3S_4K_5S_6F_7$ (Figure 1).[15]

The darobactin biosynthetic gene cluster (BGC) in *P. khanii* consists of six open reading frames (ORFs), *darABCDE* and a homolog of the global translation inhibitor *relE* from *E. coli*.[15,19] The *darA* ORF encodes the propeptide sequence and *darBCD* encode a tripartite ABC-type trans-envelope exporter system, consisting of an ABC transporter permease (DarB), a membrane fusion protein (DarC) and an ATP binding domain (DarD). The *darE* gene encodes a radical *S*-adenosyl methionine (SAM) enzyme, which was proposed to catalyse two consecutive aryl-alkyl couplings between the aromatic parts of the tryptophan side chain leading to two ring formations. The first ring is formed by connection of the indole group of W_1 with C_β of W_3 via an aryl-alkylether bond and the second ring is formed by a carbon-carbon aryl-alkyl bond between the indole group of W_3

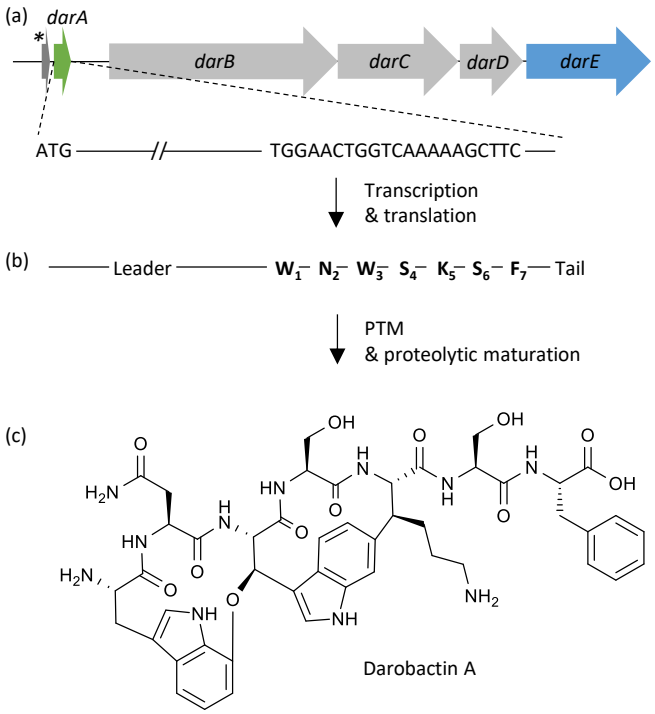

Figure 12: (a) The biosynthetic gene cluster (BGC) from *Photorhabdus khanii* HGB1456 consisting of a homolog of the global translation inhibitor gene *relE* from *E. coli* (dark grey arrow labelled with asterisk), the darobactin propeptide encoding gene *darA* (green arrow), the three ABC-type trans-envelope exporter encoding genes *darBCD* (light grey arrows) and the radical SAM enzyme encoding gene *darE* (blue arrow). (b) Transcription and translation of *darA* leads to the synthesis of the darobactin propeptide, which consists of a leader, core ($W_1N_2W_3S_4K_5S_6F_7$) and tail sequence. Two cyclization post-translational modification (PTM) reactions and proteolytic maturation result in formation of darobactin. The proteolytic maturation was recently assumed to be performed by a peptidase from *E. coli*, which is not encoded by a gene from the darobactin BGC, or by a self-cleavage mechanism catalysed by the propeptide. (c) Structural formula of the mature darobactin A.

and C_β of K_5.[15] The cyclisations were shown to give darobactin its ß-strand mimic structure and are vital for the bioactivity, as the linear $W_1N_2W_3S_4K_5S_6F_7$ peptide did not bind BamA.[15,18] A search in the National Centre for Biotechnology Information (NCBI) bacterial genome database using the darobactin propeptide sequence as query led to the identification of additional darobactin BGCs in *Photorhabdus*, *Yersinia*, *Vibrio*, and *Pseudoalteromonas* species.[15] Two additional ORFs, *darF* and *darG*, encoding proteins with unknown functions, are located in the BGC from *Pseudoalteromonas luteoviolacea*.[15] Moreover, Imai and co-workers proposed structures of the hypothetical darobactin derivatives B-E based on the darobactin A structure and the propeptide core sequences encoded in the respective *darA* homologs of those BGCs.[15] Due to the low production titre (≤3 mg/L) of darobactin A in its native producer strain, *darABCDE* were transferred into *E. coli* BW25113 and heterologously expressed under the regulation of an arabinose-inducible promoter, resulting in the production of darobactin A.[15] However, the corresponding production titre achieved in fermentations of the heterologous producer was not reported and the existence of the hypothesised darobactin derivatives B-E were not experimentally proven.

Herein, we report the *in silico* design, chemical synthesis and heterologous expression of a synthetically engineered darobactin BGC in *E. coli* BL21 (DE3) leading to an improved darobactin A production titre (13.4 (± 2.0) mg/L in 3 days). In parallel work, Wusain *et al*. published the heterologous production of darobactin A in *E. coli* reaching a similar titre.[20] We here additionally present the rational *in silico* design of *darA* variants with altered core peptide encoding sequences and their heterologous expression. The resulting darobactin derivatives include the previously hypothetical natural darobactins B-E. Most importantly, 13 new 'non-natural' derivatives were generated, including darobactin 9, which showed significantly improved antibacterial activity against some of the most problematic pathogens according to the WHO priority list, such as *P. aeruginosa*, *A. baumannii,* and *K. pneumoniae*. Furthermore, in our analysis independent targeted gene deletions of the *relE*-like gene, *darA*, *darB*, *darC*, *darD*, and *darE* revealed that only *darA* and *darE* are ultimately required for darobactin formation in *E. coli*. Moreover, the expression of *darF*, solely or in combination with *darG*, as well as purification of DarF and *in vitro* investigation of the enzyme activity identified the proteolytic degradation of darobactin as potential detoxification mechanism in the respective native producer strain.

Results & discussion

Design of a synthetic darobactin BGC modified for the heterologous production of darobactin A in *E. coli* BL21 (DE3)

Despite the strong anti-Gram-negative activity of darobactin, heterologous production in *E. coli* was previously shown to be feasible.[15] Aiming for a versatile heterologous darobactin production platform in *E. coli*, we designed a modified darobactin BGC (GenBank accessions are provided in Supplementary

Data) *in silico* based on the BGC sequence originating from *P. khanii* HGB1456 (GenBank accession WHZZ01000001.1) (see SI). The modified BGC includes the five ORFs *darABCDE* and the *relE*-like gene. We decided to include the *relE*-like gene in our initial design as it was co-localized with this darobactin BGC as well as with several other darobactin BGCs in different wild-type strains.[15] Thus, we could not exclude that this gene may play a beneficial role in darobactin biosynthesis even though its homolog *relE* was shown to be a global translation inhibitor in *E. coli*.[19] We placed the isopropyl ß-D-1-thiogalactopyranoside (IPTG)-inducible *T7lac* promoter system[21] (including the *lacI* repressor gene and *lacO* operator) upstream of *darA* intending to allow time-controlled gene expression and thus the production of darobactin. The constitutive *nptII* promoter[22] was placed upstream of *darBCDE*, since we assumed that constitutive gene expression of the *darBCD*-encoded ABC-type trans-envelope exporter system increases the capability of our *E. coli* production strain to export darobactin prior to induction of the *darA* gene expression with IPTG and therefore can improve its self-resistance to darobactin. We inserted the *tD1* terminator sequence upstream of the *nptII* promoter to prevent *T7lac* promoter-dependent gene expression affecting the transcription of the *darBCDE* operon. Furthermore, we aimed to exclude that a potential native promoter located in the 396 bp long intergenic region between *darA* and *darBCDE* influences the gene expression of *darBCDE*. In addition to the natively present unique restriction endonuclease recognition sites (R-sites), we inserted several more R-sites at strategic locations allowing to remove the *relE*-like gene, exchange promoters or *darA* and to facilitate efficient sub cloning of the modified darobactin BGC into different vector systems (see Figure 2 and Suppl. Table 2). The modified darobactin BGC DNA sequence was chemically synthesized in one part (8.5 kb), delivered in a pUC57 high-copy plasmid and cloned via restriction hydrolysis/DNA ligation into pNOSO (described in SI), which features a low-copy p15A origin of replication to allow for genetic stability of the resulting recombinant strain. The expression constructs were transformed into *E. coli* BL21 (DE3) and the heterologous production of darobactin A was initially confirmed by uHPLC-HRMS and MS^2 fragmentation after a small-scale batch cultivation (see SI). After initial evaluation of different *E. coli* expression strains, cultivation media and expression constructs, the highest relative production based on the mass peak intensity was achieved in *E. coli* BL21 (DE3) pNOSO-relEdarABCDE using FM medium for cultivation (see SI and Figure 3). Notably, darobactin A production levels were consistently higher if the *lac* promoter-regulated gene expression of the *T7* RNA polymerase, which is encoded in the genome of BL21 (DE3) and related *E. coli* strains, and the *T7lac* promoter on the plasmid remained non-induced as compared to induction with 0.1 mM IPTG. We assume that leaky *darA* gene expression by the *lac*-repressed *T7* promoter leads to a favourable amount of propeptide in the cell for optimal darobactin A production. This leaky expression might be caused by traces of lactose in the complex cultivation medium leading to slight induction of the *lac*-repressed genes. Higher *darA* gene expression levels caused by induction of the *lac*-regulated *T7* RNA polymerase expression and induction of the

T7lac promoter with IPTG might result in metabolic overburdening of the *E. coli* cell. This result is not entirely consistent with observations made in parallel in the work by Wuisan *et al*., in which an increasing *darA* to *darE* transcript ratio led to higher darobactin A production.[20] We assume that a certain *darA*:*darE* transcript ratio, which has to be determined in future experiments, is required for optimum darobactin A production. To investigate whether slight induction or repression of the *T7lac* promoter results in higher relative darobactin production, we supplemented the production broth with 10 µM, 1 µM, 100 nM, 10 nM, 1 nM and 0.1 nM concentrations of IPTG or 0.5 %, 1.5 % and 5 % of glucose. However, no production improvement with respect to non-induced *T7* polymerase and *darA* expression was achieved under any of the tested conditions (see SI, Suppl. Table 7).

Subsequently, we performed a large-scale batch cultivation with *E. coli* BL21 (DE3) pNOSO-darABCDE

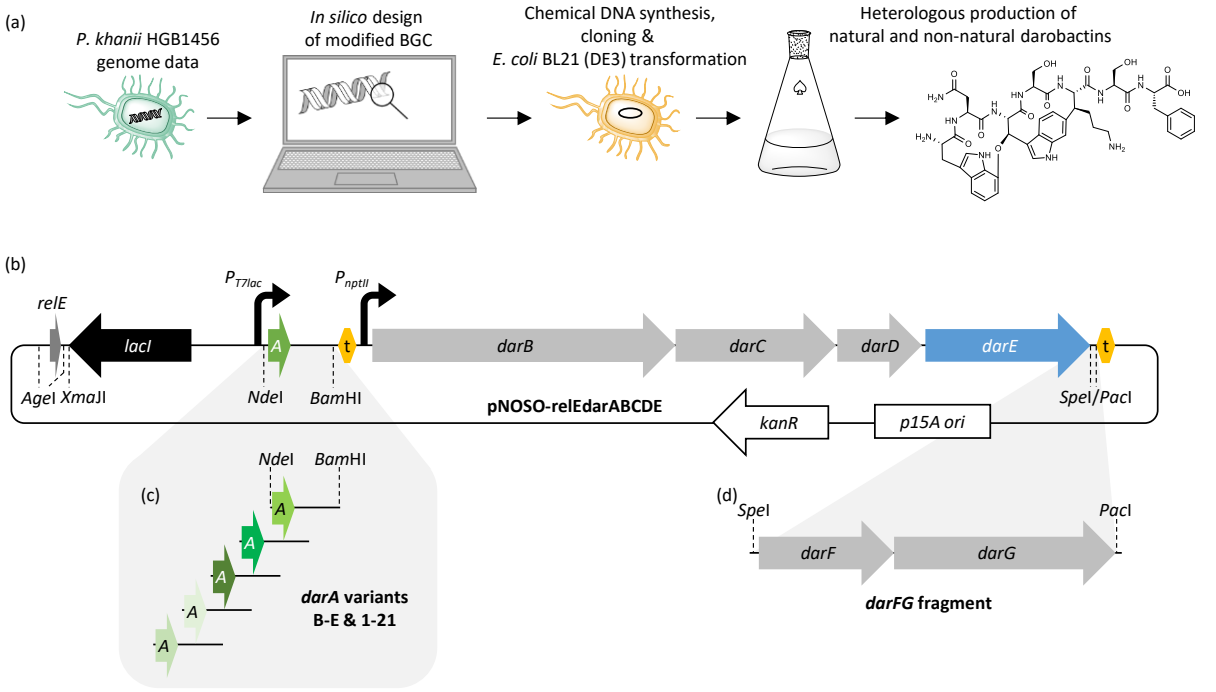

Figure 13: (a) Schematic overview of the workflow including the *in silico* design of the modified darobactin BGC based on the genome sequence from *P. khanii* HGB1456, chemical DNA synthesis and cloning of the expression construct, transformation of the expression construct into *E. coli* BL21 (DE3) and heterologous production of darobactin derivatives on the example of darobactin A. (b) Design of the darobactin BGC modified for the heterologous expression in *E. coli*. The pNOSO-relEdarABCDE expression construct contains the *relE* homologue (dark grey arrow), *lacI* repressor gene (black arrow), *T7lac* promoter (black curved arrow) upstream of *darA* (green arrow), *nptII* promoter (black curved arrow) upstream of *darBCD* (light grey arrows) and *darE* (blue arrow), *tD1* terminator (yellow hexagon), *p15A* origin of replication (ori; white box) and kanamycin resistance gene (white arrow). Selected unique restriction endonuclease recognition sites (R-sites), which were important for removal of the *relE* homologue (*Age*I), exchange of *darA* by *darA* variants with altered propeptide core sequence (*Nde*I/*Bam*HI) and introduction of *darFG* (*Spe*I/*Pac*I), are indicated by dashed lines. (c) Different *darA* variants were designed for the heterologous production of natural darobactin derivatives (B-E) and non-natural darobactin derivatives (1-21). (d) The *darFG* fragment was designed to investigate the biosynthetic function of the respective genes upon co-expression with the modified darobactin BGC.

omitting any IPTG induction to isolate darobactin A and confirm the structure and minimum inhibitory concentrations (MICs) published by Imai *et al.* for internal comparison with novel darobactins (see below).

Purification of darobactin A from the culture supernatant was done by adsorption of darobactin on XAD-16N resin followed by elution with 80 % MeOH in H_2O and several steps of preparative and semi-preparative HPLC (see SI). The purified compound was used to calculate a linear regression based on the MS peak surface areas of different stock concentrations (see SI). On this basis, an absolute quantification of the darobactin A concentration in the fermentation broth of *E. coli* BL21 (DE3) pNOSO-darABCDE was performed, providing an average production rate of 13.4 (± 2.0) mg/L.

Production of natural and non-natural darobactin derivatives.

Darobactin is a promising candidate for biosynthetic structure engineering attempts due to its excellent antibacterial activity profile, the hypothesised natural variability in its amino acid composition,[15] and its presumed insensitivity towards amino acid mutations in its binding site.[18] Thus, we investigated the plasticity of our heterologous production system aiming at the production of novel darobactin derivatives with improved antibacterial properties. To this end, we designed four DNA fragments *in silico* including the entire *darA* gene with an altered core sequence encoding the propeptides of the hypothetical natural darobactins B-E (Table 1 and Figure 4).

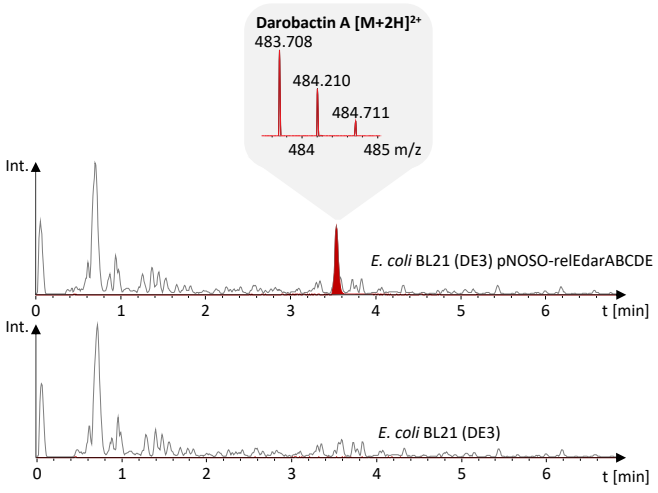

Figure 14: Darobactin A production was confirmed by uHPLC-HRMS analysis of the *E. coli* pNOSO-relEdarABCDE fermentation broth supernatant. Darobactin A is visualized as extracted ion chromatogram (EIC) at 483.71 Da (red trace) represents the $[M+2H]^{2+}$ MS peak, including the corresponding isotope pattern, which is shown in the grey field. The grey trace represents the base peak chromatogram (BPC) of the culture supernatant of *E. coli* BL21 (DE3) with and without the darobactin expression vector.

The existence of these darobactin congeners was previously assumed based on the *in silico* analysis of darobactin propeptide sequences in the respective BGCs but has not yet been confirmed.[15]

After chemical synthesis of the DNA fragments containing the chimeric *darA* genes (named *darA*-B to *darA*-E), the native *darA* sequence was replaced with *darA*-B to–E, independently, in pNOSO-darABCDE using restriction hydrolysis/DNA ligation cloning to generate pNOSO-darABCDE-B to -E. Heterologous expression of the respective constructs in *E. coli* BL21 (DE3) resulted in the production of the previously

in silico predicted native darobactins B-E, as confirmed by uHPLC-HRMS and MS^2 fragmentation analysis (see Table 1, Suppl. Figures 4-7 and 23-26).

Based on the amino acid tolerability found at positions 2 and 4-6 in the natural darobactins A-E, we designed and cloned three new expression constructs (pNOSO-darABCDE-1, -2, and –4) with altered core sequences, in which naturally occurring amino acids were combined in a non-natural manner.

Table 1: Production of darobactin derivatives after heterologous expression of the modified darobactin BGC with altered core peptide encoding *darA* sequences in *E. coli* BL21 (DE3). Changes in the *darA* core sequence and core peptide sequence with respect to the native (darobactin A) sequence are shown in red. The calculated (calc.) and measured (meas.) exact mass ($[M+2H]^{2+}$) for each derivative is given. For darobactin-related masses, which were different from the calculated masses and identified after MS^2 spectral networking analysis, the corresponding mass shifts are shown in blue. In case of darobactin 18, additionally the terminal *darA* core DNA sequence codon, which was responsible for the unplanned L-glutamine incorporation (see text), is highlighted in blue. UHPLC-HRMS chromatograms and MS^2 fragmentation data for all produced darobactin derivatives are shown in Suppl. Figures 3-21 and 22-40, respectively.

Darobactin	*darA* core DNA sequence	Core peptide	Calc. mass $[M+2H]^{2+}$	Obs. mass $[M+2H]^{2+}$	Mass deviation $[M+2H]^{2+}$ (ppm)	Mass shift (Da)
A	TGG AAC TGG TCA AAA AGC TTC	W N W S K S F	483.7089	483.7095	1.24	
B	TGG AAC TGG ACC AAA CGA TTC	W N W T K R F	525.2512	525.2511	0.19	
C	TGG TCA TGG TCA AGA AGC TTC	W S W S R S F	484.2065	484.2066	0.21	
D	TGG AAC TGG TCA AGA AGC TTC	W N W S R S F	497.7119	497.7116	0.60	
E	TGG TCA TGG TCA AAA AGC TTC	W S W S K S F	470.2034	470.2037	0.64	
1	TGG TCA TGG ACC AAA CGA TTC	W S W T K R F	511.7458	not observed		
2	TGG TCA TGG ACC AGA AGC TTC	W S W T R S F	491.2143	491.2146	0.61	
4	TGG AAC TGG ACC AAA AGC TTC	W N W T K S F	490.7167	490.7171	0.82	
5	TGG TGC TGG TCA AAA AGC TTC	W C W S K S F	478.1920	not observed		
6	TGG AAC TGG TGC AAA AGC TTC	W N W C K S F	491.6974	587.2104		+191.026
7	TGG TGC TGG TGC AAA AGC TTC	W C W C K S F	486.1806	not observed		
8	TGG AAC TGG TCA AAA TGC TTC	W N W S K C F	491.6974	587.2100		+191.0252
9	TGG AAC TGG TCA AAA AGC TGG	W N W S K S W	503.2123	503.2139	3.18	
10	TGG AAC TGG TCA AAA AGC TAC	W N W S K S Y	491.7063	491.7064	0.20	
11	TGG CAG TGG TCA AAA AGC TTC	W Q W S K S F	490.7167	490.7169	0.41	
12	TGG ACC TGG TCA AAA AGC TTC	W T W S K S F	477.2112	477.2115	0.63	
13	TGG GCA TGG TCA AAA AGC TTC	W A W S K S F	462.2059	462.206	0.22	
14	TGG AAC TGG GCA AAA AGC TTC	W N W A K S F	475.7114	475.7118	0.84	
15	TGG AAC TGG TCA GCA AGC TTC	W N W S A S F	455.1799	455.1802	0.66	
16	TGG AAC TGG TCA AAA GCT TTC	W N W S K A F	475.7114	475.7119	1.05	
17	TGG AAC TGG TCA AAA AGC GCA	W N W S K S A	445.6932	445.6936	0.90	
18	TGG AAC TGG TCA AAA AGC CAG	W N W S K S Q	410.1746 / 474.2039	474.2043	0.84	+128.0594
19	TGG AAC TGG TCA AAA	W N W S K	366.6586	not observed		
20	TGG AAC TGG TCA	W N W S	303.6190	not observed		
21	TGG AAC TGG	W N W	260.1023	not observed		

For example, in darobactins B-E position 2 is L-serine or L-asparagine, position 4 is L-serine or L-threonine, position 5 is L-lysine or L-arginine and position 6 is L-serine or L-arginine. However, natural darobactins A-E do not cover all possible combinations. The *darA* core sequence in pNOSO-darABCDE-1, on the other hand, encodes the core peptide $W_1S_2W_3T_4K_5R_6F_7$ (named darobactin 1 here), representing one of the possible non-natural combinations of natural occurring amino acids. After heterologous expression of pNOSO-darABCDE-1, -2, and –4 in *E. coli* BL21 (DE3), production of the

respective non-natural darobactins was confirmed by uHPLC-HRMS (see Table 1, Suppl. Figures 8-10 and 27-29)

Next, we aimed to investigate whether our heterologous production system also tolerates the

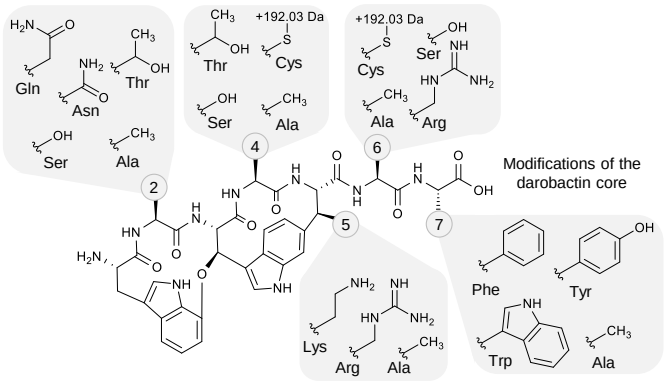

Figure 15: Structural variation among the heterologously produced darobactin derivatives. The side chain moieties of the different amino acids in positions 2, 4-6 and 7 (see numbered circles) that were observed in the heterologously produced darobactin derivatives (see also Table 1) are shown in the grey-shaded areas. Cysteine side chains in positions 4 and 6 led to formation of an adduct with a mass shift of +191.026 Da and a potential adduct sum formula of $C_6H_9NO_4S$ based on ChemCalc prediction (discussed in more detail in the text). Amino acid side chain moieties of derivatives, which were not observed upon expression of the respective pNOSO construct with altered darA sequence in *E. coli* BL21 (DE3), are not shown (darobactins 1, 5 and 7).

exchange of natively occurring amino acids in positions 2 and 4-6 of the darobactin core peptide by amino acids natively not found in the respective positions of the darobactins A-E. Therefore, numerous *darA* variants (5-8 and 11-17) were designed *in silico*, in which the core sequences encode non-natural darobactin A derivatives containing L-glutamine (darobactin 11) or L-threonine (darobactin 12) in position 2, L-cysteine in positions 2, 4, 2 and 4, or 6 (darobactins 5, 6, 7, and 8, respectively), and L-alanine in positions 2 and 4-7 (darobactins 13-17, respectively).

After chemical synthesis and subsequent cloning of the *darA* variants into pNOSO-darABCDE, generating pNOSO-darABCDE-5, -6 to -8, and –11 to -17, heterologous expression of the respective constructs in *E. coli* BL21 resulted in the production of darobactins 11-17 (see Table 1, Suppl. Figures 14-20 and 33-39), whereas darobactin-related but unexpected masses were detected after analysis via GNPS-based spectral networking[23] of the corresponding tandem MS upon expression of pNOSO-darABCDE-6 and -8 (*m/z* 587.209 and 587.212 instead of 491.697 $[M+2H]^{2+}$) (see Table 1, Suppl. Figures 10, 11 and 29, 30). Darobactin derivative production was confirmed by observation of the corresponding exact mass followed by analysis of the corresponding MS^2 spectrum that shows characteristic fragments for darobactin scaffolds (see SI). In case of expression of pNOSO-darABCDE-5, -7 and –13, no expected darobactins nor darobactin-related compounds were detected. This clearly shows that the chemical space to exchange amino acids at certain positions in darobactin is limited. For example, in position 2 the exchange of the naturally occurring amino acids L-asparagine and L-serine by the sterically and physicochemically similar amino acids L-glutamine and L-threonine was

tolerated, whereas L-alanine was not accepted in this position. The attempt to introduce one L-cysteine at different positions either resulted in production of darobactin-related compounds with unexpected masses or, similar to our attempt involving two L-cysteine residues at the same time, to complete abolishment of the production. Since the unexpected masses were higher than the expected masses, we assume that the reactive cysteine side chain thiol group underwent chemical reactions leading to adduct formation. Based on the measured exact mass we observe a mass shift of +191.02 Da with respect to the expected darobactin 6 mass. ChemCalc[24] analysis predicted a potential sum formula of $C_6H_9NO_4S$ based on the exact mass of the adduct, taking into account the seven golden rules for heuristic sum formula prediction.[25]

We assume that the presence of a sulphur makes adduct formation via a disulphide bond likely, but purification of darobactins 6 and 8 with subsequent structure elucidation is required to make a precise statement about the respective structures. However, we de-prioritized these compounds as they were produced in significantly lower amounts based on comparison of the MS peak area under the curve with respect to darobactin A (see Table 2).

Furthermore, L-alanine was successfully incorporated into the darobactin scaffold in case of darobactins 14-17 (see Table 1, Suppl. Figures 17-20 and 36-39). This was surprising, since the C-terminal amino acid (position 7) occurring in natural darobactins A-E was always L-phenylalanine. Still, replacement with L-alanine in case of darobactin 17 was found possible. The L-phenylalanine moiety is conserved in natural darobactins A-E at this position[15] and was shown to bind BamA exactly where a conserved aromatic peptide side chain in the β-signal sequences of the cognate BamA substrates bind.[18] Consequently, we hypothesise that an aromatic side chain moiety in position 7 is crucial for the bioactivity of darobactins and that further amino acid exchanges in this position against other aromatic amino acids might result in active darobactin variants. We therefore designed two new *darA* variants (9 and 10), encoding L-tryptophan and L-tyrosine in position 7, respectively. After cloning of *darA*-9 and *darA*-10 into pNOSO-darABCDE and heterologous expression of the respective constructs in *E. coli* BL21 (DE3), the production of darobactins 9 and 10 exhibiting a terminal L-tryptophan and L-tyrosine moiety, respectively, was confirmed by uHPLC-HRMS (see Table 1, Suppl. Figures 12, 13 and 31, 32).

As the heterologous production system tolerated the majority of amino acid exchanges in the darobactin precursor peptide, we subsequently aimed for a truncation of the core structure. This experiment might provide first insights into a possible structure-activity-relationship, which will be investigated in more detail in the future, the mechanism of tail sequence cleavage and pave the way for semi-synthesis on darobactin scaffolds. We designed four additional *darA* variants (18 to 21) in which the propeptide sequence length was reduced by one (*darA*-18) up to four (*darA*-21) amino acids, respectively, without removing the darobactin tail sequence. However, after cloning and heterologous

expression of the generated constructs in *E. coli* BL21(DE3), we only observed production of one unexpected darobactin derivative (darobactin 18) upon expression of pNOSO-darABCDE-18, which was shown to carry a L-glutamine at position 7 (see Table 1, Suppl. Figures 21 and 40). We had expected the production of a truncated darobactin derivative, thus having a terminal L-serine in position 6. Interestingly, the L-glutamine found in position 7 is the first amino acid of the tail sequence. Truncation of the core sequence therefore seems to lead to a maturation process in which the first amino acid of the tail sequence is recognized as part of the core and is thus not cleaved off in the proteolytic process. The attempt to truncate the darobactin core sequence by two or more amino acids resulted in a complete loss of production (see Table 1). Consequently, we assume that a core sequence of seven amino acids length is recognized by the so far unidentified protease (see below). Notably, in our experiment we did not remove the tail sequence from *darA*, but only removed one or several of the darobactin core sequence codons. In the contemporaneously performed work of Wuisan and co-workers a darobactin BGC with a *darA* variant without the tail sequence was heterologously expressed in in *E. coli*, showing that darobactin A was still produced.[20] Future experiments, in which the entire tail encoding sequence plus additional core amino acid encoding sequences are removed from *darA* might thus result in the formation of truncated darobactin congeners.

In summary, 18 natural and non-natural darobactin derivatives were successfully heterologously produced in *E. coli* BL21 (DE3) after expression of the darobactin BGC with different *darA* core sequences. Five out of the 18 produced derivatives were native darobactins (A-E), four of which (darobactins B-E) were not previously observed, and 11/19 were non-natural derivatives (1, 2, 4, 9-12, and 14-17), whereas the remaining three showed unexpected masses (6, 8, and 18).

Purification and antibacterial activity profiling of darobactin 9

Since the purification of highly water-soluble darobactin A was a time- and resource-intensive process, we assumed that purification of the newly produced derivatives to be similarly challenging. Thus, we devised a prioritization and preselection strategy enabling us to categorize the newly produced derivatives over others according their anti-Gram-negative activity. Therefore, we performed MIC assays using a small panel of Gram-negative pathogens (*K. pneumoniae* DSM-30104, *P. aeruginosa* PAO1, *E. coli* ATCC25922 and *A. baumannii* DSM-30008) using crude extracts of all heterologous producer strains (Table 2). Each crude extract was tested in serial dilutions and the given values are the concentration factor for which no visible growth was observed. The assignment of the concentration factor and the interpretation of the estimated antimicrobial activity of the crude extract is described in more detail in the legend of Table 2 and in SI (see Supplementary Figure 41).

Table 2: Estimation of antimicrobial activity and relative production titre of the darobactin derivatives with respect to darobactin A based on crude extracts (see SI). The antimicrobial activity of each darobactin derivative-containing crude extract against *K. pneumoniae* DSM-30104, *P. aeruginosa* PAO1, *E. coli* ATCC25922 and *A. baumannii* DSM-30008 is given as

concentration factor (100x concentration caused by the extraction process) divided by the lowest dilution factor (1:15 – 1:240 dilutions applied in the MIC assay) where growth inhibition was last observed. The lower the crude extract concentration factor at which growth inhibition of a certain pathogen was last observed, the stronger the antimicrobial activity. Weak activity is highlighted in light green colors (e.g. growth inhibition at 6.67x and 3.34x concentration of the crude extract) and strong activity is highlighted in green to dark-green colors (e.g. 1.67x – 0.42x concentration), whereas "-" means no activity even at 6.67x concentration. Crude extract concentrations of 0.83x and 0.42x are synonymous with a total crude extract dilution of 1:1.2 and 1:2.4, respectively. The assignment of a concentration factor as measure of the antimicrobial activity is described in more detail in SI (see Supplementary Figure 41). The area under curve (AUC) ratio serves as measure of the production titre of the respective derivative in the crude extract based on the MS peak surface compared to the AUC of darobactin A. trraces" means an AUC ratio below 0.01. It should be noted, however, that without purification of all congeners an exact quantification is not possible.

Darobactin in crude extract	Concentration/dilution of crude extract at which full growth inhibition is observed				AUC ratio (derivative/ Dar. A)
	***K. pneumoniae* DSM-30104**	***P. aeruginosa* PAO1**	***E. coli* ATCC25922**	***A. baumannii* DMS-30008**	
A	**0.83x**	**0.42x**	**0.83x**	**1.67x**	**1**
B	**3.34x**	**1.67x**	**1.67x**	**1.67x**	**0.03**
C	-	-	-	-	**traces**
D	-	**3.34x**	**3.34x**	**6.67x**	**0.14**
E	-	-	-	-	**0.02**
2	-	**6.67x**	**6.67x**	**6.67x**	**0.06**
4	**1.67x**	**0.83x**	**0.83x**	**0.83x**	**0.69**
6	**6.67x**	**3.34x**	**3.34x**	**3.34x**	**0.06**
8	-	**6.67x**	**6.67x**	**6.67x**	**0.02**
9	**1.67x**	**1.67x**	**0.83x**	**0.83x**	**0.55**
10	-	**6.67x**	-	-	**0.41**
11	**6.67x**	**6.67x**	**6.67x**	**3.34x**	**0.07**
12	-	**6.67x**	**6.67x**	**6.67x**	**0.04**
13	-	-	-	-	**traces**
14	**1:1,2**	**1.67x**	**1:1,2**	**1.67x**	**0.82**
15	-	-	-	-	**traces**
16	**1.67x**	**1.67x**	**1.67x**	**1.67x**	**1.01**
17	-	-	-	-	**0.21**
18	-	-	-	**6.67x**	**0.26**

However, we could not assign absolute quantities and exact concentrations of novel darobactins without isolating all of them. Thus, the concentration of the darobactin derivatives differed in each crude extract and this experiment does not allow direct comparison of the bioactivity observed for a certain darobactin derivative with the antibiotic activity of darobactin A. Nevertheless, we were able to de-prioritise darobactin derivatives for which no bioactivity

was observed (darobactins C, E, 5, 7, 13, 15 and 17), even though this might be caused by low concentration of the respective compound in the crude extract. In order to further narrow down the pool of the remaining darobactin derivatives of interest and select a candidate for isolation and biological assessment based on the pure compound, we calculated the area under curve (AUC) of the respective darobactin derivative MS peaks (Table 2). As the darobactin derivatives differ in their ionisability in the ESI process, this analysis can only serve as a rough estimate of the amount of compound in each crude extract. For instance, darobactin B, in which the L-serine at amino acid position 6 was replaced by the well-ionisable L-arginine, showed a higher MS signal provided from the $[M+3H]^{3+}$ ions than the MS signal provided from $[M+2H]^{2+}$ ions, whereas $[M+3H]^{3+}$ ions were only barely observed for darobactin A. Since we cannot predict the ionisation behaviour of the derivatives we cannot provide an absolute quantification of each congener. We therefore refrained from calculating mg/L values for each analog based on the absolute quantification of the darobactin A production titre. The largest AUC values were calculated for darobactins 4, 9, 10, 14 and 16. Due to the challenges associated with isolation and purification of compounds for follow up experiments by NMR and bioactivity assays we therefore prioritized compounds likely to exhibit good activity at reasonable productivity.

Since L-phenylalanine is conserved in position 7 in native darobactins and an essential structural feature to mimic the β-signal of native BamA substrates,[18] we were surprised that the extract containing darobactin 9, in which the L-phenylalanine was replaced by L-tryptophan, showed similar antibacterial activity to the darobactin A-containing sample (Table 2). On the contrary, the extract containing darobactin 10 with L-tyrosine in position 7 showed only weak activity despite its structural similarity to darobactin A and similar production level based on the AUC of the respective MS peaks. This indicates that the additional OH-group in L-tyrosine compared to L-phenylalanine negatively affects the interaction of darobactin with BamA, whereas expansion of the side chain π-system by introducing an indole moiety, as it is the case for L-tryptophan, potentially enables stronger aromatic interaction with the BamA target site. Since darobactin 9 was produced in similar quantities to darobactin A based on comparison of the respective AUCs, we classified darobactin 9 as promising starting point for further investigations and purified the compound from a large-scale production culture (see SI). The purified compound was used to determine the production titre of darobactin 9 in the fermentation broth of *E. coli* BL21 (DE3) pNOSO-darABCDE-9 (see SI), providing an average production rate of 2.9 (± 0.6) mg/L. The predicted structure (Figure 5) was verified by acquisition of tandem MS data followed by acquisition of multidimensional NMR experiments. Next, we assessed the MICs of pure darobactin 9, showing that this derivative exhibits superior antibacterial activity against

the strains of a larger pathogen panel being on average two-fold more potent than darobactin A (Table 3).

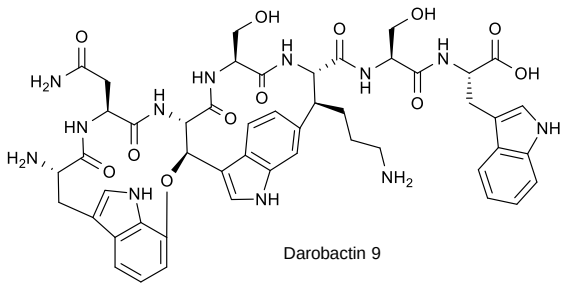

Figure 16: Structural formula of darobactin 9 carrying a C-terminal L-tryptophan.

Encouragingly, most Gram-negative bacterial strains were inhibited by sub to low µg/mL concentrations of darobactin 9, and the new derivative was particularly active against *E. coli* (0.125-2 µg/mL), *Citrobacter freundii* (0.5 µg/mL), *Enterobacter cloacae* (1 µg/mL), and *K. pneumoniae* (1-2 µg/mL). Among the species displaying high MICs for darobactin A, we observed significant improvements for darobactin 9, where MICs on *A. baumannii* of 1-2 µg/mL and MICs on *P. aeruginosa* of 0.125-2 µg/mL were obtained, which corresponds to an approximately 8-fold improvement over darobactin A. Darobactin 9 also gained some activity against *Proteus* spp. (8-64 µg/mL) and *Serratia marcescens* (64 µg/mL) both being gaps in the antibacterial spectrum of darobactin A. Intriguingly, darobactin 9 was equally active against recent clinical MDR isolates (see SI) and MICs were as low as 1-2 µg/mL and 1-4 µg/mL on *E. coli* and *K. pneumoniae*, respectively, further highlighting the potential of darobactins as new broad-spectrum and resistance-breaking antibiotics. Thus, darobactin 9 is a very promising starting point for further structure engineering attempts in the future in which we attempt to further engineer darobactin 9. Especially with respect to difficult-to-treat *A. baumannii* and *P. aeruginosa* infections, the improvement in MICs is highly encouraging for such efforts.

Targeted gene deletions and co-expression of *darF* and *darG*.

Even though hypothetical biosynthetic functions were previously assigned to *darBCD*, encoding a tripartite ABC-type trans-envelope exporter, and *darE*, encoding a radical SAM enzyme proposed to catalyse both ring formations in darobactins, experimental confirmation has yet to be performed on a molecular basis. Thus, we conducted targeted, seamless gene deletions of *darB*, *darC*, *darD*, and *darE*, independently, with subsequent heterologous expression of the deletion constructs in *E. coli* BL21 (DE3). UHPLC-HRMS analysis of the fermentation broth supernatant (described in SI) showed that

deletions of *darB*, *darC* and *darD* led to a two- to four-fold decrease in darobactin A production with titres of ca. 6 mg/L, 5 mg/L and 3 mg/L, respectively, compared to the control.

Table 3: Minimal inhibitory concentration (MIC in µg mL^{-1}) of darobactin 9 in an extended panel of clinically relevant Gram-negative pathogens. Darobactin A served as control. The heterologous darobactin producer strain *E. coli* BL21 (DE3) + BGC contains the pNOSO-darABCDE plasmid. [a] MDR clinical isolates (see SI).

Strain		Dar. 9	Dar. A
E. coli	**BL21 (DE3)**	**0.25**	**0.5-1**
	BL21 (DE3) + BGC	**2-4**	**8-16**
	ATCC-25922	**1-2**	**2**
	JW0451-2 (ΔacrB)	**0.125**	**0.5**
	K12 ΔtolC	**0.125**	**0.5**
	ECO24[a]	**1-2**	**8**
	ECO25[a]	**1-2**	**8**
A. baumannii	**DSM-30007**	**2**	**16**
	DSM-30008	**1-2**	**4**
C. freundii	**DSM-30039**	**0.5**	**1**
E. cloacae	**DSM-30054**	**1**	**2**
K. pneumoniae	**DSM-30104**	**1-2**	**2-4**
	KPN12[a]	**4**	**8**
	KPN19[a]	**1**	**2**
	KPN62[a]	**2**	**4**
P. aeruginosa	**PAO1**	**0.125**	**0.5-1**
	PA14	**2**	**16**
	PA14 ΔmexAB	**1**	**4**
P. mirabilis	**DSM-4479**	**32-64**	**64**
P. vulgaris	**DSM-2140**	**8**	**16**
S. marcescens	**DSM-30121**	**64**	**> 64**
E. faecalis	**ATCC-29212**	**> 64**	**> 64**
S. aureus	**ATCC-29213**	**> 64**	**> 64**

Given that the gene products of *darBCD* encode an efflux transporter machinery, which is presumably non-functional after deletion of one of its components, the removal of darobactin A from the cell is likely impaired, leading to lower extracellular concentrations as detected by mass spectrometry. Similar observations were made by Wuisan and co-workers, who measured 50 % reduced extracellular darobactin A concentration upon heterologous expression of only *darA* and *darE* in *E. coli*, compared to the control strain expressing *darABCDE*.[20] Interestingly, the authors could rule out that darobactin A accumulated in the cell, since intracellular concentrations were also reduced when *darBCD* was not expressed.[20] Since darobactin production was still observed despite deletion of the efflux transporter co-located with the BGC, *E. coli* BL21 (DE3) might express a *darBCD* homolog located elsewhere in the genome that partly compensates for the loss of function. Consequently, we searched for *darBCD*

homologs in the genome of *E. coli* BL21 (DE3) (GenBank accession CP001509) and found only *darD* homologs (ABC-transporter ATP-binding protein; approx. 30 hits ≥ 70 % pairwise identity), whereas no close *darB* and *darC* homologs were found. Nevertheless, we cannot exclude that another efflux system, such as AcrAB-TolC,[26] YdhE,[27] and MdtABC-TolC[28] MDR efflux transporters encoded in the *E. coli* BL21 (DE3) genome, is involved in the export of darobactin from the cell. Since *E. coli* strains with deletion of the *acrB* or *tolC* were significantly more sensitive towards darobactin A and darobactin 9 as compared to strains harbouring those genes (Table 3), we assume that involvement of both of these broad-spectrum efflux systems in darobactin export is likely. In parallel work, a cooperation of DarBCD with TolC, both being involved in the export of darobactin, was discussed.[20] However, deletion of *tolC* from the genome of the heterologous darobactin producer *E. coli* BAP-1 did not affect the ratio between intra- and extracellular darobactin concentrations.[20]

Deletion of *darE* in our heterologous expression construct resulted in complete abolishment of darobactin A production, confirming its essential function in darobactin biosynthesis. To identify potential darobactin-related compounds in the fermentation broth, we performed a MS^2 spectral similarity analysis, but no darobactin-related compounds, such as truncated derivatives, monocyclised, or linear darobactin, were detected. Even though we are not able to confirm the involvement of DarE in the cyclisation reactions on an enzyme level *in vitro*, it is safe to assume that the previously hypothesised function is correct, because bicyclised darobactin was still produced after *darBCD* deletion and taking into account that *darA* encodes the darobactin propeptide, which was proven by Wuisan and coworkers.[20] Furthermore, alkyl-arylic couplings like the ones observed for darobactin are usually formed in radical reactions catalysed by radical-SAM-type enzymes or Cytochrome P450 enzymes, which supports the previous hypothesis.[29] As no further genes are located within the BGC, we assume the involvement of other genes in the cyclization reactions to be unlikely since those genes would need to be located elsewhere in the genomes of both the native and heterologous producer strains.

Some of the darobactin BGCs found by genome mining in potential producer strains like *Pseudoalteromonas luteoviolacea* S4054 include two additional ORFs of unknown function, *darF* and *darG*. A BLAST (Basic Local Alignment Search Tool)[30] search in the non-redundant protein database (nr) using the protein sequence of DarF and DarG as query provided only hypothetical proteins of unknown function and ABC transporters as respective hits (see Supplementary Data). HHpred[31] analysis of DarF however, revealed homology to zinc-dependent metalloproteases (see Supplementary Data), making it a potential candidate protease involved in the darobactin maturation process which was not yet described. Since *darF* is not part of the darobactin BGC in *P. khanii* HGB1456, many other native producer strains and the heterologous producer, a homolog would have to be located elsewhere in these genomes. In parallel work, Wuisan and coworkers speculated that the proteolytic maturation of

the darobactin propeptide is indeed performed by a protease elsewhere in the genome of *E. coli* even though they could not rule out an autoproteolytic function of DarA itself.[20] Thus, we performed a BLAST search in the genomes of *P. khanii* HGB1456 and *E. coli* BL21 (DE3) using the DarF protein sequence as query, however without identification of potential homologs. To investigate the function of *darF* and *darG*, we co-expressed both genes under the regulation of the *nptII* promoter in combination with *darABCDE* in *E. coli* BL21 (DE3) and observed complete abolishment of darobactin A production. In order to investigate whether this effect is caused by combined co-expression of *darFG* or whether it can be related to *darF* or *darG* alone, we co-expressed both genes independently with *darABCDE*. While co-expression of *darG* only slightly decreased darobactin yields, co-expression of *darF* led to complete production abolishment. Since a spectral networking analysis did not identify any darobactin-related compounds upon expression of *darF*, we hypothesised that DarF acts as a protease degrading either the mature darobactin A itself or the corresponding propeptide, thus impeding formation of mature darobactin. To investigate this hypothesis, we heterlogously expressed and purified DarF from *E. coli* BL21 (DE3) and incubated the enzyme with darobactin A or darobactin 9 *in vitro* (see SI). We indeed observed degradation of darobactins A and 9 after 12 h of incubation with DarF, whereas no degradation was seen in the control experiments without DarF (see Supplementary Figures 49-50). These observations supported that DarF is a darobactin-degrading enzyme. A possible function of DarF in *P. luteoviolacea* S4054 might be a feedback-regulated self-detoxification or self-resistance mechanism, in which high darobactin A concentrations lead to *darF* gene expression and consequently the degradation of darobactin A, thereby setting a limit to darobactin concentrations not harmful for the native producer. In our heterologous expression system, however, the potential feedback-regulated gene expression might be impaired, because *darF* is constitutively overexpressed under the regulation of the *nptII* promoter, which seems to lead to complete degradation of darobactin.

In summary, *darA* and *darE* are the only genes essential for darobactin production in *E. coli* BL21 (DE3), which was also shown in parallel work by Wuisan *et al*.[20] Co-expression of *darBCD* increases the production level of darobactin A by a factor of 2-4, whereas *darG* co-expression reduces the production level, as judged by comparison of the darobactin A mass peak. Since co-expression of *darF* led to complete abolishment of darobactin production and no homologs were identified in the genomes of *P. khanii* HGB1456 and *E. coli* BL21 (DE3), we rule out that DarF is the protease involved in the proteolytic maturation process of the compound, in which the leader peptide or tail sequence are removed. Both the mechanism of action of DarF and the proteolytic maturation mechanism of darobactin, performed by a so far unidentified protease enzyme in the native producer strain and a similar enzyme in *E. coli* BL21 (DE3) have to be investigated in future experiments.

Conclusions

In this work, we developed a versatile heterologous production platform for darobactin derivatives based on a darobactin BGC from *P. khanii* HGB1456 modified for the expression in *E. coli* BL21 (DE3). Excluding the previously published darobactin A,[15] 17 new darobactin derivatives were produced after expression of *darA* variants encoding different core peptide sequences. Every position in the molecule was shown to be reasonably flexible for structure engineering by incorporation of different amino acids, except of the two L-tryptophans in positions 1 and 3, which are required for formation of the bicyclic darobactin core structure, proving the versatility of the presented system. Likewise, high substrate tolerance has been observed for biosynthetic enzymes in other RiPP pathways, e.g. in lanthipeptide, thiopeptide, lasso peptide and sactipeptide biosynthesis,[32] underlining the potential of RiPP structure engineering to generate new antibiotics.

However, due to difficulties in the isolation and compound purification process that will have to be addressed in the future, we were so far only able to purify our most promising congener darobactin 9, which showed favourable activity against MDR clinical pathogens and significantly improved antibacterial activity towards *P. aeruginosa* and *K. pneumoniae* strains with respect to darobactin A. For the other darobactin derivatives, we relied on appearance of the corresponding mass peak after heterologous expression of the respective plasmid-based BGC, followed by comparison of the calculated to the measured exact mass and corresponding MS^2 fragmentation pattern to assign the predicted structures for the remaining derivatives not isolated so far. However, for the L-cysteine-containing derivatives we observed an unexpected mass shift of +191.02 Da that we were not able to account for, while the MS^2 spectrum indicates the molecule contains the darobactin core structure including the L-cysteine. It therefore seems likely that the sulphur nucleophile in the respective darobactin derivatives has reacted with a metabolite in the cell in order to detoxify the sulphur nucleophile. Nevertheless, future experiments will address the optimization of cultivation conditions and downstream purification steps, finally allowing characterization of the remaining derivatives, which showed promising antibacterial activity in the crude extract-based MIC assay.

Even though the production titre of darobactin A in our heterologous host (>13 mg/L in 3 days) was improved compared to the native producer strain *P. khanii* HGB1456, parallel work of Wusain *et al*. reached a titre of >30 mg/L in 2 days.[20] Nevertheless, the production titres of darobactin A and of a few derivatives achieved with our system is sufficient for isolation and purification, with the production resulted from leaky expression of *darA* by an uninduced *T7lac* promoter. Furthermore, it is unlikely that the codon usage in the biosynthetic genes responsible for darobactin production are optimal for translation in *E. coli*, since the GC content of the darobactin BGC is only 32 % as compared to *E. coli* genome with about 50 % GC content. As we did not perform codon optimization so far, it is likely that

production improvement can be achieved on both transcriptional and translational level after further optimizations of the darobactin expression vector.

Moreover, determination of the MIC of darobactin A and darobactin 9 against the heterologous producer strain *E. coli BL21* (DE3) pNOSO-darABCDE showed that growth inhibition occurred at concentrations of 8-16 and 2-4 µg/mL (see Table 3), respectively, indicating that the maximum production titres of both compounds (>13 mg/L darobactin A and <3 mg/L darobactin 9) might be limited by self-resistance of the producer. In order to achieve industrial scale production titres, the self-resistance of the producer might be improved through targeted mutation of BamA in the genome, since it was previously shown that certain BamA mutations confer resistance towards darobactin A.[15] As experiments that occurred in parallel to this work showed BamA mutations to lead to a significant loss in fitness and darobactin A productivity,[20] the co-expression of mutated BamA contemporaneously with native BamA might be an alternative route to be explored. Furthermore, utilizing a phylogenetically more distant heterologous producer strain, e.g. of Gram-positive or eukaryotic origin, could circumvent the self-resistance issue completely as these organisms do not rely on BamA.

Targeted gene deletions and the attempts to produce truncated darobactins provided a first insight into the biosynthesis of this compound class. Interestingly, only two genes, *darA* and *darE*, are required for the formation of darobactin, a result also observed in parallel work by Wuisan and coworkers.[20] Deletion of the *relE*-like gene, which is associated with the darobactin BGC in some of the native producer strains, had no impact on the darobactin A production in *E. coli* BL21 (DE3). However, as the gene expression of the *relE* homologue was still regulated by its native promotor, its expression might be weak or totally absent in *E. coli* BL21, which prevented us to elucidate its actual function and influence on darobactin biosynthesis. In future experiments, the *relE* homologue might be re-introduced into pNOSO-darABCDE downstream of *darBCDE* under the regulation of the *nptII* promoter for further investigation into its biological role. Moreover, despite the identification of *darF* and *darG* as genes associated with the darobactin BGC in several native producer strains, their role in darobactin biosynthesis was previously not discussed. Co-expression of *darF* and *darG* in the heterologous producer and the *in vitro* investigation of purified DarF showed that DarF is a protease leading to degradation of darobactin, whereas the function of DarG remains unclear. We hypothesise that the expression of *darF* in the native producer strain might be feedback-regulated, thereby limiting the darobactin production. However, experimental evidence has to be provided in future experiments. The proteolytic maturation process of darobactin however, including the enzymes that are potentially involved, still remains unclear.

Taken together, this work provided experimental evidence for darobactin biosynthesis processes, which was in part also confirmed by parallel work by Wuisan *et al.*.[20] Importantly, we achieved efficient

structure engineering of darobactin and heterologous production of new and superior bioactive derivatives like darobactin 9 in good yields. Therefore, the work reported further advances the darobactin natural product class towards a potential use as an antibiotic drug.

Conflicts of interest

There are no conflicts to declare.

Acknowledgements

We thank Stefanie Schmidt for performing the MIC assays and Dr. F. P. Jake Haeckl for helpful proofreading of the manuscript. The authors would also like to thank Dr. Patrick Chhatwal, Leonard Knegendorf, and Prof. Dr. Dirk Schlüter from the Institute for Medical Microbiology and Hospital Epidemiology of Hannover Medical School (MHH), Germany, for providing clinical isolates.

References

1 a) E. Tacconelli, E. Carrara, A. Savoldi, S. Harbarth, M. Mendelson, D. L. Monnet, C. Pulcini, G. Kahlmeter, J. Kluytmans, Y. Carmeli, M. Ouellette, K. Outterson, J. Patel, M. Cavaleri, E. M. Cox, C. R. Houchens, M. L. Grayson, P. Hansen, N. Singh, U. Theuretzbacher, N. Magrini, A. O. Aboderin, S. S. Al-Abri, N. Awang Jalil, N. Benzonana, S. Bhattacharya, A. J. Brink, F. R. Burkert, O. Cars, G. Cornaglia, O. J. Dyar, A. W. Friedrich, A. C. Gales, S. Gandra, C. G. Giske, D. A. Goff, H. Goossens, T. Gottlieb, M. Guzman Blanco, W. Hryniewicz, D. Kattula, T. Jinks, S. S. Kanj, L. Kerr, M.-P. Kieny, Y. S. Kim, R. S. Kozlov, J. Labarca, R. Laxminarayan, K. Leder, L. Leibovici, G. Levy-Hara, J. Littman, S. Malhotra-Kumar, V. Manchanda, L. Moja, B. Ndoye, A. Pan, D. L. Paterson, M. Paul, H. Qiu, P. Ramon-Pardo, J. Rodríguez-Baño, M. Sanguinetti, S. Sengupta, M. Sharland, M. Si-Mehand, L. L. Silver, W. Song, M. Steinbakk, J. Thomsen, G. E. Thwaites, J. W. M. van der Meer, N. van Kinh, S. Vega, M. V. Villegas, A. Wechsler-Fördös, H. F. L. Wertheim, E. Wesangula, N. Woodford, F. O. Yilmaz and A. Zorzet, *Lancet Infect. Dis.*, 2018, **18**, 318; b) Global Antimicrobial Surveillance System (GLASS) Report 2016-2017, https://apps.who.int/iris/bitstream/handle/10665/279656/9789241515061-eng.pdf?ua=1, (accessed 27 November 2020);

2 K. Kupferschmidt, *Science*, 2016, **352**, 758.

3 D. van Duin and R. A. Bonomo, *Clin. Infect. Dis.*, 2016, **63**, 234.

4 R. G. Wunderink, E. J. Giamarellos-Bourboulis, G. Rahav, A. J. Mathers, M. Bassetti, J. Vazquez, O. A. Cornely, J. Solomkin, T. Bhowmick, J. Bishara, G. L. Daikos, T. Felton, M. J. L. Furst, E. J. Kwak, F. Menichetti, I. Oren, E. L. Alexander, D. Griffith, O. Lomovskaya, J. Loutit, S. Zhang, M. N. Dudley and K. S. Kaye, *Infect. Dis. Ther.*, 2018, **7**, 439.

5 J. R. Smith, J. M. Rybak and K. C. Claeys, *Pharmacotherapy*, 2020, **40**, 343.

6 L. D. Saravolatz and G. E. Stein, *Clin. Infect. Dis.*, 2020, **70**, 704.

7 J. A. Sutcliffe, W. O'Brien, C. Fyfe and T. H. Grossman, *Antimicrob. Agents Chemother.*, 2013, **57**, 5548.

8 A. Ito, T. Sato, M. Ota, M. Takemura, T. Nishikawa, S. Toba, N. Kohira, S. Miyagawa, N. Ishibashi, S. Matsumoto, R. Nakamura, M. Tsuji and Y. Yamano, *Antimicrob. Agents Chemother.*, 2018, **62**.

9 U. Theuretzbacher, K. Bush, S. Harbarth, M. Paul, J. H. Rex, E. Tacconelli and G. E. Thwaites, *Nat. Rev. Microbiol.*, 2020, **18**, 286.

10 N. Srinivas, P. Jetter, B. J. Ueberbacher, M. Werneburg, K. Zerbe, J. Steinmann, M. B. van der, F. Bernardini, A. Lederer, R. L. Dias, P. E. Misson, H. Henze, J. Zumbrunn, F. O. Gombert, D. Obrecht, P. Hunziker, S. Schauer, U. Ziegler, A. Kach, L. Eberl, K. Riedel, S. J. DeMarco and J. A. Robinson, *Science*, 2010, **327**, 1010.

11 M. Kaul, L. Mark, Y. Zhang, A. K. Parhi, Y. L. Lyu, J. Pawlak, S. Saravolatz, L. D. Saravolatz, M. P. Weinstein, E. J. LaVoie and D. S. Pilch, *Antimicrob. Agents Chemother.*, 2015, **59**, 4845.

12 A. Kling, P. Lukat, D. V. Almeida, A. Bauer, E. Fontaine, S. Sordello, N. Zaburannyi, J. Herrmann, S. C. Wenzel, C. König, N. C. Ammerman, M. B. Barrio, K. Borchers, F. Bordon-Pallier, M. Brönstrup, G. Courtemanche, M. Gerlitz, M. Geslin, P. Hammann, D. W. Heinz, H. Hoffmann, S. Klieber, M. Kohlmann, M. Kurz, C. Lair, H. Matter, E. Nuermberger, S. Tyagi, L. Fraisse, J. H. Grosset, S. Lagrange and R. Müller, *Science*, 2015, **348**, 1106.

13 a) G. S. Basarab, G. H. Kern, J. McNulty, J. P. Mueller, K. Lawrence, K. Vishwanathan, R. A. Alm, K. Barvian, P. Doig, V. Galullo, H. Gardner, M. Gowravaram, M. Huband, A. Kimzey, M. Morningstar, A. Kutschke, S. D. Lahiri, M. Perros, R. Singh, Schuck, Virna J A, R. Tommasi, G. Walkup and J. V. Newman, *Nat. Sci. Rep.*, 2015, **5**, 11827; b) S. Baumann, J. Herrmann, R. Raju, H. Steinmetz, K. I. Mohr, S. Hüttel, K. Harmrolfs, M. Stadler and R. Müller, *Angew. Chem. Int. Ed.*, 2014, **53**, 14605;

14 E. M. Hart, A. M. Mitchell, A. Konovalova, M. Grabowicz, J. Sheng, X. Han, F. P. Rodriguez-Rivera, A. G. Schwaid, J. C. Malinverni, C. J. Balibar, S. Bodea, Q. Si, H. Wang, M. F. Homsher, R. E. Painter, A. K. Ogawa, H. Sutterlin, T. Roemer, T. A. Black, D. M. Rothman, S. S. Walker and T. J. Silhavy, *Proc. Nat. Acad. Sci. USA*, 2019, **116**, 21748.
15 Y. Imai, K. J. Meyer, A. Iinishi, Q. Favre-Godal, R. Green, S. Manuse, M. Caboni, M. Mori, S. Niles, M. Ghiglieri, C. Honrao, X. Ma, J. J. Guo, A. Makriyannis, L. Linares-Otoya, N. Böhringer, Z. G. Wuisan, H. Kaur, R. Wu, A. Mateus, A. Typas, M. M. Savitski, J. L. Espinoza, A. O'Rourke, K. E. Nelson, S. Hiller, N. Noinaj, T. F. Schäberle, A. D'Onofrio and K. Lewis, *Nature*, 2019, **576**, 459.
16 Anatol Luther, Matthias Urfer, Michael Zahn, Maik Müller, Shuang-Yan Wang, Milon Mondal, Alessandra Vitale, Jean-Baptiste Hartmann, Timothy Sharpe, Fabio Lo Monte, Harsha Kocherla, Elizabeth Cline, Gabriella Pessi, Parthasarathi Rath, Seyed Majed Modaresi, Petra Chiquet, Sarah Stiegeler, Carolin Verbree, Tobias Remus, Michel Schmitt, Caroline Kolopp, Marie-Anne Westwood, Nicolas Desjonquères, Emile Brabet, Sophie Hell, Karen LePoupon, Annie Vermeulen, Régis Jaisson, Virginie Rithié, Grégory Upert, Alexander Lederer, Peter Zbinden, Achim Wach, Kerstin Moehle, Katja Zerbe, Hans H. Locher, Francesca Bernardini, Glenn E. Dale, Leo Eberl, Bernd Wollscheid, Sebastian Hiller, John A. Robinson and Daniel Obrecht, *Nature*, 2019, **576**, 452.
17 A. Konovalova, D. E. Kahne and T. J. Silhavy, *Annu. Rev. Microbiol.*, 2017, **71**, 539.
18 H. Kaur, R. P. Jakob, J. K. Marzinek, R. Green, Y. Imai, J. R. Bolla, E. Agustoni, C. V. Robinson, P. J. Bond, K. Lewis, T. Maier and S. Hiller, *Nature*, 2021, **593**, 125.
19 S. K. Christensen, M. Mikkelsen, K. Pedersen and K. Gerdes, *Proc. Nat. Acad. Sci. USA*, 2001, **98**, 14328.
20 Z. G. Wuisan, I. D. M. Kresna, N. Böhringer, K. Lewis and T. F. Schäberle, *Metab. Eng.*, 2021, **66**, 123.
21 J. W. Dubendorff and F. W. Studier, *J. Mol. Biol.*, 1991, **219**, 45.
22 D. Pogorevc, F. Panter, C. Schillinger, R. Jansen, S. C. Wenzel and R. Müller, *Metab. Eng.*, 2019, **55**, 201.
23 M. Wang, J. J. Carver, V. V. Phelan, L. M. Sanchez, N. Garg, Y. Peng, D. D. Nguyen, J. Watrous, C. A. Kapono, T. Luzzatto-Knaan, C. Porto, A. Bouslimani, A. V. Melnik, M. J. Meehan, W.-T. Liu, M. Crusemann, P. D. Boudreau, E. Esquenazi, M. Sandoval-Calderon, R. D. Kersten, L. A. Pace, R. A. Quinn, K. R. Duncan, C.-C. Hsu, D. J. Floros, R. G. Gavilan, K. Kleigrewe, T. Northen, R. J. Dutton, D. Parrot, E. E. Carlson, B. Aigle, C. F. Michelsen, L. Jelsbak, C. Sohlenkamp, P. Pevzner, A. Edlund, J. McLean, J. Piel, B. T. Murphy, L. Gerwick, C.-C. Liaw, Y.-L. Yang, H.-U. Humpf, M. Maansson, R. A. Keyzers, A. C. Sims, A. R. Johnson, A. M. Sidebottom, B. E. Sedio, A. Klitgaard, C. B. Larson, C. A. Boya P, D. Torres-Mendoza, D. J. Gonzalez, D. B. Silva, L. M. Marques, D. P. Demarque, E. Pociute, E. C. O'Neill, E. Briand, E. J. N. Helfrich, E. A. Granatosky, E. Glukhov, F. Ryffel, H. Houson, H. Mohimani, J. J. Kharbush, Y. Zeng, J. A. Vorholt, K. L. Kurita, P. Charusanti, K. L. McPhail, K. F. Nielsen, L. Vuong, M. Elfeki, M. F. Traxler, N. Engene, N. Koyama, O. B. Vining, R. Baric, R. R. Silva, S. J. Mascuch, S. Tomasi, S. Jenkins, V. Macherla, T. Hoffman, V. Agarwal, P. G. Williams, J. Dai, R. Neupane, J. Gurr, A. M. C. Rodriguez, A. Lamsa, C. Zhang, K. Dorrestein, B. M. Duggan, J. Almaliti, P.-M. Allard, P. Phapale, L.-F. Nothias, T. Alexandrov, M. Litaudon, J.-L. Wolfender, J. E. Kyle, T. O. Metz, T. Peryea, D.-T. Nguyen, D. VanLeer, P. Shinn, A. Jadhav, R. Muller, K. M. Waters, W. Shi, X. Liu, L. Zhang, R. Knight, P. R. Jensen, B. O. Palsson, K. Pogliano, R. G. Linington, M. Gutierrez, N. P. Lopes, W. H. Gerwick, B. S. Moore, P. C. Dorrestein and N. Bandeira, *Nat. Biotechnol.*, 2016, **34**, 828.
24 L. Patiny and A. Borel, *J. Chem. Inf. Model.*, 2013, **53**, 1223.
25 T. Kind and O. Fiehn, *Bmc Bioinform.*, 2007, **8**, 105.
26 N. Weston, P. Sharma, V. Ricci and L. J. V. Piddock, *Res. Microbiol.*, 2017.
27 F. Long, C. Rouquette-Loughlin, W. M. Shafer and E. W. Yu, *Antimicrob. Agents Chemother.*, 2008, **52**, 3052.

28 S. Nagakubo, K. Nishino, T. Hirata and A. Yamaguchi, *J. Bacteriol.*, 2002, **184**, 4161.
29 a) J. J. Hug, J. Dastbaz, S. Adam, O. Revermann, J. Koehnke, D. Krug and R. Müller, *ACS Chem. Biol.*, 2020, **15**, 2221; b) Y. Ye, H. Fu and T. K. Hyster, *J. Ind. Microbiol. Biotechnol.*;
30 S. F. Altschul, W. Gish, W. Miller, E. W. Myers and D. J. Lipman, *J. Mol. Biol.*, 1990, **215**, 403.
31 L. Zimmermann, A. Stephens, S.-Z. Nam, D. Rau, J. Kübler, M. Lozajic, F. Gabler, J. Söding, A. N. Lupas and V. Alva, *J. Mol. Biol.*, 2018, **430**, 2237.
32 G. A. Hudson and D. A. Mitchell, *Curr. Opin. Microbiol.*, 2018, **45**, 61.

2.2 Supporting Information

Improved broad-spectrum antibiotics against Gram-negative pathogens via darobactin biosynthetic pathway engineering

Previously published in:

Sebastian Groß,[abce] Fabian Panter,[abcde] Domen Pogorevc,[abce] Carsten E. Seyfert,[abce]

Selina Deckarm,[abc] Chantal D. Bader,[abc] Jennifer Herrmann,[abc] Rolf Müller*[abcd]

Chem. Sci., 2021 August 12; **12:** 11882-11893

DOI: 10.1039/D1SC02725E

Affilitation:

[a] Helmholtz Institute for Pharmaceutical Research Saarland (HIPS), Helmholtz Centre for Infection Research, Saarland University Campus, 66123 Saarbrücken, Germany

[b] Department of Pharmacy, Saarland University, 66123 Saarbrücken, Germany

[c] DZIF - German Centre for Infection Research, Partnersite Hannover-Braunschweig

[d]Helmholtz International Lab for Anti-Infectives, Campus E8 1, 66123 Saarbrücken, Germany

[e] These authors contributed equally

* Corresponding author

The printed version of the Supporting Information does not contain data that cannot be visualized satisfactorily on paper. To access this data please refer to the enclosed storage medium or the on-line version of this research paper.

In silico design of the modified BGC, darA variants and pNOSO vector

The *Photorhabdus khanii* HGB1456 BGC sequence (GenBank accession WHZZ01000001.1) was used as template sequence to design the modified BGC. The modified BGC was organized in three transcriptional units, the first and second consisting only of the *relE* homologue and *darA*, respectively, and the third contains *darBCDE*. No recombinant promoter was placed upstream of the *relE*-like gene, whereas recombinant *T7lac*[1] and *nptII*[2,3] promoter systems (including *lacI* repressor gene and *lacO* operator in case of *T7lac* and RBSs in both cases) were placed upstream of *darA* and *darBCDE*, respectively. Two *tD1* terminator sequences were inserted upstream of the *nptII* promoter and downstream of *darBCDE*. Suppl. Table 1 lists all genetic elements including sequence origin used for the design of the modified BGC.

Suppl. Table 1. Genetic elements used in the design of the modified darobactin BGC.

Genetic element	Nucleotide position	Sequence origin (GenBank accession)	Nucleotide position in original sequence
pNOSO-relEdarABCDE			
*Sgr*DI	10,239 – 6	-	-
p15A ori	7 – 839	pACYC177 (X06402)[4]	766 - 1,598
kanR (*aph(3')-Ia*)	840 - 1,821	pACYC177 (X06402)[4]	1,816 - 2,797
*Mau*BI - ATTCTA - *Age*I	1,822 - 1,841	-	-
relE + intergenic region (including *Age*I)	1,842 - 2,153	*P. khanii* HGB1456 darobactin BGC(WHZZ01000001.1)	1,236,669 - 1,236,980
*Mre*I - ATTATC - *Xma*JI	2,154 - 2,173	-	-
T7lac promoter (including *lacI* and *lacO*)	2,174 - 3,734	pET-10[1]	3498 - 5732
darA + intergenic region	3,735 - 4,307	*P. khanii* HGB1456 darobactin BGC(WHZZ01000001.1)	1,236,987 - 1,237,559
*Pst*I – TCCTGA - *Bam*HI	4,308 - 4,325	-	-
tD1 terminator	4,326 - 4,386	*Myxococcus xanthus* phage Mx8[5]	-
*Not*I	4,387 - 4,394	-	-
nptII promoter	4,395 - 4,548	pUC18-Zeo-mx8-nptII-corO[2] / neomycin phosphotransferase II resistance gene from Tn5[3]	-
darBCDE	4,549 - 10,169	*P. khanii* HGB1456 darobactin BGC(WHZZ01000001.1)	1,237,560 - 1,243,180
*Spe*I - TCCTGA - *Pac*I	10,170 - 10,189	-	-
tD1 terminator	10,190 - 10,238	*M. xanthus* phage Mx8[5]	-
darFG			
*Spe*I	1 - 6	-	-
darF	7 - 1,083	*P. luteoviolacea* S4054 (NZ_CP015412)	976,996 - 975,920 (reverse DNA strand)
darG	1,084 - 2,847	*P. luteoviolacea* S4054 (NZ_CP015412)	970,404 - 968,641 (reverse DNA strand
*Pac*I	2,848 - 2,855	-	-

Additional to natively present unique restriction endonuclease recognition sites (R-sites), numerous R-sites were introduced into the modified BGC to allow genetic manipulation using restriction hydrolysis/DNA ligation cloning techniques. Furthermore, two *Nde*I R-sites were removed from the BGC by synonymous codon substitutions, since *Nde*I was required as unique R-site downstream of the

T7lac promoter for *darA* exchange or exchange of the *T7lac* promoter itself. Suppl. Table 2 summarizes unique R-sites and their function.

Suppl. Table 2. Function of important R-sites in the modified darobactin BGC. [a] R-site upstream of *Mau*BI R-site in pUC57-relEdarABCDE (not present in pNOSO-relEdarABCDE), [b] R-site present two times in the modified darobactin BGC, [c] R-sites was not used for cloning experiments in this work, [d] R-site downstream of *SgrD*I R-site in pUC57-relEdarABCDE (not present in pNOSO-relEdarABCDE).

R-site	Function
*Kpn*I[a]	pSynbio1 subcloning
*Mau*BI	pNOSO subcloning
*Age*I[b]	Removal of *relE* homologue
*Mre*I[c]	Exchange of *T7lac* promoter
*Xma*JI	Exchange of *T7lac* promoter
*Nde*I	Exchange of *T7lac* promoter or *darA*
*Pst*I[c]	Exchange of *darA*
*Bam*HI	Exchange of *darA*
*Not*I	Exchange of *nptII* promoter
*Xho*I	Exchange of *nptII* promoter
*Spe*I	Introduction of *darFG*
*Pac*I	Introduction of *darFG*
*Sgr*DI	pNOSO subcloning
*Pme*I[d]	pSynbio1 subcloning

The *darA* sequence plus 396 bp downstream intergenic region was used as template for the design of *darA* variants with altered core sequences. The three nucleotides CAT were placed upstream of *darA*, thus generating a *Nde*I R-site together with the adjacent ATG start codon. *Nco*I, *Pst*I and *Bam*HI R-sites (with short random spacers in between) were placed downstream of the intergenic region. The mutations that were introduced into the core sequence of *darA* are listed in Table 1 of the manuscript.

The pNOSO vector contains the *p15A* origin of replication (ori) and the *aph(3')-Ia* gene encoding aminoglycoside-3'-phosphotransferase-Ia (mediating kanamycin resistance) for maintenance in *E. coli* and selection, respectively. Two unique R-sites, *Sal*I and *Sgr*DI (with short random spacer in between), were placed upstream of the *p15A* ori. Furthermore, a unique *Mau*BI R-site was placed downstream of the *aph(3')-Ia* terminator. The genetic elements of pNOSO are listed in Suppl. Table 1.

The *darFG* fragment was designed based on the template sequence from *Pseudoalteromonas luteoviolacea* S4054 (GenBank accession NZ_CP015412) (Suppl. Figure 1). We placed a *Spe*I R-site upstream of *darF* and a *Pac*I R-site downstream of *darG*, allowing cloning of *darFG* into pNOSO-darABCDE. Genetic elements of *darFG* are listed in Suppl. Table 1.

Suppl. Figure 1. Schematic overview of the darobactin BGC from *P. luteoviolacea* S4054 including *darF* and *darG* (purple arrows), *darA* (green arrow), *darBCD* (light grey arrows) and *darE* (blue arrow).

All sequences were deposited in GenBank database under the accession numbers provided in Supplementary Data.

Cloning of expression constructs

All DNA sequences designed *in silico* were chemically synthesized by GenScript Biotech Corporation (Piscataway, New Jersey (US)). Sequence-verified DNA synthesis fragments were delivered in pUC57 standard vectors harbouring an *ampR* (*bla*) gene for selection on ampicillin. Restriction endonuclease hydrolysis and DNA ligation were performed according to the manufacturer`s information protocols. Handling of DNA and PCRs were performed according to standard protocols.[6] *E. coli* transformation was carried out via electroporation in cuvettes with 1 mm electrode distance using 1,350 Vcm^{-1}, 10 µF and 600 Ω as conditions. The transformed cells were resuspended in 1 mL LB medium (composition described below) and incubated for 90 min before selection on LB agar medium overnight. Selected clones were cultivated in 5 mL of liquid LB medium for 16 h and plasmid DNA was subsequently isolated from 2 mL culture using alkaline lysis. The correctness of the isolated constructs was verified by restriction hydrolysis. pSynbio1-relEdarABCDE was generated by ligation of the modified BGC into pSynbio1 after restriction hydrolysis of pSynbio1 and pUC57-relEdarABCDE with *Kpn*I and *Pme*I. pNOSO-relEdarABCDE was generated by ligation of the modified BGC into pNOSO after restriction hydrolysis of pNOSO and pUC57-relEdarABCDE with *Mau*BI and *Sgr*DI. pNOSO-darABCDE was generated after removal of the *relE*-like gene by restriction hydrolysis with *Age*I and subsequent vector re-ligation. pNOSO-darABCDEFG was generated by ligation of *darFG* into pNOSO-darABCDE after restriction hydrolysis of pNOSO-darABCDE and pUC57-darFG with *Spe*I and *Pac*I. pNOSO-darABCDE-B to –E, and pNOSO-darABCDE-1 to -21 were generated by restriction hydrolysis of pNOSO-darABCDE with *Nde*I and *Bam*HI to remove *darA* and introduction of the respective *darA*-variants by ligation. Suppl. Table 3 summarizes all restriction hydrolysis/DNA ligation cloning steps performed in this study.

For heterologous expression, purification and *in vitro* characterisation of DarF (see subsection below), the *darF* gene was amplified from pUC57-darFG via PCR using the primers darF-fw (ATACCCATGGG GCATACACTTACCAATGAACTAC) and darF-rv (ATACCCTCGAGTTATTTTAAGCGCTCTAATGTTTCT), which contain additional sequence overhangs with *Nco*I and *Xho*I R-sites, respectively. The pHisSUMOTEV-darF expression construct was generated by ligation of *darF* into pHisSUMOTEV[7] after restriction hydrolysis with *Nco*I and *Xho*I.

All strains and plasmids generated in this work are listed in the Supplementary Data file.

Suppl. Table 3. Summary of restriction hydrolysis/DNA ligation cloning steps. GSP: gene synthesis product.

Cloning product	Vector	Insert	Insert source	Restriction endonuclease
pSynbio1-relEdarABCDE	pSynbio1	relEdarABCDE	pUC57-relEdarABCDE (GSP)	*Kpn*I/*Pme*I
pNOSO-relEdarABCDE	pNOSO	relEdarABCDE	pUC57-relEdarABCDE (GSP)	*Mau*BI/*Sgr*DI
pNOSO-darABCDE	pNOSO-relEdarABCDE	-	-	*Age*I
pNOSO-darABCDE-nptII-syncor	pNOSO-darABCDE	nptII-syncor	PCR	*Xma*JI/*Nde*I
pNOSO-darABCDE-nptII-synarg	pNOSO-darABCDE	nptII-synarg	PCR	*Xma*JI/*Nde*I
pNOSO-darABCDE-nptII-T7	pNOSO-darABCDE	nptII-T7	PCR	*Xma*JI/*Nde*I
pNOSO-darABCDE-Pm-synarg	pNOSO-darABCDE	Pm-synarg	PCR	*Xma*JI/*Nde*I
pNOSO-darABCDE-Pm-T7	pNOSO-darABCDE	Pm-T7	PCR	*Xma*JI/*Nde*I
pNOSO-darABCDE-tet-synarg	pNOSO-darABCDE	tet-synarg	PCR	*Xma*JI/*Nde*I
pNOSO-darACDE	pNOSO-darACDE-cmR	-	-	*Bsa*I
pNOSO-darABDE	pNOSO-darABDE-cmR	-	-	*Bsa*I
pNOSO-darABCE	pNOSO-darABCE-cmR	-	-	*Bsa*I
pNOSO-darABCD	pNOSO-darABCD-cmR	-	-	*Bsa*I
pNOSO-darABCDEF	pNOSO-darABCDEF-cmR	-	-	*Bsa*I
pNOSO-darABCDEG	pNOSO-darABCDEG-cmR	-	-	*Bsa*I
pNOSO-darABCDEFG	pNOSO-darABCDE	*darFG*	pUC57-darFG (GSP)	*Spe*I/*Pac*I
pNOSO-darABCDE-B	pNOSO-darABCDE	*darA*-B	pUC57-darA-B (GSP)	*Nde*I/*Bam*HI
pNOSO-darABCDE-C	pNOSO-darABCDE	*darA*-C	pUC57-darA-C (GSP)	*Nde*I/*Bam*HI
pNOSO-darABCDE-D	pNOSO-darABCDE	*darA*-D	pUC57-darA-D (GSP)	*Nde*I/*Bam*HI
pNOSO-darABCDE-E	pNOSO-darABCDE	*darA*-E	pUC57-darA-E (GSP)	*Nde*I/*Bam*HI
pNOSO-darABCDE-1	pNOSO-darABCDE	*darA*-1	pUC57-darA-1 (GSP)	*Nde*I/*Bam*HI
pNOSO-darABCDE-2	pNOSO-darABCDE	*darA*-2	pUC57-darA-2 (GSP)	*Nde*I/*Bam*HI
pNOSO-darABCDE-4	pNOSO-darABCDE	*darA*-4	pUC57-darA-4 (GSP)	*Nde*I/*Bam*HI
pNOSO-darABCDE-5	pNOSO-darABCDE	*darA*-5	pUC57-darA-5 (GSP)	*Nde*I/*Bam*HI
pNOSO-darABCDE-6	pNOSO-darABCDE	*darA*-6	pUC57-darA-6 (GSP)	*Nde*I/*Bam*HI
pNOSO-darABCDE-7	pNOSO-darABCDE	*darA*-7	pUC57-darA-7 (GSP)	*Nde*I/*Bam*HI
pNOSO-darABCDE-8	pNOSO-darABCDE	*darA*-8	pUC57-darA-8 (GSP)	*Nde*I/*Bam*HI
pNOSO-darABCDE-9	pNOSO-darABCDE	*darA*-9	pUC57-darA-9 (GSP)	*Nde*I/*Bam*HI
pNOSO-darABCDE-10	pNOSO-darABCDE	*darA*-10	pUC57-darA-10 (GSP)	*Nde*I/*Bam*HI
pNOSO-darABCDE-11	pNOSO-darABCDE	*darA*-11	pUC57-darA-11 (GSP)	*Nde*I/*Bam*HI
pNOSO-darABCDE-12	pNOSO-darABCDE	*darA*-12	pUC57-darA-12 (GSP)	*Nde*I/*Bam*HI
pNOSO-darABCDE-13	pNOSO-darABCDE	*darA*-13	pUC57-darA-13 (GSP)	*Nde*I/*Bam*HI
pNOSO-darABCDE-14	pNOSO-darABCDE	*darA*-14	pUC57-darA-14 (GSP)	*Nde*I/*Bam*HI
pNOSO-darABCDE-15	pNOSO-darABCDE	*darA*-15	pUC57-darA-15 (GSP)	*Nde*I/*Bam*HI
pNOSO-darABCDE-16	pNOSO-darABCDE	*darA*-16	pUC57-darA-16 (GSP)	*Nde*I/*Bam*HI
pNOSO-darABCDE-17	pNOSO-darABCDE	*darA*-17	pUC57-darA-17 (GSP)	*Nde*I/*Bam*HI
pNOSO-darABCDE-18	pNOSO-darABCDE	*darA*-18	pUC57-darA-18 (GSP)	*Nde*I/*Bam*HI
pNOSO-darABCDE-19	pNOSO-darABCDE	*darA*-19	pUC57-darA-19 (GSP)	*Nde*I/*Bam*HI
pNOSO-darABCDE-20	pNOSO-darABCDE	*darA*-20	pUC57-darA-20 (GSP)	*Nde*I/*Bam*HI
pNOSO-darABCDE-21	pNOSO-darABCDE	*darA*-21	pUC57-darA-21 (GSP)	*Nde*I/*Bam*HI

Targeted gene deletions

Independent seamless deletions of *darB*, *darC*, *darD* and *darE* from pNOSO-darABCDE (to obtain pNOSO-darACDE, pNOSO-darABDE, pNOSO-darABCE and pNOSO-darABCD) and deletions of *darF* and

darG from pNOSO-darABCDEFG (to obtain expression constructs with *darABCDEF* or *darABCDEG*) were carried out using Red/ET recombineering[8] in combination with restriction hydrolysis and vector re-ligation (Suppl. Figure 2).

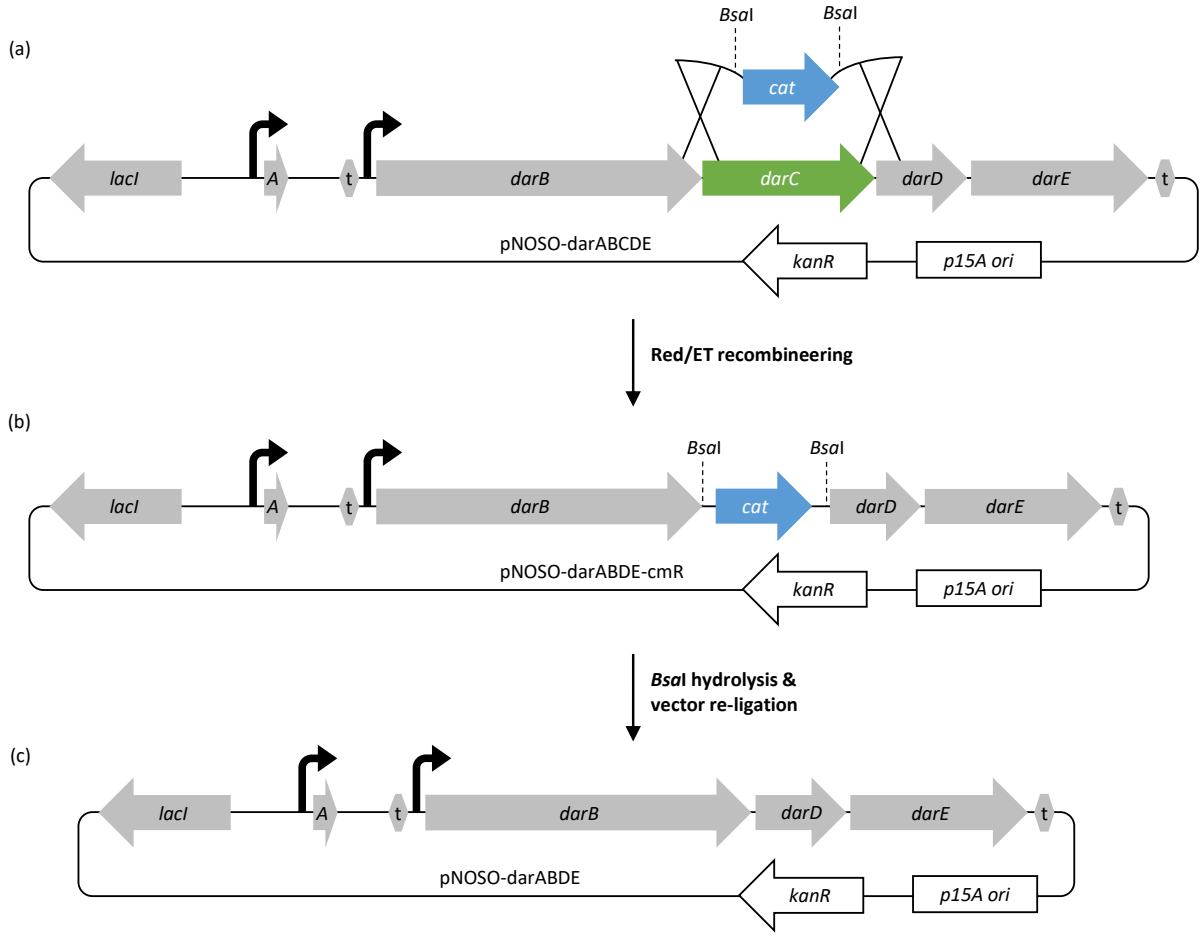

Suppl. Figure 2. Seamless gene deletion on the example of darC. (a) Replacement of darC (shown in green) in pNOSO-darABCDE by chloramphenicol resistance-mediating cat gene PCR product (shown in blue) via Red/ET recombineering. (b) Removal of cat via restriction hydrolysis using *Bsa*I. (c) Re-ligation of the vector yields pNOSO-darABDE.

First, the *cat* gene encoding chloramphenicol *O*-acetyltransferase (mediating chloramphenicol resistance) was amplified by PCR using pMYC20[9] as template. Apart from pMYC20 binding sites, primers contained tail sequences with *Bsa*I R-sites and 50 bp sequences that are homologous to the deleted gene. *Bsa*I is a type IIS restriction endonuclease cutting outside of its recognition sequence, thereby allowing the generation of variable and unique 5 bp sticky ends for ligation. All oligonucleotide primers used for the gene deletion experiments and a summary of all PCRs performed are listed in Suppl. Table 4 and Suppl. Table 5, respectively.

Suppl. Table 4. Oligonucleotides used in seamless gene deletion experiments.

Oligonucleotide	Sequence (5'-3')
Cm-DarB-F	GCGCAGGGGATCAAGATCTGATCAAGAGACAGGATAAGGAGGTACAGATTGGAGACCTACCTGTGACGGAAGATCACTTCG
Cm-DarB-R	CTCTCTGTTATGTATGCCTTTTTTTCTGATTTCTATATCCATAATTAATCAATCCGAGACCGCACACGGTCACACTGCTTC
Cm-DarC-F	CTACCTATTTGGTGAATTATAGAAAATTATCCGCCACTAAATTTTTGTGAGGAGACCTACCTGTGACGGAAGATCACTTCG
Cm-DarC-R	TTTATATGATTTACAGATATTCATCATGCTAATCATTTTATTCAATCCTTTCACCGAGACCGCACACGGTCACACTGCTTC
Cm-DarD-F	GCTTTGGTAAGAATAAATTAGTTAATAATGATACAGTAAGGATTGAATAAGGAGACCTACCTGTGACGGAAGATCACTTCG
Cm-DarD-R	TATGGGGATTATTGTGTCCATAAAGAACTCCTTTATTATGTTATTTATGCTTATCGAGACCGCACACGGTCACACTGCTTC
Cm-DarE-F	CGTTTTCTGACAGAATATTAACGATGAGGGATGGCCACTTGCTTGTTTGAGGAGACCTACCTGTGACGGAAGATCACTTCG
Cm-DarE-R	CGGTTCCGGGCCCTTGCAGGGTGGTTAATTAATCAGGAACTAGTTAGAATTCAACGAGACCGCACACGGTCACACTGCTTC
Cm-DarF-F	GTGGAACCGGCGGTTTGTTGGAGACAATAAAACAAACCATCGCGGCGTAAGGAGACCTACCTGTGACGGAAGATCACTTCG
Cm-DarF-R	TGATAAACGATGCCTTGTGCACTGATCTGCATGTTTTAAATCGACTCTTCTTACCGAGACCGCACACGGTCACACTGCTTC
Cm-DarG-F	ATGACATCATAAACACAAAACTCATAGAAACATTAGAGCGCTTAAAATAAGGAGACCTACCTGTGACGGAAGATCACTTCG
Cm-DarG-R	CCCGGAACCTTGCGGTTCCGGGCCCTTGCAGGGTGGTTAATTAATAGAATTTATCGAGACCGCACACGGTCACACTGCTTC

Suppl. Table 5. Summary of PCRs performed in seamless gene deletion experiments.

PCR product	Template DNA	Forward primer	Reverse primer
cmR (*darB*)	pMYC20	Cm-DarB-F	Cm-DarB-R
cmR (*darC*)	pMYC20	Cm-DarC-F	Cm-DarC-R
cmR (*darD*)	pMYC20	Cm-DarD-F	Cm-DarD-R
cmR (*darE*)	pMYC20	Cm-DarE-F	Cm-DarE-R
cmR (*darF*)	pMYC20	Cm-DarF-F	Cm-DarF-R
cmR (*darG*)	pMYC20	Cm-DarG-F	Cm-DarG-R

For Red/ET recombineering, 1.4 mL LB medium was inoculated with *E. coli* GB05-red and grown at 37 °C to OD_{600} 0.2. After addition of 40 µL 10 % (w/v) L-arabinose, the cultivation was continued until OD_{600} 0.4 was reached. The cells were harvested, washed twice in ice-cold ddH_2O and finally re-suspended in 30 µL of ddH_2O. The *cat* PCR product was transformed into *E. coli* GB05-red pNOSO-darABCDE or *E. coli* GB05-red pNOSO-darABCDEFG via electroporation as described above. Plasmid DNA from the fully overgrown LB agar selection plate (kanamycin and chloramphenicol) was isolated using alkaline lysis, followed by another transformation step of 100 ng of the isolated plasmid mixture into *E. coli* NEB10β. Again, we selected clones harbouring the correct recombination products on kanamycin and chloramphenicol. After the plasmid isolation, we verified the clones by restriction analysis. Next, the recombination product was hydrolysed with *Bsa*I and re-ligated to remove *cat* from the construct, leading to a clean deletion without leftover R-sites. Clones which lost their resistance towards chloramphenicol were selected for plasmid isolation and restriction analysis. Suppl. Table 6 lists all gene deletion plasmids that were generated in this work.

Suppl. Table 6. Constructs generated after Red/ET recombineering and removal of cat (cmR) by restriction hydrolysis with *Bsa*I.

Product generated	Description	Vector used for Red/ET	Red/ET product
pNOSO-darACDE	Deletion of *darB*	pNOSO-darABCDE	pNOSO-darACDE-cmR
pNOSO-darABDE	Deletion of *darC*	pNOSO-darABCDE	pNOSO-darABDE-cmR
pNOSO-darABCE	Deletion of *darD*	pNOSO-darABCDE	pNOSO-darABCE-cmR
pNOSO-darABCD	Deletion of *darE*	pNOSO-darABCDE	pNOSO-darABCD-cmR
pNOSO-darABCDEG	Deletion of *darF*	pNOSO-darABCDEFG	pNOSO-darABCDEG-cmR
pNOSO-darABCDEF	Deletion of *darG*	pNOSO-darABCDEFG	pNOSO-darABCDEF-cmR

Cultivation of strains to screen for production of darobactins

E. coli HS996, NEB10β and GB05-red strains were used for cloning and manipulation of the modified BGC. Cultivation of cloning strains was exclusively performed in LB medium (10 g/L tryptone, 5 g/L NaCl, 5 g/L yeast extract, pH 7.6) at 30 °C. *E. coli* BL21 (DE3) was used as heterologous expression host. All small scale fermentations to screen for the production of darobactins were performed in 50 mL scale in unbaffled 300 mL shaking flasks at 30 °C for 3 days and 180 rpm on an orbital shaker (Orbitron/Multitron, Infors HT) using FM cultivation medium (12.54 g/L K_2HPO_4, 2.31 g/L KH_2PO_4, 5 g/L NaCl, 12 g/L yeast extract, 4 g/L D(+) glucose, 1 g/L NH_4Cl, 0.24 g/L $MgSO_4$, pH 7.6) supplemented with 1 mg/L vitamin B_{12} after sterilization. Production screening cultures were inoculated with 5 mL of a 25 mL LB seed culture that grew for 16 h at 30 °C and 180 rpm. Ampicillin (100 µg/mL; pUC57- and pSynbio1-based expression constructs), chloramphenicol (34 µg/mL; Red/ET deletion constructs prior *cat* removal) and kanamycin (50 µg/mL; pNOSO-based expression constructs) were used as selection markers.

The initial evaluation of different media, *E. coli* strains and expression constructs is described in the respective section below. Cultivation of strains for purification of darobactins A and 9 and DarF, as well as cultivation of strains used for determination of the MICs are described in the respective sections below.

UHPLC-HRMS analysis of production screening cultures

The fermentation broth of 50 mL screening cultures was centrifuged at 7,750 × g for 15 min at 4 °C. The supernatant was directly analysed using uHPLC-HRMS. An UltiMate 3000 LC System (Dionex, Sunnyvale, California (US)) with a Acquity UPLC BEH C-18 column (1.7 µm, 100 x 2 mm; Waters Corporation, Milford, Massachusetts (US)), equipped with a VanGuard BEH C-18 (1.7 µm; Waters Corp.) guard column, was coupled to an Apollo II ESI source (Bruker Daltonics; Billerica, Massachusetts (US)) and hyphenated to maXis 4G ToF mass spectrometer (Bruker Daltonics). Separation was performed at a flow rate of 0.6 mL/min (eluent A: deionised H_2O + 0.1 % formic acid (FA), eluent B:

acetonitrile + 0.1 % FA) at 45 °C using the following gradient: 5 % B for 30 s, followed by a linear gradient up to 95 % B in 18 min and a constant percentage of 95 % B for further 2 min. Original conditions were adjusted with 5 % B within 30 s and kept constant for 1.5 min. The LC flow was split to 75 µL/min before entering the mass spectrometer. Mass spectra were acquired in centroid mode ranging from 150–2,500 m/z at a 2 Hz full scan rate. Mass spectrometry source parameters were set to 500 V as end plate offset, 4000 V as capillary voltage, 1 bar nebulizer gas pressure, 5 L/min dry gas flow and 200 °C dry temperature. For MS^2 experiments, CID (collision-induced dissociation) energy was ramped from 35 eV for 500 m/z to 45 eV for 1,000 m/z. MS full scan acquisition rate was set to 2 Hz and MS^2 spectra acquisition rates were ramped from 1 to 4 Hz for precursor ion intensities of 10 kcts to 1,000 kcts.

Initial evaluation of different heterologous expression constructs, strains and cultivation conditions

Initially we evaluated different *E. coli* expression strains, cultivation media and expression constructs to reach a darobactin A production titre sufficient for compound purification. All cultivations were performed in 50 mL scale in unbaffled 300 mL shaking flasks at 30 °C for 3 days and 180 rpm on an orbital shaker as described in the Cultivation of strains section. *E. coli* BL21 (DE3), *E. coli* Lemo21 (DE3) and *E. coli* Rosetta2 (DE3) were evaluated as expression strains. LB medium (described above), 2TY medium (16 g/L tryptone, 5 g/L NaCl, 10 g/L yeast extract, pH 7.0), SB medium (32 g/L peptone, 5 g/L NaCl, 20 g/L yeast extract, pH 7.0), M medium (10 g/L tryptone, 10 g/L NaCl, 5 g/L yeast extract, 10 g/L KH_2PO_4, pH 6.5), TB medium (10 g/L tryptone, 4 g/L glycerol, 20 g/L yeast extract, 10 g/L, 50 mM KH_2PO_4 (pH 8.0), pH 7.2), TSB medium (17 g/L peptone from casein, 3 g/L peptone from soymeal, 2.5 g/L D(+) glucose, 5 g/L NaCl, 2.5 g/L K_2HPO_4, pH 7.3), SB2-2Y medium (SB medium with 40 g/L yeast extract), FM medium (described above) and FM-2Y medium (FM medium with 24 g/L yeast extract) were evaluated as cultivation media. Each medium was supplemented with 1 mg/L vitamin B_{12} after sterilization and the gene expression of *darA* and the T7 RNA polymerase was induced by addition of 0.1 mM isopropyl ß-D-1-thiogalactopyranoside (IPTG) after an OD_{600} 0.7 was reached. Furthermore, we compared the darobactin A production upon expression of the high-copy plasmids pUC57-relEdarABCDE and pSynbio1-relEdarABCDE, as well as the low-copy plasmid pNOSO-relEdarABCDE in *E. coli* BL21 (DE3). Since we observed more impurities in the base peak chromatograms (BPC) after expression of the high-copy plasmids (Suppl. Figure 3) and the highest relative darobactin A production (based on the mass peak intensity) in *E. coli* BL21 (DE3) pNOSO-relEdarABCDE, we used this strain cultivated in FM medium as basis for all following experiments.

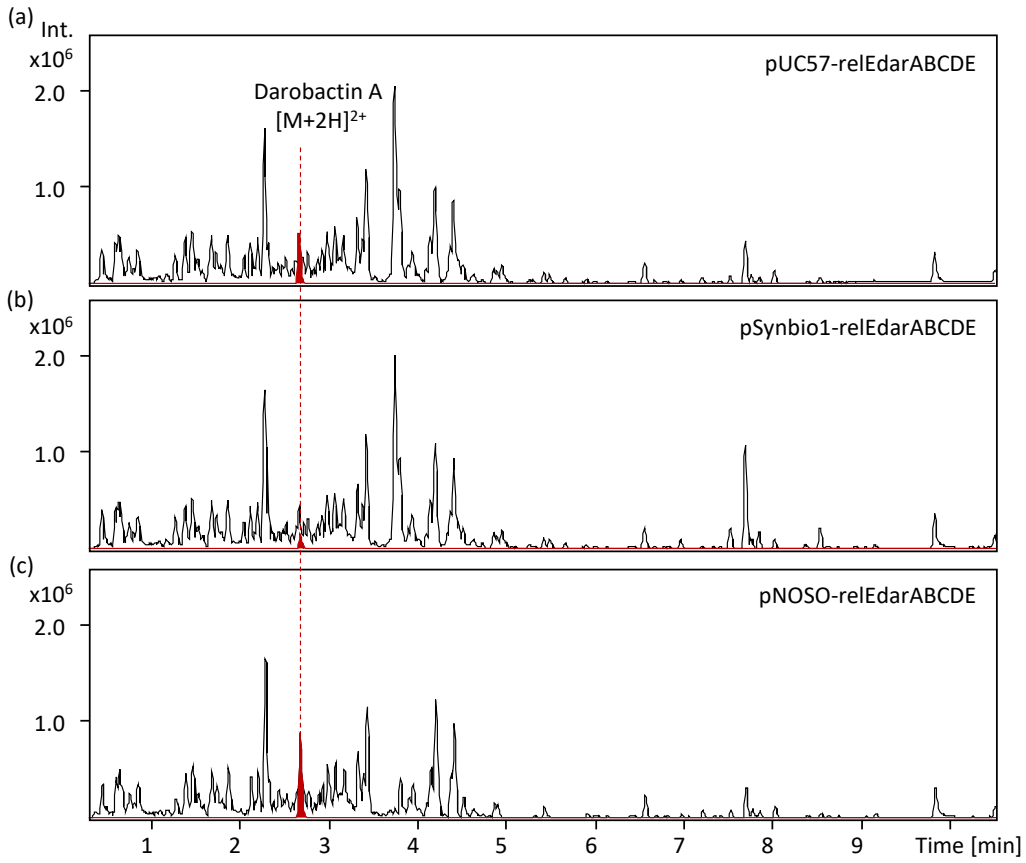

Suppl. Figure 3. Chromatogram of the *E. coli* BL21 (DE3) pUC57-relEdarABCDE (a), *E. coli* BL21 (DE3) pSynbio1-relEdarABCDE (b) and *E. coli* BL21 (DE3) pNOSO-relEdarABCDE culture supernatant. The red trace displays the darobactin A EIC for the $[M+2H]^{2+}$ species at m/z 483.710 ±0.02 Da. The black trace displays the BPC of the fermentation supernatant.

Induction and repression of T7 RNA polymerase expression and T7lac promoter-regulated darA gene expression

Since we observed higher darobactin A production (based on peak intensity in the MS) after not inducing the *darA* and T7 RNA polymerase gene expression compared to induction with 0.1 mM IPTG (data not shown), we tested how different inducer concentrations (10 nM, 1 nM, 0.1 nM IPTG) or repressor concentrations (0.5 %, 1.5 %, 5 % D(+) glucose) during cultivation of *E. coli* BL21 (DE3) pNOSO-darABCDE in FM medium affect the production level of darobactin A. uHPLC-HRMS analysis of the culture supernatant and determination of the darobactin A peak surface area (described in section Determination of the MS peak area under curve (AUC) ratio) revealed that the tested IPTG concentrations had no significant impact on the darobactin A production level (Suppl. Table 7). The supplementation of 1.5 % and 5 % D(+) glucose) resulted in a ten-fold reduction of the darobactin A production titre.

Suppl. Table 7. Influence of different IPTG and D(+) glucose concentrations on the darobactin A production level after cultivation of *E. coli* BL21 (DE3) pNOSO-darABCDE in FM medium. In the control no IPTG and D(+) glucose were supplemented during cultivation. AUC: area under curve.

IPTG/ D(+) glucose conc.	AUC relative to control [%]
Control	100
10 nM IPTG	101
1 nM IPTG	92
0.1 nM IPTG	95
0.5 % D(+) glucose	106
1.5 % D(+) glucose	11
5 % D(+) glucose	10

UHPLC-HRMS chromatograms displaying all observed darobactin derivatives

This section displays extracted ion chromatogram (EIC) traces displaying the most abundant $[M+2H]^{2+}$ ion for all observed darobactin derivatives. The EIC traces are depicted in red, the corresponding BPCs are depicted in black. All UuHPLC-HRMS EIC chromatograms were also traced in the *E. coli* BL21 (DE3) blank extract to double check for the absence of the corresponding peak in the blank. In case of darobactins 6, 8 and 18, the masses of the respective expected darobactins (without the adducts) shown in the chromatograms and main text Table 1 have not been detected.

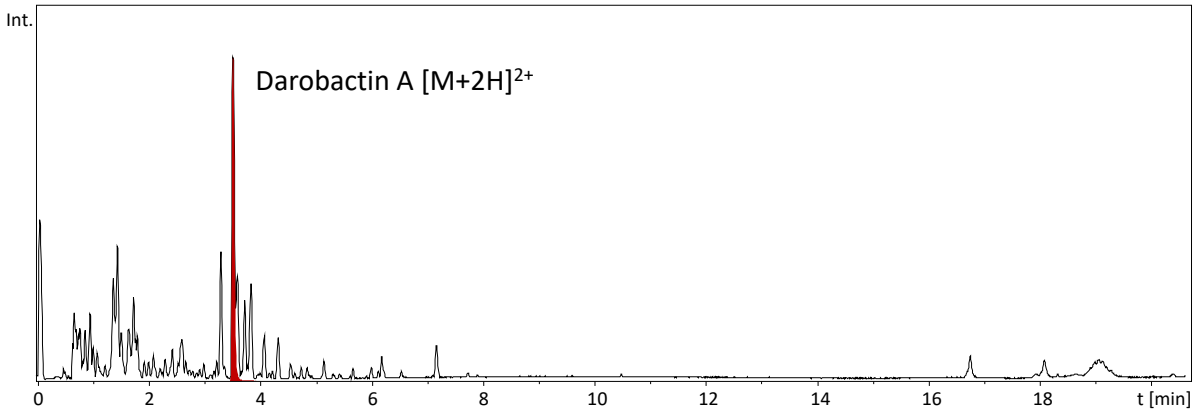

Suppl. Figure 4. Chromatogram of the *E. coli* BL21 (DE3) pNOSO-darABCDE culture supernatant. The red trace displays the darobactin A EIC for the $[M+2H]^{2+}$ species at m/z 483.710 ±0.02 Da. The black trace displays the BPC of the fermentation supernatant.

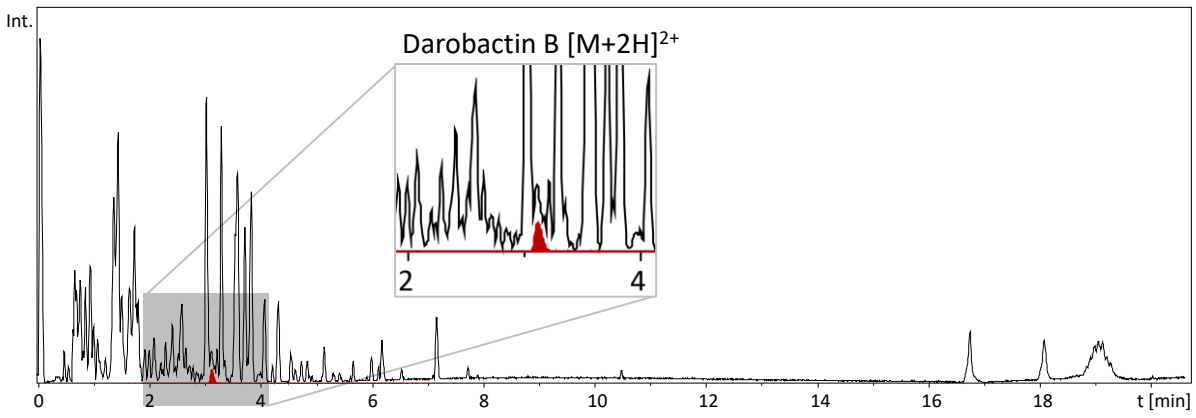

Suppl. Figure 5. Chromatogram of the *E. coli* BL21 (DE3) pNOSO-darABCDE-B culture supernatant. The red trace displays the darobactin B EIC for the $[M+2H]^{2+}$ species at m/z 525.251 ±0.02 Da. The black trace displays the BPC of the fermentation supernatant. The grey area highlights the magnification area.

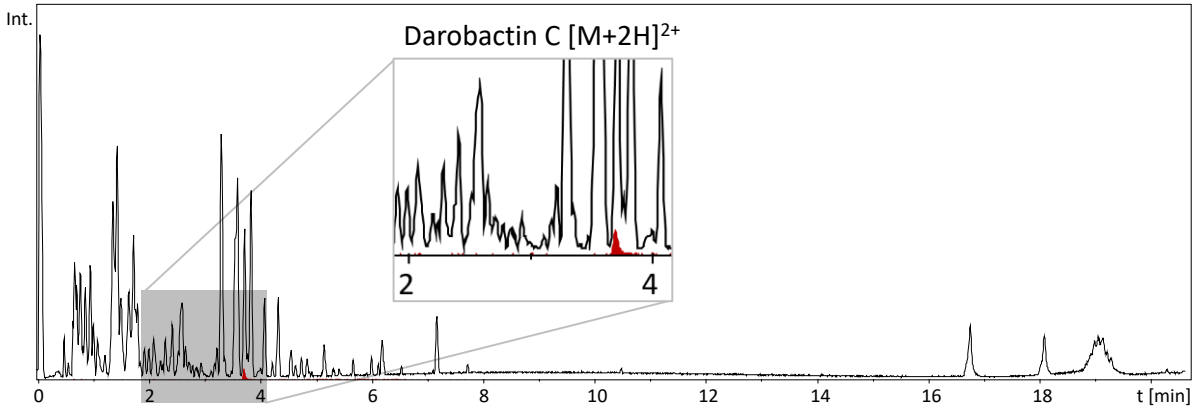

Suppl. Figure 6. Chromatogram of the *E. coli* BL21 (DE3) pNOSO-darABCDE-C culture supernatant. The red trace displays the darobactin C EIC for the $[M+2H]^{2+}$ species at m/z 484.207 ±0.02 Da. The black trace displays the BPC of the fermentation supernatant. The grey area highlights the magnification area.

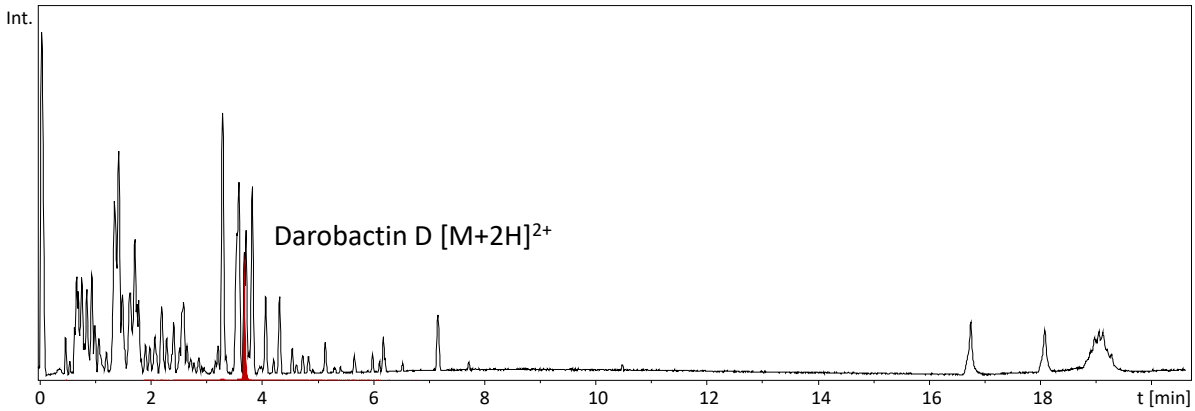

Suppl. Figure 7. Chromatogram of the *E. coli* BL21 (DE3) pNOSO-darABCDE-D culture supernatant. The red trace displays the darobactin D EIC for the $[M+2H]^{2+}$ species at m/z 491.712 ±0.02 Da. The black trace displays the BPC of the fermentation supernatant.

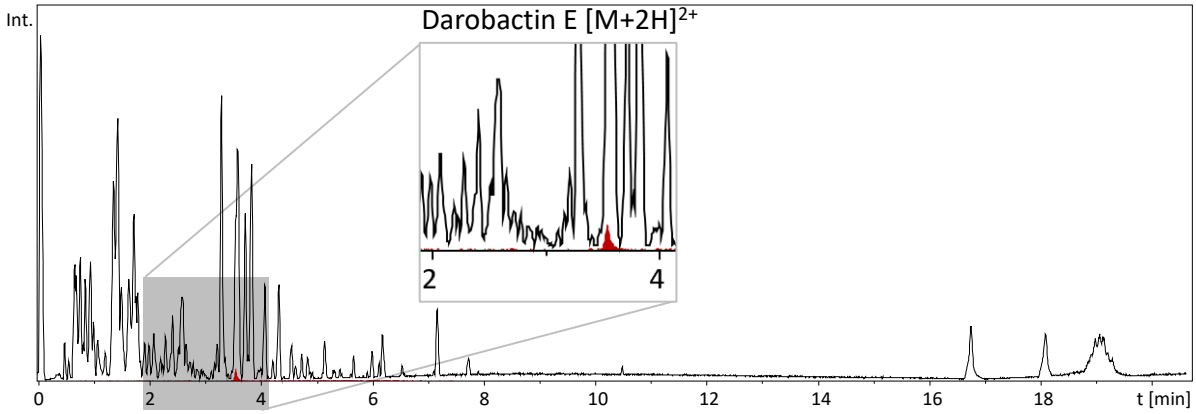

Suppl. Figure 8. Chromatogram of the *E. coli* BL21 (DE3) pNOSO-darABCDE-E culture supernatant. The red trace displays the darobactin E EIC for the $[M+2H]^{2+}$ species at m/z 470.204 ±0.02 Da. The black trace displays the BPC of the fermentation supernatant. The grey area highlights the magnification area.

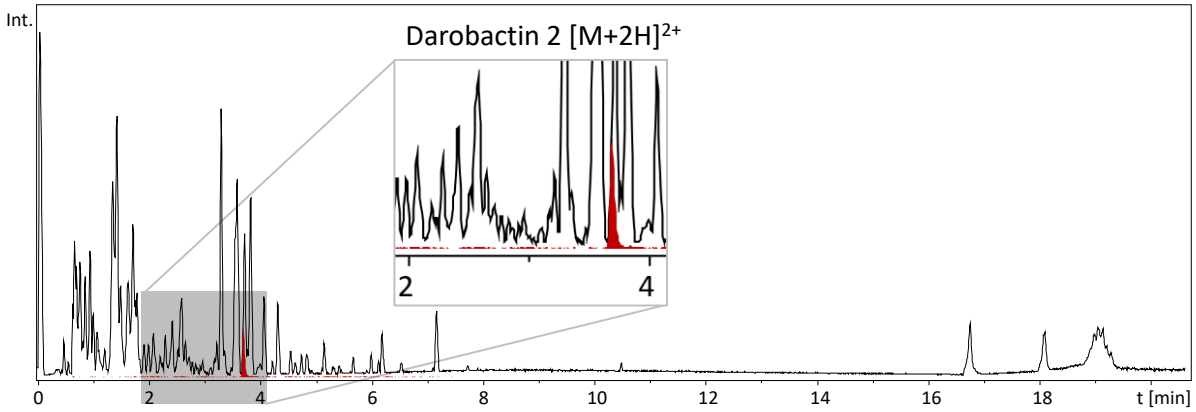

Suppl. Figure 9. Chromatogram of the *E. coli* BL21 (DE3) pNOSO-darABCDE-2 culture supernatant. The red trace displays the darobactin 2 EIC for the $[M+2H]^{2+}$ species at m/z 491.215 ±0.02 Da. The black trace displays the BPC of the fermentation supernatant. The grey area highlights the magnification area.

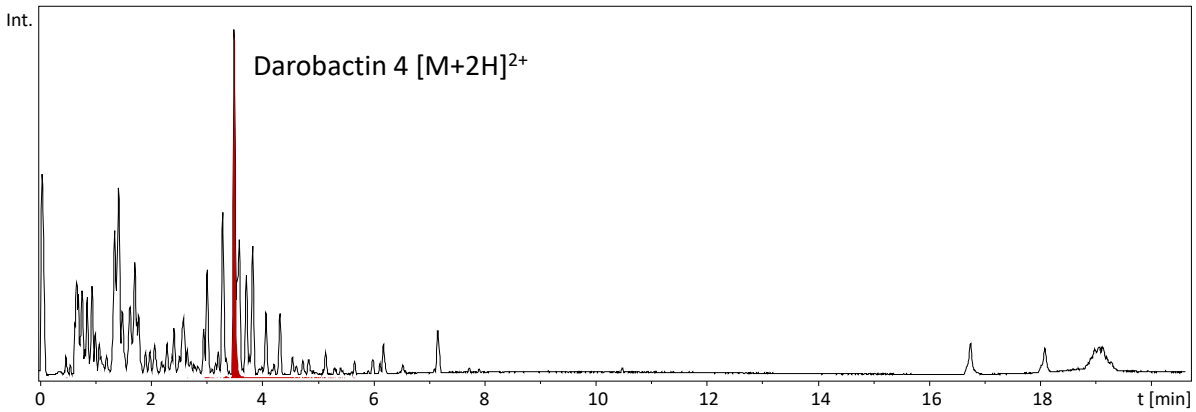

Suppl. Figure 10. Chromatogram of the *E. coli* BL21 (DE3) pNOSO-darABCDE-4 culture supernatant. The red trace displays the darobactin 4 EIC for the $[M+2H]^{2+}$ species at m/z 490.717 ±0.02 Da. The black trace displays the BPC of the fermentation supernatant.

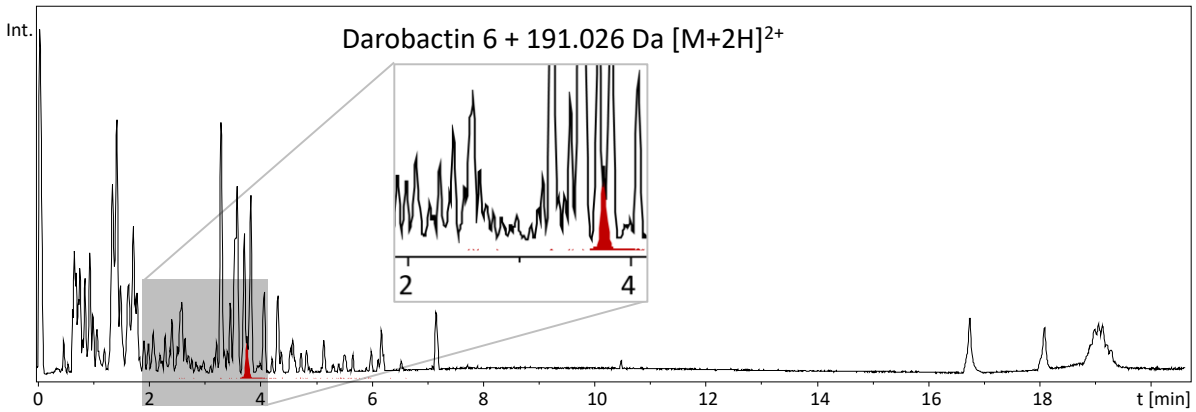

Suppl. Figure 11. Chromatogram of the *E. coli* BL21 (DE3) pNOSO-darABCDE-6 culture supernatant. The red trace displays the darobactin 6 + 191.026 EIC for the $[M+2H]^{2+}$ species at m/z 587.210 ±0.02 Da. The black trace displays the BPC of the fermentation supernatant. The grey area highlights the magnification area.

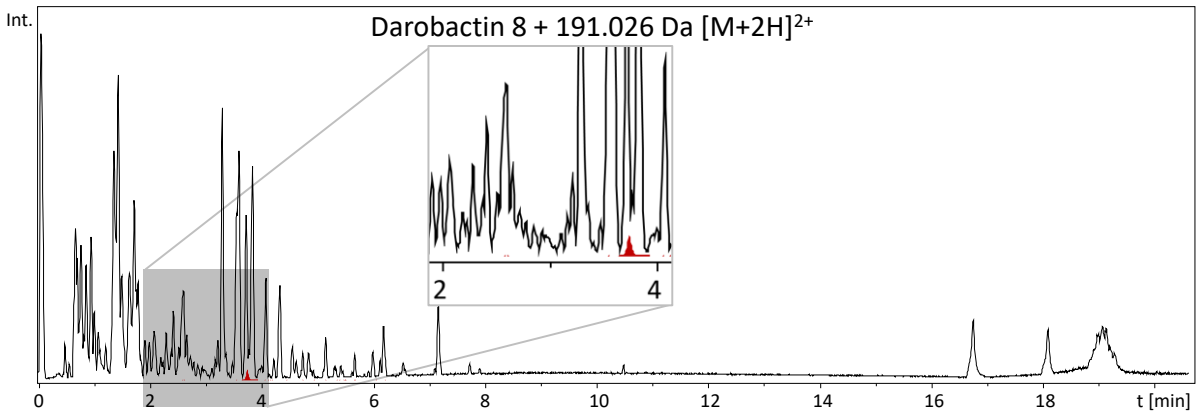

Suppl. Figure 12. Chromatogram of the *E. coli* BL21 (DE3) pNOSO-darABCDE-8 culture supernatant. The red trace displays the darobactin 8 + 191.026 EIC for the $[M+2H]^{2+}$ species at m/z 587.210 ±0.02 Da. The black trace displays the BPC of the fermentation supernatant. The grey area highlights the magnification area.

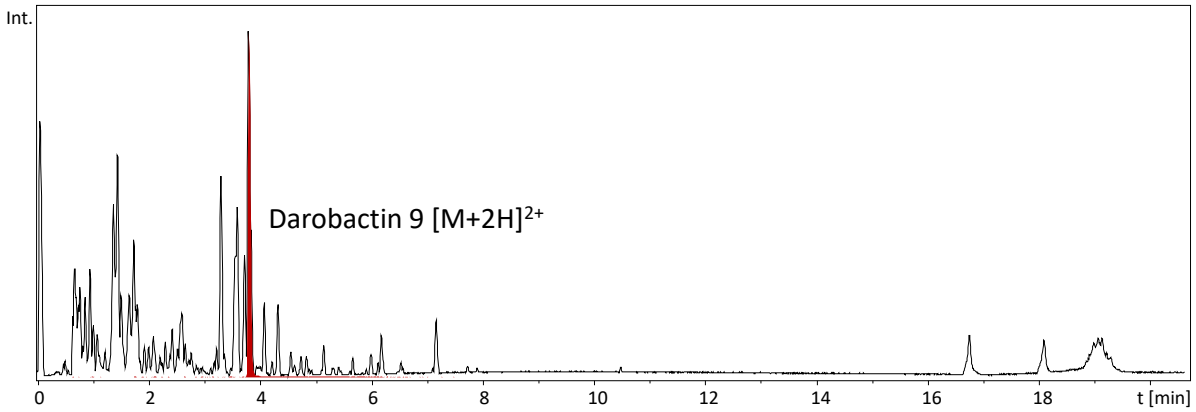

Suppl. Figure 13. Chromatogram of the *E. coli* BL21 (DE3) pNOSO-darABCDE-9 culture supernatant. The red trace displays the darobactin 9 EIC for the $[M+2H]^{2+}$ species at m/z 503.214 ±0.02 Da. The black trace displays the BPC of the fermentation supernatant.

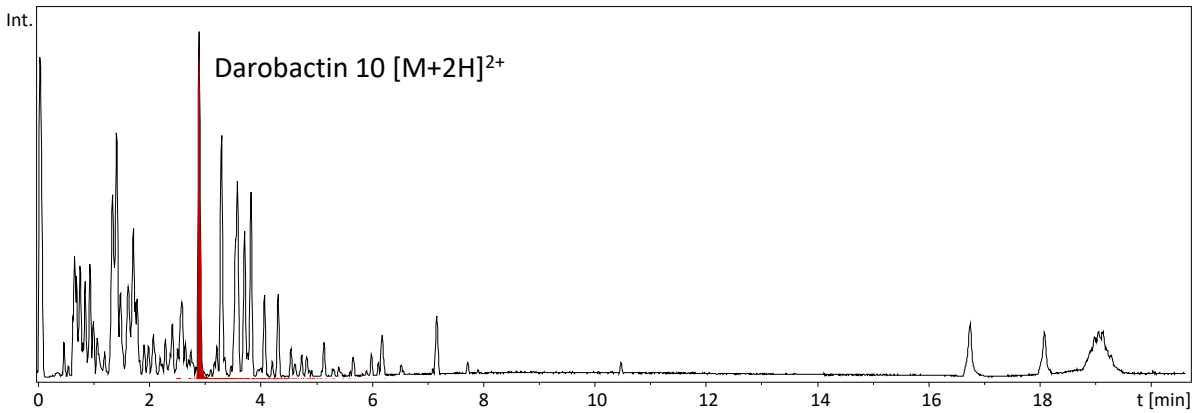

Suppl. Figure 14. Chromatogram of the *E. coli* BL21 (DE3) pNOSO-darABCDE-10 culture supernatant. The red trace displays the darobactin 10 EIC for the $[M+2H]^{2+}$ species at m/z 491.706 ±0.02 Da. The black trace displays the BPC of the fermentation supernatant.

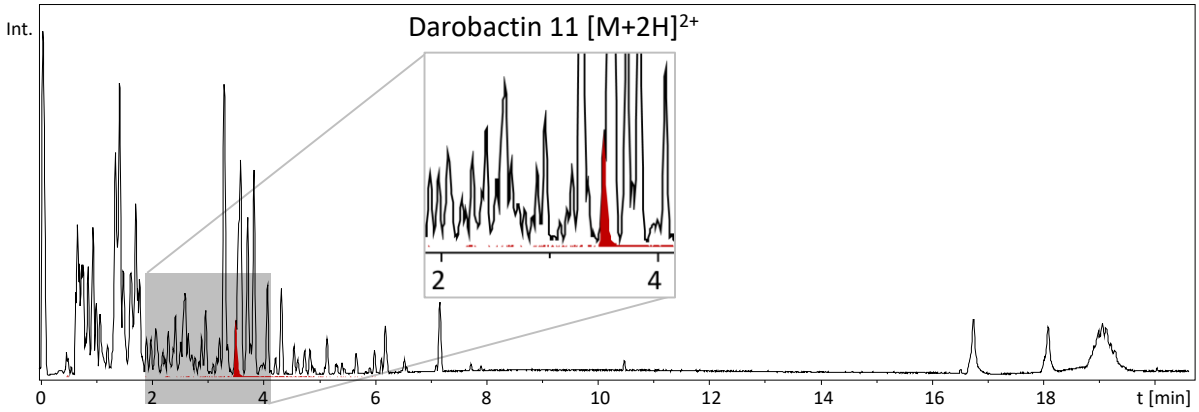

Suppl. Figure 15. Chromatogram of the *E. coli* BL21 (DE3) pNOSO-darABCDE-11 culture supernatant. The red trace displays the darobactin 11 EIC for the $[M+2H]^{2+}$ species at m/z 490.717 ±0.02 Da. The black trace displays the BPC of the fermentation supernatant. The grey area highlights the magnification area.

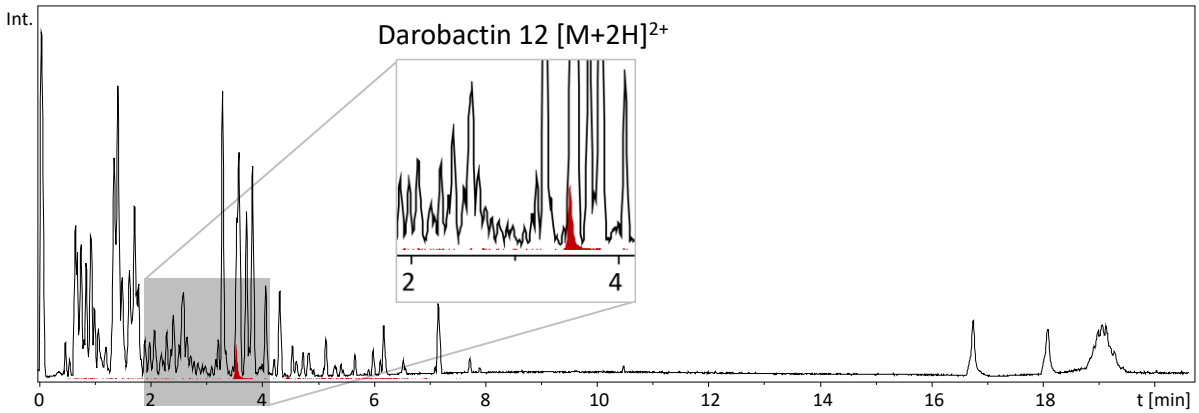

Suppl. Figure 16. Chromatogram of the *E. coli* BL21 (DE3) pNOSO-darABCDE-12 culture supernatant. The red trace displays the darobactin 12 EIC for the $[M+2H]^{2+}$ species at m/z 477.211 ±0.02 Da. The black trace displays the BPC of the fermentation supernatant. The grey area highlights the magnification area.

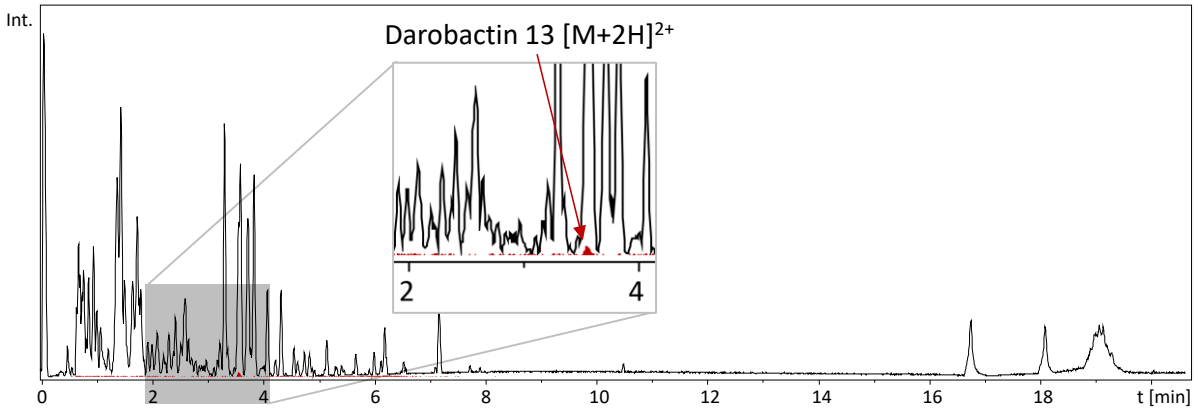

Suppl. Figure 17. Chromatogram of the *E. coli* BL21 (DE3) pNOSO-darABCDE-13 culture supernatant. The red trace displays the darobactin 13 EIC for the $[M+2H]^{2+}$ species at m/z 462.206 ±0.02 Da. The black trace displays the BPC of the fermentation supernatant. The grey area highlights the magnification area and the red arrow points towards the darobactin 13 EIC peak.

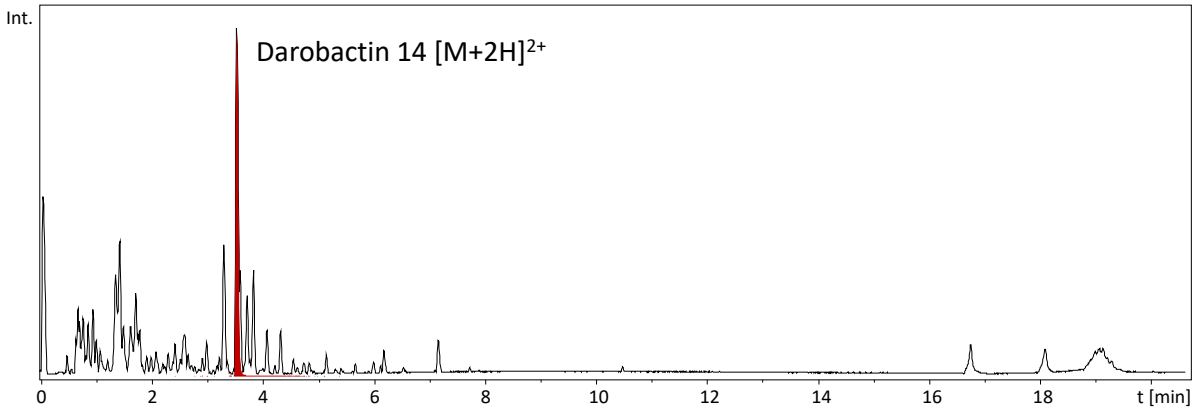

Suppl. Figure 18. Chromatogram of the *E. coli* BL21 (DE3) pNOSO-darABCDE-14 culture supernatant. The red trace displays the darobactin 14 EIC for the $[M+2H]^{2+}$ species at m/z 475.712 ±0.02 Da. The black trace displays the BPC of the fermentation supernatant.

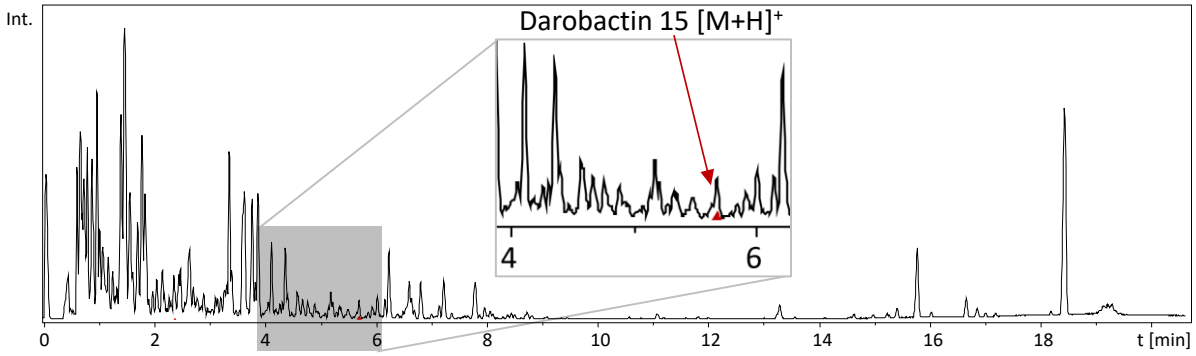

Suppl. Figure 19. Chromatogram of the *E. coli* BL21 (DE3) pNOSO-darABCDE-15 culture supernatant. The red trace displays the darobactin 15 EIC for the $[M+H]^{+}$ species at m/z 909.351 ±0.02 Da. The black trace displays the BPC of the fermentation supernatant. The grey area highlights the magnification area and the red arrow points towards the darobactin 15 EIC peak.

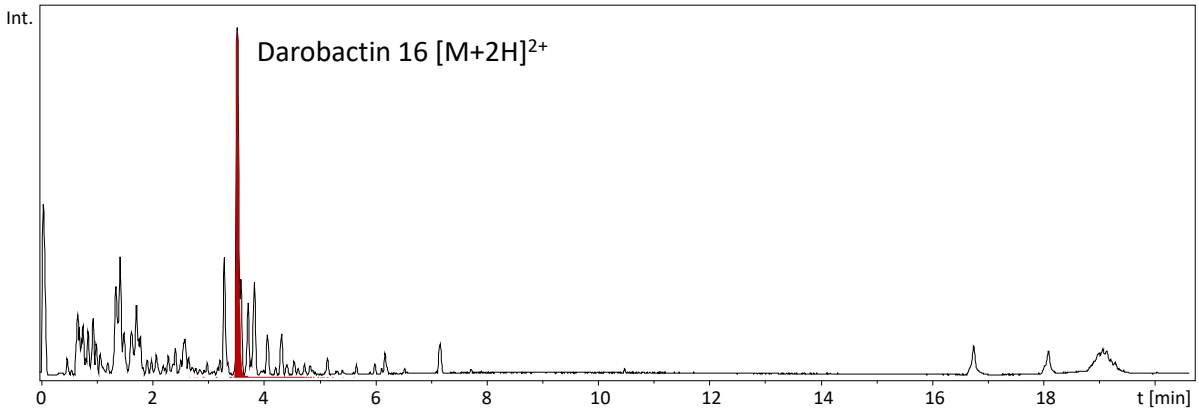

Suppl. Figure 20. Chromatogram of the *E. coli* BL21 (DE3) pNOSO-darABCDE-16 culture supernatant. The red trace displays the darobactin 16 EIC for the $[M+2H]^{2+}$ species at m/z 475.712 ±0.02 Da. The black trace displays the BPC of the fermentation supernatant.

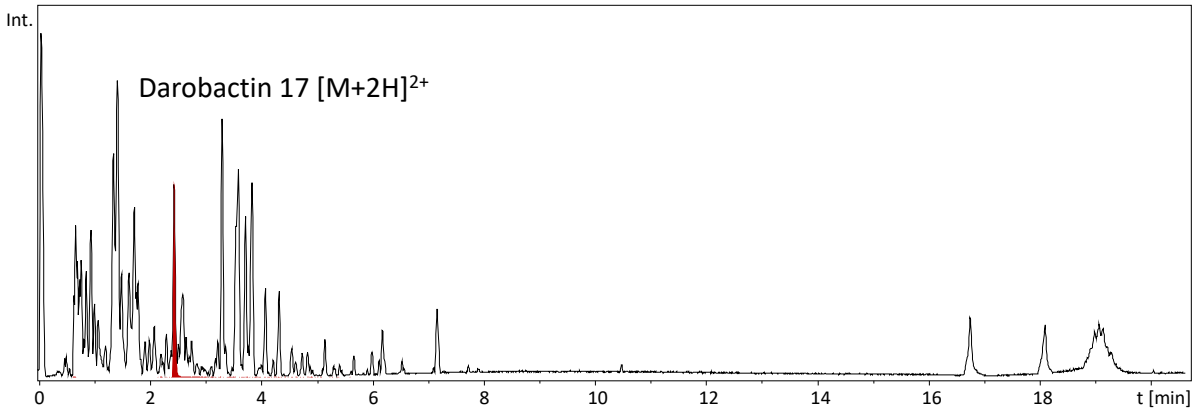

Suppl. Figure 21. Chromatogram of the *E. coli* BL21 (DE3) pNOSO-darABCDE-17 culture supernatant. The red trace displays the darobactin 17 EIC for the $[M+2H]^{2+}$ species at m/z 445.693 ±0.02 Da. The black trace displays the BPC of the fermentation supernatant.

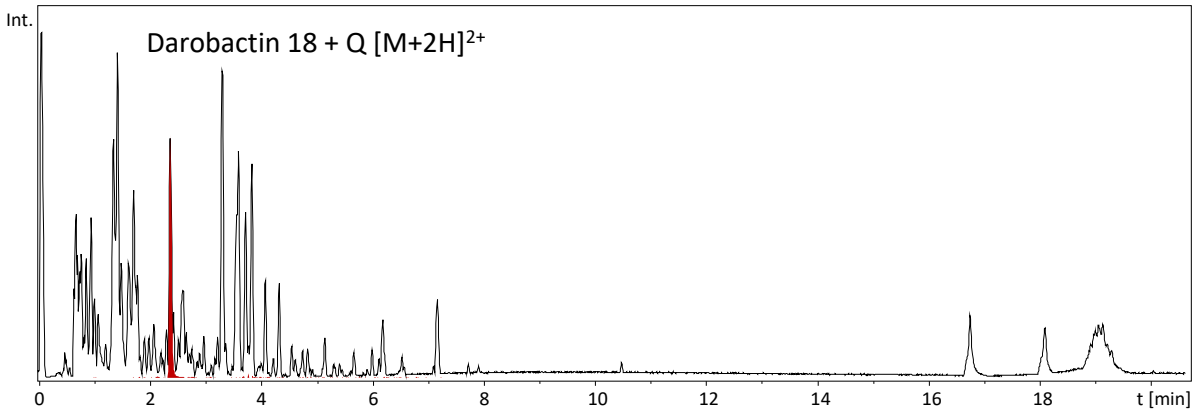

Suppl. Figure 22. Chromatogram of the *E. coli* BL21 (DE3) pNOSO-darABCDE-18 culture supernatant. The red trace displays the darobactin 18 + Q EIC for the $[M+2H]^{2+}$ species at m/z 474.204 ±0.02 Da. The black trace displays the BPC of the fermentation supernatant.

MS^2 spectral networking

All supporting GNPS clustering data to search for darobactins with unexpected precursor masses were created based on exported .mzML files from the uHPLC-$HRMS^2$ chromatograms using the parameters specified in the experimental section of the main text. The MS^2 chromatograms were exported containing all MS^2 data as an .mzML data file and uploaded to the GNPS server at University of California San Diego via FileZilla FTP upload to ftp:// ccms-ftp01.ucsd.edu and all acquired SPL MS^2 spectra are used for spectral network creation.[10] A molecular network was created using the online workflow at GNPS. The data were filtered by removing all MS^2 peaks within +/- 4 Da of the precursor m/z. MS^2 spectra were window filtered by choosing only the top six peaks in the +/- 50 Da window throughout the spectrum. The data were subsequently clustered with a parent mass tolerance of 0.05 Da and a MS^2 fragment ion tolerance of 0.1 Da to create consensus spectra. Further, no spectra were discarded based on consensus spectra calculation. Subsequently, a network was created, in which edges were filtered to have a cosine score above 0.65 and more than four matched peaks. Further

edges between two nodes were kept in the network if and only if each of the nodes appeared in each other's respective top 10 most similar nodes.[10] The dataset was downloaded from the server and subsequently visualised using Cytoscape 3.7.2. In the data set, we searched for MS² spectra that clustered to the MS² spectrum of darobactin A or other identified darobactins. Confirmation of the respective darobactin core structure was done by manual inspection of the MS² spectrum. Notably, the darobactins 6 and 8 that feature a mass shift of +191.026 and darobactin 18 that features an additional L-glutamine were uncovered using this spectral networking approach.

MS² spectra for every observed darobactin derivative for structure confirmation

In this section, we list all observed MS² spectra for the produced darobactin derivatives. Differences in intensity of the spectra that directly correlate to the number of visible fragment ions are due to the significant differences in the production titres observed among the darobactin derivatives. Darobactin MS² spectra always display a prominent, doubly charged $[M\text{-}H_2O+2H]^{2+}$ ion as well as characteristic 160.08 and 300.09 fragments used for identification. The only exception was observed for darobactin 15 displaying a singly charged $[M\text{-}H_2O+H]^{+}$ ion and only the characteristic 300.09 fragment ion.

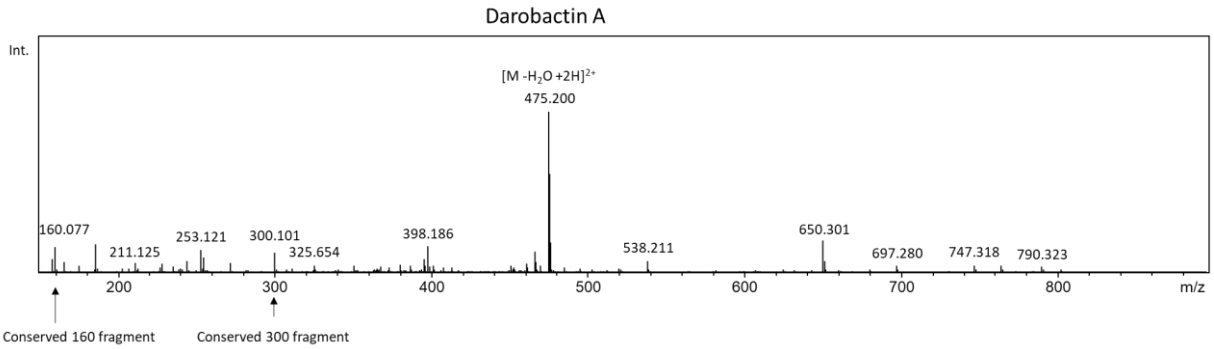

Suppl. Figure 23. MS² spectrum of darobactin A.

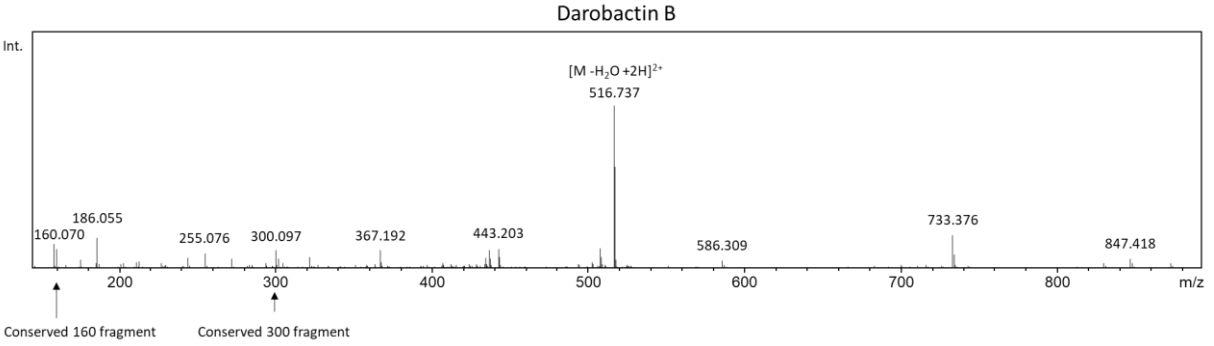

Suppl. Figure 24. MS² spectrum of darobactin B.

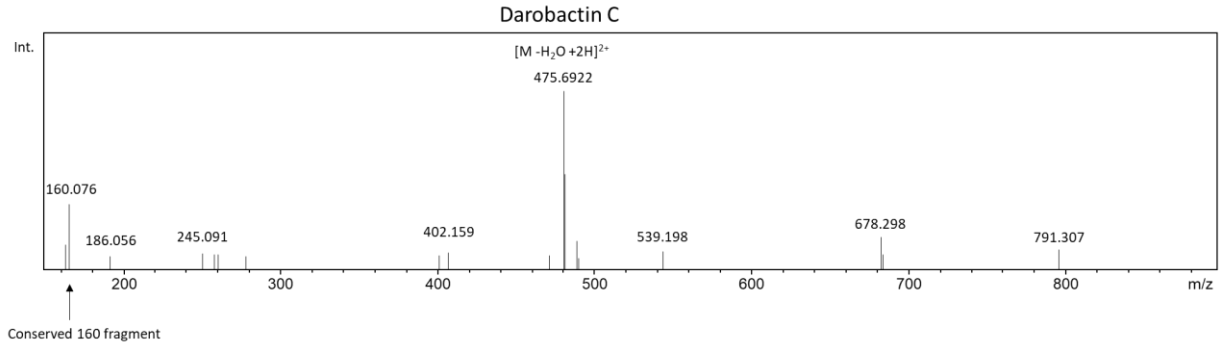

Suppl. Figure 25. MS² spectrum of darobactin C.

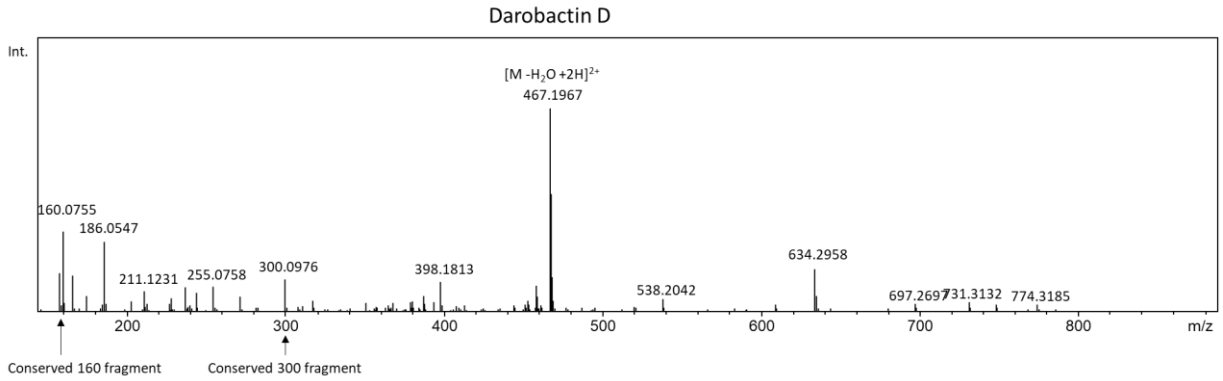

Suppl. Figure 26. MS² spectrum of darobactin D.

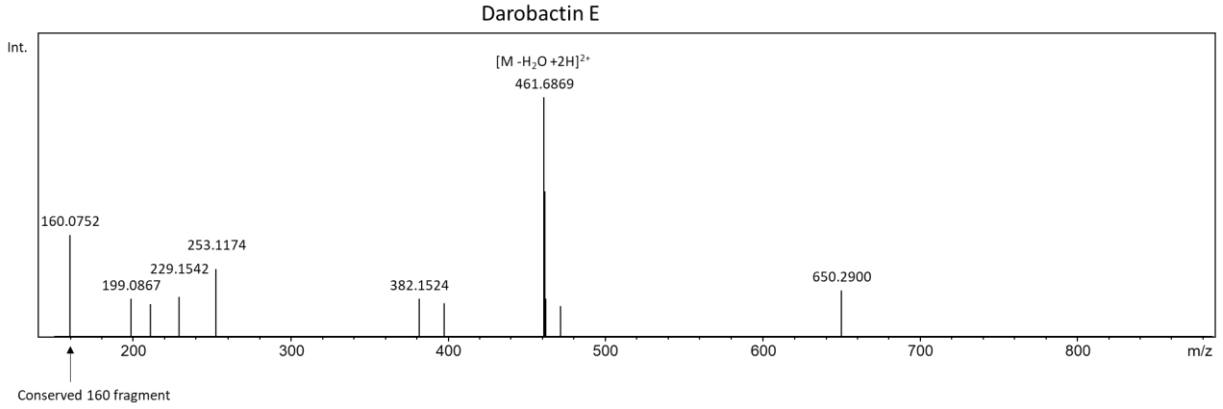

Suppl. Figure 27. MS² spectrum of darobactin E.

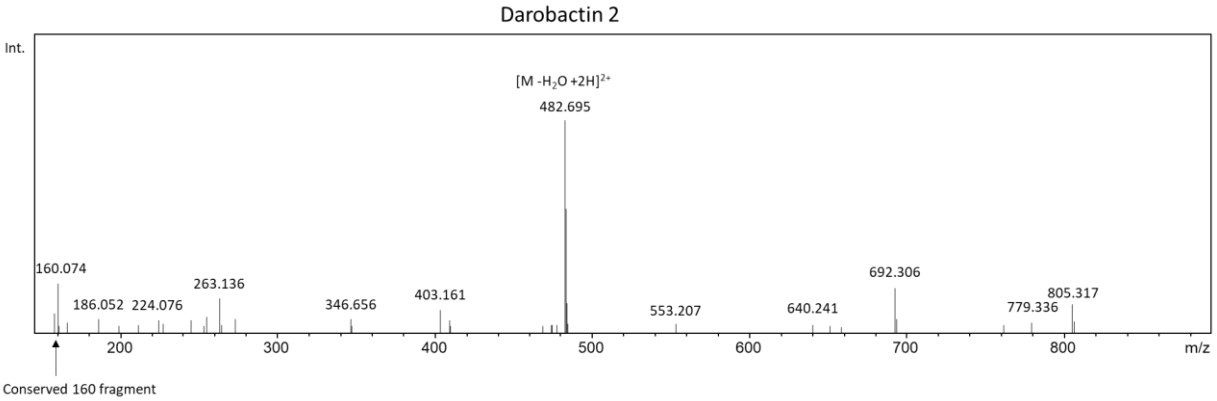

Suppl. Figure 28. MS² spectrum of darobactin 2.

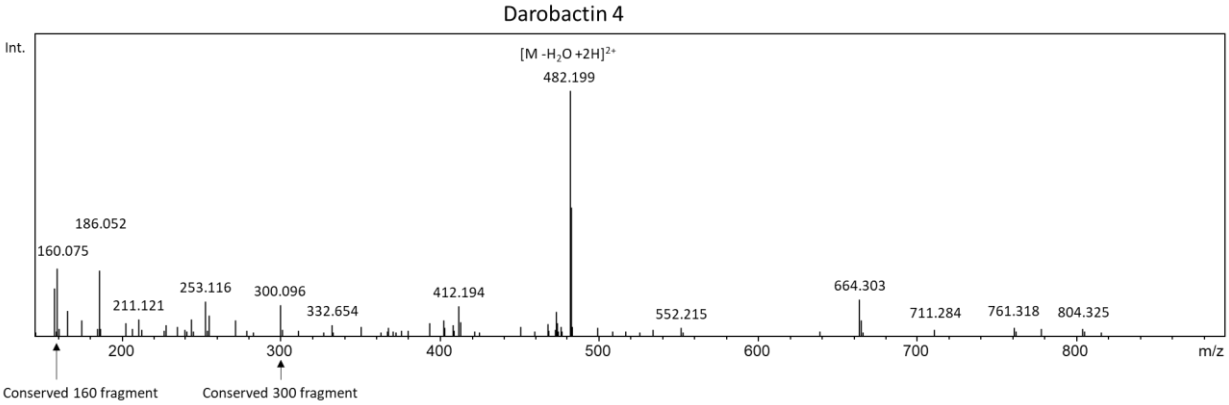

Suppl. Figure 29. MS² spectrum of darobactin 4.

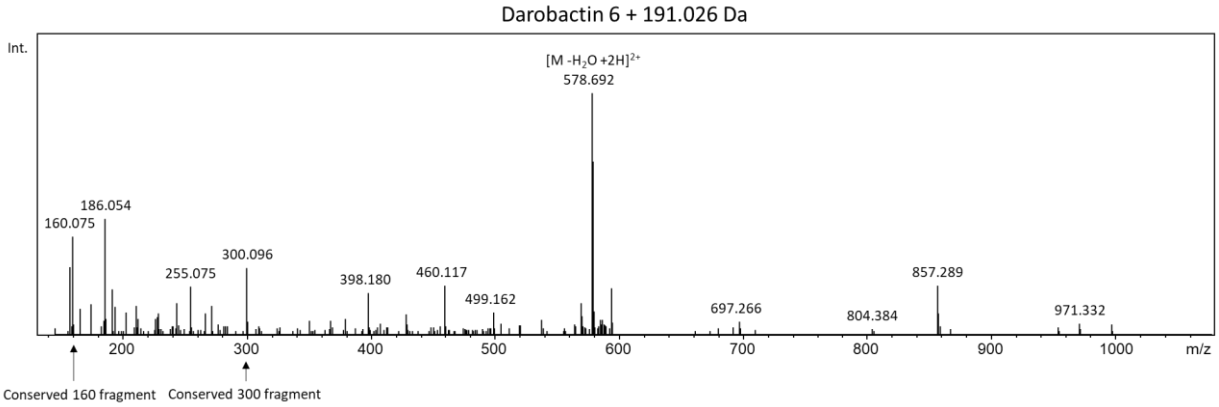

Suppl. Figure 30. MS² spectrum of darobactin 6 + the 191.026 Da adduct.

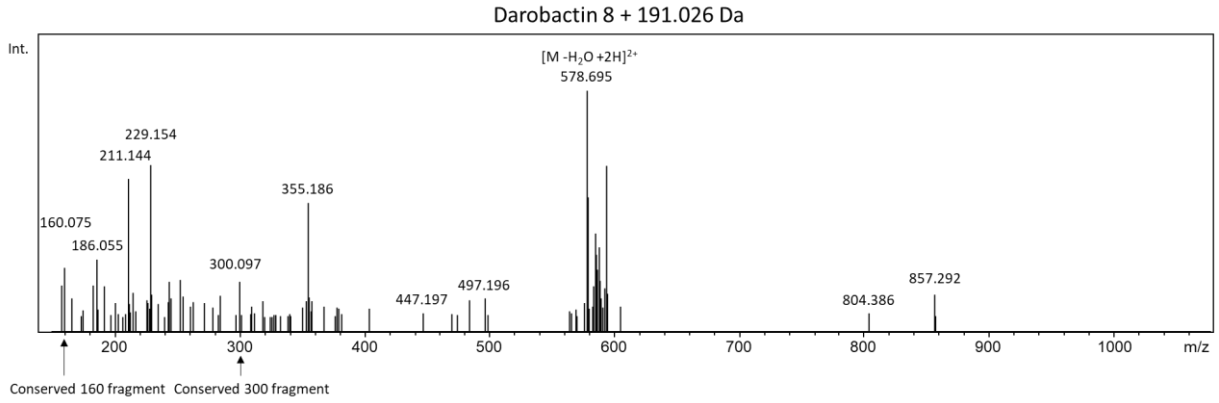

Suppl. Figure 31. MS² spectrum of darobactin 8 + the 191.026 Da adduct.

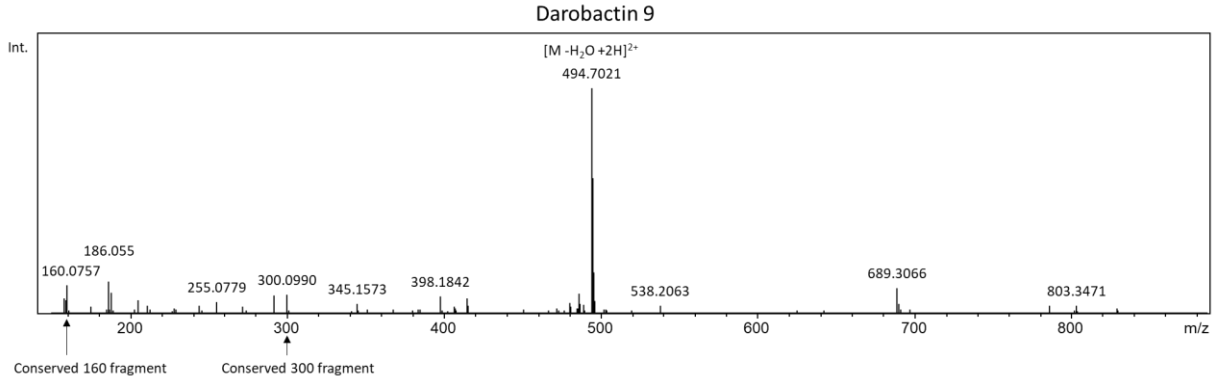

Suppl. Figure 32. MS² spectrum of darobactin 9.

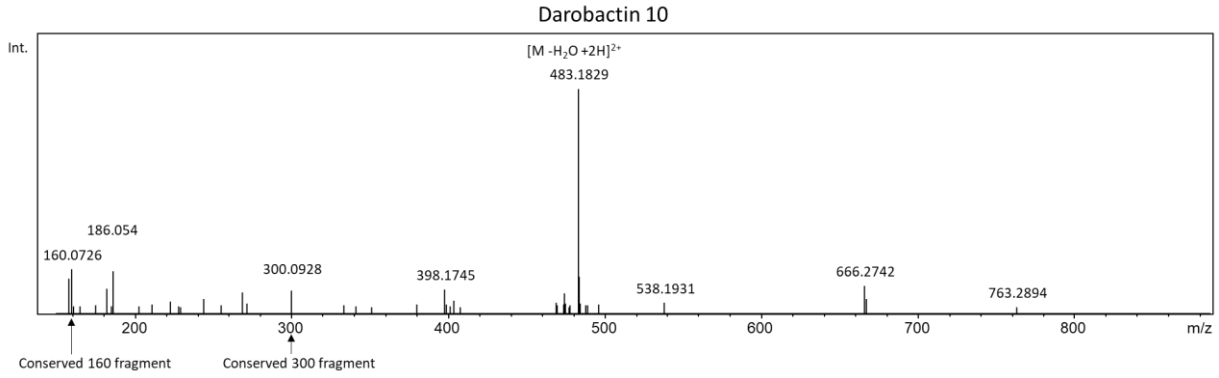

Suppl. Figure 33. MS² spectrum of darobactin 10.

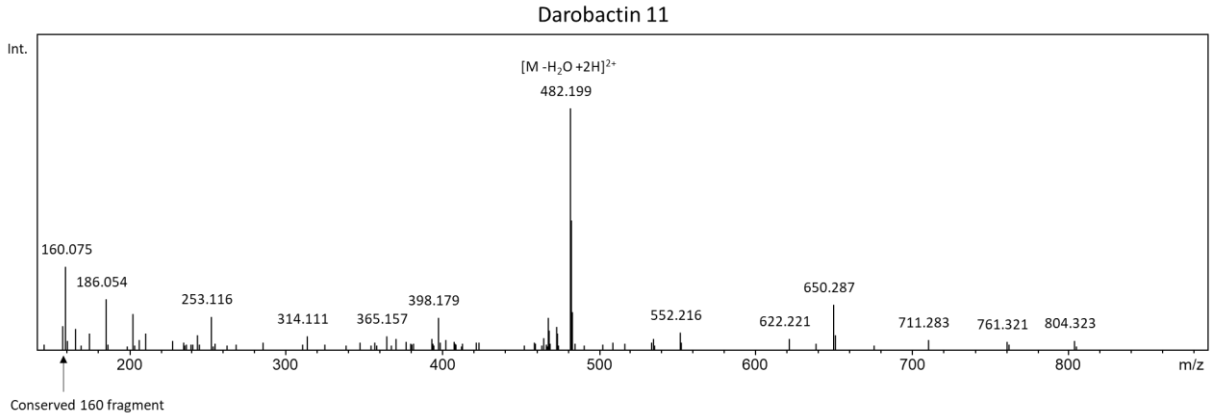

Suppl. Figure 34. MS² spectrum of darobactin 11.

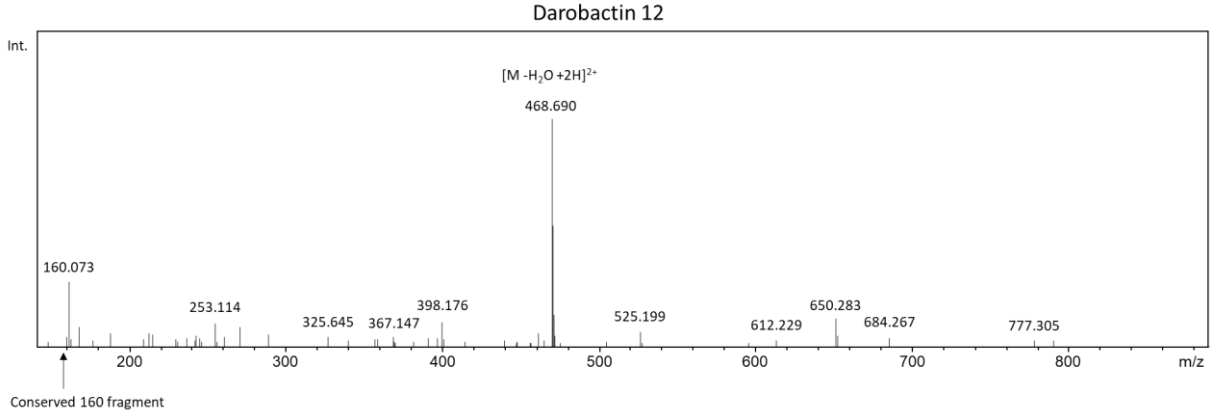

Suppl. Figure 35. MS² spectrum of darobactin 12.

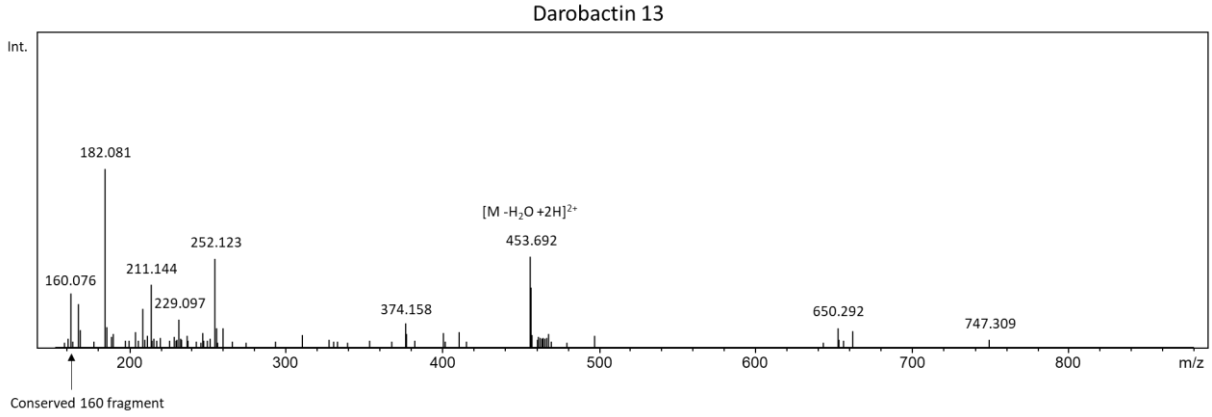

Suppl. Figure 36. MS² spectrum of darobactin 13.

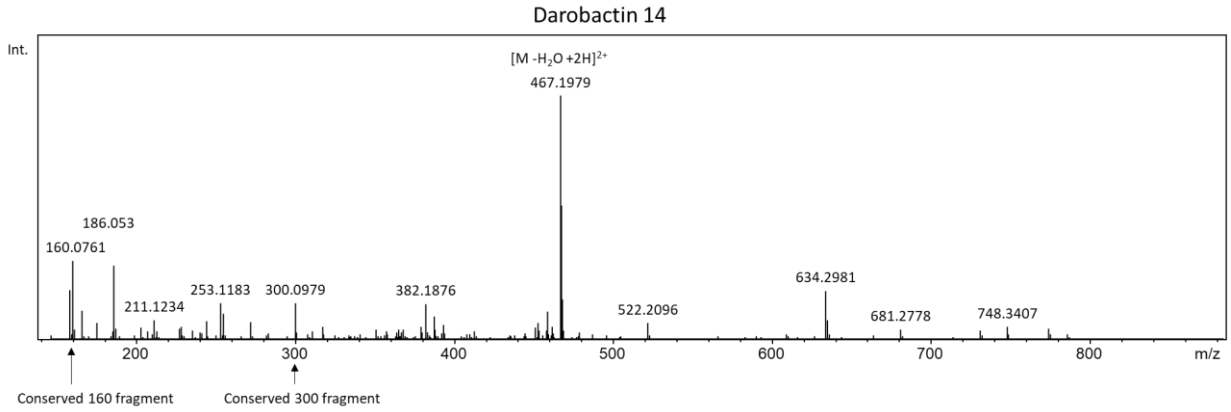

Suppl. Figure 37. MS² spectrum of darobactin 14.

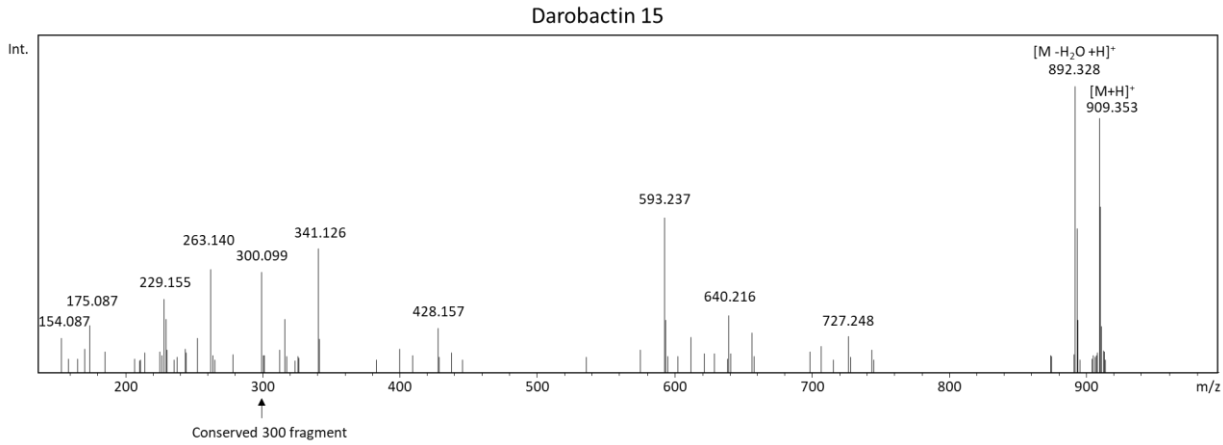

Suppl. Figure 38. MS² spectrum of darobactin 15.

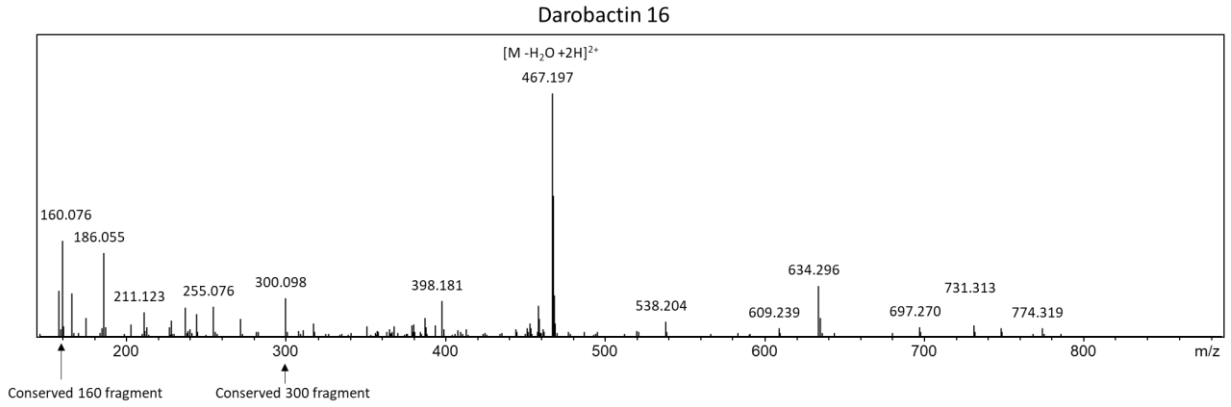

Suppl. Figure 39. MS² spectrum of darobactin 16.

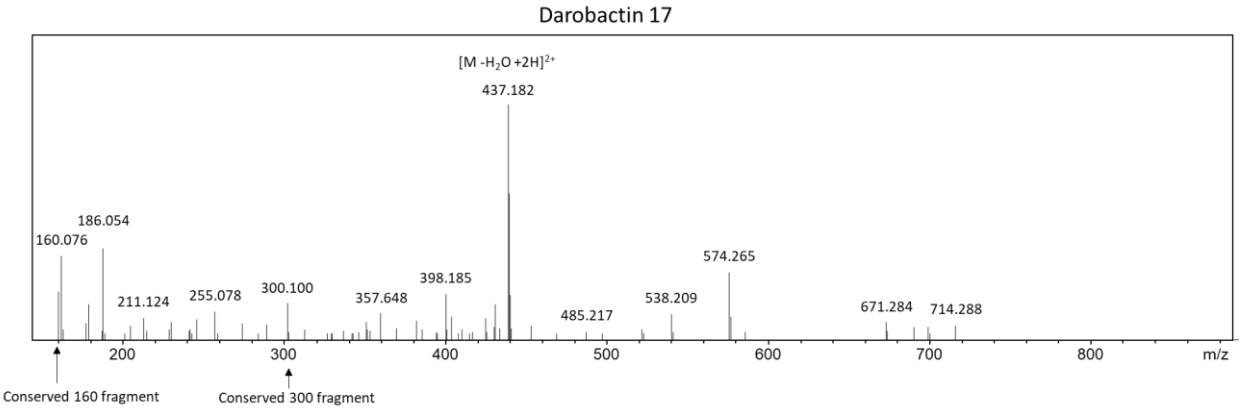

Suppl. Figure 40. MS² spectrum of darobactin 17.

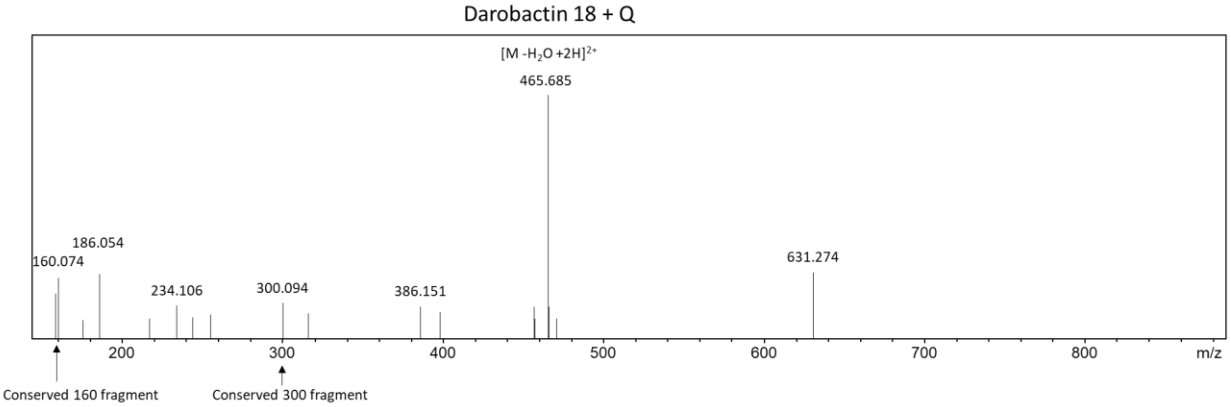

Suppl. Figure 41. MS² spectrum of darobactin 18 + L-glutamine from the follower peptide.

Evaluation of the relative minimal inhibitory concentration (MIC) of darobactin derivatives based on tested crude extracts

In order to determine the relative MIC of darobactin derivatives with respect to darobactin A, the supernatant of the fermentation broth from 50 mL screening cultures was collected after centrifugation at 7,750 x g for 10 min at 4 °C. Next, 10 % (v/v) XAD-16N resin was added with subsequent incubation for 2 h at room temperature and 180 rpm on an orbital shaker (Orbitron/Multitron, Infors HT). After passive sedimentation of the absorber resin, the supernatant was carefully decanted and the absorber resin was incubated in 80 % (v/v) MeOH/H_2O for 2 h at room temperature and shaking at 180 rpm. The crude extract was subsequently filtered using folded filter paper (8 – 12 µm pore size) and dried using a rotary evaporator. The dried extract was dissolved in 500 µL 50 % (v/v) MeOH in H_2O, resulting in a 100 x concentration factor, and was subsequently analysed using uHPLC-HRMS (described above) prior its use in MIC evaluation assay. For uHPLC-HRMS analysis, each extract was further diluted 1:5 in H_2O. The MS peak surface of each respective darobactin derivate was determined by automated peak integration using *Compass DataAnalysis* version 4.4 (Bruker Daltonics).

For MIC evaluation, 20 µL of the prepared extract were transferred into a well of the first row of a 96-well plate. After passive MeOH evaporation at room temperature, 70 µL Mueller-Hinton broth (MHB; 2 g/L beef infusion solids, 1.5 g/L starch, 17.5 g/L casein hydrolysates, final pH 7.4) or TSB medium were added to the remaining 5 µl concentrated extracts in the wells of row A, and 75 µL MHB medium or TSB medium were added into all wells. Starting from the extract/medium mixture in the first row, serial dilutions were prepared in corresponding subjacent rows of the 96-well plate (Suppl. Figure 42).

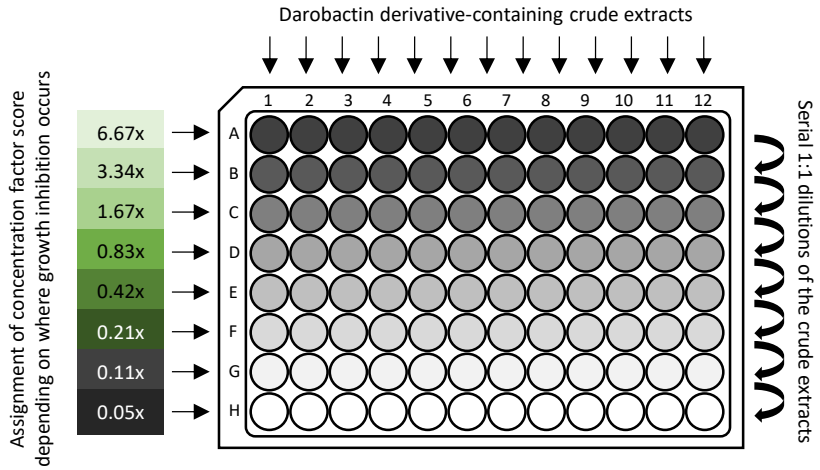

Suppl. Figure 42. The darobactin derivative-containing crude extracts (100x concentrated) were serially 1:1 diluted in a 96-well plate starting from well A (1:15 dilution) to well H (1:1,920 dilution). The concentration factor was calculated from the crude extract concentration divided by the dilution in the respective row. The well position, in which an activity of the compound against the strain was last (visually) detected, was assigned to the concentration factor score.

Next, bacterial cell suspensions of *Acinetobacter baumannii* DSM-30008, *Pseudomonas aeruginosa* PA01, *E. coli* ATCC25922 and *Klebsiella pneumoniae* DSM-30104 were prepared. Single colonies of the bacterial strains were suspended in 0.9 % (w/v) NaCl and McFarland was adjusted to 0.5. The bacterial suspension was diluted 1:100 in MHB (in case of *A. baumannii* DSM-30008, *P. aeruginosa* PA01 and *E. coli* ATCC25922) or TSB (*K. pneumoniae* DSM-30104) to achieve a final inoculum of approximately 10^6 colony-forming units (CFU)/mL. 75 µL of these suspensions were added to each well of the 96-well plates containing the extracts in serial dilution (final inoculum of 5 x 10^5 CFU/mL). Growth inhibition was assessed after 24 h incubation under static conditions at either 30°C (*A. baumannii*) or 37°C (all others). MIC was evaluated visually by determining the dilution factor (row A = 1:15; row B = 1:30; etc.) where visible growth of the respective strain was no longer observed. Finally, the concentration facor of the tested extract was calculated by division of the concentration (100x caused by the extraction process) by the dilution factor in which visible growth of the respective strain was no longer observed. For example, if the darobactin derivative-containing crude extract in column 1 (see Suppl. Figure 42) resulted in growth inhibition of the respective strain from wells A1 to E1, but not anymore in F1, we assigned the concentration factor score 0.42x to the darobactin derivative. If the darobactin derivative-containing crude extract in column 2 resulted in growth inhibition only from wells A2 to B2, but not anymore in C2, we assigned the concentration factor score 3.34x, meaning that the crude extract in

column 1 showed stronger antibacterial activity (assuming that the compound concentration is similar).

Determination of the MS peak area under curve (AUC) ratio

To calculate the relative quantity of each darobactin derivative compared to darobactin A in the crude extracts (crude extract preparation is described in previous section), the MS peak surface areas of the respective $[M+2H]^{2+}$ EICs were determined by automated peak integration using *Compass Data Analysis* version 4.4 (Bruker Daltonics). Next, the AUC of each derivative was divided by the AUC of the darobactin A peak. Raw data and calculations are supplied in the Source data file.

Large scale fermentation of darobactins A and 9 for purification

Large scale fermentation of *E. coli* BL21 (DE3) pNOSO-darABCDE and *E. coli* BL21 (DE3) pNOSO-darABCDE-9 in 6 x 1 L FM medium (supplemented with 1 mg/L vitamin B_{12} after medium sterilization) was performed in 5 L baffled shake flasks for 3 days at 30 °C and 160 rpm on an orbital shaker (Orbitron/Multitron, Infors HT). Each 1 L production culture was inoculated with 50 mL of an LB seed culture grown overnight in a 300 mL unbaffled shaking flask at 30 °C and 180 rpm. After large scale fermentation, the cells were separated from the supernatant by centrifugation on an Avanti J-26 XP centrifuge (Beckman Coulter, Brea, California (US)) with the JLA 8.1 rotor at 6,000 rcf. XAD-16N resin was added to the clarified supernatant and the mixture was shaken on an orbital shaker (Orbitron/Multitron, Infors HT) at 160 rpm for 2 h. This extraction step was performed two to three times and the combined resin subsequently extracted using 3 x 500 mL of 80% MeOH in H_2O. After solvent evaporation using a rotary evaporator, the dried extract was redissolved in H_2O and the purity was analysed by uHPLC-HRMS.

Purification of darobactins A and 9

As both darobactins, darobactin A and darobactin 9, show similar behavior in chromatographic separation, they can be purified using the same set of methods. The dried extract (extract preparation described in the section before) was taken up in a minimum of milliQ H_2O and purified on a preparative Autopurifier HPLC-MS (Waters Corp.) system with H_2O and ACN (+0.1 % FA) on a XBridge C_{18} column (5 µm, 19x150 mm; Waters Corp.) at a flow rate of 25 mL/min going from 2-25% ACN in 24 min followed by a ramp to a flushing step at 95% ACN and a ramp back to the initial conditions. Darobactins were detected by their respective mass signals of 483.70 $[M+2H]^{2+}$ and 503.21 $[M+2H]^{2+}$ for darobactins A and 9, respectively, on the built-in single quadrupole mass analyzer. Darobactin A eluted at 10 min and darobactin 9 eluted at 12 min. The darobactin-containing fractions were collected and dried using a

rotary evaporator. The samples were subsequently dissolved in a minimum of milliQ H_2O and purified on the same preparative Autopurifier HPLC-MS system with H_2O and ACN (+0.1 % FA) on a Kinetex Biphenyl column (5 µm, 19x250 mm; Phenomenex Inc., Torrance, California (US)) at a flow rate of 25 mL/min going from 2-20% ACN in 24 min followed by a ramp to a flushing step at 95% ACN and a ramp back to the initial conditions. Darobactin A eluted at 15 min and darobactin 9 eluted at 21 min. The third step of the purification of darobactins A and 9 was carried out using an Ultimate 3000 SDLC low pressure gradient system (Dionex) equipped with an Acquity CSH Phenyl-hexyl column (250x10mm 5µm; Waters Corp.). The eluents were H_2O + 0.1% FA as A and ACN + 0.1% FA as B, at a flow rate of 5 mL/min and a column thermostatic at 45 °C. The darobactins were detected by UV absorption at 280 nm and the purification was done by time-dependent fraction collection. The separation was started with a plateau at 2% B for 2 min followed by a ramp to 15% B during 20 min and a ramp to 95% B during 1 min. The A content was kept at 5% B for 2 min. The B content was ramped back to starting conditions during 30 seconds and the column was re-equilibrated for 2 min. Darobactin A elutes at 14.8 min and darobactin 9 elutes at 16.7 min. After evaporation, the darobactins were obtained as pale yellowish amorphous solids. After purification, uHPLC-HRMS analysis shows a single peak with an exact mass of 483.701 $[M+2H]^{2+}$ and 503.212 $[M+2H]^{2+}$ for darobactins A and 9, respectively. The purity of the isolated compounds was assessed on the one hand by uHPLC-HRMS as judged from the MS trace as well as the UV trace from 200 to 600 nm. In addition to that, the compounds purity was provided by the 'cleanliness' meaning the absence of non-darobactin signals in the NMR spectrum.

Structure elucidation of darobactins A and 9

1D and 2D NMR data used for the structure elucidation of darobactin 9 were acquired in a 2:1 mixture of H_2O-d_2 acetonitrile-d_3-containing 2 % formic acid-d_2 on an UltraShield 500 spectrometer (Bruker Daltonics) equipped with a 5 mm TCI cryoprobe (^1H at 500 MHz, ^{13}C at 125 MHz). The spectra were recorded at 45 °C and calibrated on the remaining non-deuterated acetonitrile signals. All observed chemical shift values (δ) are given in ppm and the coupling constant values (J) in Hz. Standard pulse programs were used for HMBC, HSQC, and gCOSY experiments. HMBC experiments were optimized for $^{2,3}J_{C\text{-}H}$ = 6 Hz. The NMR signals were grouped in the tables below and correspond to the numbering in the schemes corresponding to every table. All structure formulae devised by NMR will be made publicly available under their corresponding name in NPApatlas[11].

Quantification of darobactins A and 9 production

The quantification of darobactin A in the heterologous producers *E. coli* BL21 (DE3) pNOSO-darABCDE, *E. coli* BL21 (DE3) pNOSO-darACDE, *E. coli* BL21 (DE3) pNOSO-darABDE and *E. coli* BL21 (DE3) pNOSO-darABCE, as well as the quantification of darobactin 9 in *E. coli* BL21 (DE3) pNOSO-darABCDE-9 was done using an amaZon speed 3D ion trap MS system (Bruker Daltonics) with an Apollo II ESI source. The LC system, column and settings as well as the ESI source settings were identical as described above. We measured darobactin A and darobactin 9 standard solutions with concentrations of 1000 mg/mL, 500 mg/mL, 250 mg/mL, 125 mg/mL, 62.5 mg/mL, 31.25 mg/mL, 15.63 mg/mL, 7.81 mg/mL, 3.91 mg/mL, 1.95 mg/mL, 0.98 mg/mL. Solutions for each concentration were prepared three times and measured two times. The EICs m/z 483.70 $[M+2H]^{2+}$ as peak surface of darobactin A and m/z 503.20 $[M+2H]^{2+}$ as peak surface area of darobactin 9 were determined by automated peak integration using *Compass Data Analysis* version 4.4 (Bruker Daltonics). All standard solutions were measured in duplicates to ensure reproducibility. The linear range of the setup was experimentally determined to be between 0.98 mg/mL and 62.5 mg/mL for darobactin A and 0.98 mg/mL and 15.63 mg/mL for darobactin 9. The mean values of each measurement were used to construct a regression line that was used to calculate the quantity of darobactin A and darobactin 9 in the cultivation extract. Source data are supplied in the Source data file.

Evaluation of MICs of pure darobactins A and 9

All strains were handled according to standard procedures and were purchased from the German Collection of Microorganisms and Cell Cultures (DSMZ), the American Type Culture Collection (ATCC) and the Coli Genetic Stock Centre (CGSC; Keio collection).[12] *E. coli* BL21 (DE3) is part of our internal strain collection and *P. aeruginosa* strains were kindly provided by Prof. D. S. Häußler. The clinical isolates were kindly provided by Dr. P. Chhatwal, L. Knegendorf, and Prof. Dr. D. Schlüter from Hannover Medical School. Darobactins were prepared as DMSO stock solutions and MICs were established using microbroth dilution as described elsewhere.[13] In brief, serial dilutions of compounds (0.03-64 µg/mL) in MHB were prepared in sterile 96-well plates. Bacterial suspensions in MHB were added to achieve a final inoculum of 5×10^5 CFU/mL. Depending on the growth requirements of tested bacteria, the plates were incubated for 24 h at either 30 °C or 37 °C. MICs were defined as lowest concentration of antibiotic at which no visible growth was observed.

Sample information and antibiograms of clinical bacterial isolates

Suppl. Table 8. Sampling data of used clinical isolates. [a] 3MRGN: multi-resistant gram-negative bacteria, non-susceptible to three specific groups of antibiotics; ESBL: Extended spectrum β-lactamases.

Strain ID	Sample type	Month/year of isolation	Resistance phenotype[a]
E. coli ECO24	Midstream urine	02/2020	Quinolone resistant
E. coli ECO25	Permanent catheter urine	02/2020	3MRGN
K. pneumoniae KPN12	Permanent catheter urine	02/2020	3MRGN
K. pneumoniae KPN19	Midstream urine	02/2020	3MRGN
K. pneumoniae KPN62	Sputum	03/2020	ESBL

Suppl. Table 9. Antibiogram of clinical isolates. [a] R: resistant (shown in red); I: intermediate (shown in yellow); S: sensitive (shown in green).

	ECO24	ECO25	KPN12	KPN19	KPN62
Ampicillin	R	R	R	R	R
Ampicillin-Sulbactam	R	R	R	R	R
Piperacillin / Sulbactam		R	R	R	R
Piperacillin-Tazobactam	S	I	I	R	I
Cefuroxim	I	R	R	R	R
Cefuroxim-Axetil	S	R	R	R	R
Cefpodoxim	S	R	R	R	R
Ceftriaxon	S	R	R	R	R
Cefotaxim	S	R	R	R	R
Ceftazidim	S	R	R	R	R
Gentamicin	R	R	I	R	I
Fosfomycin	S	S	R	R	
Nitrofurantoin	S	S			
Levofloxacin	R	R	I	R	S
Ciprofloxacin	R	R	R	R	S
Moxifloxacin	R	R	R	R	S
Meropenem	S	S	S	I	S
Ertapenem					S
Cotrimoxazol	R	S	R	R	S

NMR data for darobactin 9

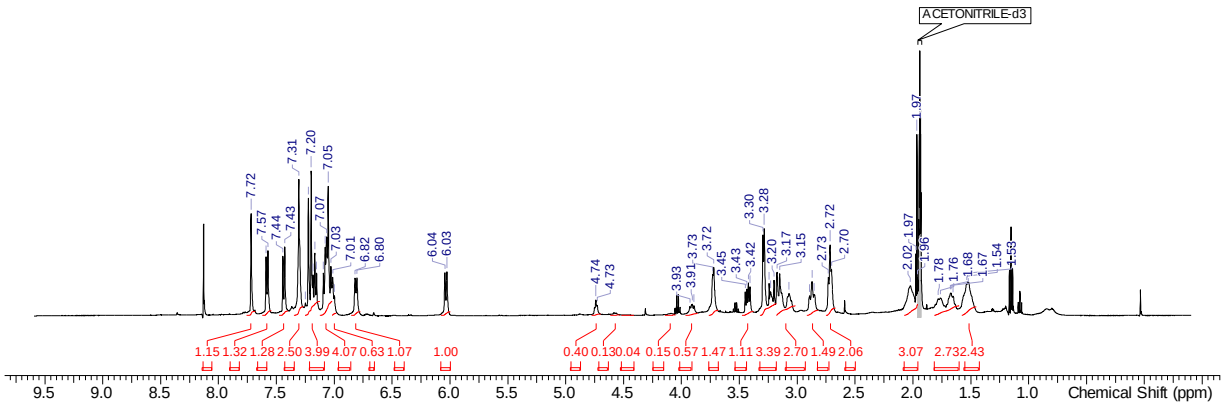

Suppl. Figure 43. Water suppressed ^{1}H spectrum of darobactin 9 in a 2:1 mixture of H_2O-d_2 acetonitrile-d_3-containing 2 % formic acid-d_2 at 45 °C and 500 MHz.

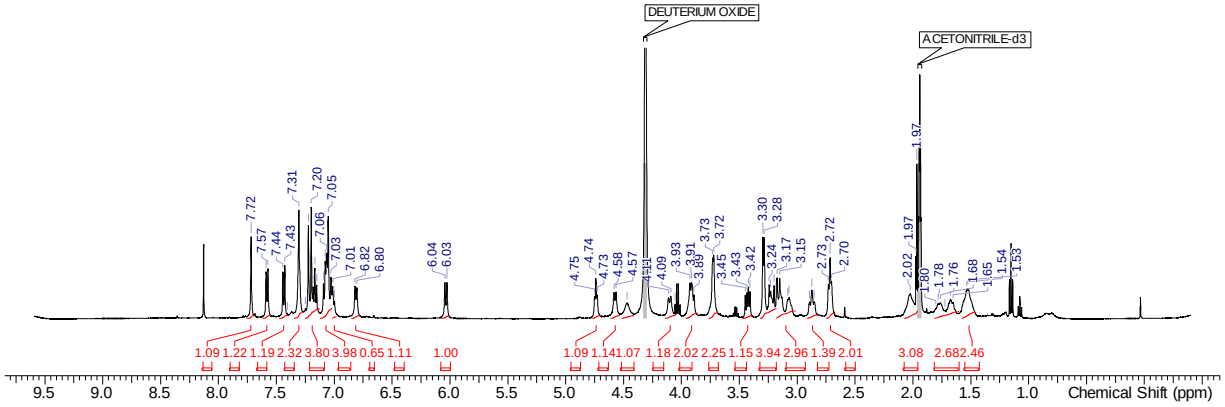

Suppl. Figure 44. ^{1}H spectrum of darobactin 9 in a 2:1 mixture of H_2O-d_2 acetonitrile-d_3-containing 2 % formic acid-d_2 at 45 °C and 500 MHz.

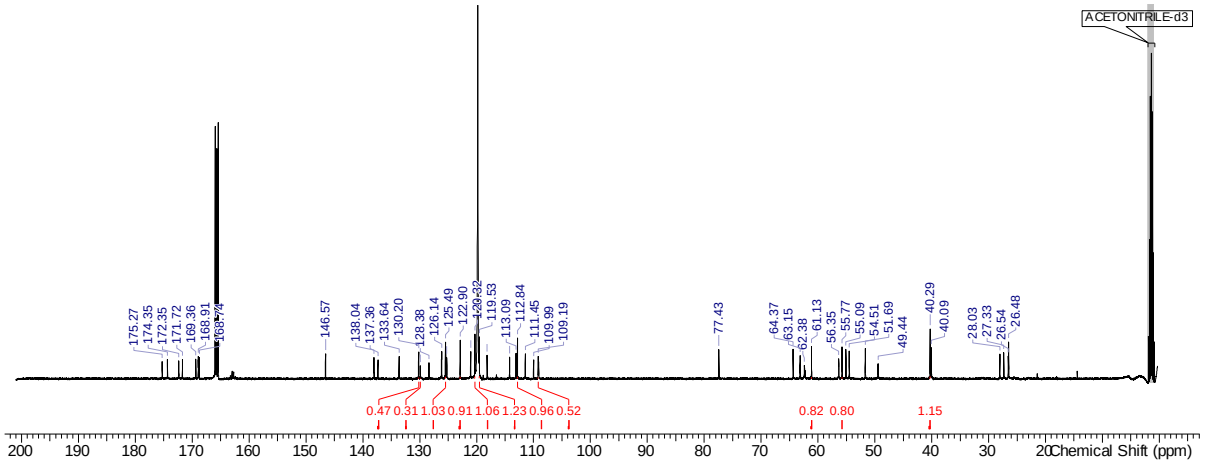

Suppl. Figure 45. ^{13}C spectrum of darobactin 9 in a 2:1 mixture of H_2O-d_2 acetonitrile-d_3-containing 2 % formic acid-d_2 at 45 °C and 125 MHz.

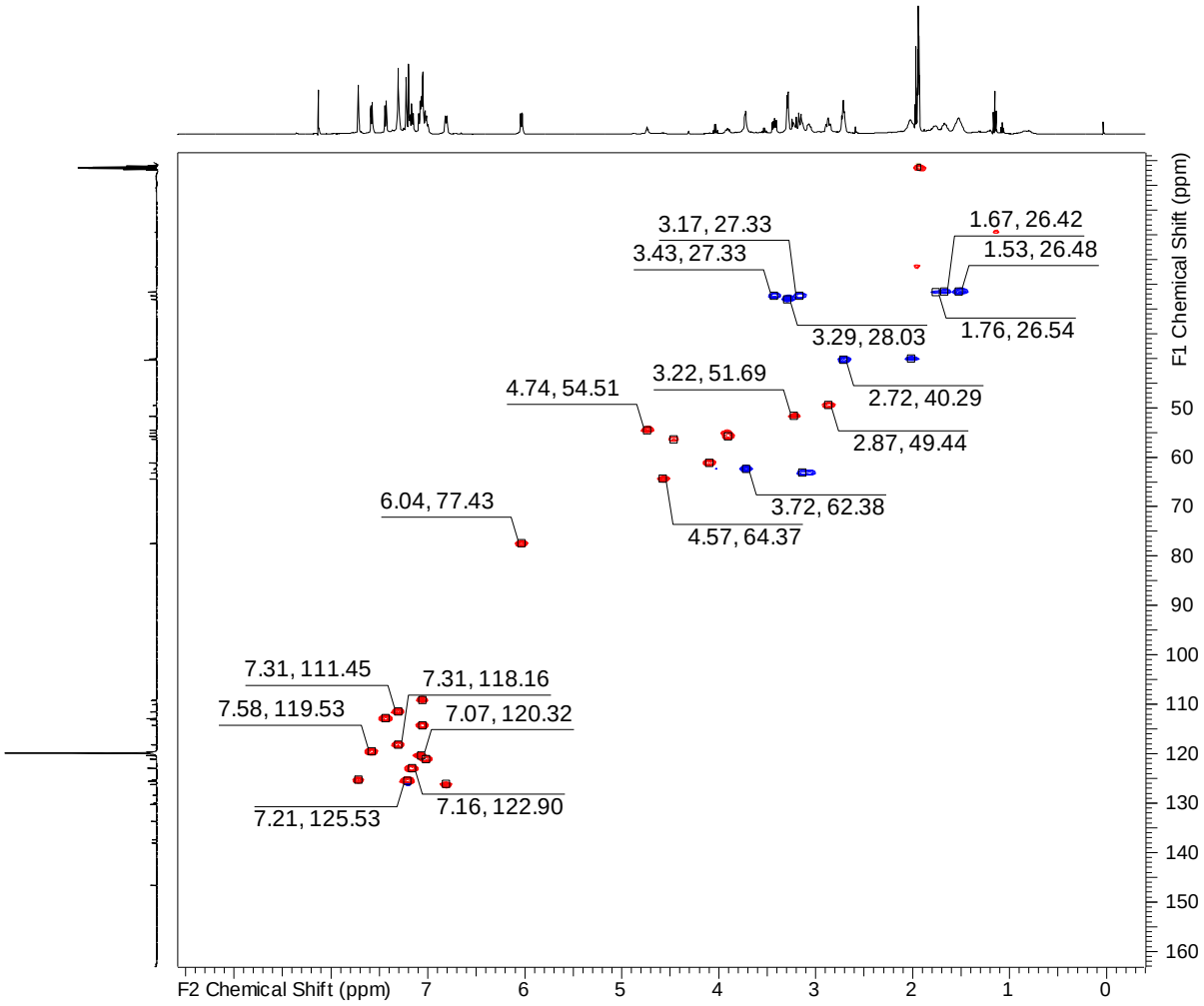

Suppl. Figure 46. HSQC spectrum of darobactin 9 in a 2:1 mixture of H_2O-d_2 acetonitrile-d_3-containing 2 % formic acid-d_2 at 45 °C and 500/125 MHz.

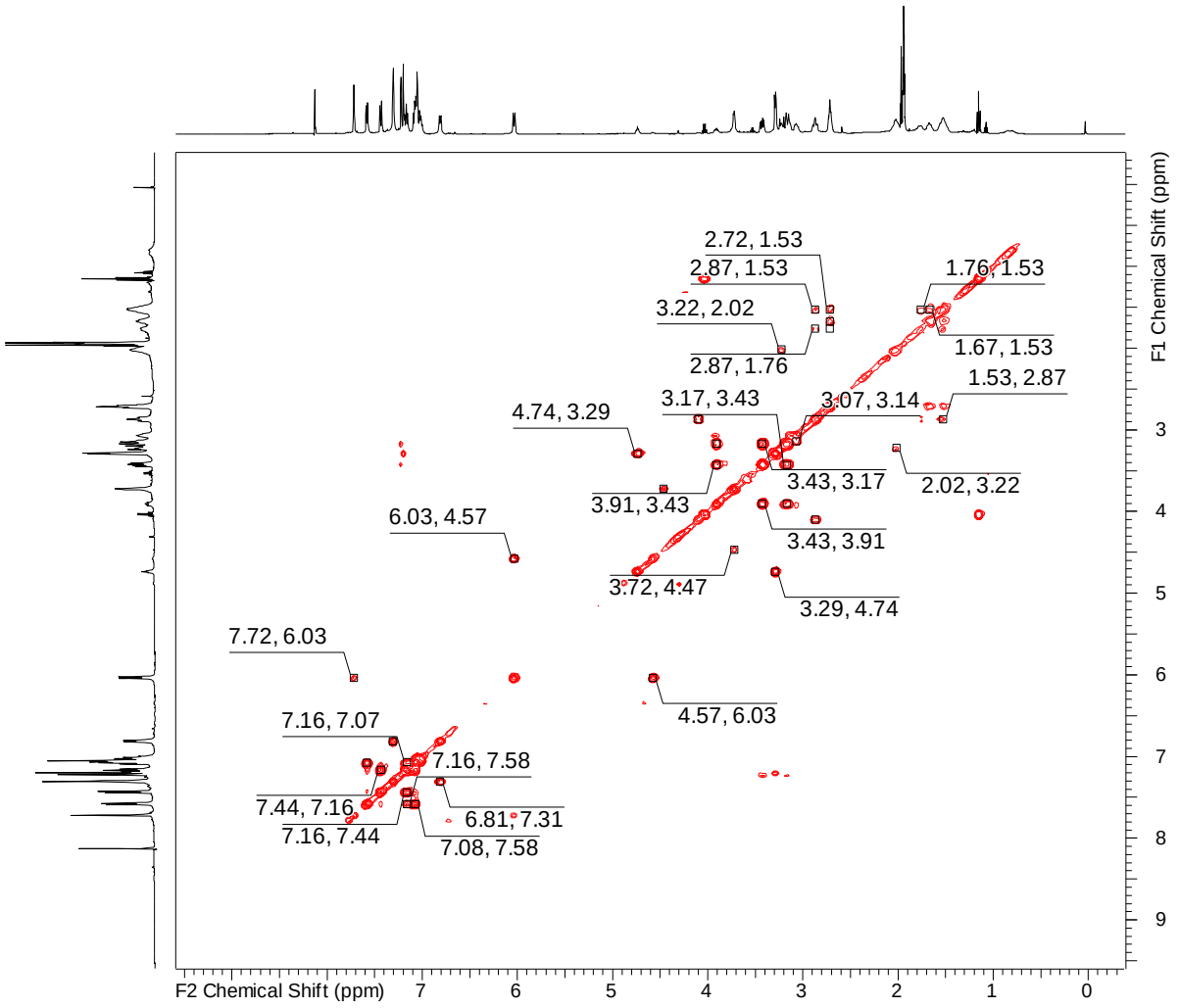

Suppl. Figure 47. COSY spectrum of darobactin 9 in a 2:1 mixture of H_2O-d_2 acetonitrile-d_3-containing 2 % formic acid-d_2 at 45 °C and 500 MHz.

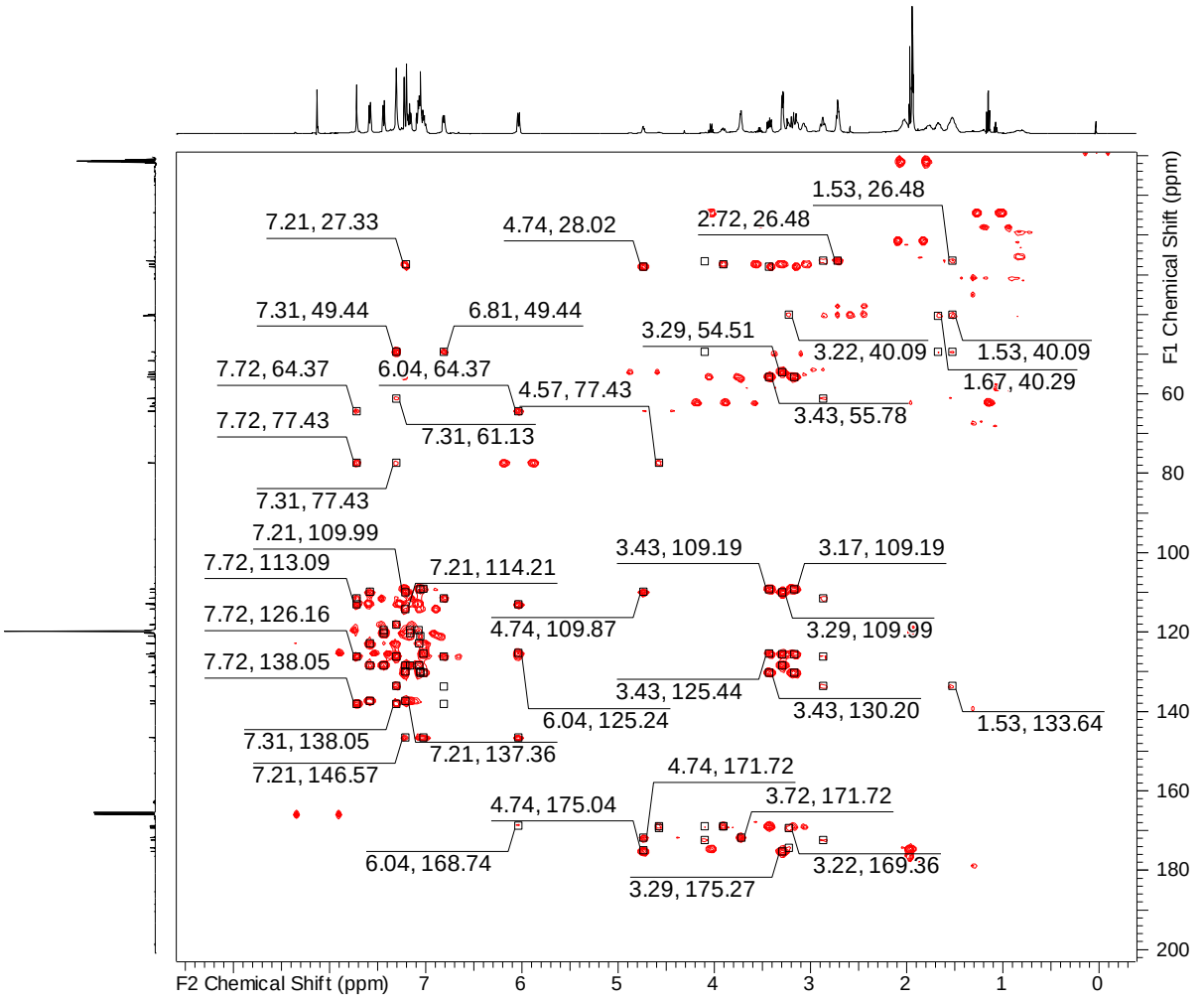

Suppl. Figure 48. HMBC spectrum of darobactin 9 in a 2:1 mixture of H_2O-d_2 acetonitrile-d_3-containing 2 % formic acid-d_2 at 45 °C and 500/125 MHz.

Suppl. Table 10. NMR chemical shifts and correlations of darobactin 9 in a 2:1 mixture of H_2O-d_2 acetonitrile-d_3-containing 2 % formic acid-d_2 at 45 °C and 500/125 MHz.

#	δ ^{13}C [ppm]	δ ^{1}H [ppm], mult (J [Hz])	COSY	HMBC
1	175.3	-	-	-
2	54.5	4.74, bt (5.6)	3	3, 4, 12
3	28.0	3.29, bd (5.8)	2	1, 2, 4, 5, 6
4	110.0	-	-	-
5	125.5	7.21, s	-	2, 3, 4, 6, 7, 8, 11
6	128.4	-	-	-
7	119.5	7.58, d (7.9)	8, 9	4, 6, 9, 11
8	120.3	7.07, m	7, 9	6, 9, 10
9	122.9	7.16, t (7.6)	8, 10	6, 7, 8, 11
10	112.8	7.44, d (8.2)	9	6, 7, 8
11	137.4	-	-	-
12	171.7	-	-	-
13	56.4	4.47, bs	14	-
14	62.4	3.72, bd (4.6)	13	12, 13
15	172.4	-	-	-
16	61.1	4.10, bd (9.8)	17	15, 17, 18, 19, 21
17	49.4	2.87, bt (9.8)	18, 19	16, 18, 19, 31, 32, 33
18	26.5	1.53/1.67, m	17, 19, 20	17, 19, 20, 33
19	26.5	1.76, m	17, 18, 20	16, 17, 33
20	40.3	2.72, bt (6.8)	18, 19	17
21	169.0	-	-	-
22	55.1	3.91, m	23	24
23	63.2	3.14/3.07, m	22	21
24	168.7	-	-	-
25	64.4	4.57, bd (8.5)	26	26, 27, 28, 46
26	77.4	6.04, bd (8.9)	25, 28	24, 25, 27, 28, 44
27	113.1	-	-	-
28	125.2	7.72, s	26	25, 26, 27, 29, 30, 31
29	126.2	-	-	-
30	138.0	-	-	-
31	111.5	7.31, m	32	17, 26, 28, 32, 33, 34
32	126.1	6.81, bd (7.9)	31	17, 29, 30, 31, 34
33	133.6	-	-	-
34	118.2	7.31, m	-	17, 29, 30, 31, 32, 33
35	168.9	-	-	-

36	55.8	3.91, m	37	37
37	27.3	3.43/3.17, dd (13.5, 7.1)/m	36	35, 36, 38, 40, 41, 45
38	109.2	-	-	-
39	114.2	7.06, m	-	38, 40, 45
40	129.9	-	-	-
41	125.4	7.21, d (12.2)	42	37, 38, 39, 40, 43, 44, 45
42	121.1	7.02, m	41, 43	40, 41, 43, 44, 45
43	109.1	7.06, m	42	41, 42, 44, 45
44	146.6	-	-	-
45	130.2	-	-	-
46	169.4	-	-	-
47	51.7	3.22, m	48	35, 46, 48, 49
48	40.1	2.02, m	47	46, 47, 49
49	174.4	-	-	-

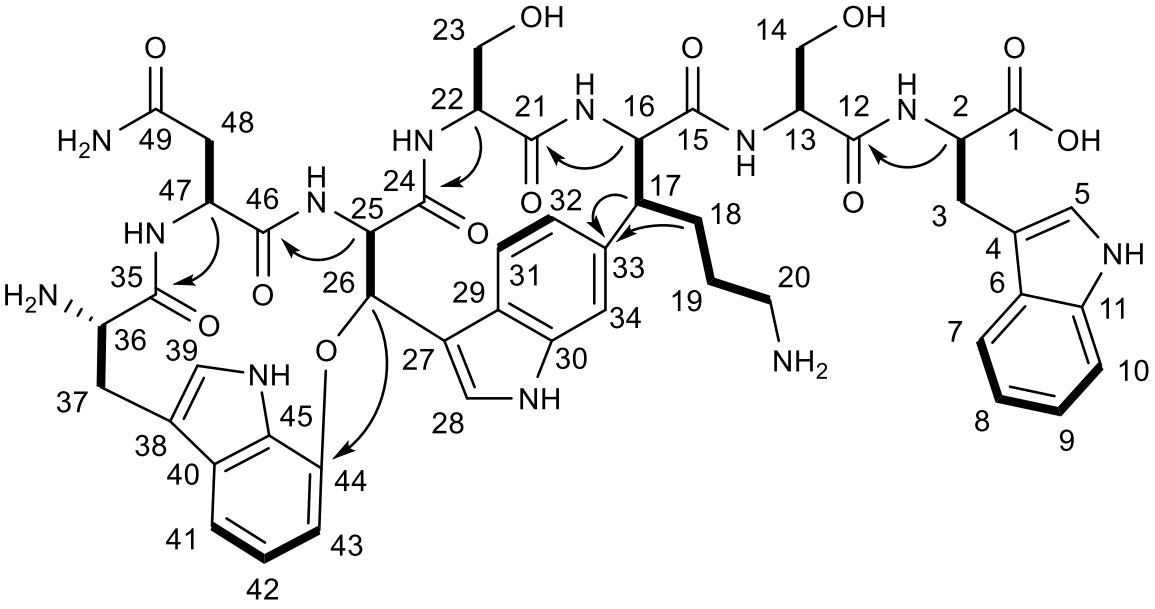

Suppl. Figure 49. Most relevant COSY (bold) and HMBC correlations (arrows) used for structure elucidation of darobactin 9 including atom numbers referred in table 8.

Protein overexpression and purification of DarF

For heterologous overexpression and purification of DarF, 6 x 1 L LB medium were inoculated with 10 mL *E. coli* BL21 (DE3) pHisSUMOTEV-darF LB seed culture each. The fermentation was performed in 5 L baffled shake flasks at 30 °C and 180 rpm (Orbitron/Multitron, Infors HT) until an OD_{600} 0.5 – 0.7 was reached. The cultures were subsequently cooled for 10 min on ice, followed by addition of 0.4 mM

IPTG to induce the *T7lac* promoter regulated *darF* gene expression. Next, the cultures were grown for 18 h at 16 °C and 180 rpm.

The cells were harvested by centrifugation on an Avanti J-26 XP centrifuge (Beckman Coulter) with the JLA 8.1 rotor at 6,000 x g for 15 min at 4 °C. All the following steps were performed on ice or at 4 °C. The cell pellets were combined and re-suspended in 100 mL lysis buffer (20 mM Bis-Tris, 200 mM NaCl, 20 mM imidazole, 1 mM TCEP, pH 6.8) and two capsule of protease inhibitor (cComplete, EDTA-free from Roche, Basel, Switzerland) were added. Cells lysis was performed by passing the cell suspension two times through a cell disrupter (Constant Systems; Daventry, UK) at 30,000 psi and spun down for 25 min on an Avanti J-26 XP centrifuge with the JA 25.50 rotor at 40,000 x g and 4 °C. The supernatant was filtered using a cellulose nitrate membrane filter (5 µm pore size) and loaded onto a pre-equilibrated (lysis buffer) 5 mL HisTrap HP column (GE Healthcare, Chicago, Illinois (US)) for affinity purification. All following purification steps were performed on an Aekta go FPLC device (GE Healthcare). The HisTrap column waswashed with lysis buffer (30 column volumes) at 5 mL/min flow rate. The elution of DarF was performed using elution buffer (20 mM Bis-Tris, 200 mM NaCl, 250 mM imidazole, 1mM TCEP, pH 6.8). The DarF-containing fractions were collected, loaded onto a pre-equilibrated (lysis buffer) Hi Prep Desalt 16/10 column (GE Healthcare) and the imidazole was removed by washing with lysis buffer (1.2 column volumes) at 10 mL/min. Subsequently, Tobacco etch virus (TEV) protease was added to the DarF-containing eluate with a ratio of 1:10 (v/v) and incubated at 4 °C for 12 h to remove the HisSUMO tag. After a second HisTrap column purification step using the same conditions as described above, the DarF-containing flow through was collected and loaded onto a pre-equilibrated (elution buffer with 10 % glycerol (w/v)) HiLoad 16/600 Superdex 200 pg gel filtration column (GE Healthcare). Size exclusion protein fractionation was performed with elution buffer plus 10 % glycerol (w/v) at 1 mL/min flow rate (1.2 column volumes). The purity of DarF was verified via SDS PAGE.

In vitro investigation of the enzyme activity of DarF

Since HHpred analysis of DarF revealed homology to zinc-dependent metalloproteases (see Supplementary Data), we tested zinc as co-factor in the *in vitro* activity assay. To remove divalent cations, which were potentially bound to DarF during the purification process, we first performed a dialysis step. The DarF eluate obtained after size exclusion chromatography had a volume of approximately 10 mL (1 mg/mL DarF) and was incubated on ice for 2 h after addition of EDTA (2 mM final concentration). After increasing the EDTA concentration (3 mM), the sample was transferred into a Slide-A Lyzer Dialysis Cassette G2, 10 MWCO (Thermo Scientific) and dialysed in 4 L elution buffer (20 mM Bis-Tris pH 6.8, 200 mM NaCl, 10 % Glycerol (w/v), 1 mM DTT) at 4 °C for 12 h under constant stirring (150 rpm, MR Hei-Standard magnetic stirrer, Heidolph Instruments, Schwabach, Germany). This dialysis step was repeated under the same conditions for another 6 h in fresh buffer.

The activity of DarF was investigated in 50 µl scale reactions (15 µM DarF, 25 µM darobactin A or 9 and 200 µM zinc in elution buffer) for 12 h at room temperature. Reactions without DarF served as controls. Each reaction was performed three times. The reactions were stopped by the addition of 150 µL acetonitrile and the samples were centrifuged at 11,000 x g for 10 min at room temperature in a table top centrifuge prior to uHPLC-MS analysis on an amaZon speed 3D ion trap MS system (Bruker Daltonics) with an Apollo II ESI source. The LC system, column and settings as well as the ESI source settings were identical as described above. Suppl. Figure 50 and Suppl. Figure 51 show representative EICs and the degradation of darobactins A and 9, respectively.

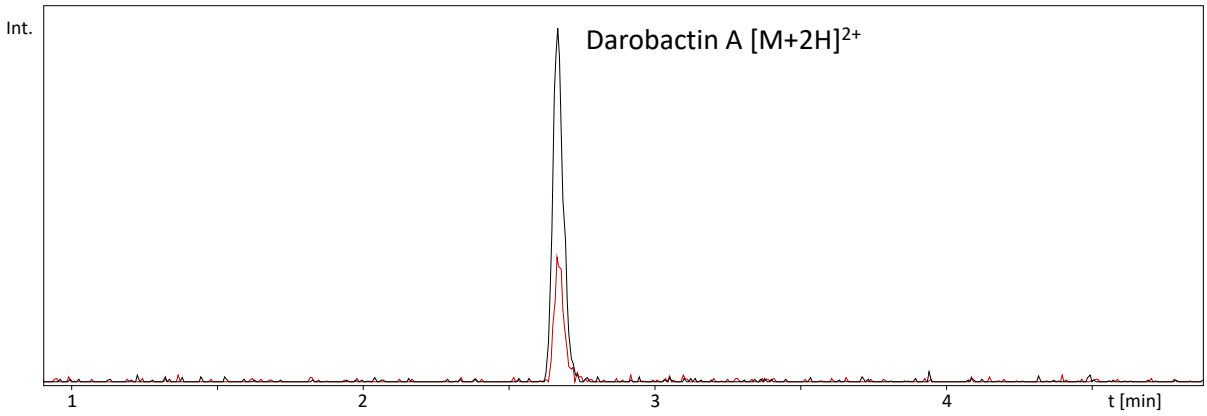

Suppl. Figure 50. Chromatogram of the in vitro darobactin A degradation reaction by DarF (red trace) and the darobactin A control without DarF (black trace). Both traces display the darobactin A EIC for the $[M+2H]^{2+}$ species at m/z 483.71 ±0.1 Da.

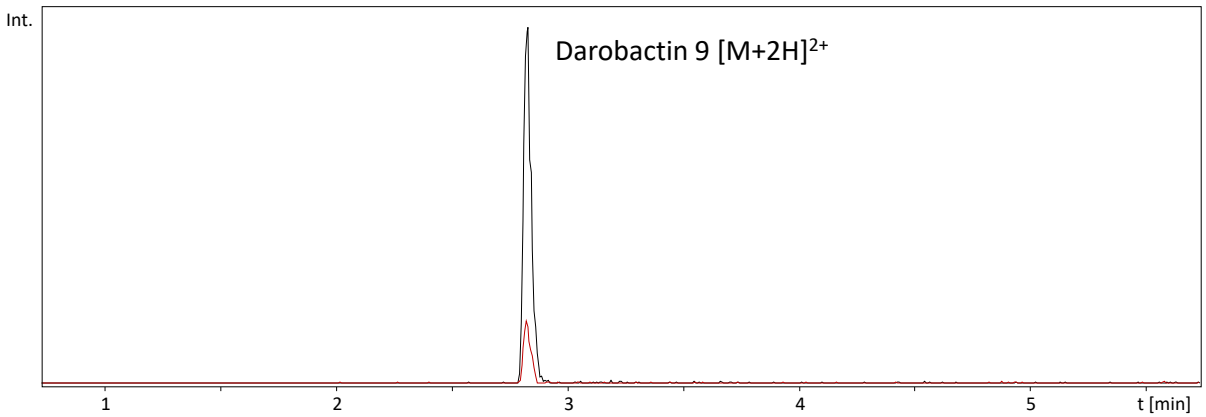

Suppl. Figure 51. Chromatogram of the in vitro darobactin 9 degradation reaction by DarF (red trace) and the darobactin A control without DarF (black trace). Both traces display the darobactin 9 EIC for the $[M+2H]^{2+}$ species at m/z 503.21 ±0.1 Da.

Software

Geneious version 10.1.3 (Biomatters Ltd.; Auckland, New Zealand) was used to design the modified darobactin BGC and the cloning and expression vector pNOSO *in silico*. *Chromeleon* version 6.80 (Thermo Fisher Scientific; Waltham, Massachusetts (US)) was used for LC control. *Compass HyStar* 3.2

Build 49.9 (Bruker Daltonics) was used for MS scan control. *Compass otof Control* version 3.4 (Bruker Daltonics) and *trap Control* version 8.0 (Bruker Daltonics) were used for data acquisition of the maXis 4G ToF and the amaZon speed 3D ion trap mass spectrometers, respectively. We used *Compass DataAnalysis* version 4.4 (Bruker Daltonics) to interpret MS data and *MS Excel* 2016 for the calculation of the absolute and relative production titers of darobactin A. *Topspin* 3.6.1 (Bruker Biospin) was used for NMR data acquisition and *Spectrus processor* 2019.2.1 (ACD Labs) for processing and assignment. *MS PowerPoint* 2016 was used for image processing and *ChemDraw Professional* version 17.1.0.105 (19) was used to create images of chemical structures.

References

1 J. W. Dubendorff and F. W. Studier, *J. Mol. Biol.*, 1991, **219**, 45.

2 D. Pogorevc, F. Panter, C. Schillinger, R. Jansen, S. C. Wenzel and R. Müller, *Metab. Eng.*, 2019, **55**, 201.

3 E. Beck, G. Ludwig, E. A. Auerswald, B. Reiss and H. Schaller, *Gene*, 1982, **19**, 327.

4 R. E. Rose, *Nucleic Acids Res.*, 1988, **16**, 356.

5 V. Magrini, M. L. Storms and P. Youderian, *J. Bacteriol.*, 1999, **181**, 4062.

6 J. Sambrook and D. W. Russell, *Molecular cloning: A laboratory manual*, Cold Spring Harbor Laboratory Press, Cold Spring Harbor, NY, 3rd edn., 2001.

7 H. Liu and J. H. Naismith, *Protein Expr. Purif.*, 2009, **63**, 102.

8 Y. Zhang, F. Buchholz, J. P. Muyrers and A. F. Stewart, *Nat. Genet.*, 1998, **20**, 123.

9 S. Groß, B. Schnell, P. A. Haack, D. Auerbach and R. Müller, *Nat. Commun.*, 2021, **12**, 1696.

10 M. Wang, J. J. Carver, V. V. Phelan, L. M. Sanchez, N. Garg, Y. Peng, D. D. Nguyen, J. Watrous, C. A. Kapono, T. Luzzatto-Knaan, C. Porto, A. Bouslimani, A. V. Melnik, M. J. Meehan, W.-T. Liu, M. Crusemann, P. D. Boudreau, E. Esquenazi, M. Sandoval-Calderon, R. D. Kersten, L. A. Pace, R. A. Quinn, K. R. Duncan, C.-C. Hsu, D. J. Floros, R. G. Gavilan, K. Kleigrewe, T. Northen, R. J. Dutton, D. Parrot, E. E. Carlson, B. Aigle, C. F. Michelsen, L. Jelsbak, C. Sohlenkamp, P. Pevzner, A. Edlund, J. McLean, J. Piel, B. T. Murphy, L. Gerwick, C.-C. Liaw, Y.-L. Yang, H.-U. Humpf, M. Maansson, R. A. Keyzers, A. C. Sims, A. R. Johnson, A. M. Sidebottom, B. E. Sedio, A. Klitgaard, C. B. Larson, C. A. Boya P, D. Torres-Mendoza, D. J. Gonzalez, D. B. Silva, L. M. Marques, D. P. Demarque, E. Pociute, E. C. O'Neill, E. Briand, E. J. N. Helfrich, E. A. Granatosky, E. Glukhov, F. Ryffel, H. Houson, H. Mohimani, J. J. Kharbush, Y. Zeng, J. A. Vorholt, K. L. Kurita, P. Charusanti, K. L. McPhail, K. F. Nielsen, L. Vuong, M. Elfeki, M. F. Traxler, N. Engene, N. Koyama, O. B. Vining, R. Baric, R. R. Silva, S. J. Mascuch, S. Tomasi, S. Jenkins, V. Macherla, T. Hoffman, V. Agarwal, P. G. Williams, J. Dai, R. Neupane, J. Gurr, A. M. C. Rodriguez, A. Lamsa, C. Zhang, K. Dorrestein, B. M. Duggan, J. Almaliti, P.-M. Allard, P. Phapale, L.-F. Nothias, T. Alexandrov, M. Litaudon, J.-L. Wolfender, J. E. Kyle, T. O. Metz, T. Peryea, D.-T. Nguyen, D. VanLeer, P. Shinn, A. Jadhav, R. Muller, K. M. Waters, W. Shi, X. Liu, L. Zhang, R. Knight, P. R. Jensen, B. O. Palsson, K. Pogliano, R. G. Linington, M. Gutierrez, N. P. Lopes, W. H. Gerwick, B. S. Moore, P. C. Dorrestein and N. Bandeira, *Nat. Biotechnol.*, 2016, **34**, 828.

11 a) Npatlas - The Natural Products Atlas, https://www.npatlas.org; b) J. A. van Santen, G. Jacob, A. L. Singh, V. Aniebok, M. J. Balunas, D. Bunsko, F. C. Neto, L. Castaño-Espriu, C. Chang, T. N. Clark, J. L. Cleary Little, D. A. Delgadillo, P. C. Dorrestein, K. R. Duncan, J. M. Egan, M. M. Galey, F. J. Haeckl, A. Hua, A. H. Hughes, D. Iskakova, A. Khadilkar, J.-H. Lee, S. Lee, N. LeGrow, D. Y. Liu, J. M. Macho, C. S. McCaughey, M. H. Medema, R. P. Neupane, T. J. O'Donnell, J. S. Paula, L. M.

Sanchez, A. F. Shaikh, S. Soldatou, B. R. Terlouw, T. A. Tran, M. Valentine, J. J. J. van der Hooft, D. A. Vo, M. Wang, D. Wilson, K. E. Zink and R. G. Linington, *ACS Cent. Sci.*, 2019, **5**, 1824;

12 T. Baba, T. Ara, M. Hasegawa, Y. Takai, Y. Okumura, M. Baba, K. A. Datsenko, M. Tomita, B. L. Wanner and H. Mori, *Mol. Syst. Biol.*, 2006, **2**, 2006.

13 I. Wiegand, K. Hilpert and R. E. W. Hancock, *Nat. Protoc.*, 2008, **3**, 163.

Chapter 3

3.1 Darobactins Exhibiting Superior Antibiotic Activity by Cryo-EM Structure Guided Biosynthetic Engineering

Previously published in:

Carsten E. Seyfert[+ [a] [b]], Christoph Porten[+ [a] [b]], Biao Yuan[+[c] [d]], Selina Deckarm[+ [a] [b]], Fabian Panter[[a] [b]], Chantal D. Bader[[a] [b]], Janetta Coetzee[[a] [b]], Felix Deschner[[a] [b]], Kamaleddin H. M. E. Tehrani[[a] [b]], Paul G. Higgins[[f] [g]], Harald Seifert[[f] [g]], Thomas Marlovits* [[c] [d] [e]], Jennifer Herrmann*[[a] [b]] and Rolf Müller*[[a] [b]]

Angew. Chem. Int. Ed. Engl. 2022 October 29; **62** (2): e202214094

DOI: 10.1002/anie.202214094

Affilitation:

[a] Microbial Natural Products Helmholtz Institute for Pharmaceutical Research Saarland (HIPS), Helmholtz Centre for Infection Research (HZI) and Department of Pharmacy at Saarland University Campus Building E8.1, 66123 Saarbrücken (Germany) E-mail: rolf.mueller@helmholtz-hips.de; jennifer.herrmann@helmholtz-hips.de

[b] German Centre for Infection Research (DZIF), partnersite Hannover-Braunschweig

[c] University Medical Center Hamburg-Eppendorf (UKE), Institute of Structural and Systems BiologyNotkestraße 85, Building 15, 22607 Hamburg (Germany); E-mail: thomas.marlovits@cssb-hamburg.de

[d] Centre for Structural Systems Biology (CSSB), Hamburg (Germany)

[e] Deutsches Elektronen-Synchrotron Zentrum (DESY), Hamburg (Germany)

[f] Microbiology, Immunology and Hygiene, Faculty of Medicine and University Hospital Cologne, University of Cologne, Cologne (Germany)

[g] German Center for Infection Research (DZIF), partner site Bonn-Cologne (Germany)

[+]These authors contributed equally; *corresponding authors

Contributions

Carsten E. Seyfert

The author significantly contributed to the conceptionalization of the study, to the methology and he performed experiments and analyzed the results. The author was responsible for the project administration. The author *in silico* designed and generated the expression constructs for the novel darobactin derivatives D22 to D39. He produced extracted and purified the described novel darobactin analogues. The author designed and established a protocol for the generation of halogenated darobactins and purified halogenated darobactin D9 analogues. The author performed targeted analysis of the MS data, evaluated, and analyzed the results of the bioactivity screens. The author led the formal analysis of all data, generated for this manuscript. The author led original writing of the draft, the visualization of the results and the review and editing. The author translated the manuscript to German for publishing the manuscript in Angewandte Chemie.

Contributions by Others:

Christoph Porten contributed to the formal analysis and the experimental investigations. He optimized darobactin purification and purified derivatives. He supported in visualization, writing, and review and editing. Biao Yuan produced and purifyed the membrane proteins BamABCDE and truncated BamA. He solved the co-structures of BamABCDE with bound darobactin 9 and darobactin 22, respectively, determined binding constants of the tested derivatives, and supported in writing, visualization of the results, and review and editing. Selina Deckarm cultivated derivatives, assisted in purification, and contributed to writing, visualization, and editing. Fabian Panter equally conceptualized the study with the author, supported in *in silico* design, generation of darobactins, formal analysis of results, the review and the editing. Chantal Bader elucidated darobactin structures via NMR, analyzed results, and contributed to visualization, writing, review, and editing. Janetta Coetzee and Felix Deschner contributed to the manuscript by performing *in vitro* activity assays against CRAB isolates and performing an *in vitro* time-kill-assay and by performing an *in vivo* toxicity assay in zebrafish larvae, respectively. They contributed to writing and editing. Kamaleddin H. M. E. Tehrani supported the methodological development of the compound purification. Paul G. Higgins and Harald Seifert assisted in formal analysis and funding. Thomas Marlovits and Jennifer Herrmann are corresponding authors, overseeing funding, resources, and project supervision and also contributing to writing and review. Rolf Müller, a corresponding author, conceptualized the project, led funding acquisition, supervised, reviewed and edited the manuscript.

Abstract

Over recent decades, the pipeline of antibiotics acting against Gram-negative bacteria is running dry, as most discovered candidate antibiotics suffer from insufficient potency, pharmacokinetic properties, or toxicity. The darobactins, a promising new small peptide class of drug candidates, bind to novel antibiotic target BamA, an outer membrane protein. Previously, we reported that biosynthetic engineering in a heterologous host generated novel darobactins with enhanced antibacterial activity. Here we utilize an optimized purification method and present cryo-EM structures of the Bam complex with darobactin 9 (D9), which served as a blueprint for the biotechnological generation of twenty new darobactins including halogenated analogs. The newly engineered darobactin 22 binds more tightly to BamA and outperforms the favorable activity profile of D9 against clinically relevant pathogens such as carbapenem-resistant *Acinetobacter baumannii* up to 32-fold, without observing toxic effects.

Introduction

The stalling development of new antibiotics in combination with an increasing human population density and rising antimicrobial resistance (AMR) in bacteria leads to an emerging antibiotic crisis across the globe.[1,2] Recent studies estimate that 1.27 million deaths in 2019 were attributed to bacterial AMR alone, while multidrug-resistant bacterial infections contributed to 5 million deaths in already diseased patients.[3] Moreover, during the current coronavirus (COVID-19) pandemic, the viral infections were often accompanied by simultaneous infection with bacterial pathogens.[4,5] Particularly, co-infections with carbapenemase-producing pathogens increase lethality rates in patients and contributed to the death of over 6 million COVID-19 patients since the pandemic outbreak in 2020.[6] The challenging research towards discovery and development of new antibiotic classes, especially against Gram-negative pathogens causing life-threatening infections, rarely results in promising candidates.[2,7] Consequently, the demand for new drugs against pathogenic Gram-negative bacteria, such as *Escherichia coli* (*E. coli*), *Acinetobacter baumannii* (*A. baumannii*), *Klebsiella pneumoniae* (*K. pneumoniae*), and *Pseudomonas aeruginosa* (*P. aeruginosa*) continuously rises.[5,8]

Presently, there are some candidates in pre-clinical and clinical development stages for the treatment of infections caused by Gram-negative pathogens. However, these mostly belong to already known compound classes or they are novel chemical entities attacking common targets, such as the broad-spectrum ribosome inhibitor odilorhabdin, originally produced by *Xenorhabdus nematophila.*[9] The darobactins, which are also produced by an entomopathogenic bacterium, *Photorhabdus khanii*,[10] however, are some of the most promising new antibacterials in the last 50 years[2] given they address a novel broad-spectrum target in Gram-negative pathogens. The mechanism of action overcomes common pathogenic resistance and is effective, not only *in vitro,* but also *in vivo.*[2] This family of bicyclic

heptapeptides belongs to the biosynthetic class of ribosomally synthesized and post-translationally modified peptides (RiPPs).[10] Darobactins distinguish themselves from other new antibiotic candidates, such as the recently published macolacin,[11] as they do not affect human gut commensals of the family *Bacteriodes*, a beneficial characteristic considering the intended use in humans.[10] Due to the selective binding to the β-barrel of the outer membrane protein (OMP) BamA, darobactin interferes with the integration of natural OMPs into the membrane by mimicking the OMP signaling peptide.[12] As a consequence, BamA is unable to close the lateral gate and, thus, affects mechanical, kinetic, and energetic properties of the entire complex.[13,14] Highlighting the value of BamA as a worthwhile antibacterial target, darobactin-resistant *E. coli* mutants without BamA generated *in vitro* resulted in substantially reduced fitness and virulence. This indicates a lack of pre-existing resistance and a reduced risk of fast resistance development, at least in *E. coli.*[12,15,16]

Darobactin has only been produced in low amounts in the native host bacterium, insufficient for larger industrial fermentation.[10] Total synthesis via multiple steps with relatively low yields was only very recently developed for darobactin A (DA) and requires the usage of toxic chemicals.[17,18] Excitingly, recently published heterologous expression platforms of the darobactin biosynthetic gene cluster (BGC) offer reasonable production rates in *E. coli* strains in low cost standard cultivation media.[10,16,19] The darobactin BGC consists of two genes essential for production. One encodes the precursor peptide DarA and the other encodes the radical *S*-adenosylmethionine (rSAM) enzyme DarE, catalyzing the bicyclic crosslinking.[20] Heterologous production rates of up to 25 mg/L in the case of DA and 3 mg/L for the more active darobactin 9 (D9), generated via biosynthetic pathway engineering, open the door for efficient large-scale production.[19] While the cryo-EM structure of DA in complex with BamA already exists,[12] no structure-activity relationship (SAR) rationale has been reported.

Herein, we describe a SAR study inspired by the structure elucidation of the BamABCDE (BAM)-D9 complex via cryo-EM, which aided the design of new darobactin core peptide sequences *in vitro*. A new, fast, and less expensive core peptide modification strategy, based on the overlap-extension polymerase chain reaction (OE-PCR) method facilitated the generation of fifteen new *darA* gene variants, including multiple halogenated tryptophans achieved through feeding experimentation, leading to promising derivatives with improved bioactivity and altered core sequences compared to DA, while conserving both tryptophan moieties critical for bicyclization.[20] Most notably, darobactin 22 (D22) shows significantly improved minimal inhibitory concentration (MIC) values against clinically relevant pathogens, such as clinical isolates of carbapenem-resistant *A. baumannii* (up to 32-fold) and *P. aeruginosa* (up to 4-fold). Single-particle cryo-EM structure elucidation explained the binding behavior of the most active new derivative compared to established DA and D9.

Results and Discussion

Five natural darobactins (DA to DE) were previously described.[10,19,21] In a recent work by our group, the non-natural derivatives D1 to D21 were produced, including a derivative in which the terminal phenylalanine (DA, $W_1N_2W_3S_4K_5S_6F_7$) is exchanged with a tryptophan (D9, $W_1N_2W_3S_4K_5S_6W_7$) as seen in Figure 1 a-b. The latter increases the antibacterial activity 2- to 8-fold against a large panel of pathogens.[19] The superior antibacterial activity of modified D9 compared to the native DA was the result of engineering the darobactin biosynthetic pathway and created a basis for new targeted structural improvements.[19] To determine if D9 shares the same binding site as DA, we first resolved the cryo-EM structure of the *E. coli* BAM complex bound to D9. While the overall average resolution was determined to be 3.4 Å, the local resolution the D9 estimated using Cryosparc revealed a resolution of 3.0 Å around binding region (Figure 1 c, d; Figure S 1 a-e; Table S 7). Binding to the β-barrel of the *E. coli* BAM complex was deciphered revealing high similarities to the binding of DA with the BAM complex shown in Figure 1 d in addition to the overlaid electron density of both compounds (Figure S 2).[15] D9 also binds to the β1 of the lateral gate of BamA with multiple hydrogen bonds in antiparallel β-sheet conformation, mimicking a β-sheet extension thereby blocking the functional region of BamA (Figure 1 c, d; Figure S 1 f, g).[12] Moreover, the N- and C-terminal ends of D9 are also tightly anchored to BamA via electrostatic and hydrophobic interactions (Figure 1 e, f). Furthermore, the distances for the establishment of hydrogen bonds of D9 to atoms of the binding site are well within the expected values and suggest that altered core peptides result in highly active darobactin derivatives such as the previously published darobactins DB, D4, D9, D11, D14, and D16.[19] Of note, D9 is more tightly bound to BamA, as shown by comparison with native DA (Figure 1 d, g, h), which could be explained by additional side chain and backbone interactions of L-tryptophan at position 1 with NH of I430, at position 6 with the carbonyl group of N422, and at position 7 with the carbonyl group of S425 (Figure 1 g, h). The novel hydrogen bond interactions and accompanied changes in D9 orientation are at the expense of L-asparagine hydrogen bond interaction on position 2 with the carbamoyl oxygen of the side chain ($O\delta_2$) of N427. Remarkably, the C-terminal carboxyl group of the terminal tryptophan forms a shorter hydrogen bond with $NH\delta_2$ of N422 in contrast to L-phenylalanine (Figure 1 g, h). Furthermore, the aromatic group of the C-terminal tryptophan of D9 is significantly extended into the hydrophobic pocket formed by residues F426 and V444, potentially generating strong hydrophobic interactions (Figure 1 e). As a consequence, this might improve the ability to seal the lateral gate compared to native DA. Taken together, the additional interaction sites of D9 result in tighter binding,[12] providing (1) structural evidence for the basis of 8-fold enhanced activity of D9 over DA and (2) proof of concept that additional chemical alterations on DA could further improve binding as well as biological activity.

For the design of new non-native darobactin derivatives, we considered currently available data, including relevant interactions of D9 (*WNWSKSW*) (Figure 1) and DA (*WNWSKSF*) with the BAM

complex and the bioactivity ranking of darobactin-containing extracts (DA to DE and D1 to D21), as well as the pure DA, DB and D9.[10,19,21] To ensure proper darobactin cyclization and ligand-receptor interaction (Figure 1 g, h), positions 1, 2 and 3 of darobactin remained unaltered. In particular, manipulations to amino acid position 2 were avoided as this has previously resulted in reduced production rates and decreased antibacterial activity.[19,21]

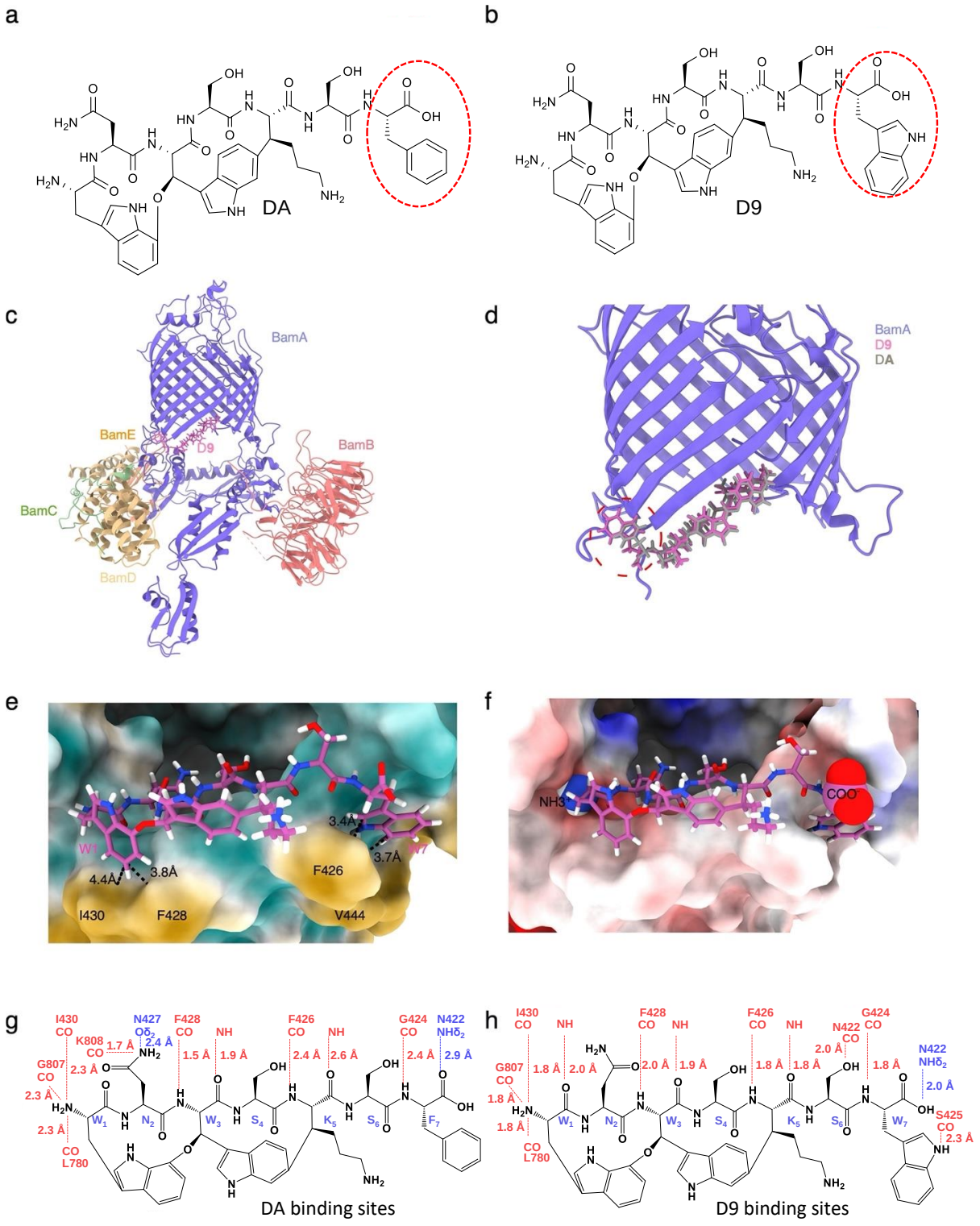

Figure 1. a-b, Structure formulae of DA and D9. The phenylalanine at the DA position 7 (F7) and the D9 tryptophan are indicated with a red dashed circle. c, Three-dimensional structure of the D9 bound BAM as resolved by cryo-EM. d, Magnified view of D9 bound to the surface of BamA and compared with DA. e-f, Magnified view of BAM-D9 showing the local (hydrophobic) environment (green = hydrophilic; orange = hydrophobic) in the binding pocket and the positive (blue) and negative (red) electrochemical potential in the BAM-D9 interaction area. g-h, 2D scheme of BamA-darobactin hydrogen bond

interactions. Canonical β-strand hydrogen bonds (red), side chain interactions (blue), and distance variations when comparing DA[12] (g) and D9 (h) were exhibited.

Consequently, the binding behavior of DA and D9 on *E. coli* BAM complex revealed positions 4, 6 and 7 as the most flexible positions for core sequence engineering, without deteriorating target binding (Figure 1 g, h). Therefore, we designed fifteen new derivatives with alterations in these positions (Table 1): The increased interaction of the C-terminal tryptophan at position 7 compared to smaller phenylalanine motivated the design of D26 to D28, which carry terminal L-histidines. The expectation was that the aromatic imidazole ring of histidine could form strong interactions with the adjacent amino acids of BamA, similar to the aromatic rings of L-phenylalanine or L-tryptophan (Figure 1 a, b).

The comparison of the three derivatives, together with native DB (*WNWTKRF*) and published non-natural derivative D16 (*WNWSKAF*)[19] enabled us to study the effect of changing L-serine at position 6 to either L-arginine or apolar L-alanine. Additionally, increased activity for DB and D4 (*WNWTKSF*) compared to DA motivated the exchange of L-serine to L-threonine at position 4.[19,21] The impressive improvement in activity due to replacing the terminal L-phenylalanine with an L-tryptophan led to the design of more derivatives derived from D9 with varying amino acids at positions 4 and 6. Consequently, derivatives D22 to D25 and D36 to D38 carrying L-arginine, L-histidine, L-serine, L-alanine, L-lysine or L-threonine on position 6 and L-threonine on position 4, as present in the more active DB,[21] were altered to evaluate the influence of each position. Replacing L-serine at position 4 with L-alanine, appeared to have less impact on activity, as observed in D14 (*WNWAKSF*),[19] possibly due to the lack of direct side chain interaction of position 4 (Figure 1 g, h). To further study the influence of position 4, D29 to D32 were designed, which correspond to related D22 to D24 and D6.

Notably, change of the amino acid in position 5 from L-lysine to L-arginine resulted in lower production yields and reduced activity, as shown by the extract activity in our previous publication and by analyzing pure DD (*WNWTRSF*) by Böhringer *et al.*[19,21] However, this data is contradictory to the darobactin binding mode determined in our cryo-EM experiments.[21] The backbone of L-lysine at position 5 is only involved in interaction with the BamA β1-strand on F426 with its carbonyl- and on A427 by the nitrogen of the amide group (Figure 1 g, h).[12] The L-lysine side chain with its terminal amino group is not involved in darobactin-BamA interaction, but is oriented into the exterior region of the β-barrel (Figure 1 d-f; Figure S 1 f). Kaur *et al.* found that the positive charge of lysine side chain interacts with phosphate moieties of cardiolipin and 1-palmitoyl-2-oleoyl-*sn*-glycero-3-phosphoglyc-erol,[12] which should also hold true for arginine. Accordingly, we were interested in the design of D39 with L-threonine at position 4, L-arginine at position 5 and 6 and L-tryptophan at position 7 (*WNWTRRW*). The designed darobactin core sequences encoding for D22 to D32 and D36 to D39 (Figure S 3) were generated by introducing point mutations via OE-PCR in pNOSO-*darABCDE*-9 (DSM 33802). A detailed

explanation can be found in the methods (Figure S 4; Table S 2). Subsequent mass spectrometry (MS) analysis (Table S 3; Figure S 5-36) and bioactivity ranking of the crude extracts for prioritization of the most active derivatives were performed as described in our previous publication, which led to the discovery of D9.[19] Different molecular ions observable in electrospray ionization (ESI) MS were used in combined extracted ion chromatograms (EIC) to obtain comparable data for the area under the curve (AUC), since introduction of basic amino acids shifted the most abundant ion species from the doubly charged to the triply charged species (Table 1). The activity screening clearly showed an improvement of antibacterial activity of all newly generated derivatives in comparison to DA and at least comparable activity to D9, except for derivatives exhibiting the terminal L-histidine (D26 to D28).

Table 4. Darobactins with modified core peptide sequences and activity screen against K. pneumoniae DSM-30104, P. aeruginosa PAO1, E. coli ATCC 25922 and A. baumannii DSM-30008. Changes in the core peptide sequence to the native DA sequence are shown in red. Relative production titers of D9 and of its derivatives with respect to DA based on crude extracts were calculated by comparing area under the curve (AUC) ratios of new derivatives relative to DA. The antimicrobial activity of each derivative-containing crude extract against tested pathogens is highlighted as a color code (bright green to dark green), depending on the highest dilution factor of standardized extract with respect to the assay volume [two-fold serial dilution from 1:15 (A) (concentration factor: 6.67x) to 1:3,840 (H) (concentration factor: 0.05x)] in which full growth inhibition was detected (compare to Groß et al.[19]). UHPLC-HRMS chromatograms and MS2 fragmentation pattern of produced darobactin derivatives are shown in Figure S 5-32 and Figure S 35-36, respectively. Derivatives D33 (WNWCKSW), D34

(WNWCKAW) and D35 (WQWTKAW) were designed but not generated due to purification issues of cysteine derivative D32 (D33, D34) or the expected low activity (D35).[21]

Darobactin	Core peptide	*K. pneumoniae* DSM-30104	*P. aeruginosa* PAO1	*E. coli* ATCC25922	*A. baumannii* DSM-30008	AUC ratio (derivative/ DA)
DA	W N W S K S F	0.83x	0.42x	0.83x	1.67x	1
D9	W N W S K S W	1.67x	3.34x	1.67x	0.83x	0.57
D22	W N W **T** K **R** W	0.83x	0.05x	0.42x	0.05x	0.73
D23	W N W **T** K **H** W	0.83x	0.11x	0.83x	0.11x	1.00
D24	W N W **T** K S W	0.83x	0.05x	0.83x	0.21x	0.96
D25	W N W **T** K **A** W	3.34x	0.11x	3.34x	0.42x	0.98
D26	W N W **T** K **R** H	6.67x				0.23
D27	W N W **T** K **A** H					0.81
D28	W N W **T** K S H	6.67x				0.86
D29	W N W **A** K **H** W	0.83x	0.21x	1.67x	0.42x	0.64
D30	W N W **A** K S W	1.67x	0.11x	0.83x	0.83x	0.75
D31	W N W **A** K **R** W	0.83x	0.05x	0.21x	0.05x	0.73
D32	W N W **C** K **R** W	0.83x	0.42x	0.42x	0.42x	0.04
D36	W N W **T** K **K** W	3.34x	0.05x	0.83x	0.11x	0.55
D37	W N W **S** K **T** W	1.67x	0.11x	0.42x	0.42x	0.71
D38	W N W **T** K **T** W	1.67x	0.11x	0.42x	0.42x	0.99
D39	W N W **T R R** W	0.42x	0.11x	0.42x	0.05x	0.96

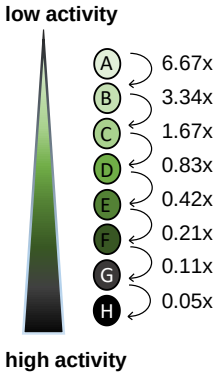

The exchange to L-histidine seems to abolish potency, which could be due to the slightly positive electro-chemical potential in the C-terminal binding area of BamA (Figure 1 f) and, in turn, may prevent histidine from binding into the hydrophobic binding pocket. Nevertheless, the activity of every other tested derivative with a terminal L-tryptophan is auspicious. Interestingly, activity testing indicated a strong effect elicited by changes at position 6, which is detectable when comparing activity data of D22 to D25 and D36. This effect was most pronounced in *A. baumannii* DSM-30008 and less obvious in *P. aeruginosa* due to generally higher potency. Overall, the SAR due to changes at position 6 in *E. coli* and *K. pneumoniae* was less obvious. Notably, the SAR of D37 and D38 suggests that *A. baumannii* is more sensitive to the modification of position 6, particularly when the residue is changed from the positively charged side chain of L-lysine or L-arginine. This could hint at more pathogen-specific interactions or other factors affecting the antibacterial potency of darobactins. Based on the direct comparison of D22 with D31 and D32, it can be concluded that changes on position 4 from L-threonine to L-alanine or extended L-cysteine residues as described previously,[19] have only minor effects on activity. NMR structure elucidation determined that the L-cysteine in these cases is connected via a disulfide bond to another L-cysteine and lactic acid (Figure S 76-85, Table S 13, S 14). Interestingly, D39, with L-arginine instead of L-lysine as a ring-forming amino acid exhibited stronger antibacterial activity.

This finding is contradictory to the 16-fold decrease in activity when comparing DA and DD,[19,21] but in line with predictions based on the expected binding mode (Figure 1 d, h), suggesting a different reason for the activity decrease of DD.[21] Our findings regarding SAR of crude extracts are summarized in Figure 2. While crude extract data should be taken with caution,[19] MIC assays done with purified darobactin derivatives were completely in line with extract data (see below).

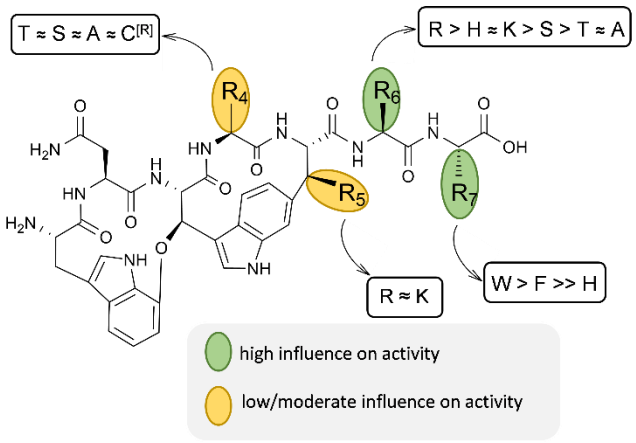

Figure 2. Summary of amino acid modifications and their influence on antibacterial activity. SAR study results in altered amino acids on position 4, 5, 6 and 7 of the heptapeptide. Tested amino acids are shown as one letter abbreviations (whereas $C^{[R]}$ indicates the L-cysteine adduct) and ordered depending on their antibacterial bioactivity against A. baumannii DSM-30008, based on a MIC assay using crude extracts (Table 1). "≈" comparable activity; ">" or "»" higher activity.

Another approach to darobactin modification is the altering of tryptophans e.g., through halogenation. The tryptophan indole ring positioning is integral for darobactin blocking of the β-barrel lateral gate.[12] We considered the possibility that halogenation of these essential elements could significantly change bioactivity. Five new halogenated derivatives of D9 were indeed produced through feeding (see SI) of halogenated L-tryptophans, two of them harboring 5-chloro- and three 6-fluoro-L-tryptophan (Figure S 37-40). However, the initial yields prohibited isolation of all derivatives. The highest yield derivative with 6-fluoro-L-tryptophan at position 3 of the core-peptide could be purified and its structure was confirmed via NMR spectroscopy (Figure S 86-90; Table S 15). The corresponding activity analysis of purified, single fluorinated derivatives D9-6F1 and D9-6F7 showed comparable activity to pure D9 with slightly improvedactivity against *E. coli* and *K. pneumoniae* and slightly diminished activity against *P. aeruginosa*. (Figure S 41). In general, modifications to darobactin amino acids, such as halogenation, expand the structural diversity spectrum of new darobactins, potentially influencing binding behavior and pharmacokinetic characteristics as known for fluoroquinolones.[22] This assessment, along with developing a workflow to improve the yield of halogenated darobactins, will be part of a separate study. Thus, for the current phase of this project, we chose to focus on purification and characterization of new non-halogenated derivatives with promising crude extract activity (Table 1, Figure 2).

To verify the promising activity data of crude extracts, certain derivatives with increased activity were selected for large-scale production and isolation. During the production optimization of D22, the commercially available *E. coli* BL21-Gold (DE3), engineered for reduced leaky expression (Agilent Technologies, California, USA), was evaluated and found to be favorable for production control of darobactins, due to their autotoxicity against the Gram-negative host. While there was no significant difference in D22 production titer when comparing *E. coli* BL21 (DE3) (10.5 (±1.0) mg/L) to *E. coli* BL21-Gold (DE3) (9.0 (±1.2) mg/L), we opted to use *E. coli* BL21-Gold (DE3). This allowed for a more controlled fermentation, and thus better reproducibility in contrast to significantly increased leaky expression in uninduced *E. coli* BL21 (DE3), as shown in Groß *et al.*[19] An optimized purification procedure utilized weak cation-exchange resin Dowex MAC-3 and ammonia elution instead of XAD16-N as previously published.[19] With this modified workflow, following an initial C18 flash chromatography step, we were able to reduce the purification effort of the darobactins to a single preparative C18 step that resulted in an increase in D22 yield from 0.8 mg/L culture to 3.0 to 3.7 mg/mL (3.8 to 4.6-fold). The detailed purification procedure can be found in the Supplementary Information.

Table 5. Antibacterial activity of pure darobactins: Compounds D22, D23, D31, D32, D36, D37 and D38 were tested in a MIC assay (in µg/mL) against clinically relevant Gram-negative pathogens. Superior activity of the new designed derivatives was analyzed by comparing them to DA data[19] as control.

Bacterial strains		MIC [µg/mL]							
		Darobactin							
		DA*	D22	D23	D31	D32	D36	D37	D38
A. baumannii	DSM-30007	16	2	4	2	1-2	2-4	16	8
	DSM-30008	4	0.25-0.5	1-2	0.5-1	1	0.5	4-8	4
	NCTC 13301 (MDR)	32-64	4-8	4-8	4-8	2-4	4-8	32-64	16-64
Citrobacter freundii	DSM-30039	1	1	2-4	1	2-4	4-8	4	4
E. coli	ATCC-25922	2	1	8	1	2	2-4	4-8	8
	BW25113	1-2	1	4	0.5-1	1	2-4	4-8	4-8
	JW0451-2 (Δ*acrB*)	0.5	0.25	0.5-1	0.125-0.5	1	0.5-1	1-2	1-2
	K12 Δ*tolC*	0.5	0.125	0.5-1	0.125-0.25	0.5-1	0.25-1	1-2	0.5-2
K. pneumonia	DSM-30104	2-4	2-4	4-8	2-4	8	16	16-32	16-32
Morganella morganii	DSM-30164	> 64	16	> 64	16	> 64	32-64	> 64	> 64
P. mirabilis	DSM-4479	> 64	64	> 64	> 64	> 64	> 64	> 64	> 64
Proteus vulgaris	DSM-2140	16	32	> 64	32-64	> 64	> 64	> 64	> 64
P. aeruginosa	PAO1 (DSM-22644)	0.5-1	0.25	1	0.25	2	0.25-0.5	2	1
	PA14 (DSM-19882)	16	2-4	4	2-4	8	2-4	8-16	8-16
	PA14 Δ*mexAB*	4	1-2	2-4	1-2	4	2-4	8-16	8
	DSM-1117	16	4-8	64	4-8	16	32	32	16-32
	NCTC 13437 (MDR)	16-32	2-4	16	2-4	16	4	32	16
S. marcescens	DSM-30121	> 64	32-64	> 64	16-32	> 64	> 64	> 64	> 64
		IC_{50} [µg/mL]							
HepG2		> 37	> 37	> 37	> 37	> 37	> 37	> 37	> 37

The purified darobactins D22, D23, D31, D32, D36, D37 and D38 were structurally verified via NMR (Figure S 46-75, Table S 7-12) and tested against a panel of different Gram-negative pathogens including *A. baumannii, E. coli, K. pneumoniae,* and *P. aeruginosa.* The activity was compared to previously published DA activity data[10] and the crude extract data shown above (Table 1). Darobactins are not active against pathogens with phylogenetically distant BamA gene loci, like *Proteus mirabilis* or *Serratia marcescens* (Table 2; Figure S 42), as expected.[12] However, many new derivatives depict promising antibacterial activity against the majority of tested pathogens (Table 2) and are in line with the previously generated MIC data of crude extracts (Table 1). Compounds D22 and D31 stand out by demonstrating up to an eight-fold increased activity against the panel of pathogens compared to native DA. Additionally, there was up to a two-fold improved activity compared to D9, most interestingly against *Acinetobacter* strains.[19] Moreover, direct comparison of D22, D31 and D32 emphasizes the minor influence of manipulations made in core sequence corresponding to amino acid position 4. The substantial influence of changes to position 6 is reflected by comparing the differing activities of D22 and D38 in addition to the activities of D9[19] and D37. Changing L-serine to L-threonine or L-arginine to

L-threonine decreased bactericidal activity significantly (Table 2), whereas a basic side chain can enhance the activity demonstrated by comparison of DA with D36. However, these effects are generally species-specific, most notably for the *K. pneumoniae* strains. Furthermore, no cytotoxicity was observed against the human cell line HepG2 as published for DA and D9.[10,19]

To investigate the SAR of D22, which exhibited the best activity profile of all known darobactins,[10,19,21] a cryo-EM co-structure determination of D22 bound BAM complex was initiated to study the potentially changed mode of binding (MoB). The structural basis of superior activity of D22 was analyzed by single-particle co-structure elucidation via cryo-EM of *E. coli* BAM-D22 complex (Figure 3) and compared to the co-structure of BAM-D9 (Figure 1). The cryo-EM structure of the *E. coli* BAM complex was resolved with an overall resolution of 3.0 Å (Figure 3 a; Figure S 43; Table S 6). The MoB of D22 is comparable to D9, but with N_2 and W_7 conformational changes, which is probably caused by substitution of T_4 and R_6, respectively (Figure 3 b). The C-terminal tryptophan is pushed deeper into the hydrophobic binding pocket and forms a closer hydrogen bond with the nitrogen of the indole ring and S425, compared to BamA-D9 (Figure 3 b-e; Figure 1 h). N422 of BamA still pairs with the C-terminal D22 carbonyl group via $NH\delta_2$ side chain interaction. Moreover, N422 forms one additional bond with the guanidine group of R_6, probably causing the tighter seal of C-terminal tryptophan into the binding pocket. A side chain interaction of Q441 from β-strand 2 is formed due to its side chain remodeling (Figure 3 e).

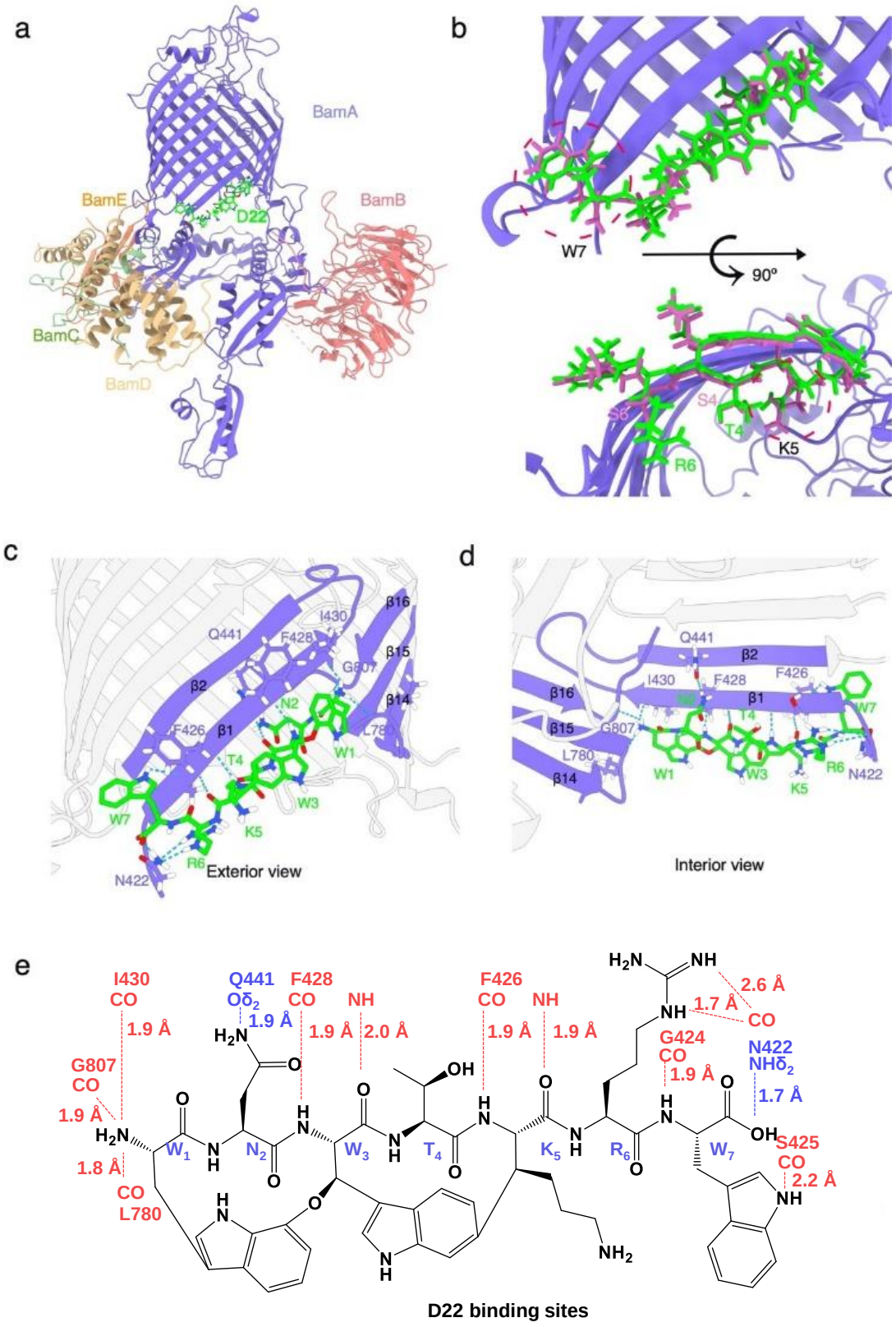

Figure 3. a, Cryo-EM structure of the D22 bound to the BAM complex. b, Magnified view of D22 (lime) bound to the surface of BamA compared to D9 (pink). The positions with variable conformations were indicated in red dashed circle. The variable amino acids at the same position were also indicated with residue name in different colors. c-d, Magnified view of BamA-D22 from exterior and interior views. Amino acids involved in hydrogen bond interaction are displayed as sticks and indicated by one letter abbreviation. Green dashes highlight hydrogen bond pairs. e, 2D scheme of BamA-D22 hydrogen bond interactions. Canonical ß-strand hydrogen bonds are shown in red and side chain interactions in blue color.

These conformational changes are likely to be responsible for increased binding affinity and consequently improved bioactivity at least in *A. baumannii* strains. Furthermore, the significantly changed interaction and orientation at the C-terminal end is not at the expense of one of three N-terminal hydrogen bond interactions, maintaining proper closing of the lateral gate of BAM (Figure 3 c, d). The fact that T_4 is not involved in direct binding with BamA β-barrels makes this residue attractive for evaluating other amino acids or other moieties for improving pharmacological properties.

Taken together, the different darobactin-BamA binding interactions of DA, D9, and D22 likely reveal the structural basis for enhanced activity of engineered darobactins, which are more closely paired with BamA to mimic the β-sheet prolongation and to lock the BAM complex in the inactive state by sealing the lateral gate tightly (Figure 1, 3).[14] These structure-activity based findings are reinforced by the results of analyzing the different binding kinetics for DA and D9 versus D22 on purified *E. coli* BamA revealing K_D values of 0.278 µM, 0.3 µM and 0.159 µM, respectively (Figure S 44). Nevertheless, more extensive activity profiling assays must be performed to generate a more valid correlation between the increased activity of D22 and the structural changes compared to DA and D9.

As D22 distinguishes itself by its superior activity, especially against tested *Acinetobacter* strains (Table 2), this derivative was tested in a MIC assay using hard-to-treat clinical isolates of carbapenem-resistant *Acinetobacter baumannii* (CRAB), where most of the commonly used antibiotics are not active (Table S 4). Here, the activities of DA, D9 and D22 were compared to colistin (COL), the antibiotic of last resort to treat infections caused by CRAB, which can cause nephrotoxicity.[23]

Table 6. Bioactivity of DA, D9 and D22 against clinical CRAB isolates compared with colistin (COL). MIC in µg/mL.

		MIC [µg/mL]			
		DA	**D9**	**D22**	**COL**
A. baumannii	038 (OXA-23)	16	4	0.5	0.25
	045 (OXA-58)	16-32	8	0.5	0.125
	046 (OXA-40)	8-16	4	0.5	0.25
	047 (OXA-235)	16-32	4-8	0.25	0.25
	070 (NDM-1)	8	2	0.0625	0.125
	054 (OXA-51-ISAba1)	16-32	8	0.125	0.125

Intriguingly, D22 was found to be highly active against all nine tested clinical CRAB strains (MICs 0.06 to 0.5 µg/mL) (Table 3), displaying significantly higher potency than the previous frontrunner D9 (and DA) and nearly equipotent antibacterial activity with colistin plus showing much better activity than other clinically used antibiotics (Table S 4).[24] In particular, the *in vitro* potency of D22 against CRAB was at least one order of magnitude better than for D9. This marked improvement is even more impressive as D9 displays already four-fold improved activity compared to native DA.

In addition, time-kill kinetics of DA and D22 at 2x, 4x and 8x MIC in *E. coli* MG1655 (Figure 4 a, b) and in *A. baumannii* NCTC13301 (Figure 4 c, d) were assessed over a period of 24 hours. D22 shows rapid bacterial killing of *E. coli* MG1655 at 4x and 8x MIC after an early static phase of up to 2 hours followed by bactericidal activity with more than 3-log killing exhibited in the reduced colony-forming units (CFU/mL) within 2 to 4 h. The observed initial bacteriostatic effect can possibly be explained by Ritzmann *et al.*, which demonstrated that binding of darobactin on the lateral gate leads to an increased stability by "freezing" BamA and consequently no immediate bactericidal effect.[14] However, DA and D22 at 2x, 4x and 8x MIC acted bactericidal over the first 8 h in time-kill experiments using *E. coli* MG1655, and the extent of bactericidal activity was concentration-dependent. Nevertheless, re-growth of bacteria was observed at 2x and 4x MIC conditions after 24 h, while this was not the case at 8x MIC (MIC values reported for DA and D22 were 2 µg/mL and 1 µg/mL, respectively). Imai *et al.* did not report re-growth of *E. coli* after DA treatment, however, the timeframe in their reported experiment was limited to 8 h with 16x MIC, making direct comparison challenging.[10] They also determined a minimum bactericidal concentration (MBC) of 8 µg/mL in *E. coli*, which is fully in line with our findings for DA and D22 having MBCs of 16 and 8 µg/mL, respectively.[10] Encouragingly, upon repeating the time-kill experiment using high inoculum conditions (~$5x10^8$ CFU/mL) we were able to show that surviving bacteria are likely persisters[25] and did not gain resistance, as representative colonies from this experiment showed no MIC shifts (Table S 5). In a comparison of time-kill kinetics of both darobactins in *A. baumannii* NCTC13301, D22 shows its clear superiority over DA (Figure 4 c, d). For the latter, we determined a lasting bacteriostatic effect at 2x MIC, and re-growth was observed at both initially bactericidal concentrations (4x and 8x MIC). In contrast, D22 showed bactericidal activity and concentrations as low as 4x MIC and fully prevented re-growth at 24 h post-treatment (MBC of 32 µg/mL).

Considering that *A. baumannii* easily acquires resistance, making CRAB a WHO priority one pathogen for antibiotic development,[8,26] the results of D22 are highly promising. It displays equipotent *in vitro* activity with colistin against clinical CRAB isolates, while colistin exhibits severe side effects. D22 did, however, not show toxic effects tested *in vitro* with HepG2 cells (Table 2) and *in vivo* using the highly sensitive zebrafish larvae model up to 500 µg/mL (Figure S 45), which emphasizes the potential for application and encourages further development towards proof of concept in humans.

Conclusion

Preceding darobactin SAR studies focused on native darobactins[16,21] or were based upon observations from them.[19] Elucidation of the MoB of DA and D9 to BamA, combined with structural data of recently published darobactins,[12,14,19,21] enabled a more guided approach, in which we constructed twenty new derivatives, including twelve derivatives with terminal L-tryptophan exhibiting similar or higher activity

than DA (Figure S 3). According to our findings, structural changes at position 4 appears to have only a minor influence, while positions 6 and 7, necessary for interactions with β-hairpins of BamA, seem to have a major influence on activity and could be used as a potential starting point for improvement of pharmaceutical properties through structural changes. The most promising compound developed to date, based on our SAR study is the biosynthetically engineered new darobactin D22, which surpasses the antibacterial activity of all identified native darobactins. This is remarkable, as natural products are produced in co-evolution over millions of years, resulting in structural diversity and target specificity for fungi, eukaryotes and bacteria.[27]

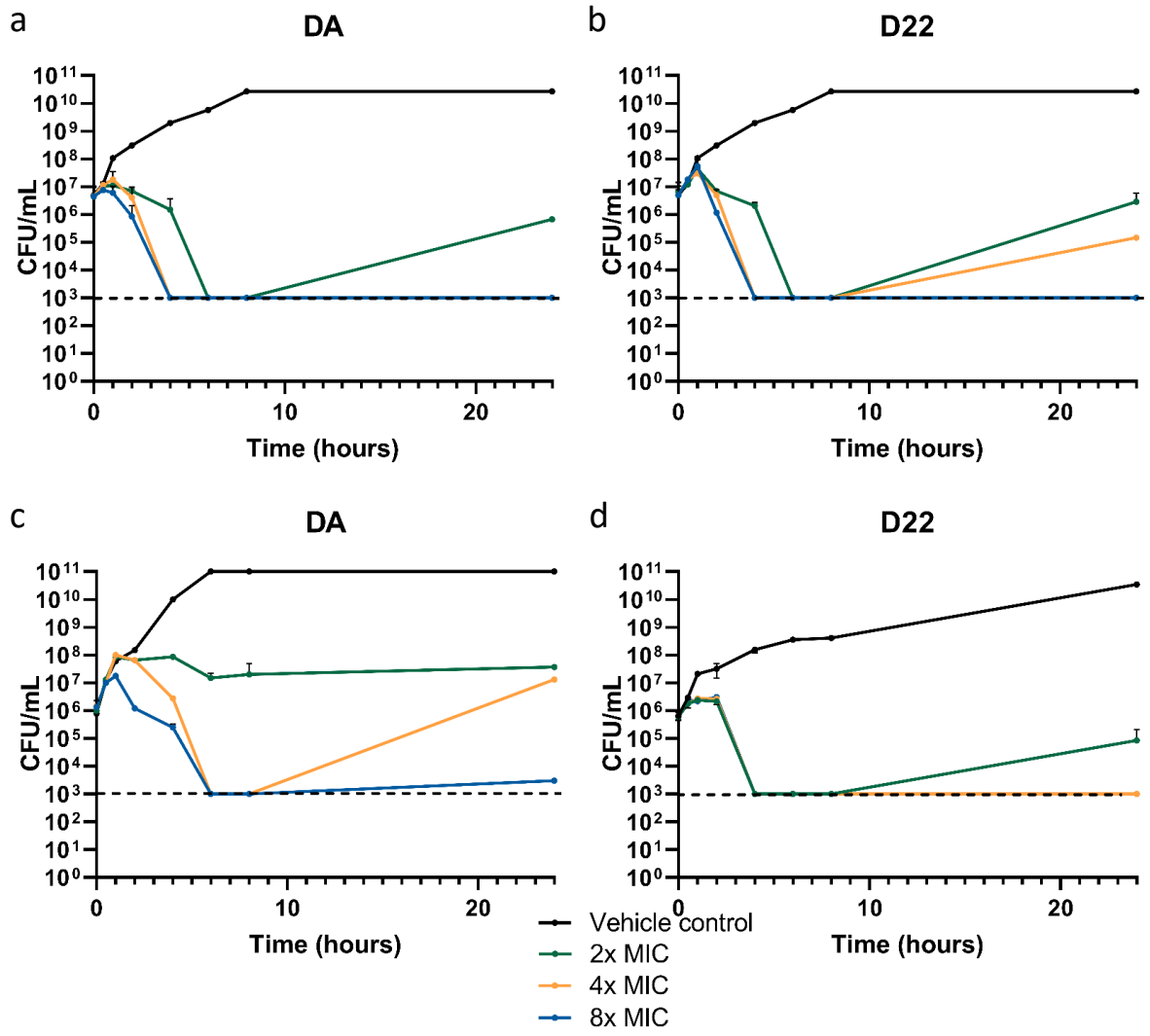

Figure 4. Time-kill curves (TKCs) support bactericidal MoA of darobactins. a-b, TKC of *E. coli* MG1655 with DA and D22 using 2x, 4x and 8x MIC. c-d, TKC of *A. baumannii* NCTC13301 with DA and D22 using 2x, 4x and 8x MIC. Data are shown as mean ± SD (n = 3).

The engineered derivative D22 is highly active against a broad range of Gram-negative bacterial pathogens demonstrating superiority even to the previous, biosynthetically engineered frontrunner D9, which already surpassed the activity of originally reported native DA.[19] In particular, D22 displays bactericidal activity against hard-to-treat CRAB and is equipotent to the highly active, yet nephrotoxic, last resort antibiotic colistin. Furthermore, D22 was shown to be non-toxic in initial assays *in vitro* (HepG2) and *in vivo* (zebrafish larvae). Further studies will explore the optimized effects of D22 regarding mechanistic, kinetic, and energetic properties, e.g. regarding the linker region and the eight β-hairpins, as detailed by Ritzmann *et al.*[14] for DA.

Future studies should also include a comparison to the structurally variable BAM complex of *A. baumannii* strains, of which a co-structure with darobactins has not yet been solved. However, our activity and toxicity data of D22 are encouraging to advance into further preclinical studies. While currently established protocols for cultivation in *E. coli* are favorable for fast and robust generation of novel, even halogenated, darobactins in quantities suitable for research and development purposes,[16,19] they are hard-pressed to satisfy supply demands for such future studies, because of low self-resistance of the Gram-negative heterologous host *E. coli.* Changing the heterologous producer to a Gram-positive strain such as *Bacillus subtilis*, which has been successfully applied in industrial fermentations, might enable higher darobactin titers. Alternatively, very recently published total syntheses reported for DA may be applicable but currently suffer from yield issues as well.[17,18]

To summarize, our SAR approach presented structural knowledge about the MoB of the darobactins and resulted in novel derivatives with up to 32-fold increased activity against CRAB, compared to the most potent known derivative D9.[19] The new, distinguished D22 was found to be comparable to clinically used antibiotics in its activity against certain Gram-negative pathogens. Consequently, our approach led to a new frontrunner molecule of darobactins showing more favorable antibacterial activity. Compound D22 is particularly active against critically prioritized Gram-negative pathogens encouraging further preclinical studies with this highly promising scaffold to hopefully and eventually achieve proof of efficacy in humans for this exciting and promising molecule class.

Acknowledgements

We thank Alexandra Amann and Viktoria George for performing the MIC assays and Dr. F. P. Jake Haeckl, Dr. Daniel Krug, Dr. Peter Sullivan and Dr. Jordan Espenshade for helpful proofreading. CryoEM optimizations and data collection were performed at the Cryo-EM Facility at CSSB Hamburg (supported by the University of Hamburg, the University Medical Center Hamburg–Eppendorf and DFG grant

numbers INST152/772-1, 152/774-1, 152/775-1, 152/776-1 and 152/777-1 FUGG.). High performance computing was possible through access to the HPC at DESY/Hamburg (Germany). This project was supported by funds available to T.C.M. through the Behörde für Wissenschaft, Forschung und Gleichstellung of the city of Hamburg at the Institute of Structural and Systems Biology at the University Medical Center Hamburg–Eppendorf (UKE), Deutsches Elektronen Synchrotron (DESY). We specially thank Dr. Rory Hennell James for giving suggestions in ligands modeling. We also thank Dr. Stephan Niebling from EMBL at CSSB for help with the ITC data analysis and Prof. Dr. Sebastian Hiller for supplying the expression plasmid for BamABCDE.

References

1 a) E. D. Brown and G. D. Wright, *Nature*, 2016, **529**, 336; b) M. McKenna, *Nature*, 2013, **499**, 394;

2 K. Lewis, *Cell*, 2020, **181**, 29.

3 C. J. L. Murray, K. S. Ikuta, F. Sharara, L. Swetschinski, G. Robles Aguilar, A. Gray, C. Han, C. Bisignano, P. Rao, E. Wool, S. C. Johnson, A. J. Browne, M. G. Chipeta, F. Fell, S. Hackett, G. Haines-Woodhouse, B. H. Kashef Hamadani, E. A. P. Kumaran, B. McManigal, R. Agarwal, S. Akech, S. Albertson, J. Amuasi, J. Andrews, A. Aravkin, E. Ashley, F. Bailey, S. Baker, B. Basnyat, A. Bekker, R. Bender, A. Bethou, J. Bielicki, S. Boonkasidecha, J. Bukosia, C. Carvalheiro, C. Castañeda-Orjuela, V. Chansamouth, S. Chaurasia, S. Chiurchiù, F. Chowdhury, A. J. Cook, B. Cooper, T. R. Cressey, E. Criollo-Mora, M. Cunningham, S. Darboe, N. P. J. Day, M. de Luca, K. Dokova, A. Dramowski, S. J. Dunachie, T. Eckmanns, D. Eibach, A. Emami, N. Feasey, N. Fisher-Pearson, K. Forrest, D. Garrett, P. Gastmeier, A. Z. Giref, R. C. Greer, V. Gupta, S. Haller, A. Haselbeck, S. I. Hay, M. Holm, S. Hopkins, K. C. Iregbu, J. Jacobs, D. Jarovsky, F. Javanmardi, M. Khorana, N. Kissoon, E. Kobeissi, T. Kostyanev, F. Krapp, R. Krumkamp, A. Kumar, H. H. Kyu, C. Lim, D. Limmathurotsakul, M. J. Loftus, M. Lunn, J. Ma, N. Mturi, T. Munera-Huertas, P. Musicha, M. M. Mussi-Pinhata, T. Nakamura, R. Nanavati, S. Nangia, P. Newton, C. Ngoun, A. Novotney, D. Nwakanma, C. W. Obiero, A. Olivas-Martinez, P. Olliaro, E. Ooko, E. Ortiz-Brizuela, A. Y. Peleg, C. Perrone, N. Plakkal, A. Ponce-de-Leon, M. Raad, T. Ramdin, A. Riddell, T. Roberts, J. V. Robotham, A. Roca, K. E. Rudd, N. Russell, J. Schnall, J. A. G. Scott, M. Shivamallappa, J. Sifuentes-Osornio, N. Steenkeste, A. J. Stewardson, T. Stoeva, N. Tasak, A. Thaiprakong, G. Thwaites, C. Turner, P. Turner, H. R. van Doorn, S. Velaphi, A. Vongpradith, H. Vu, T. Walsh, S. Waner, T. Wangrangsimakul, T. Wozniak, P. Zheng, B. Sartorius, A. D. Lopez, A. Stergachis, C. Moore, C. Dolecek and M. Naghavi, *Lancet*, 2022, **399**, 629.

4 a) B. Gonzalez-Zorn, *Clin. Microbiol. Infect.*, 2021, **27**, 646; b) B. J. Langford, M. So, S. Raybardhan, V. Leung, D. Westwood, D. R. MacFadden, J.-P. R. Soucy and N. Daneman, *Clin. Microbiol. Infect.*, 2020, **26**, 1622; c) S. Perez, G. K. Innes, M. S. Walters, J. Mehr, J. Arias, R. Greeley and D. Chew, *Morb. Mortal. Wkly. Rep.*, 2020, **69**, 1827; d) WHO Coronavirus Disease (COVID-19) Dashboard | WHO Coronavirus Disease (COVID-19) Dashboard, https://covid19.who.int/, (accessed 2020);

5 Global Antimicrobial Surveillance System (GLASS) Report 2016-2017, https://apps.who.int/iris/bitstream/handle/10665/279656/9789241515061-eng.pdf?ua=1, (accessed 27 November 2020).

6 a) E. Sharifipour, S. Shams, M. Esmkhani, J. Khodadadi, R. Fotouhi-Ardakani, A. Koohpaei, Z. Doosti and S. EJ Golzari, *BMC Infect. Dis.*, 2020, **20**, 646; b) C. Ayoub Moubareck and D. Hammoudi Halat, *Front. Cell. Infect. Microbiol.*, 2022, **12**, 823626; c) M. Karataş, M. Yaşar-Duman, A. Tünger, F. Çilli, Ş. Aydemir and V. Özenci, *Ann. Clin. Microbiol. Antimicrob.*, 2021, **20**, 51; d) J. Armstrong, G. Hickey, M. Diekhans, I. T. Fiddes, A. M. Novak, A. Deran, Q. Fang, D. Xie, S. Feng, J. Stiller, D. Genereux, J. Johnson, V. D. Marinescu, J. Alföldi, R. S. Harris, K. Lindblad-Toh, D. Haussler, E. Karlsson, E. D. Jarvis, G. Zhang and B. Paten, *Nature*, 2020, **587**, 246; e) G. Zhang, C. Hu, L. Luo, F. Fang, Y. Chen, J. Li, Z. Peng and H. Pan, *J. Clin. Virol.*, 2020, **127**, 104364; f) R. Kousovista, C. Athanasiou, K. Liaskonis, O. Ivopoulou, G. Ismailos and V. Karalis, *Pathogens*, 2021, **10**, 480; g) E. Dong, H. Du and L. Gardner, *Lancet Infect Dis*, 2020, **20**, 533;

7 a) J. A. Al-Tawfiq, H. Momattin, A. Y. Al-Ali, K. Eljaaly, R. Tirupathi, M. B. Haradwala, S. Areti, S. Alhumaid, A. A. Rabaan, A. Al Mutair and P. Schlagenhauf, *Infection*, 2021, **50**, 553; b) World Health Organization, *2019 Antibacterial agents in clinical development. an analysis of the antibacterial clinical development pipeline*, 2019;

8 E. Tacconelli, E. Carrara, A. Savoldi, S. Harbarth, M. Mendelson, D. L. Monnet, C. Pulcini, G. Kahlmeter, J. Kluytmans, Y. Carmeli, M. Ouellette, K. Outterson, J. Patel, M. Cavaleri, E. M. Cox, C. R. Houchens, M. L. Grayson, P. Hansen, N. Singh, U. Theuretzbacher, N. Magrini, A. O. Aboderin, S. S. Al-Abri, N. Awang Jalil, N. Benzonana, S. Bhattacharya, A. J. Brink, F. R. Burkert, O. Cars, G. Cornaglia, O. J. Dyar, A. W. Friedrich, A. C. Gales, S. Gandra, C. G. Giske, D. A. Goff, H. Goossens, T. Gottlieb, M. Guzman Blanco, W. Hryniewicz, D. Kattula, T. Jinks, S. S. Kanj, L. Kerr, M.-P. Kieny, Y. S. Kim, R. S. Kozlov, J. Labarca, R. Laxminarayan, K. Leder, L. Leibovici, G. Levy-Hara, J. Littman, S. Malhotra-Kumar, V. Manchanda, L. Moja, B. Ndoye, A. Pan, D. L. Paterson, M. Paul, H. Qiu, P. Ramon-Pardo, J. Rodríguez-Baño, M. Sanguinetti, S. Sengupta, M. Sharland, M. Si-Mehand, L. L. Silver, W. Song, M. Steinbakk, J. Thomsen, G. E. Thwaites, J. W. M. van der Meer, N. van Kinh, S. Vega, M. V. Villegas, A. Wechsler-Fördös, H. F. L. Wertheim, E. Wesangula, N. Woodford, F. O. Yilmaz and A. Zorzet, *Lancet Infect. Dis.*, 2018, **18**, 318.

9 a) L. Pantel, T. Florin, M. Dobosz-Bartoszek, E. Racine, M. Sarciaux, M. Serri, J. Houard, J.-M. Campagne, R. M. de Figueiredo, C. Midrier, S. Gaudriault, A. Givaudan, A. Lanois, S. Forst, A. Aumelas, C. Cotteaux-Lautard, J.-M. Bolla, C. Vingsbo Lundberg, D. L. Huseby, D. Hughes, P. Villain-Guillot, A. S. Mankin, Y. S. Polikanov and M. Gualtieri, *Mol. Cell*, 2018, **70**, 83; b) E. Racine, P. Nordmann, L. Pantel, M. Sarciaux, M. Serri, J. Houard, P. Villain-Guillot, A. Demords, C. Vingsbo Lundberg and M. Gualtieri, *Antimicrob. Agents Chemother.*, 2018, **62**, e01016; c) M. Sarciaux, L. Pantel, C. Midrier, M. Serri, C. Gerber, R. Marcia de Figueiredo, J.-M. Campagne, P. Villain-Guillot, M. Gualtieri and E. Racine, *J Med Pharm Chem*, 2018, **61**, 7814;

10 Y. Imai, K. J. Meyer, A. Iinishi, Q. Favre-Godal, R. Green, S. Manuse, M. Caboni, M. Mori, S. Niles, M. Ghiglieri, C. Honrao, X. Ma, J. Guo, A. Makriyannis, L. Linares-Otoya, N. Böhringer, Z. G. Wuisan, H. Kaur, R. Wu, A. Mateus, A. Typas, M. M. Savitski, J. L. Espinoza, A. O'Rourke, K. E. Nelson, S. Hiller, N. Noinaj, T. F. Schäberle, A. D'Onofrio and K. Lewis, *Nature*, 2019, **576**, 459.

11 Z. Wang, B. Koirala, Y. Hernandez, M. Zimmerman, S. Park, D. S. Perlin and S. F. Brady, *Nature*, 2022, **601**, 606.

12 H. Kaur, R. P. Jakob, J. K. Marzinek, R. Green, Y. Imai, J. R. Bolla, E. Agustoni, C. V. Robinson, P. J. Bond, K. Lewis, T. Maier and S. Hiller, *Nature*, 2021, **593**, 125.

13 A. Konovalova, D. E. Kahne and T. J. Silhavy, *Annu. Rev. Microbiol.*, 2017, **71**, 539.

14 N. Ritzmann, S. Manioglu, S. Hiller and D. J. Müller, *Structure*, 2022, **30**, 350.

15 S. S. Walker and T. A. Black, *Drug Discov. Today*, 2021, **26**, 2152.

16 Z. G. Wuisan, I. D. M. Kresna, N. Böhringer, K. Lewis and T. F. Schäberle, *Metab. Eng.*, 2021, **66**, 123.

17 Y.-C. Lin, F. Schneider, K. J. Eberle, D. Chiodi, H. Nakamura, S. H. Reisberg, J. Chen, M. Saito and P. S. Baran, *J. Am. Chem. Soc.*, 2022, **144**, 14458.

18 M. Nesic, D. B. Ryffel, J. Maturano, M. Shevlin, S. R. Pollack, D. R. Gauthier, P. Trigo-Mouriño, L.-K. Zhang, D. M. Schultz, J. M. McCabe Dunn, L.-C. Campeau, N. R. Patel, D. A. Petrone and D. Sarlah, *J. Am. Chem. Soc.*, 2022, **144**, 14026.

19 S. Groß, F. Panter, D. Pogorevc, C. E. Seyfert, S. Deckarm, C. D. Bader, J. Herrmann and R. Müller, *Chem. Sci.*, 2021, **12**, 11882.

20 S. Guo, S. Wang, S. Ma, Z. Deng, W. Ding and Q. Zhang, *Nat Commun*, 2022, **13**, 2361.

21 N. Böhringer, R. Green, Y. Liu, U. Mettal, M. Marner, S. M. Modaresi, R. P. Jakob, Z. G. Wuisan, T. Maier, A. Iinishi, S. Hiller, K. Lewis and T. F. Schäberle, *Microbiol Spectr*, 2021, **9**, e0153521.

22 F. J. Candel and M. Peñuelas, *Drug Des. Devel. Ther.*, 2017, **11**, 881.

23 a) L. S. Elias, D. Konzen, J. M. Krebs and A. P. Zavascki, *J. Antimicrob. Chemother.*, 2010, **65**, 2231; b) A. Ordooei Javan, S. Shokouhi and Z. Sahraei, *Eur. J. Clin. Pharmacol.*, 2015, **71**, 801;

24 a) M. H.-Y. Wong, B. K.-W. Chan, E. W.-C. Chan and S. Chen, *Front. Microbiol.*, 2019, **10**, 2809; b) B.-C. Jeon, S. H. Jeong, I. K. Bae, S. B. Kwon, K. Lee, D. Young, J. H. Lee, J. S. Song and S. H. Lee, *J.*

Clin. Microbiol., 2005, **43**, 2241; c) R. Zarrilli, D. Vitale, A. Di Popolo, M. Bagattini, Z. Daoud, A. U. Khan, C. Afif and M. Triassi, *J. Antimicrob. Chemother.*, 2008, **52**, 4115; d) J. Koirala, I. Tyagi, L. Guntupalli, S. Koirala, U. Chapagain, C. Quarshie, S. Akram, V. Sundareshan, S. Koirala, J. Lawhorn, Y. Doi and M. Olson, *Diagn. Microbiol. Infect. Dis.*, 2020, **97**, 114999; e) P. G. Higgins, F. J. Pérez-Llarena, E. Zander, A. Fernández, G. Bou and H. Seifert, *J. Antimicrob. Chemother.*, 2013, **57**, 2121; f) Y. Chen, Z. Zhou, Y. Jiang and Y. Yu, *J. Antimicrob. Chemother.*, 2011, **66**, 1255;

25 N. Q. Balaban, S. Helaine, K. Lewis, M. Ackermann, B. Aldridge, D. I. Andersson, M. P. Brynildsen, D. Bumann, A. Camilli, J. J. Collins, C. Dehio, S. Fortune, J.-M. Ghigo, W.-D. Hardt, A. Harms, M. Heinemann, D. T. Hung, U. Jenal, B. R. Levin, J. Michiels, G. Storz, M.-W. Tan, T. Tenson, L. van Melderen and A. Zinkernagel, *Nat Rev Microbiol*, 2019, **17**, 441.

26 M. R. Galac, E. Snesrud, F. Lebreton, J. Stam, M. Julius, A. C. Ong, R. Maybank, A. R. Jones, Y. I. Kwak, K. Hinkle, P. E. Waterman, E. P. Lesho, J. W. Bennett and P. Mc Gann, *J. Antimicrob. Chemother.*, 2020, **64**, e00840.

27 a) M. I. Hutchings, A. W. Truman and B. Wilkinson, *Curr. Opin. Microbiol.*, 2019, **51**, 72; b) G. D. Wright, *Nat. Prod. Rep.*, 2017, **34**, 694;

3.2 Supporting information

Darobactins Exhibiting Superior Antibiotic Activity by Cryo-EM Structure Guided Biosynthetic Engineering

Previously published in:

Carsten E. Seyfert[+ [a] [b]], Christoph Porten[+ [a] [b]], Biao Yuan[+[c] [d]], Selina Deckarm[+ [a] [b]], Fabian Panter[[a] [b]], Chantal D. Bader[[a] [b]], Janetta Coetzee[[a] [b]], Felix Deschner[[a] [b]], Kamaleddin H. M. E. Tehrani[[a] [b]], Paul G. Higgins[[f] [g]], Harald Seifert[[f] [g]], Thomas Marlovits* [[c] [d] [e]], Jennifer Herrmann*[[a] [b]] and Rolf Müller*[[a] [b]]

Angew. Chem. Int. Ed. Engl. 2022 October 29; **62** (2): e202214094

DOI: 10.1002/anie.202214094

Affilitation:

[a] Microbial Natural Products Helmholtz Institute for Pharmaceutical Research Saarland (HIPS), Helmholtz Centre for Infection Research (HZI) and Department of Pharmacy at Saarland University Campus Building E8.1, 66123 Saarbrücken (Germany) E-mail: rolf.mueller@helmholtz-hips.de; jennifer.herrmann@helmholtz-hips.de

[b] German Centre for Infection Research (DZIF), partnersite Hannover-Braunschweig

[c] University Medical Center Hamburg-Eppendorf (UKE), Institute of Structural and Systems BiologyNotkestraße 85, Building 15, 22607 Hamburg (Germany); E-mail: thomas.marlovits@cssb-hamburg.de

[d] Centre for Structural Systems Biology (CSSB), Hamburg (Germany)

[e] Deutsches Elektronen-Synchrotron Zentrum (DESY), Hamburg (Germany)

[f] Microbiology, Immunology and Hygiene, Faculty of Medicine and University Hospital Cologne, University of Cologne, Cologne (Germany)

[g] German Center for Infection Research (DZIF), partner site Bonn-Cologne (Germany)

[+]These authors contributed equally; *corresponding authors

The printed version of the Supporting Information does not contain data that cannot be visualized satisfactorily on paper. To access this data please refer to the enclosed storage medium or the on-line version of this research paper.

3.2.1 Methods

1. In silico design and generation of novel darobactin derivatives by overlap-extension polymerase chain reaction

Due to time and cost reduction, the generation of new derivatives was performed by insertion of point mutations into *darA* gene in three independent polymerase chain reactions (PCRs) (Figure S 4). In our approach, four different primers, named pr1dar_fw, pr2darXX_rv, pr3dartrp/his_fw and pr4dar_rv, were designed to generate one new darobactin derivative. Except of primer pr2darXX_rv (where XX stands for appropriate derivative, Table S 1), all primers can be re-used no matter which derivative is produced. Primer pr1dar_fw binds to a region located in the T7 lac promoter. Primer variants of pr2darXX_rv and primer pr3dartrp/his_fw are binding in the core region of *darA* and carry an overlapping region of 13 base pairs. Primer pr4dar_rv is binding in front of the termination region on the end of the intergenic region between *darA* and *darB* (Figure S 4). As depicted in Figure S 4, PCR reaction I with pr1dar_fw and pr2dar22_rv and PCR reaction II with pr3dartrp/his_fw and pr4dar_rv were performed in parallel, using pNOSO-darABCDE-9 (DSM 33802) as a template (Figure S 4). The two resulting PCR products, harboring homologous regions (highlighted in blue), were mixed in a 1 to 1 ratio and used as template for an overlap-extension PCR reaction (PCR reaction III). For PCR reaction III, primer pr1dar_fw and pr4dar_rv were re-used. The OE-PCR reaction consists of two amplification cycles performed at low and thirty-two at high annealing temperature. All used primers are listed in Table S 2. The DNA fragment amplified in PCR reaction III was gel-purified, restriction hydrolyzed and cloned into pNOSO-darABCDE-9 using standard restriction hydrolysis/DNA ligation cloning techniques. New plasmids with modified *darA* core DNA sequences were verified via Sanger sequencing at LGS biosynthetic. Figure S 3 shows the generated darobactin derivatives.

2. Overproduction of novel darobactin derivatives

Escherichia coli (*E. coli*) NEB10β strain was used for transformation of ligation mixtures with digested, modified *darA* gene fragment and pNOSO-darABCDE-9[1] backbone to generate new artificial darobactin BGC. Cultivation of bacterial cloning strain was performed in LB medium (10 g/L tryptone, 5 g/L NaCl, 5 g/L yeast extract, pH 7.6) at 30 °C. *E. coli* BL21 (DE3) or *E. coli* BL21-Gold (DE3) were taken as heterologous production hosts. Overnight culture with single colony of producer strain, previously transformed with generated expression vector (e.g. pNOSO-darABCDE-22 to 34 and 36 to 39), was incubated for 16 hours at 30 °C and 180 rpm on an orbital shaker (Orbitron/Multitron, Infors HT). 0.5 mL of seeded overnight culture was used for inoculation of 50 mL FM medium (12.54 g/L K_2HPO_4, 2.31 g/L KH_2PO_4, 5 g/L NaCl, 12 g/L yeast extract, 4 g/L D(+) glucose, 1 g/L NH_4Cl, 0.24 g/L $MgSO_4$, pH 7.0) including 1 mg/L sterile filtered vitamin B_{12}. 300 mL round bottom flasks were shaken at 30 °C

for 3 days and 180 rpm on an orbital shaker (Orbitron/Multitron, Infors HT). Kanamycin (50 µg/mL; pNOSO-based expression constructs) was used as antibiotic selection marker.

3. Analysis and quantification of production titer

The 50 mL production broth was centrifuged at 7000 x g for 10 min at 4 °C and supernatant was collected. Production of darobactin in the supernatant was analyzed using an amaZon speed 3D ion trap MS system (Bruker Daltonics) with an Apollo II ESI source uHPLC-HRMS. The extracted ion chromatogram (EIC) was calculated using DataAnalysis software as previously described.[1] Darobactins in crude extract were measured via analytic ultra-high-performance liquid chromatography-high-resolution mass spectrometry (uHPLC-HRMS) using m/z values of $[M+2H]^{2+}$, $[M+3H]^{3+}$, $[M+3H\text{-}NH_3]^{3+}$ and MS2 fragmentation analysis of $[M+2H]^{2+}$ (Figure S 5 - Figure S 36) as calculated (Table S 3). Different ionization states were used in combined extracted ion chromatograms (EIC) to receive comparable data, because introduction of basic amino acids shifted the most abundant ion species from twofold charged $[M+2H]^{2+}$ to two threefold charged states ($[M+3H]^{3+}$ and $[M+3H\text{-}NH_3]^{3+}$). The novel cysteine derivative $D32^{[R]}$, carries the identical major protection group [R], as previously published $D6^{[R]}$, indicated by their identical +191.026 Da mass shifts and as confirmed via nuclear magnetic resonance (NMR) structure elucidation of pure $D6^{[R]}$ and $D32^{[R]}$ (Table S 3, Figure S 76 - Figure S 85). For determination of compound present in the extract relative to DA extract, MS peak area under the curve (AUC) of each crude extracts was computed by automated peak integration of combined EIC values using *Compass Data Analysis* version 5.3 (Bruker Daltonics) and divided through AUC of DA (Table 1 of the manuscript).

4. Overproduction of novel darobactin derivatives with induction

The established fermentation protocol of DA and **9**[1] was taken to produce D22, D23, D31, D32, D36, D37, D38 in *E. coli* BL21 (DE3) after transformation of electro-competent *E. coli* BL21 (DE3) with pNOSO-darABCDE-22, -23, -31, -32, -36, -37 and -38. Using *E. coli* BL21-Gold (DE3) pNOSO-darABCDE-22 as a producer strain for D22 production, the *T7* RNA polymerase was induced by 0.4 mM isopropyl β-D-1-thiogalactopyranoside (IPTG) after an OD_{600} 0.8 to 1.0 was reached to allow a controlled gene expression of *darA* variant compared to *E. coli* BL21 (DE3).

5. Overproduction of halogenated darobactins

15 mL LB medium, including 30 µg/mL Kanamycin (Kan30), was inoculated with single colony of *E. coli* BL21 (DE3) harboring pNOSO-darABCDE-9. After overnight incubation at 30 °C, 180 rpm (Infors HT), 0.2 mL of seeded culture was used to inoculate 20 mL FM medium (1.254 % K_2HPO_4, 0.231 % KH_2PO_4, 0.4 % D(+)-glucose, 0.1 % NH_4Cl, 1.2 % yeast extract, 0.5 % NaCl and 0.0492 % $MgSO_4$(*$7H_2O$); pH 7.1) including Kan30 and 1 mg/L Vitamin B_{12}. Cultures were supplemented with 6-fluoro-L-tryptophane to a final concentration of 2.1 mM in 20 mL of production culture after continually feeding over a period of 3 days. Feeding of 5-chloro-L-trytrophan, was tested in concentrations of 0.1 to 10 mM end

concentration. The overproduction culture was grown under constant conditions at 30 °C and 180 rpm on an orbital shaker. For large scale production of fluorinated D9, volumes were up-scaled to 4 times 1 L cultures in 5 L un-baffled flasks and with a final concentration of 1 mM 6-fluoro-L-tryptophan. Extracts were analyzed by UHPLC-MS and -MS-MS as described before[1], while adjusting the gradient to 10-20 % B over 17 minutes, to get separation of different isomers and multiple halogenated darobactins. The derivatives were named according to the following pattern: "darobactin #" (e.g. darobactin 9), position of fluorine on tryptophan according to IUPAC (e.g. 6F for 6-fluoro-L-tryptophan"), followed by the position of the halogenated tryptophan in the core peptide (e.g. 1, 3 or 7). As an example, D9-6F3 indicates darobactin 9 with a 6-fluoro-L-tryptophan at position 3 (WNW$_F$SKSW).

6. Purification of novel darobactin derivatives

The darobactin derivatives D6, D23, D31 and D36 were purified as described before for DA and D9 using a two-step purification protocol.[1] The previously used Biphenyl column was switched for an XBridge Phenyl column in the first purification step (5 µm, 19x150 mm; Waters Corp.). For D9, the gradient was additionally adjusted to 2-16 % B from minute 2-24 during the second purification step. Detection was accomplished by their respective mass signals (Table S 3) using the built-in single quadrupole mass analyzer of the preparative Autopurifier HPLC-MS system by Waters Corp. Retention times were as follows: D6: C_{18}: 14.3 min, Phenyl: 14 min, D23: C_{18}: 11.8 min, Phenyl: 11.6 min, D31: C_{18}: 13 min, Phenyl: 14.5 min, D36: C_{18}: 12.5 min, Phenyl: 13 min.

D22 is the only derivative, where both purification protocols were used. To highlight improvements in the process, the old protocol used for D22 is described here in detail:

After elution from the absorbent resin XAD-16N with 80 % MeOH and reuptake in H_2O after evaporation, the darobactin crude extracts were purified by three chromatographic steps (two preparative-scale and one semi-preparative scale) using gradients of H_2O (eluent A) and ACN (eluent B) both containing 0.1 % FA. First, crude extracts were separated by preparative reverse-phase (RP) HPLC-MS using an AutoPurification system (Waters Corp.) equipped with built-in single quadrupole mass analyzer. Separation of 900 µL injections was achieved with an XBridge BEH C18 column (130 Å, 5 µm, 19 mm X 150 mm; Waters Corp.) with a gradient of 2-25 % B for D22 over 22 minutes. The second step utilized the same HPLC-MS instrument equipped with a XBridge Phenyl OBD (130 Å, 5 µm, 19 mm X 150 mm; Waters Corp.) and a gradient of 5-15 % B for D22 over 22 minutes. Finally, pure compounds were isolated using an Ultimate 3000 semi-preparative HPLC (Thermo Scientific) equipped with an XSelect CSH OBD Phenyl-Hexyl column (130 Å, 5 µm, 10 mm X 250 mm; Waters Corp.) and a HCT plus Mass Analyzer (Bruker) and a gradient of 2-10 % B for D22 over 20 minutes. Several chromatographic steps involving diversion of sample to an MS analyzer and the choice of adsorbent resin may limit

compound recovery. Therefore, we elected to optimize our procedure for darobactin purification. This method yielded 9.8 mg D22 from 12x 1 L culture (0.8 mg/L). In two different batches with the new purification method for D22, as described below, yields varied from 3.0-3.7 mg/L culture (3.8- to 4.6-fold increase).

The purification protocol was optimized for D9-6F, D37, D38, D22 and D32, adapting the cation-exchange protocol of Tehrani *et al.,*[2] which was then used also for D22 and D32. XAD-16N was exchanged by 2 % (w/V) weak cation exchange resin Dowex MAC-3 (hydrogen form, Sigma Aldrich) during the extraction step. The resin was incubated with the culture for 2 hours on orbital shaker (Orbitron/Multitron, Infors HT) at 160 rpm. Supernatant was decanted and MAC-3 washed with dH_2O, ethyl acetate and eluted using 3-5x 1 L of 2 M ammonia per 200-400 g of resin and decanting the supernatant after each step. For the elution steps, decanted supernatant was also filtrated through paper filter. The solvent was then neutralized on ice with 37 % HCl (Sigma Aldrich) and loaded onto a 130 g C_{18} flash column (CHROMABOND Flash RS 120 C_{18} ec, 40–63 µm) using a peristaltic pump (Ismatec). Salts and highly polar compounds were removed using 3 column volumes (CV) of dH_2O on a Biotage flash (Isolera One), which was followed by elution with 20 CV of 5 % Eluent A (dH_2O + 0.1 % FA) to 20 % Eluent B (ACN + 0.1 % FA), followed by a ramp of 3 CV to 95 % B and 3 CV of 95 %B for cleaning. Detection was performed at 220 and 280 nm UV adsorption. The darobactin-containing fractions were collected and dried using a rotary evaporator. Purification on the preparative Autopurifier HPLC-MS system by Waters Corp was achieved using XBridge C_{18} column (5 µm, 19x150 mm; Waters Corp.) with the following gradients:

After 2 min equilibration at 2 % B and 98 % A, for D32$^{[R]}$, D37 and D38 a gradient from 2-25 % B was used for 22 min, followed by a 2 min ramp to 95 % B, 1 min hold at 95 % B and ramp down to 2 % B again. D32$^{[R]}$ eluted at 11.5 min, D37 at 15.5 min and D38 at 15 min.

D22 was purified using 2 min of equilibration at 5 % B and 95 % A, a separation gradient from 5-15 % B was used for 22 min, followed by a 2 min ramp to 95 % B, 1 min hold at 95 % B and ramp down to 5 % B again. D22 eluted approximately at 15 min.

D9-6F was purified using 2 min of equilibration at 11 % B and 89 % A, a separation gradient from 11-17 % B was used for 22 min, followed by a 2 min ramp to 95 % B, 1 min hold at 95 % B and ramp down to 11 % B again. D9-6F eluted together as mixture of the two isomers approximately at 17.1.

H_2O and ACN (+0.1 % FA) were used as mobile phases A and B for all methods with a flow rate of 25 mL/min. The darobactin-containing fractions were collected and dried using a rotary evaporator.

D36 and D9-6F required a second purification step on an Ultimate 3000 SDLC low pressure gradient system (Dionex) equipped with XSelect Peptide CSH C_{18} column (250x10mm 5µm; Waters Corp.), while

for the other derivatives (D6, D23, D31) an Acquity CSH Phenyl-hexyl column (250x10mm 5µm; Waters Corp.) was used. The eluents were H_2O + 0.1 % FA as A and ACN + 0.1 % FA as B, at a flow rate of 5 mL/min (6 mL/min for D9-6F) and a column temperature of 45 °C (35 °C for D32$^{[R]}$). The darobactins were detected by UV absorption at 280 nm using time-dependent fraction collection.

The following gradients were applied:

For D36 the separation was started with a plateau of 8 % B for 1 min, followed by ramp to 15 % B for 20 min and a cleaning step using a ramp to 95 % B of 1 min, keeping 95 % B for 1 min and ramping back to the starting conditions of 8 % B for 1 min again, followed by re-equilibration for 1 min. Elution occurred at 5.3 min.

For D9-6F the separation was started with a plateau of 11 % B for 1 min, followed by ramp to 17 % B for 20 min and a cleaning step using a ramp to 95 % B of 1 min, keeping 95 % B for 1 min and ramping back to the starting conditions of 11 % B for 1 min again, followed by reequilibration for 1 min. Elution of the two isomers occurred at 12 and 13 min.

For D6 the separation was started with a plateau of 2 % B for 1 min, followed by ramp to 30 % B for 17 min and a cleaning step using a ramp to 95 % B of 3 min, keeping 95 % B for 1 min and ramping back to the starting conditions of 2 % B for 1 min again, followed by reequilibration for 1 min. Elution occurred at 13.5 min.

For D23 the separation was started with a plateau of 2 % B for 1 min, followed by ramp to 10 % B for 20 min and a cleaning step using a ramp to 95 % B of 1 min, keeping 95 % B for 1 min and ramping back to the starting conditions of 2 % B for 1 min again, followed by reequilibration for 1 min. Elution occurred at 17.8 min.

For D31 the separation was started with a plateau of 2 % B for 1 min, followed by ramp to 15 % B for 20 min and a cleaning step using a ramp to 95 % B of 1 min, keeping 95 % B for 1 min and ramping back to the starting conditions of 2 % B for 1 min again, followed by reequilibration for 1 min. Elution occurred at 12.8 min.

After evaporation, the darobactins were obtained as pale yellowish to brownish amorphous solids. Purity was confirmed by uHPLC-MS and NMR.

7. Determination of antibacterial activity

The antibacterial activity of novel darobactins was established by determining the minimum inhibitory concentration (MIC) as previously described for crude extracts and for pure compounds.[1] For determining the activity of selected darobactins against Carbapenem-resistant *Acinetobacter baumannii* (CRAB) in the presence of lung surfactant, the medium for the MIC assay was supplemented

with 1% (*v/v*) lung surfactant (Alveofact® 45 mg/mL suspension; phospholipids from bovine lung, reconstituted with provided vehicle).

8. Characterization of darobactin 22

8.1 Maximum tolerated concentration (MTC)

Husbandry of the adult zebrafish was performed according to internal protocols in accordance with the German Animal Welfare Act (§11 Abs. 1 TierSchG). Zebrafish larvae of the wildtype AB line were used for the study and all experiments were done within the first 120 hours post fertilization (hpf). The MTC assay was designed to determine acute and developmental toxicity (genotoxicity) of tested compounds on different embryonic developmental stages of zebrafish larvae.

For this purpose, the dechorinated larvae (1 day post fertilization, dpf) were incubated at 28°C in the presence of various compound concentrations (10, 50, 100, 250 and 500 µg/mL, n=10 per condition) dissolved in 0.3x Danieau's solution (17 mM NaCl, 2 mM KCl, 0.12 mM $MgSO_4$, 1.8 mM $Ca(NO_3)_2$, 1.5 mM HEPES, pH 7.1 - 7.3, and 1.2 µM methylene blue). The embryos were monitored daily and developmental stages, hatching behavior, pigmentation, heartbeat, blood flow, locomotor response, and body shape were observed.[3] If more than one dead larva was found in the untreated control, the experiment was rejected. An embryo was considered *dead* once there was no heartbeat recorded. Images were taken using a Leica M205FA stereomicroscope equipped with a Leica DFC 7000T camera. The assay was terminated when larvae reached 5 dpf (120 hpf).

8.2 Time-kill assay

Overnight bacterial cultures were prepared from a cryo-preserved stock in fresh medium and incubated in a shaking incubator at 180 rpm and at 30 °C for *Acinetobacter baumannii* (*A. baumannii*) strains and 37 °C for *E. coli* strains. The OD_{600} was determined and the initial inoculum was adjusted to approximately 5 x 10^6 colony-forming units (CFU)/mL. Time-kill kinetics were determined at 2x, 4x, 8x MIC of DA and D22, respectively, and compared to vehicle-treated cultures as control. Treated bacterial cultures were incubated in a shaking incubator at 180 rpm at the appropriate temperatures. Aliquots were taken at the assigned time points (0, 0.5, 1, 2, 4, 6, 8 and 24 hours) and CFU/mL were determined by plating the culture onto non-selective CASO agar in serial dilution. The plates were incubated in a static incubator at the appropriate temperature for 24 hours. The following day the colonies were counted and CFU/mL was determined, which was then plotted against time to obtain a time-kill curve (TKC). All TKCs were done with three technical repeats of two independent biological replicates.

9. NMR spectroscopy of D6, D22, D23, D31, D32, D36, D37 and D38

1D and 2D NMR data were recorded as described previously in a 2:1 mixture of D2O:ACN-d3 + 1 % FA-d2,[1] while modifying the temperature to 308.15 K for D32. NMR signals were assigned using ACD/labs NMR workbook suite. Color-coding in the 2D NMR spectra reflects fit of the experimental chemical shifts to the calculated chemical shifts: Green = experimental value perfectly matches the calculated chemical shift, yellow = experimental value matches predicted area of calculated chemical shift, red = experimental value differs from calculated chemical shift. All structure formulae devised by NMR will be made publicly available under their corresponding name in NPAtlas[4] upon acceptance of the manuscript.

10. Protein expression and purification

Protein expression and purification of the *E. coli* BAM complex was performed as described previously[5] with minor modification. The BAM complex was extracted with 1% (v/v) DDM, and further purified in presence of 0.05%DDM. Finally, the BAM complex protein was purified on a 16/600 Superose 6 increase column using 50 mM Tris pH 7.5, 50 mM NaCl, 0.01% (w/v) n-dodecyl β-D-maltopyranoside (DDM) and concentrated to 5.0 mg/mL. The freshly purified protein was directly used for cryo-EM without freezing.

The BamA barrel domain (BamA-β) (residues 421–810, C690S, C700S), with an N-terminal His6 tag and overexpressed and purified as described previously with small modifications.[5] In brief, *bamA-β* was cloned into pROEX vector and overexpressed in inclusion bodies using Top10. The inclusion bodies were solubilized in 8 M urea and purified using Ni-NTA with 6 M urea. The purified protein was dialyzed against ultrapure H_2O and the precipitated protein was collected by centrifugation at 100,000 xg for 30 min. The remaining soluble fraction was further concentrated using 10 kDa cut-off centrifugal into 1 mL. The remaining soluble fraction was further concentrated using 10 kDa cut-off centrifugal into 1 mL. Next, 0.6 g Guanidine hydrochloride was added and dissolved in the concentrated sample and further used for solubilizing the pellet. The subsequent refolding process was performed as described.[5]

11. Electron microscopy sample preparation and data processing, collecting and analyzing

The BAM complex incubated with a fivefold molar excess of darobactin was applied to a glow-discharged quantifoil R1.2/1.3 AU 300. The grids were blotted for 3-5 s (blot force: minus 5 to 5; 100 % humidity) and plunge-frozen in liquid ethane/propane using a Vitrobot Mark V. The grids were first screened to get the best vitrified grid using Talos Arctica. Then, the best vitrified specimens were imaged on an FEI Titan Krios, operated at 300 kV, and equipped with a Gatan K3 camera. The data were acquired with a defocus range of 0.6-3.0 µm and nominal magnification of 105,000x (a pixel size of 0.85 Å) using Thermo Fisher Scientific EPU software. For individual frames, an electron dose of 1.2 e/A2

was used, corresponding to a cumulative electron dose of 60 e/A2 equally distributed over a 3-sec movie.

The data were processed using relion3.1[6] and the final polished particles were further imported into cryoSPARC.[7] A heterogeneous classification was carried out and the particles from good classes were further submitted for non-uniform refinement to get a final 3D reconstruction map. The summary of data processing is provided in Figure S 1 and Figure S 43. Previously the BAM complex with DA (PDB: 7NRI[5]) was used as initial model to fit chimeraX1.3.[8] The BAM complex was refined in Phenix.[9] The geometry restraints of D9 and D22 were generated by using eLBOW from Phenix. The darobactins and the darobactin binding regions of the BAM complex were further refined with ISOLDE.[10] Validation was done using the cryo-EM validation tools in Phenix. The map resolution range was determined from local resolution calculation in cryoSPARC.

12. Thermal titration calorimetry

The ITC experiments on darobactins binding to BamA-β were carried out at 25 °C with the Microcal PEAQ-ITC instrument in duplicate. The ITC was performed in the buffer solution as described in previous study (20 mM NaPi, 150 mM NaCl, 0.1% w/v LDAO, pH 7.5).[5] 300 μM darobactin in the syringe was injected 13 times into the sample cell containing 20 μM BamA-β with a spacing of 150 s and a stirring rate of 750 rpm. The injection volume is 3 μl with a 6s duration, except for the first injection (0.4 μl, 0.8 s). The control experiment was performed in the absence of BamA-β. The resulting data were analyzed using the integrated public-domain software packages NITPIC, SEDPHAT and GUSSI.

13. List of bacterial strains

Table S 1: List of bacterial strains used or generated in this study.

Bacterial strain	Genotype	Reference
Cloning strains		
E. coli HS996	F$^-$, *mcr*A, Δ(*mrr-hsd*RMS-*mcr*BC), Φ80*lac*ZΔM15, Δ*lac*X74, *rec*A1, *ara*D139, Δ(*ara-leu*)7697, *gal*U, *gal*K, *rps*L (Str^R), *end*A1, *nup*G, *fhu*A::IS2	Invitrogen
E. coli NEB10β	*mcr*A, spoT1Δ(*mrr-hsd*RMS-*mcr*BC), Φ80d(*lac*ZΔM15)*rec*A1, *rel*A1, Δ*lac*X74, *rec*A1, *ara*D139, Δ(*ara-leu*)7697, *gal*K16, *gal*E15, *rps*L (Str^R), *end*A1, *nup*G, *fhu*A	New England Biolabs
E. coli BL21 (DE3)	F$^-$, *ompT, gal, dcm, lon,* Δ*hsdS*$_B$($r_B^-m_B^-$), λ(DE3 [*lacI lacUV5-T7p07 ind1 sam7 nin5*]), [*malB*$^+$]$_{K-12}$(λ^S)	Invitrogen
E. coli BL21-Gold (DE3)	*E. coli* B F– ompT hsdS(rB– mB–) dcm+ Tetr gal λ(DE3) endA The	Agilent Technologies
E. coli HS996 pNOSO-darABCDE-A	*E. coli* HS996 with pNOSO-darABCDE-A, kan^R	Groß *et al.* 2021
E. coli HS996 pNOSO-darABCDE-9	*E. coli* HS996 with pNOSO-darABCDE-9, kan^R	Groß *et al.* 2021
E. coli HS996 pNOSO-darABCDE-6	*E. coli* HS996 with pNOSO-darABCDE-6, kan^R	Groß *et al.* 2021
E. coli NEB10β pNOSO-darABCDE-22	*E. coli* NEB10β with pNOSO-darABCDE-22, kan^R	This work
E. coli NEB10β pNOSO-darABCDE-23	*E. coli* NEB10β with pNOSO-darABCDE-23, kan^R	This work
E. coli NEB10β pNOSO-darABCDE-24	*E. coli* NEB10β with pNOSO-darABCDE-24, kan^R	This work
E. coli NEB10β pNOSO-darABCDE-25	*E. coli* NEB10β with pNOSO-darABCDE-25, kan^R	This work
E. coli NEB10β pNOSO-darABCDE-26	*E. coli* NEB10β with pNOSO-darABCDE-26, kan^R	This work
E. coli NEB10β pNOSO-darABCDE-27	*E. coli* NEB10β with pNOSO-darABCDE-27, kan^R	This work
E. coli NEB10β pNOSO-darABCDE-28	*E. coli* NEB10β with pNOSO-darABCDE-28, kan^R	This work
E. coli HS996 pNOSO-darABCDE-29	*E. coli* HS996 with pNOSO-darABCDE-29, kan^R	This work

Bacterial strain	Genotype	Reference
Cloning strains		
E. coli HS996 pNOSO-darABCDE-30	*E. coli* HS996 with pNOSO-darABCDE-30, kan^R	This work
E. coli HS996 pNOSO-darABCDE-31	*E. coli* HS996 with pNOSO-darABCDE-31, kan^R	This work
E. coli HS996 pNOSO-darABCDE-32	*E. coli* HS996 with pNOSO-darABCDE-32, kan^R	This work
E. coli HS996 pNOSO-darABCDE-36	*E. coli* HS996 with pNOSO-darABCDE-36, kan^R	This work
E. coli HS996 pNOSO-darABCDE-37	*E. coli* HS996 with pNOSO-darABCDE-37, kan^R	This work
E. coli HS996 pNOSO-darABCDE-38	*E. coli* HS996 with pNOSO-darABCDE-38, kan^R	This work
E. coli HS996 pNOSO-darABCDE-39	*E. coli* HS996 with pNOSO-darABCDE-39, kan^R	This work
Heterologous producer strains		
E. coli BL21 (DE3) pNOSO-darABCDE-9	*E. coli* BL21 (DE3) with pNOSO-darABCDE-9, kan^R	Groß *et al.* 2021
E. coli BL21 (DE3) pNOSO-darABCDE-6	*E. coli* BL21 (DE3) with pNOSO-darABCDE-6, kan^R	Groß *et al.* 2021
E. coli BL21 (DE3) pNOSO-darABCDE-22	*E. coli* BL21 (DE3) with pNOSO-darABCDE-22, kan^R	This work
E. coli BL21-Gold (DE3) pNOSO-darABCDE-22	*E. coli* BL21-Gold (DE3) with pNOSO-darABCDE-22, kan^R	This work
E. coli BL21 (DE3) pNOSO-darABCDE-23	*E. coli* BL21 (DE3) with pNOSO-darABCDE-23, kan^R	This work
E. coli BL21 (DE3) pNOSO-darABCDE-24	*E. coli* BL21 (DE3) with pNOSO-darABCDE-24, kan^R	This work
E. coli BL21 (DE3) pNOSO-darABCDE-25	*E. coli* BL21 (DE3) with pNOSO-darABCDE-25, kan^R	This work
E. coli BL21 (DE3) pNOSO-darABCDE-26	*E. coli* BL21 (DE3) with pNOSO-darABCDE-26, kan^R	This work
E. coli BL21 (DE3) pNOSO-darABCDE-27	*E. coli* BL21 (DE3) with pNOSO-darABCDE-27, kan^R	This work

Bacterial strain	Genotype	Reference
Heterologous producer strains		
E. coli BL21 (DE3) pNOSO-darABCDE-28	*E. coli* BL21 (DE3) with pNOSO-darABCDE-28, kan^R	This work
E. coli BL21 (DE3) pNOSO-darABCDE-29	*E. coli* BL21 (DE3) with pNOSO-darABCDE-29, kan^R	This work
E. coli BL21 (DE3) pNOSO-darABCDE-30	*E. coli* BL21 (DE3) with pNOSO-darABCDE-30, kan^R	This work
E. coli BL21 (DE3) pNOSO-darABCDE-31	*E. coli* BL21 (DE3) with pNOSO-darABCDE-31, kan^R	This work
E. coli BL21 (DE3) pNOSO-darABCDE-32	*E. coli* BL21 (DE3) with pNOSO-darABCDE-32, kan^R	This work
E. coli BL21 (DE3) pNOSO-darABCDE-36	*E. coli* BL21 (DE3) with pNOSO-darABCDE-36, kan^R	This work
E. coli BL21 (DE3) pNOSO-darABCDE-37	*E. coli* BL21 (DE3) with pNOSO-darABCDE-37, kan^R	This work
E. coli BL21 (DE3) pNOSO-darABCDE-38	*E. coli* BL21 (DE3) with pNOSO-darABCDE-38, kan^R	This work
E. coli BL21 (DE3) pNOSO-darABCDE-39	*E. coli* BL21 (DE3) with pNOSO-darABCDE-39, kan^R	This work
E. coli BL21 (DE3) C43 pBAM	*E. coli* BL21 (DE3) C43 with pBAM, amp^R	Kaur *et al.* 2021
E. coli BL21 (λ DE3) Lemo cells pET15b-BamAβ421-810	*E. coli* BL21 (λ DE3) Lemo cells with pET15b-BamAβ421-810, amp^R	This work

3.2.2 Supplementation figures and tables

Cryo-EM of BAM-D9

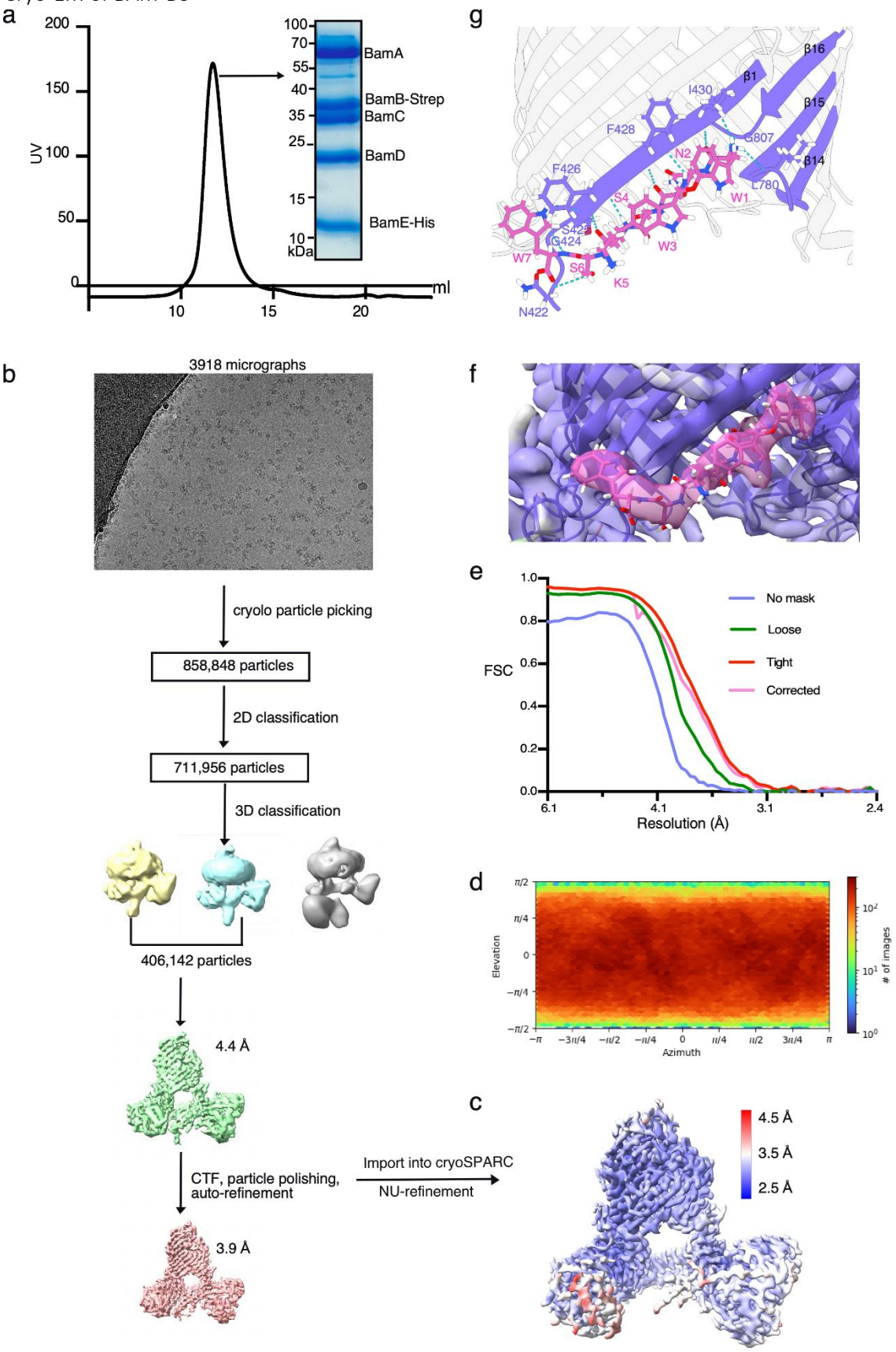

Figure S 1: Cryo-EM structure of BAM-D9 complex.a, SDS page analysis of purified BAM sample used for cryo-EM. b, Workflow of data generation, processing and refinement to decipher BAM-D9 complex. c, BAM overview map with resolution of the EM reconstruction, highlighting local variations from 2.5 Å (blue) to 4.5 Å (red). d, angular distribution of D9 bound to BAM complex was calculated in cryoSPARC for particle projections. Heat map shows number of particles for each viewing angle. e, resolution estimation by Fourier shell correlation (FSC) curves (CryoSparc). f, magnified BAM-D9 interaction area showing electron density surface of D9 (pink) bound on BAM (blue). g, magnified BAM-D9 interaction area, D9 (pink) and interacting amino acids of BamA (blue) are highlighted in stick representation. Potential hydrogen bond interactions are shown as green dashes. Involved ß-sheets (ß1, ß14, ß15, ß16) were labeled as interaction amino acids of BamA and D9.

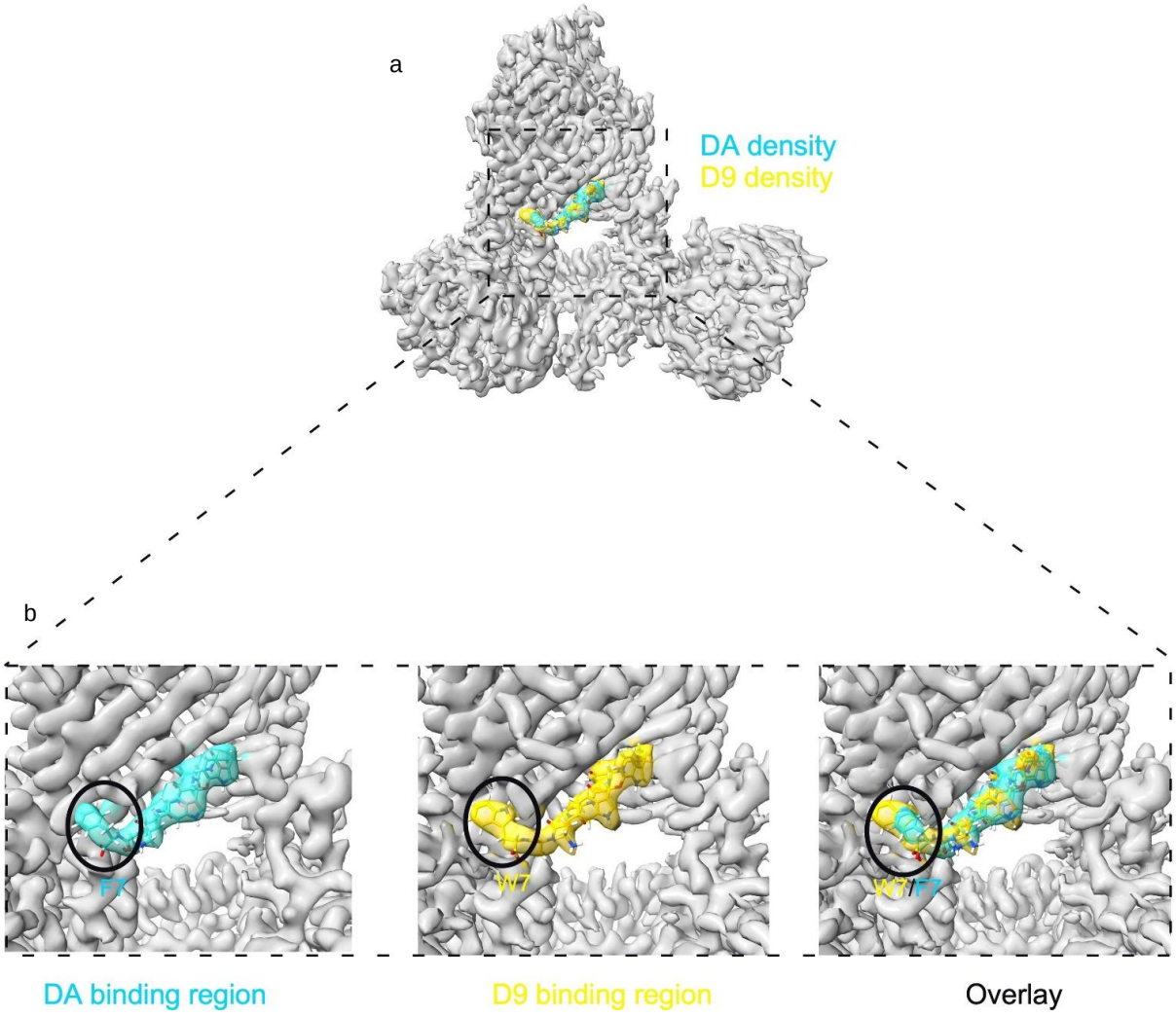

Figure S 2: EM density comparison of DA and D9. a, Overlay of BAM-DA (blue) and BAM-D9 (yellow) electron density. For the density maps, the raw data of BAM-DA were taken from Kaur *et al.*.[5] The raw data of BAM-D9 were generated in this study. b, Magnified view of DA, D9 and overlaid binding region. DA and D9 are fitted (stick presentation) to show consistent matching of DA and D9 into the electron densities.

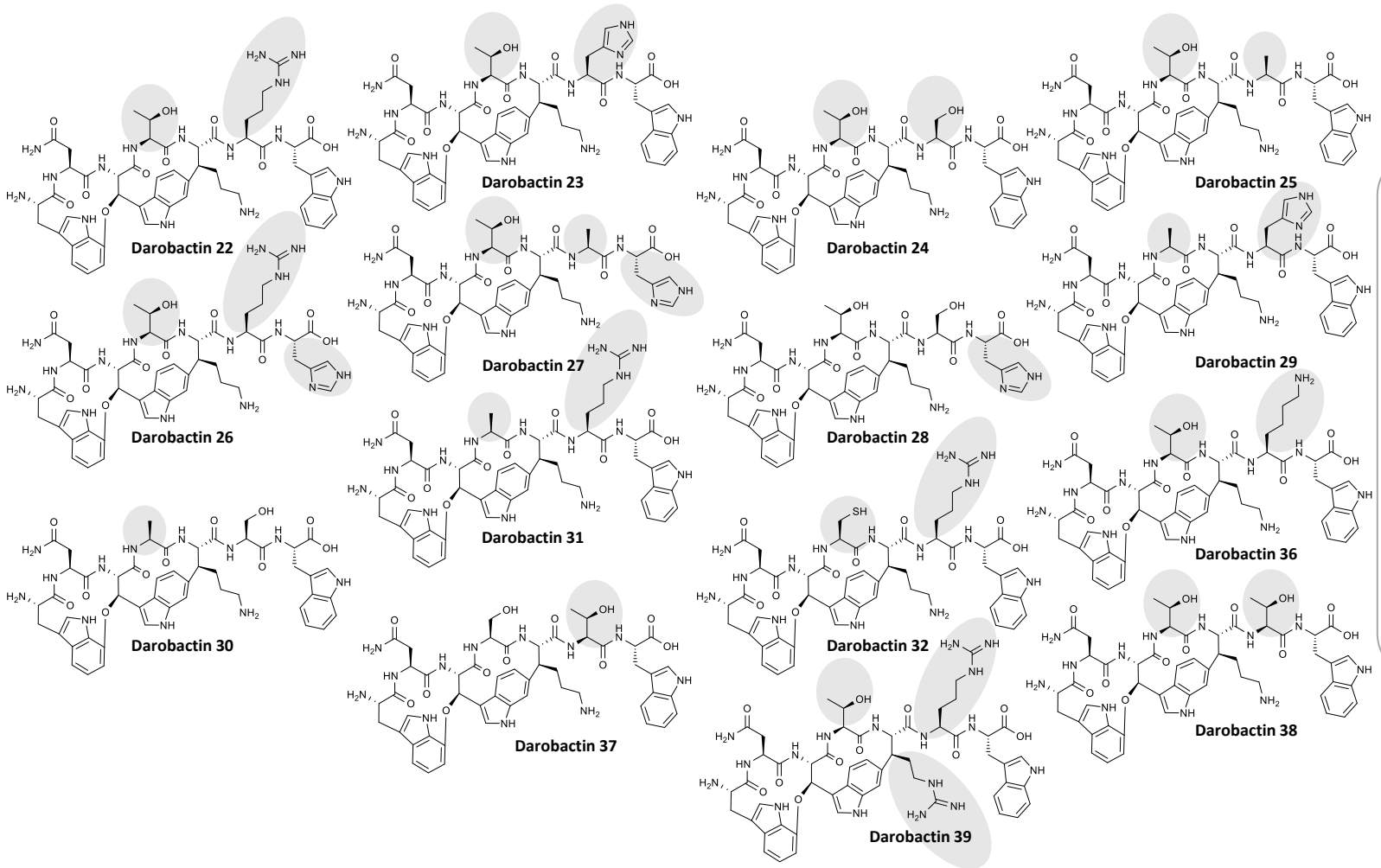

Darobactin	Core peptide
9	W N W S K S W
22	W N W **T** K **R** W
23	W N W **T** K **H** W
24	W N W **T** K S W
25	W N W **T** K **A** W
26	W N W **T** K **R H**
27	W N W **T** K **A H**
28	W N W **T** K S **H**
29	W N W **A** K **H** W
30	W N W **A** K S W
31	W N W **A** K **R** W
32	W N W **C** K **R** W
36	W N W **T** K **K** W
37	W N W S K **T** W
38	W N W **T** K **T** W
39	W N W **T R R** W

Figure S 3 : Overview of all generated non-halogenated novel darobactin derivatives. D22 to D32 and D36 to D39 are displayed and positions of hepta-peptide with amino acid changes compared to D9 amino acid sequence were highlighted in grey. Table with core peptide sequences itemize differences between the darobactin derivatives to D9.

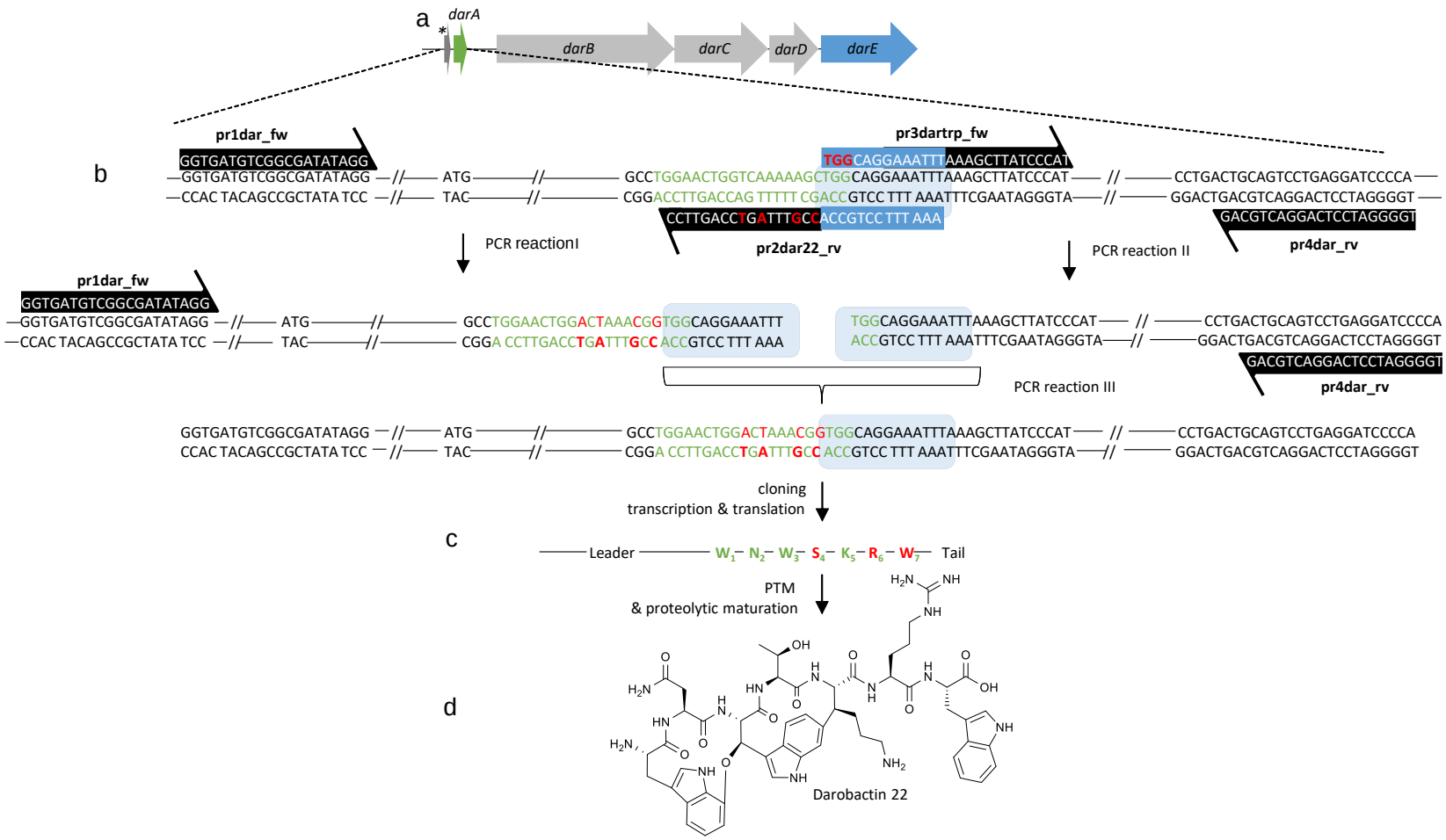

Figure S 4: Generation of new darobactin derivatives via overlap-extension PCR. a, Biosynthetic gene cluster of D9 b, Exemplified PCR reaction workflow with primer pr1dar_fw and pr2dar22_rv (harboring mismatches (red) compared to template sequence to introduce mutations during PCR amplification, leading into D22) to generate DNA fragment of PCR reaction I and with pr3dartrp_fw and pr4dar_rv to generate DNA fragment of PCR reaction II. Primer pr2dar22_rv and pr3dartrp_fw sharing homologous region (highlighted in blue). Using DNA fragments of PCR reaction I & II as template, overlap extension PCR reaction, named as PCR reaction III, was performed to generate fragment harboring modified *darA* core sequence. Unique restriction sites on 3' and 5'end enable to clone the mutated *darA* gene into pNOSO-darABCDE-9 for generating pNOSO-darABCDE-22. c, core peptide sequence of D22 with changed amino acids (red) compared to DA/D9. d, D22 structure based on NMR data, page 48-53.

Table S 2: Oligonucleotides used for overlap extension (OE) polymerase chain reaction I, II and III. Homologous regions of pr3darhis_fw and pr3dartrp_fw with pr2darXX_rv are highlighted in blue. Mismatches of pr2darXX_rv compared to template to generate the new darobactin derivatives are highlighted in red.

Oligonucleotide	Sequence (5'-3')
pr1dar_fw	**GGTGATGTCGGCGATATAGG**
pr3darhis-fw	CAT**CAGGAAATTTAAAGCTTATCCCAT**
pr3dartrp-fw	TGG**CAGGAAATTTAAAGCTTATCCCAT**
pr4dar_rv	**TGGGGATCCTCAGGACTGCAG**
pr2dar22_rv	**AAATTTCCTGCCACCGTTTAGTCCAGTTCC**
pr2dar23_rv	**AAATTTCCTGCCAATGTTTAGTCCAGTTCC**
pr2dar24_rv	**AAATTTCCTGCCATGATTTAGTCCAGTTCC**
pr2dar25_rv	**AAATTTCCTGCCACGCTTTAGTCCAGTTCC**
pr2dar26_rv	**AAATTTCCTGATGCCGTTTAGTCCAGTTCC**
pr2dar27_rv	**AAATTTCCTGATGCGCTTTAGTCCAGTTCC**
pr2dar28_rv	**AAATTTCCTGATGTGATTTAGTCCAGTTCC**
pr2dar29_rv	**AAATTTCCTGCCAATGTTTCGCCCAGTTCC**
pr2dar30_rv	**AAATTTCCTGCCATGATTTCGCCCAGTTCC**
pr2dar31_rv	**AAATTTCCTGCCACCGTTTCGCCCAGTTCC**
pr2dar32_rv	**AAATTTCCTGCCACCGTTTACACCAGTTCC**
pr2dar36_rv	**AAATTTCCTGCCATTTTTTAGTCCAGTTCC**
pr2dar37_rv	**AAATTTCCTGCCAAGTTTTTGACCAGTTCC**
pr2dar38_rv	**AAATTTCCTGCCAAGTTTTAGTCCAGTTCC**
pr2dar39_rv	**AAATTTCCTGCCACCGCCGAGTCCAGTTCCA**

Table S 3: Calculated and observed masses of the darobactin derivatives. Core peptide sequence of each novel darobactin derivative in comparison to core sequence of DA and D9 are summarized (differences highlighted in red). Calculated and observed masses in the XAD16-N extracts of the different charge states ($[M+H]^{1+}$, $[M+2H]^{2+}$, $[M+3H]^{3+}$, $[M+3H-NH_3]^{3+}$). For D6 and D32, a mass shift of 95.5126 for the $[M+2H]^{2+}$ mass (191.0252 neutral mass), was observed depicted as cysteine ($C^{[R]}$) and derivatives with residue $D6^{[R]}$ and $D32^{[R]}$. When reducing with 10 % β-mercaptoethanol, the expected masses are found (D6 and D32). For some derivatives only selected charge states could be found.

Darobactin	Core peptide	Calc. mass $[M+1H]^{1+}$	Obs. mass $[M+1H]^{1+}$	Calc. mass $[M+2H]^{2+}$	Obs. mass $[M+2H]^{2+}$	Calc. mass $[M+3H]^{3+}$	Obs. mass $[M+3H]^{3+}$	Calc. mass $[M+3H-NH_3]^{3+}$	Obs. mass $[M+3H-NH_3]^{3+}$
DA	W N W S K S F	966.4104	966.4111	483.7089	483.7095	322.8083	322.8082	317.1328	317.1324
$D6^{[R]}$	W N W $C^{[R]}$ K S F	1173.4128	1173.4123	587.2101	587.2102	391.8091	391.8088	386.1336	no
D6	W N W C K S F	982.3876	982.3865	491.6974	491.6970	328.1341	no	322.4585	no
D9	W N W S K S W	1005.4213	1005.4209	503.2143	503.2139	335.8120	335.8118	330.1364	no
D9-6F7	W N W S K S W_F	1023.4119	no	512.2096	512.2096	341.8088	no	336.1333	no
D9-6F1	W_F N W S K S W	1023.4119	1023.4103	512.2096	512.2095	341.8088	341.8084	336.1333	336.1338
D9-6F1-7	W_F N W S K S W_F	1041.4025	1041.4020	521.2049	521.2043	347.8057	347.8052	342.1302	no
D9-5Cl3	W N W_{Cl} S K S W	1039.3824	1039.3802	520.1948	520.1942	347.1323	no	341.4568	no
D9-5Cl7	W N W S K S W_{Cl}	1039.3824	1039.3811	520.1948	520.1937	347.1323	347.1309	341.4568	no
D22	W N W **T** K **R** W	1088.5061	1088.5430	544.7567	544.7912	363.5069	363.5297	357.8314	357.8540
D23	W N W **T** K **H** W	1069.4639	1069.4644	535.2356	535.2457	357.1595	357.1662	351.4840	351.4906
D24	W N W **T** K S W	1019.4370	1019.4790	510.2221	510.2450	340.4838	no	334.8083	no
D25	W N W **T** K **A** W	1003.4421	1003.4520	502.2247	502.2415	335.1522	no	329.4767	no
D26	W N W **T** K **R** H	1039.4857	1039.4851	520.2465	520.2463	347.1667	347.1667	341.4912	341.4911
D27	W N W **T** K **A** H	954.4217	954.4226	477.7145	477.7146	318.8121	318.8121	313.1366	313.1366
D28	W N W **T** K S H	970.4166	970.4174	485.7119	485.7122	324.1437	324.1439	318.4682	318.4683
D29	W N W **A** K **H** W	1039.4533	1039.4545	520.2303	520.2308	347.1560	347.1563	341.4804	341.4808
D30	W N W **A** K S W	989.4264	989.4256	495.2169	495.2169	330.4803	no	324.8048	no
D31	W N W **A** K **R** W	1058.4955	1058.4998	529.7514	529.7537	353.5034	353.5047	347.8278	347.8292
$D32^{[R]}$	W N W $\mathbf{C}^{[R]}$ K **R** W	1281.4928	no	641.2500	641.2489	427.8358	427.8351	422.1603	422.1597
D32	W N W **C** K **R** W	1090.4676	1090.4712	545.7374	545.7376	364.1607	364.1613	358.4852	358.4854
D36	W N W **T** K **K** W	1060.4999	1060.4988	530.7536	530.7539	354.1715	354.1716	348.4960	348.4961
D37	W N W **S** K **T** W	1019.4370	1019.4356	510.2221	510.2206	340.4838	340.4834	334.8083	334.8085
D38	W N W **T** K **T** W	1033.4526	1033.4515	517.2300	517.2299	345.1557	345.1554	339.4802	339.4795
D39	W N W **T R R W**	1116.5122	no	558.7597	558.7597	372.8423	372.8422	367.1667	367.1667

Chromatograms of darobactin extracts

This section displays either extracted ion chromatogram (EIC) traces of the most abundant $[M+2H]^{2+}$ ion for darobactin derivatives, with similar ionization behavior compared to DA. For some derivatives (D22, D26, D31, D39) the additional introduced arginine led to the $[M+3H]^{3+}$ being more abundant. To keep comparability, combined extracted ion chromatograms (EICs) of the two charge states were used to determine AUC. The combined EICs are depicted in red, the corresponding BPCs of the extracts in black.

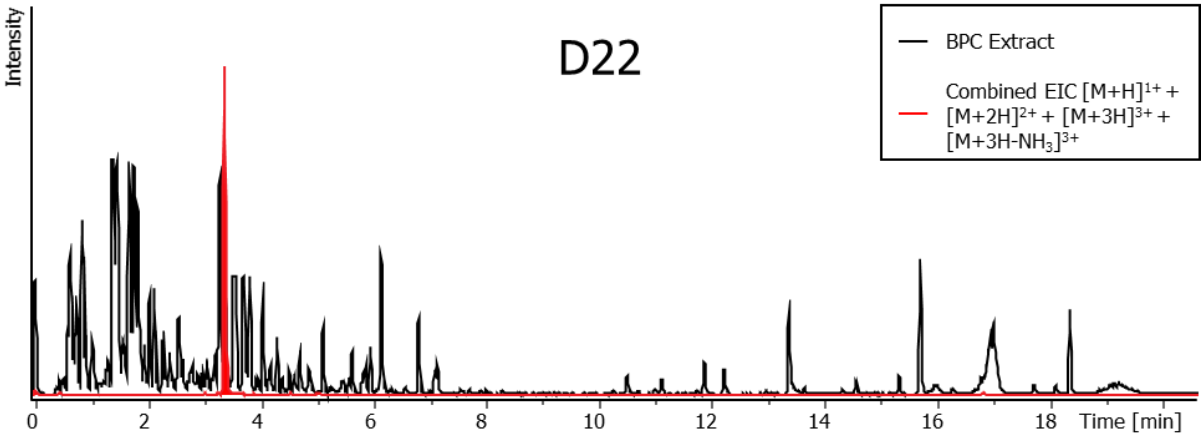

Figure S 5: Chromatogram of the *E. coli* BL21 (DE3) pNOSO-darABCDE-22 culture XAD16-N extract. The red trace displays the D22 combined EIC for the $[M+H]^{1+}$, $[M+2H]^{2+}$, $[M+3H]^{3+}$ and $[M+3H-NH_3]^{3+}$ species at their respective calculated masses (Table S 3) ±0.05 Da. The black trace displays the BPC of the whole extract from fermentation supernatant.

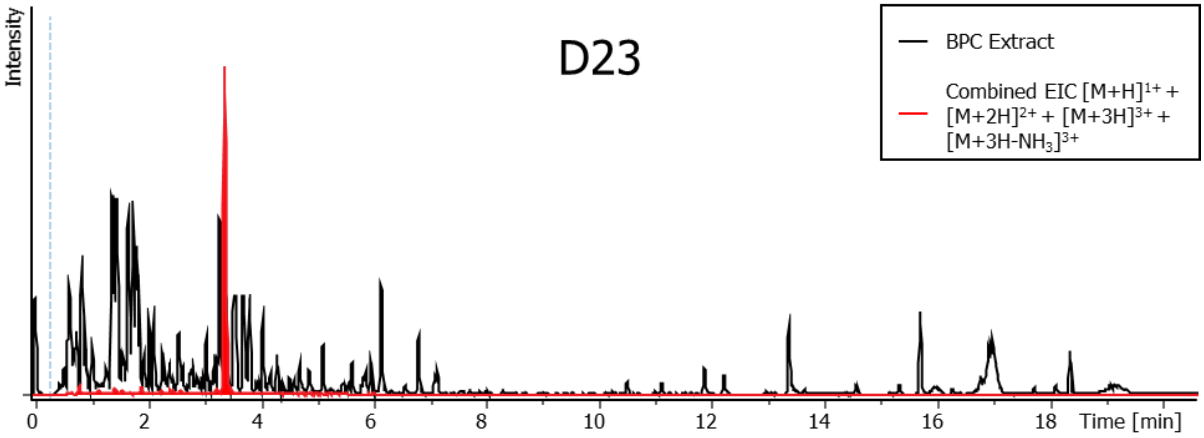

Figure S 6: Chromatogram of the *E. coli* BL21 (DE3) pNOSO-darABCDE-23 culture XAD16-N extract. The red trace displays the D23 combined EIC for the $[M+H]^{1+}$, $[M+2H]^{2+}$, $[M+3H]^{3+}$ and $[M+3H-NH_3]^{3+}$ species at their respective calculated masses (Table S 3) ±0.02 Da. The black trace displays the BPC of the whole extract from fermentation supernatant.

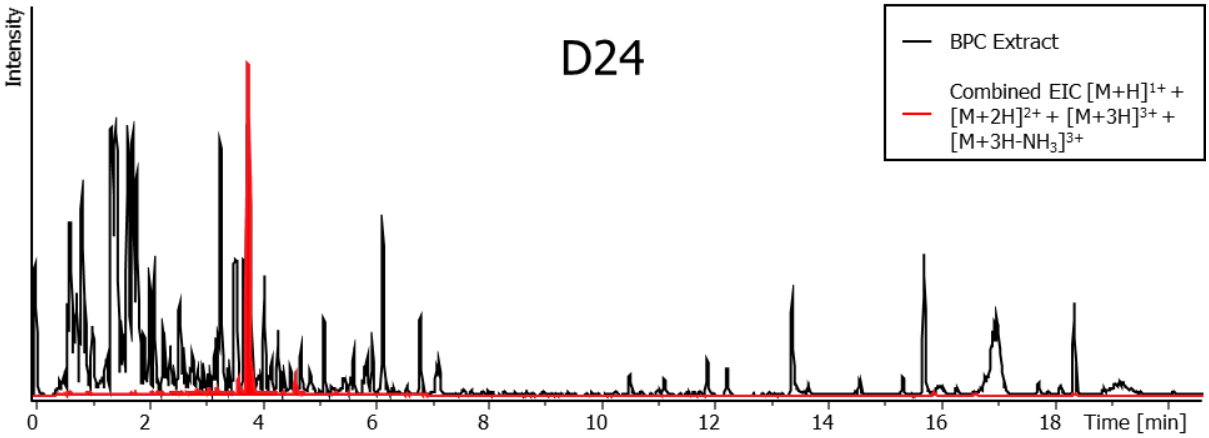

Figure S 7: Chromatogram of the *E. coli* BL21 (DE3) pNOSO-darABCDE-24 culture XAD16-N extract. The red trace displays the D24 combined EIC for the $[M+H]^{1+}$, $[M+2H]^{2+}$, $[M+3H]^{3+}$ and $[M+3H-NH_3]^{3+}$ species at their respective calculated masses (Table S 3) ±0.05 Da. The black trace displays the BPC of the whole extract from fermentation supernatant.

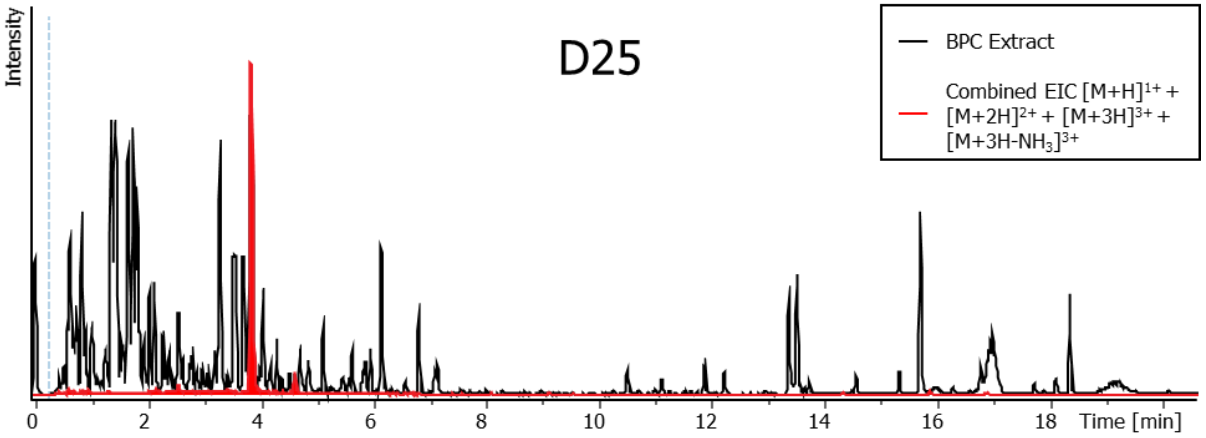

Figure S 8: Chromatogram of the *E. coli* BL21 (DE3) pNOSO-darABCDE-25 culture XAD16-N extract. The red trace displays the D25 combined EIC for the $[M+H]^{1+}$, $[M+2H]^{2+}$, $[M+3H]^{3+}$ and $[M+3H-NH_3]^{3+}$ species at their respective calculated masses (Table S 3) ±0.02 Da. The black trace displays the BPC of the whole extract from fermentation supernatant.

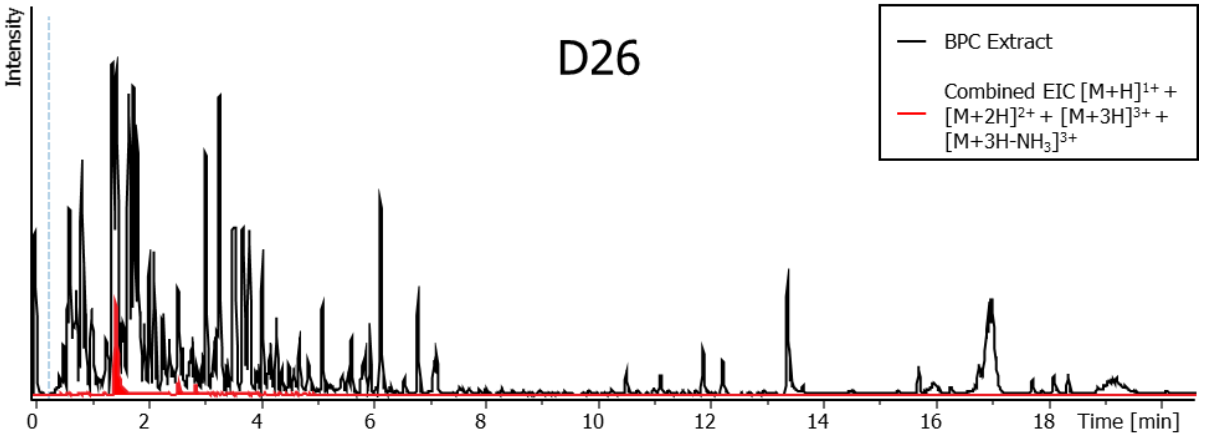

Figure S 9: Chromatogram of the *E. coli* BL21 (DE3) pNOSO-darABCDE-26 culture XAD16-N extract. The red trace displays the D26 combined EIC for the $[M+H]^{1+}$, $[M+2H]^{2+}$, $[M+3H]^{3+}$ and $[M+3H-NH_3]^{3+}$ species at their respective calculated masses (Table S 3) ±0.02 Da. The black trace displays the BPC of the whole extract from fermentation supernatant.

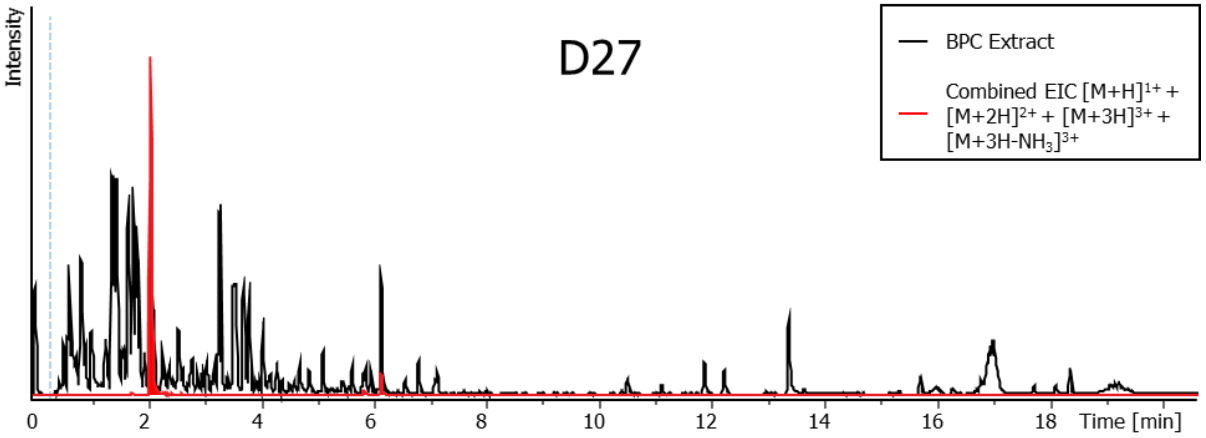

Figure S 10: Chromatogram of the *E. coli* BL21 (DE3) pNOSO-darABCDE-27 culture XAD16-N extract. The red trace displays the D27 combined EIC for the $[M+H]^{1+}$, $[M+2H]^{2+}$, $[M+3H]^{3+}$ and $[M+3H-NH_3]^{3+}$ species at their respective calculated masses (Table S 3) ±0.02 Da. The black trace displays the BPC of the whole extract from fermentation supernatant.

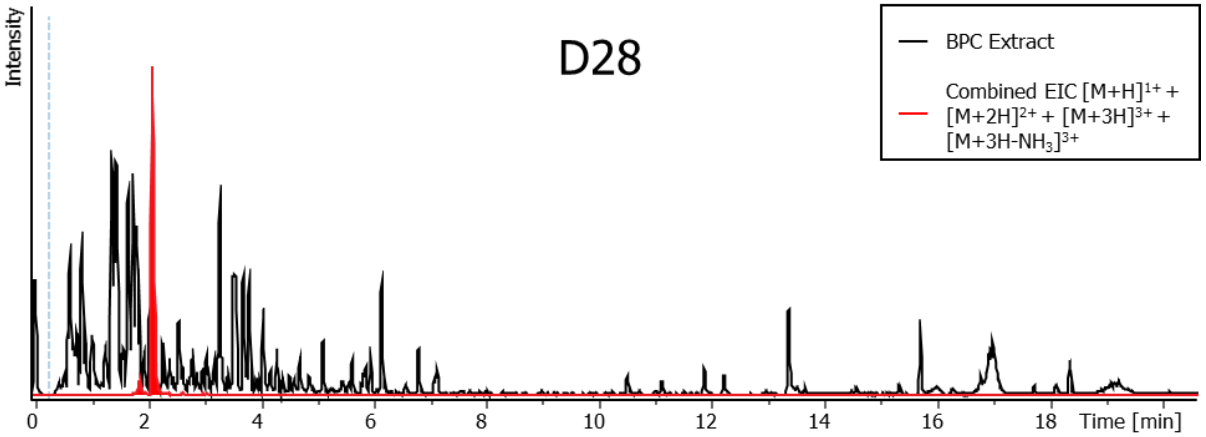

Figure S 11: Chromatogram of the *E. coli* BL21 (DE3) pNOSO-darABCDE-28 culture XAD16-N extract. The red trace displays the D28 combined EIC for the $[M+H]^{1+}$, $[M+2H]^{2+}$, $[M+3H]^{3+}$ and $[M+3H-NH_3]^{3+}$ species at their respective calculated masses (Table S 3) ±0.02 Da. The black trace displays the BPC of the whole extract from fermentation supernatant.

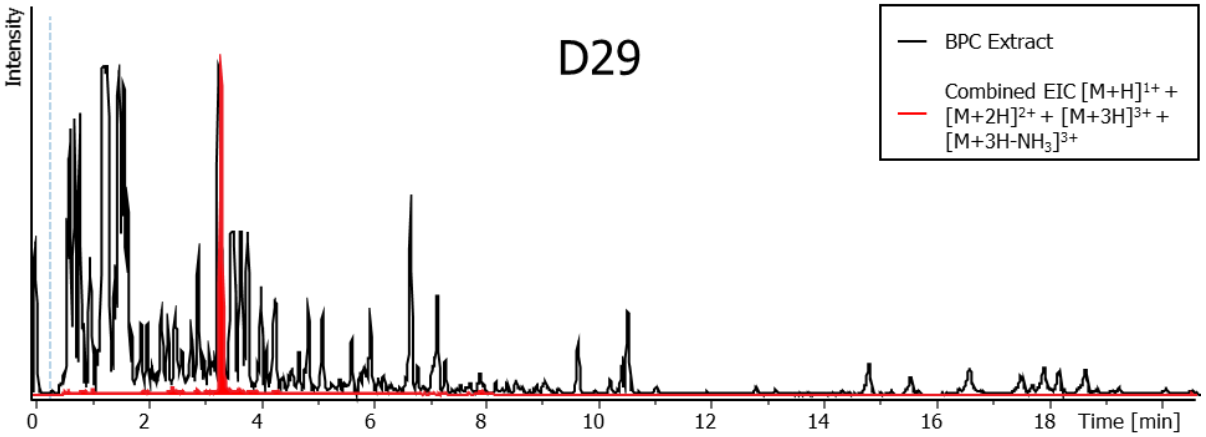

Figure S 12: Chromatogram of the *E. coli* BL21 (DE3) pNOSO-darABCDE-29 culture XAD16-N extract. The red trace displays the D29 combined EIC for the $[M+H]^{1+}$, $[M+2H]^{2+}$, $[M+3H]^{3+}$ and $[M+3H-NH_3]^{3+}$ species at their respective calculated masses (Table S 3) ±0.02 Da. The black trace displays the BPC of the whole extract from fermentation supernatant.

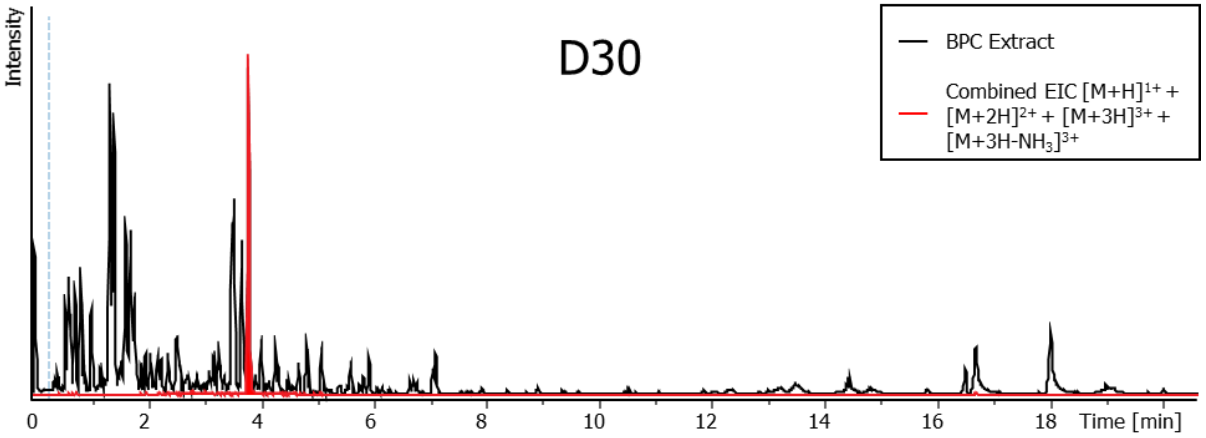

Figure S 13: Chromatogram of the *E. coli* BL21 (DE3) pNOSO-darABCDE-30 culture XAD16-N extract. The red trace displays the D30 combined EIC for the $[M+H]^{1+}$, $[M+2H]^{2+}$, $[M+3H]^{3+}$ and $[M+3H\text{-}NH_3]^{3+}$ species at their respective calculated masses (Table S 3) ±0.02 Da. The black trace displays the BPC of the whole extract from fermentation supernatant.

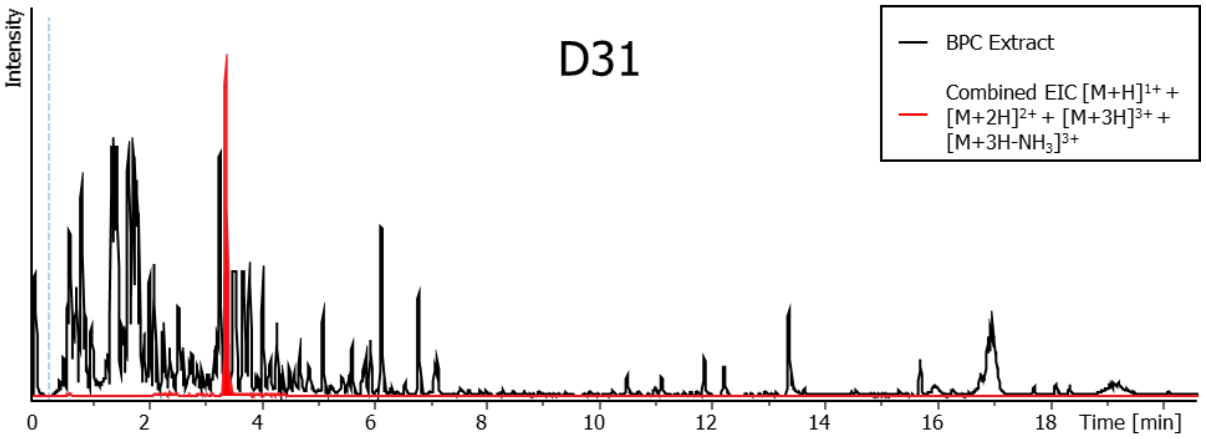

Figure S 14: Chromatogram of the *E. coli* BL21 (DE3) pNOSO-darABCDE-31 culture XAD16-N extract. The red trace displays the D31 combined EIC for the $[M+H]^{1+}$, $[M+2H]^{2+}$, $[M+3H]^{3+}$ and $[M+3H\text{-}NH_3]^{3+}$ species at their respective calculated masses (Table S 3) ±0.02 Da. The black trace displays the BPC of the whole extract from fermentation supernatant.

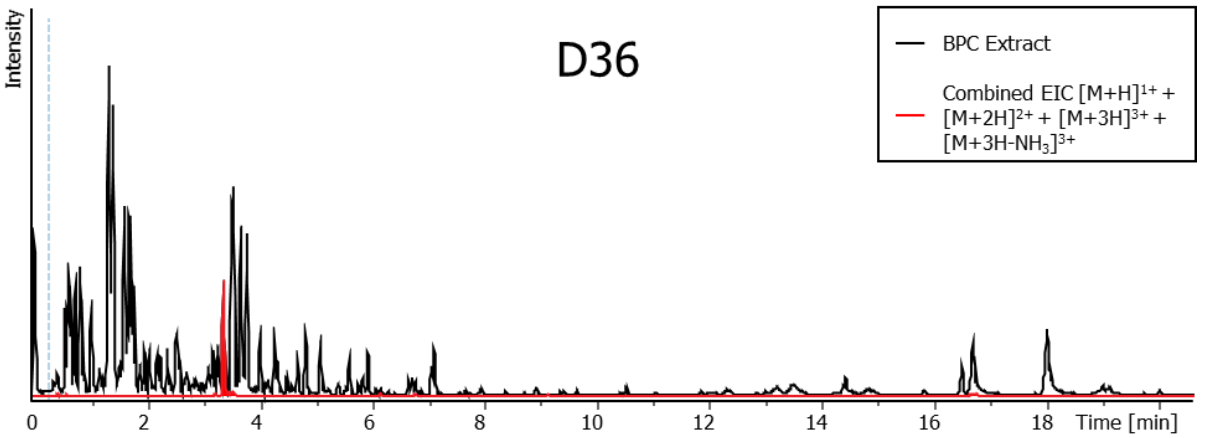

Figure S 15: Chromatogram of the *E. coli* BL21 (DE3) pNOSO-darABCDE-36 culture XAD16-N extract. The red trace displays the D36 combined EIC for the $[M+H]^{1+}$, $[M+2H]^{2+}$, $[M+3H]^{3+}$ and $[M+3H\text{-}NH_3]^{3+}$ species at their respective calculated masses (Table S 3) ±0.02 Da. The black trace displays the BPC of the whole extract from fermentation supernatant.

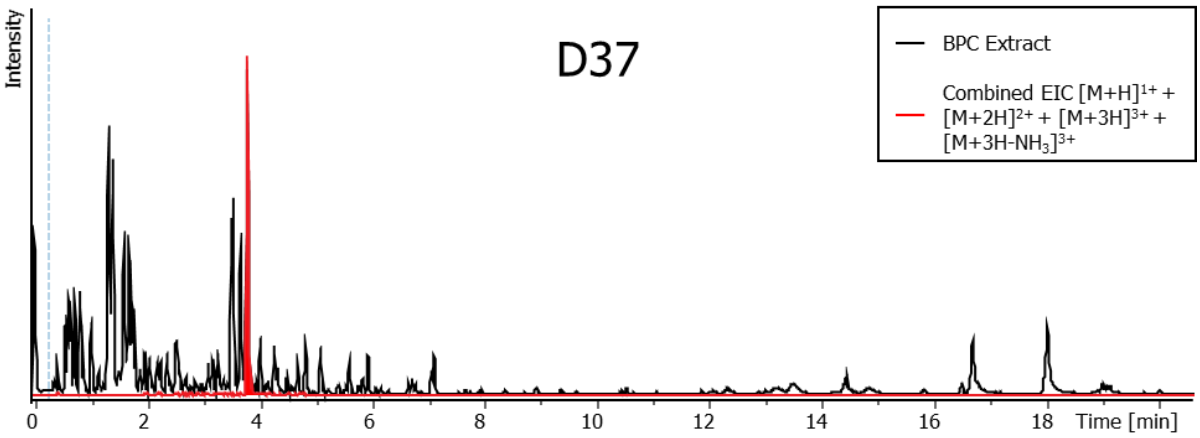

Figure S 16: Chromatogram of the *E. coli* BL21 (DE3) pNOSO-darABCDE-37 culture XAD16-N extract. The red trace displays the D37 combined EIC for the $[M+H]^{1+}$, $[M+2H]^{2+}$, $[M+3H]^{3+}$ and $[M+3H-NH_3]^{3+}$ species at their respective calculated masses (Table S 3) ±0.02 Da. The black trace displays the BPC of the whole extract from fermentation supernatant.

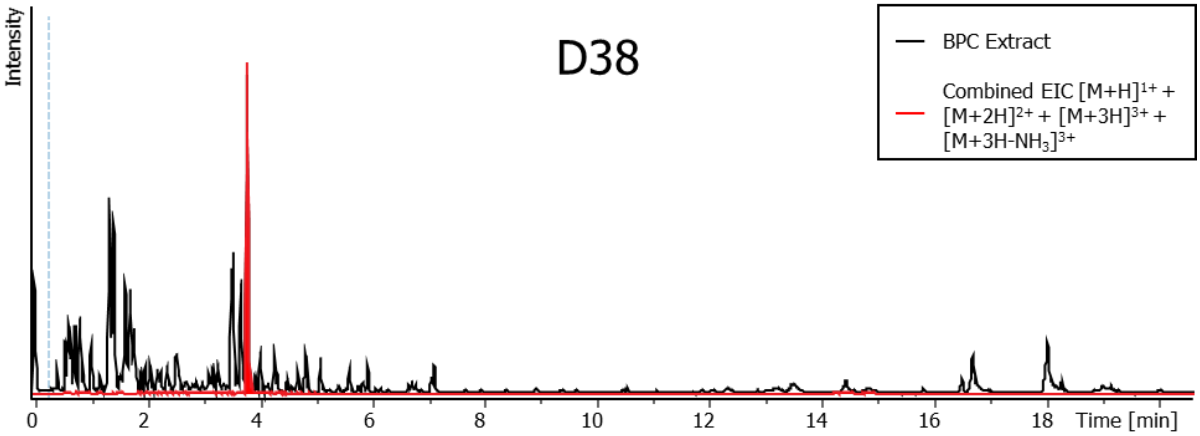

Figure S 17: Chromatogram of the *E. coli* BL21 (DE3) pNOSO-darABCDE-38 culture XAD16-N extract. The red trace displays the D38 combined EIC for the $[M+H]^{1+}$, $[M+2H]^{2+}$, $[M+3H]^{3+}$ and $[M+3H-NH_3]^{3+}$ species at their respective calculated masses (Table S 3) ±0.02 Da. The black trace displays the BPC of the whole extract from fermentation supernatant.

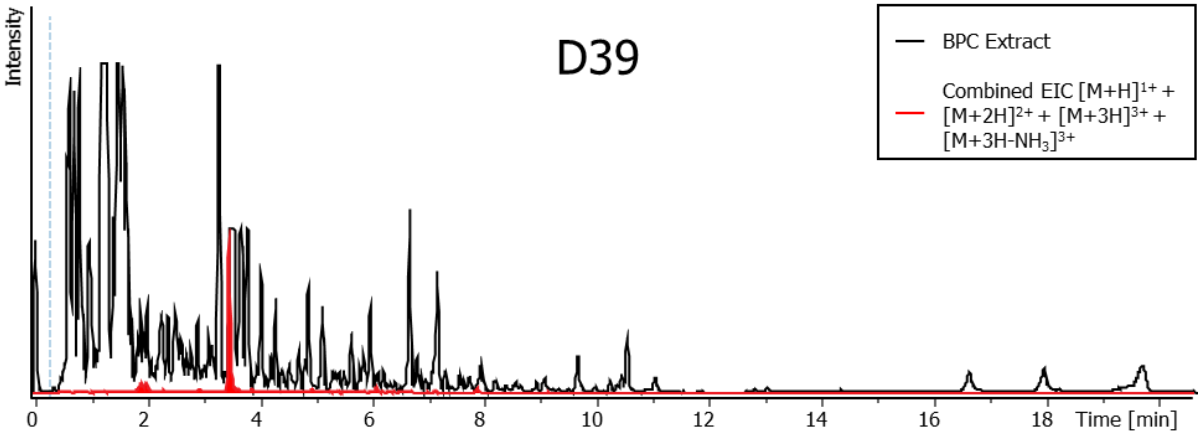

Figure S 18: Chromatogram of the *E. coli* BL21 (DE3) pNOSO-darABCDE-39 culture XAD16-N extract. The red trace displays the D39 combined EIC for the $[M+H]^{1+}$, $[M+2H]^{2+}$, $[M+3H]^{3+}$ and $[M+3H-NH_3]^{3+}$ species at their respective calculated masses (Table S 3) ±0.02 Da. The black trace displays the BPC of the whole extract from fermentation supernatant.

Analyses of darobactin derivative MS2 spectra

Here, all MS2 spectra of the derivatives are displayed. The blue square symbols the precursor ion, which was picked for fragmentation. In all spectra, the $[M\text{-}NH_3+2H]^{2+}$ fragment and the typical b2-ion with ammonia loss (theoretical mass of 300.0979) can be observed. Fragmentation pattern is shown in detail for the halogenated derivatives (Figure S 38 and Figure S 40).

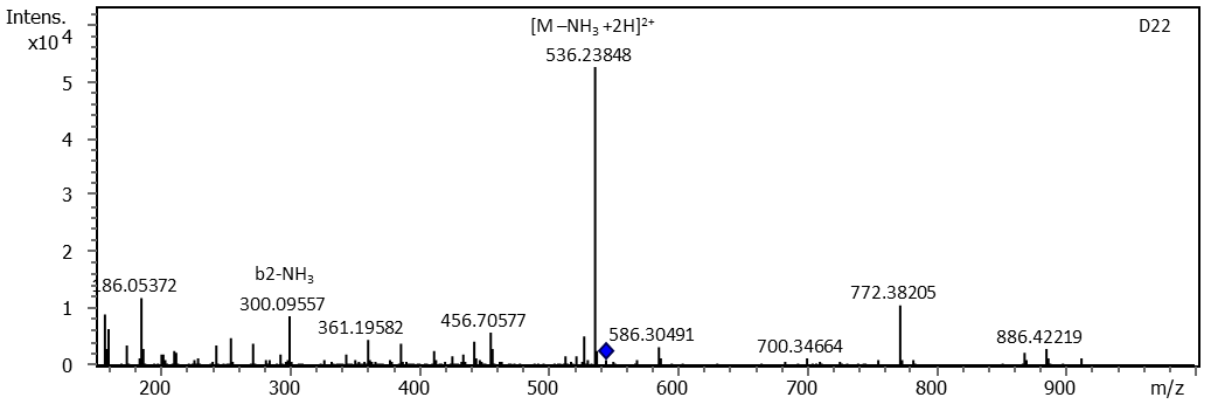

Figure S 19: MS2 spectrum of D22.

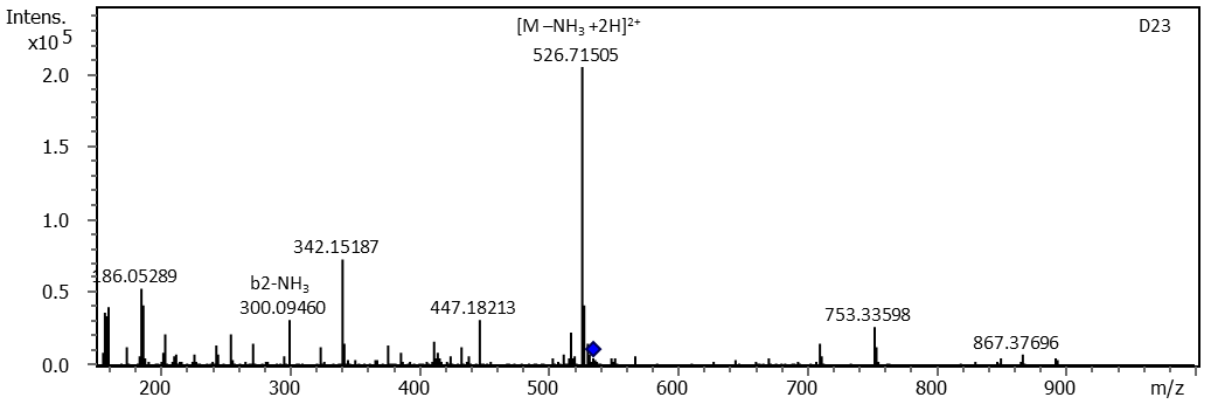

Figure S 20: MS2 spectrum of D23.

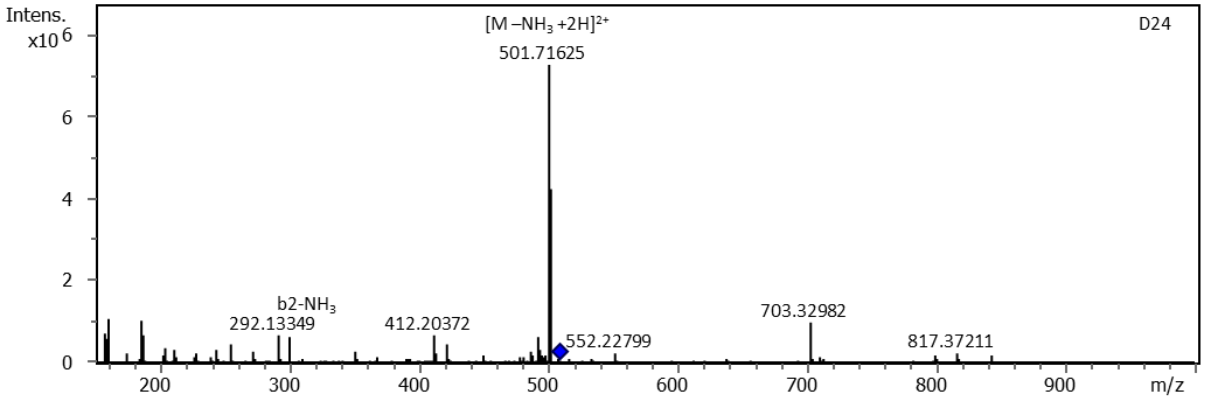

Figure S 21: MS2 spectrum of D24.

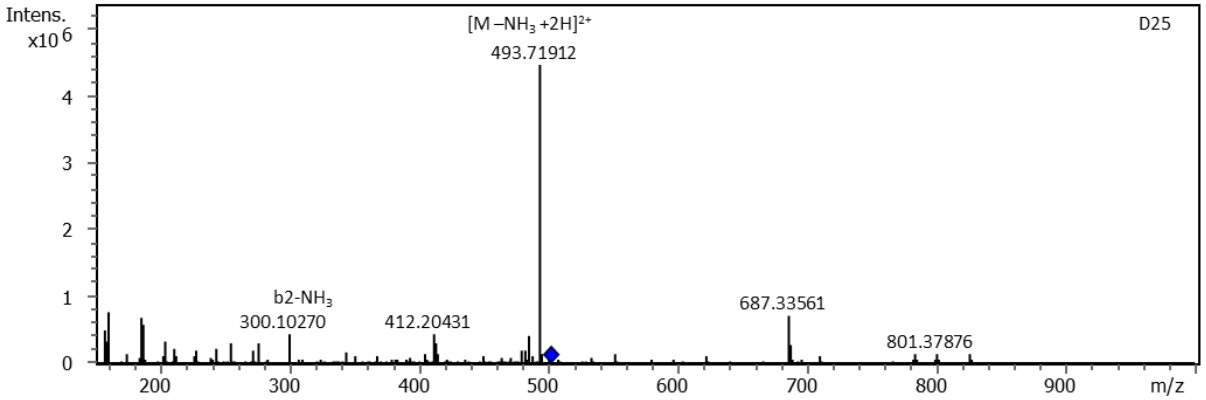

Figure S 22: MS2 spectrum of D25.

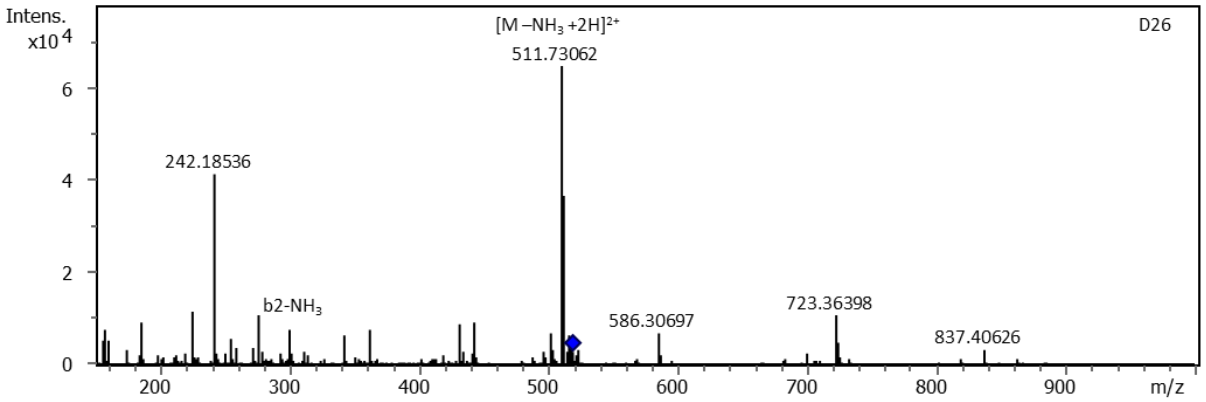

Figure S 23: MS2 spectrum of D26.

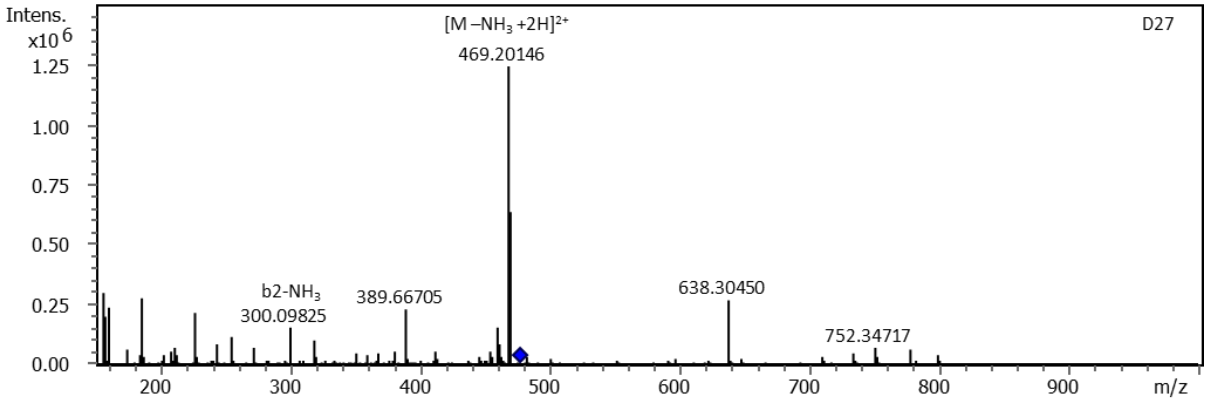

Figure S 24: MS2 spectrum of D27.

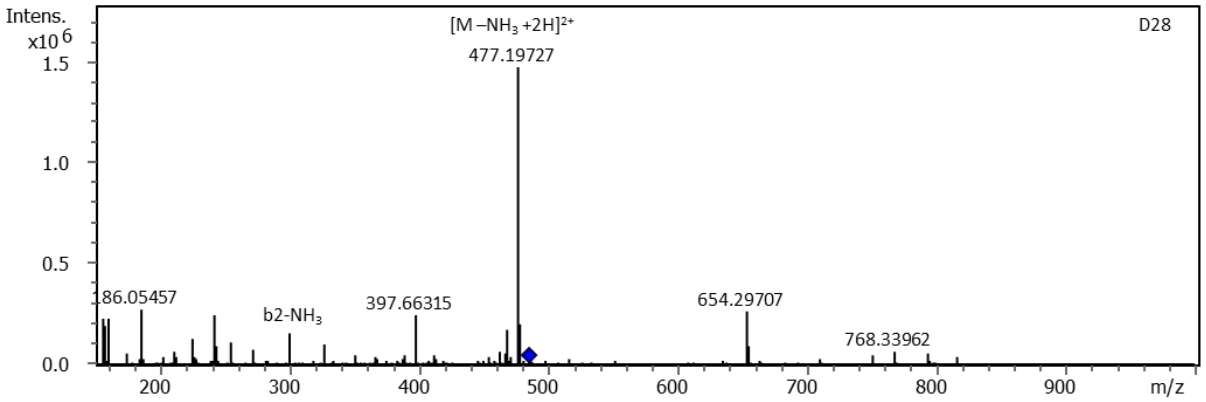

Figure S 25: MS2 spectrum of D28.

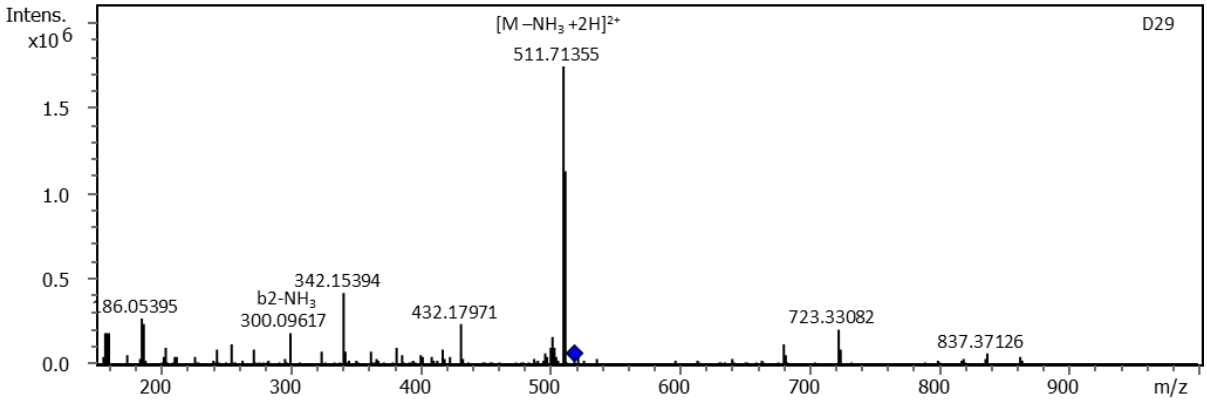

Figure S 26: MS2 spectrum of D29.

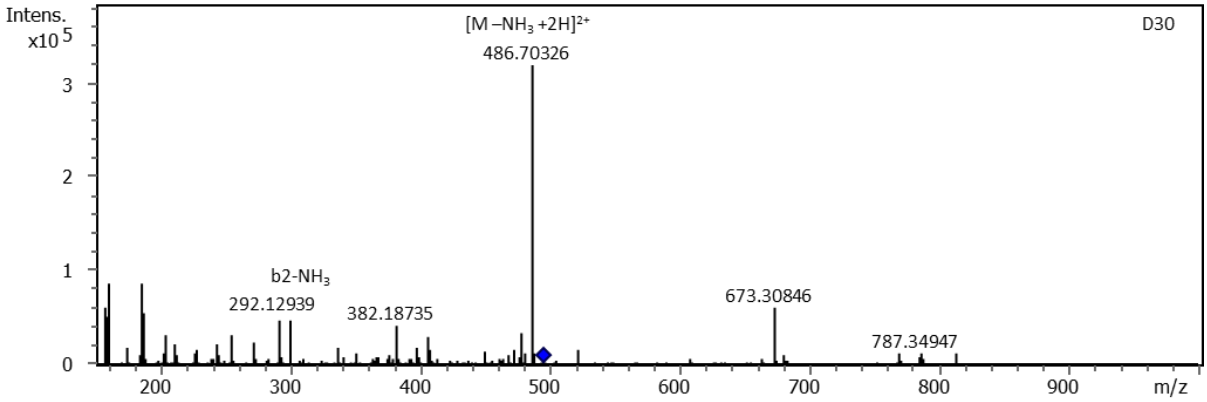

Figure S 27: MS2 spectrum of D30.

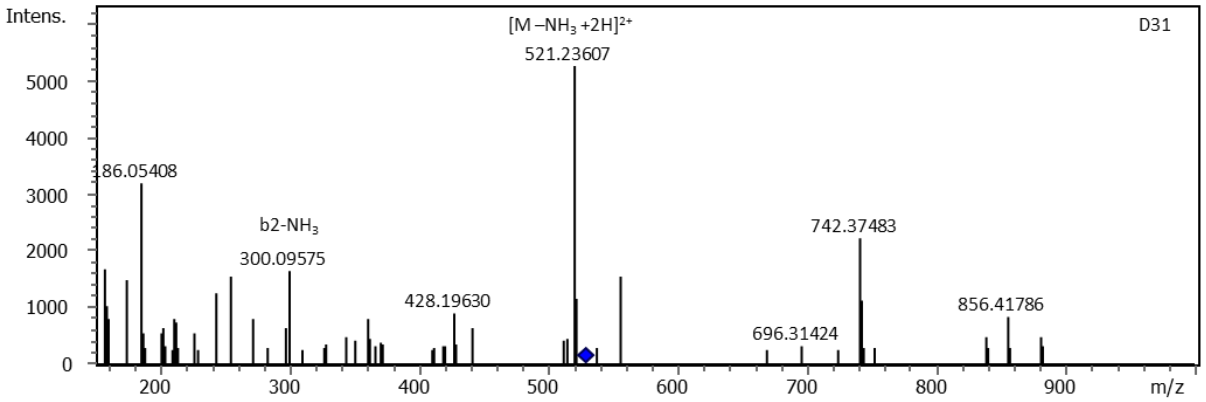

Figure S 28: MS2 spectrum of D31.

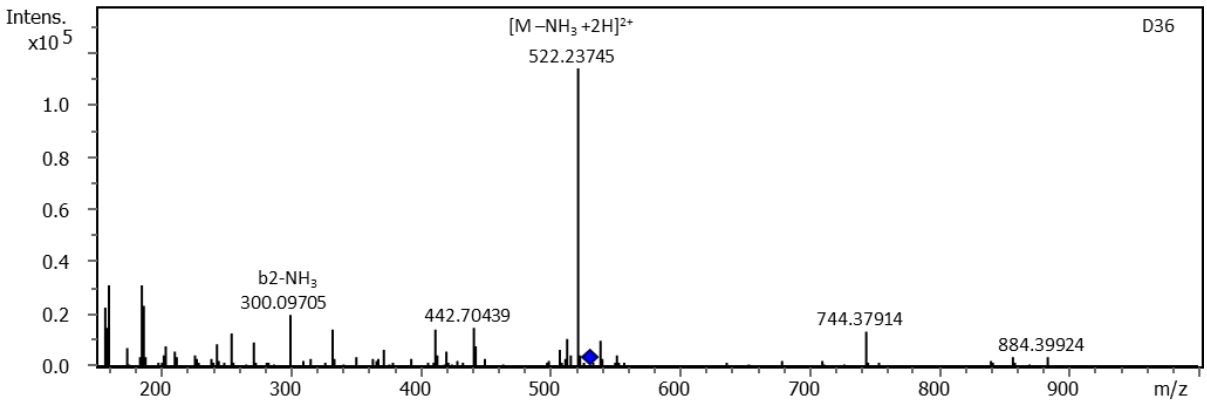

Figure S 29: MS2 spectrum of D36.

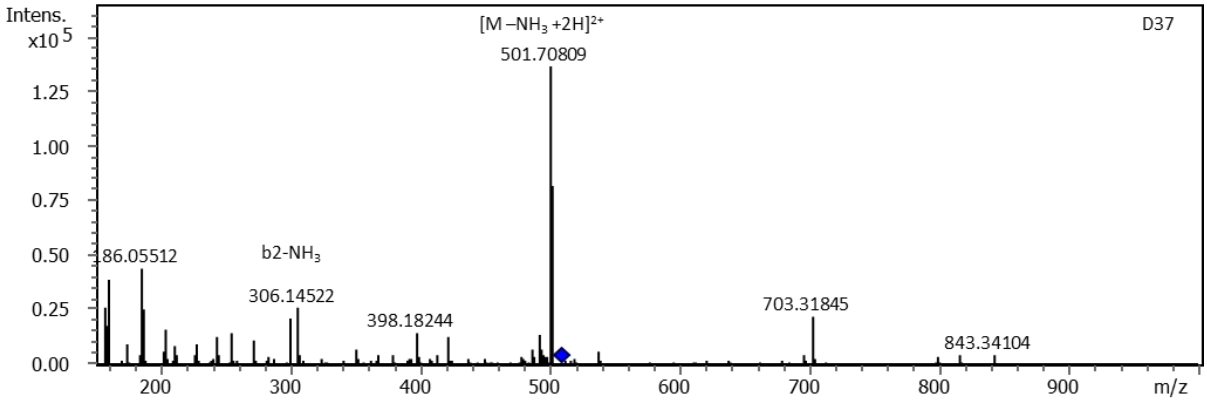

Figure S 30: MS2 spectrum of D37.

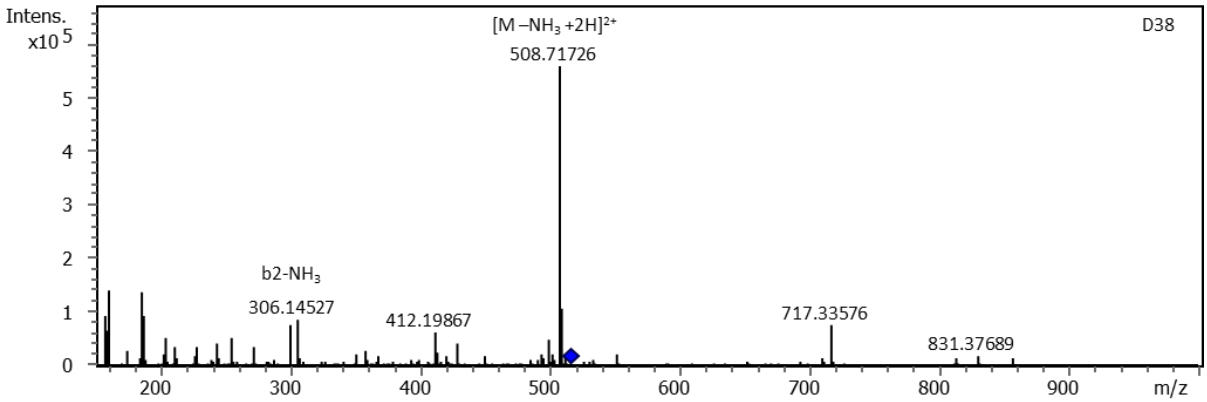

Figure S 31: MS2 spectrum of D38.

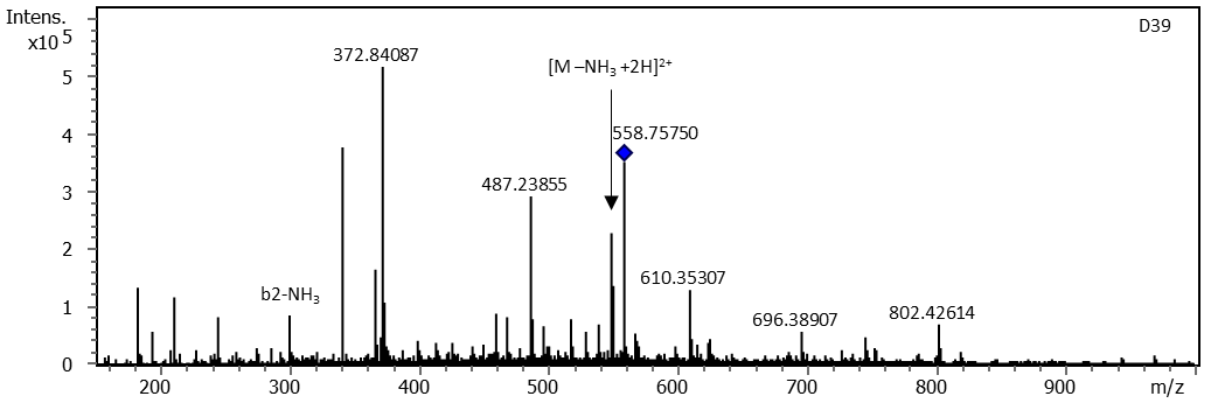

Figure S 32: MS2 spectrum of D39.

Analyses of cysteine derivatives D6 and D32 MS and MS2 spectra

The cysteine derivatives D6 and D32 had an expected mass shift of 95.5126 for the $[M+2H]^{2+}$ mass (191.0252 neutral mass), as observed before.[1] Treatment with 10 % β-mercaptoethanol and heating to 85 °C for 10 min results in appearance of the expected mass (Figures S 33 and 35). Judging from the higher AUC of the reduced $D6^{[R]}$ and $D32^{[R]}$ (Figure S 33 and Figure S 35, b), it is possible, that different,

unreported protection groups are present. The main protection group, which was identified using NMR (Figure S 76 - Figure S 85) consists of cysteine and lactic acid. Chirality of lactic acid was deemed unimportant for our conclusions, based only on the overall length of position 4 sidechain, which was prolonged through residue.

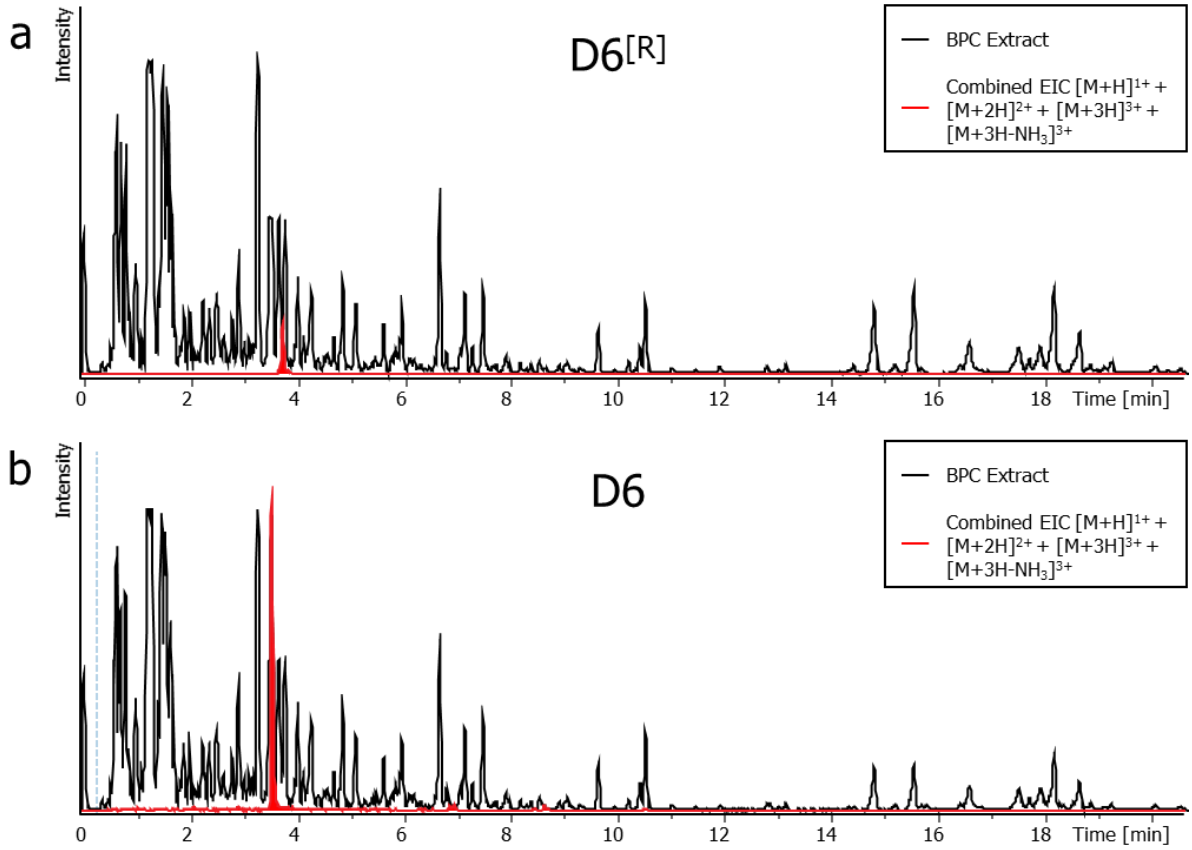

Figure S 33: Chromatogram of the *E. coli* BL21 (DE3) pNOSO-darABCDE-6 culture XAD16-N extract. The red trace displays the D6 combined EIC for the $[M+H]^{1+}$, $[M+2H]^{2+}$, $[M+3H]^{3+}$ and $[M+3H-NH_3]^{3+}$ species with expected protection group [R] on cysteine (a) and without protection group via reduction (b) at their respective calculated masses (Table S 3) ±0.02 Da. A displays the 1:5 reconstituted extract, diluted additionally with 1/10 dH_2O, while B was diluted with 1/10 β-mercaptoethanol. Both were heated 10 min at 85 °C, centrifuged and measured. The black trace displays the BPC of the whole extract from fermentation supernatant.

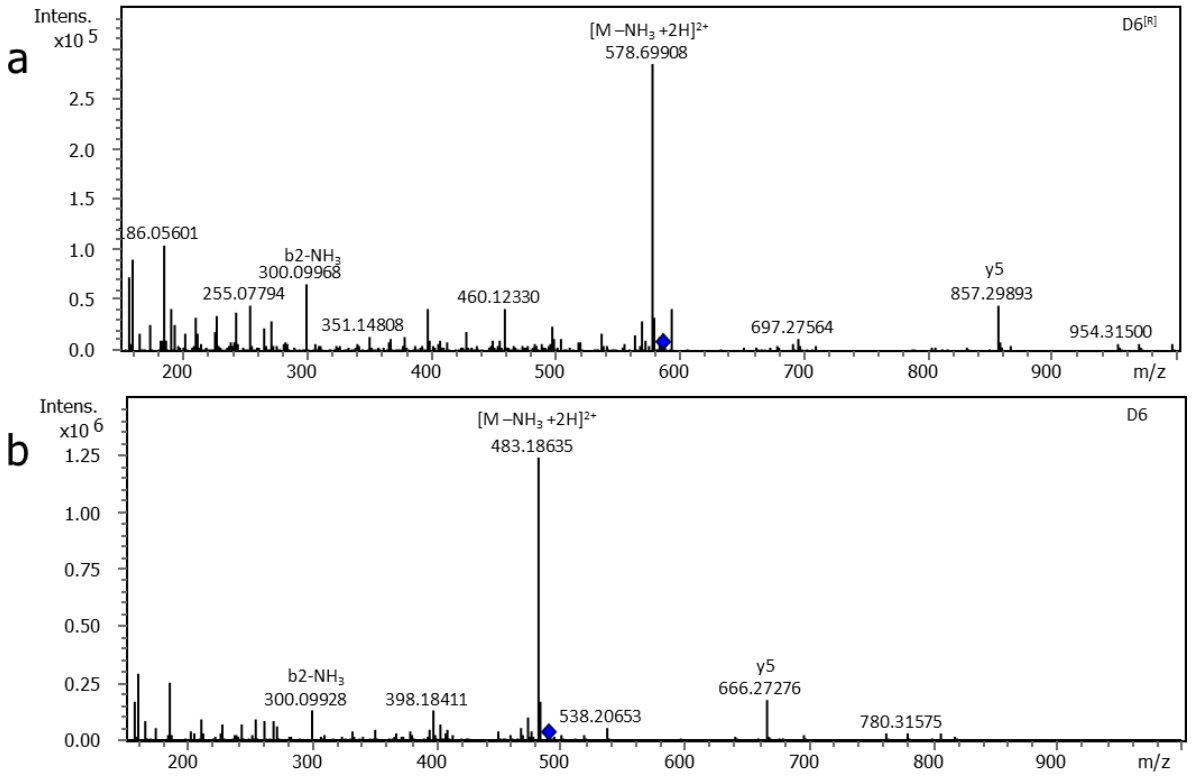

Figure S 34: MS2 spectrum of D6 before cleaving of with its most abundant protection group (a) and after reduction with β-mercaptoethanol (b).

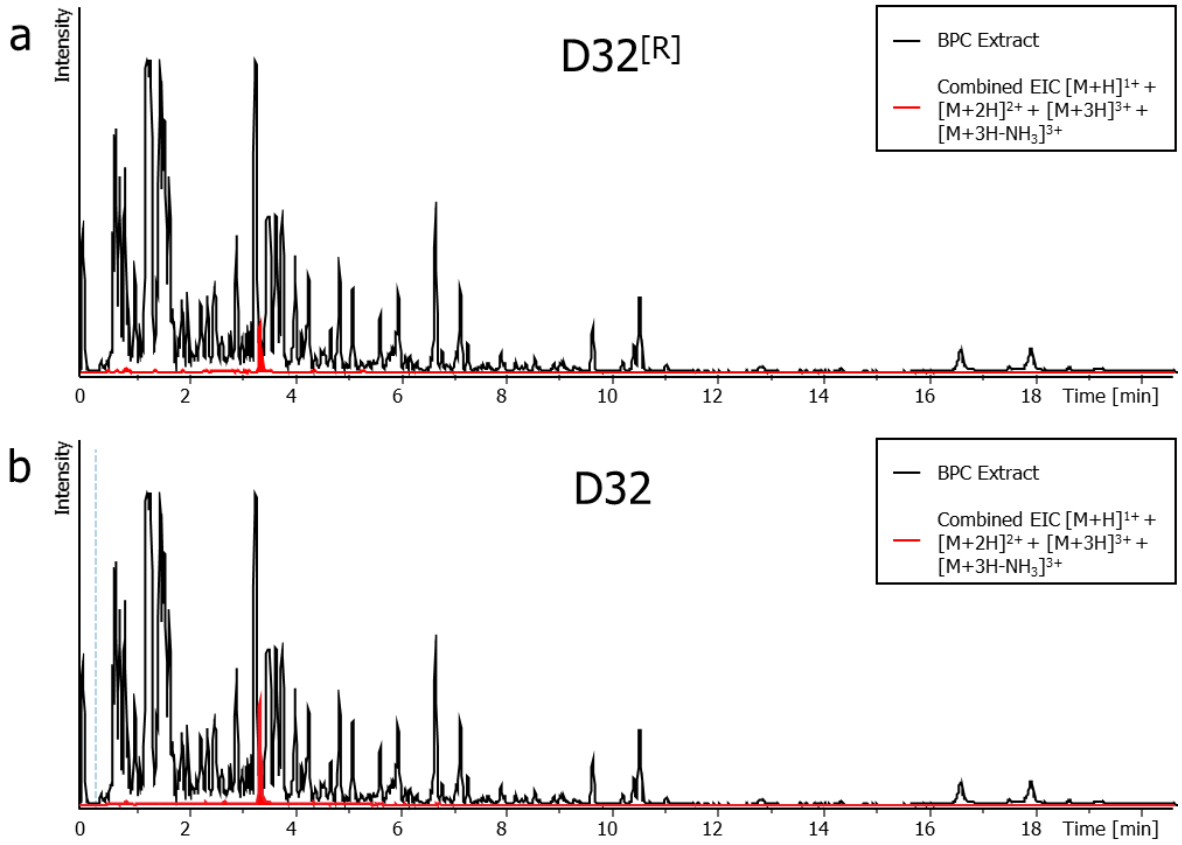

Figure S 35: Chromatogram of the *E. coli* BL21 (DE3) pNOSO-darABCDE-32 culture XAD16-N extract. The red trace displays the D32 combined EIC for the $[M+H]^{1+}$, $[M+2H]^{2+}$, $[M+3H]^{3+}$ and $[M+3H\text{-}NH_3]^{3+}$ species with expected protection group [R] on cysteine (a) and without protection group via reduction (b) at their respective calculated masses (Table S 3) ±0.02 Da. A displays the 1:5 reconstituted extract, diluted additionally with 1/10 dH_2O, while B was diluted with 1/10 β-mercaptoethanol. Both were heated 10 min at 85 °C, centrifuged and measured. The black trace displays the BPC of the whole extract from fermentation supernatant.

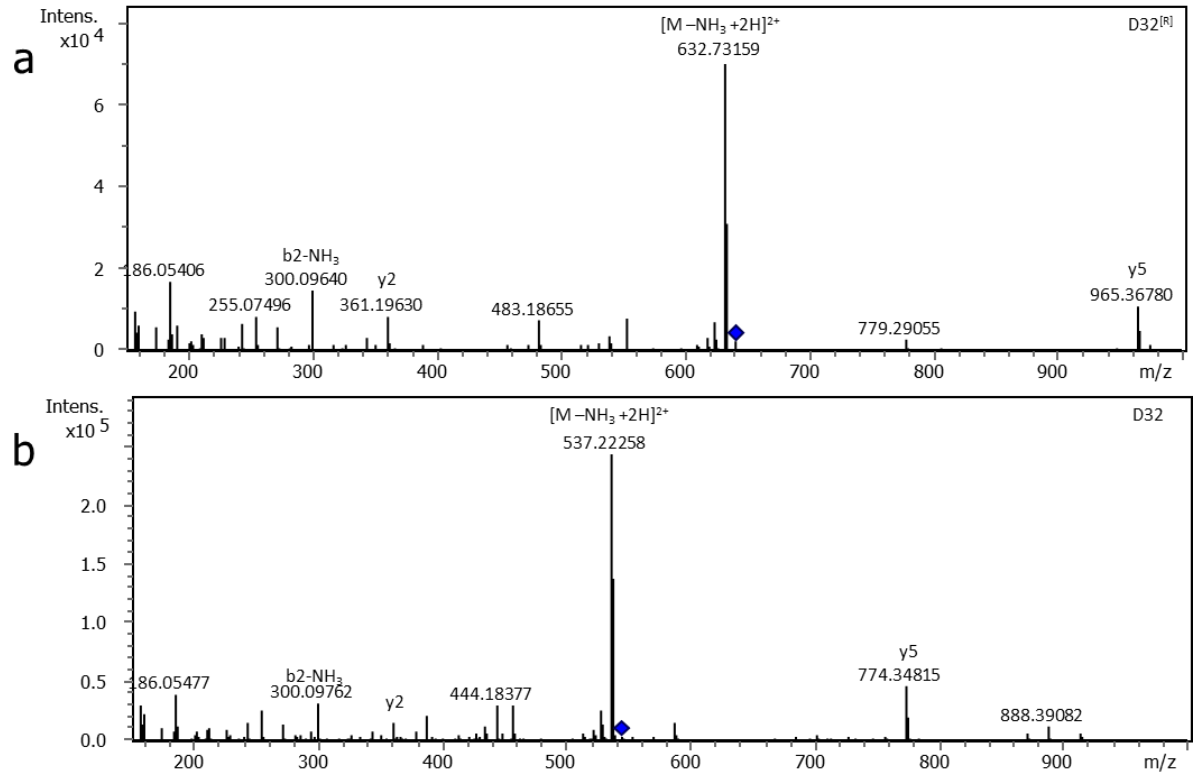

Figure S 36: MS2 spectrum of D32 before cleaving of with its most abundant protection group (a) and after reduction with β-mercaptoethanol (b).

Analyses of halogenated D9

MS and MS2 spectra

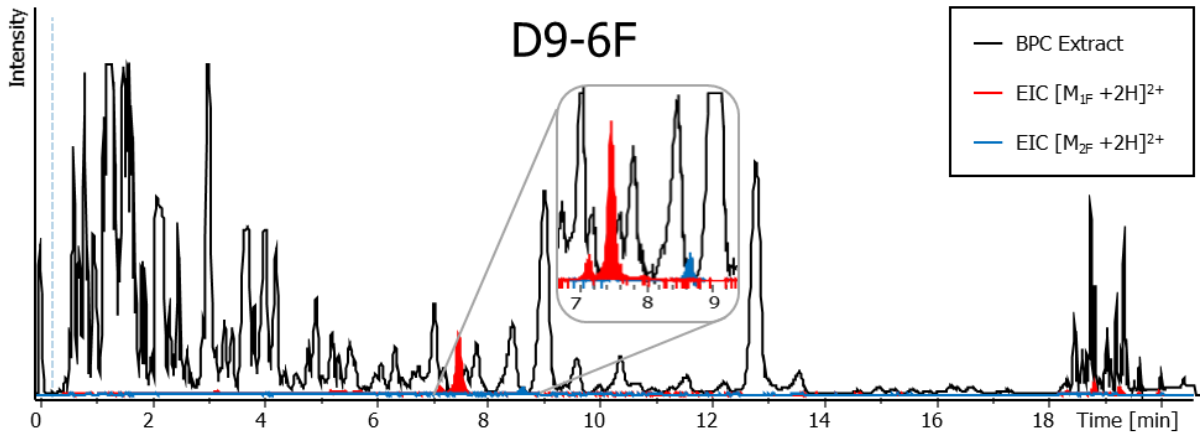

Figure S 37: Chromatogram of *E. coli* BL21 (DE3) pNOSO-darABCDE-9-6F culture XAD-16N extract. The red trace displays the two single fluorinated isomers and the blue trace the twofold fluorinated one at 7-9 min (grey: Zoom into the relevant area). Corresponding masses for fluorination on middle tryptophan (W3) differ, because of prevented ring formation between W3 and K5 and were not found with darobactin specific charge states.

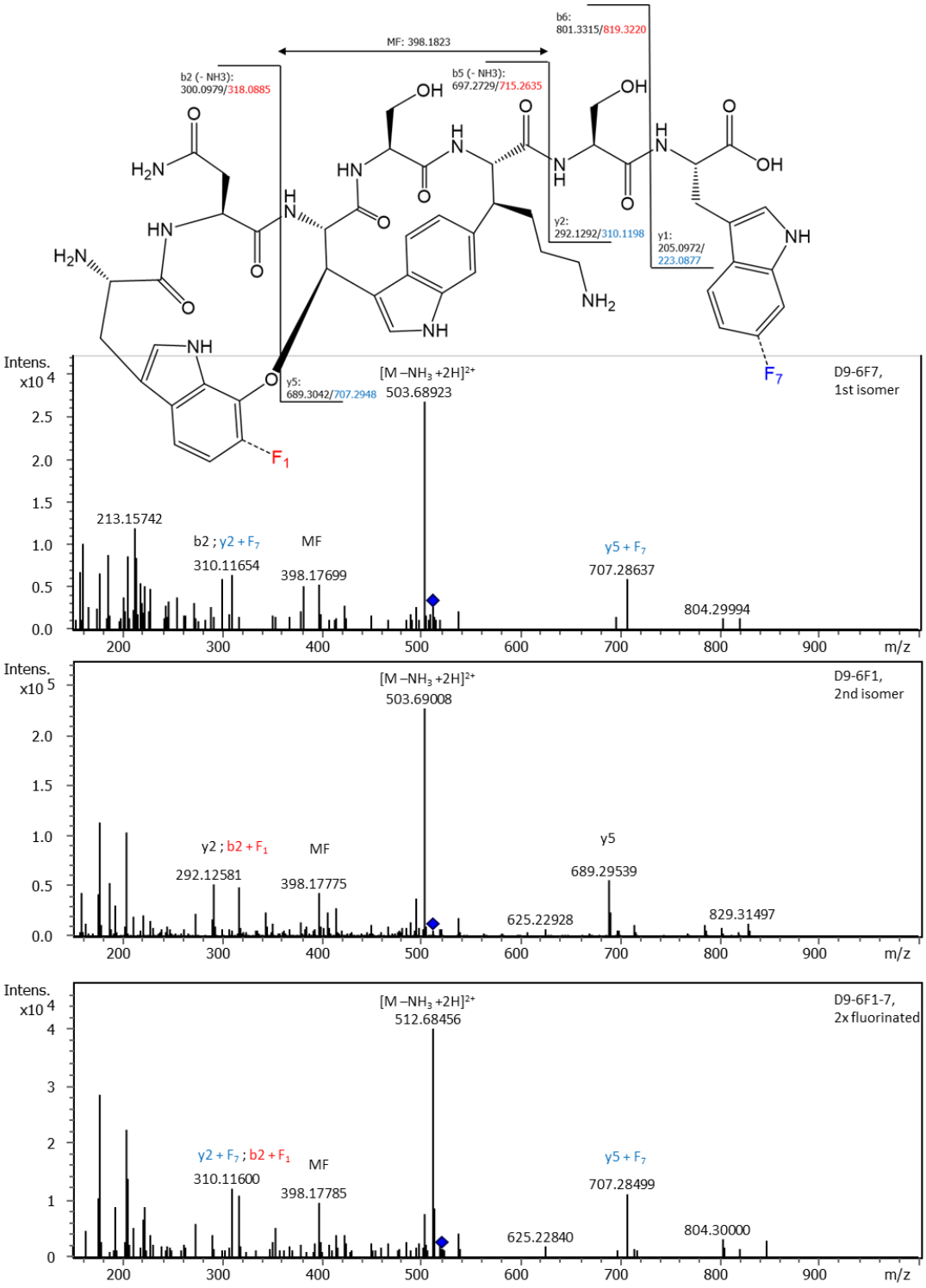

Figure S 38: MS2 fragmentation pattern of D9-6F. Possible fluorination sites from feeding 6-fluoro-L-tryptophan are highlighted in colors red (W1) and blue (W7). The colors are reflected in the potential mass shifts, which could be overserved of different b- and y- ions and (not of) middle fragment (MF). As fluorination on W3 would prevent the ring formation on this position its mass would differ by 2 hydrogens and was not observed. All ions can be assigned one of the two positions. Found mass shifts indicating the real position of fluorination are highlighted in their respective colors.

For fluorinated D9, fluorination on W3 would prevent ring formation, therefore differ in mass. The respective masses for fluorination on this position (and with other positions together) could not be

found with a m/z of $[M+2H]^{2+}$ (513.2174, 522.2127, 531.2080). The other two fluorinations are present and could be identified from their masses (Figure S 37) and MS2 fragmentation pattern (Figure S 38). First eluting, single fluorinated isomer (top) shows mass shifts of +17.99 (+F-H) on the y2 and y5 ion, therefore fluorination is only possible on last tryptophan (W7). Second eluting, single fluorinated isomer (middle) shows fluorine mass shift for b2-ion only, only possible for fluorination on W1. Two times fluorinated D9 (bottom) shows fluorine mass shifts of b2, y2 and y5 ions, so it is fluorinated on frontal and terminal tryptophans (W1,7). The main isomer (2nd eluting) was purified and was confirmed using NMR structure elucidation.

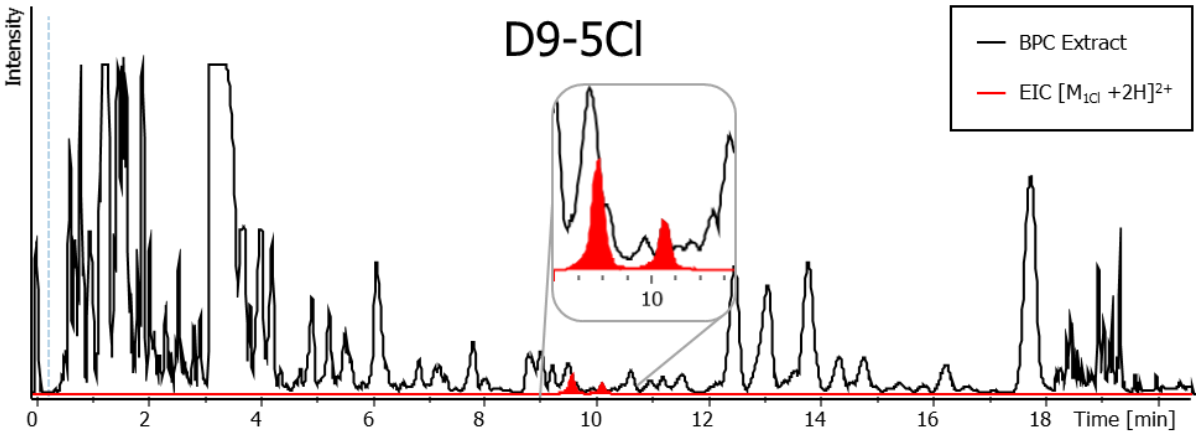

Figure S 39: Chromatogram of *E. coli* BL21 (DE3) pNOSO-darABCDE-9-5Cl culture XAD-16N extract. The red trace displays the two single chlorinated isomers between 9-10.2 min (grey: Zoom into the relevant area). Twofold and threefold chlorinated D9 could not be observed with darobactin specific charge state.

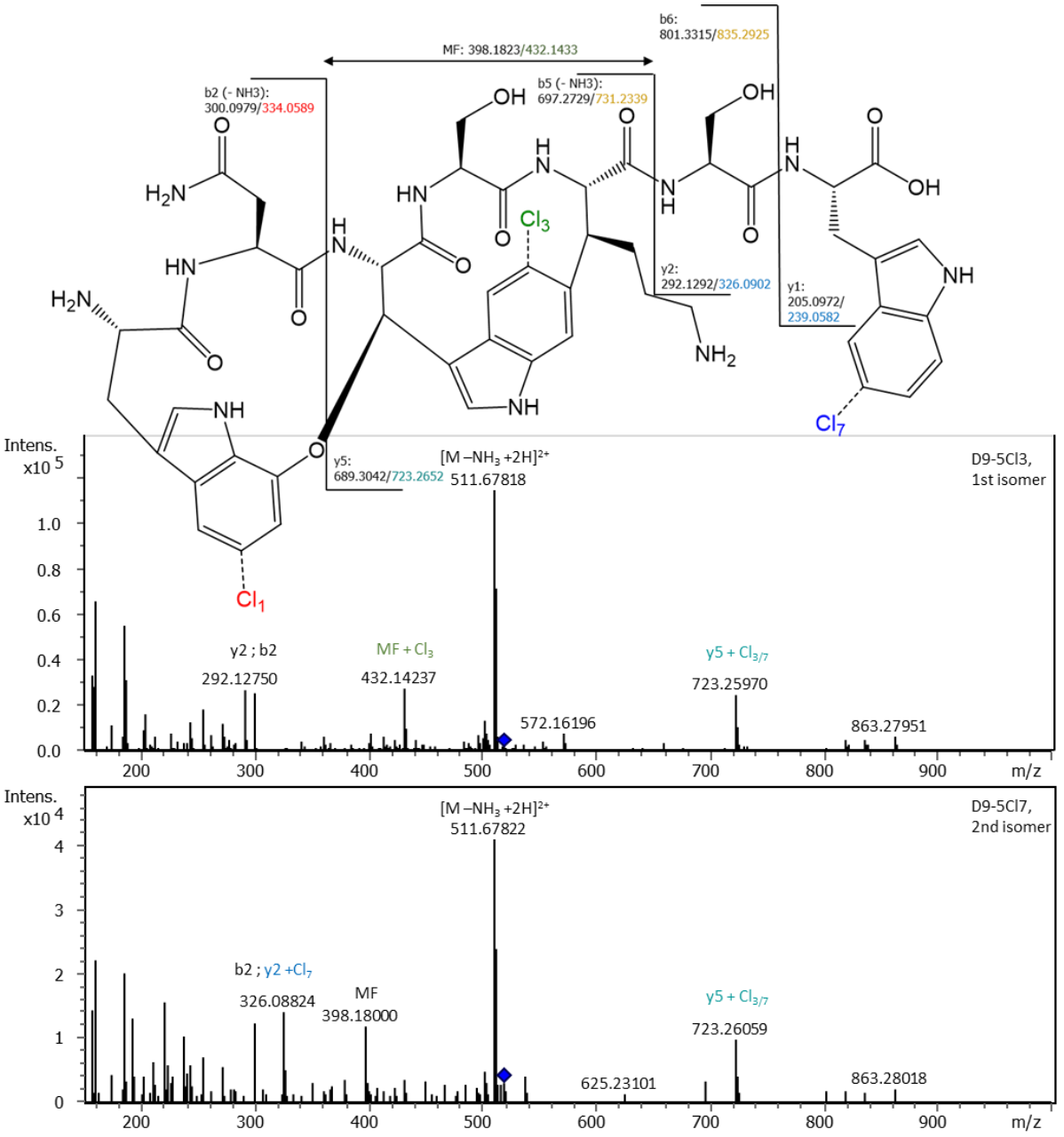

Figure S 40: MS2 fragmentation pattern of D9-5Cl. Possible chlorination sites from feeding 5-chloro-L-tryptophans are highlighted in colors red (W1), green (W3) and blue (W7). The colors are reflected in the potential mass shifts, which could be overserved of different b- and y- ions and middle fragment (MF). Found mass shifts indicating the real position of chlorination are highlighted in their respective colors. As some fragment masses indicate ambiguous chlorination sites, they are marked in the mixed colors of the two respective sites (blue + green equals turquoise, red + green equals orange).

For chlorinated D9, no two-fold (537.1753) or three-fold (554.1559) could be identified. However, two one-fold chlorinated isomers were observed (Figure S 39 and Figure S 40). The first eluting, single chlorinated isomer (top) shows a mass shift of +33.96 (+Cl-H) of middle fragment (MF) ion, and no mass shifts of y2- and b2-ions, therefore chlorination is only possible on second tryptophan (W3). Second eluting, single chlorinated isomer (bottom) shows chlorine mass shift for y2-ion only, as only possible for chlorination on W7. Two and three times chlorinated D9 could not be observed. While the chlorinated y5-ion fragment indicates chlorination on either W3 or W7 (turquoise), based on the y2-

ion and MF-ion, the position W3 for the first eluting isomer and the position W7 for the second isomer can be safely assumed.

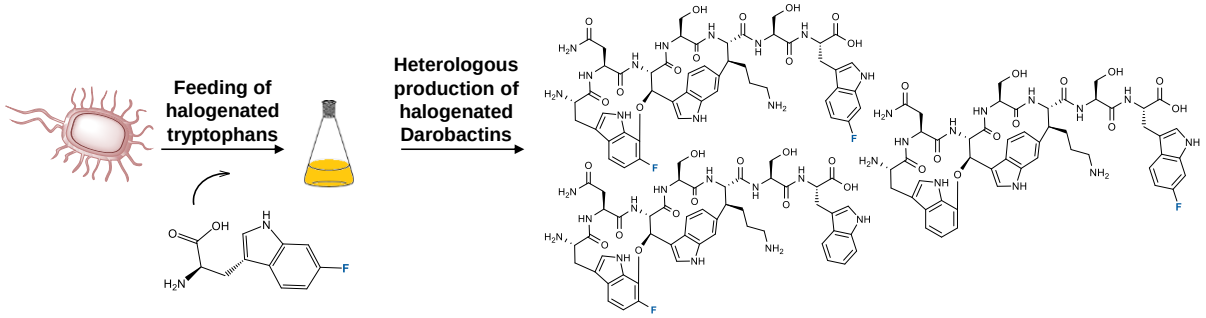

MIC [µg/mL]	*A. baumannii*		*E. coli*	*K. pneumoniae*	*P. aeruginosa*		
Darobactin	DSM-30007	DSM-30008	ATCC25922	DSM-301204	DSM-22644	DSM-19882	PA14 Δ*mexAB*
D9-6F1	2 – 4	1	1	1	1	8	4
D9-6F7	2 - 4	1	0.5	0.5 - 1	0.5	8	4 - 8
D9	2	1	2	2	0.25	2	1
DA	16	2	2	2 - 4	0.5 - 1	16	4

Figure S 41: Generation and activity of fluorinated D9 against Gram-negative bacteria. *Acinetobacter baumannii* (*A. baumannii*), *Escherichia coli* (*E. coli*), *Klebsiella pneumoniae* (*K. pneumoniae*) and *Pseudomonas aeruginosa* (*P. aeruginosa*). Feeding of 6-fluoro-L-tryptophan to the production culture led to multiple halogenated D9 derivatives, where the fluorinated compound is incorporated into either the first (F1) or the terminal (F7) tryptophan. F1 and F7 are show approximately equipotent antibacterial activity to D9.

BamA interaction site

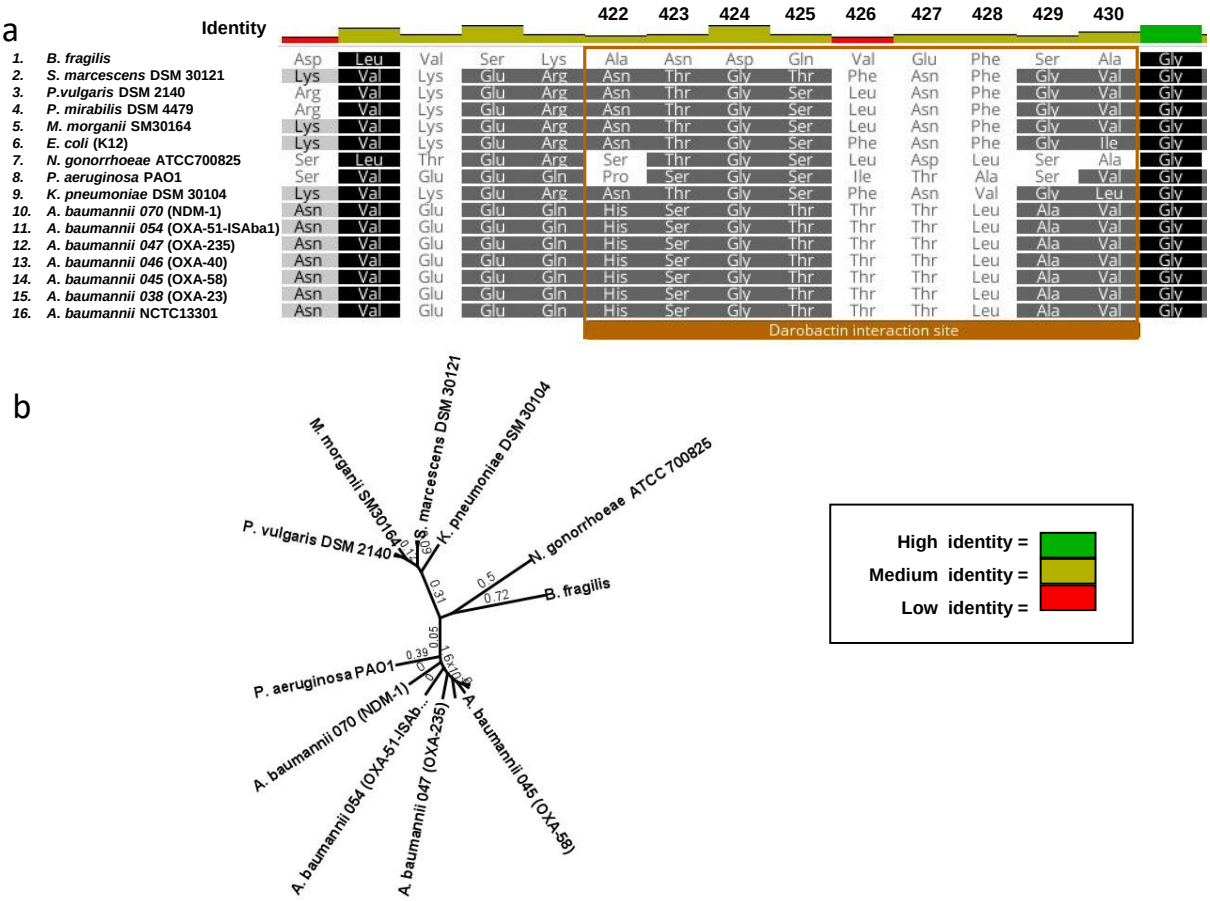

Figure S 42: Alignment of BamA sequence variations. a, BamA sequence alignment of, at least, one represent of each tested Gram-negative species (Table 2 and 3 of the manuscript) and of *Bacteroides fragilis* (*B. fragilis*) as control. b, phylogenetic tree of BamA amino acid sequences of selected bacteria. The color legend shows 100 % identity across all amino acid

sequences in green, 30 % to below 100 % identity in yellow and less than 30 % in red. The graph was created with Geneious software 2021.2.2.

Cryo-EM of BAM-D22

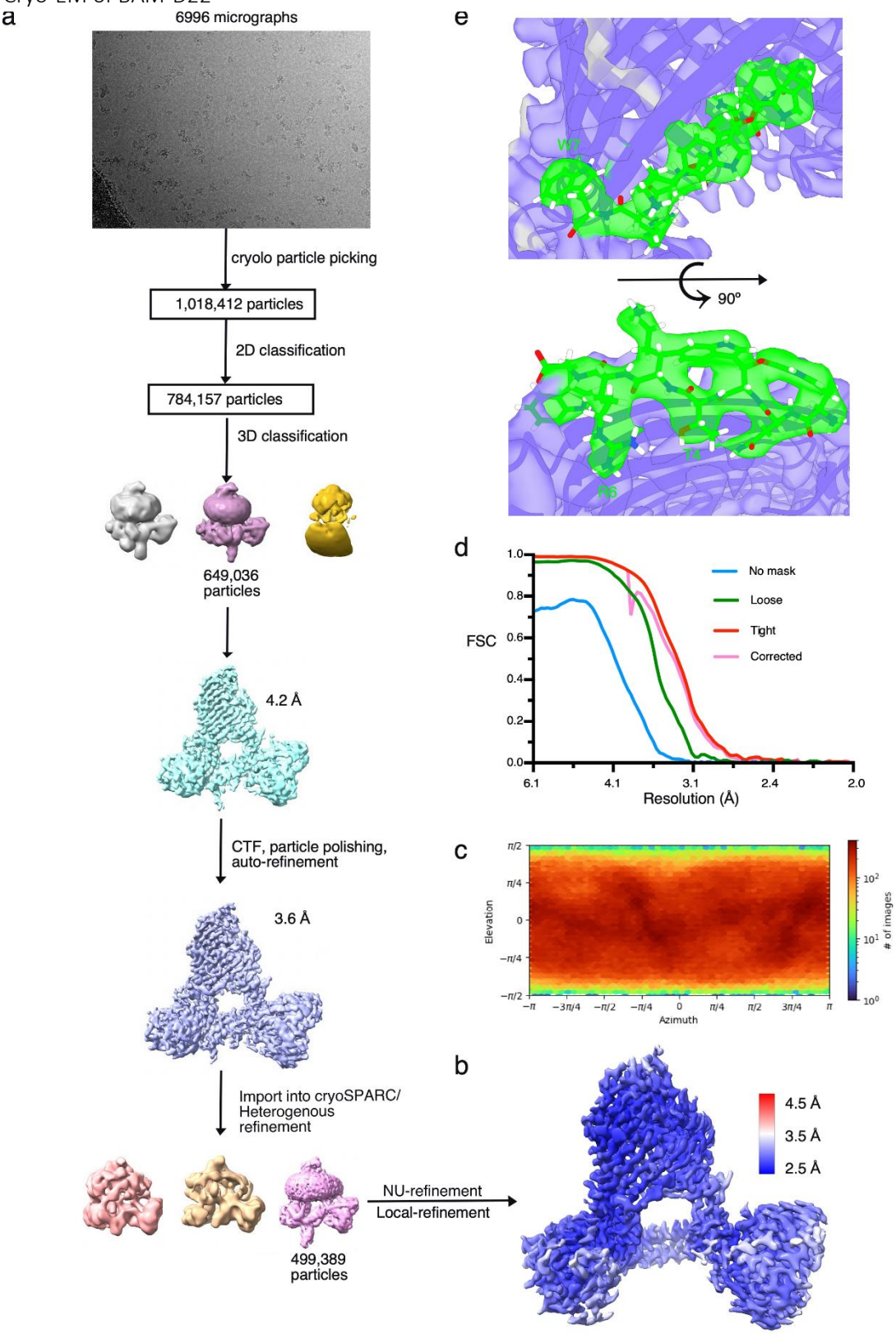

Figure S 43: Cryo-EM structure of BAM-D22 complex. a, workflow of data generation, processing and refinement to decipher BAM-D22 complex. b, BAM overview map with resolution of the EM reconstruction, highlighting local variations from 2.5 Å (blue) to 4.5 Å (red). c, angular distribution of D22 bound to BAM complex was calculated in cryoSPARC for particle projections. Heat map shows number of particles for each viewing angle. d, Fourier shell correlation (FSC) curves for

corrected, tight, loose and unmasked masks. e, front (top) and 90 ° rotated (bottom) view of magnified BAM-D22 interaction area showing electron density surface of D22 (green) bound on BAM (blue). Modified positions of D22 compared to D9 were labeled (one letter code) as well as the terminal tryptophan (W_7).

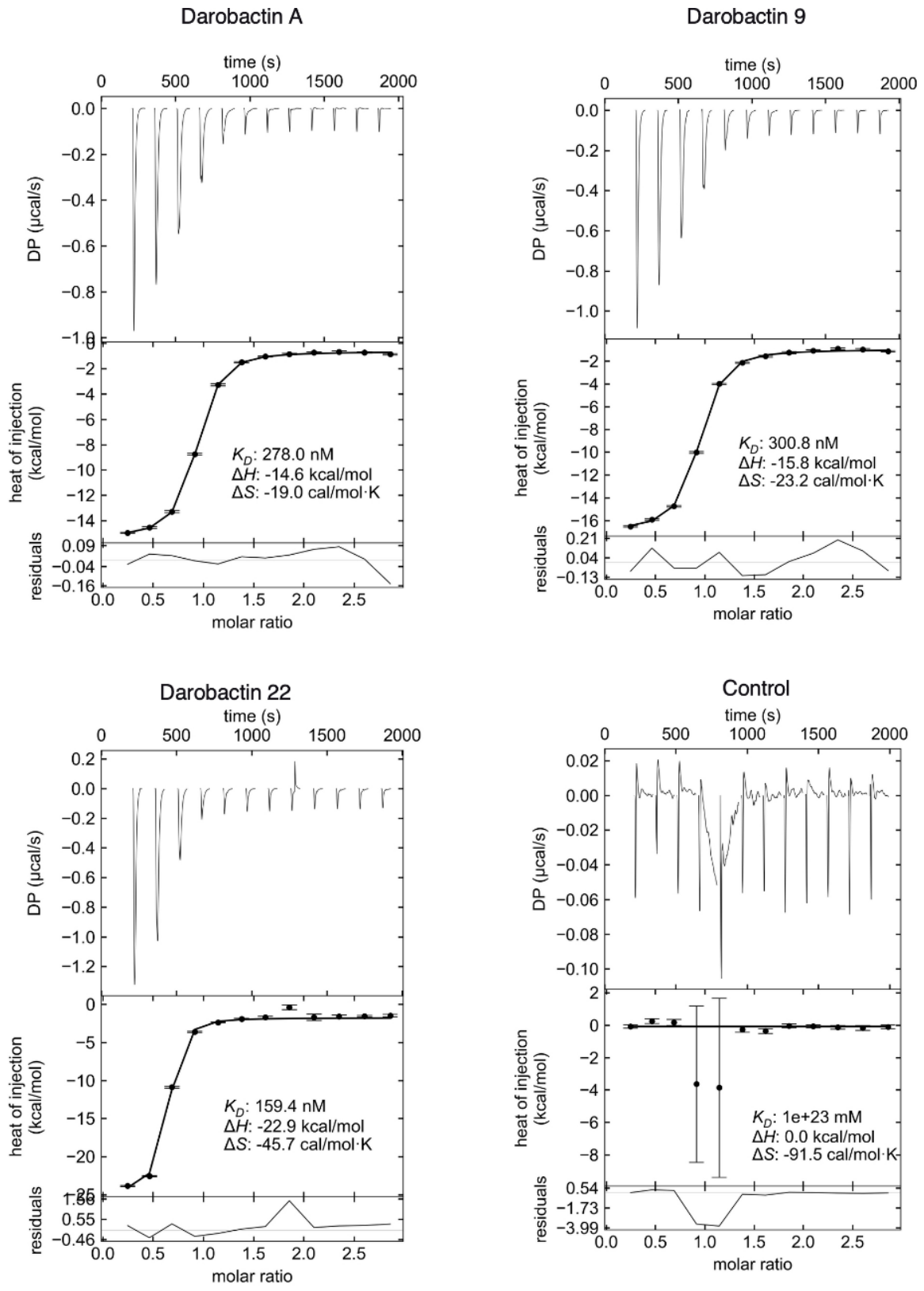

Figure S 44: Thermal titration calorimetry assays. Specific binding kinetics (K_D, Δ*H* and Δ*S*) of DA, D9 and D22 to *E. coli* BamA-β barrel were analyed and represented in the appropriate plot. Experiment was done in duplicates and repeated with similar results. Control assay was performed in absence of BamA-β barrel.

CRAB profiling

Antibiograms of clinical CRAB isolates

Table S 4: Antibiograms of clinical CRAB isolates. IMP: Imipenem; IMR: Imipenem/Relebactam; LEV: Levofloxacin; AMK: Amikacin; TOB: Tobramycin; MNO: Minocycline; TGC: Tigecyline; COL: Colistin

CRAB clinical isolate	MIC [µg/mL]							
	IMP	IMR	LEV	AMK	TOB	MNO	TGC	COL
038 (OXA-23)	32	32/4	8	16	32	1	2	0.5
045 (OXA-58)	8	8/4	8	128	1	4	1	0.5
046 (OXA-40)	64	64/4	8	>256	>128	4	1	0.5
047 (OXA-235)	8	8/4	8	>256	>128	16	1	0.5
070 (NDM-1)	32	64/4	4	>256	>128	≤0.0625	0.125	0.5
054 (OXA-51-ISAba1)	4	16/4	32	2	0.25	1	1	0.5

Table S 5: Activity assessment using 24 h population of TKC. Determining a MIC shift of *Acinetobacter baumannii* (*A. baumannii*) NCTC 13301 clones selected after a 24 h TKC experiment with high inoculum D22 at 2x, 4x and 8x MIC. No MIC shift was observed for the selected clones compared to the wild-type strain.

Activity assessment using 24 h population of TKC, MIC [µg/mL]	D22
A. baumannii NCTC 13301	8
A. baumannii NCTC 13301 (2x MIC)	8
A. baumannii NCTC 13301 (4x MIC)	8
A. baumannii NCTC 13301 (8x MIC)	8

a

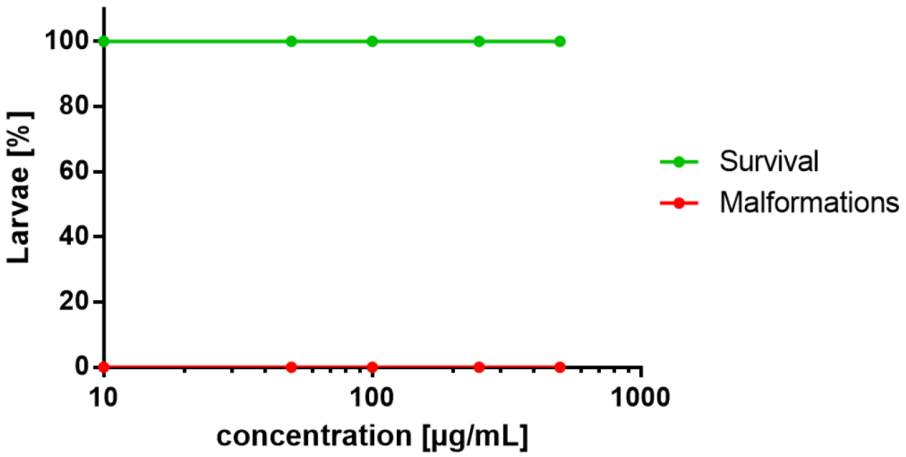

b

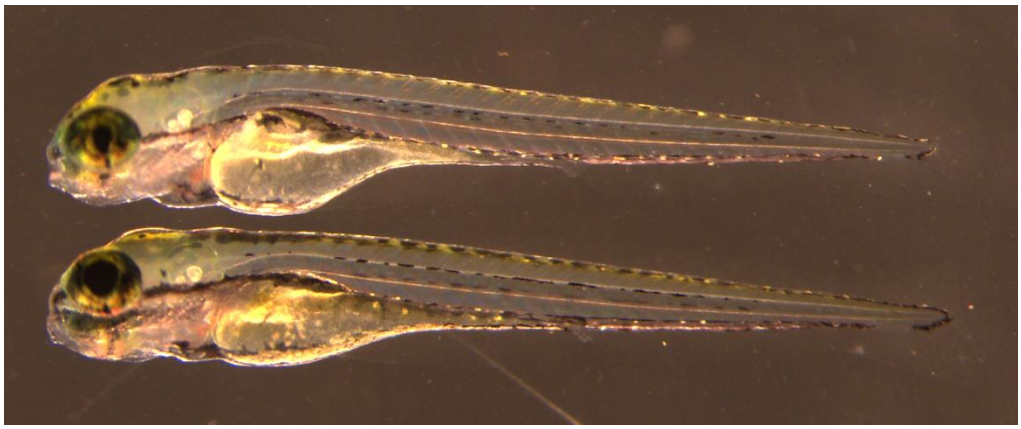

c

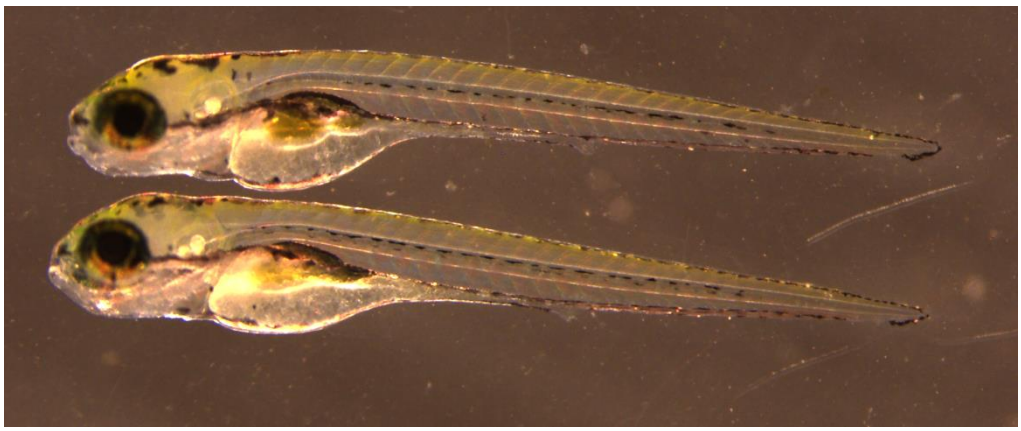

Figure S 45: No *in vivo* cytotoxicity against zebrafish larvae. D22 was added to surrounding fish water one day post fertilization (dpf) and left for four consecutive days (96 h) until five dpf. Tested concentrations were: 10, 50, 100, 250 and 500 µg/mL. Ten dechorinated larvae were tested per concentration. a, surviving rate : all zebrafish larvae survived. b, control zebrafish larvae. c, zebrafish larvae tested with 500 µg/mL. No malformation detected and no signs of toxicity detected.

Cryo-EM data collection, refinement, and validation statistics.

Table S 6: Cryo-EM data collection and refinement statistics and validation statistics of BAM-D9 and BAM-D22 data collection.

	BAM-D9 (EMDB-15363, PDB:8ADI)	BAM-D22 (EMDB-15362, PDB:8ADG)
	Data collection and processing	
Microscope	Titan Krios	Titan Krios
Voltage (kV)	300	300
Detector	K3	K3
Magnification	105,000	105,000
Does per frame (e^{-}/Å^2)	1.2	1.2
Exposure rate (e^{-}/pixel/ s)	15	15
Calibrated pixel size (Å)	0.85	0.85
Defocus range (μm)	–0.8 to –3	–0.6 to -3
symmetry	C1	C1
Initial particles (no.)	858,848	1,018,412
Final particles (no.)	406,142	499,389
Map resolution (Å)	3.4	3.0
FSC threshold	0.143	0.143
	Refinement	
Initial model (PDB ID)	7NRI	7NRI
Model resolution (Å)	3.5	3.1
FSC threshold	0.5	0.5
Model composition	5 chains, 1 ligand	5 chains, 1 ligand
Non-hydrogen atoms	11802	11,822
Protein residues	1499	1500
Ligands	D**9**	D**22**
	B factors (Å^2)	
Protein	7.35	42.32
Ligand	5.00	29.87
Bond lengths (Å)	0.003(0)	0.003 (0)
Bond angles (°)	0.538 (2)	0.557(3)
	Validation	
MolProbity score	1.44	1.12
Clash score	4.54	2.64
Poor rotamers (%)	0.0	0.00
	Ramachandran plot	
Favored (%)	96.7	96.9
Allowed (%)	3.3	3.1
Disallowed (%)	0.00	0.00

D22

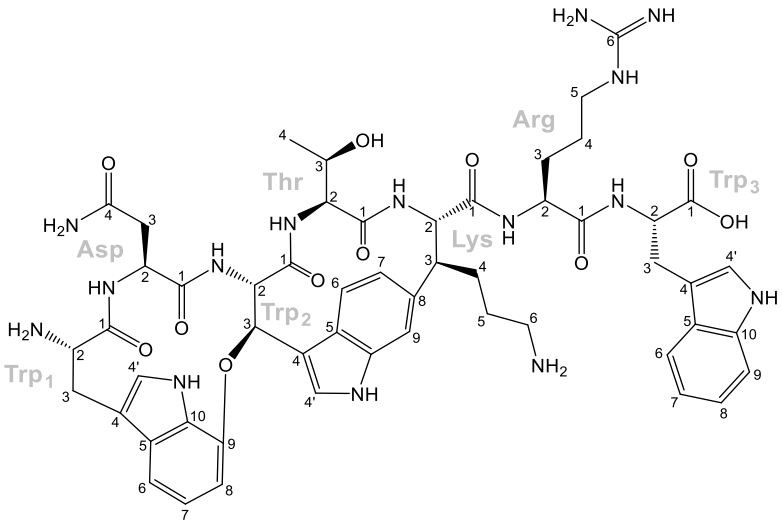

Table S 7: NMR spectroscopic data of D22.

	NMR data in ACN/D_2O + 1% FA-d_4			
position	δ ^{13}C	δ ^{1}H, mult (*J* in Hz)	COSY correlations	HMBC correlations
Trp3				
1	175.0	-	-	-
2	53.8	5.05, t (6.5)	3	1, 3, 4, *Arg*-1
3	26.7	3.70, m	2	1, 2, 3
4	109.1	-	-	-
4’	124.2	7.63, s	-	3, 4, 5, 9, 10
5	127.2	-	-	-
6	118.3	8.02, d (7.9)	7	8, 10
7	119.0	7.53, m	6, 8	5, 9
8	121.6	7.61, m	7, 9	6, 10
9	111.5	7.88, d (8.2)	8	5, 7
10	136.0	-	-	-
Arg				
1	172.0	-	-	-
2	53.0	4.66, dd (8.6, 5.6)	3	1, *Lys*-1, 3
3	27.9	1.93, 2.10, m	2, 4	1, 2, 4, 5
4	24.2	1.79, m	3, 5	3, 5
5	40.2	3.40, t (7.0)	4	3, 4, 6
6	156.4	-	-	-

NMR data in ACN/D_2O + 1% FA-d_4				
position	δ ^{13}C	δ ^{1}H, mult (*J* in Hz)	COSY correlations	HMBC correlations
Lys				
1	171.0	-	-	-
2	59.8	4.44, d (10.6)	3	1, 3, 4, *Thr*-1, *Trp₂*-8
3	47.7	3.29, dt (10.6, 3.0)	2, 4	1, 2, 4, 5, *Trp₂*-7, *Trp₃*-8, *Trp₂*-9
4	25.2	1.88, m	3, 5	3, 5, 6, *Trp₂*-8
5	25.3	2.13, m	4, 6	3, 4, 6
6	39.0	3.15, dq (11.6, 6.0)	5	4, 5
Thr				
1	167.5	-	-	-
2	57.7	4.08, d (6.3)	3	1, 3, 4, *Trp₂*-1
3	67.7	3.71, m	2, 4	2, 4
4	18.0	1.12, d (6.3)	3	2, 3
Trp₂				
1	167.7	-	-	-
2	63.2	4.99, d (8.9)	3	1, 3, 4, *Asp*-1
3	76.3	6.50, d (8.9)	2, 4‘	2, 4, 4‘, *Trp₃*-9
4	111.7	-	-	-
4‘	124.0	8.17, s	3	3, 4, 5, 10
5	124.6	-	-	-
6	117.0	7.74, d (8.3)	7	4, 8, 10
7	124.6	7.24, d (8.3)	6	5, 9, *Lys*-3
8	132.4	-	-	-
9	110.1	7.73, s	-	5, 7, *Lys*-3
10	136.8	-	-	-
Asp				
1	168.2	-	-	-
2	50.4	3.63, m	3	1, 3, 4, *Trp3*-1
3	38.6	2.49, d (6.8)	2	1, 2, 4
4	173.0	-	-	-
Trp₁				
1	168.0	-	-	-
2	54.5	4.33, dd (10.8, 7.2)	3	1, 3
3	26.0	3.61, 3.87, dd (13.4, 7.2)	2	1, 2, 4, 4‘, 5
4	107.9	-	-	-
4‘	124.7	7.68, s	-	3, 4, 5, 9, 10
5	128.9	-	-	-
6	119.8	7.52, m	7	4, 8, 10
7	113.1	7.53, m	6, 8	5, 9
8	108.12	7.53, m	7	6, 10
9	145.2	-	-	-
10	128.7	-	-	-

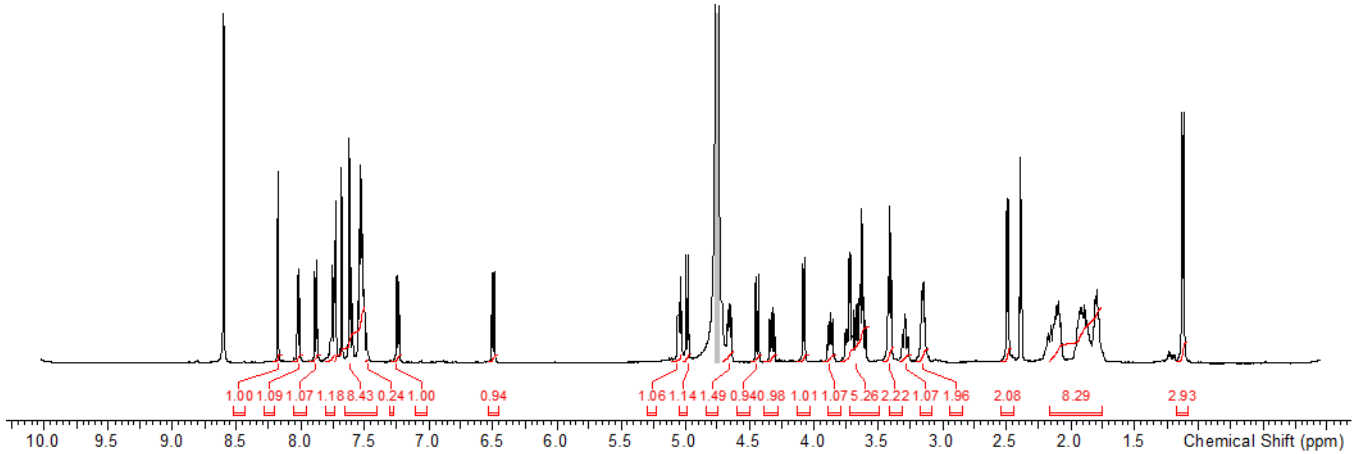

Figure S 46: ^{1}H spectrum of D22 in ACN/D2O + 1% FA at 45 °C and 500 MHz.

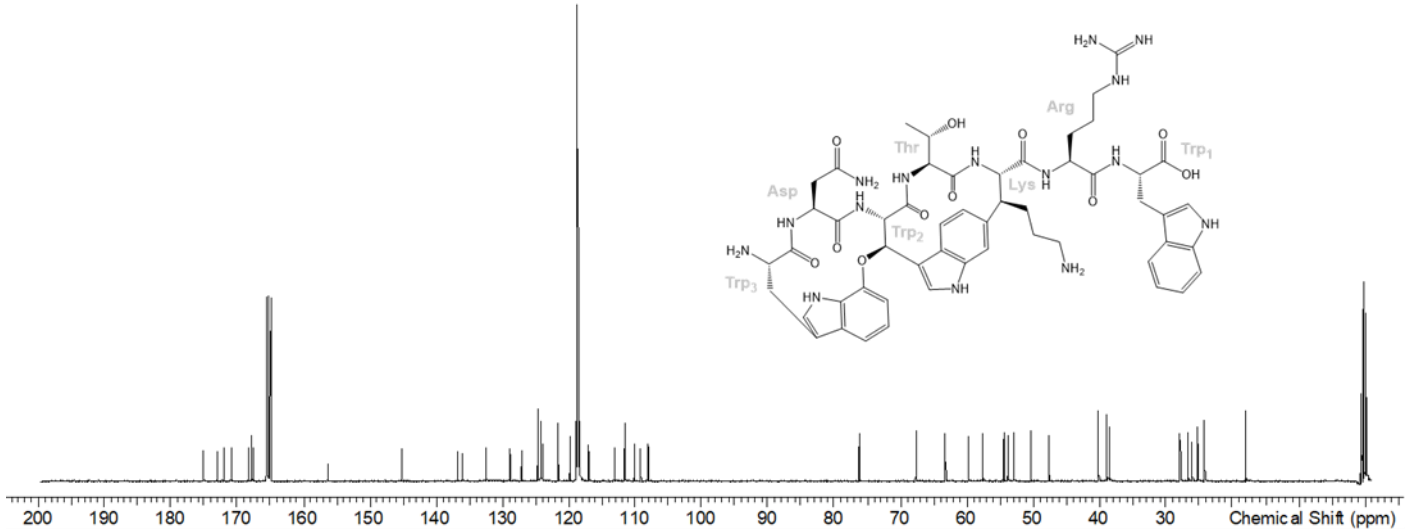

Figure S 47: ^{13}C spectrum of D22 in ACN/D2O + 1% FA at 45 °C and 125 MHz.

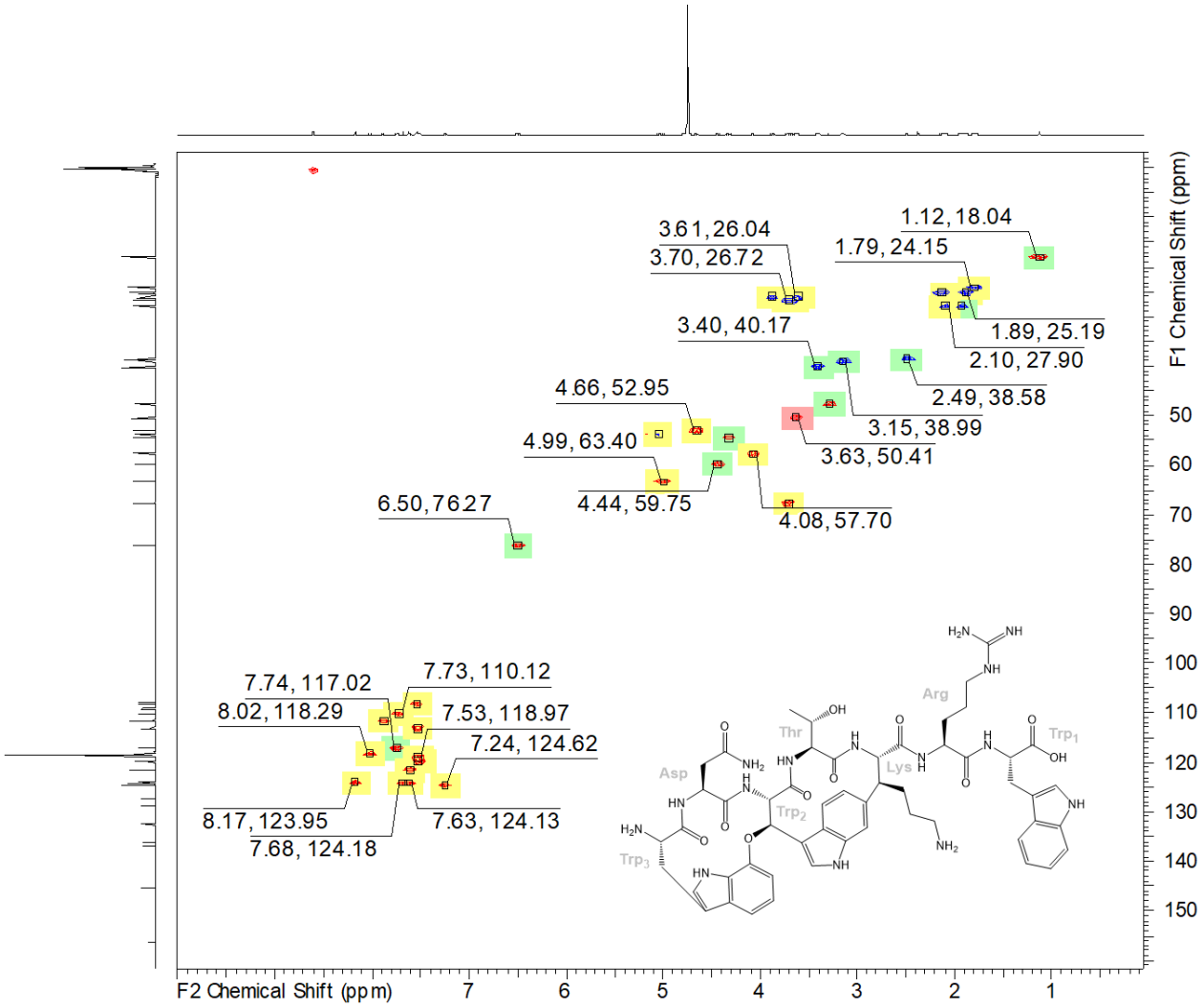

Figure S 48: HSQC spectrum of D22 in ACN/D2O + 1% FA at 45 °C and 500/125 MHz.

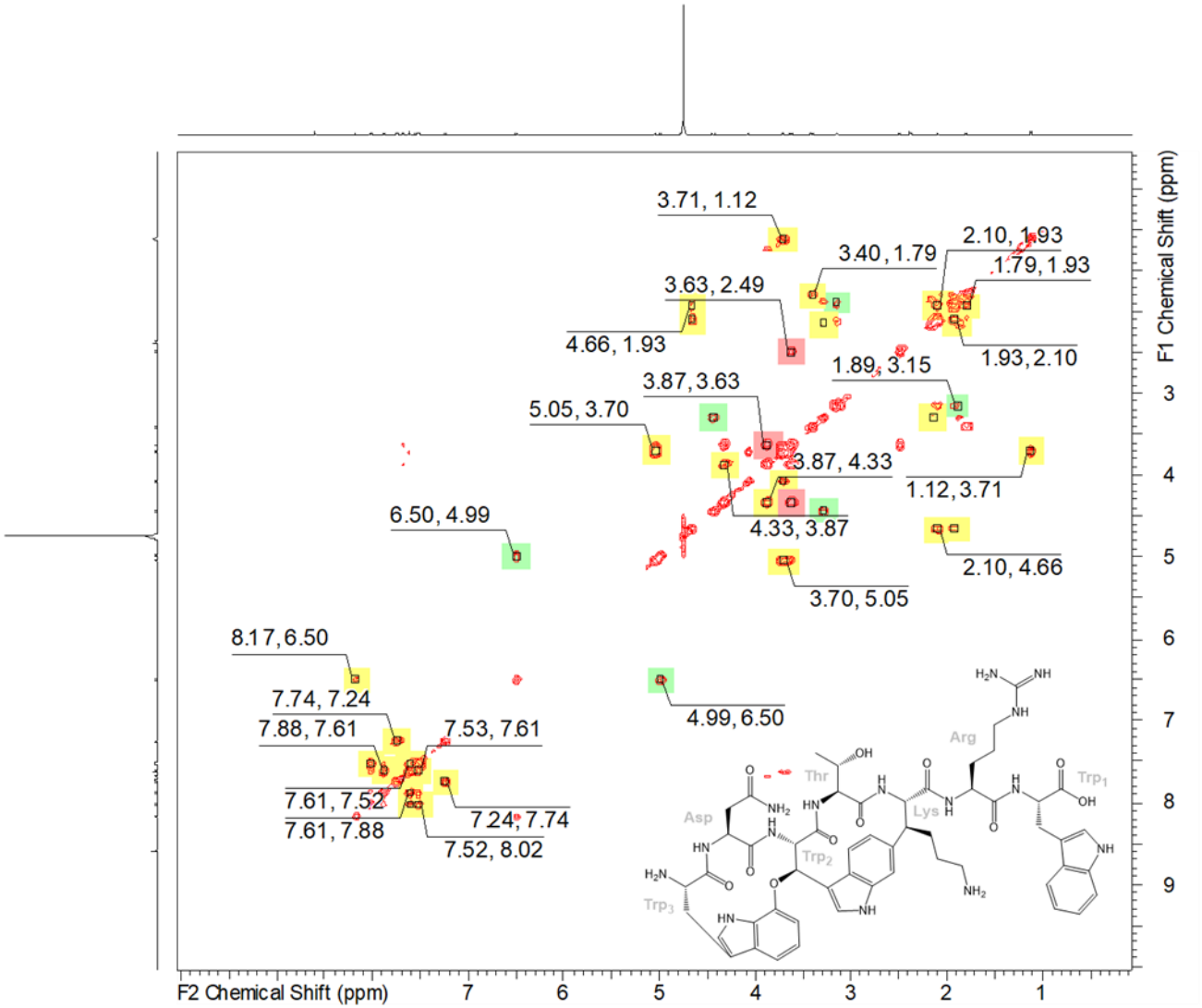

Figure S 49: COSY spectrum of D22 in ACN/D2O + 1% FA at 45 °C and 500/125 MHz.

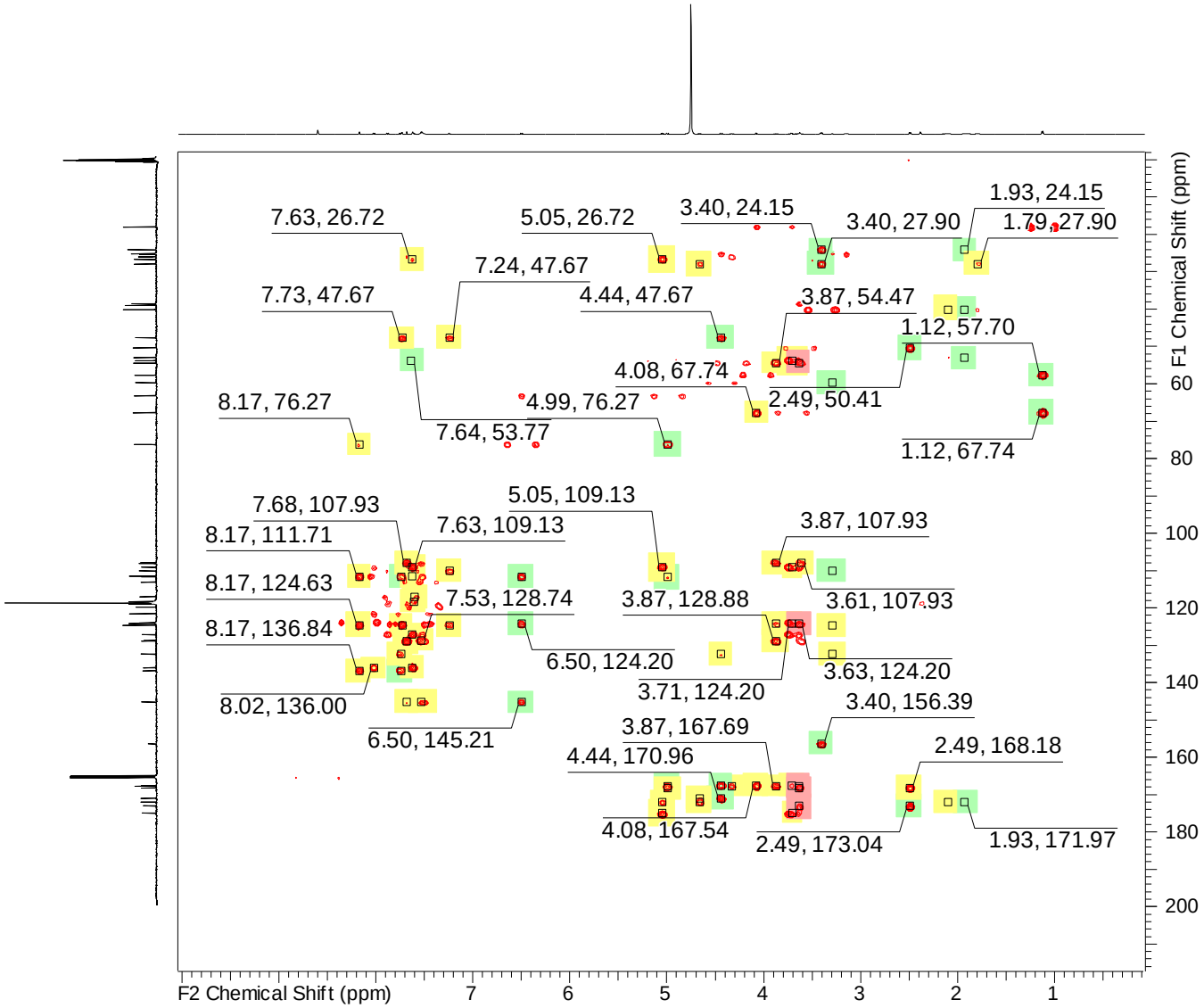

Figure S 50: HMBC spectrum of D22 in ACN/D2O + 1% FA at 45 °C and 500/125 MHz.

D23

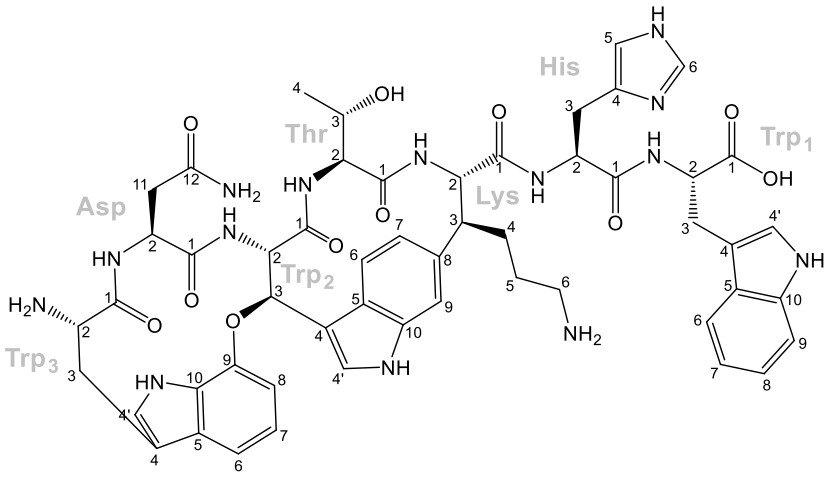

Table S 8: NMR spectroscopic data of D23.

		NMR data in ACN/D_2O + 1% FA-d_4		
position	δ ^{13}C	δ ^{1}H, mult (*J* in Hz)	COSY correlations	HMBC correlations
Trp$_3$				
1	176.3	-	-	-
2	55.4	5.04, m	3	1, 3, 4, *His*-1
3	27.9	3.71, m	2	1, 2, 3
4	110.4	-	-	-
4’	125.4	7.62, s	-	3, 4, 5, 9, 10
5	128.4	-	-	-
6	119.5	8.02, d (7.6)	7	8, 10
7	120.3	7.53, m	6, 8	5, 9
8	122.9	7.61, m	7, 9	6, 10
9	112.9	7.89, d (7.9)	8	5, 7
10	136.0	-	-	-
His				
1	171.5	-	-	-
2	53.1	5.05, m	3	1, *Lys*-1, 3, 4
3	27.4	3.39, 3.55, m	2	2, 4, 5
4	24.2	-	-	-
5	118.1	7.49, s	6	3, 4, 6
6	134.6	8.81, s	5	4, 5

NMR data in ACN/D_2O + 1% FA-d_4				
position	δ ^{13}C	δ ^{1}H, mult (*J* in Hz)	COSY correlations	HMBC correlations
Lys				
1	171.2	-	-	-
2	60.9	4.41, d (9.8)	3	1, 3, 4, *Thr*-1, *Trp₂*-8
3	49.1	3.23, m	2, 4	1, 2, 4, 5, *Trp₂*-7, *Trp₃*-8, *Trp₂*-9
4	26.5	2.10, m	3, 5, 6	3, 5, 6, *Trp₂*-8
5	26.4	1.84, m	4, 6	3, 4, 6
6	40.2	3.10, m	4, 5	4, 5
Thr				
1	168.8	-	-	-
2	58.8	4.05, d (4.6)	3	1, 3, 4, *Trp₂*-1
3	69.2	3.67, m	2, 4	2, 4
4	19.3	1.04, d (4.8)	3	2, 3
Trp₂				
1	169.0	-	-	-
2	64.5	4.99, bd (8.2)	3	1, 3, 4, *Asp*-1
3	77.5	6.49, d (8.2)	2, 4‘	2, 4, 4‘, *Trp₃*-9
4	113.0	-	-	-
4‘	125.3	8.17, s	3	3, 4, 5, 10
5	125.9	-	-	-
6	118.3	7.74, d (7.7)	7	4, 8, 10
7	125.9	7.22, d (7.7)	6	5, 9, *Lys*-3
8	133.5	-	-	-
9	111.4	7.71, s	-	5, 7, *Lys*-3
10	138.1	-	-	-
Asp				
1	169.5	-	-	-
2	51.7	3.63, m	3	1, 3, 4, *Trp3*-1
3	39.8	2.49, d (6.4)	2	1, 2, 4
4	174.3	-	-	-
Trp₁				
1	169.0	-	-	-
2	55.7	4.33, m	3	1, 3
3	27.3	3.61, 3.87, dd (12.8, 6.0)	2	1, 2, 4, 4‘, 5
4	109.2	-	-	-
4‘	125.5	7.68, s	-	3, 4, 5, 9, 10
5	130.0	-	-	-
6	121.1	7.51, m	7	4, 8, 10
7	114.4	7.52, m	6, 8	5, 9
8	109.4	7.54, m	7	6, 10
9	146.5	-	-	-
10	130.1	-	-	-

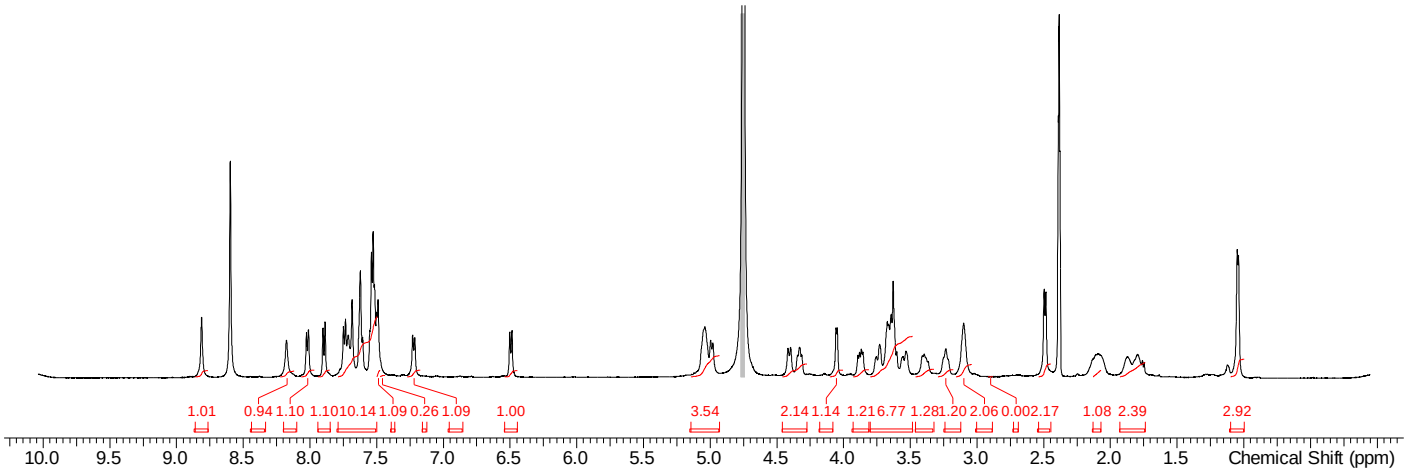

Figure S 51: ^{1}H spectrum of D23 in ACN/D2O + 1% FA at 45 °C and 500 MHz.

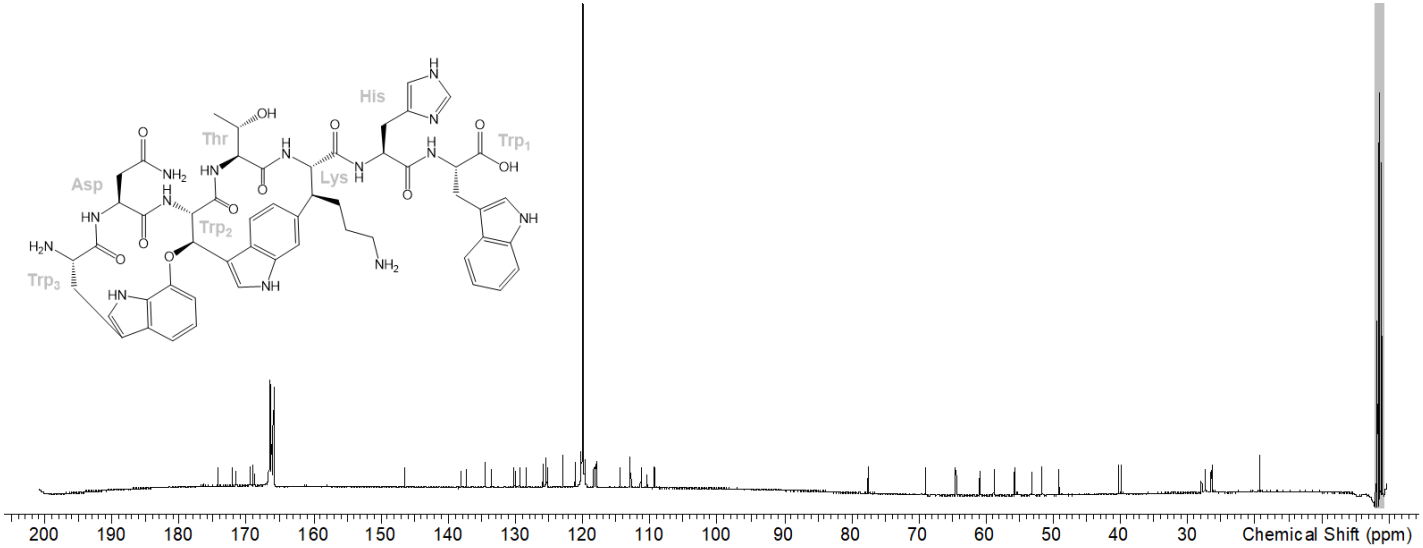

Figure S 52: ^{13}C spectrum of D23 in ACN/D2O + 1% FA at 45 °C and 125 MHz.

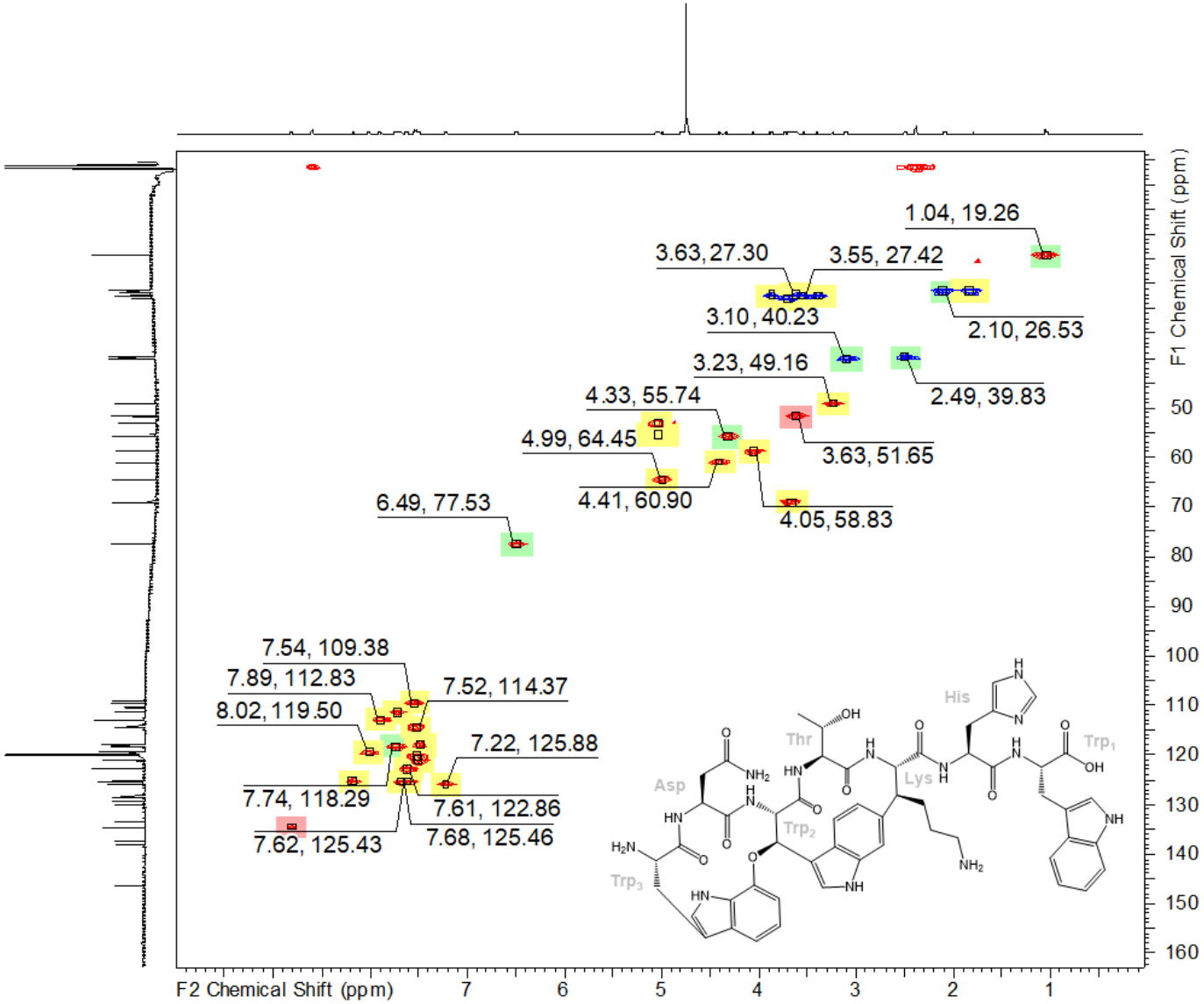

Figure S 53: HSQC spectrum of D23 in ACN/D2O + 1% FA at 45 °C and 500/125 MHz.

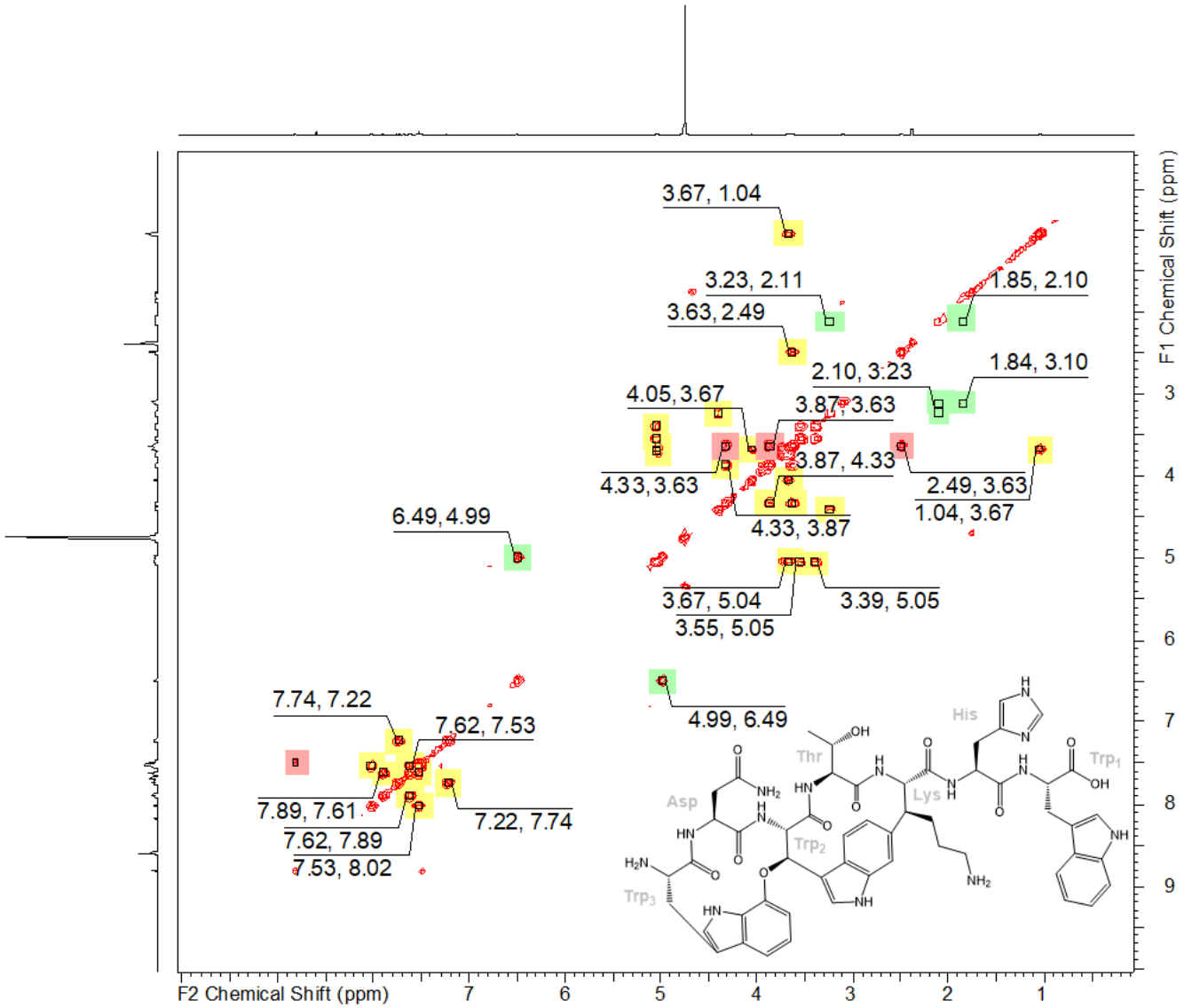

Figure S 54: COSY spectrum of D23 in ACN/D2O + 1% FA at 45 °C and 500/125 MHz.

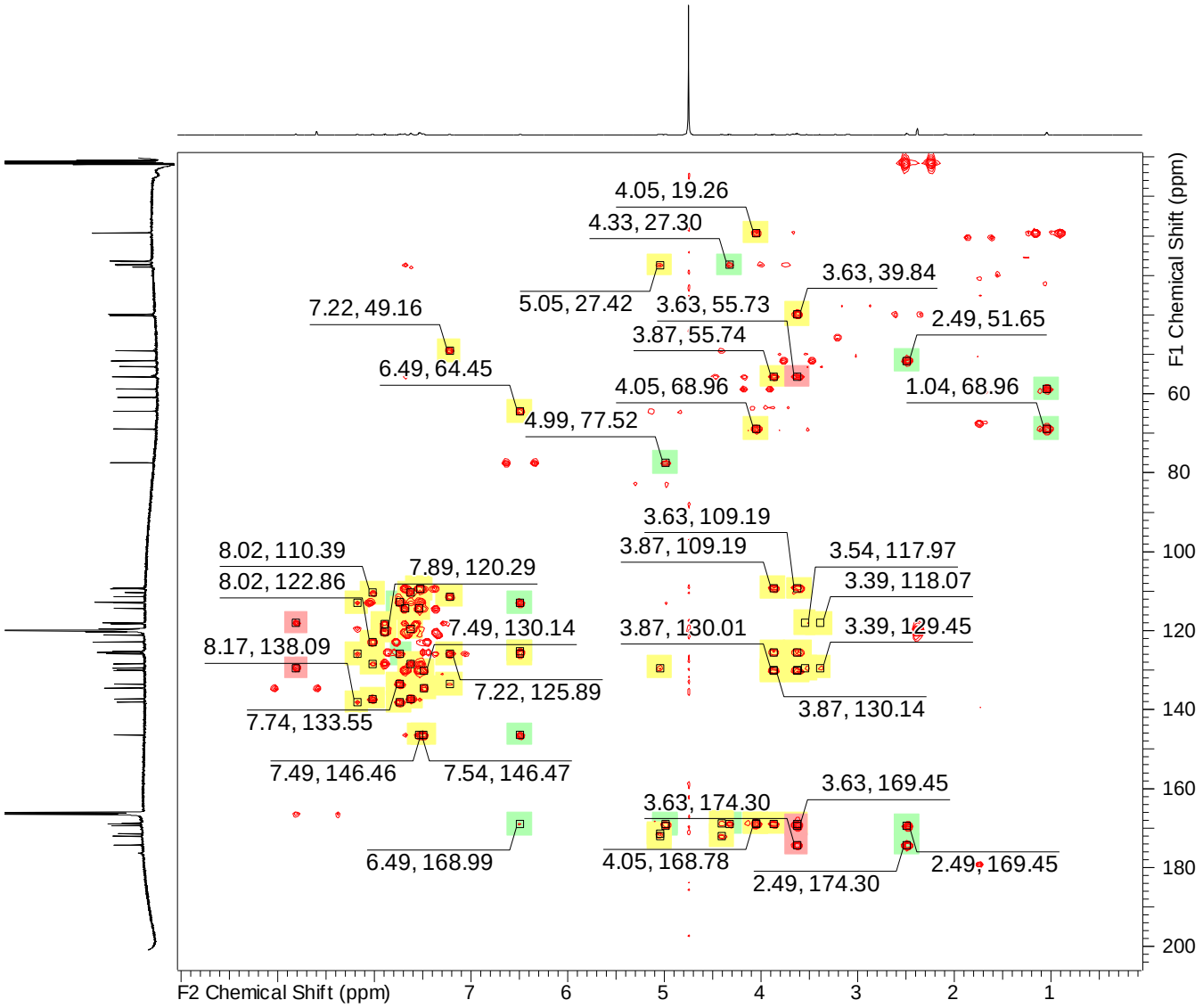

Figure S 55: HMBC spectrum of D23 in ACN/D2O + 1% FA at 45 °C and 500/125 MHz.

D31

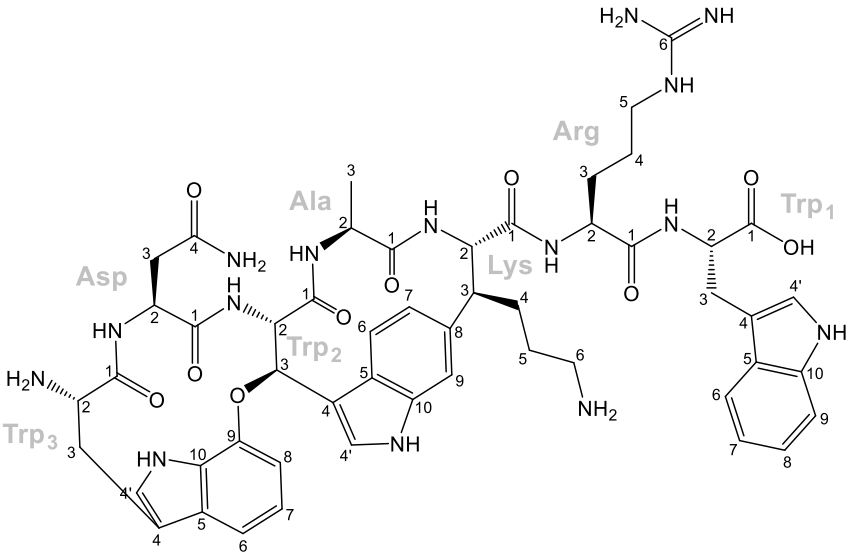

Table S 9: NMR spectroscopic data of D31.

		NMR data in ACN/D_2O + 1% FA-d_4		
position	δ ^{13}C	δ ^{1}H, mult (*J* in Hz)	COSY correlations	HMBC correlations
Trp₃				
1	175.0	-	-	-
2	53.9	5.16, bt (6.1)	3	1, 3, 4, *Arg*-1
3	26.9	3.77, 3.82, dd (14.6, 5.3)	2	1, 2, 3
4	109.4	-	-	-
4’	124.4	7.73, s	-	3, 4, 5, 9, 10
5	127.4	-	-	-
6	118.5	8.13, d (7.9)	7	8, 10
7	119.2	7.62, m	6, 8	5, 9
8	121.7	7.70, m	7, 9	6, 10
9	111.7	7.98, d (8.2)	8	5, 7
10	136.3	-	-	-
Arg				
1	172.2	-	-	-
2	53.3	4.75, q (6.9)	3	1, *Lys*-1, 3, 4
3	28.2	2.08, 2.22, m	2, 4	1, 2, 4, 5
4	24.4	1.93, m	3, 5	2, 3, 5
5	40.5	3.52, t (7.0)	3	3, 4, 6
6	156.7	-	-	-

NMR data in ACN/D_2O + 1% FA-d_4				
position	δ ^{13}C	δ ^{1}H, mult (*J* in Hz)	COSY correlations	HMBC correlations
Lys				
1	171.2	-	-	-
2	60.1	4.53, d (10.5)	3	1, 3, 4, *Ala*-1, *Trp₂*-8
3	48.2	3.37, m	2, 4	1, 2, 4, 5, *Trp₂*-7, *Trp₃*-8, *Trp₂*-9
4	22.6	2.32, 2.03, m	3, 5, 6	3, 5, 6, *Trp₂*-8
5	25.4	2.23, m	4, 6	3, 4, 6
6	39.3	3.28, m	4, 5	4, 5
Ala				
1	170.9	-	-	-
2	48.1	4.36, q (6.9)	3	1, 3, *Trp₂*-1
3	18.4	1.26, d (6.9)	2	1, 2
Trp₂				
1	166.9	-	-	-
2	63.4	5.04, d (8.9)	3	1, 3, 4, *Asp*-1
3	76.3	6.58, d (8.9)	2, 4‘	2, 4, 4‘, *Trp₃*-9
4	112.1	-	-	-
4‘	124.2	8.28, s	3	3, 4, 5, 10
5	125.1	-	-	-
6	117.1	7.86, d (8.2)	7	4, 8, 10
7	125.0	7.35, d (8.2)	6	5, 9, *Lys*-3
8	132.6	-	-	-
9	110.4	7.84, s	-	5, 7, *Lys*-3
10	137.0	-	-	-
Asp				
1	168.3	-	-	-
2	50.7	3.72, m	3	1, 3, 4, *Trp3*-1
3	39.0	2.59, m	2	1, 2, 4
4	173.4	-	-	-
Trp₁				
1	167.9	-	-	-
2	54.8	4.43, dd (10.8, 7.2)	3	1, 3
3	26.3	3.97, 3.72, dd (13.5, 7.2)	2	1, 2, 4, 4‘, 5
4	108.2	-	-	-
4‘	124.4	7.79, s	-	3, 4, 5, 9, 10
5	128.9	-	-	-
6	120.1	7.61, m	7	4, 8, 10
7	113.2	7.62, m	6, 8	5, 9
8	108.0	7.62, m	7	6, 10
9	145.5	-	-	-
10	129.2	-	-	-

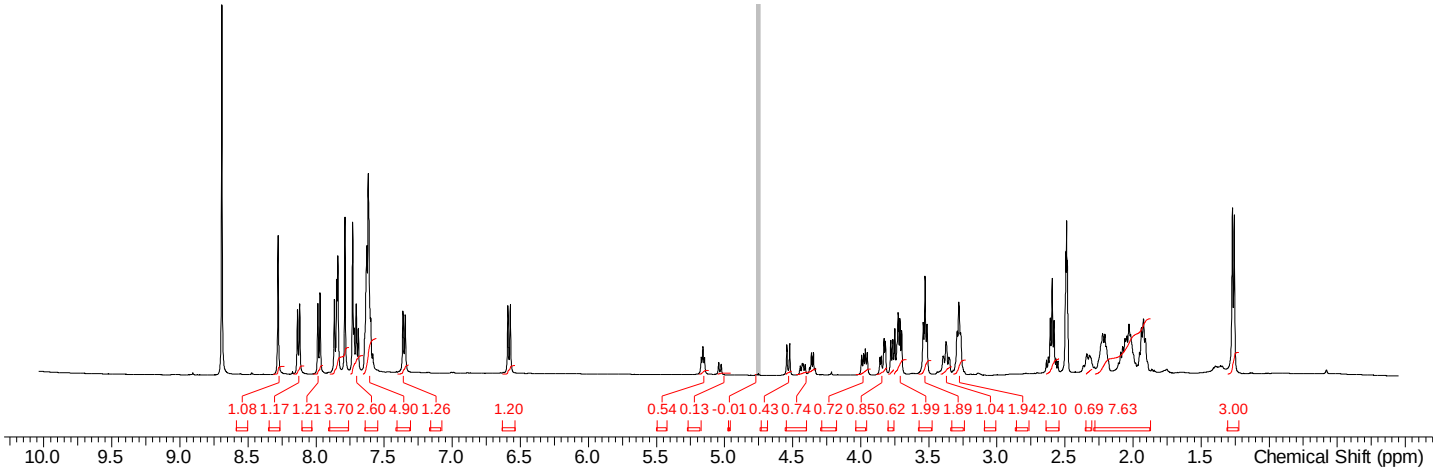

Figure S 56: Water suppressed ^{1}H spectrum of D31 in ACN/D2O + 1% FA at 45 °C and 500 MHz.

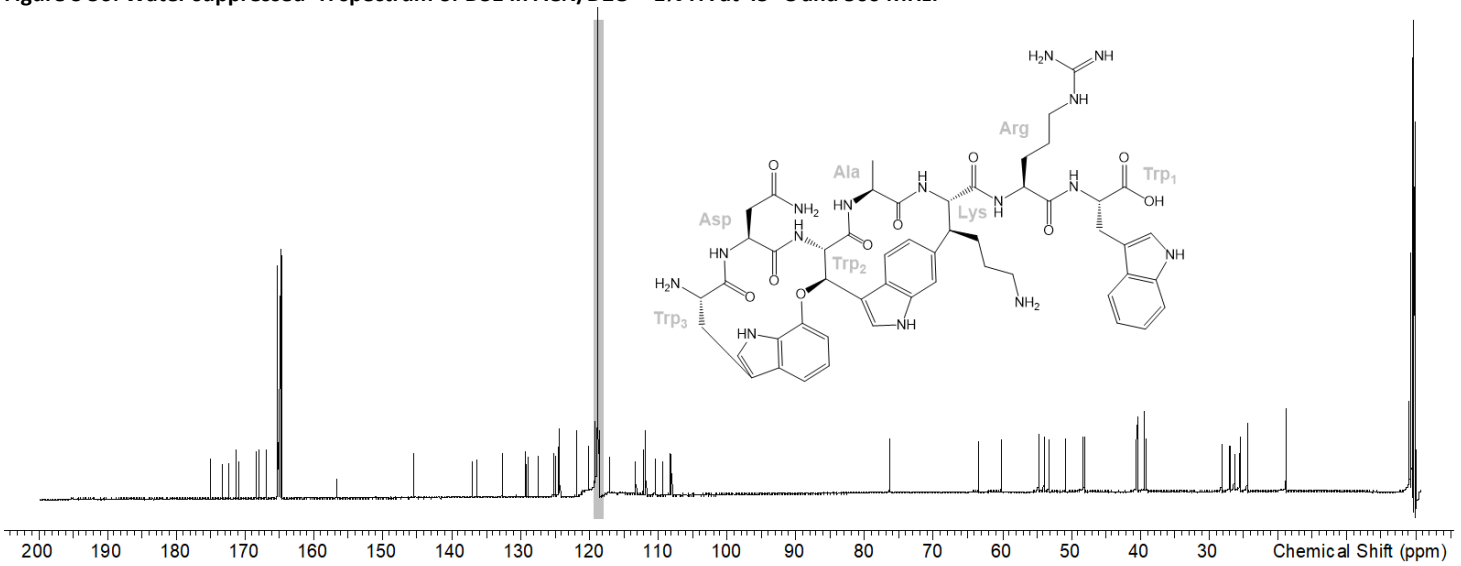

Figure S 57: ^{13}C spectrum of D31 in ACN/D2O + 1% FA at 45 °C and 125 MHz.

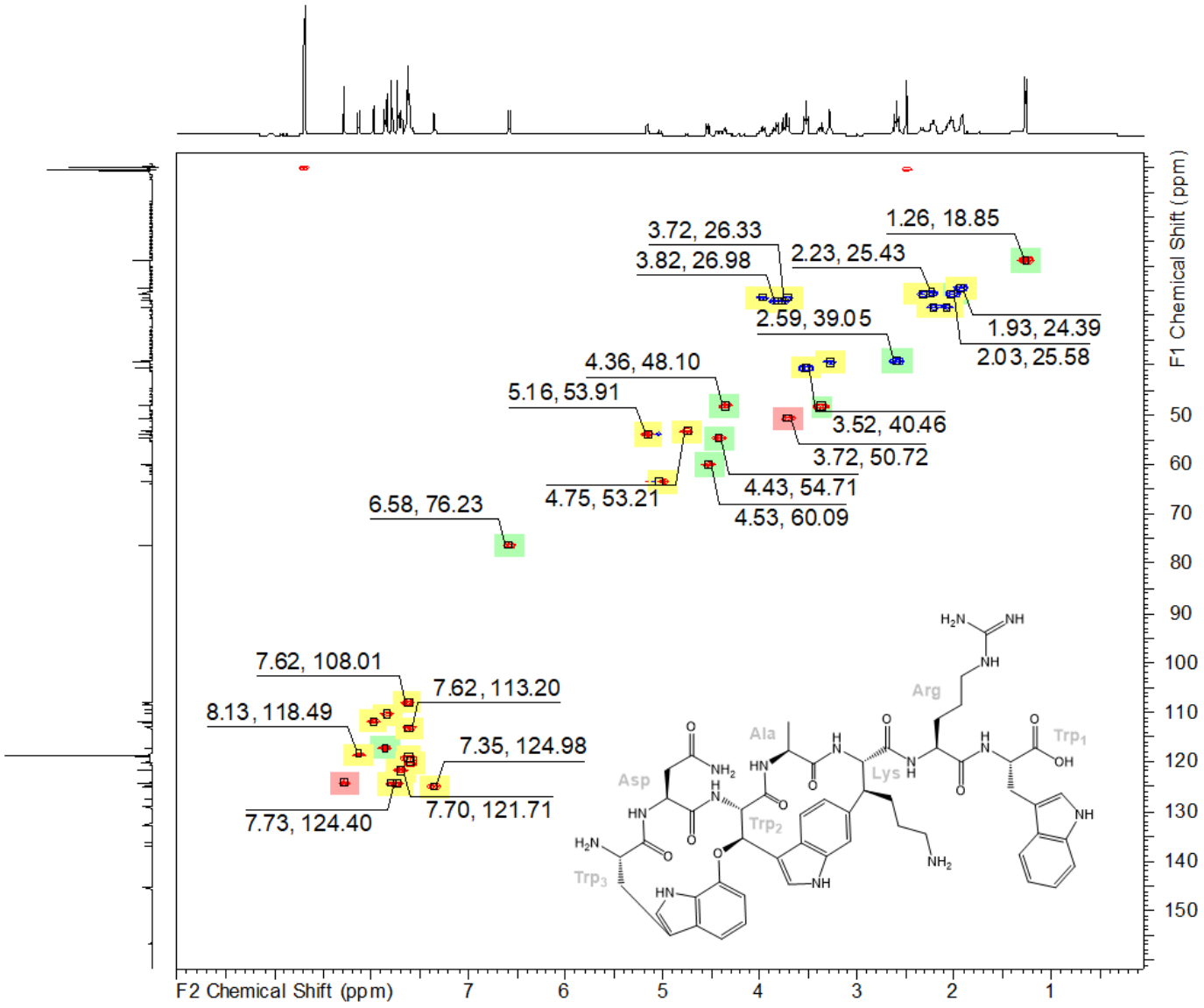

Figure S 58: HSQC spectrum of D31 in ACN/D2O + 1% FA at 45 °C and 500/125 MHz.

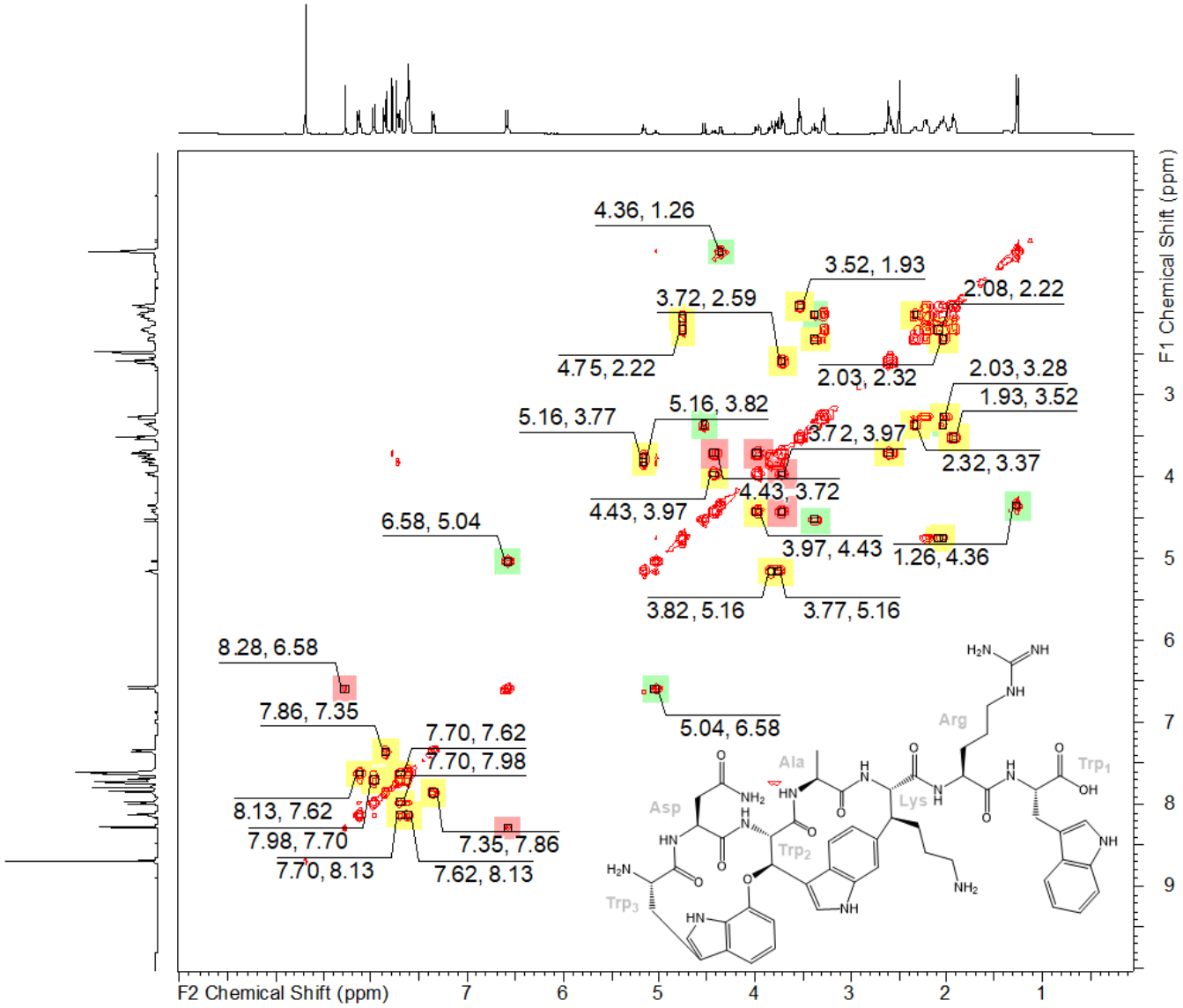

Figure S 59: COSY spectrum of D31 in ACN/D2O + 1% FA at 45 °C and 500/125 MHz.

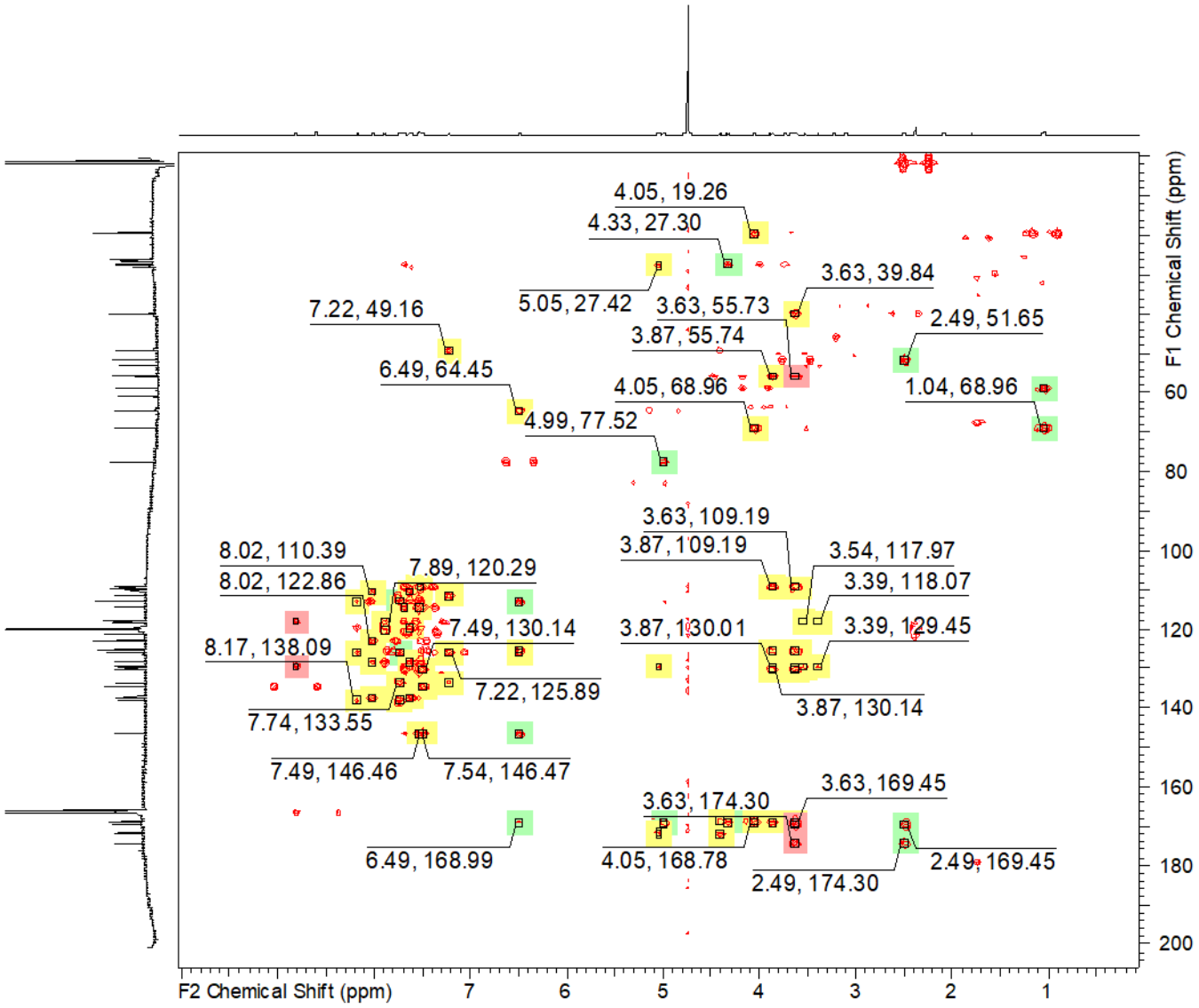

Figure S 60: HMBC spectrum of D31 in ACN/D2O + 1% FA at 45 °C and 500/125 MHz.

D36

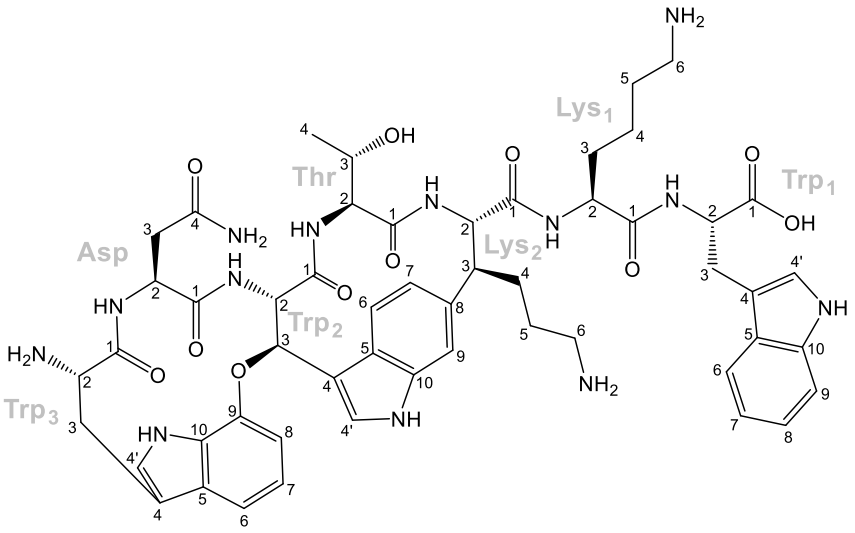

Table S 10: NMR spectroscopic data of D36.

		NMR data in ACN/D_2O + 1% FA-d_4		
position	δ ^{13}C	δ ^{1}H, mult (*J* in Hz)	COSY correlations	HMBC correlations
Trp₃				
1	175.0	-	-	-
2	53.7	5.03, bt (6.2)	3	1, 3, 4, *Lys₁*-1
3	26.7	3.66, m	2	1, 2, 3
4	109.1	-	-	-
4’	124.2	7.62, s	-	3, 4, 5, 9, 10
5	127.1	-	-	-
6	118.3	8.02, d (7.9)	7	8, 10
7	119.0	7.51, m	6, 8	5, 9
8	121.5	7.61, m	7, 9	6, 10
9	111.5	7.88, d (8.1)	8	5, 7
10	135.9	-	-	-
Lys₁				
1	172.2	-	-	-
2	53.1	4.62, dd (8.6, 5.7)	3	1, 3, 4, *Lys₂*-1
3	30.1	2.06, 1.91, m	2, 4	1, 2, 4
4	21.7	1.59, m	3, 5	2, 3, 5, 6
5	25.8	1.88, m	4, 6	2, 3, 6
6	38.8	3.17, t (7.7)	5	4, 5

NMR data in ACN/D_2O + 1% FA-d_4				
position	δ ^{13}C	δ ^{1}H, mult (*J* in Hz)	COSY correlations	HMBC correlations
Lys₂				
1	170.9	-	-	-
2	59.7	4.42, d (10.5)	3	1, 3, 4, *Thr*-1, *Trp₂*-8
3	47.7	3.27, dt (10.9, 2.9)	2, 4	1, 2, 4, 5, *Trp₂*-7, *Trp₃*-8, *Trp₂*-9
4	25.1	1.85, m	3, 5	3, 5, 6, *Trp₂*-8
5	25.2	2.09, m	4, 6	3, 4, 6
6	38.9	3.12, m	5	4, 5
Thr				
1	167.5	-	-	-
2	57.6	4.06, d (6.1)	3	1, 3, 4, *Trp₂*-1
3	67.7	3.70, m	2, 4	2, 4
4	18.0	1.12, d (6.3)	3	2, 3
Trp₂				
1	167.6	-	-	-
2	63.2	4.98, d (8.7)	3	1, 3, 4, *Asp*-1
3	76.2	6.49, d (8.8)	2, 4‘	2, 4, 4‘, *Trp₃*-9
4	111.6	-	-	-
4‘	123.9	8.16, s	3	3, 4, 5, 10
5	124.	-	-	-
6	117.0	7.74, d (8.3)	7	4, 8, 10
7	124.6	7.24, d (8.2)	6	5, 9, *Lys₂*-3
8	132.4	-	-	-
9	110.1	7.73, s	-	5, 7, *Lys₂*-3
10	136.8	-	-	-
Asp				
1	168.1	-	-	-
2	50.4	3.61, m	3	1, 3, 4, *Trp3*-1
3	38.5	2.48, d (6.8)	2	1, 2, 4
4	173.0	-	-	-
Trp₁				
1	167.7	-	-	-
2	54.4	4.32, dd (10.8, 7.2)	3	1, 3
3	26.0	3.61, 3.86, dd (13.4, 7.1)	2	1, 2, 4, 4‘, 5
4	107.9	-	-	-
4‘	124.1	7.67, s	-	3, 4, 5, 9, 10
5	128.7	-	-	-
6	119.8	7.49, m	7	4, 8, 10
7	113.1	7.52, m	6, 8	5, 9
8	108.1	7.52, m	7	6, 10
9	145.1	-	-	-
10	128.8	-	-	-

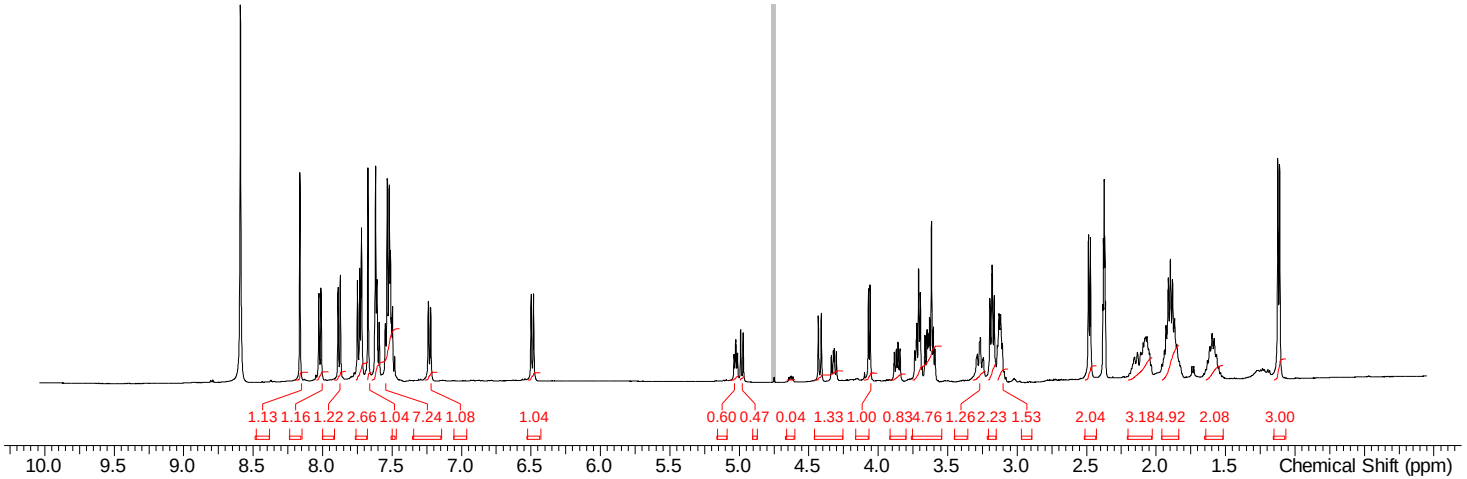

Figure S 61: Water suppressed ^{1}H spectrum of D36 in ACN/D2O + 1% FA at 45 °C and 500 MHz.

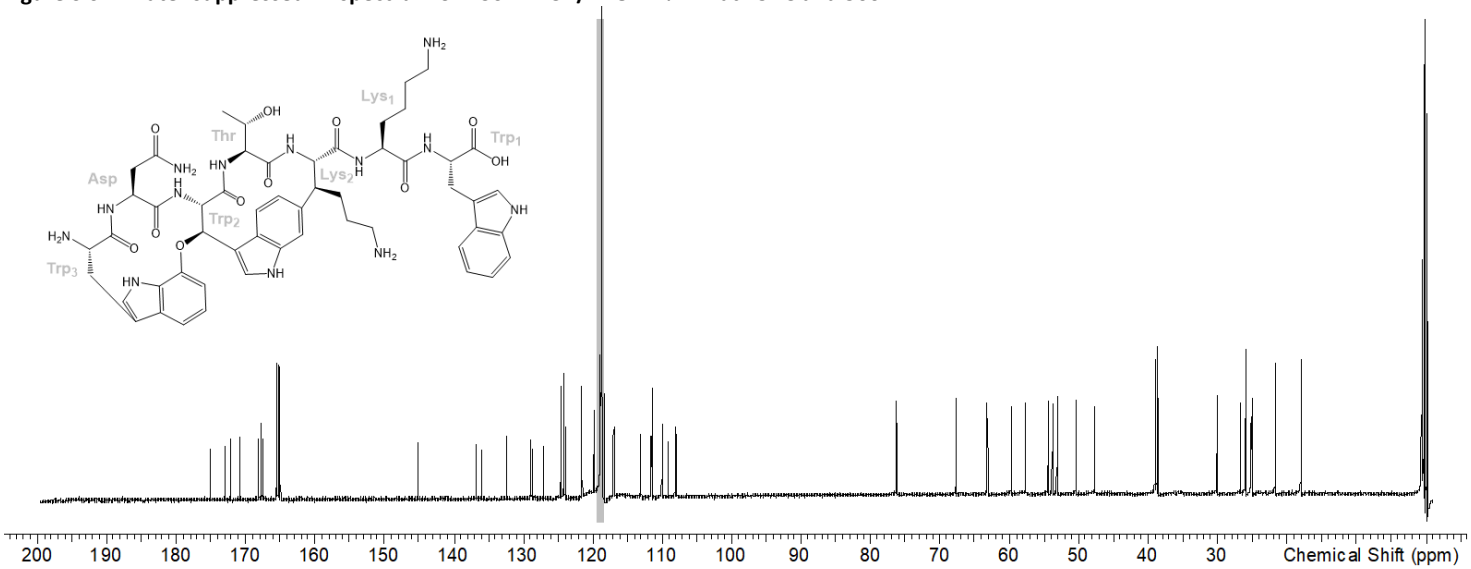

Figure S 62: ^{13}C spectrum of D36 in ACN/D2O + 1% FA at 45 °C and 125 MHz.

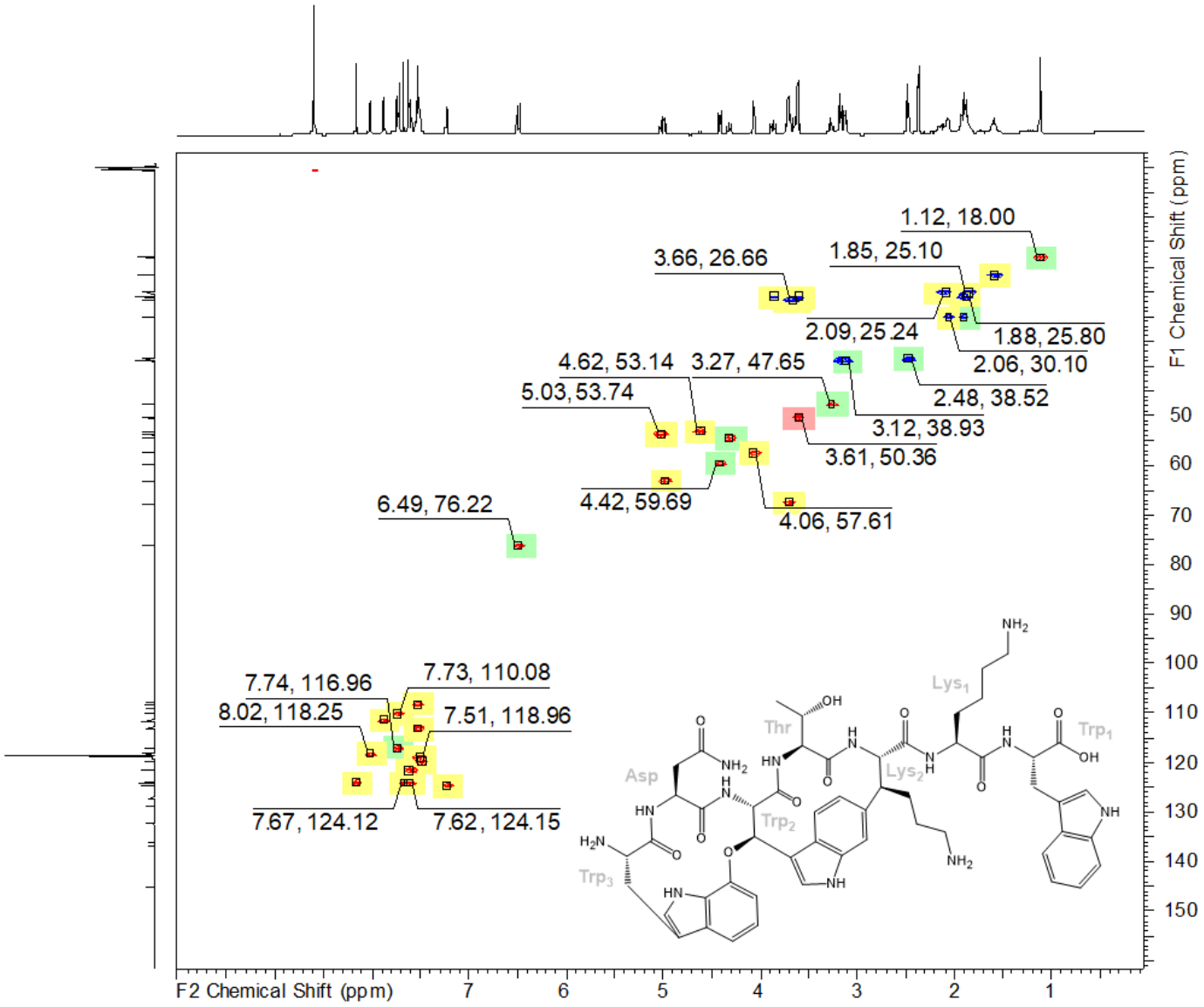

Figure S 63: HSQC spectrum of D36 in ACN/D2O + 1% FA at 45 °C and 500/125 MHz.

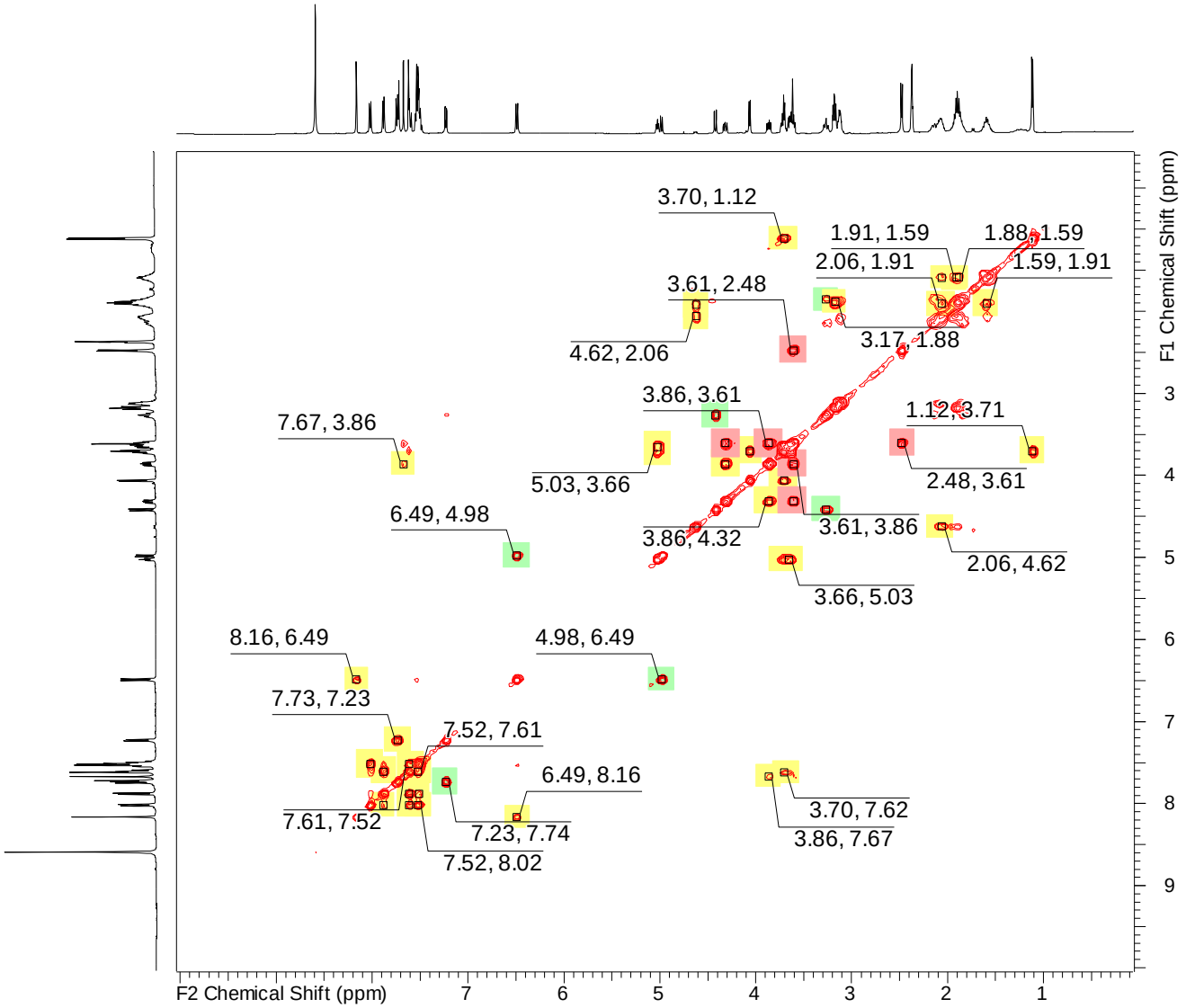

Figure S 64: COSY spectrum of D36 in ACN/D2O + 1% FA at 45 °C and 500/125 MHz.

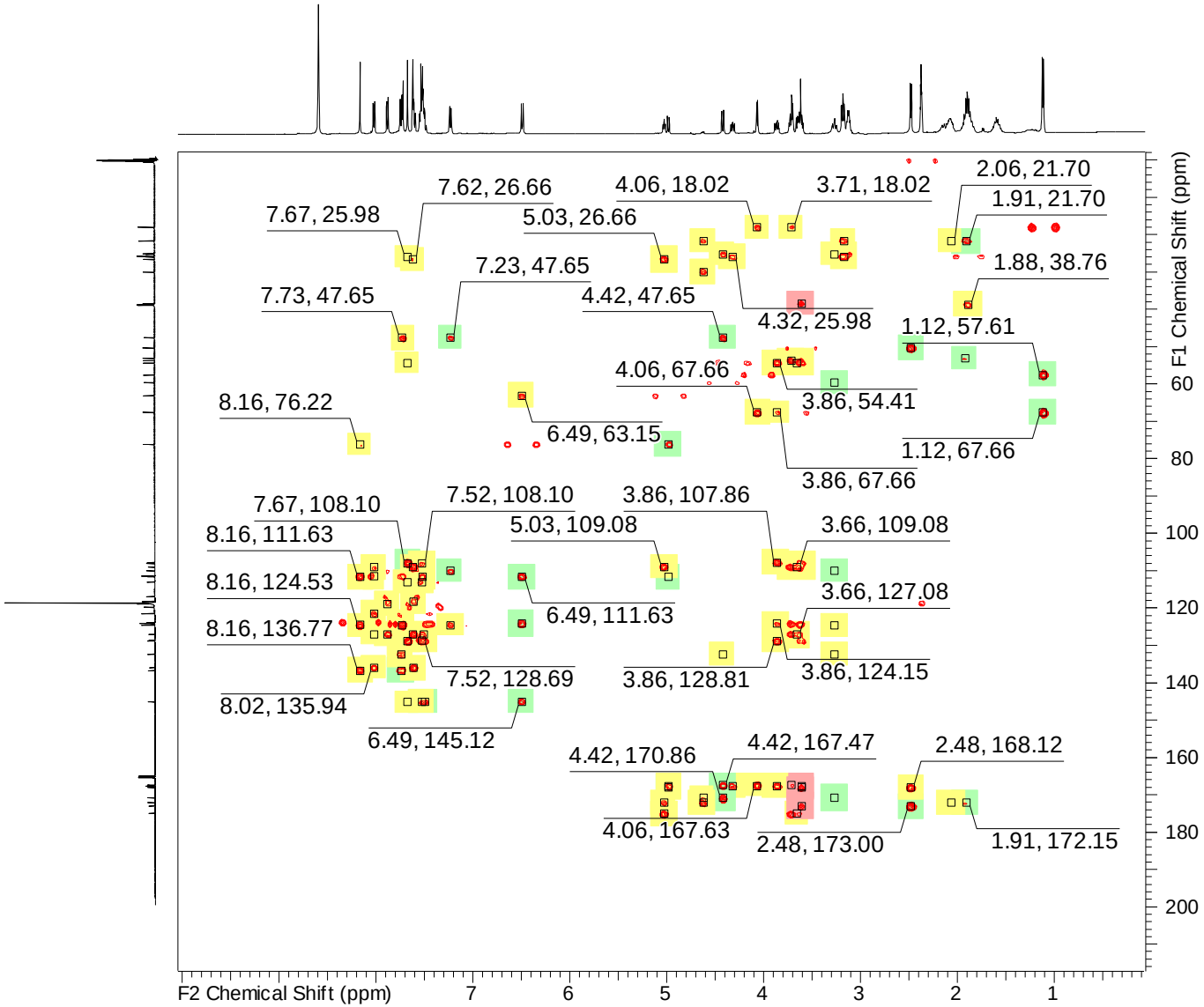

Figure S 65: HMBC spectrum of D36 in ACN/D2O + 1% FA at 45 °C and 500/125 MHz.

D37

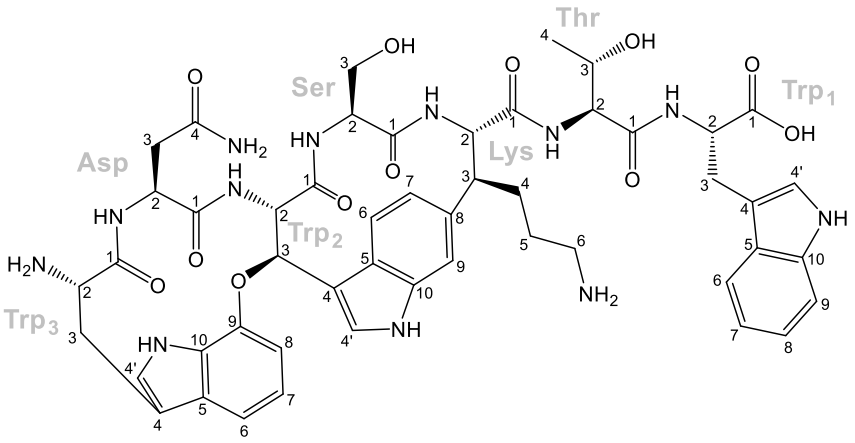

Table S 11: NMR spectroscopic data of D37.

		NMR data in ACN/D_2O + 1% FA-d_4		
position	δ ^{13}C	δ ^{1}H, mult (*J* in Hz)	COSY correlations	HMBC correlations
Trp₃				
1	174.9	-	-	-
2	53.9	5.17, t (5.8)	3	1, 3, 4, *Thr*-1
3	27.0	3.79, m	2	1, 2, 3
4	109.2	-	-	-
4’	124.3	7.72, s	-	3, 4, 5, 9, 10
5	127.4	-	-	-
6	118.6	8.12, d (7.9)	7	8, 10
7	119.1	7.61, m	6, 8	5, 9
8	121.8	7.71, m	7, 9	6, 10
9	111.7	7.99, d (8.2)	8	5, 7
10	136.2	-	-	-
Thr				
1	170.4	-	-	-
2	58.7	4.80, m	3	1, 3, 4, *Lys*-1
3	66.7	4.62, m	2, 4	1, 2, 4
4	18.6	1.51, d (6.3)	3	2, 3
Lys				
1	171.4	-	-	-
2	60.1	4.58, bd (10.7)	3	1, 3, 4, *Ser*-1, *Trp₂*-8
3	48.1	3.39, m	2, 4	1, 2, 4, 5, *Trp₂*-7, *Trp₃*-8, *Trp₂*-9
4	25.3	1.97, 2.18, m	3, 5	3, 5, 6, *Trp₂*-8
5	26.1	2.08, m	4, 6	3, 4, 6
6	39.1	3.21, m	5	4, 5

position	NMR data in ACN/D_2O + 1% FA-d_4 δ ^{13}C	δ ^{1}H, mult (*J* in Hz)	COSY correlations	HMBC correlations
Ser				
1	167.9	-	-	-
2	53.9	4.40, m	3	1, 3, *Trp₂*-1
3	61.9	3.63, 3.55, m	2	1, 2
Trp₂				
1	167.6	-	-	-
2	63.3	5.07, d (8.9)	3	1, 3, 4, *Asp*-1
3	76.3	6.56, d (9.0)	2, 4‘	2, 4, 4‘, *Trp₃*-9
4	111.9	-	-	-
4‘	124.1	8.25, s	3	3, 4, 5, 10
5	124.9	-	-	-
6	117.0	7.84, bd (8.1)	7	4, 8, 10
7	124.9	7.34, bd (8.2)	6	5, 9, *Lys*-3
8	132.6	-	-	-
9	110.3	7.82, s	-	5, 7, *Lys*-3
10	136.9	-	-	-
Asp				
1	168.2	-	-	-
2	50.5	3.74, m	3	1, 3, 4, *Trp3*-1
3	38.6	2.56, bd (6.0)	2	1, 2, 4
4	173.0	-	-	-
Trp₁				
1	167.8	-	-	-
2	54.6	4.42, m	3	1, 3
3	26.2	3.69, 3.95, dd (13.7, 7.3)	2	1, 2, 4, 4‘, 5
4	108.1	-	-	-
4‘	124.3	7.73, s	-	3, 4, 5, 9, 10
5	128.8	-	-	-
6	119.9	7.56, m	7	4, 8, 10
7	113.1	7.59, m	6, 8	5, 9
8	108.0	7.59, m	7	6, 10
9	145.4	-	-	-
10	128.5	-	-	-

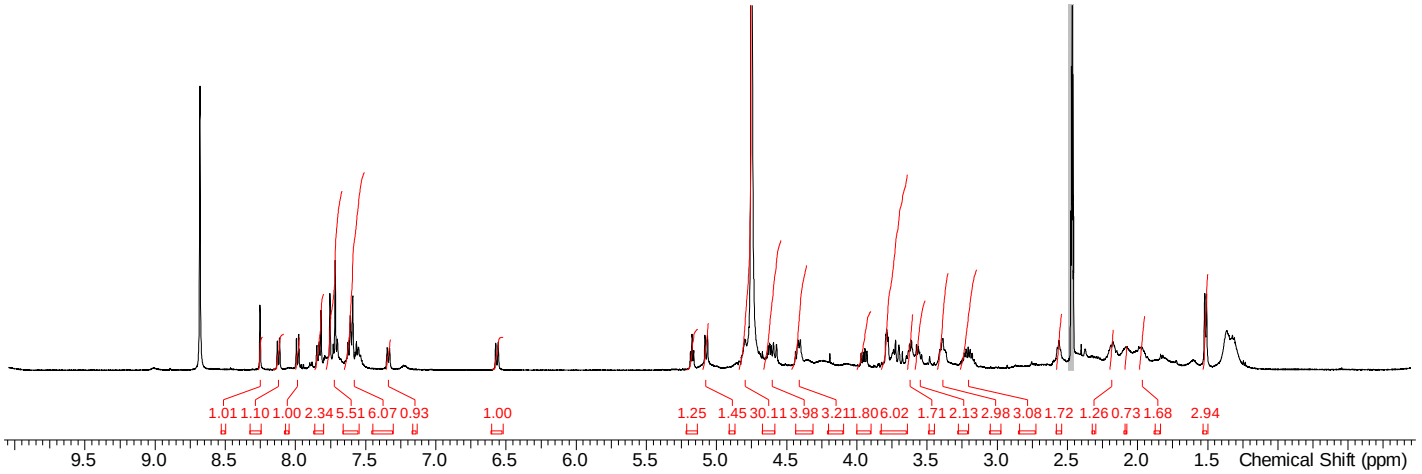

Figure S 66: ^{1}H spectrum of D37 in ACN/D2O + 1% FA at 45 °C and 500 MHz.

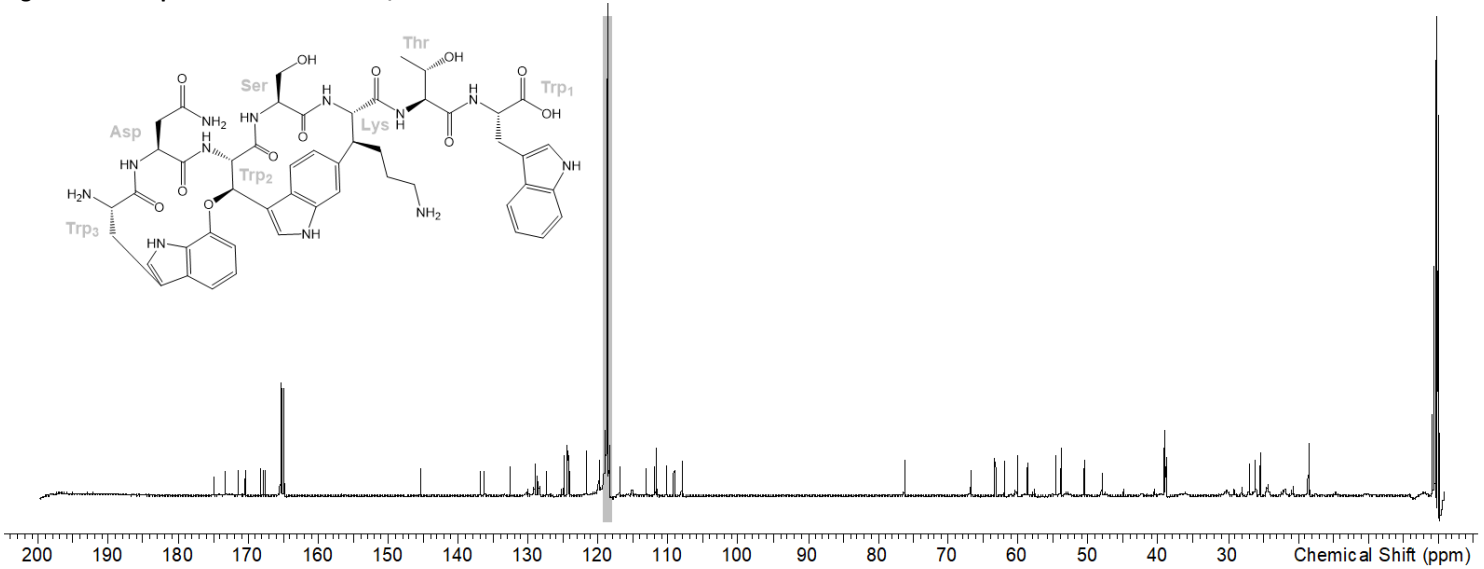

Figure S 67: ^{13}C spectrum of D37 in ACN/D2O + 1% FA at 45 °C and 125 MHz.

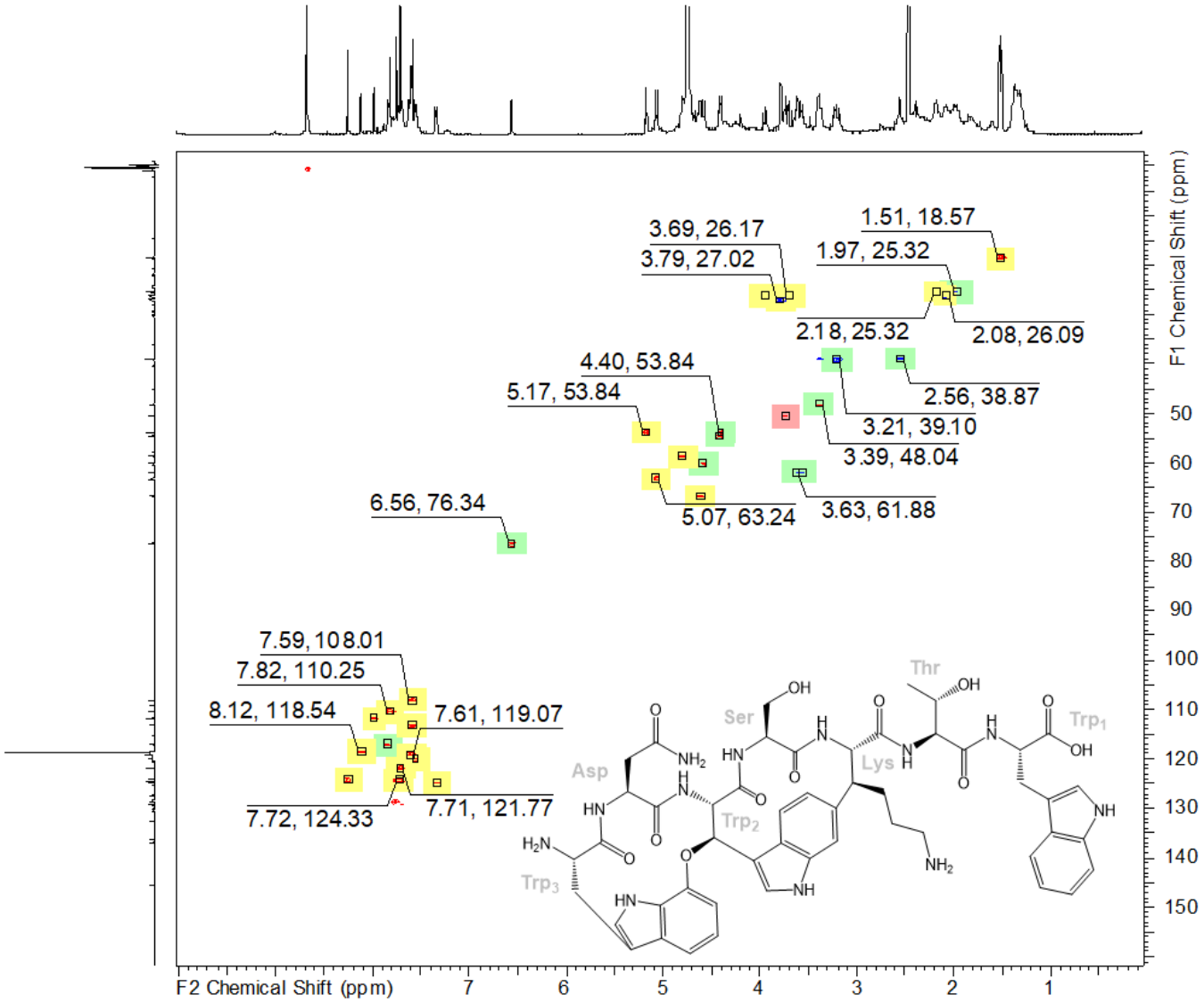

Figure S 68: HSQC spectrum of D37 in ACN/D2O + 1% FA at 45 °C and 500/125 MHz.

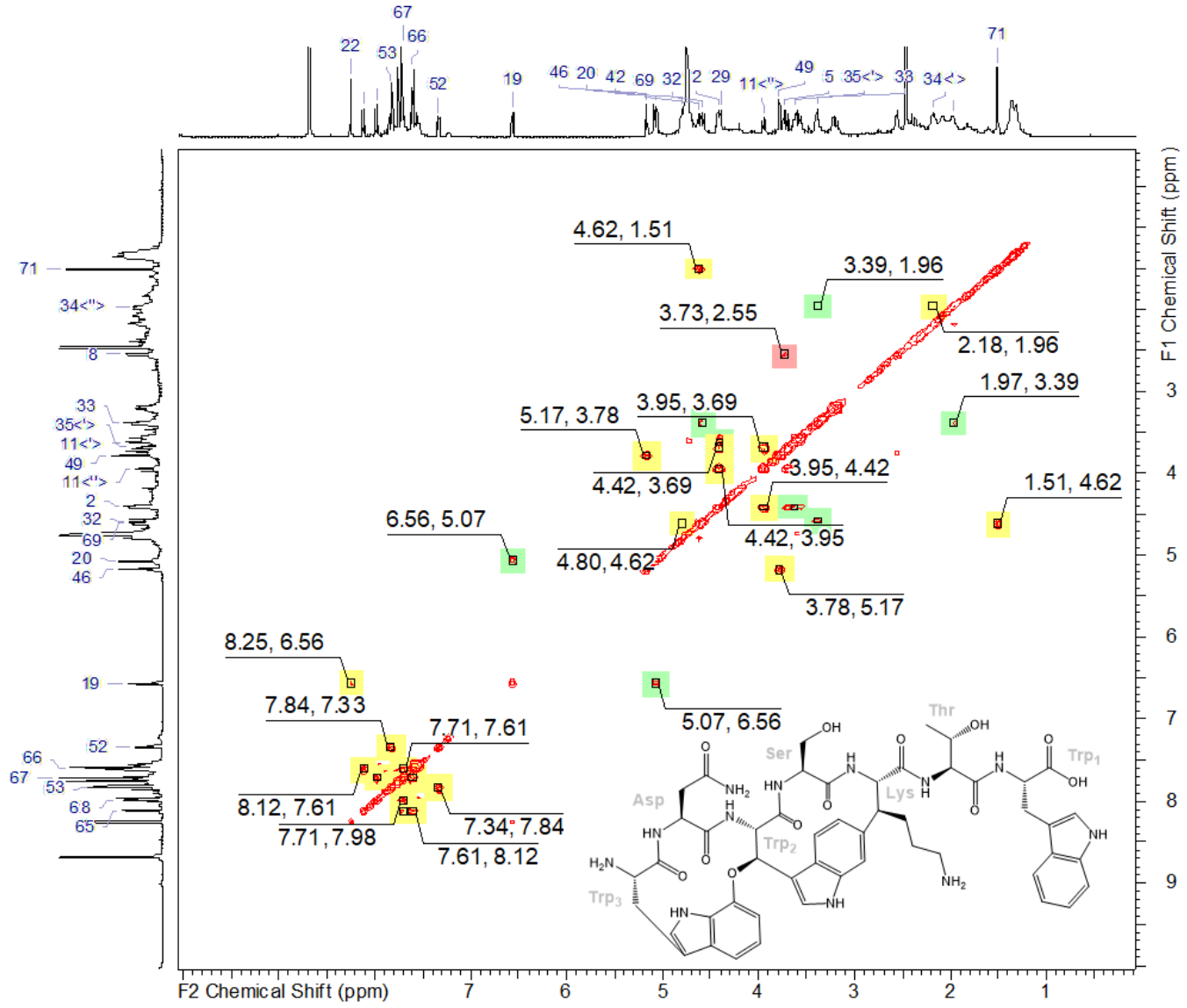

Figure S 69: COSY spectrum of D37 in ACN/D2O + 1% FA at 45 °C and 500/125 MHz.

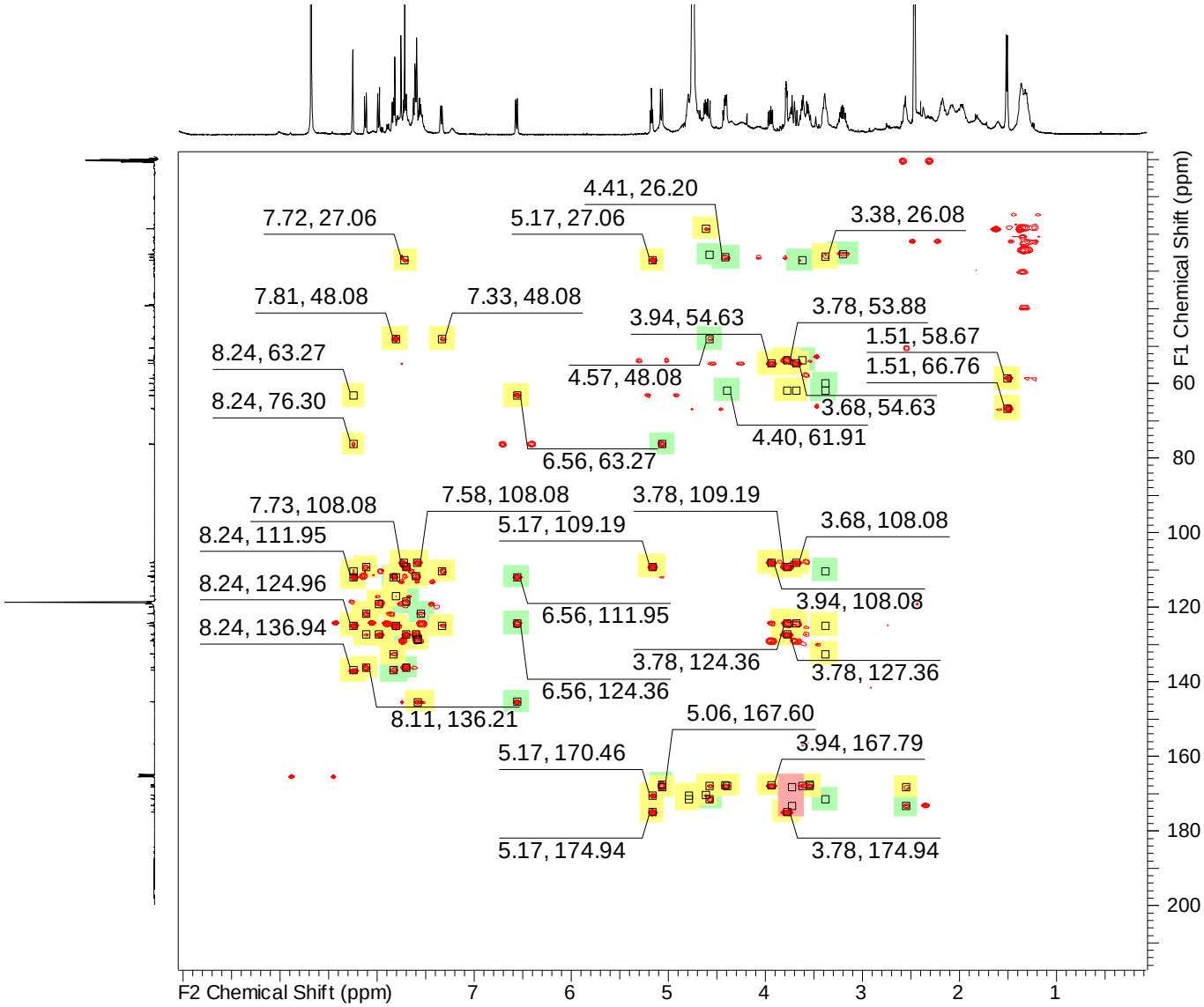

Figure S 70: HMBC spectrum of D37 in ACN/D2O + 1% FA at 45 °C and 500/125 MHz.

D38

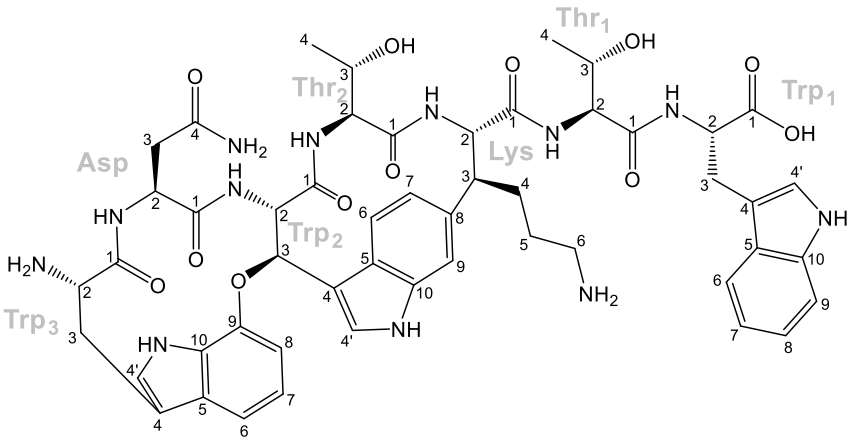

Table S 12: NMR spectroscopic data of D38.

	NMR data in ACN/D_2O + 1% FA-d_4			
position	δ ^{13}C	δ ^{1}H, mult (*J* in Hz)	COSY correlations	HMBC correlations
Trp₁				
1	174.7	-	-	-
2	53.5	5.05, t (6.7)	3	1, 3, 4, *Thr₁*-1
3	26.7	3.66, m	2	1, 2, 3
4	108.8	-	-	-
4'	124.2	7.60, s	-	3, 4, 5, 9, 10
5	127.0	-	-	-
6	118.3	8.00, d (7.9)	7	8, 10
7	118.9	7.50, m	6, 8	5, 9
8	121.6	7.60, m	7, 9	6, 10
9	111.5	7.87, d (8.2)	8	5, 7
10	135.9	-	-	-
Thr₁				
1	170.2	-	-	-
2	58.4	4.66, bd (3.9)	3	1, 3, 4, *Lys*-1
3	66.3	4.48, m	2, 4	1, 2, 4
4	18.3	1.35, d (6.4)	3	2, 3
Lys				
1	171.1	-	-	-
2	59.7	4.38, d (10.5)	3	1, 3, 4, *Thr₂*-1, *Trp₂*-8
3	47.6	3.25, m	2, 4	1, 2, 4, 5, *Trp₂*-7, *Trp₃*-8, *Trp₂*-9
4	25.0	1.89, 2.00, m	3, 5	3, 5, 6, *Trp₂*-8
5	25.9	1.94, m	4, 6	3, 4, 6
6	38.8	3.03, m	5	4, 5

	NMR data in ACN/D_2O + 1% FA-d_4			
position	δ ^{13}C	δ ^{1}H, mult (*J* in Hz)	COSY correlations	HMBC correlations
Thr₂				
1	167.4	-	-	-
2	57.6	4.04, d (6.3)	3	1, 3, 4, *Trp₂*-1
3	67.6	3.66, m	2, 4	2, 4
4	18.0	1.06, d (6.3)	3	2, 3
Trp₂				
1	167.5	-	-	-
2	63.0	4.95, d (8.9)	3	1, 3, 4, *Asp*-1
3	76.2	6.43, d (8.9)	2, 4‘	2, 4, 4‘, *Trp₃*-9
4	111.5	-	-	-
4‘	123.9	8.12, s	3	3, 4, 5, 10
5	124.1	-	-	-
6	116.9	7.68, d (8.2)	7	4, 8, 10
7	124.5	7.18, d (8.2)	6	5, 9, *Lys*-3
8	132.3	-	-	-
9	110.0	7.67, s	-	5, 7, *Lys*-3
10	136.7	-	-	-
Asp				
1	168.0	-	-	-
2	50.3	3.58, m	3	1, 3, 4, *Trp3*-1
3	38.4	2.43, d (6.9)	2	1, 2, 4
4	172.9	-	-	-
Trp₃				
1	167.6	-	-	-
2	54.3	4.28, dd (10.9, 7.3)	3	1, 3
3	25.9	3.58, 3.82, dd (13.3, 7.1)	2	1, 2, 4, 4‘, 5
4	107.7	-	-	-
4‘	124.1	7.62, s	-	3, 4, 5, 9, 10
5	128.6	-	-	-
6	119.7	7.44, m	7	4, 8, 10
7	113.0	7.47, m	6, 8	5, 9
8	108.0	7.46, m	7	6, 10
9	145.0	-	-	-
10	128.7	-	-	-

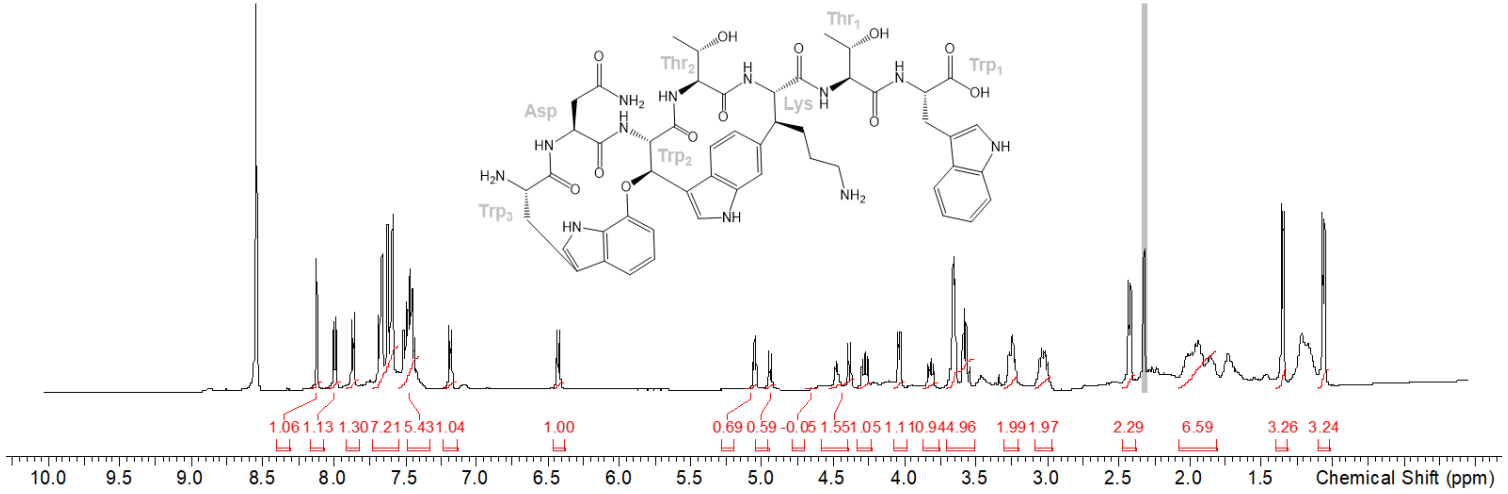

Figure S 71: Water-suppressed ^{1}H spectrum of D38 in ACN/D2O + 1% FA at 45 °C and 500 MHz.

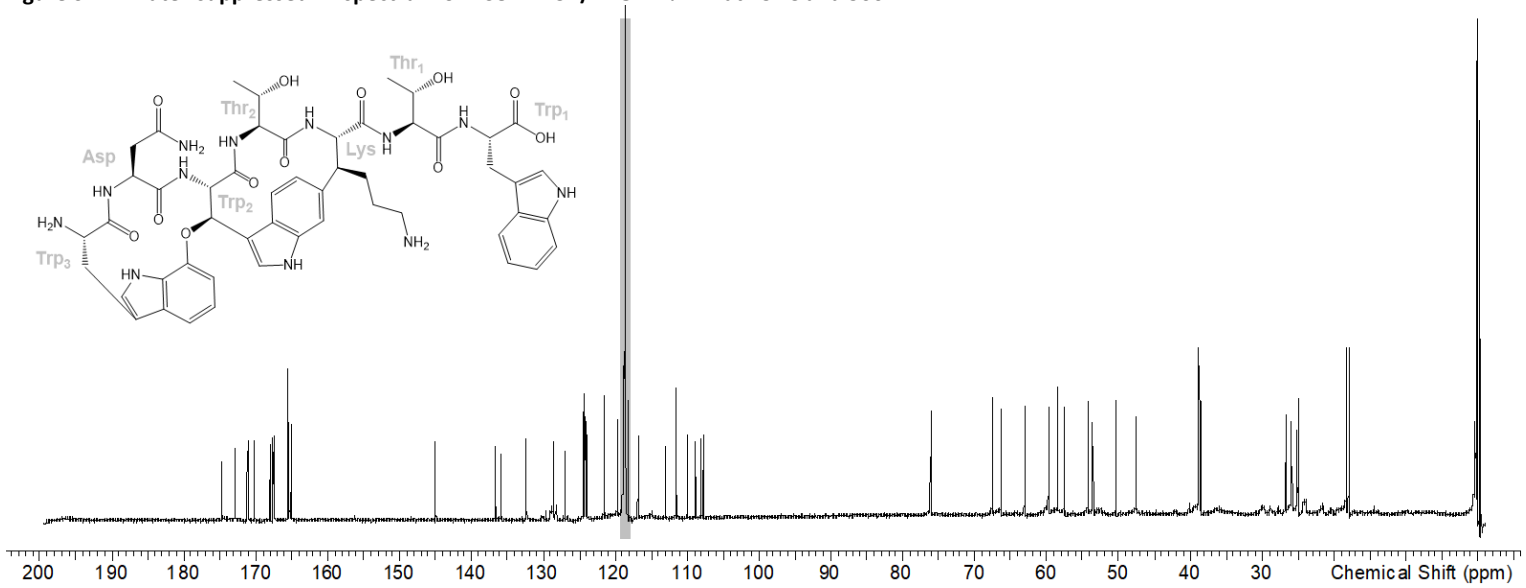

Figure S 72: ^{13}C spectrum of D38 in ACN/D2O + 1% FA at 45 °C and 125 MHz.

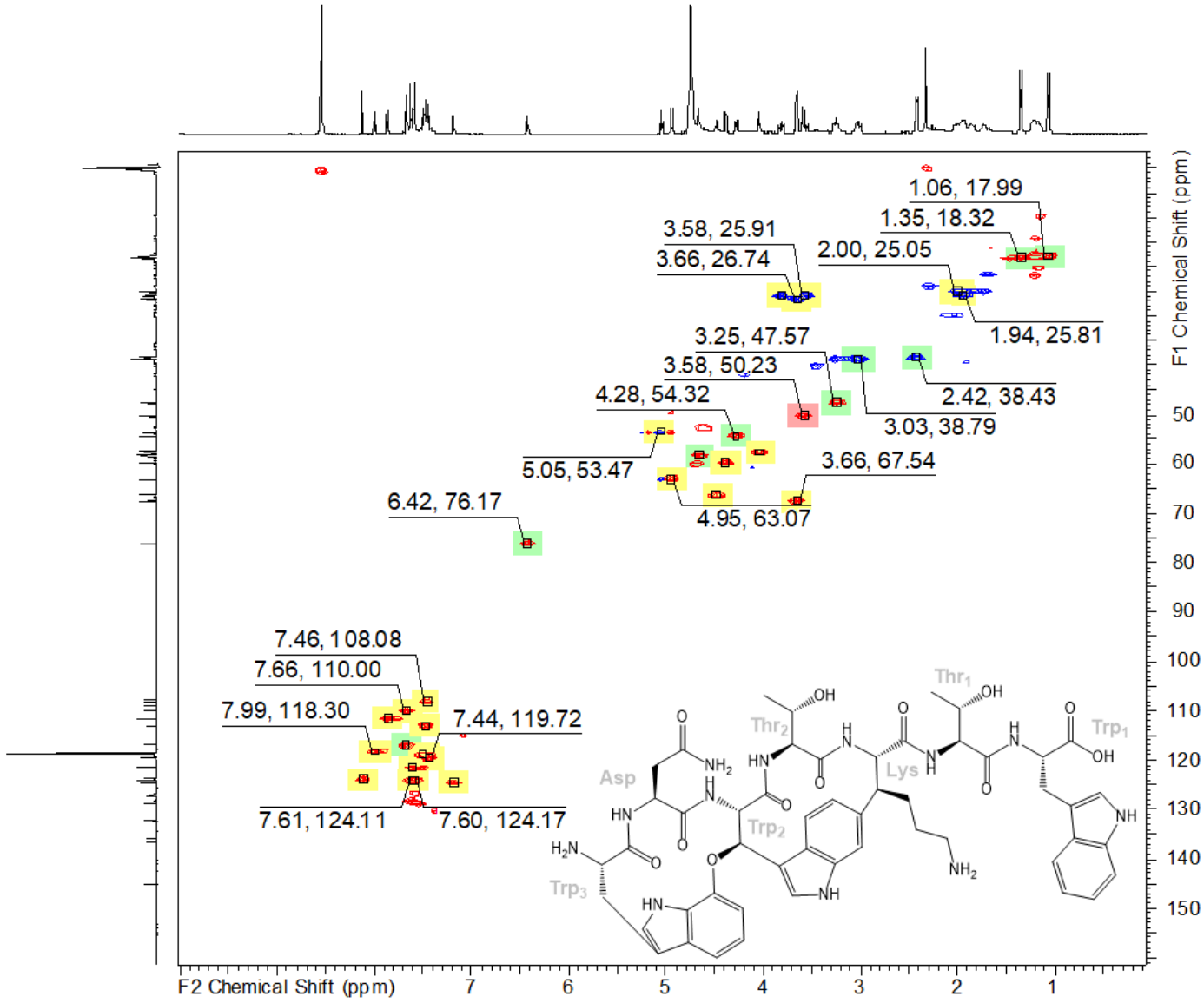

Figure S 73: HSQC spectrum of D38 in ACN/D2O + 1% FA at 45 °C and 500/125 MHz.

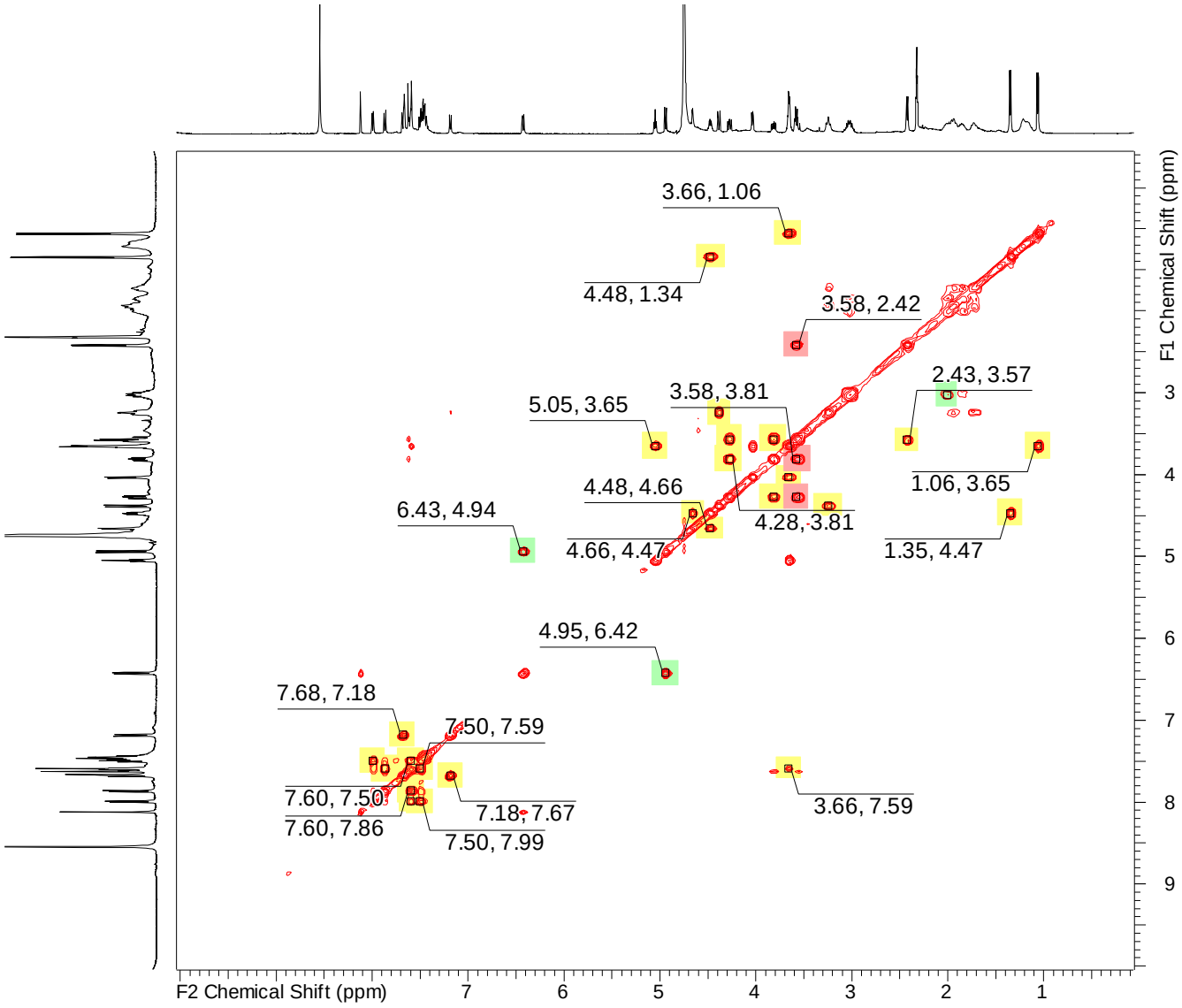

Figure S 74: COSY spectrum of D38 in ACN/D2O + 1% FA at 45 °C and 500/125 MHz.

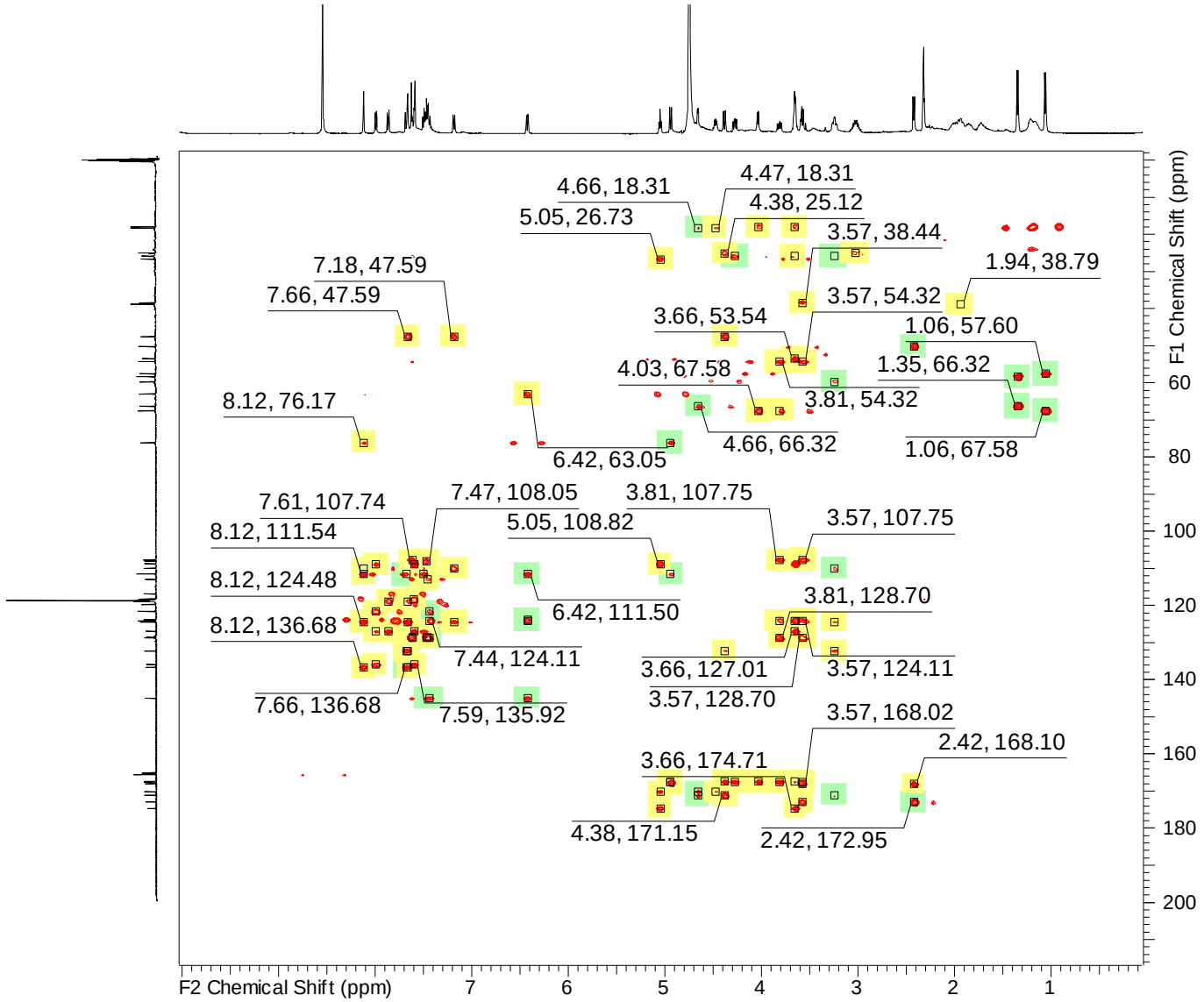

Figure S 75: HMBC spectrum of D38 in ACN/D2O + 1% FA at 45 °C and 500/125 MHz.

D6[R]

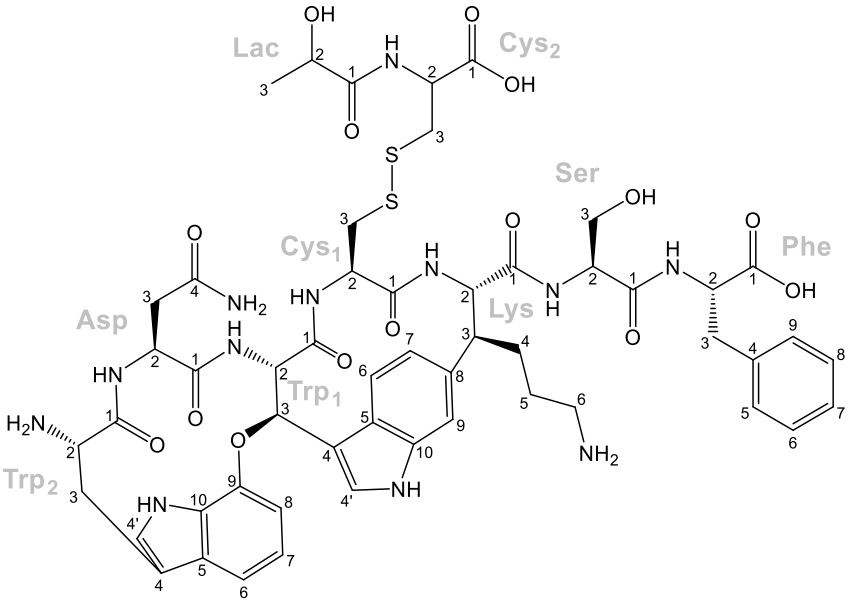

Table S 13: NMR spectroscopic data of D6[R].

	NMR data in ACN/D_2O + 1% FA-d_4			
position	δ ^{13}C	δ ^{1}H, mult (*J* in Hz)	COSY correlations	HMBC correlations
Phe				
1	174.0	-	-	-
2	54.3	5.07, m	3	1, 3, 4, *Ser*-1
3	36.7	3.64, 3.51, m	2	1, 2, 4, 5/9
4	136.7	-	-	-
5/9	129.4	7.70, m	6/8	3, 7
6/8	129.4	7.80, m	5/9, 7	4, 6/8
7	127.0	7.75, m	6/8	5/9
Ser				
1	167.8	-	-	-
2	54.2	4.35, m	3	1, 3, *Lys*-1
3	62.2	3.61, 3.49, m	2	1, 2
Lys				
1	167.7	-	-	-
2	60.2	4.58, m	3	1, 3, 4, *Cys*-1, *Trp*$_1$-8
3	48.2	3.41, m	2, 4	1, 2, 4, 5, *Trp*$_1$-7, *Trp*$_3$-8, *Trp*$_1$-9
4	25.8	2.48, 2.13, m	3, 5	3, 5, 6, *Trp*$_1$-8
5	25.5	2.29, m	4, 6	3, 4, 6
6	39.4	3.40, m	5	4, 5

NMR data in ACN/D_2O + 1% FA-d_4				
position	δ ^{13}C	δ ^{1}H, mult (*J* in Hz)	COSY correlations	HMBC correlations
Cys₁				
1	171.2	-	-	-
2	52.6	5.07, m	3	1, 3, *Trp₁*-1
3	39.0	3.29, 3.50, m	2	1, 2, *Cys₂*-3
Cys₂				
1	173.4	-	-	-
2	52.6	5.10, m	3	1, 3, *Lac*-1
3	39.3	3.46, 3.67, m	2	1, 2, *Cys₁*-3
Lac				
1	176.7	-	-	-
2	67.6	4.65, m	3	1, 3
3	19.8	1.75, t (5.3)	2	1, 2
Trp₁				
1	170.6	-	-	-
2	63.4	5.03, d (9.0)	3	1, 3, 4, *Asp*-1
3	76.4	6.54, d (8.9)	2, 4‘	2, 4, 4‘, *Trp₂*-9
4	112.0	-	-	-
4‘	124.2	8.23, s	3	3, 4, 5, 10
5	125.0	-	-	-
6	117.2	7.82, d (8.3)	7	4, 8, 10
7	125.0	7.32, d (8.2)	6	5, 9, *Lys*-3
8	132.6	-	-	-
9	110.4	7.83, s	-	5, 7, *Lys*-3
10	137.1	-	-	-
Asp				
1	168.3	-	-	-
2	50.7	3.67, m	3	1, 3, 4, *Trp₂*-1
3	39.0	2.54, t (6.1)	2	1, 2, 4
4	173.3	-	-	-
Trp₂				
1	167.8	-	-	-
2	54.7	4.38, m	3	1, 3
3	26.3	3.67, 3.92, m	2	1, 2, 4, 4‘, 5
4	108.1	-	-	-
4‘	120.0	7.55, s	-	3, 4, 5, 9, 10
5	129.4	-	-	-
6	124.4	7.73, m	7	4, 8, 10
7	113.2	7.57, m	6, 8	5, 9
8	108.2	7.59, m	7	6, 10
9	145.5	-	-	-
10	129.1	-	-	-

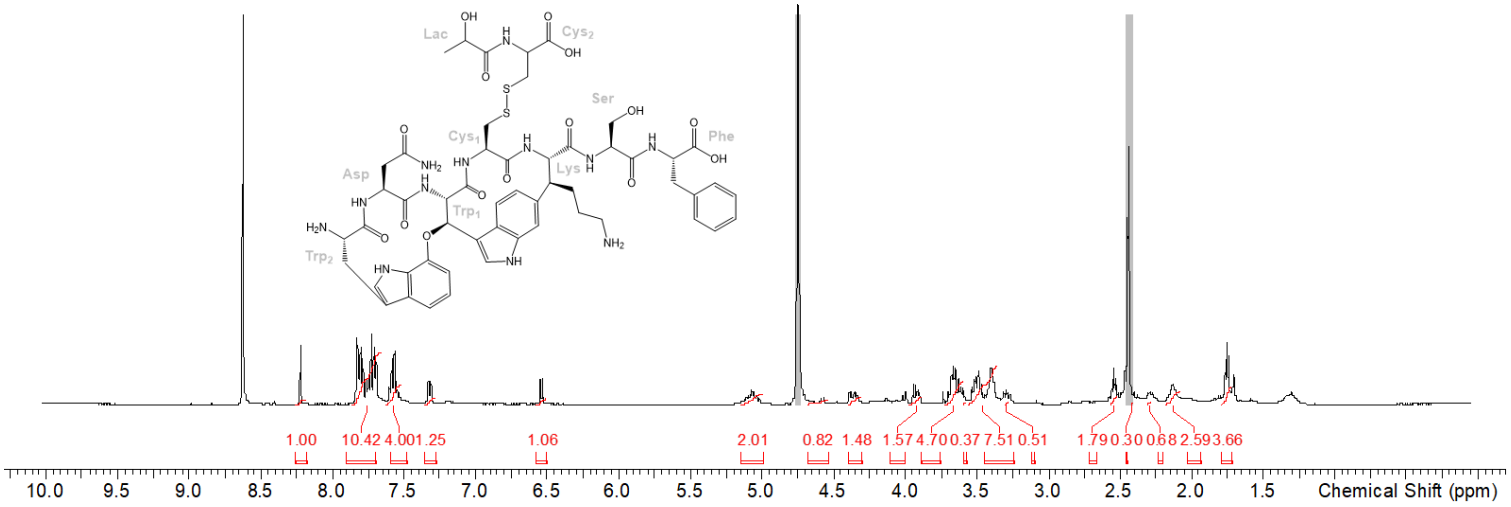

Figure S 76: ^{1}H spectrum of D6$^{[R]}$ in ACN/D2O + 1% FA at 45 °C and 500 MHz.

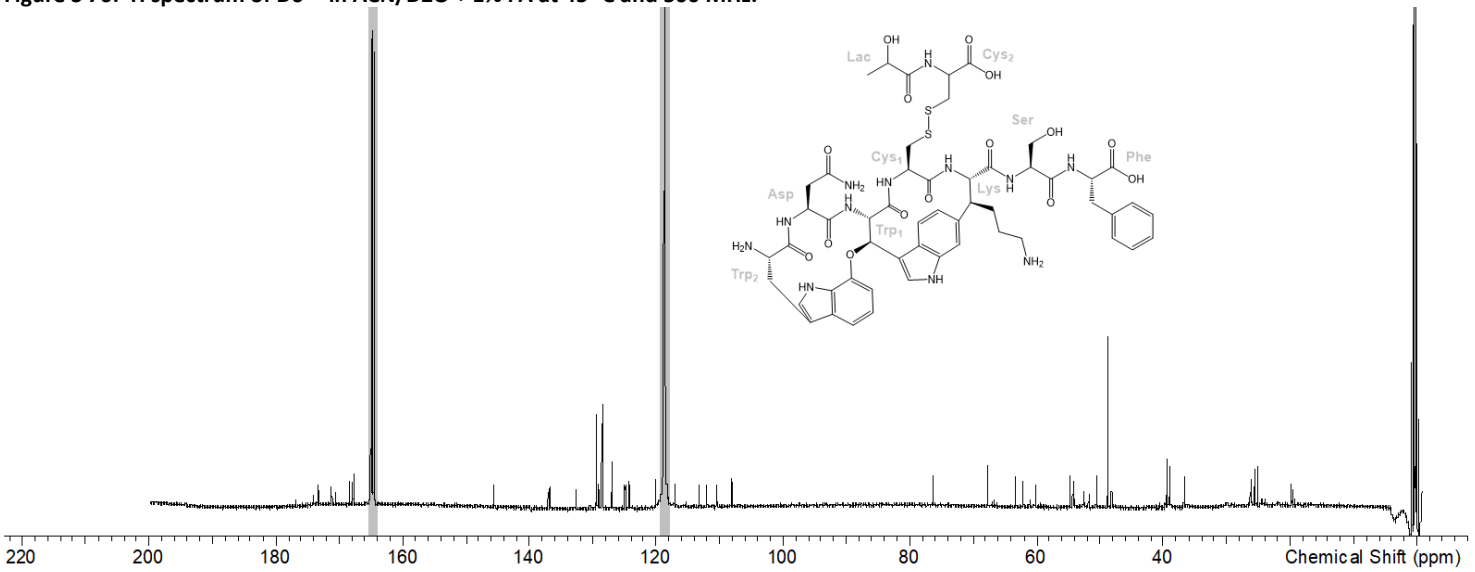

Figure S 77: ^{13}C spectrum of D6$^{[R]}$ in ACN/D2O + 1% FA at 45 °C and 125 MHz.

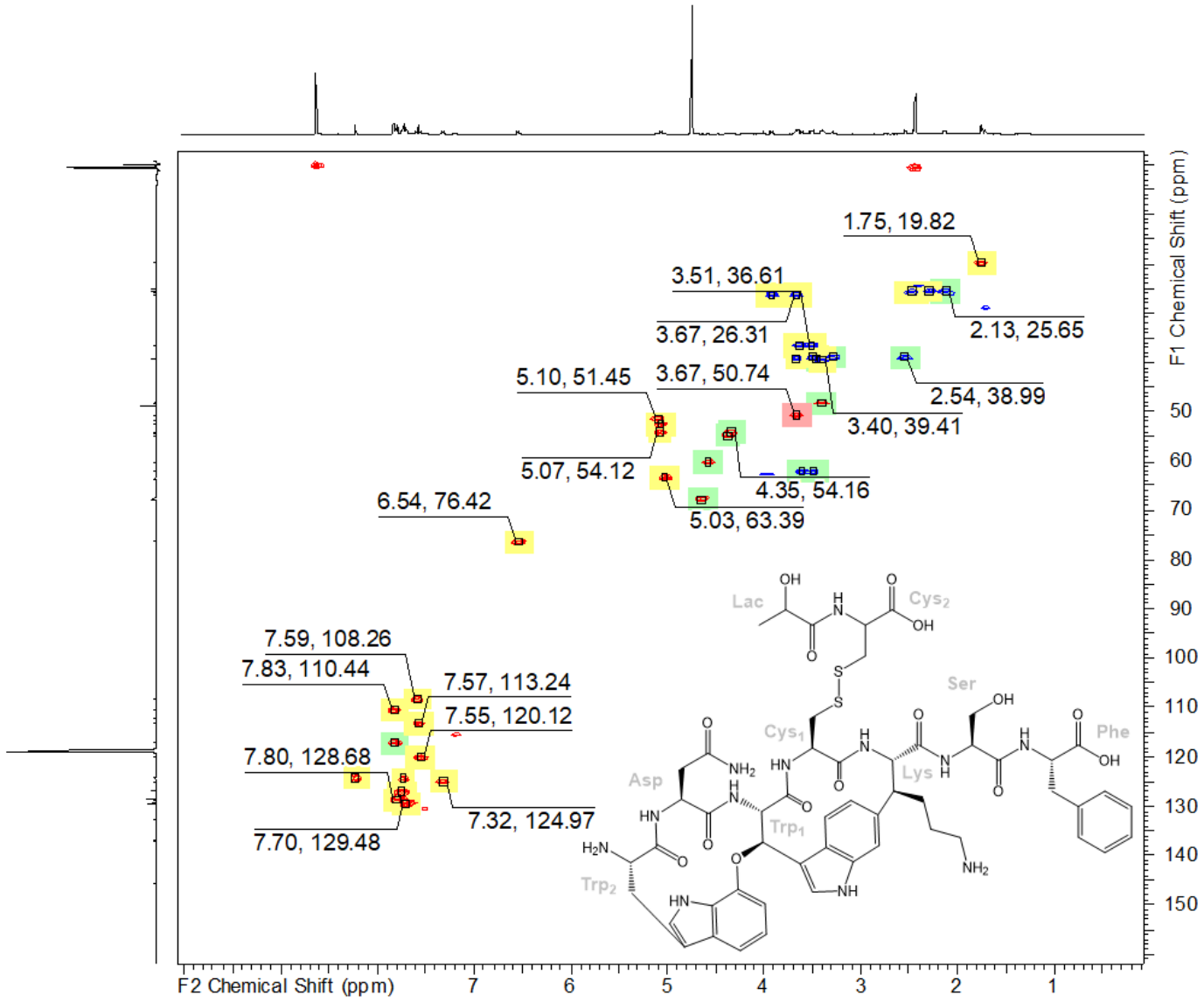

Figure S 78: HSQC spectrum of D6[R] in ACN/D2O + 1% FA at 45 °C and 500/125 MHz.

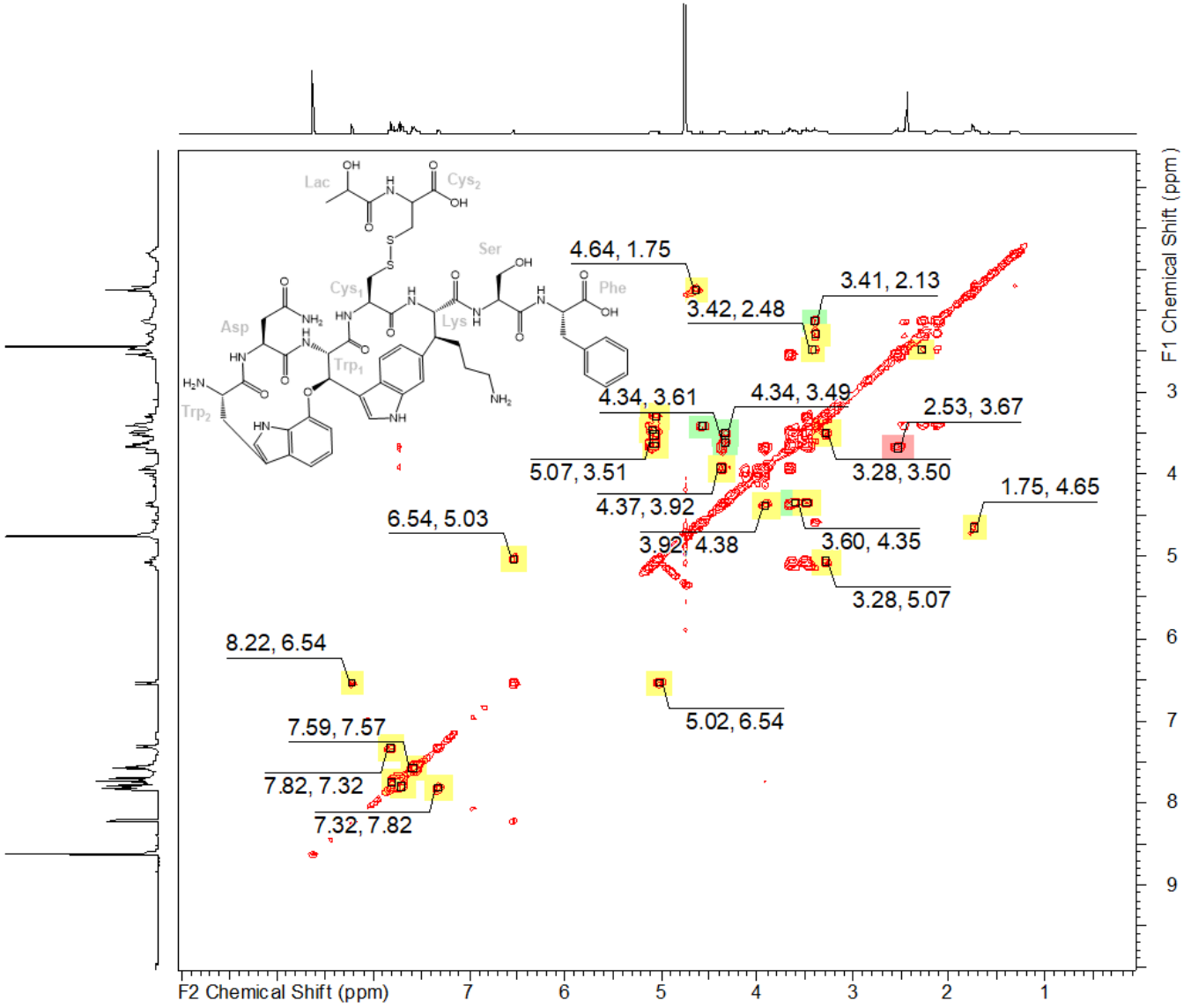

Figure S 79: COSY spectrum of D6[R] in ACN/D2O + 1% FA at 45 °C and 500/125 MHz.

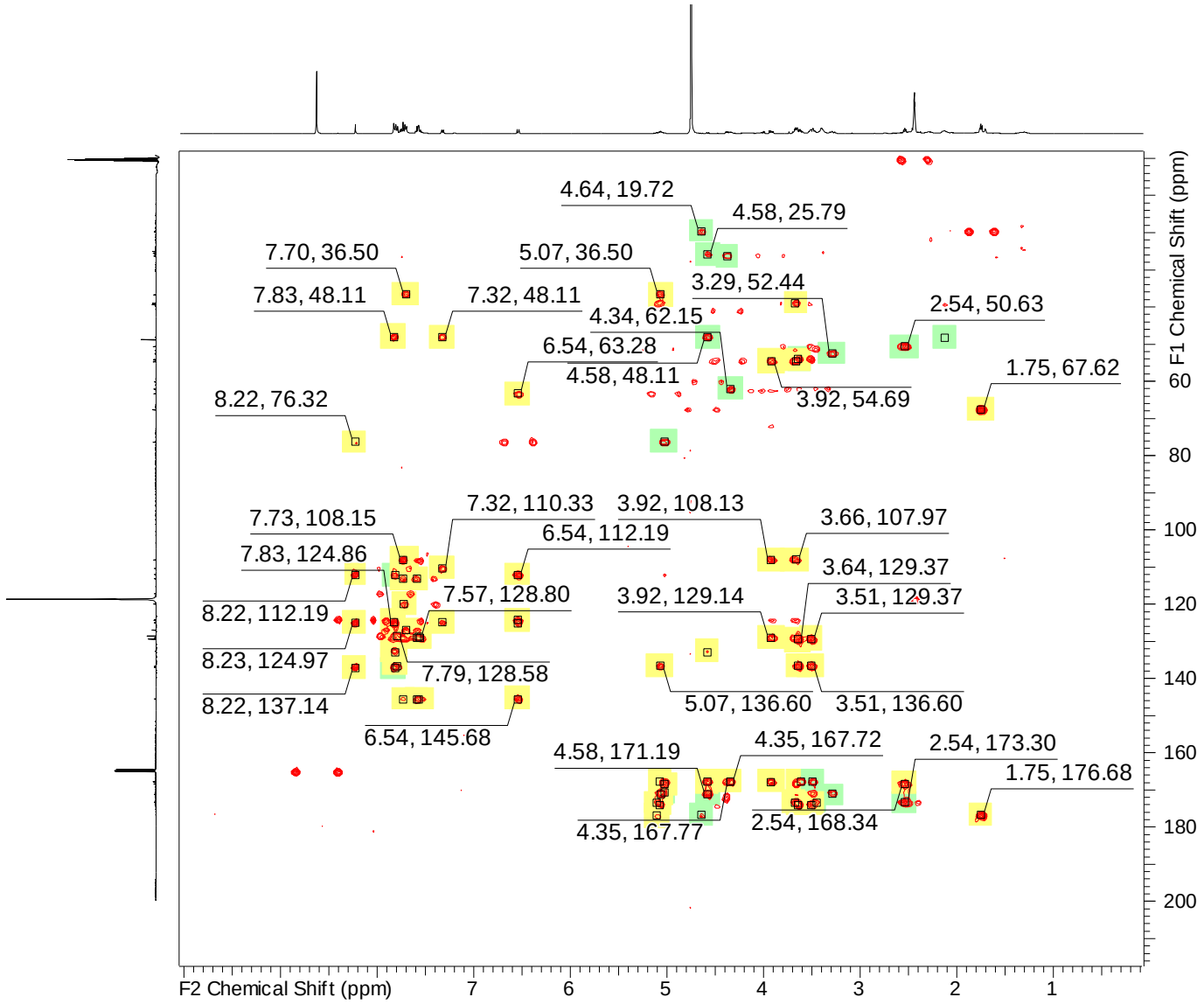

Figure S 80: COSY spectrum of D6[R] in ACN/D2O + 1% FA at 45 °C and 500 MHz.

D32[R]

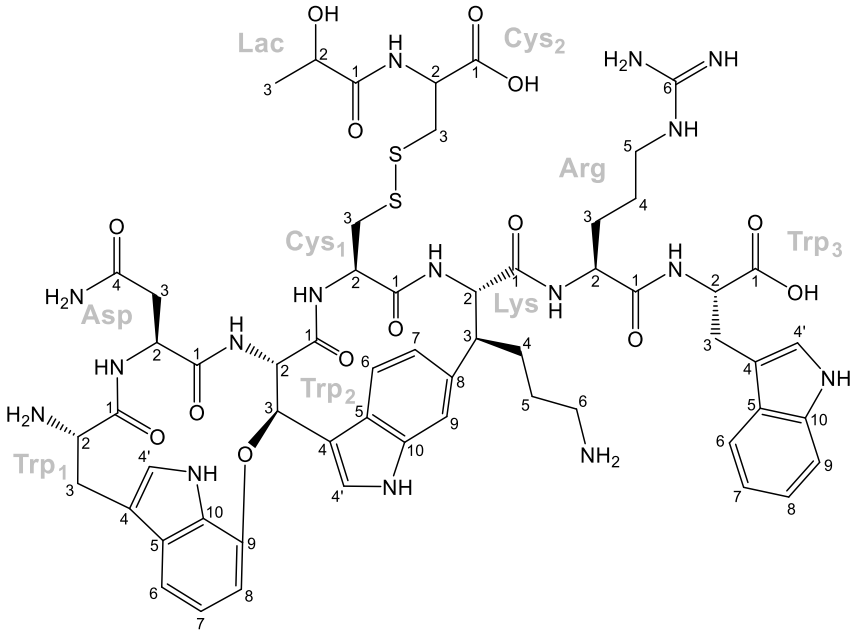

Table S 14: NMR spectroscopic data of D32[R].

	NMR data in ACN/D_2O + 1% FA-d_4			
position	δ ^{13}C	δ ^{1}H, mult (*J* in Hz)	COSY correlations	HMBC correlations
Trp3				
1	175.1	-	-	-
2	53.6	4.61, t (5.8)	3	1, 3, 4, 4‘, *Asp*-1
3	26.8	3.26, m	2, 4‘	1, 2, 4, 4‘, 5
4	109.1	-	-	-
4‘	124.2	7.19, s	3	3, 4, 5, 10
5	127.2	-	-	-
6	118.3	7.57, d (7.9)	7	4, 5, 8, 9, 10
7	119.8	7.06, m	6, 8	5, 8, 9
8	111.6	7.43, d (8.0)	7, 9	5, 6, 8, 10
9	121.6	7.17, t (5.6)	8	5, 6, 7, 8, 10
10	136.0	-	-	-
Arg				
1	172.1	-	-	-
2	53.0	4.26, m	3	3, 4
3	28.2	1.64, 1.49, m	2, 4	1, 2, 4, 5
4	24.3	1.35, m	3, 5	2, 3, 5
5	40.3	2.96, m	4	3, 4, 6
6	156.4	-	-	-

NMR data in ACN/D_2O + 1% FA-d_4				
position	δ ^{13}C	δ ^{1}H, mult (*J* in Hz)	COSY correlations	HMBC correlations
Lys				
1	170.8	-	-	-
2	59.7	4.01, bd (9.9)	3	1, 3, 4, *Cys*-1, *Trp*$_1$-8
3	47.7	2.88, m	2, 4	1, 2, 4, 5, *Trp*$_1$-7, *Trp*$_3$-8, *Trp*$_1$-9
4	25.3	1.46, 1.65, m	3, 5	2, 3, 5, 6
5	25.5	1.73, m	4, 6	3, 4, 6
6	39.0	2.68, bd (4.8)	5	4, 5
Cys$_1$				
1	167.7	-	-	-
2	51.3	4.00, m	3	1, 3, *Trp*$_1$-1
3	40.6	2.31, 2.42, m	2	1, 2
Cys$_2$				
1	174.3	-	-	-
2	52.3	4.35, m	3	1, 3, *Lac*-1
3	39.4	2.98, 2.81, m	2	1, 2
Lac				
1	176.3	-	-	-
2	67.4	4.08, m	3	1, 3
3	19.6	1.19, d (6.9)	2	1, 2
Trp$_2$				
1	167.1	-	-	-
2	63.1	4.51, bd (9.2)	3	1, 3, 4, *Asp*-1
3	76.2	6.01, d (8.7)	2, 4‘	2, 4, 4‘, *Trp*$_1$-9
4	111.7	-	-	-
4‘	124.0	7.70, s	3	3, 4, 5, 6, 9, 10
5	124.7	-	-	-
6	109.9	7.27, m	7	4, 5, 7, 8, 9, 10
7	124.8	6.81, d (7.5)	6	5, 6, 8, 9, 10, *Lys*-3
8	132.4	-	-	-
9	117.1	7.28, s	-	6, 7, *Lys*-3
10	136.8	-	-	-
Asp				
1	168.0	-	-	-
2	50.4	3.23, m	3	1, 3, 4, *Trp*$_1$-1
3	38.8	2.03, m	2	1, 2, 4
4	173.3	-	-	-

NMR data in ACN/D_2O + 1% FA-d_4				
position	δ ^{13}C	δ ^{1}H, mult (*J* in Hz)	COSY correlations	HMBC correlations
Trp₁				
1	167.8	-	-	-
2	54.4	3.90, m	3	1, 3
3	26.1	3.16, 3.42, m	2, 4‘	1, 2, 4, 4‘, 5
4	107.9	-	-	-
4‘	124.2	7.22, s	3	3, 4, 5, 9
5	128.9	-	-	-
6	113.2	7.06, m	7	4, 8, 9
7	119.0	7.08, m	6, 8	5, 9
8	108.1	7.04, m	7	6, 9, 10
9	145.2	-	-	-
10	128.7	-	-	-

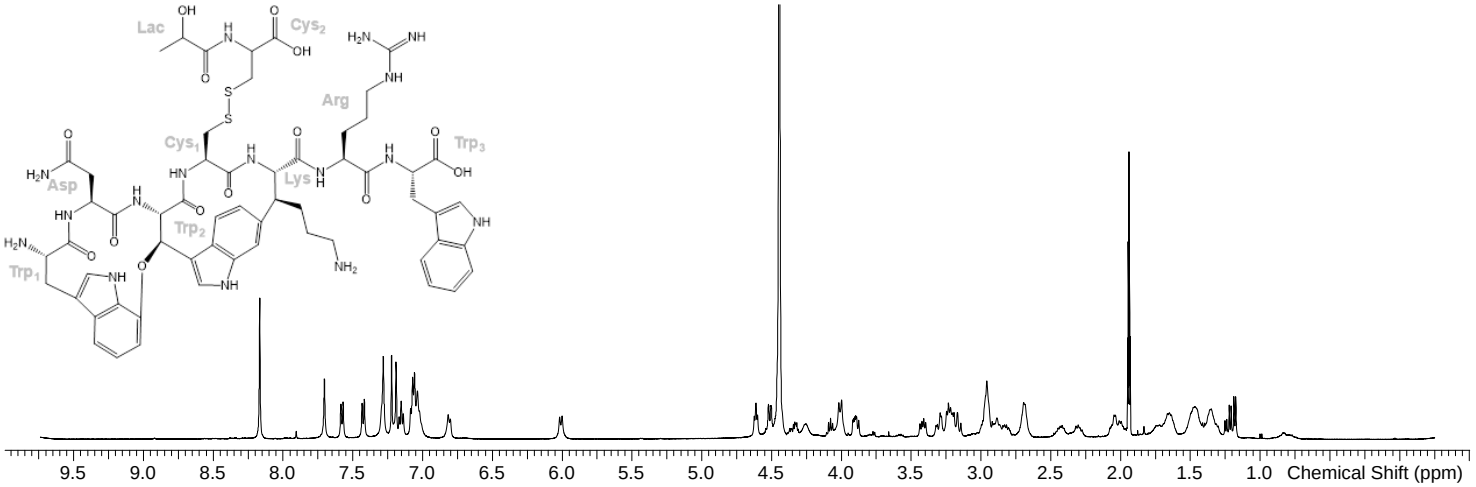

Figure S 81: ^{1}H spectrum of D32$^{[R]}$ in ACN/D2O + 1% FA at 35 °C and 500 MHz.

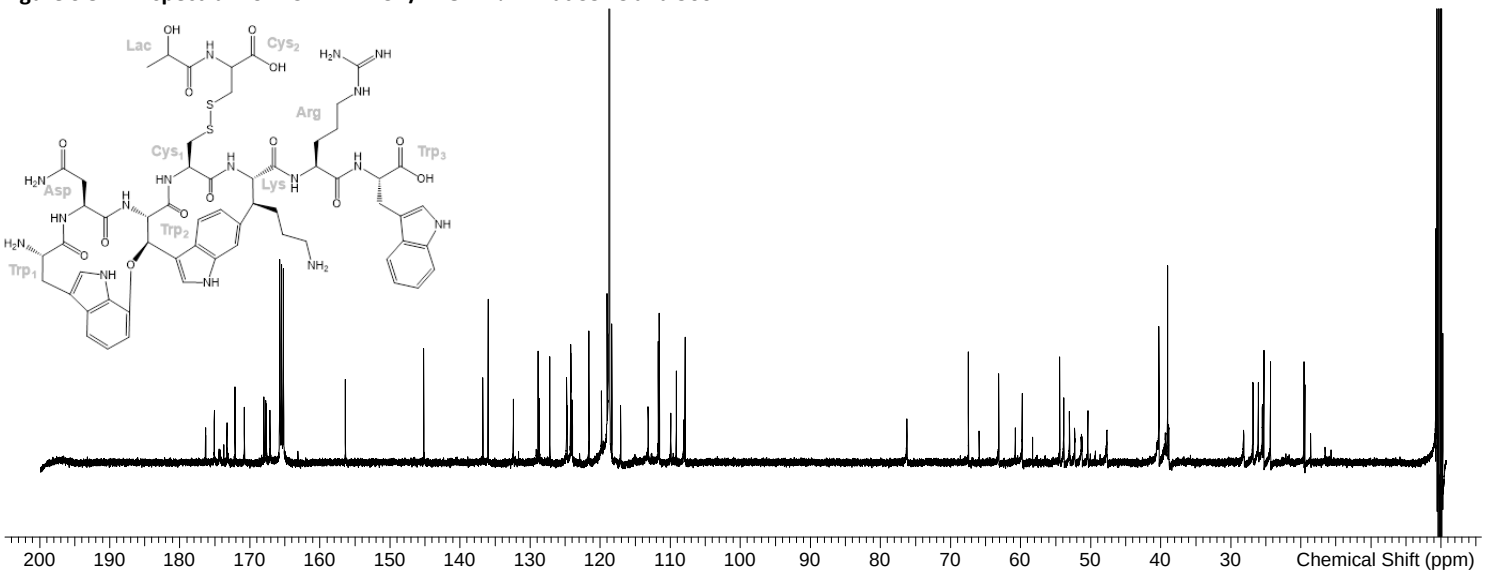

Figure S 82: ^{13}C spectrum of D32$^{[R]}$ in ACN/D2O + 1% FA at 35 °C and 125 MHz.

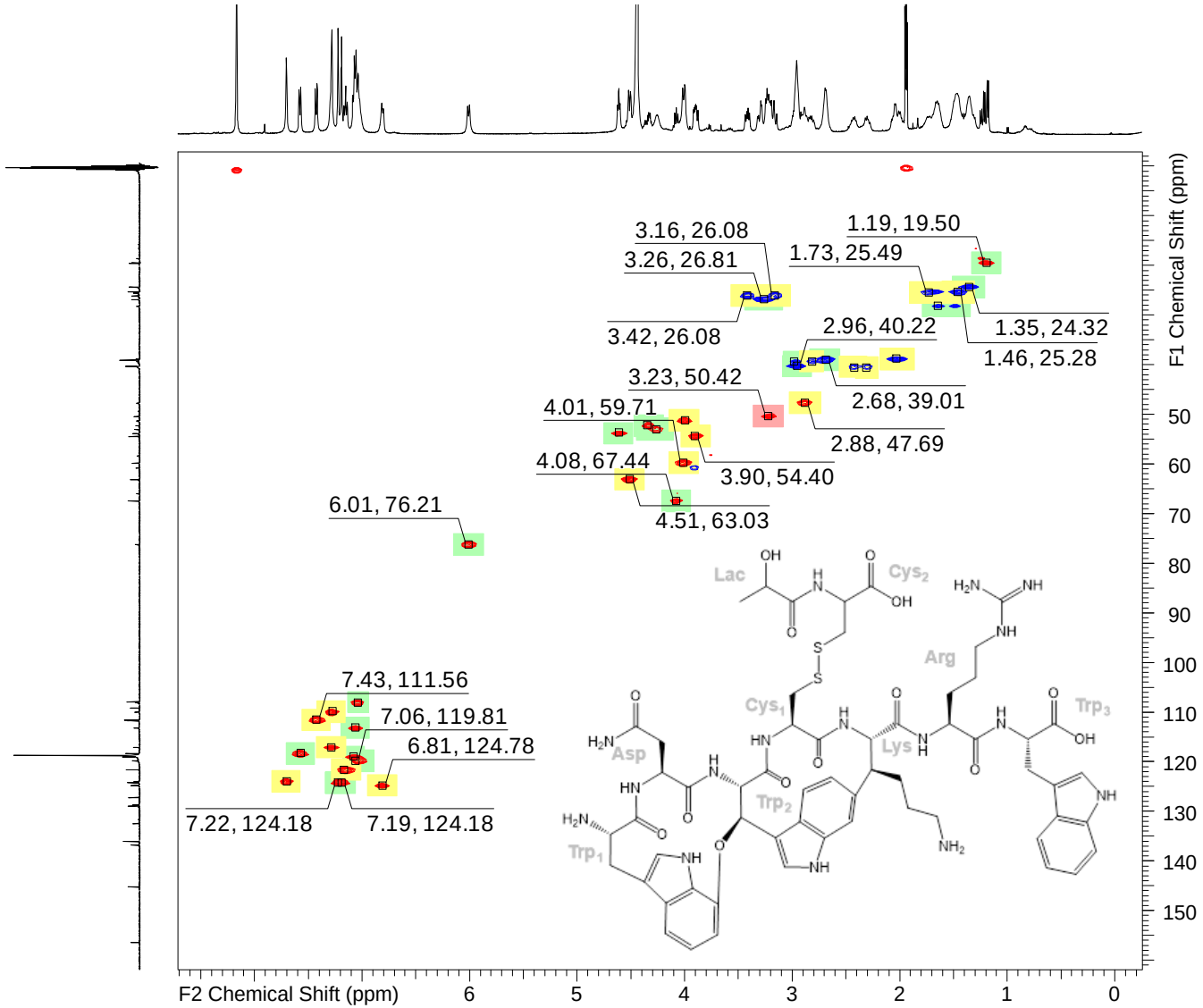

Figure S 83: HSQC spectrum of D32[R] in ACN/D2O + 1% FA at 35 °C and 500/125 MHz.

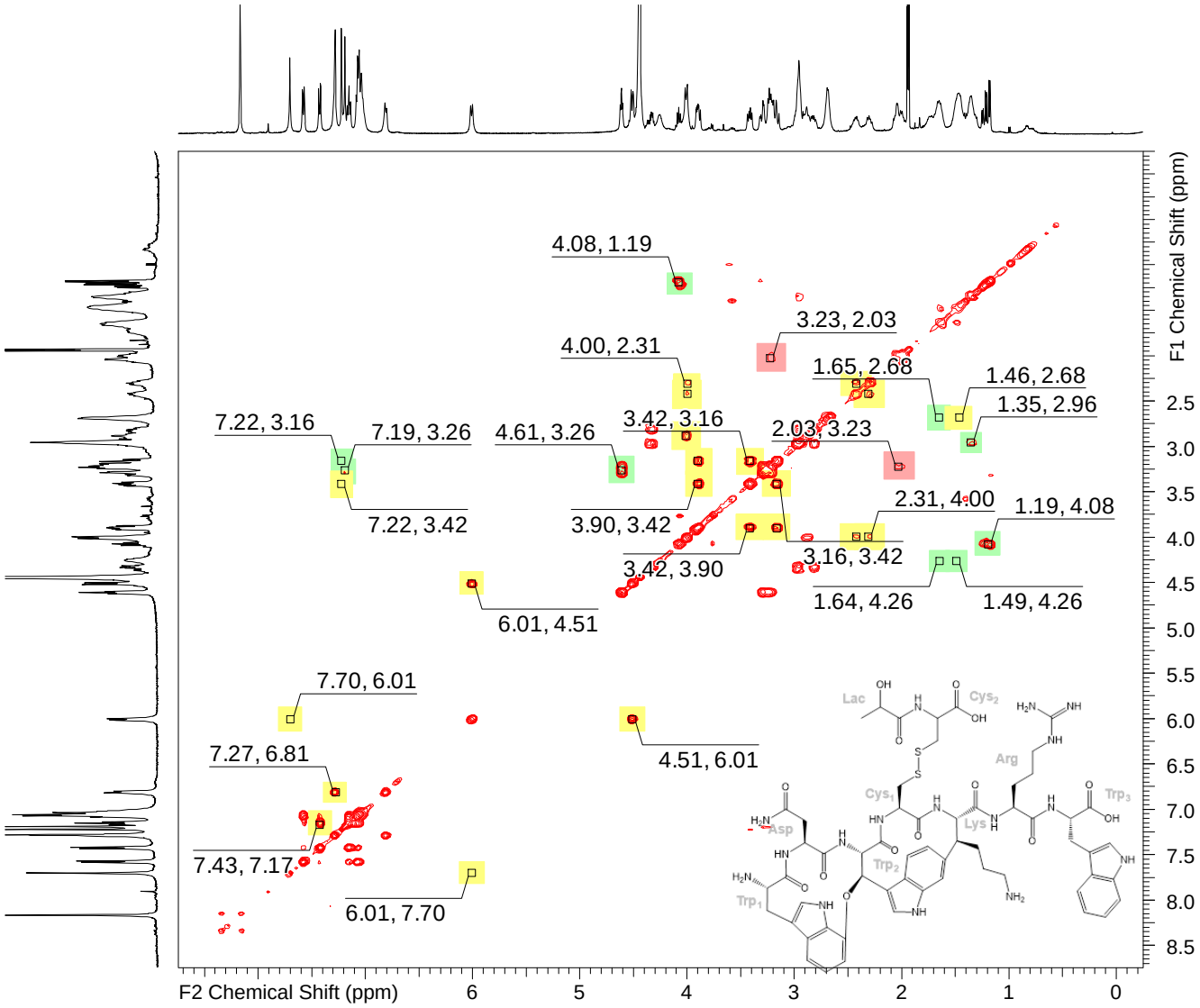

Figure S 84: COSY spectrum of D32[R] in ACN/D2O + 1% FA at 35 °C and 500 MHz.

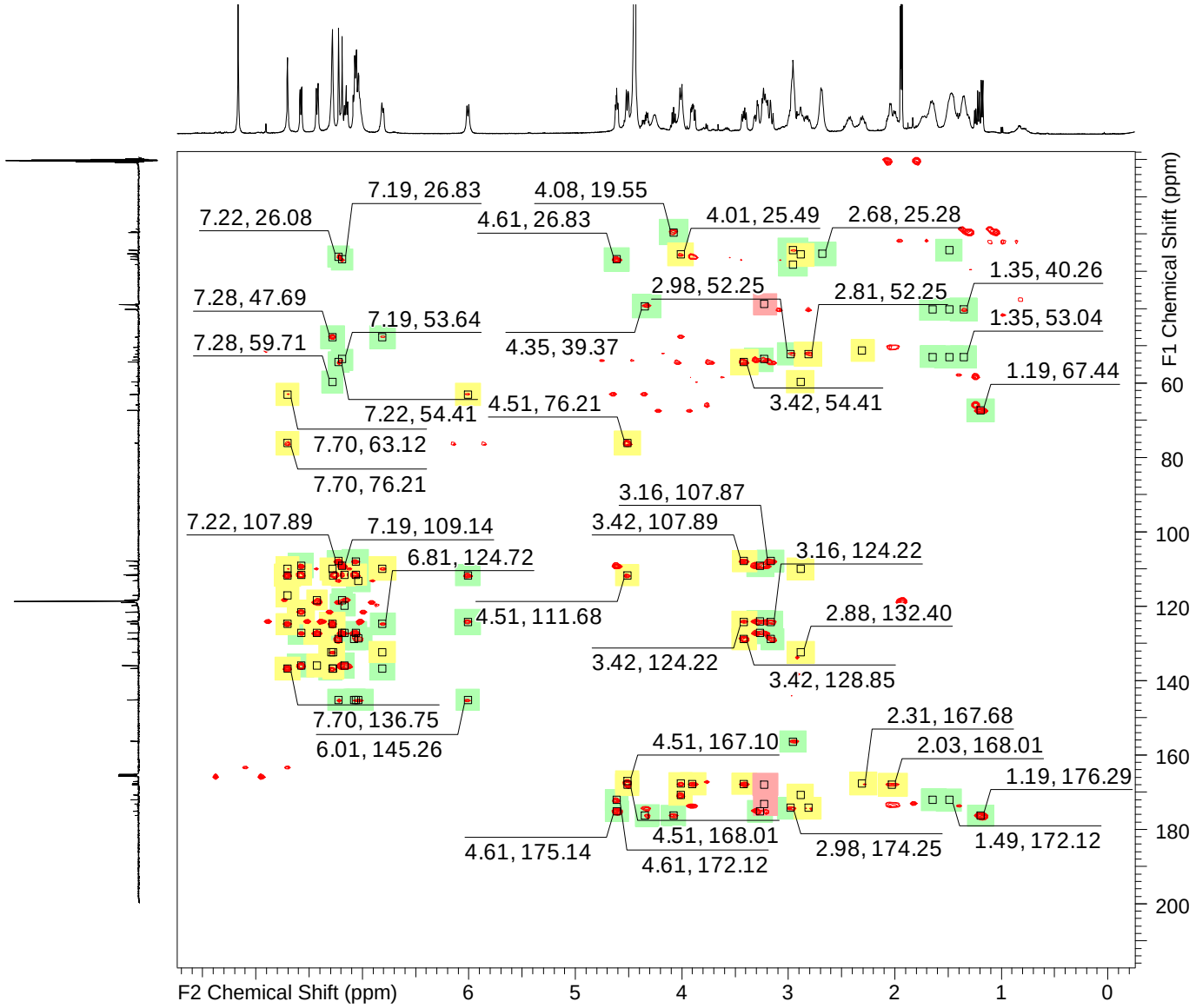

Figure S 85: HMBC spectrum of D32[R] in ACN/D2O + 1% FA at 35 °C and 500/125 MHz.

D9-6F

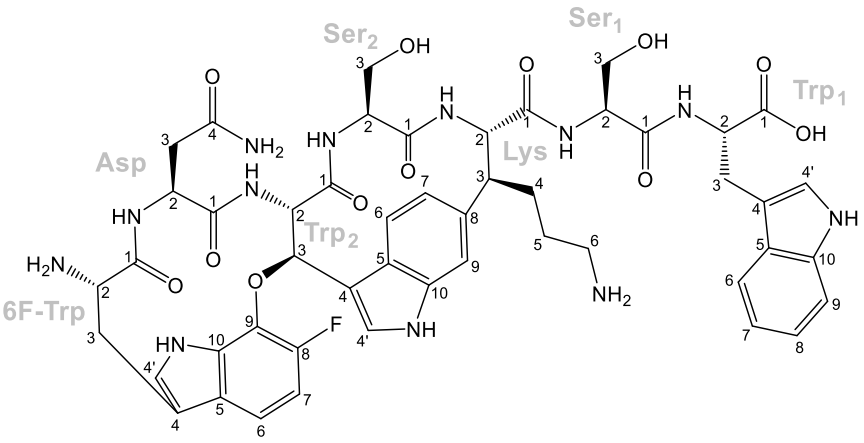

Table S 15: NMR spectroscopic data of D9-6F.

		NMR data in ACN/D_2O + 1% FA-d_4		
position	δ ^{13}C	δ ^{1}H, mult (*J* in Hz)	COSY correlations	HMBC correlations
Trp$_1$				
1	174.5	-	-	-
2	53.5	5.20, t (5.9)	3	1, 3, 4, *Ser*-1
3	26.8	3.80, m	2	1, 2, 3
4	108.9	-	-	-
4'	124.3	7.72, s	-	3, 4, 5, 9, 10
5	127.2	-	-	-
6	118.2	8.13, d (7.9)	7	8, 10
7	119.1	7.62, m	6, 8	5, 9
8	121.7	7.71, m	7, 9	6, 10
9	111.6	7.99, d (8.4)	8	5, 7
10	136.1	-	-	-
Ser$_1$				
1	170.4	-	-	-
2	55.3	4.89, m	3	1, 3, *Lys*-1
3	61.0	4.22, m	2	1, 2
Lys				
1	171.2	-	-	-
2	59.9	4.57, d (10.2)	3	1, 3, 4, *Ser$_2$*-1, *Trp$_2$*-8
3	48.0	3.38, m	2, 4	1, 2, 4, 5, *Trp$_2$*-7, *Trp$_2$*-8, *Trp$_2$*-9
4	25.3	2.22, 2.03, m	3, 5	3, 5, 6, *Trp$_2$*-8
5	25.4	2.14, m	4, 6	3, 4, 6
6	39.1	3.25, m	5	4, 5

NMR data in ACN/D_2O + 1% FA-d_4				
position	δ ^{13}C	δ ^{1}H, mult (*J* in Hz)	COSY correlations	HMBC correlations
Ser₂				
1	167.7	-	-	-
2	53.9	4.36, m	3	1, 3, *Trp₂*-1
3	61.8	3.54, dd (11.3, 6.4)	2	1, 2
Trp₂				
1	167.8	-	-	-
2	62.9	5.14, d (9.1)	3	1, 3, 4, *Asp*-1
3	76.0	6.54, bd (8.9)	2, 4‘	2, 4, 4‘, *Trp₃*-9
4	111.7	-	-	-
4‘	124.0	8.27, s	3	3, 4, 5, 10
5	124.8	-	-	-
6	117.0	7.79, d (7.6)	7	4, 8, 10
7	124.8	7.33, d (7.3)	6	5, 9, *Lys*-3
8	132.6	-	-	-
9	110.4	7.83, s	-	5, 7, *Lys*-3
10	136.9	-	-	-
Asp				
1	168.5	-	-	-
2	50.4	3.89, m	3	1, 3, 4, *Trp₃*-1
3	38.9	2.60, t (7.4)	2	1, 2, 4
4	173.1	-	-	-
6F-Trp				
1	167.5	-	-	-
2	54.4	4.44, m	3	1, 3
3	25.9	3.65, 3.96, m	2	1, 2, 4, 4‘, 5
4	108.0	-	-	-
4‘	124.7	7.75, s	-	3, 4, 5, 9, 10
5	124.8	-	-	-
6	114.0, d (*J* = 9.3)	7.59, m	7	4, 10
7	109.5, d (*J* = 22.4)	7.44, m	6	5, 8, 9
8	149.4, d (*J* = 235.1)	-	-	-
9	130.9	-	-	-
10	130.3	-	-	-

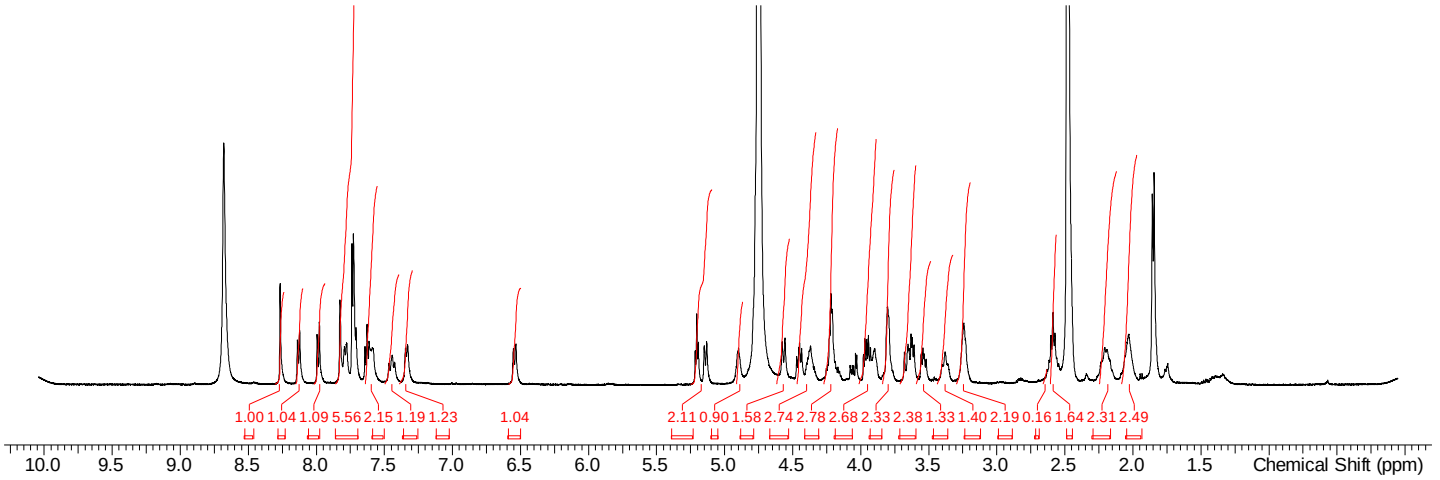

Figure S 86: ^{1}H spectrum of D9-6F in ACN/D2O + 1% FA at 45 °C and 500 MHz.

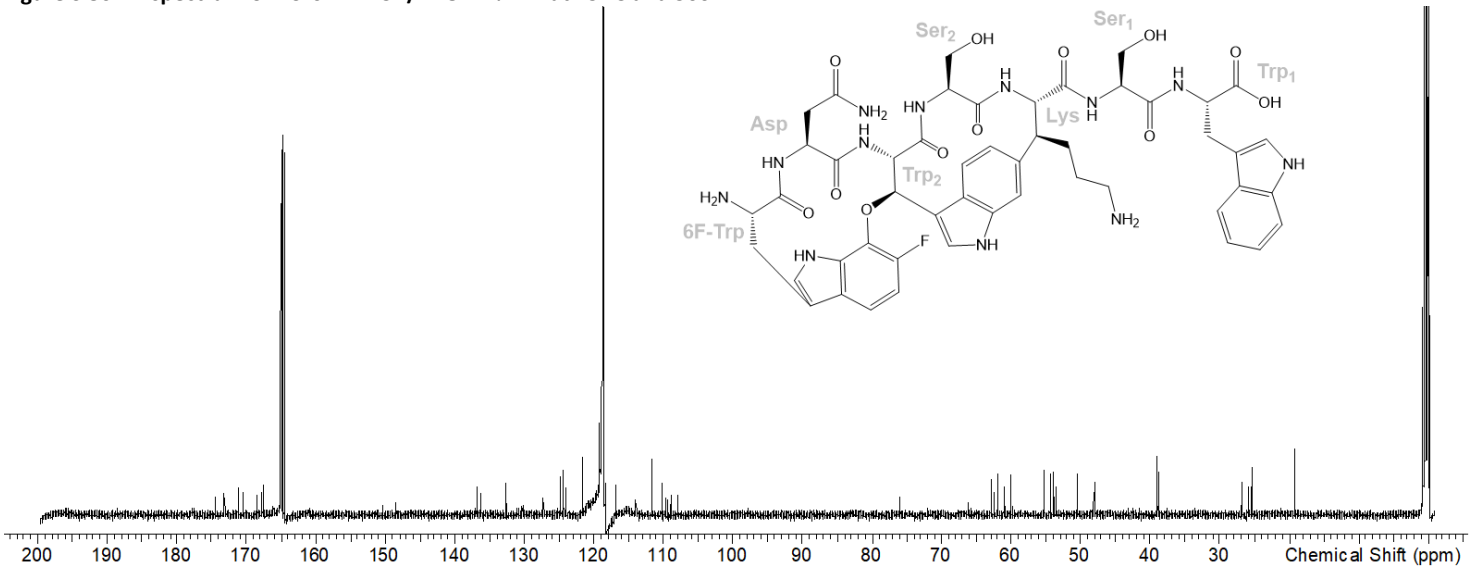

Figure S 87: ^{13}C spectrum of D9-6F in ACN/D2O + 1% FA at 45 °C and 125 MHz.

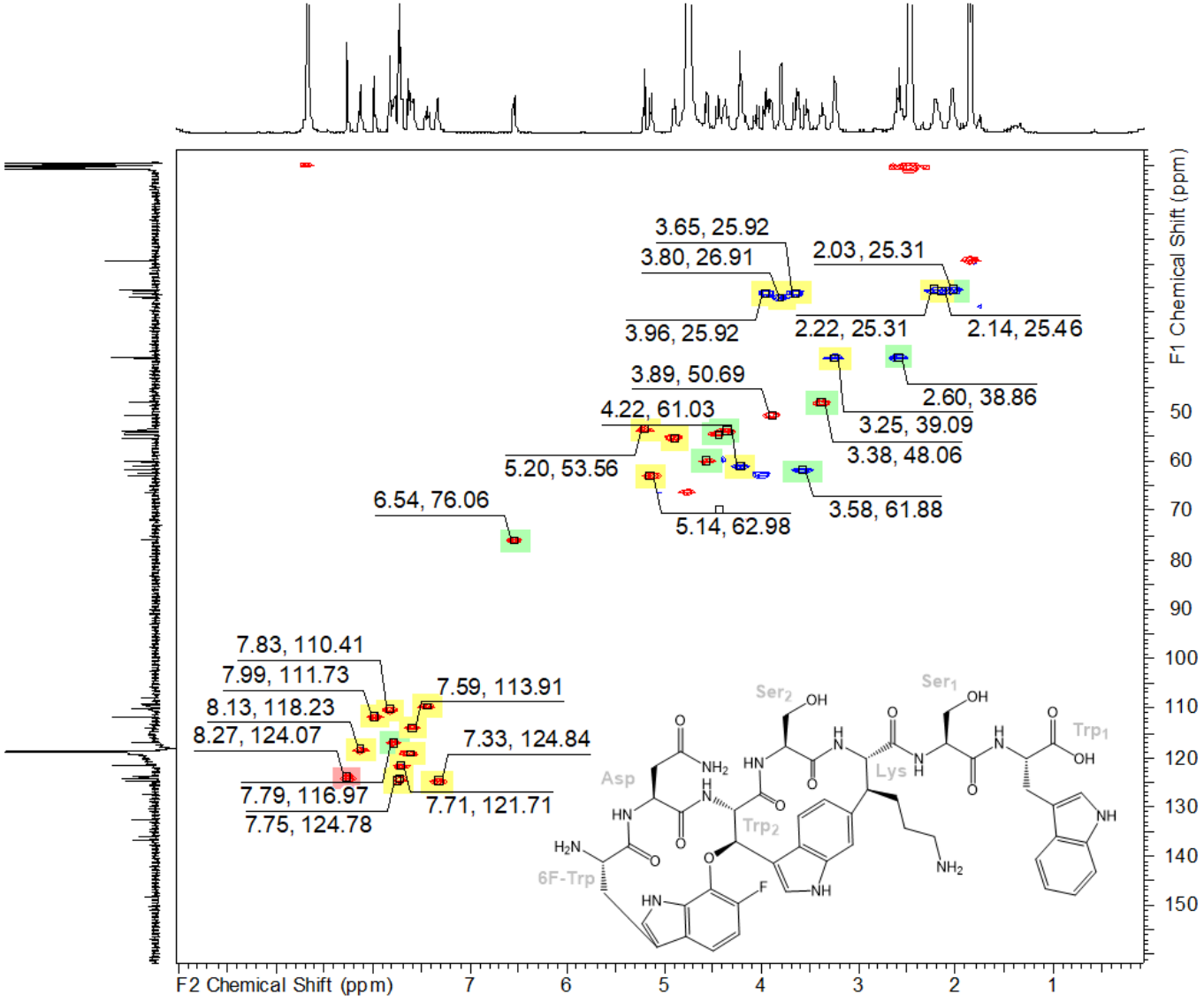

Figure S 88: HSQC spectrum of D9-6F in ACN/D2O + 1% FA at 45 °C and 500/125 MHz.

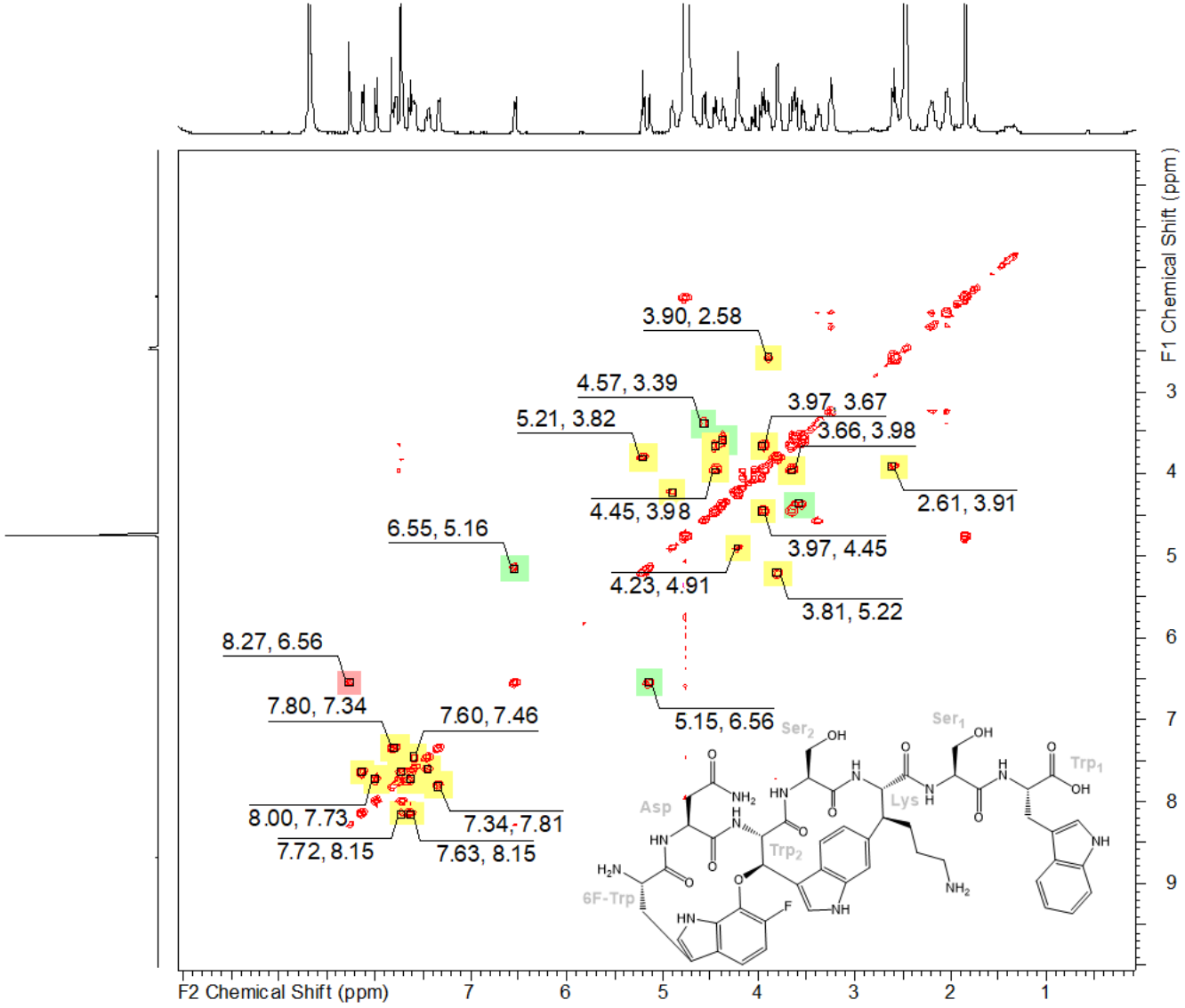

Figure S 89: COSY spectrum of D9-6F in ACN/D2O + 1% FA at 45 °C and 500/125 MHz.

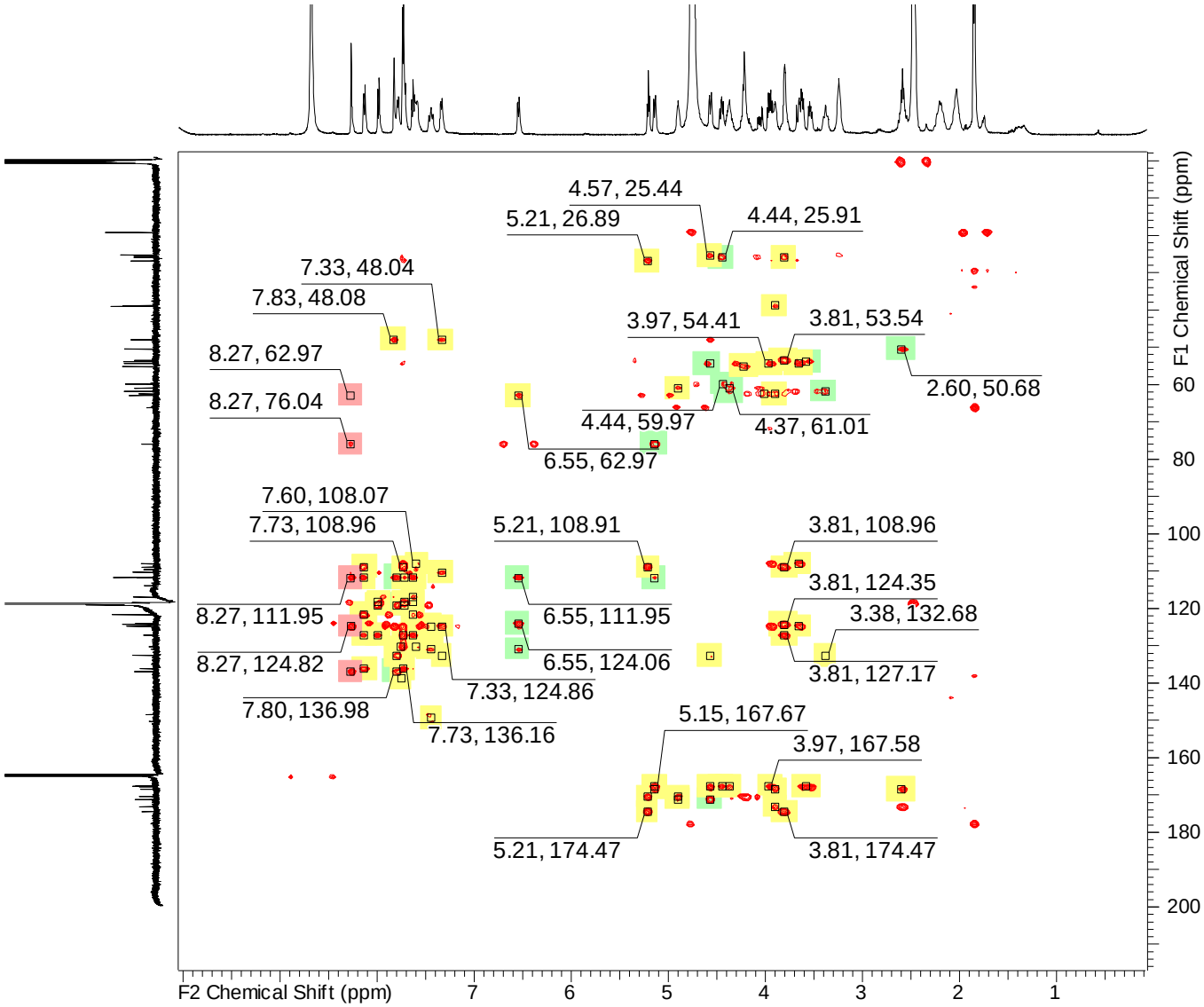

Figure S 90: HMBC spectrum of D9-6F in ACN/D2O + 1% FA at 45 °C and 500/125 MHz.

References

1 S. Groß, F. Panter, D. Pogorevc, C. E. Seyfert, S. Deckarm, C. D. Bader, J. Herrmann and R. Müller, *Chem. Sci.*, 2021, **12**, 11882.

2 K. H. M. E. Tehrani, H. Fu, N. C. Brüchle, V. Mashayekhi, A. Prats Luján, M. J. van Haren, G. J. Poelarends and N. I. Martin, *ChemComm*, 2020, **56**, 3047.

3 C. B. Kimmel, W. W. Ballard, S. R. Kimmel, B. Ullmann and T. F. Schilling, *Dev. Dyn.*, 1995, **203**, 253.

4 J. A. van Santen, G. Jacob, A. L. Singh, V. Aniebok, M. J. Balunas, D. Bunsko, F. C. Neto, L. Castaño-Espriu, C. Chang, T. N. Clark, J. L. Cleary Little, D. A. Delgadillo, P. C. Dorrestein, K. R. Duncan, J. M. Egan, M. M. Galey, F. J. Haeckl, A. Hua, A. H. Hughes, D. Iskakova, A. Khadilkar, J.-H. Lee, S. Lee, N. LeGrow, D. Y. Liu, J. M. Macho, C. S. McCaughey, M. H. Medema, R. P. Neupane, T. J. O'Donnell, J. S. Paula, L. M. Sanchez, A. F. Shaikh, S. Soldatou, B. R. Terlouw, T. A. Tran, M. Valentine, J. J. J. van der Hooft, D. A. Vo, M. Wang, D. Wilson, K. E. Zink and R. G. Linington, *ACS Cent. Sci.*, 2019, **5**, 1824.

5 H. Kaur, R. P. Jakob, J. K. Marzinek, R. Green, Y. Imai, J. R. Bolla, E. Agustoni, C. V. Robinson, P. J. Bond, K. Lewis, T. Maier and S. Hiller, *Nature*, 2021, **593**, 125.

6 S. H. W. Scheres, *J. Struct. Biol.*, 2012, **180**, 519.

7 A. Punjani, J. L. Rubinstein, D. J. Fleet and M. A. Brubaker, *Nat Methods*, 2017, **14**, 290.

8 E. F. Pettersen, T. D. Goddard, C. C. Huang, E. C. Meng, G. S. Couch, T. I. Croll, J. H. Morris and T. E. Ferrin, *Protein Sci.*, 2021, **30**, 70.

9 P. D. Adams, R. W. Grosse-Kunstleve, L. W. Hung, T. R. Ioerger, A. J. McCoy, N. W. Moriarty, R. J. Read, J. C. Sacchettini, N. K. Sauter and T. C. Terwilliger, *Acta Crystallogr D Biol Crystallogr*, 2002, **58**, 1948.

10 T. I. Croll, *Acta Crystallogr. D Biol Crystallogr*, 2018, **74**, 519.

Chapter 4

4.1 New Genetically Engineered Derivatives of Antibacterial Darobactins Underpin their Potential for Antibiotic Development.

Previously published in:

Carsten E. Seyfert[a,b], Alison V. Müller[a,b], Danica J. Walsh[a,b], Joy Birkelbach[a,b], Andreas M. Kany[a,b], Christoph Porten[a,b], Biao Yuan[c,d,f], Daniel Krug[a,b], Jennifer Herrmann[a,b], Thomas C. Marlovits[c,d,f], Anna K. H. Hirsch[a,b,e] and Rolf Müller[a,b,e]

J. Med. Chem., 2023 November 21

DOI: acs.jmedchem.3c01660

Affilitaton:

[a]Helmholtz Institute for Pharmaceutical Research Saarland (HIPS), Helmholtz Centre for Infection Research (HZI) and Saarland University Department of Pharmacy, Saarbrücken, Germany

[b]German Centre for Infection Research (DZIF), partner site Hannover-Braunschweig

[c]University Medical Center Hamburg-Eppendorf (UKE), Institute of Structural and Systems Biology and Centre for Structural Systems Biology (CSSB), Hamburg, Germany

[d]Deutsches Elektronen-Synchrotron Zentrum (DESY), Hamburg

[e]Helmholtz International Lab for Anti-Infectives

[f]Centre for Structural Systems Biology (CSSB), 22607 Hamburg, Germany

Contributions

Carsten E. Seyfert

The author significantly contributed to the conceptionalization of the study, to the methodology and the performance of experiments and interpretation of the results. The author was responsible for the project administration. The author designed *in silico* expression constructs for the novel darobactin derivatives D58 to D74. He produced, extracted and purified the described novel darobactin analogues and evaluated the activity data. He supported the establishment of MST assay for the determination of the binding constants of darobactins. The author led the formal analysis of all data generated for this manuscript. The author wrote the original draft and visualized the results. He directed the review and editing.

Contributions of by Others:

Alison V. Müller contributed to the formal analysis and the experimental investigations. She generated the expression constructs for darobactins 58 to 74. She significantly contributed to the production, extraction and purification of analogues and analyzed their bioactivity data. She supported with visualization, review and editing. Danica Walsh established a MST assay to determine the binding constants of darobactin to its target protein BamA and supported in reviewing and editing. Joy Birkelbach supported the investigations by *de novo* structural elucidation of darobactin 69, and in review, and editing. Andreas M. Kany performed the *in vitro* ADME profiling of D22 and D69 and supported the writing by reviewing and editing. The other authors contributed to the formal analysis of the results, provided resources and/or edited and reviewed the draft. Rolf Müller is the corresponding author of the manuscript. He conceived the project together with the author. He was responsible for raising funds and resources. He led the supervision, reviewed and edited the manuscript.

ABSTRACT: Biosynthetic engineering of bi–cyclic darobactins, selectively sealing the lateral gate of the outer membrane protein BamA, lead to active analogues which are up to 128–fold more potent against Gram–negative pathogens compared to native counterparts. Because of their excellent antibacterial activity, darobactins represent one of the most promising new antibiotic classes of the last decades. Here we present a series of structure-driven biosynthetic modifications of our current frontrunner, darobactin 22 (**D22**), to investigate modifications at the understudied positions 2, 4 and 5 for their impact on bioactivity. Novel darobactins were found highly active against critical pathogens from the WHO priority list. Antibacterial activity data were corroborated by dissociation constants with BamA. The most active derivatives **D22** and **D69** were subjected to ADMET profiling, showing promising features. We further evaluated **D22** and **D69** for bioactivity against multidrug–resistant clinical isolates and found them to have strong activity.

Introduction

In the coming years increasing antimicrobial resistance (AMR) is expected to induce a rise in the number of deaths of the growing global population from roughly 1.3 million to up to 10 million annually.[1–5] In particular, resistant pathogens appear in clinics more often, among other factors in combination with nosocomial infections, leading to increased mortality rates.[5,6] Most new antibiotics reaching the development stage are derivatives of known chemical classes with a known target and mode of binding (MoB), resulting in potentially rapid development of cross-resistance.[7] Thus, the search for antibacterial compounds acting on innovative target sites is urgently required. The recently discovered darobactins are a novel class of antibiotics showing promise for meeting that demand.[8,9] Native darobactins found in *Photorhabdus khanii* are ribosomally produced and post–translationally modified peptides (RiPPs).[8,10] They selectively target the outer membrane protein (OMP) BamA, the major component of the BamABCDE (BAM) complex, and inhibit the insertion and folding of OMPs, ultimately resulting in cell lysis.[11,12,13] The target site of darobactins is not addressed by commercially available antibiotics. Consequently, the risk of cross-resistance is lower and they are proven to exhibit an auspicious broad–spectrum Gram–negative activity against clinically relevant and multiresistant pathogens such as *Pseudomonas aeruginosa*, *Escherichia coli*, *Acinetobacter baumannii* or *Klebsiella pneumoniae*, against which many other antibiotics are not effective anymore.[8,9,12,14] Two derivatization series of darobactins published by Groß *et al.* and

Seyfert *et al.* have confirmed the efficacy of scaffold modification by biotechnological engineering of the fully synthetic darobactin biosynthetic gene cluster (BGC) to enhance the bioactivity of analogues,[9,12] which was partly confirmed by studies of Marner *et al.*.[15] The feasibility of modifications at specific positions of the core peptide was a prerequisite for analyzing their influence on antibacterial activity and for understanding how analogues of this novel compound class interact with its unique target BamA. These new insights together with the first described co-crystal structure of darobactin A (**DA**) and BamA helped establishing the structure-activity relationships of the different derivatives.[11,12] The earlier derivatization series increased the antibacterial activity of darobactins up to 128–fold for darobactin 22 (**D22**) compared to native **DA**, even against clinical isolates of carbapenem-resistant *A. baumannii* (CRAB) and multidrug-resistant *P. aeruginosa.*[9,12,15] However, some positions, especially position 2 (Figure 1), have not yet been subject to detailed investigation. Additional efforts to engineer antibacterial darobactin derivatives as potential future drugs are therefore a promising approach to fight the antibiotic crisis.[16]

Consequently, we used our current frontrunner molecule **D22** as a starting point and considered the effects of changes at position 2 alone, as well as designed and produced analogues with additional modifications of positions 4, 5, and 6. We devised 17 novel darobactins based on the results achieved by evaluating the structure– and activity–guided outcome of our previous study[12] in order to explore the influence of amino acid changes in so far (under) –investigated positions. Notably, we found that changes at positions 2 and 5 still result in highly active darobactins, inconsistent with data from previous publications regarding native darobactin D (**DD**) and darobactin E (**DE**).[17] Changes at position 4 support the hypothesis that exchange of L-serine and L-threonine may affect activity due to a shift in molecular orientation. One new derivative showed activity comparable to **D22** with better binding to the target BamA. The first *in vitro* ADMET analyses reveal a favorable profile of the tested frontrunners, enabling selection of a suitable derivative for further *in vivo* profiling.

Results

Structural analysis of darobactin-BamA interaction sites and design of novel analogues potentially interacting with BamA. The structural elucidation of darobactin MoB using cryo–EM and crystallization techniques shed light on the complex structure of BAM–**DA** and BAM–**D9**.[11,12] Combined with an activity-guided approach, this led to highly active analogues like **D22** (Figure 1 a, c, f).[12] Subsequently, we further analyzed the BAM-darobactin co–structures to devise a blueprint for developing novel analogues, modified on previously under–investigated positions of the darobactin heptapeptide. We compared the different

interactions of **DA**, **D9**, and **D22** with BAM, utilizing the respective, recently solved co–structures (Figure 1 d - f). [11,12] In particular, variations at positions 4, 6, and 7 of the heptapeptide (Figure 1 b, c) seem to affect the hydrogen bonding interactions of L-asparagine at position 2 for **DA** (N427), **D9** (no interaction), and **D22** (Q441) (Figure 1 d - f). Therefore, the observed variability of interactions with position 2 makes this position particularly suitable for introducing amino acid modifications to alter interactions with Q441 on β-sheet 2 or N427 on β–sheet 1 (Figure 1).

Consequently, we initiated a structure-guided mutagenesis of **D22** mainly at position 2 but also including positions 4, 5, and 6 to evaluate the potential of various amino acids to build hydrogen bonding interactions with BamA. We used the Chimera[18] and PyMOL[19] rotamer and mutagenesis tools to model exchange of amino acids of **D22** within the co-structure with BamA which prompted us to explore interactions between BamA and hitherto untested amino acid residues, varying in length and polarity (Figure 2 a). Examples of modeled BamA–darobactin interactions are presented in Figure S 1 a - f and Figure S 2 a - c. Briefly, changing L-asparagine to L-glutamic acid, L-aspartic acid, L-glutamine or L-tyrosine in derivatives **D58**, **D60**, **D61**, **D67** and **D69**, respectively, might result in hydrogen bonding formation between amino acids on the first or second BamA β-sheet. Depending on the automated calculation, even multiple interactions are possible as computed for **D69** (Figure S 2 a, b). Furthermore, after a switch from L-asparagine to L- serine at position 2 similar to native darobactin **DE**,[8,9] the L-serine of the resulting **D64** does not appear to be involved in a hydrogen bonding interaction with BamA. However, we could not identify a steric hindrance that would allow conclusions about the rather inactive native analogue **DE** (WSWSKSF)[17] (Figure S 1 e). The previously detected and discussed orientation shift,[12] potentially due to change from L-serine to L-threonine at position 4, was also intended to be evaluated for its influence on antibacterial activity by directly comparing several derivatives that differed only in position 4 (**D69-D73**). Further, the hydrogen bonding interactions between BamA and **D39** – a previously described analogue that was not further investigated – are not directly influenced by changing L-lysine in position 5 to L-arginine according to our results (Figure S1 a). Since the change at position 6 has previously led to greater differences in antibacterial activity that seem to be partly correlate with variations in the production,[9,12] we also sought to generate derivatives that were characterized by changes at position 6. A less active derivative could possibly have higher production rates due to reduced intrinsic sensitivity of the Gram–negative bacterial producer. Thus, derivatives **D65** with L-lysine and **D74** with L-glutamine in this position were designed (Figure 2 b, Figure S2 c).

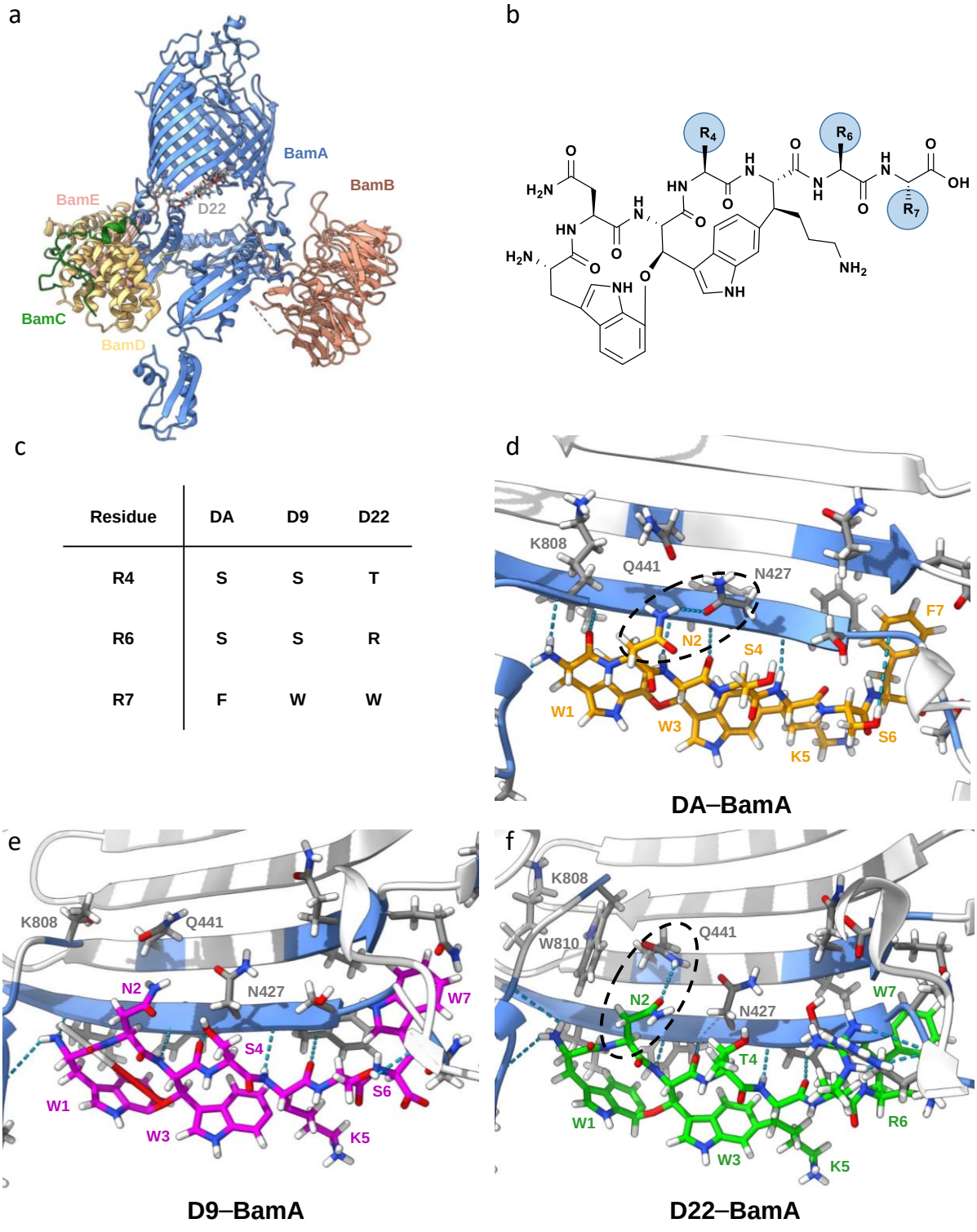

Residue	DA	D9	D22
R4	S	S	T
R6	S	S	R
R7	F	W	W

Figure 1. Analysis of darobactin – BamA interaction. a) Co-structure of **D22–**BamABCDE (BAM). b) Darobactin core structure with residues 4, 6 and 7 highlighted (R_4, R_6 and R_7). c) Overview of variations between native **DA**, derivatives **D9** and **D22** on residue 4, 6, and 7, respectively. d) BamA**–DA** (orange) interaction site. e) BamA**–D9** (pink) interaction site, f) BamA**–D22** (green) interaction site. Calculated hydrogen bonding interactions between BamA and darobactins are shown in blue. The raw data were taken from protein data bank (PDB) and originally published in Kaur *et al.*[11] and Seyfert *et al.*.[12] PDB accession codes: 7NRI (**DA**), 8ADI (**D9**) and 8ADG (**D22**).

In total, 17 novel derivatives were modeled and designed *in silico* (Figure 2 a, b). Since the novel analogues were engineered mainly based on modeled structures combined with the activity data as found in the literature,[8,9,12,17] we wanted to corroborate our hypotheses. Considering the still rather time-consuming production and purification of darobactins, we characterized the novel darobactins following the rational cascade of (1) investigating the influence of altered amino acids on the bioactivity as observed from extracts of producing strains, (2) confirming the bioactivity of selected derivatives as pure compounds and (3) profiling the most active derivative in comparison to **D22**.

a

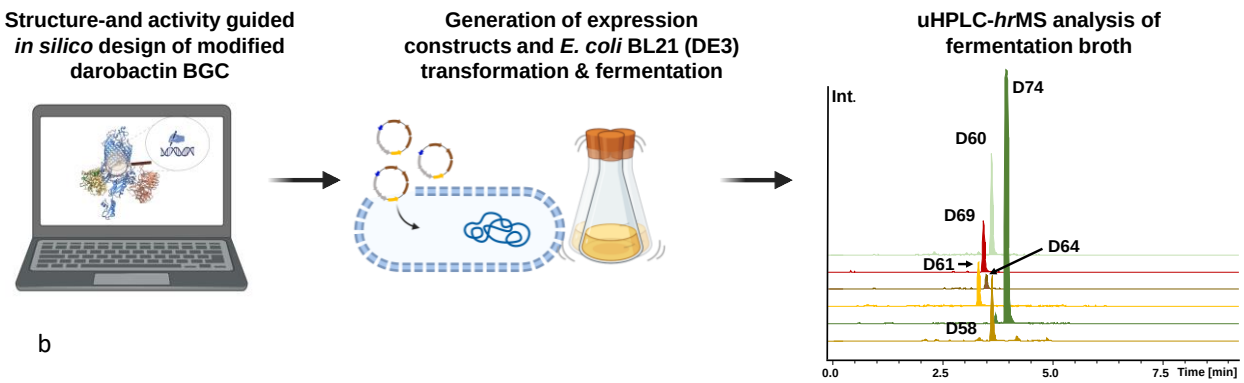

b

Residue	D22	D58	D59	D60	D61	D62	D63	D64	D65	D66	D67	D68	D69	D70	D71	D72	D73	D74
R2	N	E	K	D	Q	R	V	S	S	N	Y	L	Q	S	E	K	D	N
R4	T	T	T	T	T	T	T	T	T	T	T	T	S	S	S	S	S	T
R6	R	R	R	R	R	R	R	R	K	C	R	R	R	R	R	R	R	Q

c

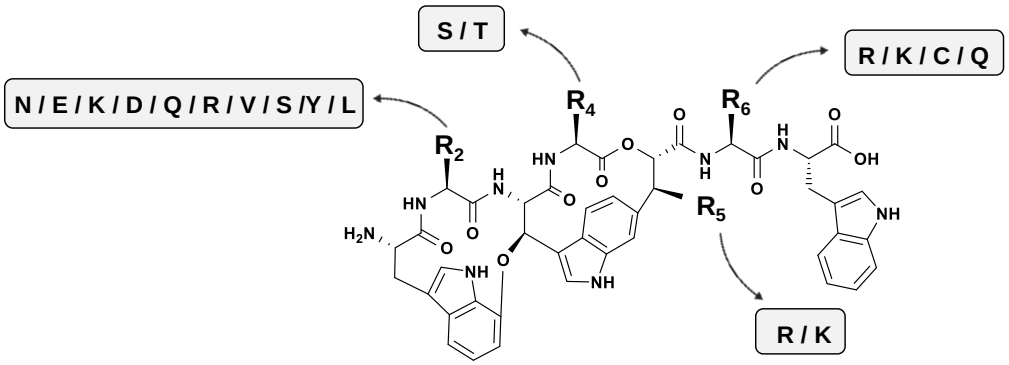

Figure 2. Structure–and–activity–guided approach to produce novel darobactins. a) workflow to design, produce and analyze novel derivatives b) novel derivatives **D58** to **D74** with modifications at positions 2, 4, and 6. c) predicted chemical structure of the darobactins, investigated in this study using MS^2 analysis (Figure S20-38, Table S5): **D58** to **D74** and previously published derivative **D39.**[12]

We generated the new darobactin expression constructs by introducing point mutations in the plasmid pNOSO–darABCDE–22, as described previously.[12] We achieved the production in *E. coli* BL21 (DE3),

extraction and analysis of darobactins as described in the methods (Figure 2 a, b). We assessed the compound production using mass spectrometry (MS) (Table S 4, Figure S 3 – S 19) and detailed MS^2 fragmentation pattern analysis (Table S 5, Figure S 20 – S 37) to validate the respective compounds. Varying molecular ions were detected in electrospray ionization (ESI) MS measurements (Table S 4, S 5), consistent with previous results.[12] All derivatives could indeed be identified and the MS^2-predicted chemical structures of all novel darobactins are displayed in Figure S 38.

Evaluation of antibacterial activity, binding kinetics and cytotoxicity of novel darobactins. The extracts of production clones for all derivatives were prepared and tested for their antibacterial activity against *E. coli* ATCC 25922, *P. aeruginosa* PA01, *K. pneumoniae* DSM-30104 and *A. baumannii* DSM-30008. The production of new darobactins was estimated based on integration of combined extracted ion chromatograms (EICs) of singly, doubly and triply charged darobactin-ions in the crude extracts and was normalized to **D22** due to variable ionization states of most prominent mass peaks[12] (Table S 4) and is presented in Table 1.

Table 1. Antibacterial activity screen of darobactin containing extracts with modified core peptide sequences against *Acinetobacter baumannii* DSM-30008, *Klebsiella pneumoniae* DSM-30104, *Pseudomonas aeruginosa* PAO1 and *Escherichia coli* ATCC 25922. Changes in the core peptide sequence compared to the **D22** sequence are shown in red. Relative production titers of **D22** and its derivatives in crude extracts were calculated by comparing area under the curve (AUC) ratios of new derivatives relative to **D22**. The antimicrobial activity of each derivative-containing crude extract against tested pathogens is highlighted as a color code (bright green to dark green), depending on the highest dilution factor of standardized extract with respect to the assay volume [two-fold serial dilution from 1 : 15 (A) (concentration factor: 6.67x) to 1 : 3,840 (H) (concentration factor: 0.05x)] in which full growth inhibition was detected (compare to Seyfert *et al.*[12]). UHPLC-HRMS chromatograms of produced new darobactins are shown in the Figure S 3 – S 19.

Darobactin	Core peptide	*A. baumannii* DSM-30008	*K. pneumoniae* DSM-30104	*P. aeruginosa* PA01	*E. coli* ATCC25922	AUC ratio (derivative/ D22)
D22	W N W T K R W	H	E	G	E	1
D58	W E W T K R W	E	B	B	C	0.39
D59	W K W T K R W	A	A	A	A	0.02
D60	W D W T K R W	E	B-C	C	C	0.62
D61	W Q W T K R W	F	D	D	D	0.28
D62	W R W T K R W	A	B	—	—	0.01
D63	W V W T K R W	C	B	A	—	0.04
D64	W S W T K R W	E	A	B	A	0.08
D65	W S W T K K W	D	A	B	A	0.08
D66	W N W T K C W	C	A	B	A	0.44
D67	W Y W T K R W	E	C	D	C	0.36
D68	W L W T K R W	D	B	B	B	0.14
D69	W Q W S K R W	G	D	E	D	0.33
D70	W S W S K R W	E	C	D	C	0.14
D71	W E W S K R W	E	C	B-C	C	0.43
D72	W K W S K R W	C	B	B	C	0.11
D73	W D W S K R W	C	A	B	A	0.38
D74	W N W T K Q W	D	C	E-F	E	2.79

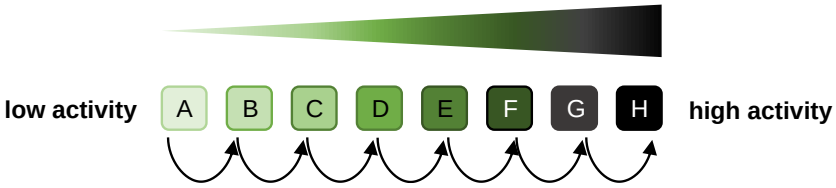

All extracts containing new analogues were active against the panel of Gram-negative pathogens tested and species specificity resembles the earlier findings for derivatives **D9** and **D22**.[9,12] Antibacterial activity differs from extract to extract but agrees with significantly varying production as determined via the area under the curve (AUC) ratio calculated from LC–MS analysis and normalized to **D22** production (Table 1). Interestingly, the changes at position 2 result in highly active analogues (*e.g.,* **D58** – **65** and **D67** – **D73**). The derivatives with changes at position 2 and an L-serine instead of L-threonine at position 4 exhibit increased antibacterial activity in extracts, but this might also be due to the different production levels (see AUC ratio in Table 1). Therefore, we selected eight representative derivatives for purification in order to conduct bioactivity profiling with pure compounds and to avoid misinterpretation of the MIC data from extracts that could arise due to significantly varying production titers. The **D22** analogues were produced at a larger scale and purified. Next, the pure darobactins **D58**, **D60**, **D61**, **D64**, **D69** and **D74** were tested against the same panel of pathogens. In addition, **D39** was produced, purified and tested in parallel to study the contradicting MIC data regarding the inactivity of native **DD** [17] compared to **D39**,[12] but also to compare it with published data of active **DA**.[8,9] The activity data of all pure compounds align well with the MIC data obtained from derivative–containing extracts (Table 1). All novel darobactins exhibit promising antibacterial activity against a range of clinically relevant pathogens (Table 2). Variations at position 2 unequivocally lead to active derivatives, in contrast to the activity profile of native darobactin **DE**. The

analogues **D58**, **D60**, **D61**, **D64** and **D69** retain high activity against *A. baumannii*, but the changes at position 2 result in slightly different activity profiles against *K. pneumoniae, P. aeruginosa* and *E. coli* (Table 2). However, the antibacterial activity of all derivatives remains potent against the tested pathogens. Derivative **D39**, which was not tested as a pure compound in a previously published assay,[12] with L-arginine instead of L-lysine at position 5 as in native analogue **DD**, displayed lower activity against *P. aeruginosa* and *K. pneumoniae* compared to **D22**. Although its activity is still low-micromolar and not completely abolished, as described for native **DD** (WNWSRSF) in Böhringer *et al.*.[17] Derivative **D39** even exhibits activity against the tested *A. baumannii* strain comparable to the current frontrunner **D22**.

Table 2. Minimal inhibitory concentration (MIC), binding kinetics (K_D) and cytotoxicity of D22 (control), of novel analogues D39, D58, D60, D61, D64, D69 and D74 and of native derivative DD. Antibacterial activity [in µg mL^{-1}; n=2] is given for representative strains of the most critical and clinically relevant Gram-negative pathogens *Acinetobacter baumannii, Klebsiella pneumoniae*, *Pseudomonas aeruginosa* and *Escherichia coli*. Binding kinetics represented by determination of K_D values (in µM) were determined via microscale thermophoresis for selected darobactins against BamA of *E. coli*; n=3. No toxicity was observed against the tested human cell line HepG2; n=2; n.d. = not determined.

MIC [µg/mL]									
darobactin analogue	**D22**	**DD**	**D39**	**D58**	**D60**	**D61**	**D64**	**D69**	**D74**
core peptide sequence	WNWTKRW	WNWSRSF	WNWTRRW	WEWTKRW	WDWTKRW	WQWTKRW	WSWTKRW	WQWSKRW	WNWTKQW
***A. baumannii* [DSM-30008]**	0.25–0.5	4–8	0.5–2	2	2	0.5	0.5	0.5	4
***K. pneumoniae* [DSM-30104]**	2–4	8-16	4–8	16	16	8	16	4	16
***P. aeruginosa* [PA01]**	0.5–1	2	2	8	4	4	2	1	2
***E. coli* [ATCC25922]**	1	1	4–8	8	16	2	4	1	4
K_D [µM]									
EcBamA	4.1 ± 1.9	7.8 ± 0.6	10.9 ± 3.5	5.1 ± 3.7	22.6 ± 2.3	3.6 ± 0.6	5.1 ± 0.7	1.4 ± 0.4	2.2 ± 0.6
IC_{50} [µg/mL]									
HepG2	> 37	n.d.	>37	> 37	> 37	> 37	> 37	> 37	> 37

The inconsistency between the published antibacterial activity of **DD** and those of **D39** prompted us to produce **DD** in our laboratory. We obtained 13 mg pure **DD** via isolation out of 9 L Formulated Medium (FM), in contrast to the yield of ~ 1 mg out of 100 L as described in Böhringer *et al.*.[17] This compound supply enabled evaluation of MICs (Table 2), which revealed high antibacterial activity for **DD** (Table 2), significantly different from previously published data.[17] Surprisingly, direct comparison between **D61** and **D69** – only differentiated by the L-serine/ L-threonine change at position 4 - shows partly enhanced activity of **D69** comparable to the current frontrunner **D22**. Further, the substitution of L-arginine to L-glutamine in **D74** affects the antibacterial activity negatively, as expected by analyzing the modeled co-structure of BamA–**D74** compared to the cryo-EM data of BamA–**D22**: **D74** is less anchored at BamA than **D22** at position 6 (Figure S 2 c). Of note, the available amount of **D74** was significantly higher in the extract

produced for initial activity assessment in comparison to the other new derivatives (Table 1) and we could quantify in follow-up experiments that the production indeed reached 33 ± 1.7 mg per L medium.

The production of **D22**[12] achieved 10.5 ± 0.9 mg per L, of **D58** 6.9 ± 2.0 mg per L, of **D61** 7.4 ± 1.1 mg per L**,** of **D69** 4.6 ± 0.6 mg per L and of **DD** 4.4 ± 1.1 mg per L, respectively (Figure S 39).

Due to the unexpectedly differing activity data, we evaluated binding constants (K_D) of each purified analogue to *E. coli* BamA (EcBamA). As an alternative to the previously published methods using isothermal titration calorimetry (ITC), we established a K_D determination assay using microscale thermophoresis (MST) to enable a higher throughput. The K_D data underpin the results of the activity screen (Table 2): K_D of all tested derivatives in fact correlated with MIC data. We observed a slightly better K_D for **D69**, bearing an L-glutamine instead of L-arginine, compared to **D22** (Figure 3). Thus, we decided to use the best derivative of our new series, **D69**, to compare its ADMET profile with **D22**, which has not been analyzed before. Moreover, we verified the chemical structure of **D69** via NMR (Figure 3, Table S 7 and Figure S 39 – S44).

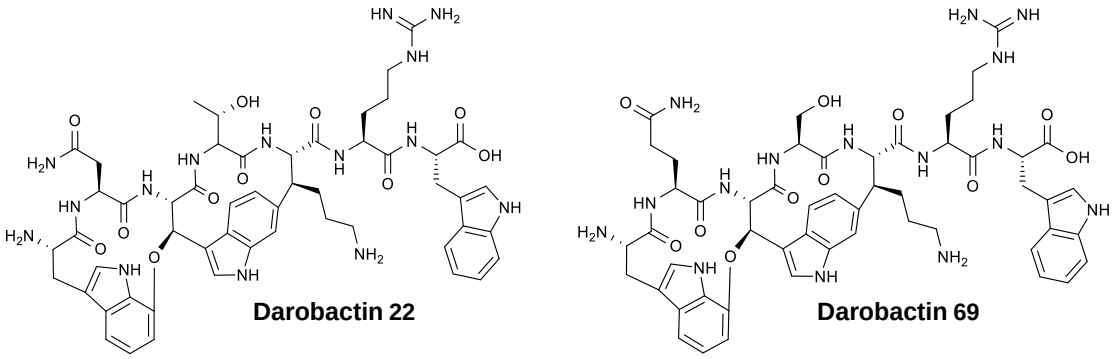

Figure 3. Chemical structures of darobactin 22 and 69.

***In vitro* ADMET profiling of D22 and D69.** The two most promising darobactin analogues, **D22** and **D69**, were evaluated regarding metabolic and plasma stability as well as plasma protein binding (PPB) in order to obtain first *in vitro* information on their pharmacokinetic properties (Table 3).

Table 3. Determination of metabolic stability, plasma stability and plasma protein binding. Darobactin derivatives D22 and D69 were compared in mouse, human and rat (Wistar) liver microsomes / plasma.

Darobactin analogue	Species	D22	D69
Liver Microsomes $t_{1/2}$ [a] [min] / Cl_{int} [b] [µL/mg/min]	Mouse[d]	>120 / <11.6	>120 / <11.6
	Human	>120 / <11.6	>120 / <11.6
	Rat	>120 / <11.6	>120 / <11.6
Plasma $t_{1/2}$ [min]	Mouse [e]	>240	>240
	Human	>240	>240
	Rat	>240	>240
PPB[c] [%]	Mouse[e]	57.5 ± 7.2	53.6 ± 10.3
	Human	46.7 ± 2.7	53.1 ± 3.7
	Rat	62.8 ± 6.3	58.4 ± 7.4

[a] half-life; [b] intrinsic clearance ; [c] plasma protein binding; [d] C57BL/6 ; [e] CD-1

Both, **D22** and **D69**, were not metabolized in murine liver microsomes over 2 h. Likewise, both compounds showed good plasma stability with no degradation over 4 h. This was also confirmed in human and rat fractions/plasma for both compounds. PPB was found to be relatively low between 46% and 63% which is correlated to the high polarity and good solubility of these RiPPs. Furthermore, all new darobactins investigated in this study did not display cytotoxicity against the human cell line HepG2, which is consistent with previous results [8,9,12] where no toxicity *in vitro* and even *in vivo* has been detected at concentrations up to 37 µg mL^{-1} and 500 µg mL^{-1}, respectively.

Activity screen against multidrug-resistant *A. baumannii* and *P. aeruginosa* strains to select the most attractive candidate for further *in vivo* profiling

Considering the superior binding affinity of **D69**, along with comparable ADMET (Table 4) and MIC data for **D22** and **D69** (Table 2), we aimed to assess the potency of **D22** and **D69** against further *A. baumannii* and *P. aeruginosa* strains, including multidrug-resistant clinical isolates in addition to laboratory strains. Therefore, we selected human pathogens isolated from the lungs and urine of patients with indwelling catheters (*P. aeruginosa* 83979, *P. aeruginosa* 84389), which are challenging to treat and exhibit resistance to four classes of antibiotics: acylureidopenicillins, cephalosporins, fourth-generation carbapenems and fluoroquinolones (Table S 6). **D22** tends to show better antibacterial activity in sub– to low–micromolar range against the tested hard–to–treat pathogens (Table 4). However, the antibacterial activity of both **D22** and **D69** against *P. aeruginosa* 83979 and 84389 is similar to meropenem (16 µg mL^{-1}) and ciprofloxacin (4 µg mL^{-1}) (Table S 6), which are clinically used.

Table 4. Minimal inhibitory concentration (MIC) in µg mL^{-1} of D22 and D69 in an extended panel of clinically relevant Gram-negative pathogens. [*] MDR clinical isolates (see SI); n=2.

Bacterial strains	MIC [µg mL^{-1}]	
	D22	**D69**
***Acinetobacter baumannii* DSM-30007**	2–4	2
***A. baumannii* DSM 30008**	0.25–0.5	0.5
***A. baumannii* NCTC 13301**	4–8	8–16
***A. baumannii* ATCC 17978**	4–8	16
***Pseudomonas aeruginosa* PA01 DSM 22644**	0.25	1
***P. aeruginosa* PA14 DSM 19882**	2–4	16
P. aeruginosa* 83979	4–8	8–16
P. aeruginosa* 84389	16	16–32

Discussion and Conclusions

Changes in the darobactin core peptide significantly influence antibacterial activity of the analogues positively or negatively.[9,12] Thus, we used existing structural data of antibiotic darobactins **DA**, **D9,** and **D22** as a guide to study the influence of scaffold modifications at underinvestigated amino acid positions. We started by simulating targeted mutagenesis of the cryo–EM co–structure of BAM-**D22**[11,12] to predict potential influences of amino acid exchanges in the darobactin heptapeptide for the formation of hydrogen bonding interactions. Indeed, the modeling predicted strong interactions at position 2 for **D69**, no interaction for **D64** and even no direct overall changes for **D39** after modifying the respective positions compared to **D22**. To create the corresponding bioactivity readouts, we used our genetic- modification and extraction platform to produce the new analogues. Through the fermentation process, we could obtain all engineered novel darobactins in titers clearly higher than those of previously published native derivatives **DD** and **DE** that share modifications at positions 2 and 5.[17] The production of darobactins however still differs significantly between derivatives. This might be attributed to the intrinsic sensitivity of the heterologous host *E. coli* but further factors could also reduce production. For example, the modifications especially in positions 2 and 5 could prevent the proper bi–cyclization of darobactins by steric hindrance of the radical SAM DarE or impair the still unknown peptidase responsible for the release of the mature

heptapeptide on the *C*– and *N*–terminal ends of the core peptide, due to the high target specificity in RiPPs[20]. Nevertheless, the heterologous production of darobactins in *E. coli* is robust and certain derivatives like **D74** (which has only one change at position 6 compared to **D22**) exhibit higher production rates than all known artificial analogues. This could be due to its lower activity against *E. coli*, yet, this observation was not made for **D60**. Thus, there might be other reasons for varying production titers. Besides the potentially better interference with DarE, this derivative might be transferred out of the bacterial cell in a more efficient process, which remains to be characterized. Nonetheless, the approximately 3- fold increase in production compared to **D22** makes **D74** an interesting candidate for potential semi–synthetic approaches. To achieve further and less restricted modifications of biosynthetically generated darobactins, semi-synthesis can become an alternative to total synthesis, which is currently costly and time–consuming.[21] Combinations of fermentation and semi-synthetic approaches might help in the future to find a path forward for large-scale production of darobactins in amounts high enough for preclinical and clinical development of this new class of antibiotics at costs acceptable for pharmaceutical development.[22]

Importantly, our biosynthetic approach enables access to a structurally diverse set of darobactins for further investigation. We were able to study modified analogues substituted with amino acids at positions that have not been tested before. Consequently, we could enhance the repertoire of artificial darobactins and our knowledge about the influence of respective modifications especially at positions 2 and 5, but also in combination with position 4. In contrast to previous reports, we showed that the change at position 2, as in **DE**, does not necessarily lead to strongly reduced antibacterial activity compared to **DA**.[17] The strain–specific antibacterial activity is in line with the findings that already single amino acid substitutions in the compound-binding site are able to completely abolish activity, which has been shown *e.g.* for the non-native derivative **D25**, but also for BamA mutants.[8,17] Although causative point mutations in the respective pathogens could easily lead to resistance, it has already been shown that such modifications are connected to severe fitness-loss of the mutants.[23] Interestingly, similar differences between native and artificial analogues as seen for **DE** and **D64** at position 2 were observed for modification at position 5. The artificial darobactin **D39** (WNWTRRW), bearing an L-arginine instead of L-lysine at position 5 as in native **DD** (WNWSRSF), was active as a pure compound, whereas pure **DD** was published to be inactive against Gram-negative bacteria.[17] The positive charge of the arginine side chain should also interact with the phosphate moieties of cardiolipin and 1–palmitoyl–2–oleoyl–sn–glycero–3–phosphoglycerol which was shown for L-lysine in Kaur *et al.*.[11] Thus, we hypothesized that **DD** should have a comparable antibacterial activity as **DA**. Differences between **DD** and **D39,** however can also be due to other positional changes (Table 2). Thus, we reproduced the **DD** purification and antibacterial characterization to gain certainty about the bioactivity

of **DD**. The production and purification process of **DD** in the previously published paper significantly differs from our methods,[12,17] which, led to considerably higher yields. Notably, the pure **DD** was highly active in our MIC assays, validated by K_D determination via MST. In general, an MIC shift between derivatives might be explained by the slight orientation shift of darobactins binding to BamA due to the change at position 4 from L-serine to L-threonine[12] and due to the terminal switch from L-phenylalanine to L-tryptophan. Especially the change of the terminal amino acid was proven to enhance the antibacterial activity of **D9** up to 8–fold compared to **DA**.[9] The binding constants now determined via MST validate MIC data of pure analogues for *Ec*BamA. By using MST for the first time to determine binding to BamA, we significantly reduced the required amount of protein and ligand per assay compared to ITC, which turned out advantageous due to the reduced production yields for these derivatives. The profiling of new analogues regarding cytotoxicity against HepG2 cells did not show any toxic effects that could be caused by an interaction with eukaryotic membrane β–barrels. Further ADMET profiling data reveal high metabolic and plasma stability and low PPB. This is in line with the high polarity of the compound class and hints at a dominance of renal excretion over hepatic metabolism, which has to be confirmed *in vivo*.

In conclusion, the two frontrunners **D22** and **D69** display properties attractive to be further evaluated *in vivo* (Table 3). Potential future steps include determination of pharmacokinetic properties, followed by studies in *in vivo* infection models focusing on *E. coli* but also *P. aeruginosa* or *A. baumannii*. The new derivatives extend the repertoire of darobactins with validated antibacterial activity data for the best characterized molecules even against clinical isolates of multidrug–resistant *A. baumannii* and *P. aeruginosa* strains. Further derivatization of darobactins has thus expanded our current knowledge of the darobactin–BAM interaction and its impact on biological activity against difficult–to–treat Gram–negative pathogens.

EXPERIMENTAL SECTION

General Procedures. *E. coli* HS996 strain was used as bacterial cloning strain for the transformation of ligation mixtures with digested, modified *darA* gene fragments and the pNOSO-darABCDE-22[12] backbone to construct novel BGC. The modified darA gene fragments were generated with the overlap-extension PCR method, as described previously.[12] The cultivation of the bacterial cloning strain was performed as described previously.[9,12] In brief, the cultivation of *E. coli* HS996 was performed in LB medium (10 g/L tryptone, 5 g/L NaCl, 5 g/L yeast extract, pH 7.0) at 30 °C. The production host *E. coli* BL21 (DE3) was grown

in FM medium (12.54 g/L K_2HPO_4, 2.31 g/L KH_2PO_4, 5 g/L NaCl, 12 g/L yeast extract, 4 g/L D(+) glucose, 1 g/L NH_4Cl, 0.24 g/L $MgSO_4$ * $7H_2O$, pH 7.1) including 1 mg/L sterile filtered vitamin B12. The producer strains, previously transformed with expression vectors (e.g. pNOSO-darABCDE-58 to 74), were separately incubated for 16 hours at 30 °C in LB medium. 0.5 mL of seeded overnight broth was used to inoculate 50 mL FM medium. The production cultures were shaken at 30 °C for 3 days with an appropriate selection marker.[9,12]

Analysis of the production of novel darobactins. The detection and verification of new artificial darobactins produced by overexpression of the mutated *darA* variants was verified using the analytical tools described in Groß *et al.*.[9] In brief, the new analogues in the fermentation broth were measured by analytic ultra-high performance liquid chromatography-high-resolution mass spectrometry (uHPLC-HRMS) using *m/z* values of $[M+2H]^{2+}$, $[M+3H]^{3+}$, $[M+3H-NH_3]^{3+}$ and MS^2 fragmentation analysis of $[M+2H]^{2+}$ (Figure S 21 - Figure S 37) as calculated (Table S 5). To obtain comparable data, multiple ionization states were recorded and combined in an extracted ion chromatogram (EIC), because the amino acid exchange, e.g. of basic amino acids, shifted the most abundant ion species from doubly charged $[M+2H]^{2+}$ to triply charged states ($[M+3H]^{3+}$ and $[M+3H-NH_3]^{3+}$. The integrated combined EIC value of each derivative, detectable in the extracted samples was computed by automated peak integration using Compass Data Analysis version 5.3 (Bruker Daltonics) and divided through the area under the curve (AUC) of **D22** (Table 1).

UHPLC-HRMS analysis.

All analyzes, except for the MS^2 spectra and quantification of production for **DD**, **D58**, **D61** were carried out as described in Groß *et al.*[9]: The fermentation broth of 50 mL screening cultures was centrifuged at 7,750 × g for 15 min at 4 °C. The supernatant was directly analyzed by uHPLC-HRMS using an UltiMate 3000 LC System (Dionex, Sunnyvale, California (US)), which was coupled to either maXis 4G ToF, timsTOF fleX, or amaZon speed mass spectrometers (Bruker Daltonics): LC conditions and couplings were as follows: An Acquity UPLC BEH C-18 column (1.7 µm, 100 x 2 mm; Waters Corporation, Milford, Massachusetts (US)), equipped with a VanGuard BEH C-18 (1.7 µm; Waters Corp.) guard column, was coupled to an Apollo II ESI source (Bruker Daltonics; Billerica, Massachusetts (US)) and hyphenated to respective mass spectrometers. Separation was performed at a flow rate of 0.6 mL/min (eluent A: deionized H_2O + 0.1 % formic acid (FA), eluent B: acetonitrile + 0.1 % FA) at 45 °C using the following gradient: 5 % B for 30 s, followed by a linear gradient up to 95 % B in 18 min and a constant percentage of 95 % B for further 2 min. Original conditions were adjusted with 5 % B within 30 s and kept constant for 1.5 min. The LC flow was split to 75 µL/min before entering the mass spectrometer. In case of maXis 4G

and timsTOF flex, each run started with a calibrant peak of basic sodium formate solution which was provided by a filled 20 µL loop switched into the LC flow at the beginning of each run.

Parameters for maXis 4G were as follows: Mass spectra were acquired in centroid mode ranging from 150–2,500 *m/z* at a 2 Hz full scan rate. Mass spectrometry source parameters were set to 500 V as end plate offset, 4000 V as capillary voltage, 1 bar nebulizer gas pressure, 5 L/min, dry gas flow and 200 °C dry temperature. For MS^2 experiments, CID (collision-induced dissociation) energy was ramped from 35 eV for 500 *m/z* to 45 eV for 1,000 *m/z*. MS full scan acquisition rate was set to 2 Hz and MS^2 spectra acquisition rates were ramped from 1 to 4 Hz for precursor ion intensities of 10 kcts to 1,000 kcts. If analyses on maXis 4G did not result in clear spectra, a timsTOF fleX was used instead: For MS^2 experiments, the same LC system, column and eluents and gradient were used, but coupled to a timsTOF fleX mass spectrometer (Bruker Daltonics) with the same ESI source and source conditions. MS^2 spectra were acquired using parallel acquisition and serial fragmentation (PASEF) mode with the following conditions: TIMS delta values were set to -20 V (delta 1), -120 V (delta 2), 80 V (delta 3), 100 V (delta 4), 0 V (delta 5), and 100 V (delta 6). The 1/K0 (inverse reduced ion mobility) range was set from 0.55 Vs/cm^2 to 1.9 Vs/cm^2, the mass range was *m/z* 100–2000. MS^2 spectra were acquired using the PASEF DDA mode with a collision energy of 30 eV. Ion charge control (ICC) was enabled and set to 7.5 Mio. counts. The analysis accumulation and ramp time was set at 100 ms with a spectra rate of 9.43 Hz and a total cycle of 0.32 sec was also selected resulting in one full TIMS-MS scan and two PASEF MS/MS scans. Precursor ions were actively excluded for 0.1 min and were reconsidered if the intensity was 2.0-fold higher than the previous selection with a target intensity of 4000 and an intensity threshold of 100. TIMS dimension was calibrated linearly using 4 selected ions from ESI Low Concentration Tuning Mix (Agilent Technologies, USA) [*m/z*, $1/k_0$: (301.998139, 0.6678 Vs cm^{-2}), (601.979077, 0.8782 Vs cm−2)] in negative mode and [*m/z*, $1/k_0$: (322.048121, 0.7363 Vs cm^{-2}), (622.028960, 0.9915 Vs cm^{-2})] in positive mode. The mobility for mobility calibration was taken from the CCS compendium.[24]

Some quality controls were run on an amaZon speed in positive ionization mode. MS settings were as follows: Capillary voltage 4500 V, end plate off-set 500 V, nebulizer 30.00 psi, dry gas flow 10 L/min and dry gas temperature 300 °C. Scan range for standard measurements was 200–2000 *m/z* with target mass at 600 *m/z*.

DD, **D58** and **D61** production was quantified using a Vanquish Flex UHPLC (Thermo Fisher, Dreieich, Germany), coupled to a TSQ Altis Plus mass spectrometer (Thermo Fisher, Dreieich, Germany). Supernatants were diluted 1:10 in PBS pH 7.4, followed by addition of 2 volumes 10% MeOH/CAN

containing 15 nM diphenhydramine as internal standard. Samples were centrifuged (15 min, 4 °C, 4000 rpm) before analysis and darobactin content quantified in SRM mode using a calibration curve. LC conditions were as follows: column: Hypersil GOLD C-18 (1.9 µm, 100 x 2.1 mm; Thermo Fisher, Dreieich, Germany); temperature 40 °C; flow rate 0.700 ml/min; solvent A: deionized H_2O + 0.1% FA; solvent B: acetonitrile + 0.1% FA; gradient: 0–0.2 min 10% B, 0.2–1.2 min 10–90% B, 1.2–1.6 min 90% B, 1.6–2.0 min 10% B. MS conditions were as follows: vaporizer temperature 350 °C, ion transfer tube temperature 380 °C, Sheath Gas 30, Aux Gas 10, Sweep Gas 2; spray voltage: 3700 V (**DD**), 3300 V (**D61, D58**) mass transitions: 497.750–489.083 (**DD**, $[M+2H]^{2+}$), 552.167–543.667 (**D61**, $[M+2H]^{2+}$); 552.300–543.883 (**D58**, $[M+2H]^{2+}$); collision energy: 10.9 V (**DD**), 13.1 V (**D61**), 9.3 V (**D58**); Tube lens offset: 59 V (**DD**), 89 V (**D61**), 96 V (**D58**).

Fermentation and purification of darobactins.

All pure darobactins were characterized by a purity of over 95%.

Fermentation of novel darobactin derivatives was achieved in 5 L shaking flasks each containing 1.5 L FM medium supplemented with 30 µg/mL kanamycin as selection marker. A total of 6 x 1.5 L main cultures were inoculated with 15 mL of a well-grown overnight culture of *E.coli* BL21 (DE3) producer strain harboring the modified darobactin BGC which was cultivated for 16 h at 30 °C and 180 rpm, in LB medium with an appropriate selection marker (30 µg/mL kanamycin). The main production cultures in 5 L shaking flasks were incubated for three days at 30 °C and 160 rpm on an orbital shaker.

After incubation, the 1.5 L production broth was centrifuged at 6000 x g for 15 minutes at 4 °C to remove the bacterial cells from the supernatant. The collected supernatant was pH adjusted to 7.0–7.3 with NaOH or HCl and mixed with 2 % (w/V) cation exchange resin Dowex MAC-3 for 5–6 hours at 4 °C and 400 rpm on an orbital shaker. The extraction of the novel darobactins was performed as described in more detail previously.[12] In brief, the resin was washed twice with H_2O_{dest} for about 15 minutes and incubated overnight at 4 °C in H_2O_{dest}. The novel darobactins were then eluted from the resin 5–7 times with 300 mL each of a 2 M ammonia solution for 30 min, where the supernatant was decanted after each elution step. The eluate containing the darobactins was then neutralized on ice with 99 % (V/V) acetic acid until a pH between 4–7 was reached. Afterwards the eluate was filtered using folded filter paper.

Purification of the darobactin containing supernatant was performed by two to three chromatographic steps, depending on purity. First, fractionation was performed by a combination of solid phase extraction and flash chromatography using a 130 g C18 flash column (CHROMABOND flash RS 120 C18 ec, 40–63 µm).

The eluate loaded C18 column was first washed with 2 column volumes (CV) of H_2O_{dest} to remove salts and highly polar compounds. Fractionation was then performed with a gradient using a mobile phase composed of deionized H_2O + 0.1 % FA (eluent A) and acetonitrile (ACN) + 0.1 % FA (eluent B) on a Biotage flash chromatographic system (Isolera One) at a flow rate of 50 mL/min under the following conditions:

1 CV H_2O_{dest} without FA, followed by elution with 20 CV of 5 % B increased to 25 % B, followed by a ramp of 2 CV to 95 % B and 2 CV of 95 % eluent B as a cleaning step. Detection was performed at 220 and 280 nm UV absorption. The darobactin containing fractions were collected and concentrated using a rotary evaporator.

In a second chromatographic step, the darobactin containing fractions were purified by a preparative reversed phase chromatography on the preparative Autopurifier HPLC-MS system by Waters Corp. using an XBridge C18 column (5 µm, 19 x 150 mm; Waters Corp.). Separation was performed using the same solvents (eluent A and eluent B) as previously described for the first purification step at a flow rate of 25 mL/min with the following gradients:

HPLC conditions for purification of **D61** and **D64** were initially an equilibration with 5 % eluent B and 95 % eluent A for 2 min, followed by a gradient from 5–20 % B for 22 min, a ramp to 95 % B for another 2 min and constant holding at 95 % B for 1 min. The initial conditions were set within 2 min ramping back to 5 % B. The elution of **D61** occurred after 13.5 min and for **D64** after 14.5 min.

D58 and **D74** and native **DD** were separated with the following gradient: equilibration step with 2 % B and 98 % A for 2 min, followed by a linear gradient to 25 % B over 22 min, an increase to 95 % B within 2 min, keeping at 95 % B for 1 min, followed by ramping back to initial 2 % B within 2 min. The elution of **D58** occurred at minute 11.4, for **D74** at minute 12.5 and for **DD** at minute 13.5.

Purification of **D60** was initially achieved with equilibration at 10 % B and 90 % A for 2 min, a linear separation gradient from 10 % B up to 17 % B for 22 min, followed by an increase to 95 % B within 2 min and holding at 95 % B for 1 min. The initial conditions were set by ramping back to 10 % B within 2 min. The elution of **D60** occurred after 12 min.

D69 and **D39** were separated using the following HPLC conditions: an equilibration step at 2 % B and 98 % A for initial 2 min followed by a linear gradient from 2 % B up to 15 % B for 22 min, an increase up to 95 % B within 2 min and keeping 95 % B for 1 min. Afterwards the initial conditions of 2 % B and 98 % A were set within 2 min. The elution of **D69** occurred after 17 min and of **D39** after 15 min. The fractions containing darobactin were collected according to their elution time and concentrated using a rotary evaporator.

For some derivatives, a further purification step was performed on an Ultimate 3000 semi-preparative HPLC system (Thermo Scientific) using an Acquity CSH Phenyl-hexyl column (250 mmx 10 mm, 5 µm; Waters Corp.) to obtain entirely pure compounds. The separation was performed using the same solvents (eluent A and eluent B) as previously described for the first and second purification step at a flow rate of 5 mL/min and a column temperature of 45 °C. Detection of darobactin was performed by UV absorption at 280 nm and the corresponding fractions were collected in a time dependent manner. The following gradients were used:

Purification of **D58** and **D60** were achieved using an initial equilibration step of 2 % eluent B and 98 % eluent A for 2 min, followed by a linear gradient from 2–25 % B for 22 min, an increase up to 95 % B within 2 min and holding at 95 % B for 1 min, followed by setting the initial conditions of 2 % B within 2 min. The elution of **D57** occurred at minute 12.1, of **D58** at minute 9.5, and of **D60** at minute 10.

Separation of **D64** was also started with an equilibration step of 2 % B for 2 min. The HPLC conditions were then an gradient from 2 % B to 15 % B for 22 min and increase to 95 % B within 2 min, holding 95 % B for 1 min and adjusting the initial conditions by ramping back to 2 % B within 2 min. Elution of **D64** occurred after 10.8 min. The corresponding fractions containing darobactin were collected, concentrated and dried using a rotary evaporator and purity was confirmed by uHPLC-HRMS analysis.

Determination of antibacterial activity. The antibacterial activity of novel darobactins was determined by the evaluation of the minimum inhibitory concentration (MIC) as previously described for crude extracts and for pure darobactin analogues.[9]

Microscale thermophoresis assay. The microscale thermophoresis (MST) (Serial no. 201709-BR-N024, Monolith NT.115 Micro Scale Thermophoresis, NanoTemper Technologies GmbH.) was performed according to the standard protocol from the manufacturer NanoTemper Technologies GmbH using the Monolith His-Tag Labeling Kit RED-tris-NTA 2nd Generation kit. The buffer used was HEPES (50 mM), pH 7.6, $MgCl_2$ (5 mM) and Tween (0.05%). The protein concentration of 50 nM was used and the ligand was tested at the highest soluble concentration, which was 2 mM for most of the compounds under the assay conditions. A 1:1 dilution of the ligand over 16 samples was performed using a stock of ligand (in water) diluted in HEPES buffer. Non-hydrophobic capillary tubes were used. A pretest to check for the labelling and compound fluorescence was performed before every sample, followed by a binding affinity (K_D) determination. Each sample was measured after 15 min incubation at RT and analyzed in MO Control version 1.6.

ADME profiling of D22 and D69.

Metabolic Stability in Liver Microsomes. For the evaluation of phase I metabolic stability, the compound (1 µM) was incubated with 0.5 mg/mL pooled C57BL/6 mouse, Wistar rat liver microsomes (Xenotech, Kansas City, USA) or human liver microsomes (Corning, New York, USA), 2 mM NADPH, 10 mM $MgCl_2$ at 37 °C for 120 min on a microplate shaker (Eppendorf, Hamburg, Germany). The metabolic stability of testosterone, verapamil and ketoconazole were determined in parallel to confirm the enzymatic activity of mouse/rat liver microsomes, for human liver microsomes testosterone, diclofenac and propranolol were used. The incubation was stopped after defined time points by precipitation of aliquots of enzymes with 2 volumes of cold acetonitrile containing internal standard (15 nM diphenhydramine). Samples were stored on ice until the end of the incubation and precipitated protein was removed by centrifugation (15 min, 4 °C, and 4,000 g). Concentration of the remaining test compound at the different time points was analyzed by HPLC-MS/MS (TSQ Altis Plus, Thermo Fisher, Dreieich, Germany) and used to determine half-life ($t_{1/2}$). **Stability in Plasma.** To determine stability in plasma, the compound (1 µM) was incubated with pooled CD-1 mouse, Wistar rat or human plasma (Neo Biotech, Nanterre, France). Samples were taken at defined time points by mixing aliquots with 4 volumes of acetonitrile containing internal standard (12.5 nM diphenhydramine). Samples were stored on ice until the end of the incubation and precipitated protein was removed by centrifugation (15 min, 4 °C, 4,000 g, and 2 centrifugation steps). Concentration of the remaining test compound at the different time points was analyzed by HPLC-MS/MS (TSQ Quantum Access MAX, Thermo Fisher, Dreieich, Germany). The plasma stability of procain, propantheline and diltiazem were determined in parallel to confirm the enzymatic activity. **Plasma Protein Binding.** Plasma protein binding was determined using the Rapid Equilibrium Dialysis (RED) system (Thermo Fisher Scientific, Waltham MA, USA). Compounds were diluted in murine (CD-1), rat (Wistar) or human plasma (Neo Biotech, Nanterre, France) to 10 µM and added to the respective chamber according to the manufacturer's protocol, followed by addition of PBS pH 7.4 to the opposite chamber. Samples were taken immediately after addition to the plate as well as after 2, 4 and 5 h by mixing 10 µL with 80 µL ice-cold acetonitrile containing 12.5 nM diphenhydramine as internal standard, followed by addition of 10 µL plasma to samples taken from PBS and vice versa. Samples were stored on ice until the end of the incubation and precipitated protein was removed by centrifugation (15 min, 4 °C, 4,000 g, and 2 centrifugation steps). Concentration of the remaining test compound at the different time points was analyzed by HPLC-MS/MS (TSQ Altis Plus, Thermo Fisher, Dreieich, Germany). The amount of compound bound to protein was calculated using the equation PPB [%] = 100 – 100 x (amount in buffer chamber/amount in plasma chamber).

Protein expression and purification. The *E. coli* BamA barrel domain (BamA-β) (residues 421–810, C690S, C700S), with an N-terminal 6 x His tag was overexpressed and purified as described previously.[12]

NMR spectroscopy of D69. NMR data were recorded on an UltraShield 500 MHz (^{1}H at 500 MHz, ^{13}C at 125 MHz) equipped with a 5 mm inverse TCI cryoprobe (Bruker, Billerica, MA, USA). Shift values (δ) were calculated in ppm, and coupling constants (J) were calculated in Hz. For the two-dimensional experiments HMBC, HSQC, and gCOSY standard pulse programs were used. HMBC experiments were optimised for $^{2,3}J_{C\text{-}H}$ = 6 Hz, and HSQC were optimised for $^{1}J_{C\text{-}H}$ = 145 Hz. NMR data of darobactin-69 showed high similarity to that of **D22** when comparing 1D and 2D NMR spectra. However, instead of the L-asparagine a glutamine moiety, and instead of the L-threonine a L-serine moiety could be identified, as evidenced by typical proton and carbon shifts as well as COSY and HMBC correlations (Table S 7). The amino acid sequence of **D69** was predetermined by the core peptide, and confirmed by HMBC correlations from α-protons to carbonyl carbons. A couple of amino acid connections that could not be established by HMBC NMR data due to missing correlations were confirmed based on ESI-HR-MS^2 analysis (Figure S39).

ASSOCIATED CONTENT

Supporting Information. Additional figures and tables including modeled BamA – darobactin interactions, MS and MS^2 fragmentation pattern of all derivatives, chromatograms of extracts, antibiogram of clinical *P. aeruginosa* isolates, quantification of pure darobactins, NMR spectroscopic data of **D69** and HPLC traces of pure compounds.

Molecular formula strings

Model of BamA-**D39**

Model of BamA-**D58**

Model of BamA-**D60**

Model of BamA-**D61**

Model of BamA-**D64**

Model of BamA-**D67**

Model of BamA-**D69**_v1

Model of BamA-**D69**_v2

Model of BamA-**D74**

This material is available free of charge via the Internet at http://pubs.acs.org."

AUTHOR INFORMATION

Corresponding Author

*Email: rolf.mueller@helmholtz-hips.de. Phone: (+49)681 98806-3002

Author Contributions

The manuscript was written through contributions of all authors. All authors have given approval to the final version of the manuscript.

Funding Sources

Helmholtz Validation Funds, Gottfried-Wilhem Leibniz Preis der Deutschen Forschungsgemeinschaft (DFG) MU1254/32-1.

Notes

C.E.S., R.M., J.H. are inventors of the patent application WO 2022/175443 A1.

ACKNOWLEDGMENT

We thank our technical stuff Alexandra Amann and Viktoria George for performing the MIC assays and Selina Wolter, Philipp Gansen and Jannine Seelbach for the ADMET profiling. We would also like to thank Prof. Dirk Schlüter and Dr. Claas Baier from Medical School Hannover for providing MDR clinical isolates of *P. aeruginosa* and Besnik Qallaku for the material support.

ABBREVIATIONS

BAM, BamABCDE complex; BGC, biosynthetic gene cluster; Cl_{int}, intrinsic clearance; CRAB, carbapenem-resistant *A. baumannii*; cryo-EM, cryogenic electron microscopy; EcBamA, *E. coli* BamA; FM, Formulated Medium; ITC, isothermal titration calorimetry; K_D, dissociation constant; MIC, minimal inhibitory concentration; MoB, Mode of binding; MST, microscale thermophoresis; OMP, outer membrane protein; PPB, plasma protein binding; RiPPs, ribosomally synthesized and post-translationally modified peptides; rSAM, radical S-adenosyl-L-methionine; $t_{1/2}$, half-life time.

References

1 E. Y. Klein, T. P. van Boeckel, E. M. Martinez, S. Pant, S. Gandra, S. A. Levin, H. Goossens and R. Laxminarayan, *PNAS*, 2018, **115**, E3463-E3470.

2 R. Mirzaei, M. Yunesian, S. Nasseri, M. Gholami, E. Jalilzadeh, S. Shoeibi and A. Mesdaghinia, *The Science of the total environment*, 2018, **619-620**, 446.
3 J. Hu, J. Zhou, S. Zhou, P. Wu and Y. F. Tsang, *Process Safety and Environmental Protection*, 2018, **113**, 483.
4 Tackling drug-resistant infections globally: final report and recommendations, https://apo.org.au/node/63983, (accessed 7 September 2023).
5 C. J. L. Murray, K. S. Ikuta, F. Sharara, L. Swetschinski, G. Robles Aguilar, A. Gray, C. Han, C. Bisignano, P. Rao, E. Wool, S. C. Johnson, A. J. Browne, M. G. Chipeta, F. Fell, S. Hackett, G. Haines-Woodhouse, B. H. Kashef Hamadani, E. A. P. Kumaran, B. McManigal, R. Agarwal, S. Akech, S. Albertson, J. Amuasi, J. Andrews, A. Aravkin, E. Ashley, F. Bailey, S. Baker, B. Basnyat, A. Bekker, R. Bender, A. Bethou, J. Bielicki, S. Boonkasidecha, J. Bukosia, C. Carvalheiro, C. Castañeda-Orjuela, V. Chansamouth, S. Chaurasia, S. Chiurchiù, F. Chowdhury, A. J. Cook, B. Cooper, T. R. Cressey, E. Criollo-Mora, M. Cunningham, S. Darboe, N. P. J. Day, M. de Luca, K. Dokova, A. Dramowski, S. J. Dunachie, T. Eckmanns, D. Eibach, A. Emami, N. Feasey, N. Fisher-Pearson, K. Forrest, D. Garrett, P. Gastmeier, A. Z. Giref, R. C. Greer, V. Gupta, S. Haller, A. Haselbeck, S. I. Hay, M. Holm, S. Hopkins, K. C. Iregbu, J. Jacobs, D. Jarovsky, F. Javanmardi, M. Khorana, N. Kissoon, E. Kobeissi, T. Kostyanev, F. Krapp, R. Krumkamp, A. Kumar, H. H. Kyu, C. Lim, D. Limmathurotsakul, M. J. Loftus, M. Lunn, J. Ma, N. Mturi, T. Munera-Huertas, P. Musicha, M. M. Mussi-Pinhata, T. Nakamura, R. Nanavati, S. Nangia, P. Newton, C. Ngoun, A. Novotney, D. Nwakanma, C. W. Obiero, A. Olivas-Martinez, P. Olliaro, E. Ooko, E. Ortiz-Brizuela, A. Y. Peleg, C. Perrone, N. Plakkal, A. Ponce-de-Leon, M. Raad, T. Ramdin, A. Riddell, T. Roberts, J. V. Robotham, A. Roca, K. E. Rudd, N. Russell, J. Schnall, J. A. G. Scott, M. Shivamallappa, J. Sifuentes-Osornio, N. Steenkeste, A. J. Stewardson, T. Stoeva, N. Tasak, A. Thaiprakong, G. Thwaites, C. Turner, P. Turner, H. R. van Doorn, S. Velaphi, A. Vongpradith, H. Vu, T. Walsh, S. Waner, T. Wangrangsimakul, T. Wozniak, P. Zheng, B. Sartorius, A. D. Lopez, A. Stergachis, C. Moore, C. Dolecek and M. Naghavi, *Lancet*, 2022, **399**, 629.
6 a) M. I. Hutchings, A. W. Truman and B. Wilkinson, *Curr. Opin. Microbiol.*, 2019, **51**, 72; b) Global antimicrobial resistance surveillance system (GLASS) report: early implementation 2017-2018, https://www.who.int/publications/i/item/9789241515061, (accessed 7 September 2023);
7 a) C. Hobson, A. N. Chan and G. D. Wright, *Chem. Rev.*, 2021; b) B. Ribeiro da Cunha, L. P. Fonseca and C. R. C. Calado, *Antibiotics*, 2019, **8**; c) S. Walesch, J. Birkelbach, G. Jézéquel, F. P. J. Haeckl, J. D. Hegemann, T. Hesterkamp, A. K. H. Hirsch, P. Hammann and R. Müller, *EMBO reports*, 2022, e56033;
8 Y. Imai, K. J. Meyer, A. Iinishi, Q. Favre-Godal, R. Green, S. Manuse, M. Caboni, M. Mori, S. Niles, M. Ghiglieri, C. Honrao, X. Ma, J. Guo, A. Makriyannis, L. Linares-Otoya, N. Böhringer, Z. G. Wuisan, H. Kaur, R. Wu, A. Mateus, A. Typas, M. M. Savitski, J. L. Espinoza, A. O'Rourke, K. E. Nelson, S. Hiller, N. Noinaj, T. F. Schäberle, A. D'Onofrio and K. Lewis, *Nature*, 2019, **576**, 459.
9 S. Groß, F. Panter, D. Pogorevc, C. E. Seyfert, S. Deckarm, C. D. Bader, J. Herrmann and R. Müller, *Chem. Sci.*, 2021, **12**, 11882.
10 G. Zhong, Z.-J. Wang, F. Yan, Y. Zhang and L. Huo, *ACS Bio & Med Chem Au*, 2023, **3**, 1.
11 H. Kaur, R. P. Jakob, J. K. Marzinek, R. Green, Y. Imai, J. R. Bolla, E. Agustoni, C. V. Robinson, P. J. Bond, K. Lewis, T. Maier and S. Hiller, *Nature*, 2021, **593**, 125.
12 C. E. Seyfert, C. Porten, B. Yuan, S. Deckarm, F. Panter, C. Bader, J. Coetzee, F. Deschner, K. Tehrani, P. G. Higgins, H. Seifert, T. Marlovits, J. Herrmann and R. Müller, *Angew. Chem. Int. Ed.*, 2022, **62**, e202214094.

13 a) N. Ritzmann, S. Manioglu, S. Hiller and D. J. Müller, *Structure*, 2022, **30**, 350; b) S. F. Haysom, J. Machin, J. M. Whitehouse, J. E. Horne, K. Fenn, Y. Ma, H. El Mkami, N. Böhringer, T. F. Schäberle, N. A. Ranson, S. E. Radford and C. Pliotas, *Angewandte Chemie*, 2023, e202218783; c) R. D. Miller, A. Iinishi, S. M. Modaresi, B.-K. Yoo, T. D. Curtis, P. J. Lariviere, L. Liang, S. Son, S. Nicolau, R. Bargabos, M. Morrissette, M. F. Gates, N. Pitt, R. P. Jakob, P. Rath, T. Maier, A. G. Malyutin, J. T. Kaiser, S. Niles, B. Karavas, M. Ghiglieri, S. E. J. Bowman, D. C. Rees, S. Hiller and K. Lewis, *Nat. Microbiol.*, 2022, **7**, 1661;

14 a) Anatol Luther, Matthias Urfer, Michael Zahn, Maik Müller, Shuang-Yan Wang, Milon Mondal, Alessandra Vitale, Jean-Baptiste Hartmann, Timothy Sharpe, Fabio Lo Monte, Harsha Kocherla, Elizabeth Cline, Gabriella Pessi, Parthasarathi Rath, Seyed Majed Modaresi, Petra Chiquet, Sarah Stiegeler, Carolin Verbree, Tobias Remus, Michel Schmitt, Caroline Kolopp, Marie-Anne Westwood, Nicolas Desjonquères, Emile Brabet, Sophie Hell, Karen LePoupon, Annie Vermeulen, Régis Jaisson, Virginie Rithié, Grégory Upert, Alexander Lederer, Peter Zbinden, Achim Wach, Kerstin Moehle, Katja Zerbe, Hans H. Locher, Francesca Bernardini, Glenn E. Dale, Leo Eberl, Bernd Wollscheid, Sebastian Hiller, John A. Robinson and Daniel Obrecht, *Nature*, 2019, **576**, 452; b) M. A. Cook and G. D. Wright, *Sci. Transl. Med.*, 2022, **14**, eabo7793;

15 M. Marner, L. Kolberg, J. Horst, N. Böhringer, J. Hübner, I. D. M. Kresna, Y. Liu, U. Mettal, L. Wang, M. Meyer-Bühn, S. Mihajlovic, M. Kappler, T. F. Schäberle and U. von Both, *Microbiol Spectr*, 2023, **11**, e0443722.

16 E. D. Brown and G. D. Wright, *Nature*, 2016, **529**, 336.

17 N. Böhringer, R. Green, Y. Liu, U. Mettal, M. Marner, S. M. Modaresi, R. P. Jakob, Z. G. Wuisan, T. Maier, A. Iinishi, S. Hiller, K. Lewis and T. F. Schäberle, *Microbiol Spectr*, 2021, **9**, e0153521.

18 E. F. Pettersen, T. D. Goddard, C. C. Huang, E. C. Meng, G. S. Couch, T. I. Croll, J. H. Morris and T. E. Ferrin, *Protein Sci.*, 2021, **30**, 70.

19 Schrödinger, The PyMOL Molecular Graphics System, Version 2.5.2 (Version 2.5.2), Schrödinger, LLC, 2022.

20 a) G. A. Hudson and D. A. Mitchell, *Curr. Opin. Microbiol.*, 2018, **45**, 61; b) P. G. Arnison, M. J. Bibb, G. Bierbaum, A. A. Bowers, T. S. Bugni, G. Bulaj, J. A. Camarero, D. J. Campopiano, G. L. Challis, J. Clardy, P. D. Cotter, D. J. Craik, M. Dawson, E. Dittmann, S. Donadio, P. C. Dorrestein, K.-D. Entian, M. A. Fischbach, J. S. Garavelli, U. Göransson, C. W. Gruber, D. H. Haft, T. K. Hemscheidt, C. Hertweck, C. Hill, A. R. Horswill, M. Jaspars, W. L. Kelly, J. P. Klinman, O. P. Kuipers, A. J. Link, W. Liu, M. A. Marahiel, D. A. Mitchell, G. N. Moll, B. S. Moore, R. Müller, S. K. Nair, I. F. Nes, G. E. Norris, B. M. Olivera, H. Onaka, M. L. Patchett, J. Piel, M. J. T. Reaney, S. Rebuffat, R. P. Ross, H.-G. Sahl, E. W. Schmidt, M. E. Selsted, K. Severinov, B. Shen, K. Sivonen, L. Smith, T. Stein, R. D. Süssmuth, J. R. Tagg, G.-L. Tang, A. W. Truman, J. C. Vederas, C. T. Walsh, J. D. Walton, S. C. Wenzel, J. M. Willey and van der Donk, Wilfred A., *Natural product reports*, 2013, **30**, 108;

21 a) M. Nesic, D. B. Ryffel, J. Maturano, M. Shevlin, S. R. Pollack, D. R. Gauthier, P. Trigo-Mouriño, L.-K. Zhang, D. M. Schultz, J. M. McCabe Dunn, L.-C. Campeau, N. R. Patel, D. A. Petrone and D. Sarlah, *J. Am. Chem. Soc.*, 2022, **144**, 14026; b) Y.-C. Lin, F. Schneider, K. J. Eberle, D. Chiodi, H. Nakamura, S. H. Reisberg, J. Chen, M. Saito and P. S. Baran, *J. Am. Chem. Soc.*, 2022, **144**, 14458;

22 a) A. K. Krome, T. Becker, S. Kehraus, A. Schiefer, M. Gütschow, L. Chaverra-Muñoz, S. Hüttel, R. Jansen, M. Stadler, A. Ehrens, D. Pogorevc, R. Müller, M. P. Hübner, T. Hesterkamp, K. Pfarr, A. Hoerauf, K. G. Wagner and G. M. König, *Natural product reports*, 2022, **39**, 1705; b) M. Miethke, M. Pieroni, T. Weber, M. Brönstrup, P. Hammann, L. Halby, P. B. Arimondo, P. Glaser, B. Aigle, H. B.

Bode, R. Moreira, Y. Li, A. Luzhetskyy, M. H. Medema, J.-L. Pernodet, M. Stadler, J. R. Tormo, O. Genilloud, A. W. Truman, K. J. Weissman, E. Takano, S. Sabatini, E. Stegmann, H. Brötz-Oesterhelt, W. Wohlleben, M. Seemann, M. Empting, A. K. H. Hirsch, B. Loretz, C.-M. Lehr, A. Titz, J. Herrmann, T. Jaeger, S. Alt, T. Hesterkamp, M. Winterhalter, A. Schiefer, K. Pfarr, A. Hoerauf, H. Graz, M. Graz, M. Lindvall, S. Ramurthy, A. Karlén, M. van Dongen, H. Petkovic, A. Keller, F. Peyrane, S. Donadio, L. Fraisse, L. J. V. Piddock, I. H. Gilbert, H. E. Moser and R. Müller, *Nat. Rev. Chem.*, 2021, **5**, 726;

23 Z. G. Wuisan, I. D. M. Kresna, N. Böhringer, K. Lewis and T. F. Schäberle, *Metab. Eng.*, 2021, **66**, 123.

24 J. A. Picache, B. S. Rose, A. Balinski, K. L. Leaptrot, S. D. Sherrod, J. C. May and J. A. McLean, *Chem. Sci.*, 2019, **10**, 983.

4.2 Supplementary Information

New Genetically Engineered Derivatives of Antibacterial Darobactins Underpin their Potential for Antibiotic Development.

Previously published in:

Carsten E. Seyfert[a,b], Alison V. Müller[a,b], Danica J. Walsh[a,b], Joy Birkelbach[a,b], Andreas M. Kany[a,b], Christoph Porten[a,b], Biao Yuan[c,d,f], Daniel Krug[a,b], Jennifer Herrmann[a,b], Thomas C. Marlovits[c,d,f], Anna K. H. Hirsch[a,b,e] and Rolf Müller[a,b,e]

J. Med. Chem., 2023 November 21

DOI: acs.jmedchem.3c01660

Affilitaton:

[a]Helmholtz Institute for Pharmaceutical Research Saarland (HIPS), Helmholtz Centre for Infection Research (HZI) and Saarland University Department of Pharmacy, Saarbrücken, Germany

[b]German Centre for Infection Research (DZIF), partner site Hannover-Braunschweig

[c]University Medical Center Hamburg-Eppendorf (UKE), Institute of Structural and Systems Biology and Centre for Structural Systems Biology (CSSB), Hamburg, Germany

[d]Deutsches Elektronen-Synchrotron Zentrum (DESY), Hamburg

[e]Helmholtz International Lab for Anti-Infectives

[f]Centre for Structural Systems Biology (CSSB), 22607 Hamburg, Germany

The printed version of the Supporting Information does not contain data that cannot be visualized satisfactorily on paper. To access this data please refer to the enclosed storage medium or the on-line version of this research paper.

BamABCDE (BAM) – darobactin cryo-EM co-structures with the accession code 7NRI (**DA**), 8ADI (**D9**) and 8ADG (**D22**) were analyzed on their appropriate interaction site using Pymol 2.5.2 and ChimeraX1.3 software 1; 2. The Pymol "Mutagenesis" and the Chimera "rotamers" tool were used to exchange the asparagine on position 2 of the darobactin heptapeptide with proteinogenic amino acids of variable length and polarity.[1,2] The potential hydrogen bonding interactions were automatically computed in the respective structural analysis software.[2,3] The orientation of the changed amino acids was calculated by the automatic rotamer tool based on the probabilities of the rotamer library. Based on the findings, novel derivatives, potentially interacting with BamA, were designed and generated using the overlap-extension PCR method previously developed to generated darobactin **D22** to **D39**.[4] In brief, oligonucleotides harboring mismatches compared to the nucleotide core sequence of pNOSOdarABCDE-D22 were externally synthesized (Sigma-Aldrich) (Table S1). In two independent PCR reactions (PCR I, PCR II) fragments, harboring point mutations in the nucleotide core region, were amplified and used as templates for an overlapping PCR (PCR III) to combine the fragments of PCR I and PCR II. The combined fragments were separated via agarose gel electrophoresis, and purified using the NucleoSpin Gel and PCR Cleanup kit (Macherey-Nagel). The purified DNA fragments were digested using restriction-ligation based techniques to generate novel expression constructs summarized in Table S2.

Table S 1: Oligonucleotides used to mutate the *darA* core region for the generation of novel expression constructs with modified darobactin BGC.

Oligonucleotide name	Sequence (5'-3')	Function	Reference
pr1_dar9_fw	GGTGATGTCGGCGATATAGG	Primer for PCR I and III	Seyfert *et al.* 2022
pr1_dar9_v2_fw	GGTGATGTCGGCGATATAGGCG	Primer for PCR I and III	Seyfert *et al.* 2022
pr2_dar22_58b_rv	GCCACCGTTTAGTCCATTCCCAGGCCGT	Primer for PCR I to insert point mutation into *darA*	This study
pr2_dar22_59b_rv	GCCACCGTTTAGTCCATTTCCAGGCCGT	Primer for PCR I to insert point mutation into *darA*	This study
pr2_dar22_60_rv	GCCACCGTTTAGTCCAATCCCAGGCCGT	Primer for PCR I to insert point mutation into *darA*	This study
pr2_dar22_61_rv	GCCACCGTTTAGTCCATTGCCAGGCCGT	Primer for PCR I to insert point mutation into *darA*	This study
pr2_dar22_62_rv	GCCACCGTTTAGTCCATCTCCAGGCCGT	Primer for PCR I to insert point mutation into *darA*	This study
pr2_dar22_63_rv	GCCACCGTTTAGTCCAAACCCAGGCCGT	Primer for PCR I to insert point mutation into *darA*	This study
pr2_dar22_64_rv	GCCACCGTTTAGTCCATGACCAGGCCGT	Primer for PCR I to insert point mutation into *darA*	This study

pr2_dar22_65_rv	GCCATTTTTTAGTCCATGAC CAGGCCGT	Primer for PCR I to insert point mutation into *darA*	This study
pr2_dar22_65_rv2	GCCATTTTTTAGTCCATGAC CAGG	Primer for PCR I to insert point mutation into *darA*	This study
pr2_dar22_66_rv	AAATTTCCTGCCAACATTTA GTCCAGTTCCA	Primer for PCR I to insert point mutation into *darA*	This study
pr2_dar22_67_rv	GCCACCGTTTAGTCCAATAC CAGGCCGT	Primer for PCR I to insert point mutation into *darA*	This study
pr2_dar22_68_rv	GCCACCGTTTAGTCCATAAC CAGGCCGT	Primer for PCR I to insert point mutation into *darA*	This study
pr2_dar22_69_rv	GCCACCGTTTTGACCATTGC CAGGCCGT	Primer for PCR I to insert point mutation into *darA*	This study
pr2_dar22_70_rv	GCCACCGTTTTGACCATGAC CAGGCCGT	Primer for PCR I to insert point mutation into *darA*	This study
pr2_dar22_71_rv	GCCACCGTTTTGACCATTCC CAGGCCGT	Primer for PCR I to insert point mutation into *darA*	This study
pr2_dar22_72_rv	GCCACCGTTTTGACCATTTC CAGGCCGT	Primer for PCR I to insert point mutation into *darA*	This study
pr2_dar22_72_rv2	GCCACCGTTTTGACCATTTC CAGGC	Primer for PCR I to insert point mutation into *darA*	This study
pr2_dar22_73_rv	GCCACCGTTTTGACCAATCC CAGGCCGT	Primer for PCR I to insert point mutation into *darA*	This study
pr2_dar22_74_rv	AAATTTCCTGCCATTGTTTA GTCCAGTTCCA	Primer for PCR I to insert point mutation into *darA*	This study
pr3_dar9_Trp_fw	TGGCAGGAAATTTAAAGCTT ATCCCAT	Primer for PCR II	Seyfert *et al.* 2022
pr3_dar22_v2_fw	CTAAACGGTGGCAGGAAAT TTAAAGCTTATC	Primer for PCR II	Seyfert *et al.* 2022
pr3_dar65b_6K_fw	CTAAAAAATGGCAGGAAAT TTAAAGCTTATCCCA	Primer for PCR II	This study
pr3_dar22_6C_fw	CTAAATGTTGGCAGGAAATT TAAAGCTTATC	Primer for PCR II	This study
pr3_dar22_4S_fw	CAAAACGGTGGCAGGAAAT TTAAAGCTTATC	Primer for PCR II	This study
pr3_dar22_6Q_fw	CTAAACAATGGCAGGAAAT TTAAAGCTTATC	Primer for PCR II	This study
pr4_dar9_rv	TGGGGATCCTCAGGACTGC AG	Primer for PCR II and III	Seyfert *et al.* 2022

Table S 2: Expression plasmids generated to express and produce novel darobactins in *E. coli* BL21 (DE3).

Plasmid	**size [kb]**	**Relevant characteristics/ construction**	**Reference**
pNOSO-darABCDE-22	9.9	*E. coli* cloning and expression vector for production of **D22**	Seyfert *et al.*
pNOSO-darABCDE-58	9.9	*E. coli* cloning and expression vector for production of **D58**	This study
pNOSO-darABCDE-59	9.9	*E. coli* cloning and expression vector for production of **D59**	This study
pNOSO-darABCDE-60	9.9	*E. coli* cloning and expression vector for production of **D60**	This study
pNOSO-darABCDE-61	9.9	*E. coli* cloning and expression vector for production of **D61**	This study

pNOSO-darABCDE-62	9.9	*E. coli* cloning and expression vector for production of **D62**	This study
pNOSO-darABCDE-63	9.9	*E. coli* cloning and expression vector for production of **D63**	This study
pNOSO-darABCDE-64	9.9	*E. coli* cloning and expression vector for production of **D64**	This study
pNOSO-darABCDE-65	9.9	*E. coli* cloning and expression vector for production of **D65**	This study
pNOSO-darABCDE-66	9.9	*E. coli* cloning and expression vector for production of **D66**	This study
pNOSO-darABCDE-67	9.9	*E. coli* cloning and expression vector for production of **D67**	This study
pNOSO-darABCDE-68	9.9	*E. coli* cloning and expression vector for production of **D68**	This study
pNOSO-darABCDE-69	9.9	*E. coli* cloning and expression vector for production of **D69**	This study
pNOSO-darABCDE-70	9.9	*E. coli* cloning and expression vector for production of **D70**	This study
pNOSO-darABCDE-71	9.9	*E. coli* cloning and expression vector for production of **D71**	This study
pNOSO-darABCDE-72	9.9	*E. coli* cloning and expression vector for production of **D72**	This study
pNOSO-darABCDE-73	9.9	*E. coli* cloning and expression vector for production of **D73**	This study
pNOSO-darABCDE-74	9.9	*E. coli* cloning and expression vector for production of **D74**	This study

Table S 3: List of bacterial strains generated or used in this study.

Bacterial strain	Genotype	Reference
Cloning strains		
***E. coli* HS996**	F^-, *mcr*A, Δ(*mrr-hsd*RMS-*mcr*BC), Φ80*lac*ZΔM15, Δ*lac*X74, *rec*A1, *ara*D139, Δ(*ara-leu*)7697, *gal*U, *gal*K, *rps*L (Str^R), *end*A1, *nup*G, *fhu*A::IS2	Invitrogen
***E. coli* NEB10β**	*mcr*A, spoT1Δ(*mrr-hsd*RMS-*mcr*BC), Φ80d(*lac*ZΔM15)*rec*A1, *rel*A1, Δ*lac*X74, *rec*A1, *ara*D139, Δ(*ara-leu*)7697, *gal*K16, *gal*E15, *rps*L (Str^R), *end*A1, *nup*G, *fhu*A	New England Biolabs
***E. coli* BL21 (DE3)**	$F^–$, *ompT, gal, dcm, lon,* $\Delta hsdS_B(r_B^-m_B^-)$, λ(DE3 [*lacI lacUV5-T7p07 ind1 sam7 nin5*]), $[malB^+]_{K\text{-}12}(\lambda^S)$	Invitrogen
***E. coli* BL21-Gold (DE3)**	*E. coli* B F– ompT hsdS(rB– mB–) dcm+ Tetr gal λ(DE3) endA	Agilent Technologies
***E. coli* NEB10β pNOSO-darABCDE-22**	*E. coli* NEB10β with pNOSO-darABCDE-22, kan^R	Seyfert *et al.* 2022
***E. coli* HS996 pNOSO-darABCDE-58**	*E. coli* HS996 with pNOSO-darABCDE-58, kan^R	This study
***E. coli* HS996 pNOSO-darABCDE-59**	*E. coli* HS996 with pNOSO-darABCDE-59, kan^R	This study
***E. coli* HS996 pNOSO-darABCDE-60**	*E. coli* HS996 with pNOSO-darABCDE-60, kan^R	This study

***E. coli* HS996 pNOSO-darABCDE-61**	*E. coli* HS996 with pNOSO-darABCDE-61, kan^R	This study
***E. coli* HS996 pNOSO-darABCDE-62**	*E. coli* HS996 with pNOSO-darABCDE-62, kan^R	This study
***E. coli* HS996 pNOSO-darABCDE-63**	*E. coli* HS996 with pNOSO-darABCDE-63, kan^R	This study
***E. coli* HS996 pNOSO-darABCDE-64**	*E. coli* HS996 with pNOSO-darABCDE-64, kan^R	This study
***E. coli* HS996 pNOSO-darABCDE-65**	*E. coli* HS996 with pNOSO-darABCDE-65, kan^R	This study
***E. coli* HS996 pNOSO-darABCDE-66**	*E. coli* HS996 with pNOSO-darABCDE-66, kan^R	This study
***E. coli* HS996 pNOSO-darABCDE-67**	*E. coli* HS996 with pNOSO-darABCDE-67, kan^R	This study
***E. coli* HS996 pNOSO-darABCDE-68**	*E. coli* HS996 with pNOSO-darABCDE-68, kan^R	This study
***E. coli* HS996 pNOSO-darABCDE-69**	*E. coli* HS996 with pNOSO-darABCDE-69, kan^R	This study
***E. coli* HS996 pNOSO-darABCDE-70**	*E. coli* HS996 with pNOSO-darABCDE-70, kan^R	This study
***E. coli* HS996 pNOSO-darABCDE-71**	*E. coli* HS996 with pNOSO-darABCDE-71, kan^R	This study
***E. coli* HS996 pNOSO-darABCDE-72**	*E. coli* HS996 with pNOSO-darABCDE-72, kan^R	This study
***E. coli* HS996 pNOSO-darABCDE-73**	*E. coli* HS996 with pNOSO-darABCDE-73, kan^R	This study
***E. coli* HS996 pNOSO-darABCDE-74**	*E. coli* HS996 with pNOSO-darABCDE-74, kan^R	This study
Heterologous producer strains		
***E. coli* BL21 (DE3) pNOSO-darABCDE-22**	*E. coli* BL21 (DE3) with pNOSO-darABCDE-22, kan^R	This study
***E. coli* BL21-Gold (DE3) pNOSO-darABCDE-22**	*E. coli* BL21-Gold (DE3) with pNOSO-darABCDE-22, kan^R	This study
***E. coli* BL21 (DE3) pNOSO-darABCDE-58**	*E. coli* BL21 (DE3) with pNOSO-darABCDE-58, kan^R	This study
***E. coli* BL21 (DE3) pNOSO-darABCDE-59**	*E. coli* BL21 (DE3) with pNOSO-darABCDE-59, kan^R	This study
***E. coli* BL21 (DE3) pNOSO-darABCDE-60**	*E. coli* BL21 (DE3) with pNOSO-darABCDE-60, kan^R	This study
***E. coli* BL21 (DE3) pNOSO-darABCDE-61**	*E. coli* BL21 (DE3) with pNOSO-darABCDE-61, kan^R	This study
***E. coli* BL21 (DE3) pNOSO-darABCDE-62**	*E. coli* BL21 (DE3) with pNOSO-darABCDE-62, kan^R	This study
***E. coli* BL21 (DE3) pNOSO-darABCDE-63**	*E. coli* BL21 (DE3) with pNOSO-darABCDE-63, kan^R	This study
***E. coli* BL21 (DE3) pNOSO-darABCDE-64**	*E. coli* BL21 (DE3) with pNOSO-darABCDE-64, kan^R	This study
***E. coli* BL21 (DE3) pNOSO-darABCDE-65**	*E. coli* BL21 (DE3) with pNOSO-darABCDE-65, kan^R	This study
***E. coli* BL21 (DE3) pNOSO-darABCDE-66**	*E. coli* BL21 (DE3) with pNOSO-darABCDE-66, kan^R	This study
***E. coli* BL21 (DE3) pNOSO-darABCDE-67**	*E. coli* BL21 (DE3) with pNOSO-darABCDE-67, kan^R	This study

***E. coli* BL21 (DE3) pNOSO-darABCDE-68**	*E. coli* BL21 (DE3) with pNOSO-darABCDE-68, kan^R	This study
***E. coli* BL21 (DE3) pNOSO-darABCDE-69**	*E. coli* BL21 (DE3) with pNOSO-darABCDE-69, kan^R	This study
***E. coli* BL21 (DE3) pNOSO-darABCDE-70**	*E. coli* BL21 (DE3) with pNOSO-darABCDE-70, kan^R	This study
***E. coli* BL21 (DE3) pNOSO-darABCDE-71**	*E. coli* BL21 (DE3) with pNOSO-darABCDE-71, kan^R	This study
***E. coli* BL21 (DE3) pNOSO-darABCDE-72**	*E. coli* BL21 (DE3) with pNOSO-darABCDE-72, kan^R	This study
***E. coli* BL21 (DE3) pNOSO-darABCDE-73**	*E. coli* BL21 (DE3) with pNOSO-darABCDE-73, kan^R	This study
***E. coli* BL21 (DE3) pNOSO-darABCDE-74**	*E. coli* BL21 (DE3) with pNOSO-darABCDE-74, kan^R	This study
***E. coli* BL21 (λ DE3) Lemo cells pET15b-BamAβ421-810**	*E. coli* BL21 (λ DE3) Lemo cells with pET15b-BamAβ421-810, amp^R	Seyfert *et al.* 2022

Supplementation figures and tables

1. Mutagenesis of the darobactin heptapeptide

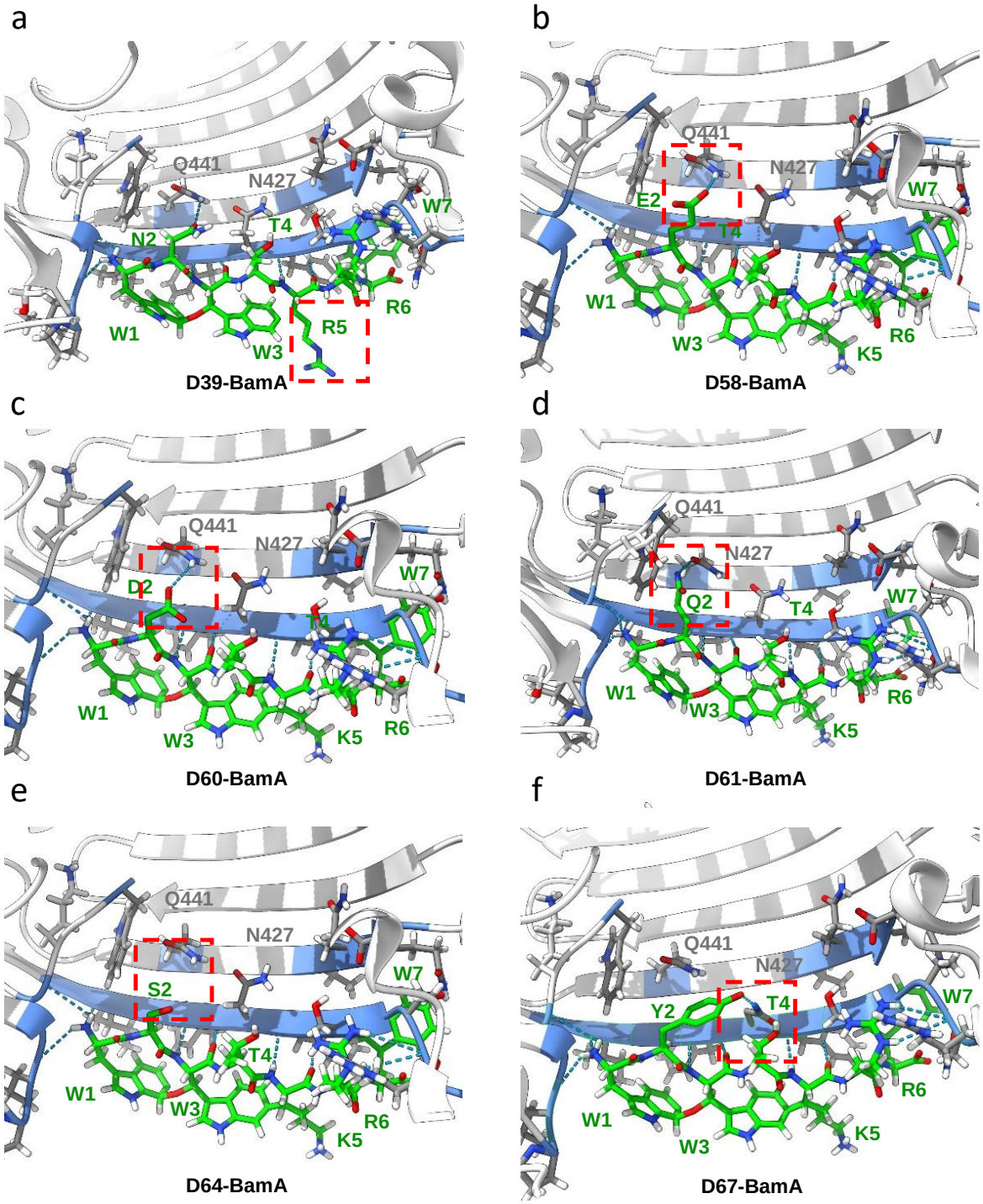

Figure S 91: Mutagenesis of D22 bound to BamABCDE to predict the possible interaction of D39, D58, D60, D61, D64 and D67 with BamA. Chimera rotamer tool was used to model potential hydrogen bonding interactions by changing a) L-arginine to L- lysine to project **D38**-BamA interaction b) L-asparagine to L-glutamic acid to project **D58**-BamA interaction c) L- asparagine to L-aspartic acid to project **D60**-BamA interaction d) L-asparagine to L-glutamine to project **D61**-BamA interaction e) L-asparagine to L-serine to project **D64**-BamA interaction f) L-asparagine to L-tyrosine to project **D67**-BamA interaction. Changes and modeled interactions were highlighted in red. The raw data of **D22** were

taken from protein data bank (PDB) for the mutagenesis and were originally published in Seyfert *et al*.[4] with the PDB accession code: 8ADG (D22).

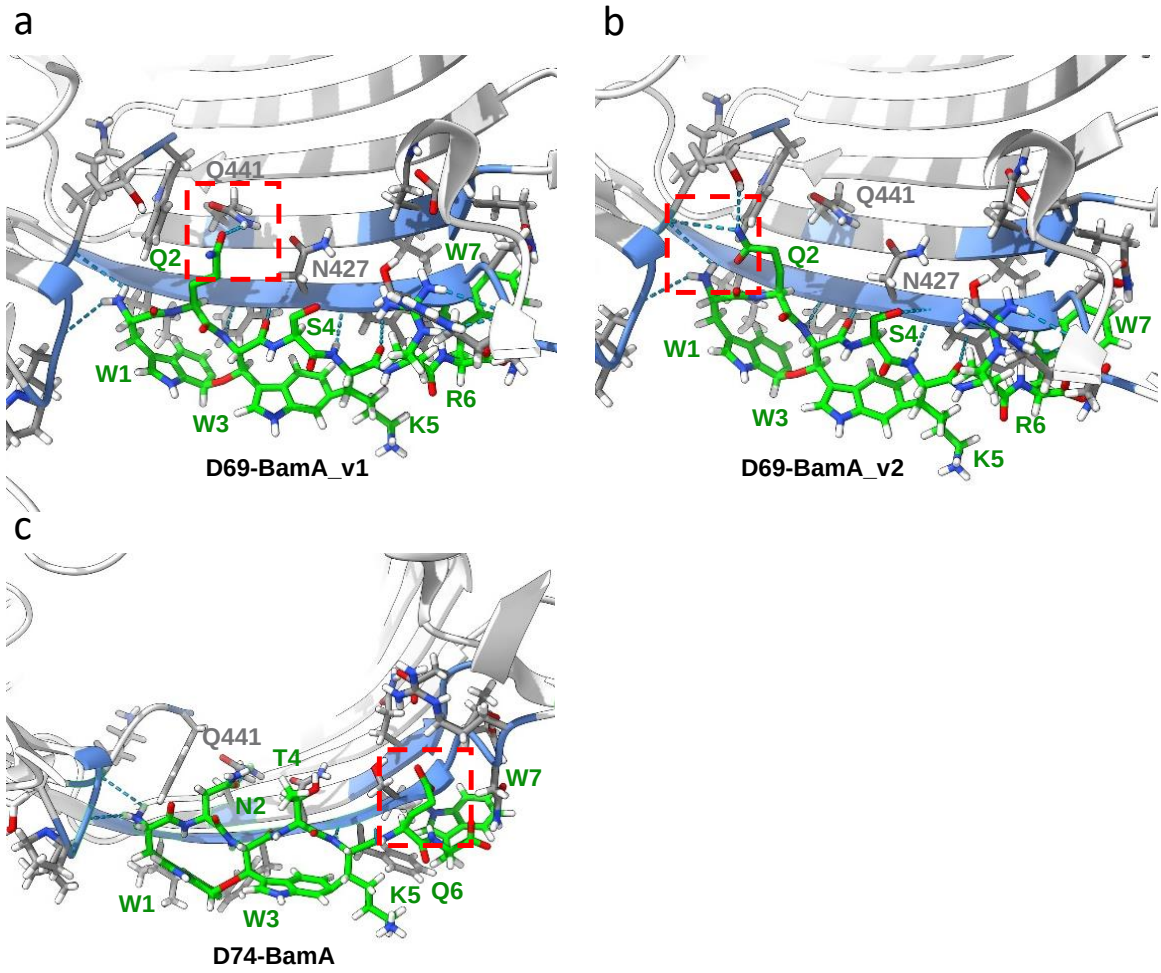

Figure S 92: Mutagenesis of D22 bound to BamABCDE to predict the possible interaction of D69 and D74 with BamA. Chimera rotamer tool was used to model the interactions by changing of a) and b) L-asparagine to L-glutamine to project **D69**-BamA interaction e) L-arginine to L-glutamine to project **D74**-BamA interaction. Changes and modeled interactions were highlighted in red. The raw data of **D22** were taken from protein data bank (PDB) as starting point for molecular modeling. The accession code is 8ADG (**D22**).

2. Chromatograms of darobactin extracts

Table S 4: The calculated (calc.) and observed (obs.) masses of the darobactin analogues. The core peptide sequence of each new derivative with highlighted (red) differences in the core peptide compared to **D22** is indicated. The calc. and obs. masses in the extracts of the different charge states ($[M+H]^{1+}$, $[M+2H]^{2+}$ and $[M+3H]^{3+}$) for each derivative are listed.

Darobactin analogue	Core peptide	Calc. mass $[M+H]^{1+}$	Obs. mass $[M+H]^{1+}$	Calc. mass $[M+2H]^{2+}$	Obs. mass $[M+2H]^{2+}$	Calc. mass $[M+3H]^{3+}$	Obs. mass $[M+3H]^{3+}$	Calc. mass $[M+3H-NH_3]^{3+}$	Obs. mass $[M+3H-NH_3]^{3+}$
D58	W E W T K R W	1103.5058	1103.5171	552.2565	552.2632	368.5068	368.5109	362.8318	362.8351
D59	W K W T K R W	1102.5582	1102.4853	551.7827	551.7889	368.1909	368.1951	362.5159	362.5204
D60	W D W T K R W	1089.4901	1089.5022	545.2487	545.2555	363.8349	363.8392	358.1599	358.1636
D61	W Q W T K R W	1102.5218	1102.5318	551.7645	551.7711	368.1788	368.1831	362.5038	362.5073
D62	W R W T K R W	1130.5643	1130.5152	565.7858	565.7906	377.5263	377.5306	371.8513	371.8691
D63	W V W T K R W	1073.5316	1073.5133	537.2694	537.2752	358.5154	358.1436	352.8404	352.8433
D64	W S W T K R W	1061.4952	1061.5028	531.2512	531.2575	354.5033	354.5071	348.8283	348.8315
D65	W S W T K K W	1033.4891	1033.4981	517.2482	517.2535	345.1679	345.1713	339.4929	339.4956
D66	W N W T K C W	1226.4394	1226.4533	613.7207	613.7307	409.4896	409.4887	403.8146	403.8122
D67	W Y W T K R W	1137.5265	1137.5359	569.2669	569.2734	379.8470	379.8510	374.1720	374.1754
D68	W L W T K R W	1087.5473	1087.5103	544.2773	544.2830	363.1873	363.1909	357.5123	357.5151
D69	W Q W S K R W	1088.5061	1088.5114	544.7567	544.7603	363.5069	363.5092	357.8319	357.8334
D70	W S W S K R W	1047.4796	1047.4822	524.2434	524.2461	349.8314	349.8328	344.1564	344.1574
D71	W E W S K R W	1089.4901	1089.4893	545.2487	545.2491	363.8349	363.8350	358.1599	358.1593
D72	W K W S K R W	1088.5425	1088.4476	544.7749	544.7741	363.5190	363.5184	357.8440	357.8430
D73	W D W S K R W	1075.4745	1075.4735	538.2409	538.2413	359.1630	359.1631	353.4880	353.4876
D74	W N W T K Q W	1060.4636	1060.4622	530.7354	530.7372	354.1594	354.1588	348.4844	348.4836

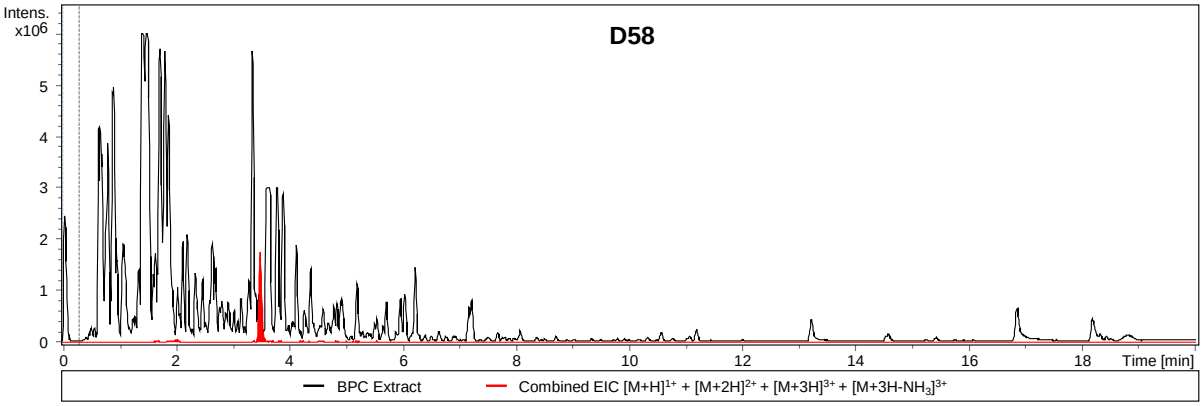

Figure S 93: Chromatogram of the *E. coli* BL21 (DE3) pNOSO-darABCDE-58 extract. The red trace shows the combined EIC for the $[M+H]^{1+}$, $[M+2H]^{2+}$, $[M+3H]^{3+}$ and $[M+3H\text{-}NH_3]^{3+}$ species of **D58** at their calculated masses, respectively (**Table S 4**) ±0.02 Da. The BPC of the whole extract from fermentation broth supernatant is presented in black.

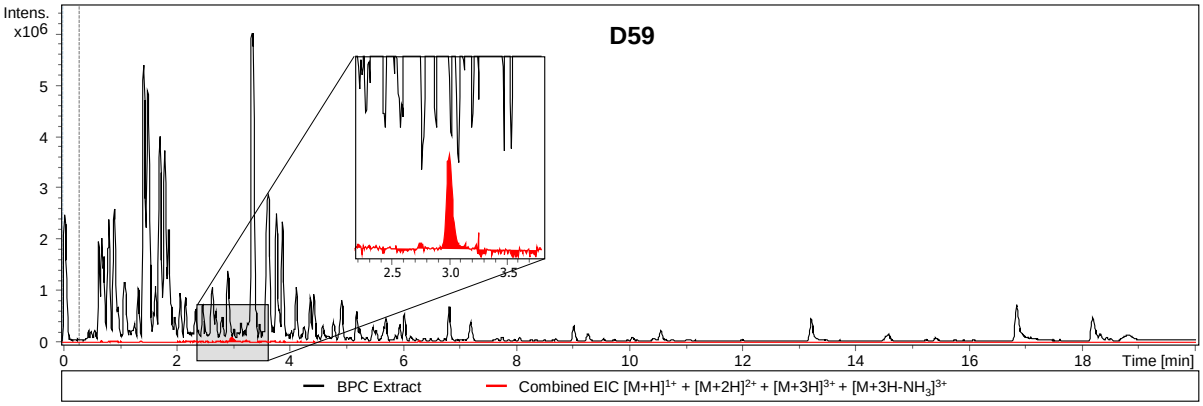

Figure S 94: Chromatogram of the *E. coli* BL21 (DE3) pNOSO-darABCDE-59 extract. The red trace shows the combined EIC for the $[M+H]^{1+}$, $[M+2H]^{2+}$, $[M+3H]^{3+}$ and $[M+3H\text{-}NH_3]^{3+}$ species of **D59** at their calculated masses, respectively (**Table S 4**) ±0.02 Da. The BPC of the whole extract from fermentation broth supernatant is presented in black.

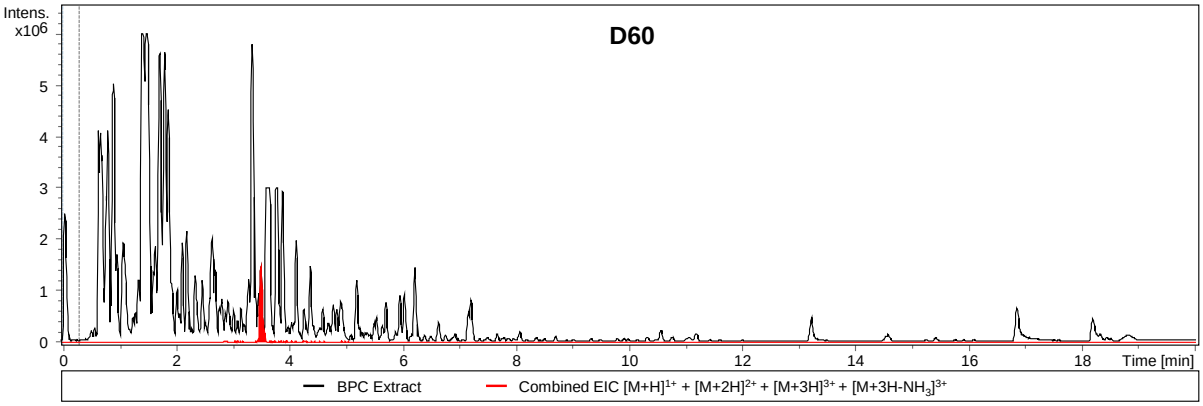

Figure S 95: Chromatogram of the *E. coli* BL21 (DE3) pNOSO-darABCDE-60 extract. The red trace shows the combined EIC for the $[M+H]^{1+}$, $[M+2H]^{2+}$, $[M+3H]^{3+}$ and $[M+3H\text{-}NH_3]^{3+}$ species of **D60** at their calculated masses, respectively (**Table S 4**) ±0.02 Da. The BPC of the whole extract from fermentation broth supernatant is presented in black.

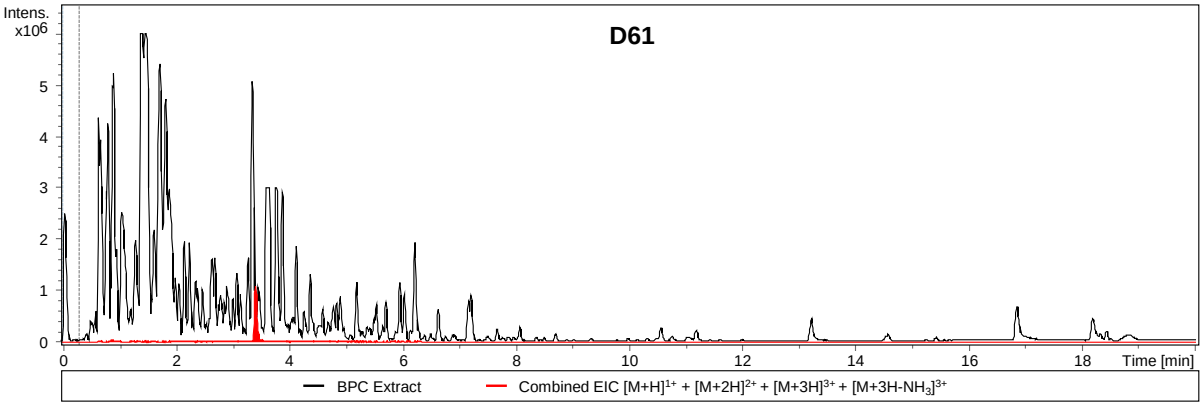

Figure S 96: Chromatogram of the *E. coli* BL21 (DE3) pNOSO-darABCDE-61 extract. The red trace shows the combined EIC for the $[M+H]^{1+}$, $[M+2H]^{2+}$, $[M+3H]^{3+}$ and $[M+3H\text{-}NH_3]^{3+}$ species of **D61** at their calculated masses, respectively (**Table S 4**) ±0.02 Da. The BPC of the whole extract from fermentation broth supernatant is presented in black.

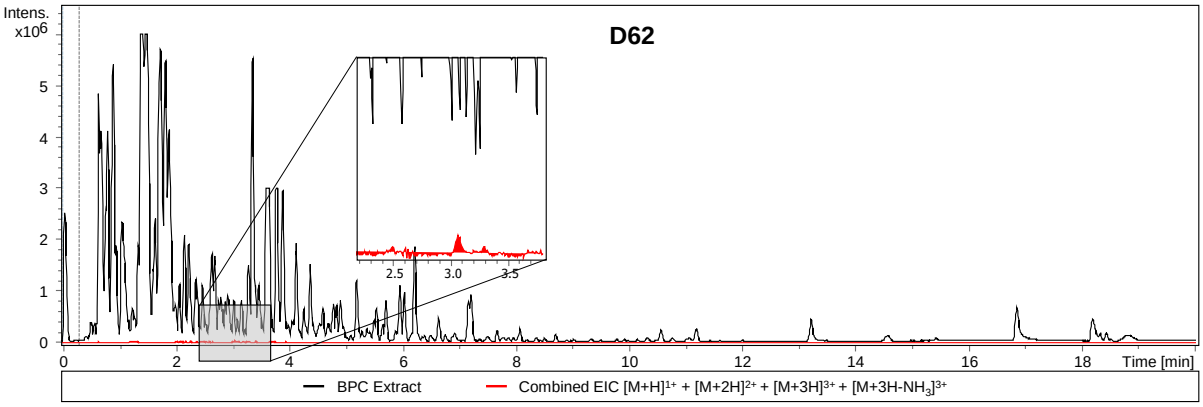

Figure S 97: Chromatogram of the *E. coli* BL21 (DE3) pNOSO-darABCDE-62 extract. The red trace shows the combined EIC for the $[M+H]^{1+}$, $[M+2H]^{2+}$, $[M+3H]^{3+}$ and $[M+3H\text{-}NH_3]^{3+}$ species of **D62** at their calculated masses, respectively (**Table S 4**) ±0.02 Da. The BPC of the whole extract from fermentation broth supernatant is presented in black.

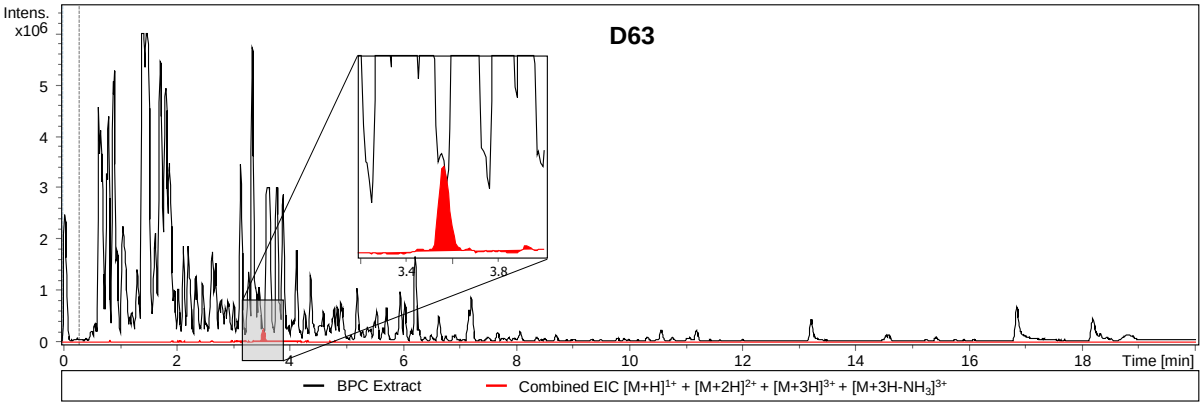

Figure S 98: Chromatogram of the *E. coli* BL21 (DE3) pNOSO-darABCDE-63 extract. The red trace shows the combined EIC for the $[M+H]^{1+}$, $[M+2H]^{2+}$, $[M+3H]^{3+}$ and $[M+3H\text{-}NH_3]^{3+}$ species of **D63** at their calculated masses, respectively (**Table S 4**) ±0.02 Da. The BPC of the whole extract from fermentation broth supernatant is presented in black.

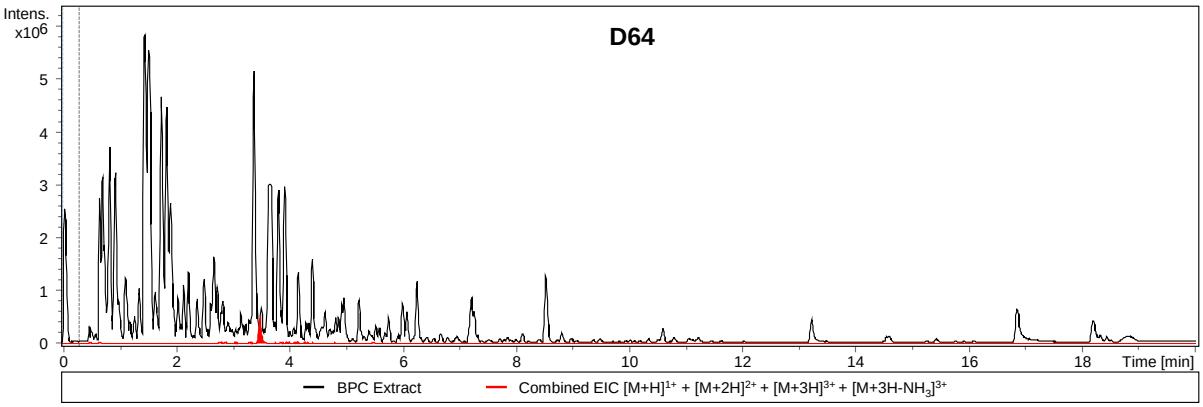

Figure S 99: Chromatogram of the *E. coli* BL21 (DE3) pNOSO-darABCDE-64 extract. The red trace shows the combined EIC for the $[M+H]^{1+}$, $[M+2H]^{2+}$, $[M+3H]^{3+}$ and $[M+3H\text{-}NH_3]^{3+}$ species of **D64** at their calculated masses, respectively (**Table S 4**) ±0.02 Da. The BPC of the whole extract from fermentation broth supernatant is presented in black.

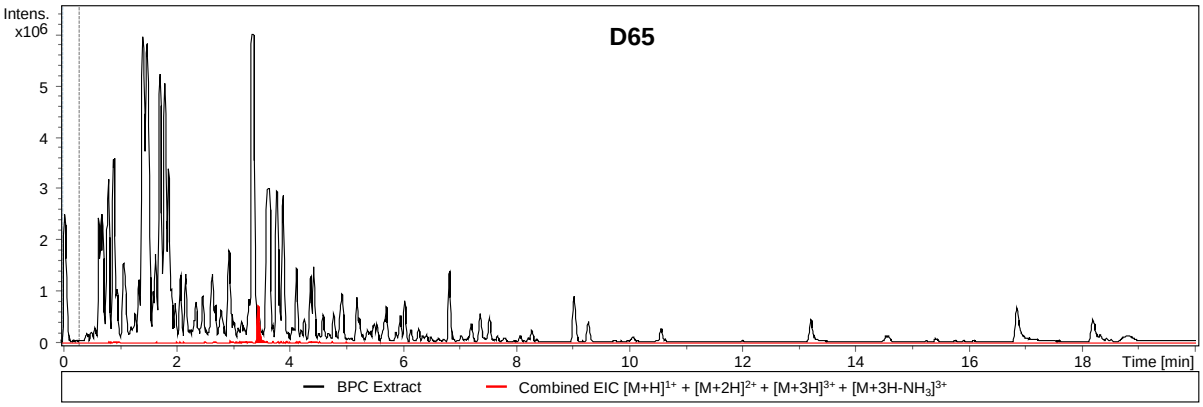

Figure S 100: Chromatogram of the *E. coli* BL21 (DE3) pNOSO-darABCDE-65 extract. The red trace shows the combined EIC for the $[M+H]^{1+}$, $[M+2H]^{2+}$, $[M+3H]^{3+}$ and $[M+3H\text{-}NH_3]^{3+}$ species of **D65** at their calculated masses, respectively (**Table S 4**) ±0.02 Da. The BPC of the whole extract from fermentation broth supernatant is presented in black.

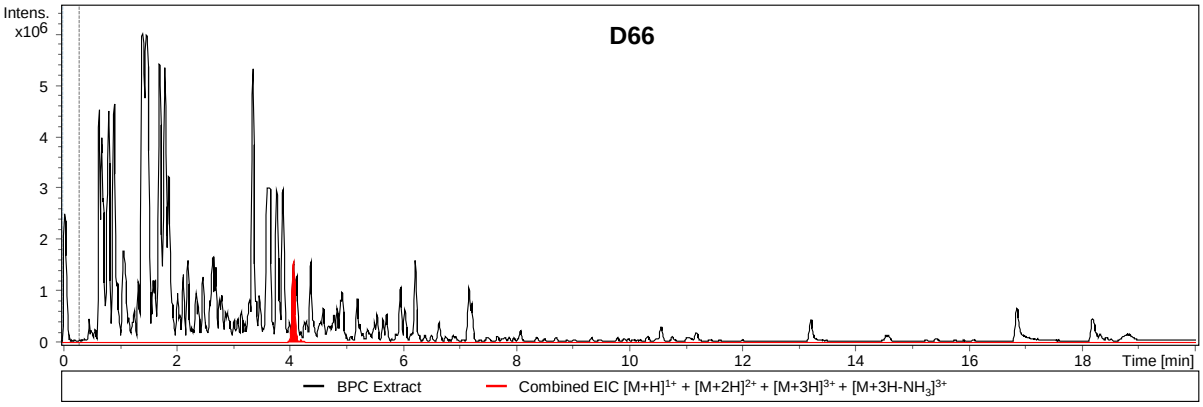

Figure S 101: Chromatogram of the *E. coli* BL21 (DE3) pNOSO-darABCDE-66 extract. The red trace shows the combined EIC for the $[M+H]^{1+}$, $[M+2H]^{2+}$, $[M+3H]^{3+}$ and $[M+3H\text{-}NH_3]^{3+}$ species of **D66** at their calculated masses, respectively (Table S 4) ±0.02 Da. The BPC of the whole extract from fermentation broth supernatant is presented in black. , The L-cysteine of **D66** is linked to another L-cysteine and lactic acid via a disulfide bond (Table S 5, Figure S 11 and S 29), as was shown for **D6** and **D32** in previous studies.[4,5]

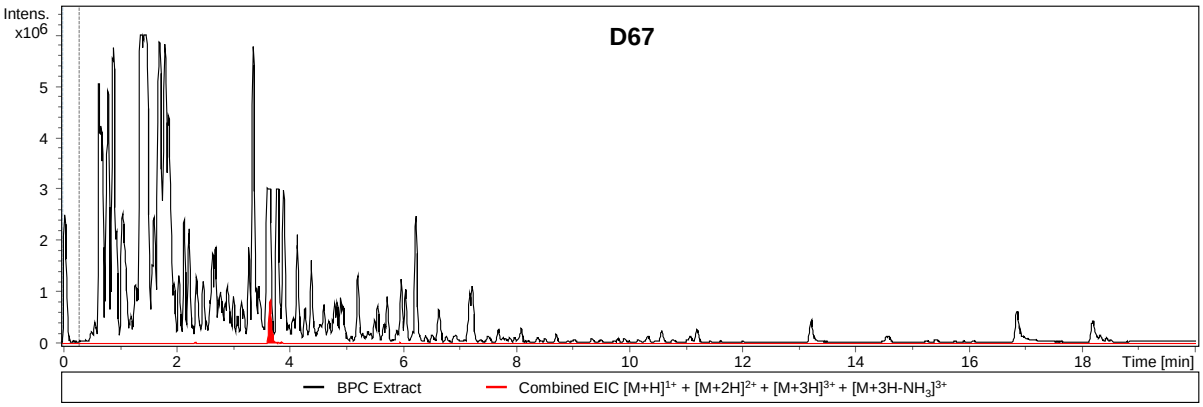

Figure S 102: Chromatogram of the *E. coli* BL21 (DE3) pNOSO-darABCDE-67 extract. The red trace shows the combined EIC for the $[M+H]^{1+}$, $[M+2H]^{2+}$, $[M+3H]^{3+}$ and $[M+3H\text{-}NH_3]^{3+}$ species of **D67** at their calculated masses, respectively (**Table S 4**) ±0.02 Da. The BPC of the whole extract from fermentation broth supernatant is presented in black.

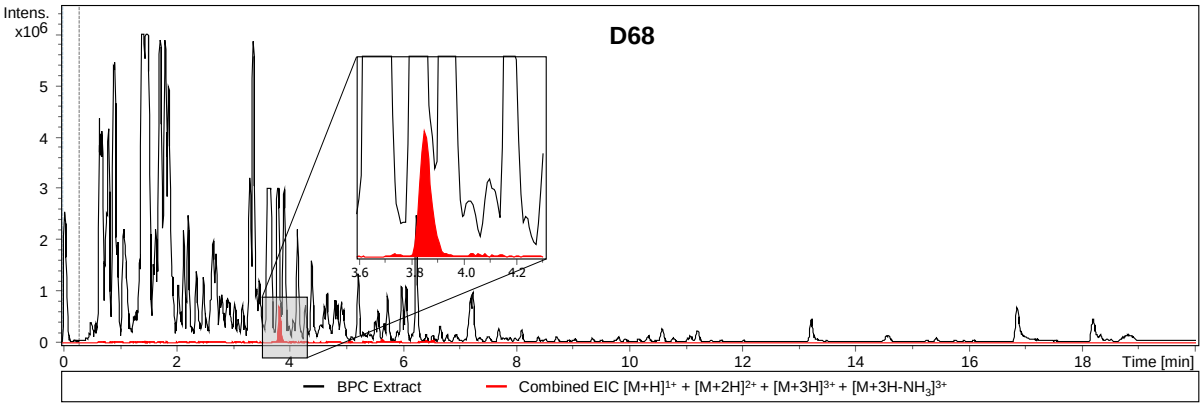

Figure S 103: Chromatogram of the *E. coli* BL21 (DE3) pNOSO-darABCDE-68 extract. The red trace shows the combined EIC for the $[M+H]^{1+}$, $[M+2H]^{2+}$, $[M+3H]^{3+}$ and $[M+3H\text{-}NH_3]^{3+}$ species of **D68** at their calculated masses, respectively (**Table S 4**) ±0.02 Da. The BPC of the whole extract from fermentation broth supernatant is presented in black.

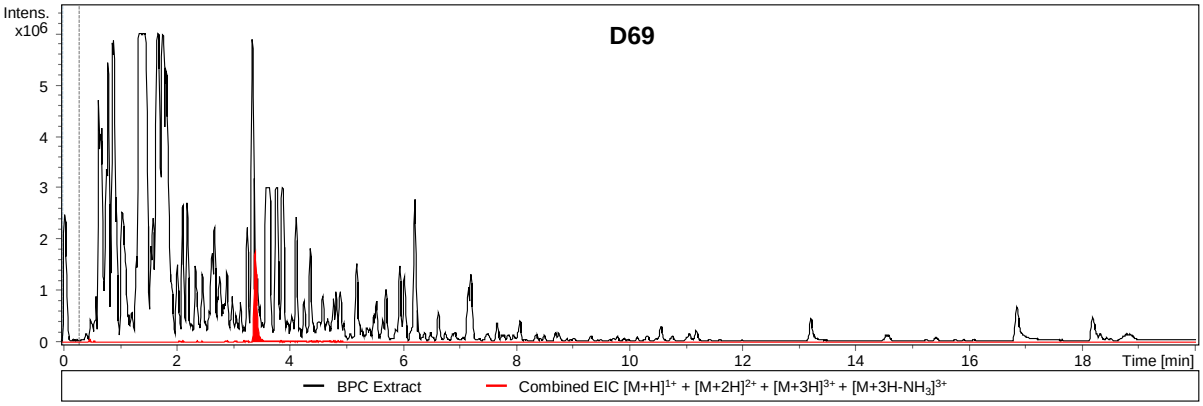

Figure S 104: Chromatogram of the *E. coli* BL21 (DE3) pNOSO-darABCDE-69 extract. The red trace shows the combined EIC for the $[M+H]^{1+}$, $[M+2H]^{2+}$, $[M+3H]^{3+}$ and $[M+3H\text{-}NH_3]^{3+}$ species of **D69** at their calculated masses, respectively (**Table S 4**) ±0.02 Da. The BPC of the whole extract from fermentation broth supernatant is presented in black.

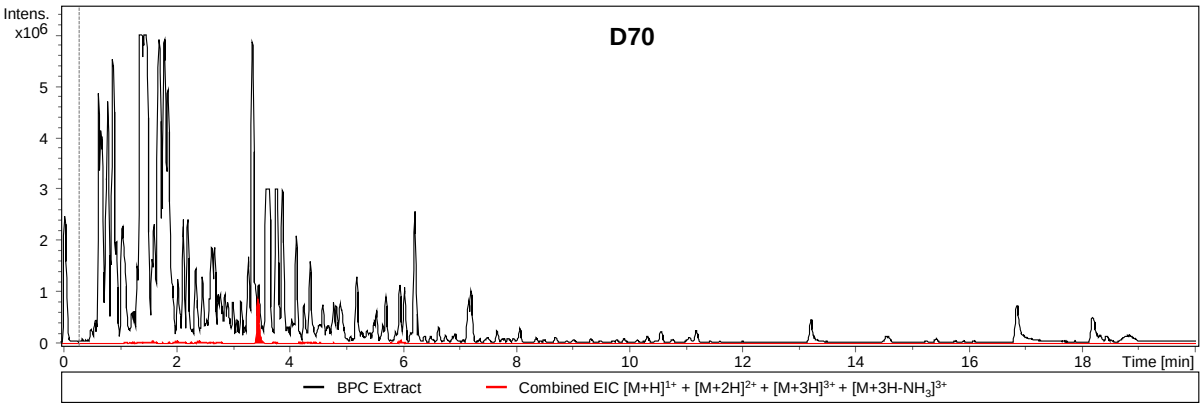

Figure S 105: Chromatogram of the *E. coli* BL21 (DE3) pNOSO-darABCDE-70 extract. The red trace shows the combined EIC for the $[M+H]^{1+}$, $[M+2H]^{2+}$, $[M+3H]^{3+}$ and $[M+3H\text{-}NH_3]^{3+}$ species of **D70** at their calculated masses, respectively (**Table S 4**) ±0.02 Da. The BPC of the whole extract from fermentation broth supernatant is presented in black.

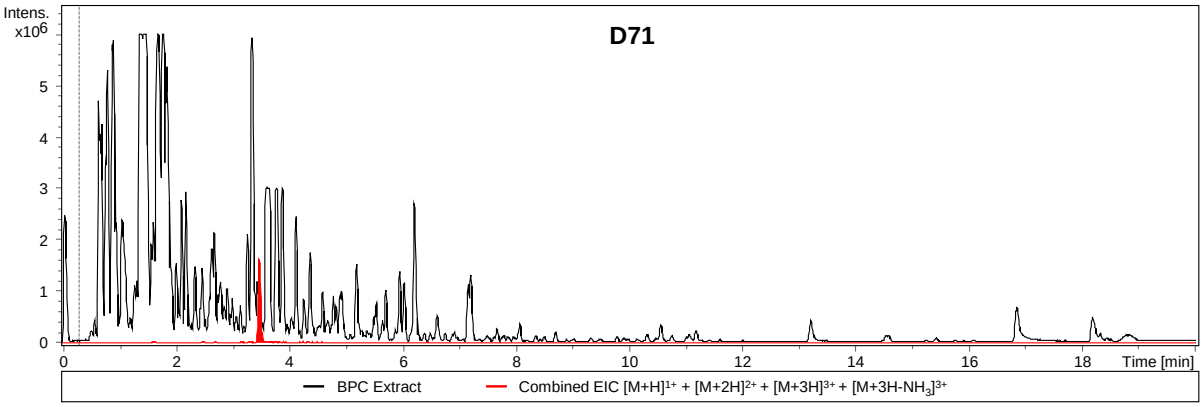

Figure S 106: Chromatogram of the *E. coli* BL21 (DE3) pNOSO-darABCDE-71 extract. The red trace shows the combined EIC for the $[M+H]^{1+}$, $[M+2H]^{2+}$, $[M+3H]^{3+}$ and $[M+3H\text{-}NH_3]^{3+}$ species of **D71** at their calculated masses, respectively (**Table S 4**) ±0.02 Da. The BPC of the whole extract from fermentation broth supernatant is presented in black.

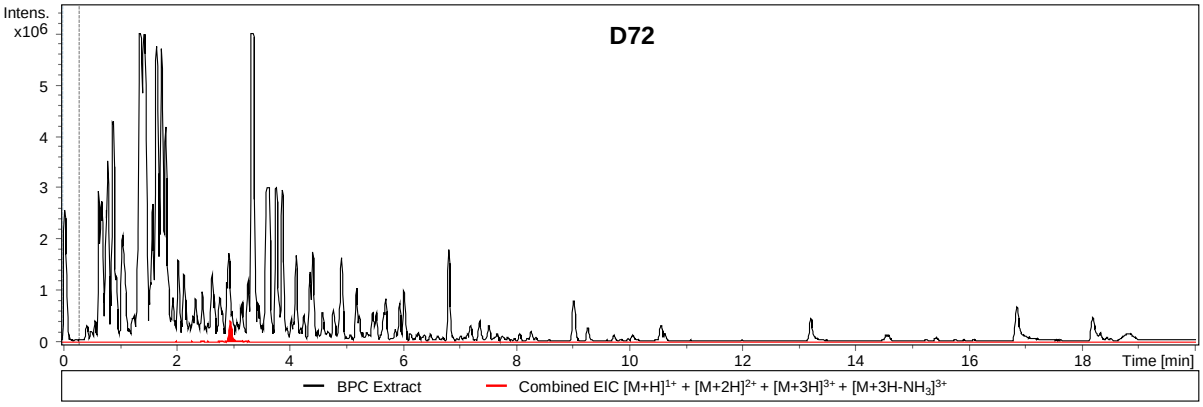

Figure S 107: Chromatogram of the *E. coli* BL21 (DE3) pNOSO-darABCDE-72 extract. The red trace shows the combined EIC for the $[M+H]^{1+}$, $[M+2H]^{2+}$, $[M+3H]^{3+}$ and $[M+3H\text{-}NH_3]^{3+}$ species of **D72** at their calculated masses, respectively (**Table S 4**) ±0.02 Da. The BPC of the whole extract from fermentation broth supernatant is presented in black.

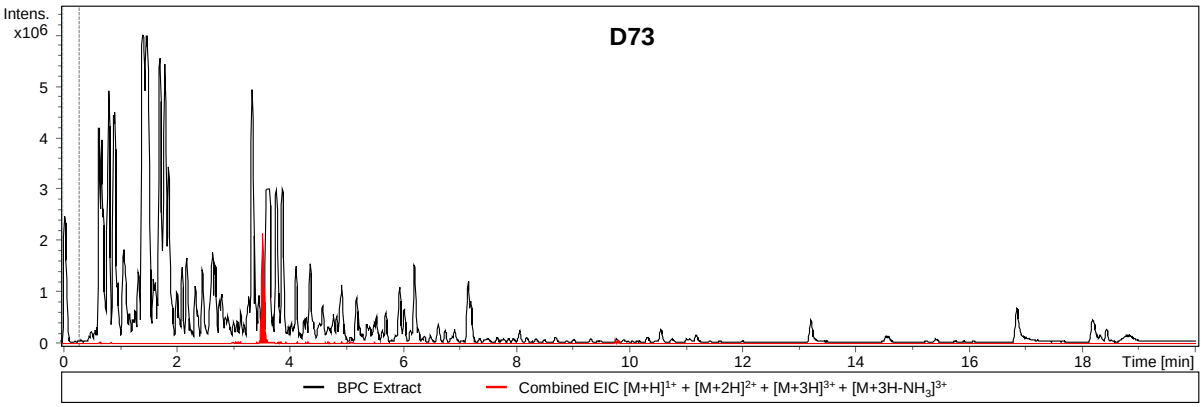

Figure S 108: Chromatogram of the *E. coli* BL21 (DE3) pNOSO-darABCDE-73 extract. The red trace shows the combined EIC for the $[M+H]^{1+}$, $[M+2H]^{2+}$, $[M+3H]^{3+}$ and $[M+3H-NH_3]^{3+}$ species of **D73** at their calculated masses, respectively (**Table S 4**) ±0.02 Da. The BPC of the whole extract from fermentation broth supernatant is presented in black.

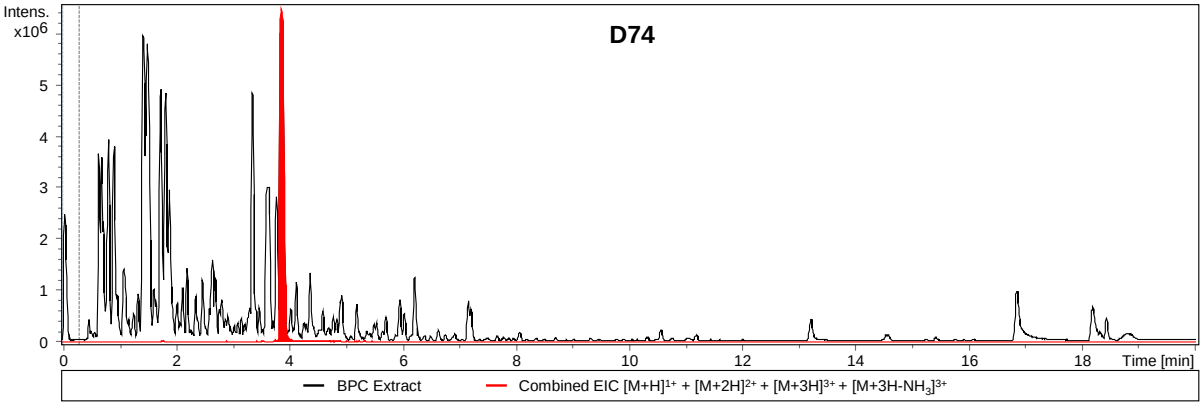

Figure S 109: Chromatogram of the *E. coli* BL21 (DE3) pNOSO-darABCDE-74 extract. The red trace shows the combined EIC for the $[M+H]^{1+}$, $[M+2H]^{2+}$, $[M+3H]^{3+}$ and $[M+3H-NH_3]^{3+}$ species of **D74** at their calculated masses, respectively (**Table S 4**) ±0.02 Da. The BPC of the whole extract from fermentation broth supernatant is presented in black.

3. MS^2 spectra analysis of darobactin analogues

The MS^2 spectra of all novel darobactin analogues are shown in Figure S 21-37. The blue quadratic symbols

display the precursor ion, which was picked for fragmentation. The $[M\text{-}NH_3+2H]^{2+}$ fragment and the derivative related typical b2-ion with ammonia loss can be observed and allow the further verification of modifications (Figure S 20). The theoretical mass of all derivatives and the ions for the most characteristic fragmentation pattern are displayed in table S 5.

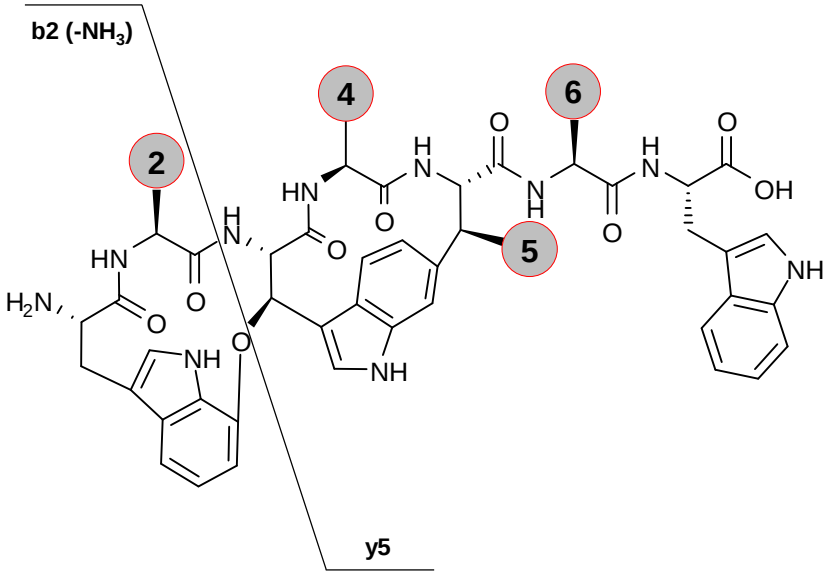

Figure S 110: MS^2 fragmentation pattern of darobactin analogues. The most characteristic ions in the MS^2 fragmentation pattern (b2 with or without ammonia loss and y5) are calculated and observed as described in the methods and displayed in Table S 5.

Table S 5: Calculated (calc.) and observed (obs.) masses of the typical b2 and y5 fragment ions. The novel darobactins with highlighted modifications in the core peptide in comparison to **D22** are summarized (differences in red). The calc. and obs. masses in the extracts of the $[M\text{-}NH_3+2H]^{2+}$ and the calc. and obs. typical b2 and y5 ion masses with ammonia loss are displayed.

Darobactin	Core peptide	calc. $[M\text{-}NH_3+2H]^{2+}$	obs. $[M\text{-}NH_3+2H]^{2+}$	calc. b2 – NH_3	obs. b2 – NH_3	calc. y5	obs. y5
58	W E W T K R W	543.7432	543.7384	315.0975	315.0959	772.3889	772.3822
59	W K W T K R W	543.2694	543.2674	314.1499	314.1434	772.3889	772.3831
60	W D W T K R W	536.7354	536.7287	301.0819	301.0796	772.3889	772.3799
61	W Q W T K R W	543.2512	543.2455	314.1135	314.1119	772.3889	772.3828
62	W R W T K R W	557.2673	557.2682	342.1561	342.1489	772.3889	772.3765
63	W V W T K R W	528.7561	528.7522	285.1234	285.1204	772.3889	772.3851
64	W S W T K R W	522.7380	522.7348	273.0870	273.0871	772.3889	772.3789
65	W S W T K K W	508.7349	508.7324	273.0870	273.1228	744.3828	744.3780
66	W N W T K C W	605.2012	605.2035	300.0979	300.0957	910.3222	910.3113
67	W Y W T K R W	560.7536	560.7478	349.1183	349.1139	772.3889	772.3809
68	W L W T K R W	535.7640	535.7581	299.1390	299.1383	772.3889	772.3808
69	W Q W S K R W	536.2434	536.2369	314.1135	314.1114	758.3733	758.3649
70	W S W S K R W	515.7301	515.7247	273.0870	273.0859	758.3733	758.3635
71	W E W S K R W	536.7354	536.7316	315.0975	315.0965	758.3733	758.3684
72	W K W S K R W	536.2616	536.2589	314.1499	314.1817	758.3733	758.3697
73	W D W S K R W	529.7276	529.7237	301.0819	301.0807	758.3733	758.3672
74	W N W T K Q W	522.2221	522.2198	300.0979	300.0967	744.3464	744.3422

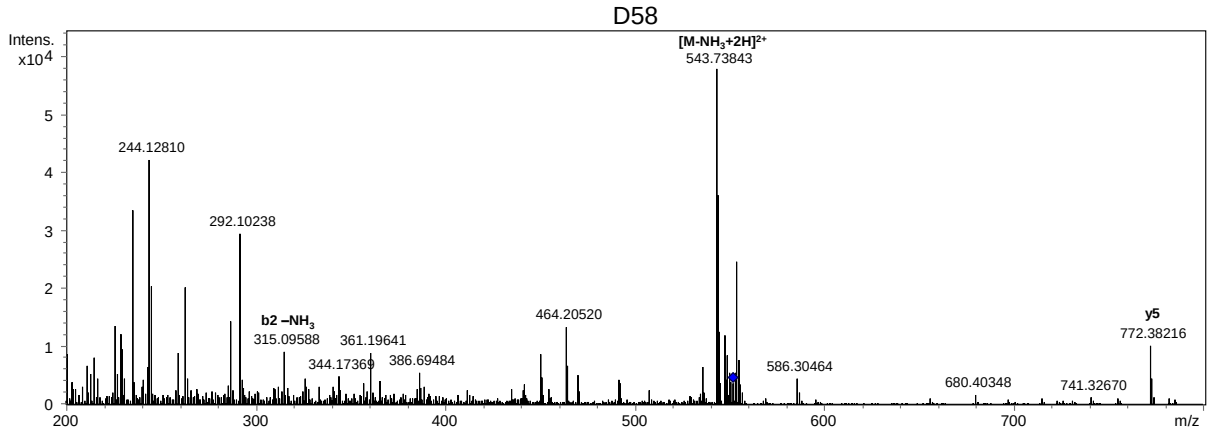

Figure S 111: MS^2 spectrum for D58.

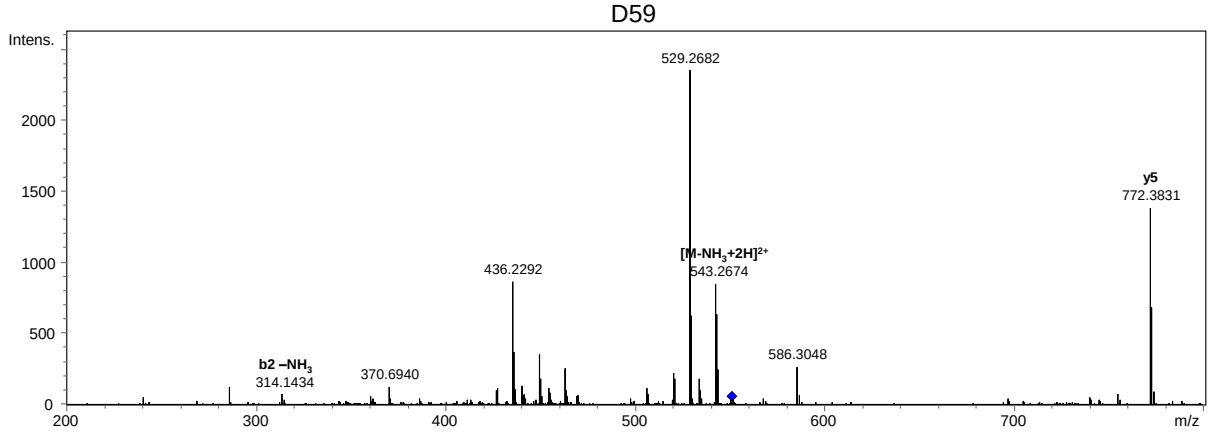

Figure S 112: MS^2 spectrum for D59.

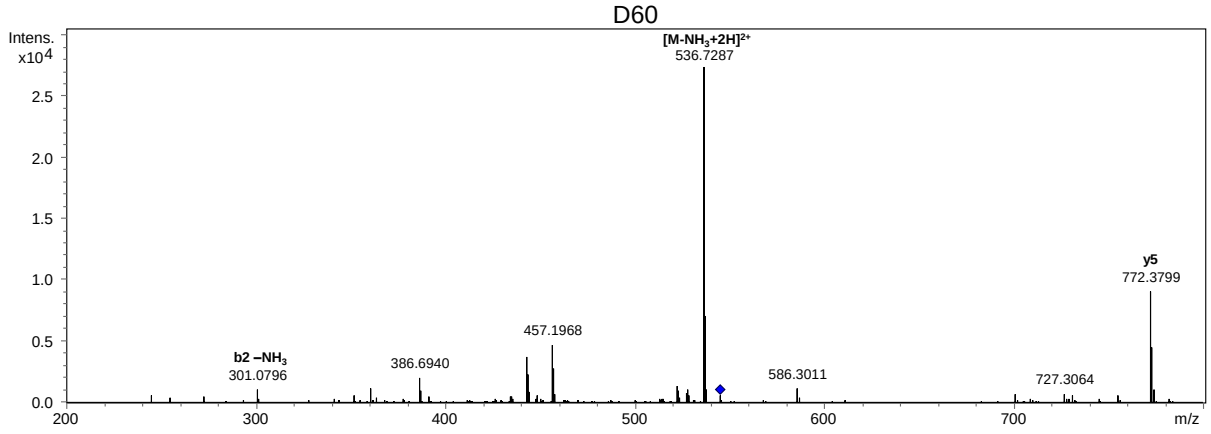

Figure S 113: MS^2 spectrum for D60.

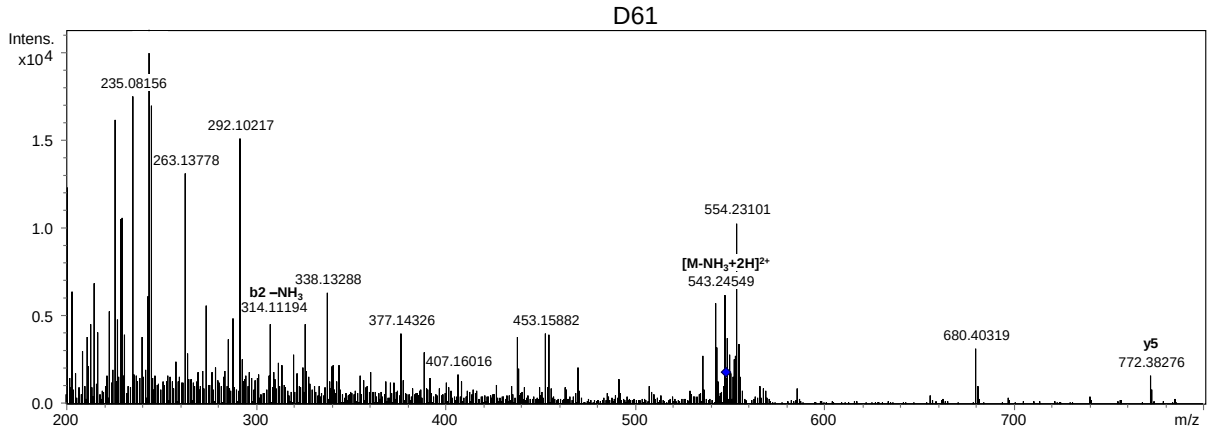

Figure S 114: MS^2 spectrum for D61.

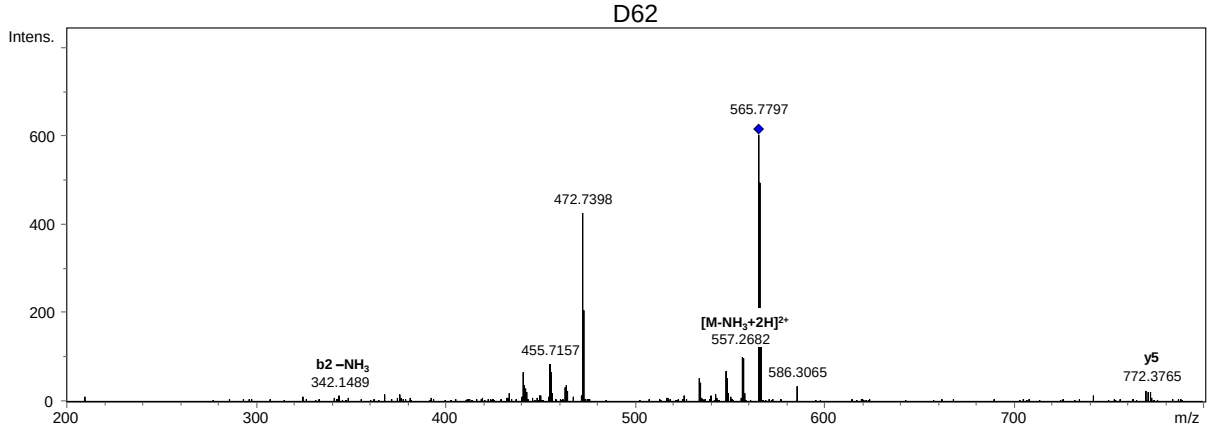

Figure S 115: MS^2 spectrum for D62.

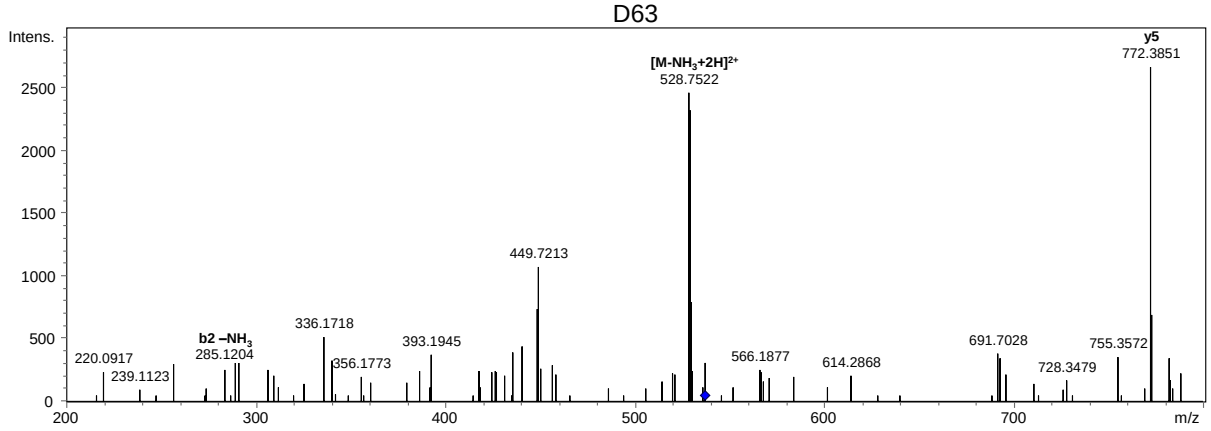

Figure S 116: MS^2 spectrum for D63.

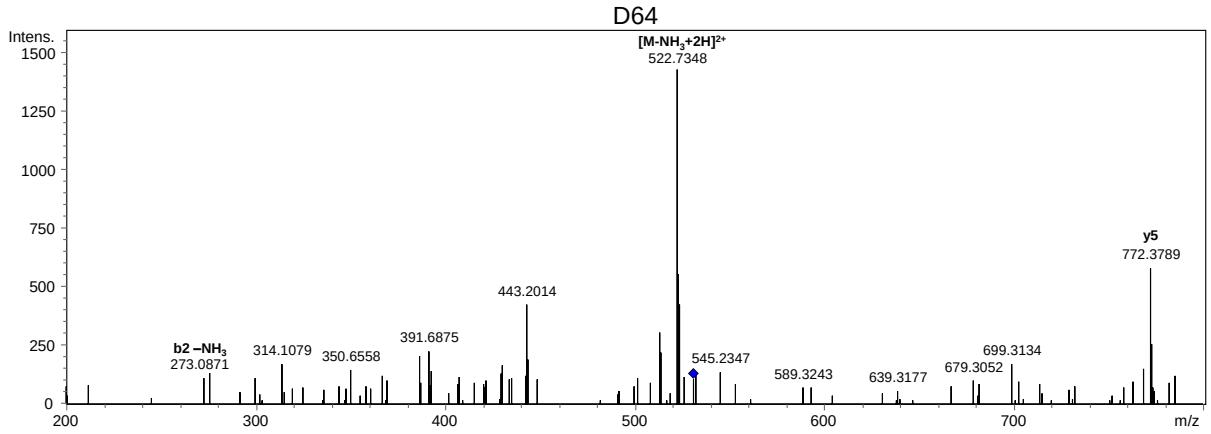

Figure S 117: MS^2 spectrum for D64.

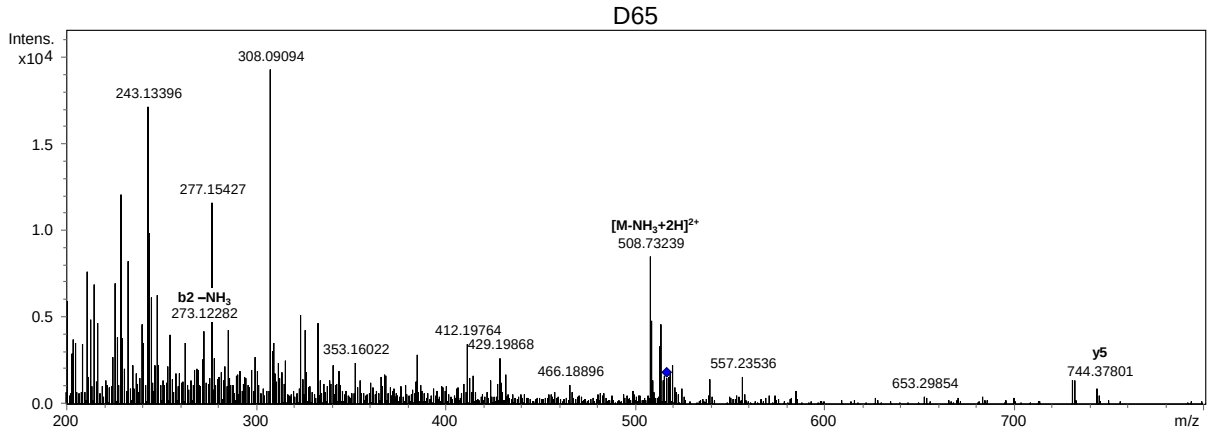

Figure S 118: MS^2 spectrum for D65.

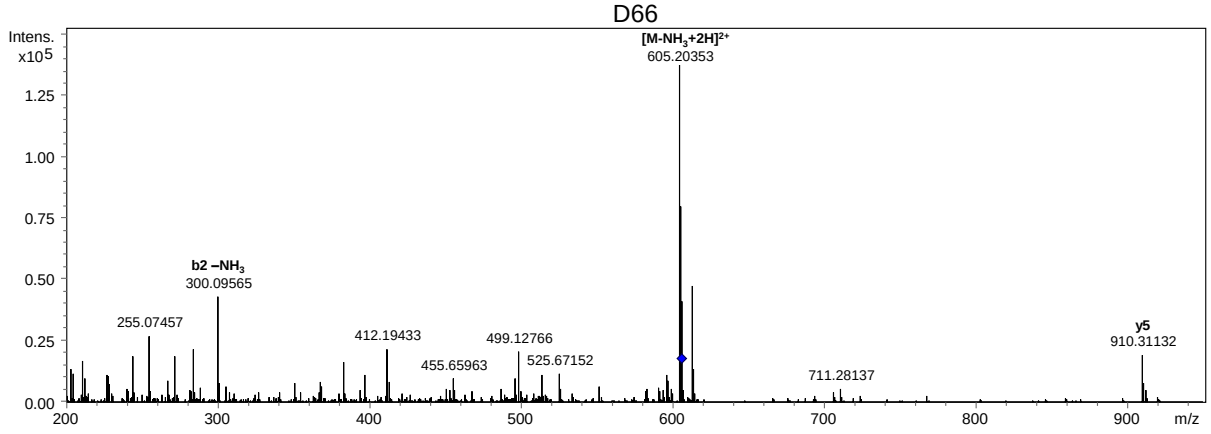

Figure S 119: MS^2 spectrum for D66.

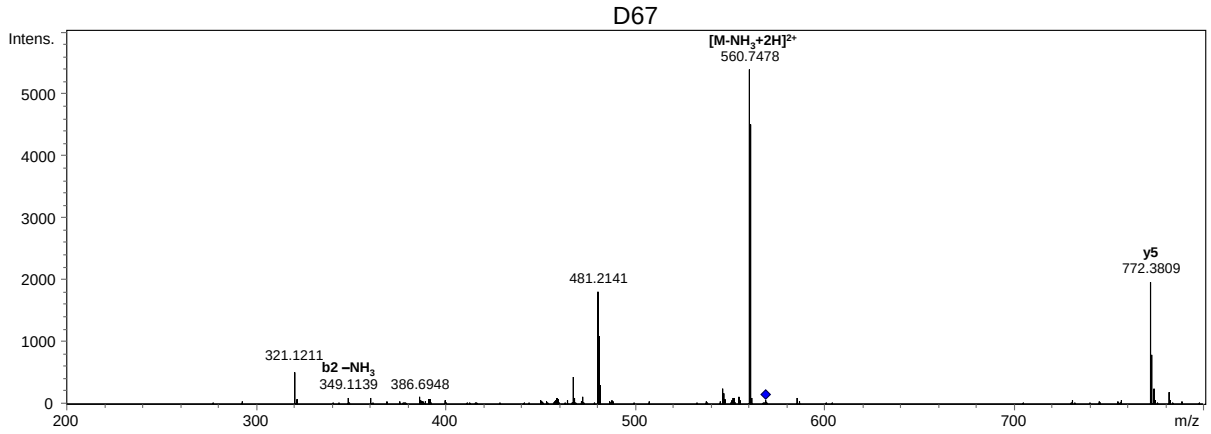

Figure S 120: MS^2 spectrum for D67.

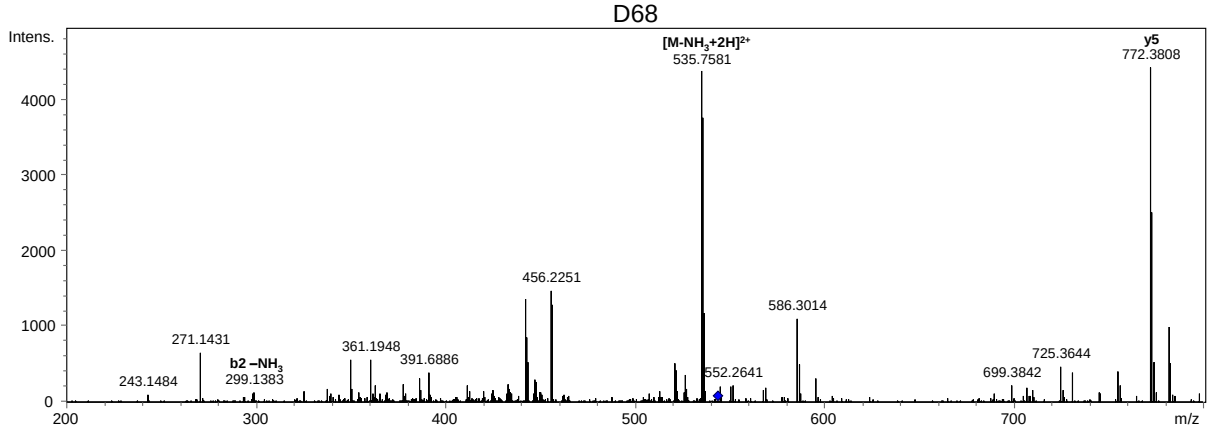

Figure S 121: MS^2 spectrum for D68.

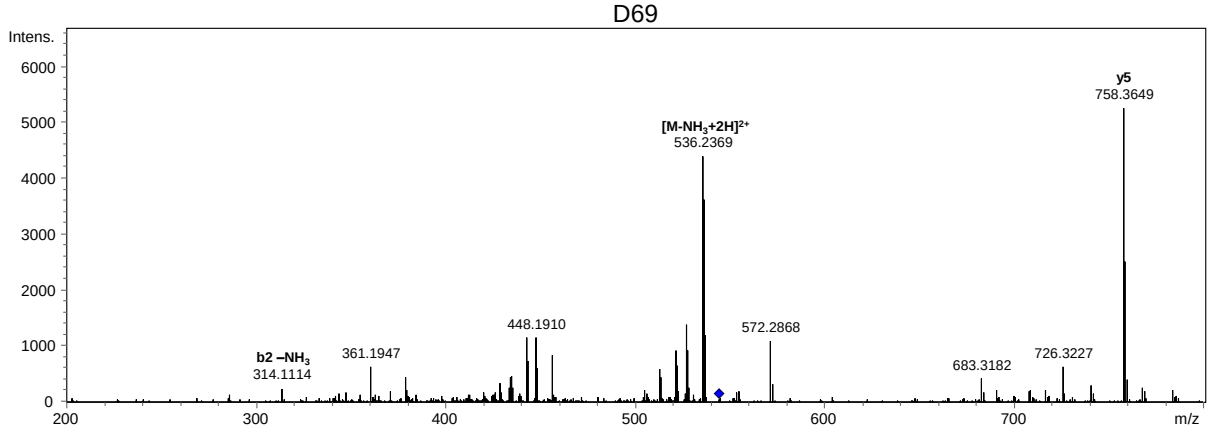

Figure S 122: MS^2 spectrum for D69.

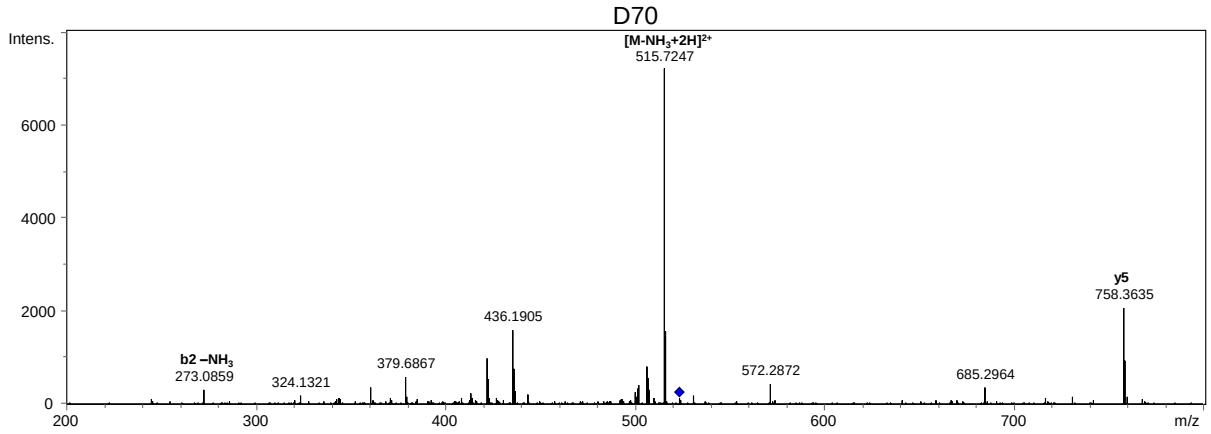

Figure S 123: MS² spectrum for D70.

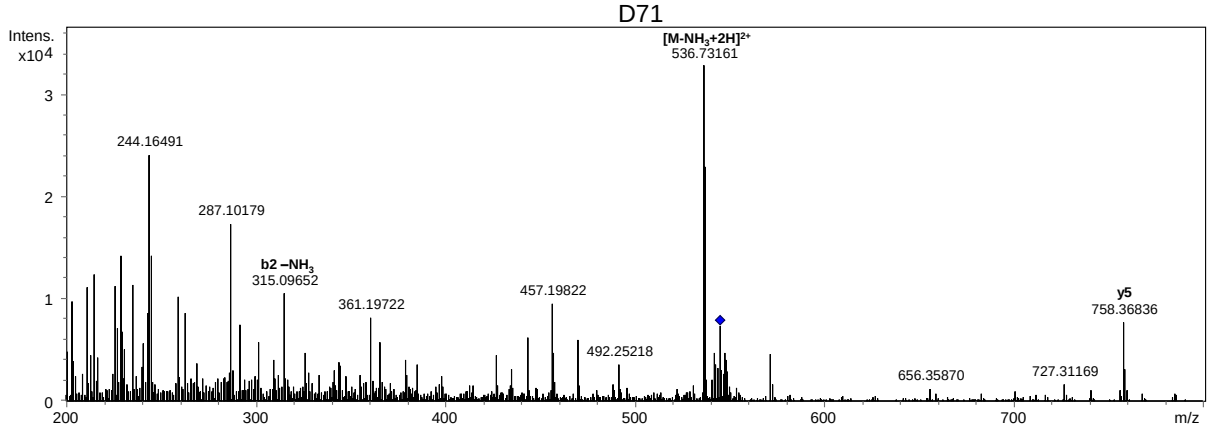

Figure S 124: MS² spectrum for D71.

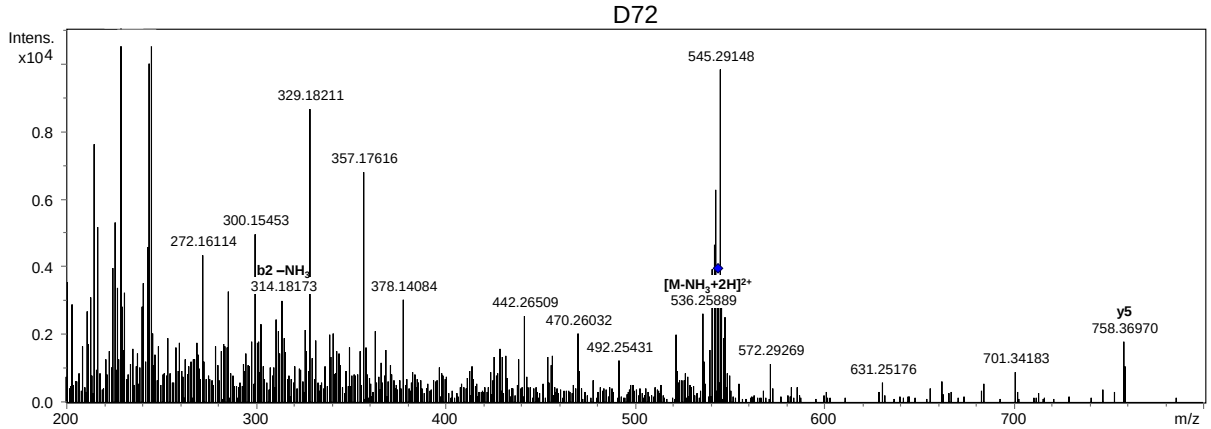

Figure S 125: MS² spectrum for D72.

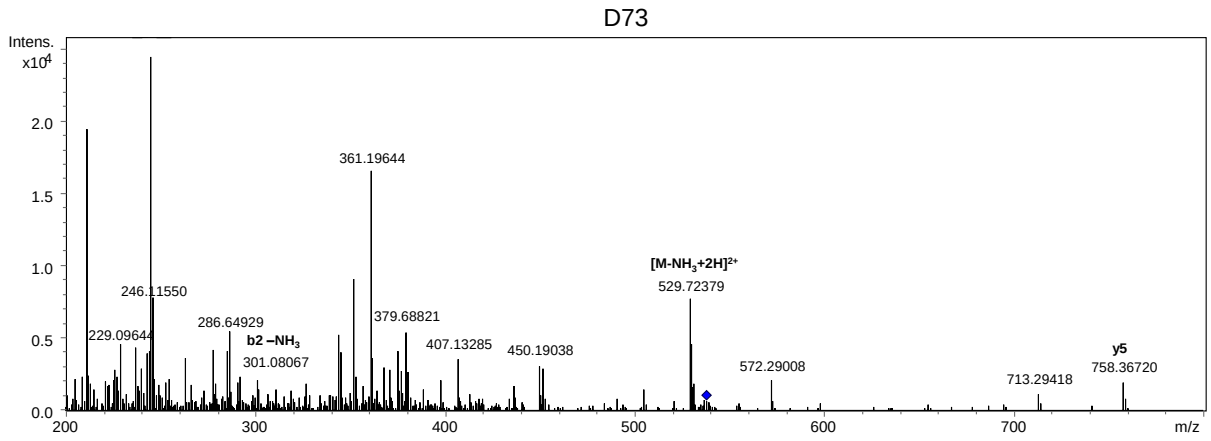

Figure S 126: MS^2 spectrum for D73.

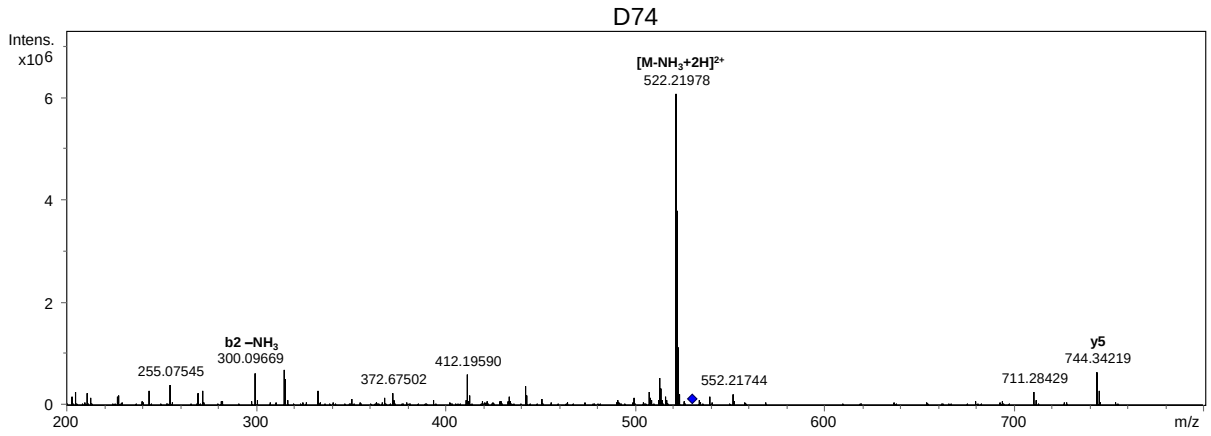

Figure S 127: MS^2 spectrum for D74.

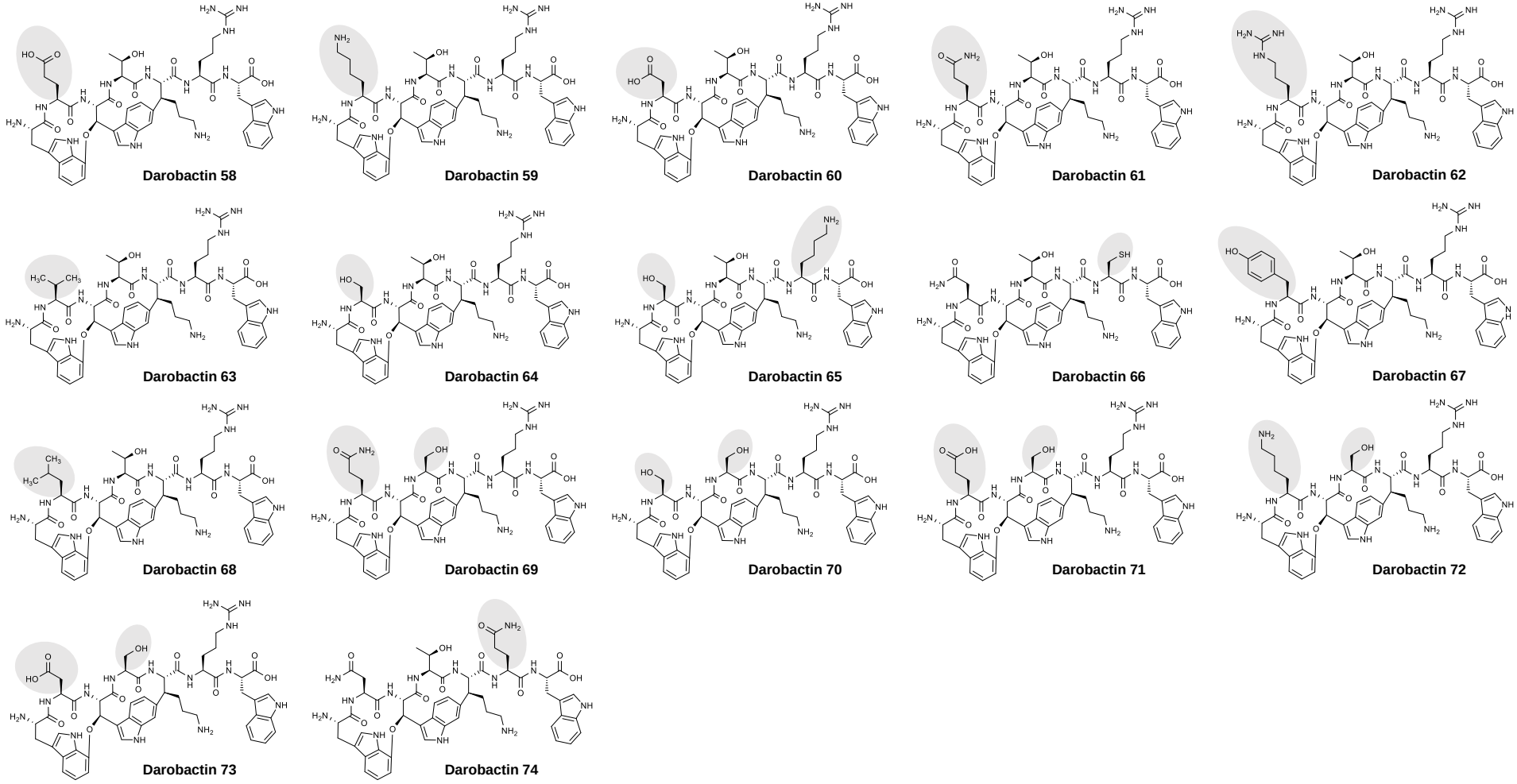

Figure S 128: Overview of all generated novel darobactin analogues. **D58** to **D74** are displayed and positions of heptapeptide with amino acid exchange compared to **D22** amino acid sequence were highlighted in grey. Structures were predicted using MS^2 analysis. **D69** was verified via NMR spectrometry (Table S 7, Figure S 39 – S44).

4. Antibiogram of clinical *P. aeruginosa* isolates

Table S 6: Antibiogram of clinical *P. aeruginosa* isolates. Antibacterial activity of **D22** and **D69** were evaluated in parallel with meropenem and ciprofloxacin (CIP) as controls (Table 4). The minimal inhibitory concentration (MIC) of **D22** and **D69** is comparable to the antibiotics Mereopenem and CIP. Broncheoalveolar lavage (BAL); permanent catheter urine (PK-urine); resistant (R); multi-resistant pathogen (MRP); multi-resistant Gram-negative pathogens with resistance against four of four groups of antibiotics (4MNGR).

		resistance profile, MIC [µg mL^{-1}]		
	material	MRP	Meropenem	CIP
P. aeroginosa 83979	BAL	4MRGN	> 16 (R)	> 4 (R)
P. aeroginosa 84389	PK-urine	4MRGN	16 (R)	4 (R)

5. Quantification of production

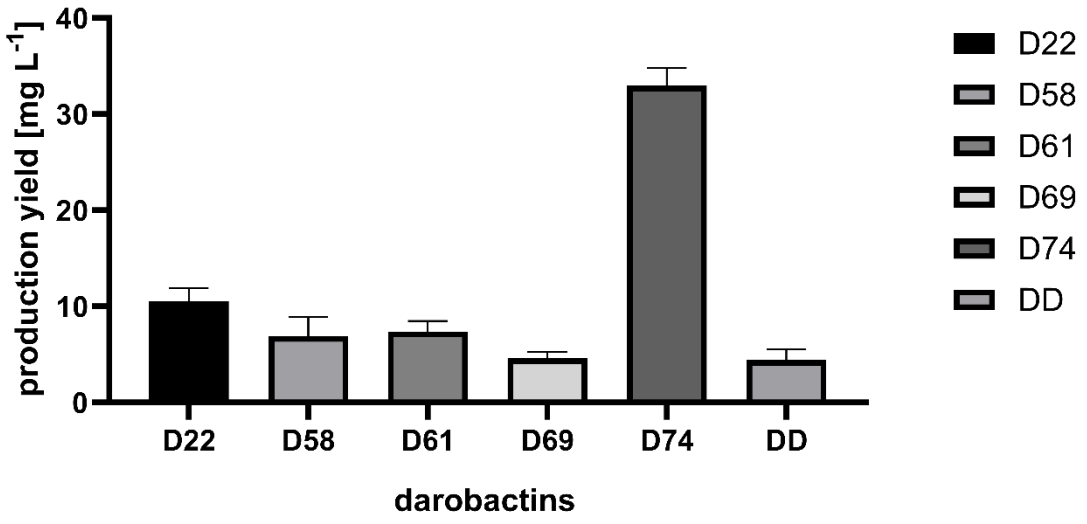

Figure S 129: Production yield of darobactin D22, D69 and D74. HPLC UV quantification of production yield was calculated by integration across the chromatographic UV peak area of each derivative. Eight (**D22**, **D69**), ten (**D74**) and twelve (**D58**, **D61**, **DD**) replicates were compared. The production yields of **D22** achieved 10.5 ± 0.9 mg per liter, of **D58** 6.9 ± 2.0 mg per liter, of **D61** 7.4 ± 1.1 mg per liter, of **D69** 4.6 ± 0.6 mg per liter**,** of **D74** 33 ± 1.7 mg per liter and of **DD** 4.4 ± 1.1 mg per liter, respectively.

6. NMR spectroscopic data

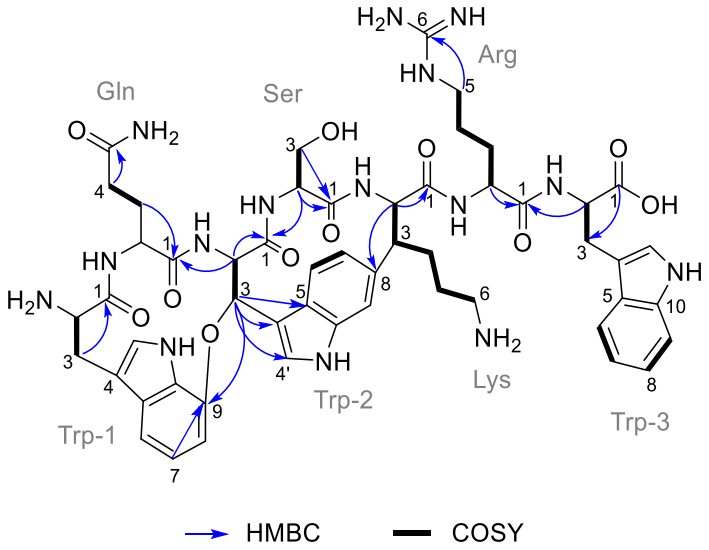

Table S 7: NMR Spectroscopic Data for D69[a].

		δ_C[b], type	δ_H[c], (J in Hz)	COSY[d]	HMBC[e]
Trp-3	1	174.9, C	-	-	-
	2	53.7, CH	4.99, t (5.5)	3	1, 3, 4, Arg-1
	3	26.6, CH_2	3.63, m	2	1, 2, 4, 4', 5
	4'	124.0, CH	7.56, s	-	3, 4, 5, 9, 10
	4	109.0, C	-	-	-
	5	127.0, C	-	-	-
	6	118.1, CH	7.95, br d (7.5)	7	4, 5, 8, 10
	7	118.9, CH	7.45, m	6, 8	5, 6, 8, 9
	8	121.4, CH	7.53, m	7, 9	6, 10
	9	111.4, CH	7.81, br d (7.9)	8	5, 7
	10	135.9, C	-	-	-
Arg	1	171.9, C	-	-	-
	2	52.9, CH	4.60, br t (6.3)	3ab	1, 3
	3a	27.8, CH_2	1.88, m	2, 3b, 4	1, 2, 4, 5
	3b		2.02, m	2, 3a, 4	1, 2, 4, 5
	4	23.9, CH_2	1.74, m	3, 5	2, 5
	5	40.0, CH_2	3.34, m	4	3, 4, 6
	6	156.3, C	-	-	-
Lys	1	170.8, C	-	-	-
	2	59.7, CH	4.39, br d (10.3)	3	1, 3, 4, Ser-1, Trp2-8
	3	47.7, CH	3.21, m	2, 4b	2, 4
	4a	25.2, CH_2	1.82, m	4b, 6	6
	4b		2.12, m	4a, 3	-
	5	25.1, CH_2	2.04, m	4ab, 6	-
	6	38.9, CH_2	3.08, m	4a, 5	4
Ser	1	167.5, C	-	-	-
	2	53.7, CH	4.24, m	3ab	1, Trp2-1

	3a	61.6, CH_2	3.40, m	2	1
	3b		3.46, m	2	1
Trp-2	1	167.6, C	-	-	-
	2	62.9, CH	4.92, d (8.9)	3	1, 3, 4, Gln-1
	3	76.2, CH	6.39, br d (8.9)	2	2, 4, 4', 5, 9
	4’	123.8, CH	8.09, s	-	3, 4, 5, 10
	4	111.6, C	-	-	-
	5	124.6, C	-	-	-
	6	116.7, CH	7.69, d (7.3)	7	8, 10
	7	124.7, CH	7.18, d (7.3)	6	5, 9, Lys-3
	8	132.3, C	-	-	-
	9	110.1, CH	7.67, s	-	5, 8, 10, Lys-3
	10	136.6, C	-	-	-
Gln	1	169.0, C	-	-	-
	2	52.3, CH	3.33, m	3	1
	3	28.7, CH_2	1.78, m	4	-
	4	30.1, CH_2	2.20, m	3	2, 3, 5
	5	177.0, C	-	-	-
Trp-1	1	167.7, C	-	-	-
	2	54.3, CH	4.27, m	3ab	1, 3
	3a	25.9, CH_2	3.80, dd (13.3, 6.8)	2, 3b	1, 2, 4, 4’, 5
	3b		3.54, m	2, 3a	2, 4, 4’, 5
	4’	124.0, CH	7.59, s	-	4, 5, 9, 10
	4	107.8, C	-	-	-
	5	128.7, C	-	-	-
	6	119.6, CH	7.40, m	7	9, 10
	7	113.0, CH	7.44, m	6	5, 8, 9
	8	108.0, CH	7.44, m	-	7, 9, 10
	9	145.0, C	-	-	-
	10	128.6, C	-	-	-

[a]Recorded in D_2O/acetonitrile-d_3 (2:1) + 1% formic acid-d_4 at 318 K. [b]Acquired at 175 MHz, adjusted to the solvent signal of acetonitrile-d_3 (δ_C 118.69 ppm). [c]Acquired at 700 MHz, adjusted to the solvent signal of D_2O (δ_H 4.75 ppm). [d]Proton showing COSY correlation to indicated protons. [e]Proton showing HMBC correlation to indicated carbon.

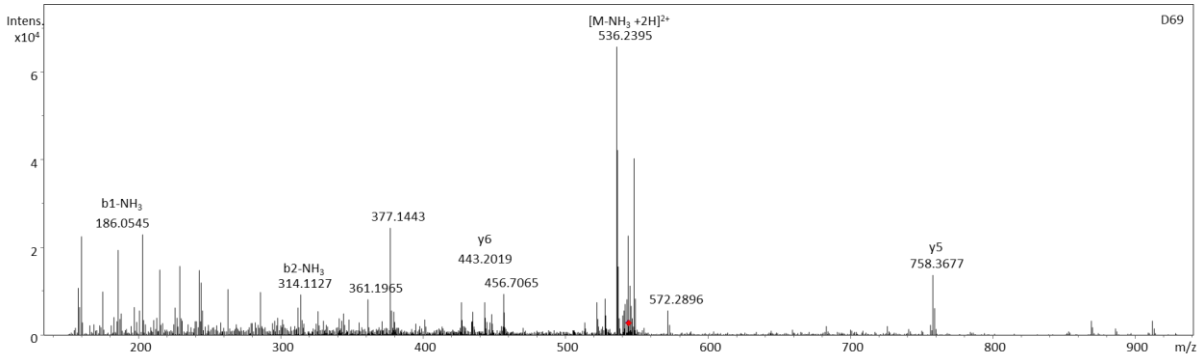

Figure S 130: MS² spectrum of D69. A red rhombus highlights the precursor ion with *m/z* 544.75490, which was picked for fragmentation. Furthermore, the $[M\text{-}NH_3+2H]^{2+}$ fragment and the characteristic b2-NH_3 and y5 fragment can be observed.

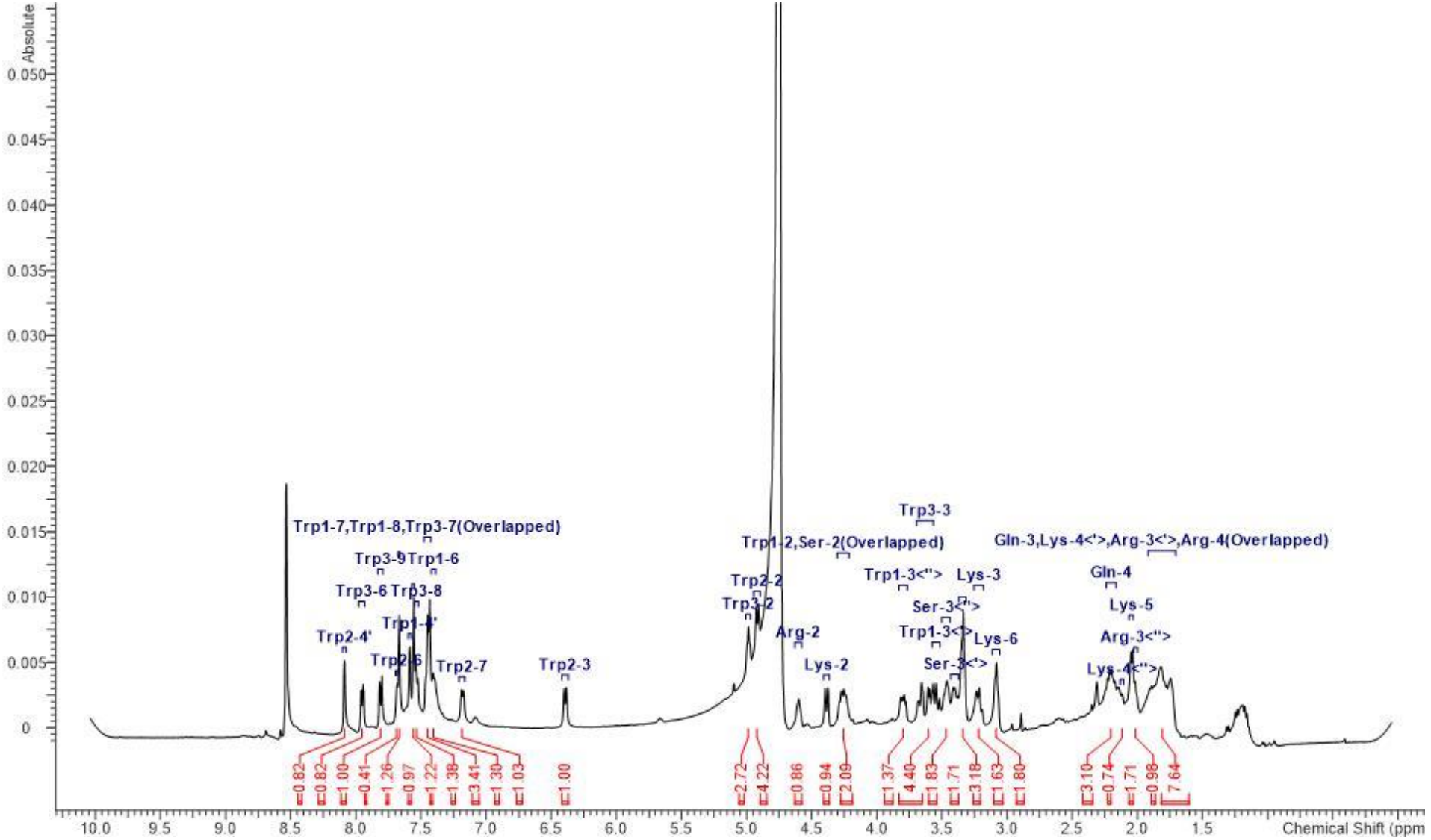

Figure S 131: ^{1}H NMR of D69 recorded in D_2O/acetonitrile-d_3 (2:1) + 1% formic acid-d_4 at 318 K.

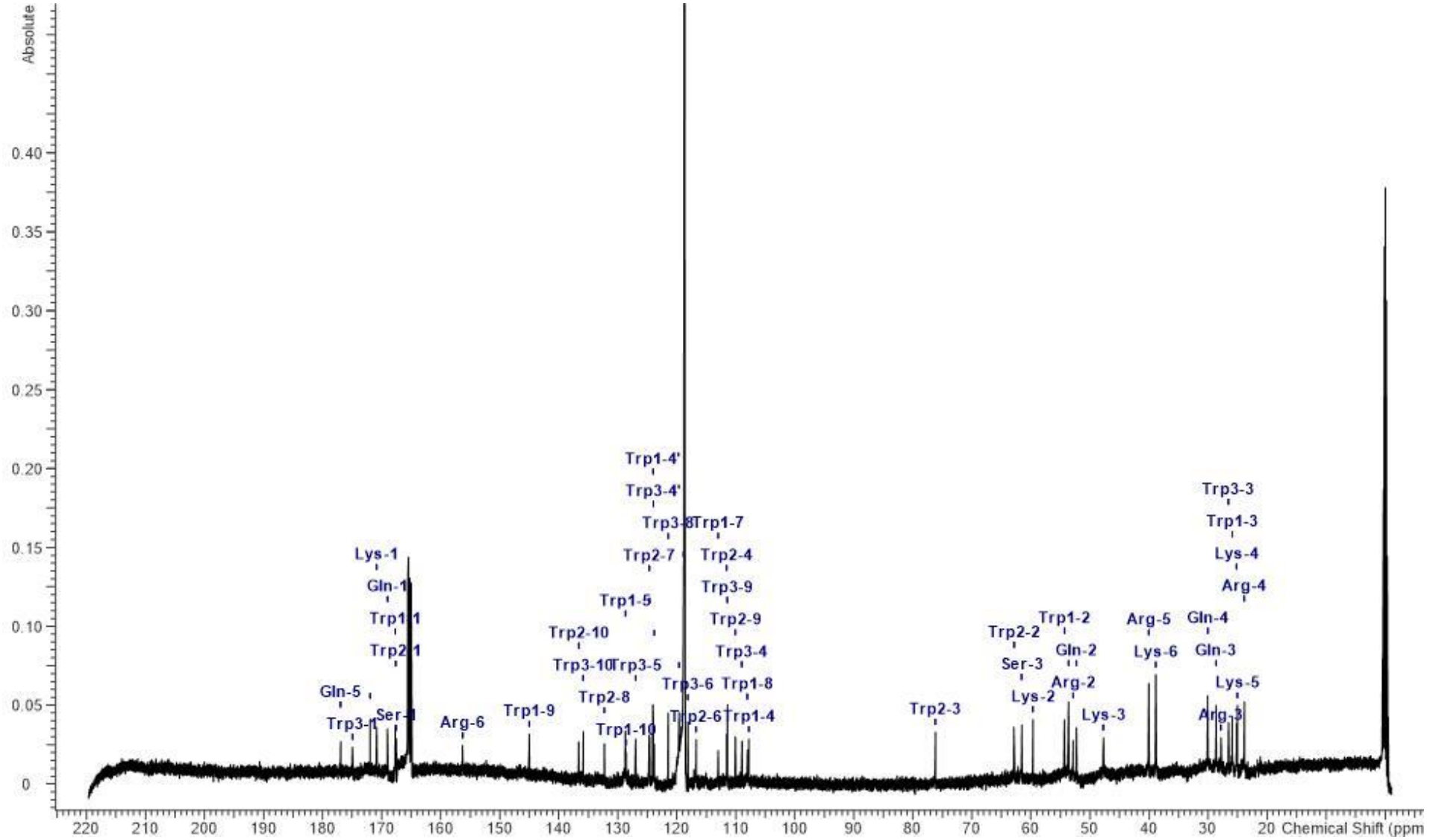

Figure S 132: ^{13}C NMR of D69 recorded in D_2O/acetonitrile-d_3 (2:1) + 1% formic acid-d_4 at 318 K.

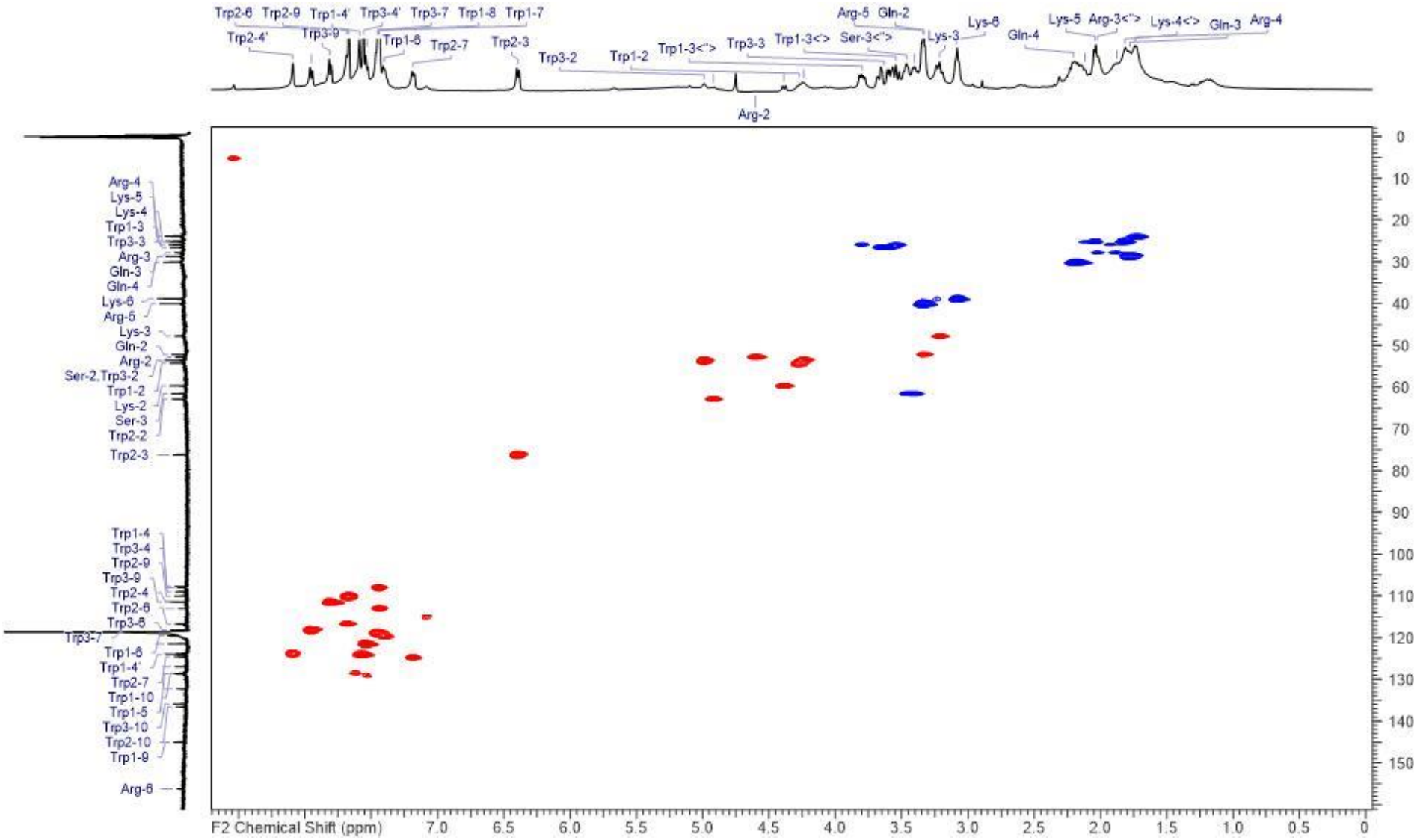

Figure S 133: HSQC NMR of D69 recorded in D_2O/acetonitrile-d_3 (2:1) + 1% formic acid-d_4 at 318 K.

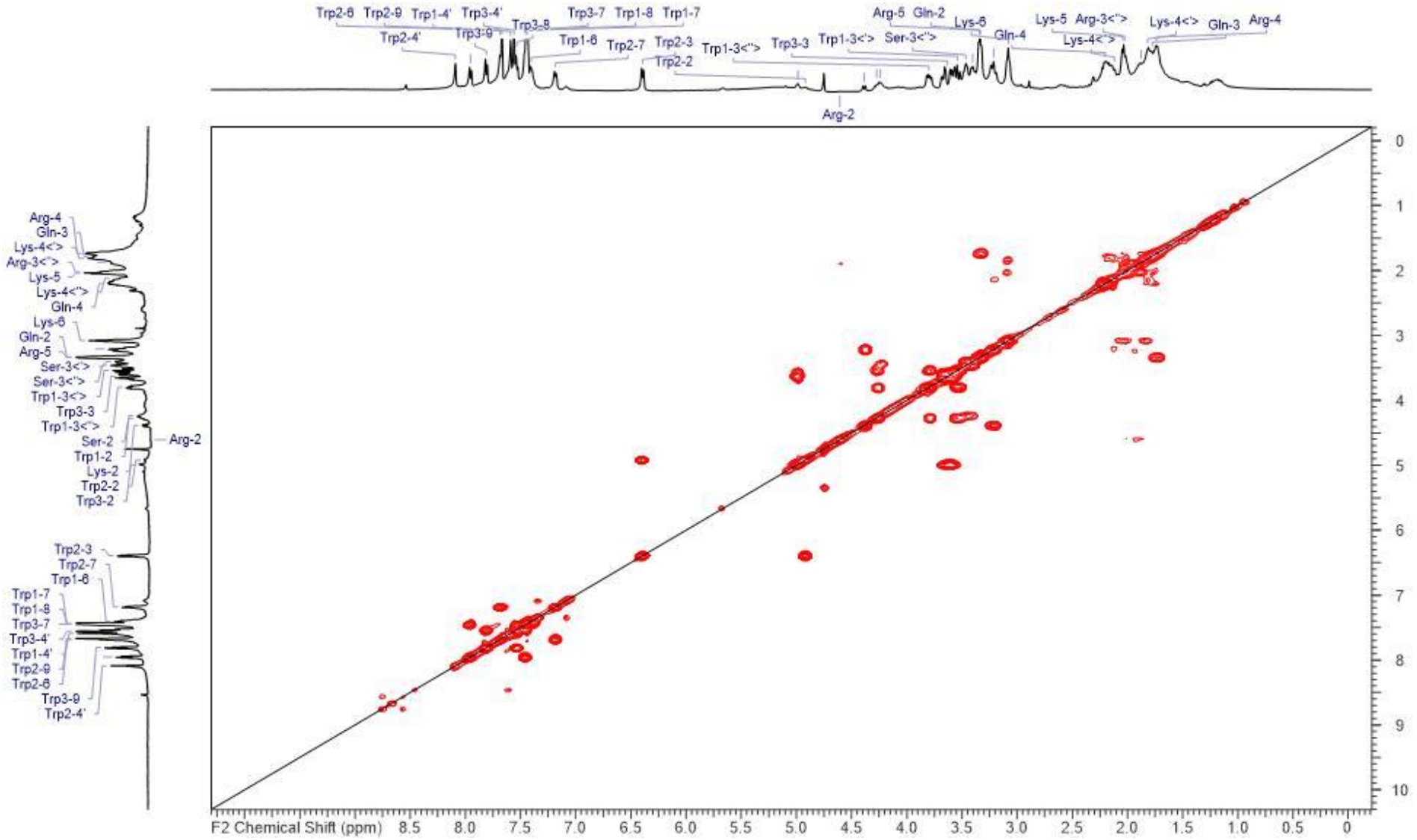

Figure S 134: COSY NMR of D69 recorded in D_2O/acetonitrile-d_3 (2:1) + 1% formic acid-d_4 at 318 K.

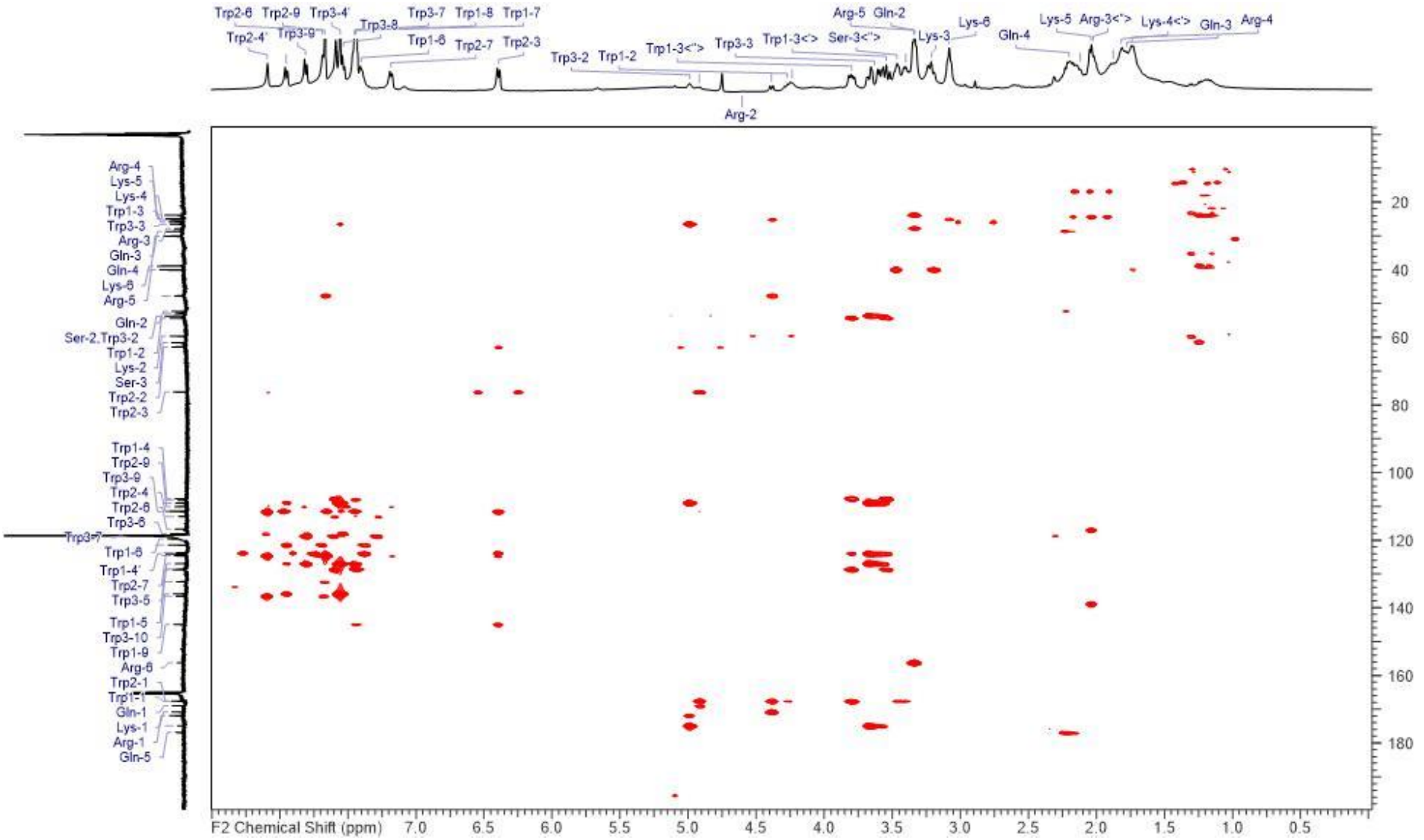

Figure S 135: HMBC NMR of D69 recorded in D_2O/acetonitrile-d_3 (2:1) + 1% formic acid-d_4 at 318 K.

7. HPLC traces of pure compounds

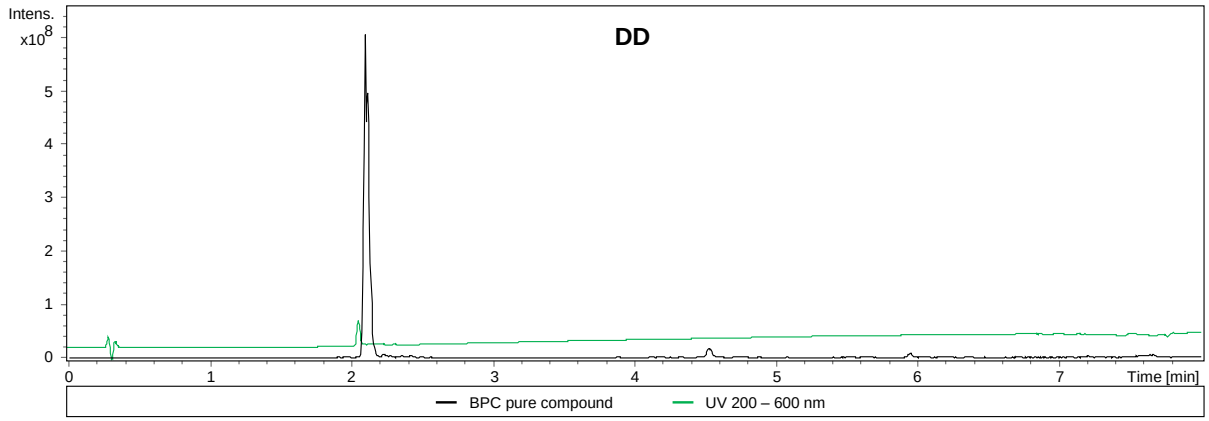

Figure S 136: Chromatogram of purified DD. The green trace shows the UV at 200–600 nm and the black trace shows the BPC. Acquired using amaZon speed.

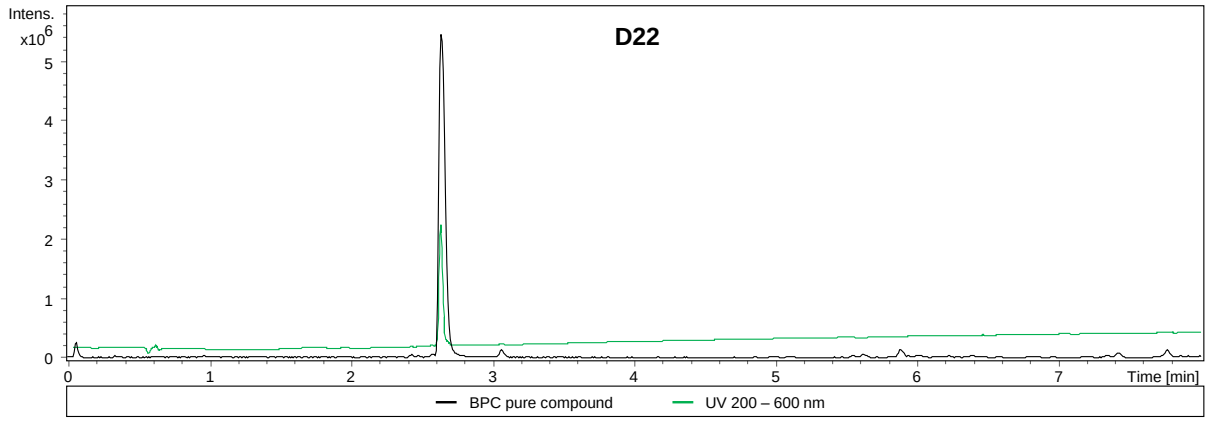

Figure S 137: Chromatogram of purified D22. The green trace shows the UV at 200–600 nm and the black trace shows the BPC. Acquired using maXis 4G.

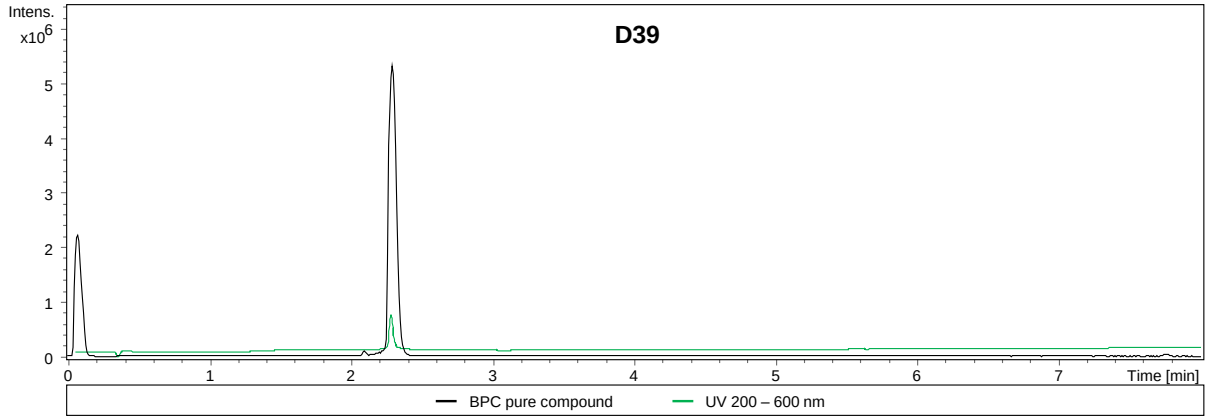

Figure S 138: Chromatogram of purified D39. The green trace shows the UV at 200–600 nm and the black trace shows the BPC. Acquired using maXis 4G.

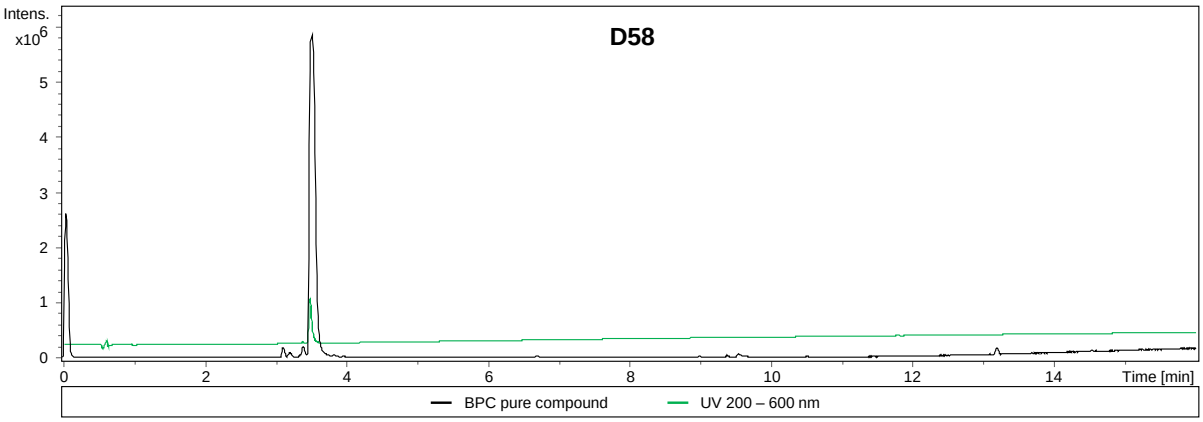

Figure S 139: Chromatogram of purified D58. The green trace shows the UV at 200–600 nm and the black trace shows the BPC. Acquired using maXis 4G.

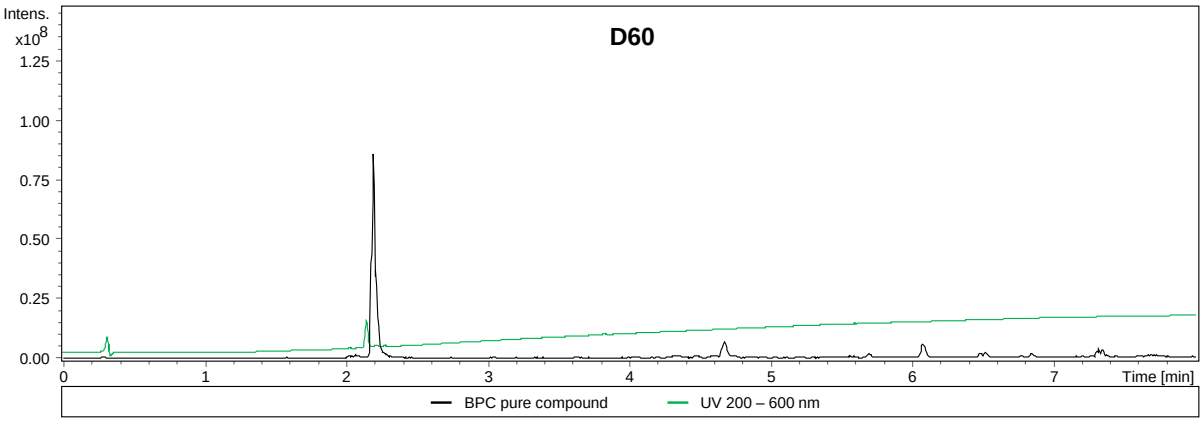

Figure S 140: Chromatogram of purified D60. The green trace shows the UV at 200–600 nm and the black trace shows the BPC. Acquired using amaZon speed.

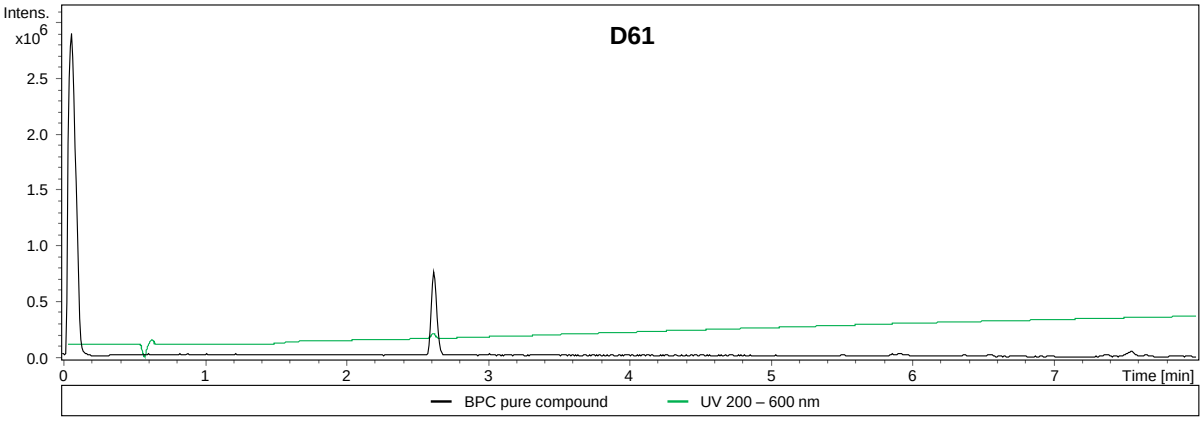

Figure S 141: Chromatogram of purified D61. The green trace shows the UV at 200–600 nm and the black trace shows the BPC. Acquired using maXis 4G.

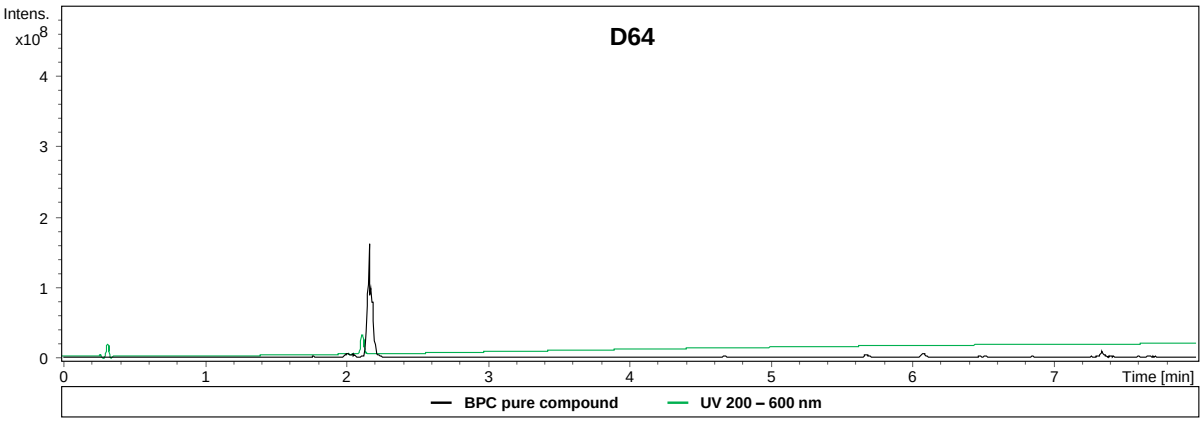

Figure S 142: Chromatogram of purified D64. The green trace shows the UV at 200–600 nm and the black trace shows the BPC. Acquired using amaZon speed.

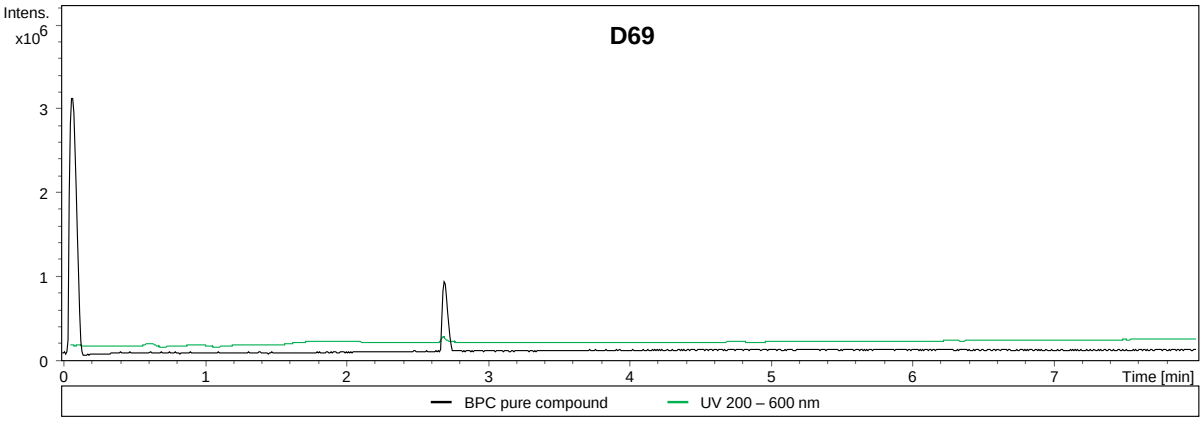

Figure S 143: Chromatogram of purified D69. The green trace shows the UV at 200–600 nm and the black trace shows the BPC. Acquired using maXis 4G.

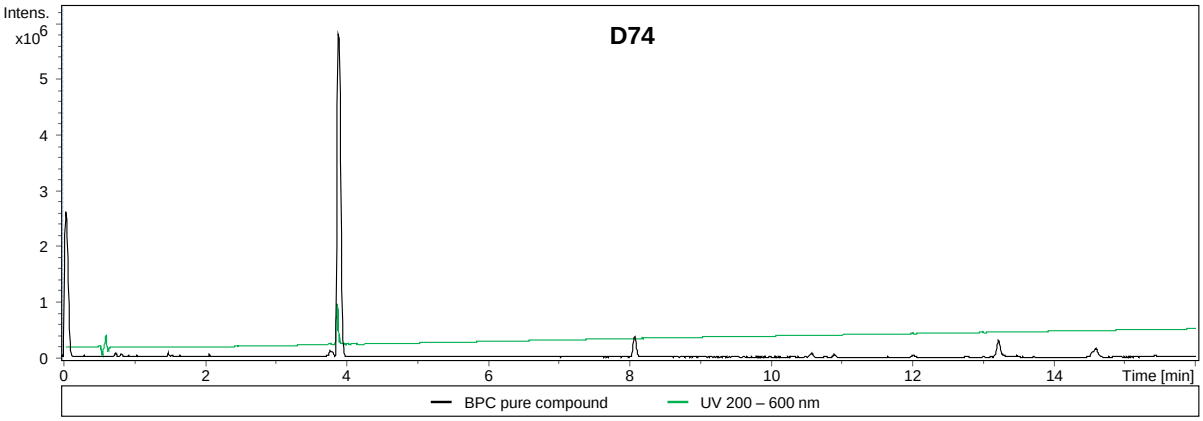

Figure S 144: Chromatogram of purified D74. The green trace shows the UV at 200–600 nm and the black trace shows the BPC. Acquired using maXis 4G.

References

1 a) T. D. Goddard, C. C. Huang, E. C. Meng, E. F. Pettersen, G. S. Couch, J. H. Morris and T. E. Ferrin, *Protein Science*, 2018, **27**, 14; b) Schrödinger, The PyMOL Molecular Graphics System, Version 2.5.2 (Version 2.5.2), Schrödinger, LLC, 2022;

2 E. F. Pettersen, T. D. Goddard, C. C. Huang, E. C. Meng, G. S. Couch, T. I. Croll, J. H. Morris and T. E. Ferrin, *Protein Sci.*, 2021, **30**, 70.

3 E. F. Pettersen, T. D. Goddard, C. C. Huang, G. S. Couch, D. M. Greenblatt, E. C. Meng and T. E. Ferrin, *J. Comput. Chem.*, 2004, **25**, 1605.

4 C. E. Seyfert, C. Porten, B. Yuan, S. Deckarm, F. Panter, C. Bader, J. Coetzee, F. Deschner, K. Tehrani, P. G. Higgins, H. Seifert, T. Marlovits, J. Herrmann and R. Müller, *Angew. Chem. Int. Ed.*, 2022, **62**, e202214094.

5 S. Groß, F. Panter, D. Pogorevc, C. E. Seyfert, S. Deckarm, C. D. Bader, J. Herrmann and R. Müller, *Chem. Sci.*, 2021, **12**, 11882.

Chapter 5 – Discussion

5.1 Establishment of a heterologous production platform for darobactins

The selective anti-Gram-negative activity of **DA** against pathogens such as *E. coli, A. baumannii*, *P. aeruginosa* and *K. pneumoniae* over eukaryotic cell lines or common microbes of the human gut microbiome, indicated the darobactins as one of the most promising novel antibiotic classes identified in recent years[1]. Upon first description of **DA**, Imai *et al.* even profiled its antibacterial activity *in vivo* showing clear efficacy in mice infected with *E. coli*, *K. pneumoniae* and *P. aeruginosa* strains [2]. These results, combined with the novel target BamA, encouraged us to identify challenges and needs for further development of the darobactins. The described purification of native **DA** was performed by cultivation of native producer *P. khanii* HGB1456 and yielded amounts only sufficient for first profiling assays of the molecule. The production titer was rather low (1–1.5 mg L^{-1}) and the fermentation time with up to two weeks relatively long[2]. Consequently, our first goal was to establish a heterologous production platform to facilitate the production of **DA** in a fast-growing host. *In silico,* we designed a BGC for the heterologous expression of **DA** and selected *E. coli* as a host, which has already shown primary positive results in attempts to heterologously produce **DA**[2]. In contrast to these initial attempts, our *in silico* design and *de novo* synthesis of the BGC enabled us to include additional unique recognition sites for restriction enzymes to the BGC, e.g. on gene boarders and on the terminal ends of the BGC. This allowed for further manipulation of the BGC and incorporation of additional, not-directly cluster-related genes. The flexible BGC design enabled us to integrate additional genes such as *darF*, *darG* or the tryptophan synthase genes encoding for TrpA and TrpB enzymes[3], as described in chapter 2 and in our patent application (see appendix), respectively[4]. Notably, we successfully expressed and produced **DA** with an over 10–fold increased production titer compared to the native producer by controlling the gene expression under two different promoters (see chapter 2 for more details) (Figure D1). Besides the increased titer, we significantly reduced the fermentation time from 14 to 3 days[5]. The establishment of the heterologous production platform with milligram titers per liter paved the way for additional investigations of the BGC and full elucidation of the darobactin biosynthesis. In parallel work, Wuisan *et al.*[6] described a similar approach to overproduce **DA** but did not adapt the BGC to gain higher flexibility in exchanging or adding of genes of interest, underscoring the significance of our engineering strategy.

5.2 Elucidation of darobactin biosynthesis and discovery of resistance gene *darF*

Our versatile heterologous expression construct enabled us to decipher the function of all cluster-related genes *darABCDE* found in native producer *P. khanii* HGB1456. Our work was confirmed by parallel work of the Schäberle lab[6]. Consistent with our data, they also determined the minimal cluster size to the precursor peptide encoding gene *darA* and to the rSAM-encoding gene *darE*. Using a BLAST search, we however were able to identify another native darobactin producer, *Pseudoalteromonas luteoviolacea* (*P. luteoviolacea*), harboring two additional genes, which were located in the same operon structure as the corresponding darobactin BGC. We named the genes *darF* and *darG,* to be consistent with the previous nomenclature. In order to functionally investigate the proteins encoded by those two genes, we co-expressed them with the darobactin BGC (Figure D1). Co-expression of *darG* only resulted in a slight reduction in **DA** production, whereas the constitutive co-expression of *darF* completely abolished **DA** production.

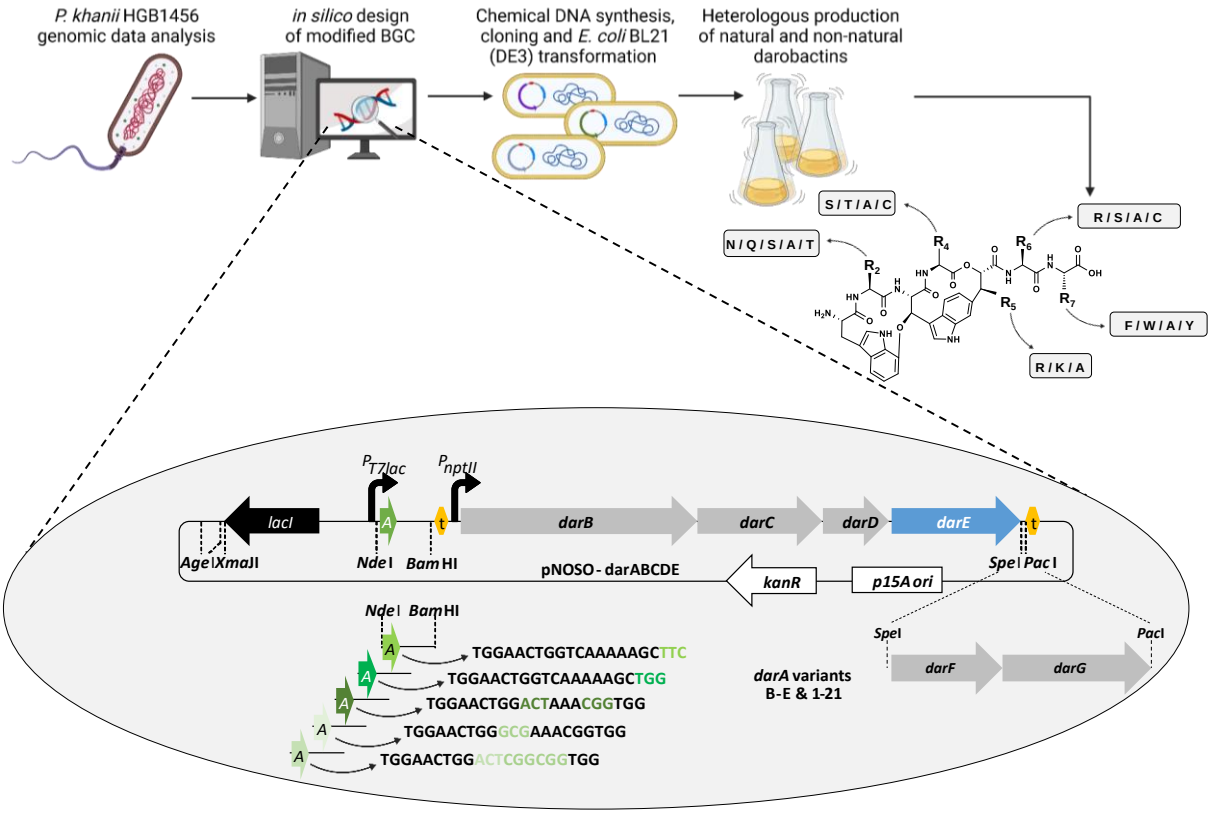

Figure D 1: Heterologous production platform for darobactins and for the elucidation of darobactin biosynthesis. The figure is adapted from Groß *et al.*[5] and Seyfert *et al.*[7].

Due to similarities with metallo-peptidases, we initially thought that *darF* might be a peptidase-encoding gene, responsible for releasing the mature peptide. This was based on the hypothesis that

specialized peptidases, involved in the release of mature RiPPs, are often but not exclusively located in one BGC[8]. Consequently, this might indicate that *E. coli* expresses a functional homolog that we could not find using bioinformatic tools but *P. luteoviolacea* require to coexpress *darF* to release the mature RiPP. However, we were unable to confirm this hypothesis in following *in vitro* assays. Subsequent investigations of the enzyme function suggested DarF to be a darobactin-degrading enzyme. Thus, we speculated that the peptidase required for the proteolytic cleavage of mature bi-cyclized darobactin, indeed, must functionally closely resemble the native producer's version, which is likely locating elsewhere in *E. coli*'s genome. The co-expression of detoxification systems to inactivate and recycle natural products by the native producer is a general wide-distributed feature of many bacteria[9]. It is advantageous to recycle the energy-rich molecules to re-use proteinogenic or non-proteinogenic building blocks. Moreover, it is even more crucial to reduce the concentration of often self-toxic molecules in the organism to guarantee the survival and fitness of the host[10], also known from diverse toxin-antitoxin systems[11,12]. In the case of DarF, it is particularly interesting that not all bacteria harboring a darobactin BGC are co-expressing a darobactin-degrading enzyme. Thus, the producer we identified could harbor an evolved BGC and might have acquired the gene from a common ancestor[9]. *Photorhabdus sp.* are known to express diverse proteolytic enzymes that are not unique for a specific cluster[13]. Therefore, another possibility is that many strains might have lost *darF* during evolution as other enzymes were taking over its function. In general, potential enzymes for regulation of the concentration of certain secondary metabolites are often modifying the bioactive compounds e.g. by adenylation[10] or acetylation[14], resulting in blocking the active site or degradation of the compound in subsequent steps, as seen – among others – for certain *Bartonella* proteins[9–11]. The genes, encoding detoxification enzymes are often transferred *via* horizontal gene transfer and can also lead to the spread of resistance[15]. In this context, the characterization of DarF as a darobactin-degrading enzyme enriches the understanding of how native producers protect themselves from the bioactive darobactins. The distinct cleavage site of DarF in mature **DA** and *de novo* generated **D9** heptapeptide has to be deciphered in upcoming studies but is likely located on a conserved position of the heptapeptide, as both tested analogues, **DA** and **D9**, were degraded. Fortunately, *darF* is only present in certain species of *P. luteoviolacea,* indicating the spread of *darF* to be a rare event, which reduces the risk of fast resistance development towards this potential new drug. Nevertheless, the finding of DarF might be important in future studies in case of upcoming resistances.

5.3 Derivatization of darobactins via BGC engineering

Our synthetic BGC allowed us to exchange the *darA* region of the darobactin BGC with artificial *darA* fragments carrying point mutations in the nucleotide core region *via* restriction ligation techniques to

heterologously express the other native analogues darobactin B, C, D and E, which have not been produced so far[2]. Furthermore, we tested the feasibility of exchanging the nucleotide core regions of the precursor peptide to potentially express and produce non-natural derivatives. Both approaches, the production of derivatives with sequences found in public databases and the generation of novel non-natural darobactins, resulted in production of the expected bicyclic derivatives (chapter 2). However, the results exhibited that the cysteine containing derivatives can react with media compounds via their reactive thiol group. Notably, these derivatizations were reversible, as described in our second publication, and we managed to purify the respective non-substituted cysteine derivatives, revealing their comparable activity to other derivatives (chapter 3).

Comparable to the BGC, the *darA* fragments to exchange the nucleotide core sequence of the RiPP were chemically synthesized, facilitated by the plummeting cost of this approach. Unfortunately, the supply chain bottlenecks during the Covid pandemic and the rising inflation led to increased prices again and significantly delayed the timeframe required to deliver the gene constructs. Thus, to keep our flexibility, we developed an alternative method to generate the darobactin BGC with mutated *darA* nucleotide core sequences using molecular biology techniques. We adapted a three-step overlap extension PCR (OE-PCR) method, explained in chapter 3, to introduce the desired mismatches. The generation of fragments, harboring mutated nucleotide core sequences to express and produce non-natural darobactins worked efficiently and we proceeded to exchange *darA* in the darobactin BGC, with standard restriction and ligation techniques as descripted in chapter 2. The process was established successfully and presented a screening rate of transformants with correct novel *darABCDE* constructs over 90 %. Compared to the laboratory that was generating novel derivatives in parallel[16], our approach required reduced time and resources. The OE-PCR methods increased our independence from external companies by using standard molecular biology equipment, material and solvents, available in our lab and enabled the generation of darobactin analogues **D22** to **D39** and **D58** to **D74** that are published and described in chapter 3 and 4, respectively.

5.4 Enhancing the bioactivity of darobactins

In contrast to the promising *in vitro* anti-Gram-negative activity of **DA**, the *in vivo* clearance of bacteria rescuing the laboratory mice from death, was less pronounced in infection models with *P. aeruginosa* and *A. baumannii* strains[2] as introduced in chapter 1. The mice survived, only after up to 25-fold increased dosing compared to infections with *E. coli*. Thus, our rationale behind the design of the new derivatives was evident: We aimed to find analogues with a broader spectrum in anti-Gram-negative activity than native **DA** and with higher potency, demonstrated in reduced MIC values, respectively. After establishing the production platform, elucidation of the biosynthesis and modulation of the BGC

to produce artificial derivatives, we tested the freshly generated analogues for their activity to inhibit Gram-negative bacteria. Our first approach described in chapter 2, started with novel derivatives carrying amino acids that were already present in native analogues plus completely artificial amino acids incorporated in the heptapeptide. This resulted in the new analogue **D9** exhibiting up to 8-fold enhanced activity against difficult to treat pathogens such as *A. baumannii* or *P. aeruginosa* and highlights the possibility and potency of darobactin derivatization. Moreover, engineering of the darobactin BGC for heterologous production of native and artificial analogues underpins the general prospects of tailoring RiPPs towards desired bioactivity. The work enlarged the knowledge about what is possible in RiPP engineering and serves as a conceptional and methodological blueprint for other RiPPs. This was emphasized in a couple of research and review articles, describing that our first approach already significantly contributed to the field of RiPPs research and could be translated to future bioengineering projects[17,18,19]. However, the darobactin target site and the mode of binding was not clear during the conceptualization and generation of our first derivatization series, and it was obvious that the options to further improve the antibacterial activity of **D9** were even more promising by developing more rational approachs[7]. During the submission process of our first darobactin publication, research in the Hiller lab was published[20] and served as inspiration to investigate the heptapeptide on a structural level to elucidate which amino acid positions might be a suitable target for exchange in **D9** to further increase the anti-Gram-negative activity of this compound in a follow-up study.

5.5 Structure – and activity guided approach to develop new highly active analogues.

The Hiller group successfully purified and investigated the target protein BamA and was able to generate a co-structure of native **DA** with the BAM complex using X-ray crystallography and cryo-EM techniques[20,21]. They provided us with the expression vector harboring *bamABCDE*, which enabled the subsequent fast structural elucidation of the co-structure of **D9** with BAM via Cryo-EM by our partner laboratory in Hamburg (Figure D2). These results had a major impact on our following strategy in developing improved darobactin derivatives. The structural analysis of the BAM-**D9** co-structure explained the increased antibacterial activity of **D9** on a structural level. As a main result the C-terminal tryptophan of **D9** clearly increases the interaction area of the molecule with the target protein, BamA. The lateral gate of the BAM complex is completely blocked, which is not the case by interaction with **DA** (chapter 3)[20]. Next, we utilized the interaction of **D9** and BAM combined with the available structural data from the Hiller lab as a blueprint for the design of derivatives **D22** to **D39** (Figure D2). Remarkably, these novel darobactins with a C-terminal tryptophan and additional modifications mainly

on position 6 showed generally enhanced bioactivity and yielded the currently most active molecule **D22**.

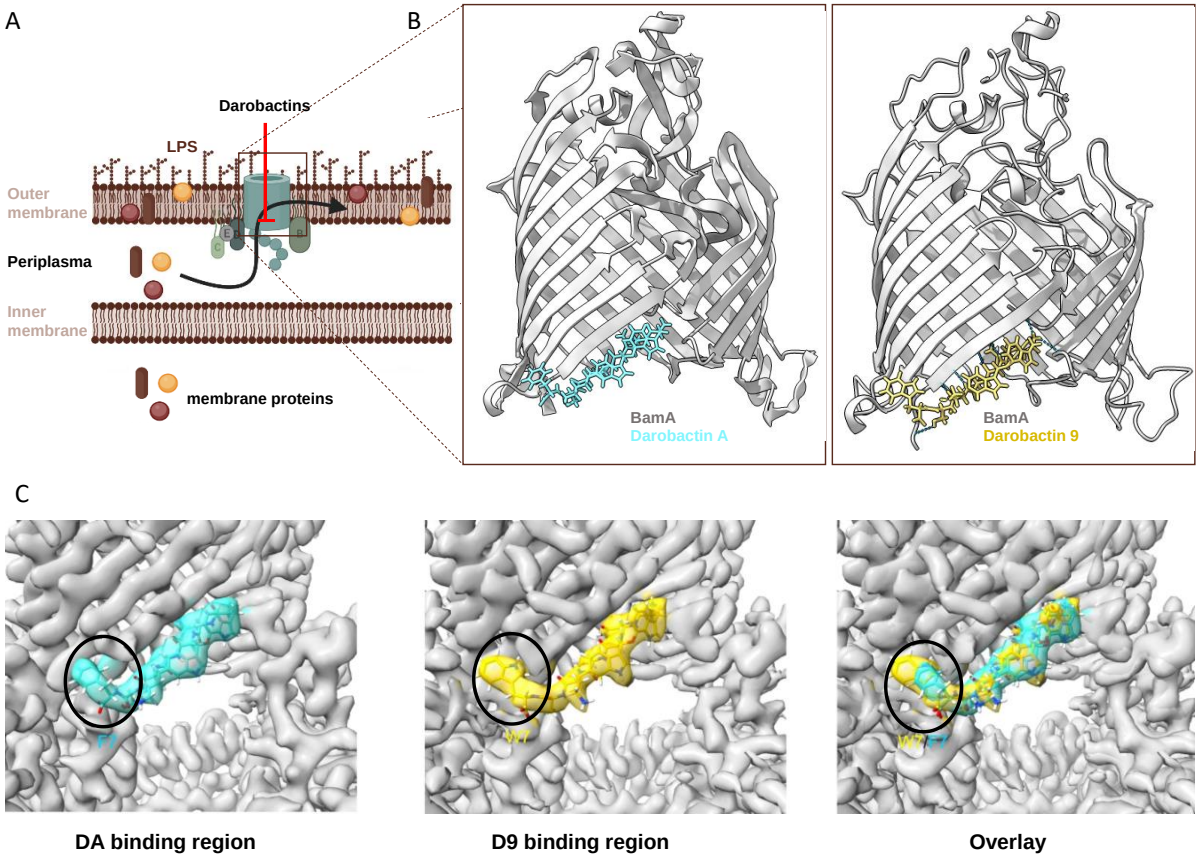

Figure D 2: Structural elucidation of DA and D9 interaction site on BamA[20,22]. **A-B** The structural data exhibited the mode of binding of darobactins and initiated the design of **D22** to **D39**. **C** Magnified interaction of **DA** and **D9** separately and overlayed exhibiting the enlarged interaction area of **D9** compared to **DA**. **A** and **B** adapted from Seyfert *et al.* 2023[7] and **C** adapted from Figure S43 (chapter 3)[22].

Thus, the structure-and activity-guided approach permitted us to generate derivatives characterized by a significant gain in antibacterial activity compared to the random approach described in chapter 2. Furthermore, we were able to underpin our results with biophysical data. In brief, the binding constant (K_D) of **D22** on EcBamA was 50 % reduced compared to **D9**. Moreover, an additional Cryo-EM co-structure of BAM with **D22** depicted the change of L-serine to L-arginine on position 6 to be particularly important to increase the hydrogen bonding interactions, ultimately leading to the whole compound being sealed tighter to the binding pocket. Of note, the activity of **D22** was 32-fold enhanced to **D9** and 128-fold enhanced to **DA** against tested CRAB isolates and in a similar range to colistin. Thus, our SAR approach (Figure D3) resulted in the generation of the first darobactin derivatives with a sub-micromolar anti-Gram negative activity against critical pathogens such as *P. aeruginosa* and *A. baumannii*[22,23]. The derivatization described in chapter 3 motivated us to proceed with our conceptual approach to genetically engineer the BGC guided by our structural data. We modelled the influences of distinct amino acid substitution patterns for a potential formation of hydrogen bond interactions

with BamA at different positions of the heptapeptide (chapter 4). We hypothesized that additional or stronger hydrogen bonding interactions might correlate with an increase in antibacterial potency of the respective derivative.

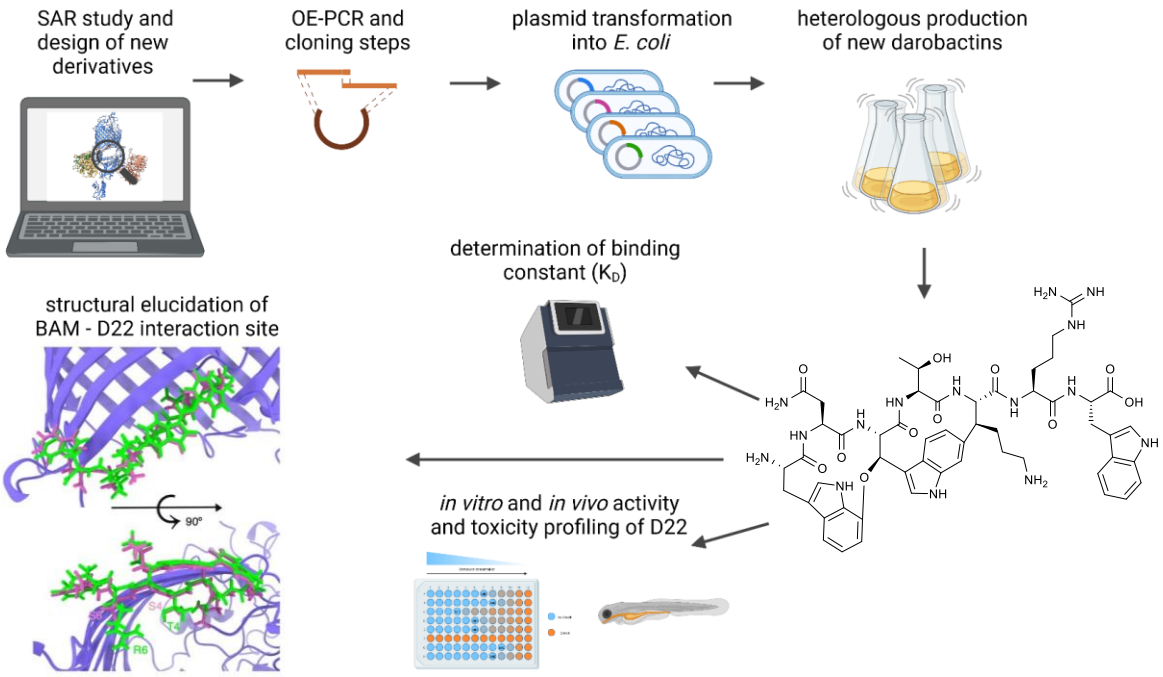

Figure D 3: Workflow of the structure – and activity guided – approach to develop new highly active darobactin analogues. The interaction site of BAM-**D22** (bottom left) is adapted from Seyfert *et al.*[22] .

In particular, we wanted to learn more about the feasibility of modifications on underinvestigated positions of the heptapeptide, e.g. position 2 and 4, and their influence on the antibacterial activity, also due to results generated by other groups that contradict our data[16,22]. This resulted in generation of derivatives **D58** to **D74** where we could prove the bioactivity of derivatives predicted to be more active by molecular modelling. Combined with the previous derivatization results shown in chapter 2 to 4 we could obtain a clear picture of the influences of amino acid substitutions on position 2, 4, 5, 6 and 7 of the darobactin heptapeptide on antibacterial activity. We generated data on modification of all positions except for position 1 and 3, the ring-closing tryptophans. These positions were not changed to retain a proper bi-cyclization, crucial for three dimensional structure and therefore bioactivity of the darobactins[8,24]. Activity improvement only through biotechnological engineering of a RiPP was described before but not in this manner and barely achieved using structure and activity-guided approaches[25]. Main reasons for this are that most RiPPs are less soluble and structural elucidation failed for many bioactive compounds due to the large complexity especially in cyclic molecules as illustrated in Figure 6[26]. Thus, our approach was a positive example of how an RiPP

antibiotic can be optimized[18,25,27] and will help in the future for additional rounds of darobactin optimization. Moreover, it should motivate researchers to adapt our strategy to their concepts of RiPP compound optimization.

5.6 *in vitro* and *in vivo* profiling of darobactins

The first *in vitro* profiling assays of the best derivative **D22** described in chapter 3 revealed promising bioactivity against MDR CRABs, faster and more sustained killing of tested *E. coli* and *A. baumannii* strains over a period of 24 hours compared to **DA,** and no toxicity against zebrafish larvae up to 500 µM **D22**. Consequently, we extended the profiling of **D22** but also proceeded with derivatization efforts to characterize additional highly active analogues such as **D69**. Noteworthy, we describe potent anti-bacterial activity against clinical and multidrug-resistant *P. aeruginosa* strains that are only susceptible to meropenem (chapter 4). Thus, in addition to the promising activity against *E. coli* and *A. baumannii* strains (chapter 2 and 3), **D22** and **D69** depict high activity against in total three Gram-negative pathogens that were categorized as critical by the WHO[28].

Even if the *in vitro* activity assays against a broad range of Gram-negative pathogens exhibited high potential for **D22** and **D69**, no data on their ADMET profiles was available yet, which is highly relevant in drug discovery and development. The ideal antibiotic is selective, orally bioavailable and is capable of crossing barriers in the body to reach its target[29]. *In vitro* ADMET profiling can help to evaluate these properties in potential drugs[236,238–240], and we obtained respective data for the most potent derivatives **D22** and **D69.** Both exhibited high metabolic and plasma stability as well as low plasma protein binding (PPB) in mouse, rat and human liver fractions/plasma. Thus, the ADMET profiling demonstrated promising properties of both darobactins and paves their way for further follow-up studies *in vivo*, *e.g.* pharmacokinetic (PK) and pharmacodynamic (PD) models to characterize the antibiotic in living organisms, such as laboratory mice. This next step is essential to determine whether darobactins might have the potential to be further developed towards (pre-) clinical studies as new drugs.

Sufficient compound supply is crucial for *in vivo* studies, and over 400 mg **D22** was produced and purified using our optimized purification method (personal communication C. Porten, S. Deckarm, C. Seyfert)[22]. *In vivo* PK/PD profiling of **D22** was performed by an external contract research organization, and the unpublished results were consistent with what we were anticipating based on our findings in the prior ADMET profiling (Selvita, Zagreb, Croatia). In brief, **D22** was administrated to mice *via* different routes and samples of different organs, urine and of feces were taken at distinct time points to determine the concentration of **D22,** indicating high levels of **D22** in the urine, bladder and kidney.

This is in line with the high polarity of the compound and hints at a dominance of renal excretion over hepatic metabolism as proposed in chapter 4.

The high concentrations of D22 in kidneys, bladder and urine of the test animals prompted us to study **D22**'s potential for the treatment of urinary tract infections (UTIs). Since there are more and more multi-resistant pathogens, especially *E. coli* strains, which lead to severe and chronic bladder infections[30], especially in women, darobactin with its new MoA and its high selectivity towards Gram-negative bacteria is a potentially suitable candidate to be used in treating these infections. We conducted an *in vivo* UTI model and compared administration of varying concentrations of **D22** in mice. The study was performed at the Statens Serum Institute (Denmark) and is not published so far. **D22** treatment significantly reduced the bacterial loads compared to the vehicle treatment in all tissues.

The initial *in vitro* and the so far unpublished *in vivo* profiling of darobactins, especially of **D22**, emphasizes the need to further investigate this new compound class. Its antibacterial activity, particularly in UTI models against hard to treat *E. coli* strains, indicates the promising potency of **D22**. At this stage of the project, the perspectives of a further development of darobactins have to be evaluated in the light of the cost of goods, especially regarding the production yields and possibilities to circumvent the, for industrial standards, still low production titer in the heterologous host.

5.7 Perspectives for further development

5.7.1 Biosynthetic production in *E. coli* and their limits

Even though we were able to produce all designed derivatives and examine the respective extracts for their bioactivity, the production of the individual derivatives that we isolated varied considerably. The possible reasons for the strong deviations were already discussed in Chapter 4. Due to the importance of achieving an increase in production to meet the demand of upcoming studies and potential (pre-) clinical trials, this aspect should be further investigated. Derivatives with higher activity against the Gram-negative producer can only be achieved in lower production titer due to the intrinsic sensitivity of the heterologous producer *E. coli*. We were able to clearly prove this in the presented studies (see chapters 2, 3 and 4). However, we also obtained derivatives such as **D58**, which, despite their reduced activity, were also produced in reduced titers. Consequently, there are additional bottelnecks influencing the production titer and leading to significantly varying production rates. One aspect, shown by Wuisan *et al.* might be the ratio between the precursor peptide DarA and the rSAM enzyme responsible for bicyclization[6]. Moreover, the presence of the transporter system *darBCD* is influencing the final production capacity of *E. coli* (chapter 2). The influence of the transporter system *darBCD* for the production titer was evaluated in Groß *et al.*[5] and Wuisan *et al.* [6] by creating expression constructs harboring the darobactin BGC without the transporter systems. This resulted in detectable but reduced

production, indicating, other efflux systems in *E. coli* seems to export and secret mature darobactins out of the cell. This analysis furthermore indicates that the proteolytic release of the mature active darobactins is not performed on DarBCD during the export out of the bacterial cell but separately. As the pellet did not show relevant concentrations of darobactins in our experiments, their export does not seem to be a limitation for production titers.

An investigation of the expression level of the peptidase was not possible so far, as we were unable to pinpoint a specific peptidase being involved in darobactin maturation. This peptidase is hypothesized to be relatively conserved in the native producers and should be present in *E. coli*. Currently, we are screening *E. coli* strains of the commercially available KEIO library, having single gene knockouts of peptidases that were not essential for survival. These knockout strains were supplemented with the darobactin BGC to correlate the lack of a certain peptidase with inability of darobactin production.

Moreover, further investigation of the rSAM enzyme might provide valuable insights here to reveal how DarE exactly works. As described in chapter 4, changes in position 2 to rather electrically charged side chains and to generally longer side chains reduce the production of the respective derivative. The same was also detected for modifications in position 5 to rather polar and uncharged side chains in contrast to the L-lysine and L-arginine bearing a positive charge at physiological pH. Sterical hindrance of the active site seems to be one plausible reason for the varying production because catalytic activity of the radical SAM enzyme could be hindered by certain amino acid substitutions in the core peptide [8,31]. This could be analyzed in future studies by targeted mutations next to the catalytic active site of DarE and successive analysis of darobactin detectable over time. To predict potential influences of mutations near to the active site of DarE, the predicted α-fold structure of DarE can be used, published by Guo *et al.* [17]. Next, an experimental workflow can be designed to evaluate potential changes in proper cyclization and production after modulation of DarE.

Feeding of amino acids to the production culture showed minor effects but can also enhance production. Main limitation therefore does not seem to be precursor supply, but intrinsic sensitivity of *E. coli*. Co-expressing of a mutated BamA version or mutation of BamA in the host reduces the intrinsic sensitivity of *E. coli* but come with significant reduction in fitness and virulence[2,6]. We observed up to three times reduction in the cell densities of *E. coli* BamA mutants that are correlated with a decrease in production titers. Furthermore, the mutants presented a short stationary phase of only one day before they started to die, contrary to the unmutated *E. coli* producer that was still viable after 3 days of fermentation. All these results indicate that a switch in host might be necessary to enhance the production titer because currently it apprears rather unlikely to engineer *E. coli* in a way to overproduce darobactins in higher titers in a short time frame.

5.7.2 Options for heterologous expression in novel hosts

For a switch of the heterologous host, Gram-negative organisms are beneficial due to their closer phylogenetic proximity, which can increase success rates of this approach. Bacteroides show a higher variance in the BAM complex in comparison to *E. coli* and *Photorhabdus sp*.[20,22] and would therefore be a suitable option. However, these symbiotic intestinal bacteria, which often live anaerobically, have not yet been described to heterologously produce high levels of natural products[32].

A switch to more well-described Gram-positive expression hosts or even eukaryotes such as yeast strains might therefore be indicated[33]. Both, yeast and Gram-positive bacteria do not comprise an outer membrane and consequently do not express the target protein of the darobactins. This would circumvent limitation of production based on sensitivity of these organisms to darobactins. However it might be necessary to co-express and produce the specialized peptidase to release the mature peptide in other hosts than *E. coli* [34]. After production in another heterologous host, modifications of the DarE enzyme to increase its catalytic efficiency or upscaling of *darA* expression might be future project parts to pave the way of darobactins forward to (pre-) clinical trials by reducing the cost of goods regarding compound supply in sufficient amounts.

Despite heterologous expression, a semi-synthetic approach could be applied to generate sufficient material of the frontrunner molecules for further studies. This could be achieved in two steps by (1) optimizing the heterologous production in *E. coli* of derivatives with weaker activity against the producer *E. coli* BL21 (DE3) but higher production rates such as **D38** or **D74** (chapter 3 and 4). In particular, **D74**, which only differs from **D22** at position 6, shows an excellent titer of up to 35 mg, which is three times the titer of **D22** (chapter 4). (2) After **D74** has been produced on a large scale, it could be used as a starting material to generate subsequent semi-synthetic modifications of **D74** to convert it into **D22** in order to circumvent the production limitation of **D22**. In the meantime, the increase of **D22** production by another host could be established in parallel to solve the problem again biotechnologically. The total synthesis is currently no effective option, due to low efficiency combined with high costs of materials and requirement of highly toxic chemicals[27,35].

5.7.3 Non-proteinogenic modifications of darobactins

A semi-synthetic approach offers an additional advantage by allowing the incorporation of non-proteinogenic amino acids to the darobactin peptide sceleton. The exemplified potential of halogenated darobactin variants produced using biotechnological methods, revealed comparable anti-Gram-negative activities of analogues with these non-proteinogenic modifications compared to current leads[22]. The chlorinated and fluorinated analogues at position 7, however only achieved relatively low production yields likely due to low ribosomal promiscuity[8]. Consequently, semi-synthesis

could provide a versatile toolkit for generating halogenated analogues, overcoming this limitation during biosynthesis.

The evaluation of potential novel proteinogenic darobactins through modeling of predicted interactions with BamA after mutagenesis on distinct positions of the compound, (utilized in chapter 4 for proteinogenic substitutions,) can be extended to non-proteinogenic building blocks. Although the ribosomal principle underlying the production is associated with more severe limitations in comparison to NRPS[36]. Post-production semi-synthesis might offer new possibilities to generaten respective non-proteinogenic substitutions, independent from the ribosomally controlled biosynthesis rules in bacterial or eukaryotic hosts. Generated analogues can be investigated in future profiling studies regarding their impact in increasing the bioactivity of darobactins as well as in changing the physical and chemical properties of this currently hydrophilic compound class.

In particular, changing the physical and chemical properties of darobactins might increase the potency of darobactins, because the ADMET profiling of **D22** and **D69** (chapter 4) and the PK/PD profile of **DA**, shown by Imai *et al.*[2] lead us conclude that the hydrophilicity of darobactins likely results in a low PPB and lead to a fast renal clearance of the compound. Therefore, semi-synthetic modifications might be an option to reduce hydrophilicity in order to prolong the half-life in the organism. To overcome that obstacle, position 4 of the heptapeptide seems to be especially suitable for modifications due to no direct interactions of the side chain with the target protein BamA[141,179]. As shown in chapter 3, this position can be modified without abolishing the activity.

Novel artificial derivatives, generated via semi-synthesis can then be further profiled using the already described models in chapter 2 to 4. The established *in-house* MST method can be used to rapidly check the binding constants of the respective new derivative on target protein BamA. In case of promising interaction, the novel compound can be tested *in vitro* for its anti-Gram-negative activity and promising candidates can be further profiled in ADMET assays to investigate potential changes in metabolic stability, plasma stability and PPB[29]. Depending on these results, potential new frontrunners can be extensively investigated by proceeding with *in vivo* PK/PD and infection studies to verify the potential advantages compared to **D22** in animals and to overcome the highlighted problems associated with the relatively high hydrophilicity[29] (Figure D5).

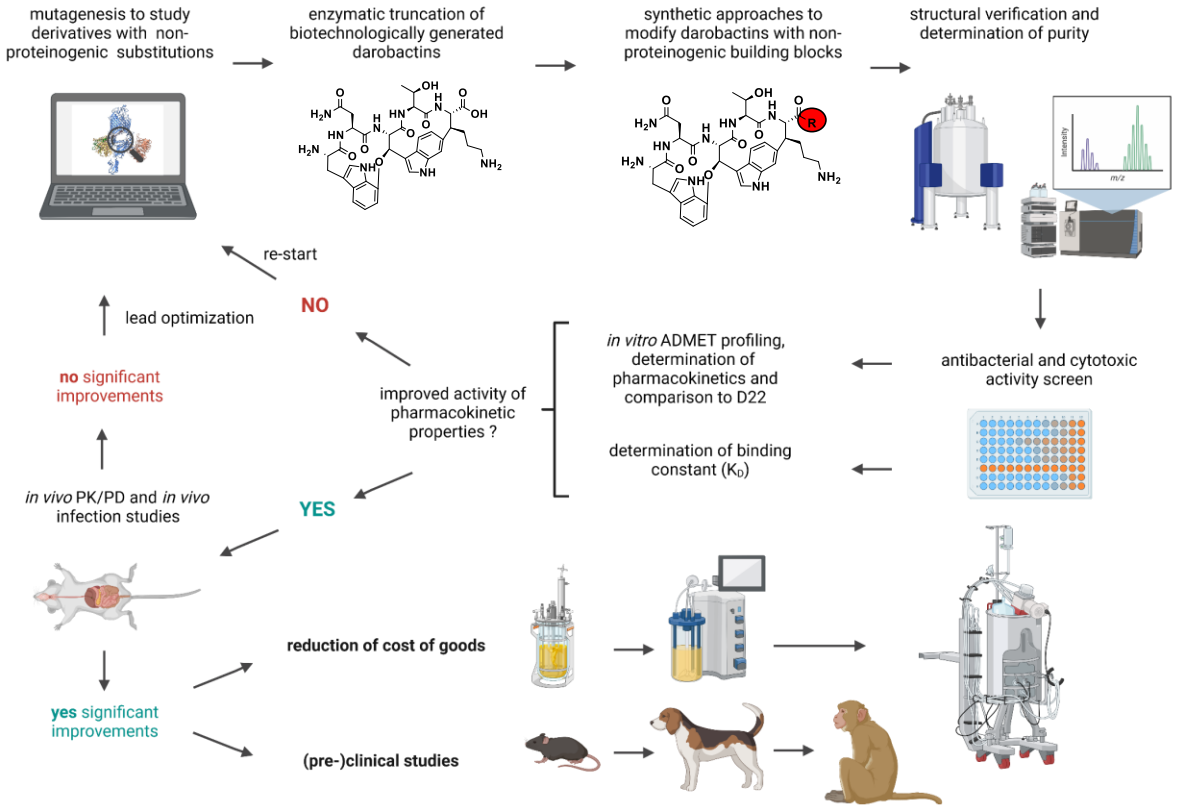

Figure D 4: Potential semi-synthetic workflow to improve the activity of darobactins to evolve this compound class towards (pre-) clinical studies.

However, it should also be noted that hydrophilicity combined with good water solubility and low risk of metabolization brings major advantages and modifications have to be carefully balanced. In addition to the problems of low production rates of new antibiotic candidates, unfavorable pharmacokinetic properties leading to unfavorable *in vivo* efficiency can cause the drug to not reach its target site. Besides toxicity issues, these are the main reasons for the low number of new molecules in the (pre-) clinical pipeline and the even lower number of compounds approved for market as safe, effective drugs[1,37].

5.8 Comparison of darobactins to other antibiotics in the pipeline

The development and market introduction of new, innovative antibiotics have been identified as crucial goals by the WHO in light of the worsening antibiotics crisis[38]. Despite this, only a minority of antibiotics that target new sites have proven to be effective and sustainable against existing resistances, leading to a limited number of market introductions in recent decades[1]. The outlook remains challenging as the significant change in investments necessary to enable research and development yielding market approvals as seen in the golden age of antibiotics still seems out of reach[39]. Within the pre-clinical pipeline, merely 40 % of the 74 antibiotic candidates (29 molecules) are

classified as "innovative antibiotics"[38]. These candidates fulfill at least one of the four WHO innovation criteria, which include a new chemical class, a new target, a new MoA, and the absence of known cross-resistances[38]. Especially the acting of innovative antibiotics on novel target sites or antibacterial activity rooted in a new MoA is recommended as characteristics of a novel antibiotic[1,40]. This should automatically reduce the likelihood of cross-resistance, which is the most critical issue with new and traditional antibiotics[1,41]. However, these candidates haven't reached all significant milestones necessary to advance these pre-clinical candidates to the clinical phases yet and final market approval remains uncertain[41,42].

Among the antibiotics currently undergoing clinical investigation (a total of twenty-seven), nearly 80% (21 agents) are derivatives of existing "traditional antibiotics"[38,42,43]. This poses a risk of rapid resistance development. A critical evaluation of the six "innovative antibiotics" situated in one of the three clinical development phases reveals that they do not represent new broad-spectrum antibiotics[38]. Their efficacy is limited, and their general spectrum of action is rather restricted, having on the other side advantages regarding development of resistancy[38,42]. Notably, only two of these antibiotics effectively combat at least one of the critically prioritized Gram-negative pathogens. These two agents, taniborbactam and VNRX-7145 in combination with ceftibuten, belong to the β-lactam/boronate BLI antibiotics category[38]. The other innovative antibiotics, zoliflodacin and gepotidacin, are topoisomerase inhibitors and already in clinical trials phase 3. Although chemically distinct, both bind to the same enzyme, raising concerns about possible cross-resistance. The next innovative agent in the clinical pipeline is the FtsZ inhibitor TXA709, which inhibits the Z-ring formation during cell division[42]. The compound is still under investigation in clinical trials phase 1[38] with the primary goal to learn more about the effects of TXA709 on the bacterial cell and the evaluation of potential off-target effects[44]. Afabicin, which addresses a novel target, the FabI enzyme[38],fulfills all four innovation criteria of the WHO. It's MoA comes with a novel target attacked by an antibiotic of a novel chemical class exhibiting a low risk of cross-resistance. Afabicin development is directed to treat bone and joint infections but also skin and skin structure infections[38]. One limitation of afabicin is its selectivity to Gram-positive pathogens, highlighting the need to find similarly promising leads targeting Gram-negative bacteria.

None of the candidate antibiotics in the clinical pipeline has the potency to effectively kill a broader spectrum of critical and clinically prioritized Gram-negative pathogens. This makes the darobactins promising for further development with their pronounced anti-Gram-negative activity, the selective MoA at the OM of Gram-negative bacteria, the new target site, the new chemical class and the low risk of cross-resistance with known antibiotics. Fortunately there are a couple of additional promising antibacterial compounds in development against pathogens prioritized by the WHO such as the cystobactamids, corramycin and corrallopyronin.[45] Other exemplary antibiotics that are not yet being

investigated in clinical trials are the teixobactins, the odilorhabdins and the macolacins. A comparison of the latter three with darobactins makes it possible to better identify the advantages and characteristics of the darobactins. Teixobactins are an example of a new antibiotic with a novel MoA that is primarily effective against Gram-positive pathogens. Odilorhabdins fulfill three of the WHO innovation criteria and are an example of a broad-spectrum antibiotic with derivatives that act against Gram-positive and Gram-negative pathogens. Interestingly, the native odilorhabdins were originally isolated from nematode symbionts of the genus *X. nematophila*, which are closely related to the native darobactin producer *P. khanii*. Macolacin is genetically and structurally related to polymyxins and exhibits potent activity against Gram-negatives, which makes it particularly interesting for this work as we have already compared the activity of our current frontrunner **D22** against CRABs with colistin, also known as polymyxin E (Chapter 3).

Teixobactin has a novel MoA by targeting two steps in the highly conserved lipid II and lipid III precursor synthesis, both crucial for the integrity of bacterial cell wall[46]. Its production is challenging due to a complex total synthesis route, and low production titers in conventional fermentation, making it less feasible for widespread use[47]. The available data regarding potential off-target effects in human body is incomplete, but it clearly affects common bacteria of the human microbiome[48]. Teixobactin activity is rather selective against Gram-positive bacteria including MRSA and vancomycin-resistant enterococci (VRE), with only minor effects on Gram-negative pathogens as CRABs or *P. aeruginosa*, *E. coli* or *K. pneumoniae.* Teixobactin exhibits no risk of cross-resistance but has similar limitations to the candidates listed in the previous paragraph when it comes to treatment of Gram-negative pathogens[48,49].

The advantages and disadvantages of odilorhabdins are similar to those of teixobactin. Odilorhabdins are targeting a site on the ribosomal 30 S subunit not exploited by known antibiotics[50]. This means they have a novel target site and the risk of cross-resistances is rather low, as shown by comparing the exact MoB with traditional antibiotics also binding on the ribosomal 30 S subunit[50]. The low risk of cross-resistance against MDR *E. coli* and *K. pneumoniae* strains and promising activity of new frontrunner molecule NOSO-502 also against *P. aeruginosa* can even be highlighted[51]. Notably, odilorhabdins exhibit activity against *Staphylococci* strains in the low sub-micromolar range. Thus, they do not only fulfill three criteria of the WHO for a novel innovative antibiotic but also target critically prioritized Gram-negative bacteria beside the Gram-positive *Staphylococci*. The main disadvantage of odilorhabdins is the complex production via total synthesis due to incorporation of multiple non-proteinogenic amino acids into the final molecule and all found to be crucial for antibacterial activity[52]. Their biosynthesis has not been published yet, hindering development of a heterologous expression platform.

Even though macolacin was advertised as innovative compound, it might rather be seen as novel derivative of the colistin family upon closer inspection[53]. It only presents three structural modifications compared to colistin and a comparable BGC. Indeed, macolacin is expressed by a new native producer *Paenibacillus xylanexedens*, which does not share the identical but a clearly cognate BGC. Despite their structural similarities, macolacin seems to break *mrc1* resistances, and inhibits critically-prioritized resistant Gram-negative bacteria showing resistance to colistin[261]. Thus, macolacin fulfills one of the WHO innovation criteria, namely the absence of known cross-resistances. The anti-Gram-negative activity of macolacin is as broad and in the similar range compared to the activity of colistin. Extensively derivatization yielded derivatives with increased *in vitro* and *in vivo* activity against Gram-negative pathogens. As macolacin shares the identical target site compared to polymyxins, it likely shares their significant side effects, making it rather a back-up choice for further development[54].

Contrary to the three exemplified antibiotics described above, darobactins depict a broad and selective anti-Gram-negative activity against pathogens critically prioritized by the WHO (Figure 4)[38]. The *in vitro* activity against difficult-to-treat clinical isolates such as multidrug resistant *E. coli*, *P. aeruginosa* and *A. baumannii* is promising[5,22,55]. The unique chemical structure[17] due to the rSAM dependent ether and carbon crosslink during the darobactin biosynthesis and the distinct target site on the OM by blocking an essential protein of the BAM complex seem to result in a low risk of cross-resistance with antibiotics on market[27]. Since darobactin can only be used to inhibit Gram-negative and not Gram-positive pathogens, by binding selectively on its target site at the OM, the number of incorrect prescriptions against infections with Gram-positive bacteria, should be comparably low, in case a darobactin analogue will reach the market. Darobactins specialization in Gram-negative bacteria give them an unique advantage in specific clinical scenarios such as in cUTI infections including kidney and bladder where most infections are caused by Gram-negative bacteria and not by Gram-positive bacteria[30,56]. Moreover, potent *in vitro* inhibition of pathogens correlating with pneumonal bacterial infections such as *P. aeruginosa* or *A. baumannii* species let us infer that darobactins should also be studied regarding their efficiency in combating infections of the respiratory tract.

5.9 Final remarks

In summary, this work describes a versatile workflow for generating and profiling novel molecules of a new antibiotic class by biosynthetic pathway engineering. The optimized production and purification platform enables proceeding with *in vitro* and *in vivo* investigations. This work delivers an important contribution to the understanding of how darobactins interact with their target protein BamA and revealed positions of the molecule that are crucial for antibacterial activity. Furthermore, this thesis provides perspectives on how the darobactin molecule class can be optimized in future studies to

improve the *in vivo* activity. So far, the darobactins seem promising candidates in the fight against the AMR crisis and might help to treat Gram-negative infections in humans one day.

References

1 K. Lewis, *Cell*, 2020, **181**, 29.

2 Y. Imai, K. J. Meyer, A. Iinishi, Q. Favre-Godal, R. Green, S. Manuse, M. Caboni, M. Mori, S. Niles, M. Ghiglieri, C. Honrao, X. Ma, J. Guo, A. Makriyannis, L. Linares-Otoya, N. Böhringer, Z. G. Wuisan, H. Kaur, R. Wu, A. Mateus, A. Typas, M. M. Savitski, J. L. Espinoza, A. O'Rourke, K. E. Nelson, S. Hiller, N. Noinaj, T. F. Schäberle, A. D'Onofrio and K. Lewis, *Nature*, 2019, **576**, 459.

3 D. Pogorevc, F. Panter, C. Schillinger, R. Jansen, S. C. Wenzel and R. Müller, *Metabolic engineering*, 2019, **55**, 201.

4 WO2022175443A1, 2022.

5 S. Groß, F. Panter, D. Pogorevc, C. E. Seyfert, S. Deckarm, C. D. Bader, J. Herrmann and R. Müller, *Chemical Science*, 2021, **12**, 11882.

6 Z. G. Wuisan, I. D. M. Kresna, N. Böhringer, K. Lewis and T. F. Schäberle, *Metab. Eng.*, 2021, **66**, 123.

7 Carsten E. Seyfert, Christoph Porten and Rolf Müller, 2023, **29**, 539.

8 G. A. Hudson and D. A. Mitchell, *Curr. Opin. Microbiol.*, 2018, **45**, 61.

9 G. D. Wright, *Adv. Drug Deliv. Rev.*, 2005, **57**, 1451.

10 P. Engel, A. Goepfert, F. V. Stanger, A. Harms, A. Schmidt, T. Schirmer and C. Dehio, *Nature*, 2012, **482**, 107.

11 A. Harms, M. Liesch, J. Körner, M. Québatte, P. Engel and C. Dehio, *PLoS genetics*, 2017, **13**, e1007077.

12 L. van Melderen, *Curr. Opin. Microbiol.*, 2010, **13**, 781.

13 M. M. M. Abd-Elgawad, *Plants (Basel, Switzerland)*, 2021, **10**.

14 A. Lanois-Nouri, L. Pantel, J. Fu, J. Houard, J.-C. Ogier, Y. S. Polikanov, E. Racine, H. Wang, S. Gaudriault, A. Givaudan and M. Gualtieri, *mBio*, 2022, e0282621.

15 A. R. Burmeister, *Evolution, medicine, and public health*, 2015, **2015**, 193.

16 N. Böhringer, R. Green, Y. Liu, U. Mettal, M. Marner, S. M. Modaresi, R. P. Jakob, Z. G. Wuisan, T. Maier, A. Iinishi, S. Hiller, K. Lewis and T. F. Schäberle, *Microbiol Spectr*, 2021, **9**, e0153521.

17 S. Guo, S. Wang, S. Ma, Z. Deng, W. Ding and Q. Zhang, *Nat Commun*, 2022, **13**, 2361.

18 A. L. Vagstad, *Current opinion in biotechnology*, 2023, **80**, 102891.

19 a) C. Ongpipattanakul, E. K. Desormeaux, A. DiCaprio, van der Donk, Wilfred A., D. A. Mitchell and S. K. Nair, *Chem. Rev.*, 2022, **122**, 14722; b) C. D. Bader, A. L. Nichols, D. Yang and B. Shen, *Curr. Opin. Microbiol.*, 2023, **75**, 102359;

20 H. Kaur, R. P. Jakob, J. K. Marzinek, R. Green, Y. Imai, J. R. Bolla, E. Agustoni, C. V. Robinson, P. J. Bond, K. Lewis, T. Maier and S. Hiller, *Nature*, 2021, **593**, 125.

21 a) J.-B. Hartmann, M. Zahn, I. M. Burmann, S. Bibow and S. Hiller, *J. Am. Chem. Soc.*, 2018, **140**, 11252; b) H. Kaur, J.-B. Hartmann, R. P. Jakob, M. Zahn, I. Zimmermann, T. Maier, M. A. Seeger and S. Hiller, *J. Biomol. NMR*, 2019, **73**, 375;

22 C. E. Seyfert, C. Porten, B. Yuan, S. Deckarm, F. Panter, C. Bader, J. Coetzee, F. Deschner, K. Tehrani, P. G. Higgins, H. Seifert, T. Marlovits, J. Herrmann and R. Müller, *Angew. Chem. Int. Ed.*, 2022, **62**, e202214094.

23 M. Marner, L. Kolberg, J. Horst, N. Böhringer, J. Hübner, I. D. M. Kresna, Y. Liu, U. Mettal, L. Wang, M. Meyer-Bühn, S. Mihajlovic, M. Kappler, T. F. Schäberle and U. von Both, *Microbiol Spectr*, 2023, **11**, e0443722.

24 J. Santos-Aberturas, G. Chandra, L. Frattaruolo, R. Lacret, T. H. Pham, N. M. Vior, T. H. Eyles and A. W. Truman, *Nucleic Acids Res.*, 2019.

25 M. M. Zdouc, J. J. J. van der Hooft and M. H. Medema, *Trends in Pharmacological Sciences*, 2023, **44**, 532.
26 M. Montalbán-López, T. A. Scott, S. Ramesh, I. R. Rahman, A. J. van Heel, J. H. Viel, V. Bandarian, E. Dittmann, O. Genilloud, Y. Goto, M. J. Grande Burgos, C. Hill, S. Kim, J. Koehnke, J. A. Latham, A. J. Link, B. Martínez, S. K. Nair, Y. Nicolet, S. Rebuffat, H.-G. Sahl, D. Sareen, E. W. Schmidt, L. Schmitt, K. Severinov, R. D. Süssmuth, A. W. Truman, H. Wang, J.-K. Weng, G. P. van Wezel, Q. Zhang, J. Zhong, J. Piel, D. A. Mitchell, O. P. Kuipers and van der Donk, Wilfred A., *Natural product reports*, 2021, **38**, 130.
27 G. Zhong, Z.-J. Wang, F. Yan, Y. Zhang and L. Huo, *ACS Bio & Med Chem Au*, 2023, **3**, 1.
28 Global Antimicrobial Resistance Surveillance System (GLASS) Report. Early implementation, http://apps.who.int/iris/bitstream/handle/10665/259744/9789241513449-eng.pdf;jsessionid=97E045EBFE3B29F286CBA3EE8360F0D1?sequence=1, (accessed 31 January 2018).
29 J. Hodgson, *Nat Biotechnol*, 2001, **19**, 722.
30 A. L. Flores-Mireles, J. N. Walker, M. Caparon and S. J. Hultgren, *Nat Rev Microbiol*, 2015, **13**, 269.
31 P. G. Arnison, M. J. Bibb, G. Bierbaum, A. A. Bowers, T. S. Bugni, G. Bulaj, J. A. Camarero, D. J. Campopiano, G. L. Challis, J. Clardy, P. D. Cotter, D. J. Craik, M. Dawson, E. Dittmann, S. Donadio, P. C. Dorrestein, K.-D. Entian, M. A. Fischbach, J. S. Garavelli, U. Göransson, C. W. Gruber, D. H. Haft, T. K. Hemscheidt, C. Hertweck, C. Hill, A. R. Horswill, M. Jaspars, W. L. Kelly, J. P. Klinman, O. P. Kuipers, A. J. Link, W. Liu, M. A. Marahiel, D. A. Mitchell, G. N. Moll, B. S. Moore, R. Müller, S. K. Nair, I. F. Nes, G. E. Norris, B. M. Olivera, H. Onaka, M. L. Patchett, J. Piel, M. J. T. Reaney, S. Rebuffat, R. P. Ross, H.-G. Sahl, E. W. Schmidt, M. E. Selsted, K. Severinov, B. Shen, K. Sivonen, L. Smith, T. Stein, R. D. Süssmuth, J. R. Tagg, G.-L. Tang, A. W. Truman, J. C. Vederas, C. T. Walsh, J. D. Walton, S. C. Wenzel, J. M. Willey and van der Donk, Wilfred A., *Natural product reports*, 2013, **30**, 108.
32 a) C. J. Smith, M. B. Rogers and M. L. McKee, *Plasmid*, 1992, **27**, 141; b) D. R. Jones, M. B. Smith, R. McLean, J. M. Grondin, C. R. Amundsen, G. D. Inglis, B. Selinger and D. W. Abbott, *Sci Rep*, 2019, **9**, 17400;
33 a) L. van Mellaert and J. Anné, in *Novel Frontiers in the Production of Compounds for Biomedical Use*, Springer, Dordrecht, 2001, pp. 277–300; b) L. Bredmose, S. M. Madsen, A. Vrang, P. Ravn, M. G. Johnsen, J. Glenting, J. Arnau and H. Israelsen, in *Recombinant Protein Production with Prokaryotic and Eukaryotic Cells. A Comparative View on Host Physiology*, ed. O.-W. Merten, D. Mattanovich, C. Lang, G. Larsson, P. Neubauer, D. Porro, P. Postma, J. T. de Mattos and J. A. Cole, Springer Netherlands, Dordrecht, 2010, pp. 269–275; c) L. J. Byrne, K. J. O'Callaghan and M. F. Tuite, *Methods in molecular biology (Clifton, N.J.)*, 2005, **308**, 51; d) R. Mokdad-Gargouri, S. Abdelmoula-Soussi, N. Hadiji-Abbès, I. Y.-H. Amor, I. Borchani-Chabchoub and A. Gargouri, *Methods in molecular biology (Clifton, N.J.)*, 2012, **824**, 359;
34 a) H. Ikeda, S. Kazuo and S. Omura, *Journal of Industrial Microbiology & Biotechnology*, 2014, **41**, 233; b) P. Bekiesch, P. Basitta and A. K. Apel, *Archiv der Pharmazie*, 2016, **349**, 594; c) C. Guan, Y. Yuan, Y. Ma, X. Wang, C. Zhang, M. Lu, R. Gu and D. Chen, *Microb Cell Fact*, 2022, **21**, 23; d) Y. Lu, H. Yan, J. Deng, Z. Huang, X. Jin, Y. Yu, Q. Hu, F. Hu and J. Wang, *Microb Cell Fact*, 2017, **16**, 154;
35 a) M. Nesic, D. B. Ryffel, J. Maturano, M. Shevlin, S. R. Pollack, D. R. Gauthier, P. Trigo-Mouriño, L.-K. Zhang, D. M. Schultz, J. M. McCabe Dunn, L.-C. Campeau, N. R. Patel, D. A. Petrone and D. Sarlah, *J. Am. Chem. Soc.*, 2022, **144**, 14026; b) Y.-C. Lin, F. Schneider, K. J. Eberle, D. Chiodi, H. Nakamura, S. H. Reisberg, J. Chen, M. Saito and P. S. Baran, *J. Am. Chem. Soc.*, 2022, **144**, 14458;
36 M. Winn, J. K. Fyans, Y. Zhuo and J. Micklefield, *Nat. Prod. Rep.*, 2016, **33**, 317.
37 a) K. Lewis, *Biochem Pharmacol*, 2017, **134**, 87; b) A. P. Li, *Drug Discov. Today*, 2001, **6**, 357;
38 World Health Organization, *World Health Organization*, 2021.

39 F. A. Bernal, P. Hammann and F. Kloss, *Current opinion in biotechnology*, 2022, **78**, 102783.
40 B. Kintses, P. K. Jangir, G. Fekete, M. Számel, O. Méhi, R. Spohn, L. Daruka, A. Martins, A. Hosseinnia, A. Gagarinova, S. Kim, S. Phanse, B. Csörgő, Á. Györkei, E. Ari, V. Lázár, I. Nagy, M. Babu, C. Pál and B. Papp, *Nature communications*, 2019, **10**, 5731.
41 M. Miethke, M. Pieroni, T. Weber, M. Brönstrup, P. Hammann, L. Halby, P. B. Arimondo, P. Glaser, B. Aigle, H. B. Bode, R. Moreira, Y. Li, A. Luzhetskyy, M. H. Medema, J.-L. Pernodet, M. Stadler, J. R. Tormo, O. Genilloud, A. W. Truman, K. J. Weissman, E. Takano, S. Sabatini, E. Stegmann, H. Brötz-Oesterhelt, W. Wohlleben, M. Seemann, M. Empting, A. K. H. Hirsch, B. Loretz, C.-M. Lehr, A. Titz, J. Herrmann, T. Jaeger, S. Alt, T. Hesterkamp, M. Winterhalter, A. Schiefer, K. Pfarr, A. Hoerauf, H. Graz, M. Graz, M. Lindvall, S. Ramurthy, A. Karlén, M. van Dongen, H. Petkovic, A. Keller, F. Peyrane, S. Donadio, L. Fraisse, L. J. V. Piddock, I. H. Gilbert, H. E. Moser and R. Müller, *Nat. Rev. Chem.*, 2021, **5**, 726.
42 S. Walesch, J. Birkelbach, G. Jézéquel, F. P. J. Haeckl, J. D. Hegemann, T. Hesterkamp, A. K. H. Hirsch, P. Hammann and R. Müller, *EMBO reports*, 2022, e56033.
43 J. D. Hegemann, J. Birkelbach, S. Walesch and R. Müller, *EMBO reports*, 2023, **24**, e56184.
44 TAXIS Pharmaceuticals, Inc., *Our Pipeline. TXA709 FtsZ Modulation*, USA, 2023.
45 a) S. Baumann, J. Herrmann, R. Raju, H. Steinmetz, K. I. Mohr, S. Hüttel, K. Harmrolfs, M. Stadler and R. Müller, *Angewandte Chemie (International ed. in English)*, 2014, **53**, 14605; b) W. A. M. Elgaher, M. M. Hamed, S. Baumann, J. Herrmann, L. Siebenbürger, J. Krull, K. Cirnski, A. Kirschning, M. Brönstrup, R. Müller and R. W. Hartmann, *Chem. Eur. J.*, 2020; c) C. Couturier, S. Groß, A. von Tesmar, J. Hoffmann, S. Deckarm, A. Fievet, N. Dubarry, T. Taillier, C. Pöverlein, H. Stump, M. Kurz, L. Toti, S. Haag Richter, D. Schummer, P. Sizun, M. Hoffmann, R. Prasad Awal, N. Zaburannyi, K. Harmrolfs, J. Wink, E. Lessoud, T. Vermat, V. Cazals, S. Silve, A. Bauer, M. Mourez, L. Fraisse, C. Leroi-Geissler, A. Rey, S. Versluys, E. Bacqué, R. Müller and S. Renard, *Angewandte Chemie (International ed. in English)*, 2022, **61**, e202210747; d) A. Ehrens, A. Schiefer, A. K. Krome, T. Becker, K. Rox, H. Neufeld, T. Aden, K. G. Wagner, R. Müller, M. Grosse, M. Stadler, G. M. König, S. Kehraus, S. Alt, T. Hesterkamp, M. P. Hübner, K. Pfarr and A. Hoerauf, *Front. Trop. Dis*, 2022, **3**; e) A. K. Krome, T. Becker, S. Kehraus, A. Schiefer, M. Gütschow, L. Chaverra-Muñoz, S. Hüttel, R. Jansen, M. Stadler, A. Ehrens, D. Pogorevc, R. Müller, M. P. Hübner, T. Hesterkamp, K. Pfarr, A. Hoerauf, K. G. Wagner and G. M. König, *Natural product reports*, 2022, **39**, 1705;
46 a) F. von Nussbaum and R. D. Süssmuth, *Angew. Chem. Int. Ed. Engl.*, 2015, **54**, 6684; b) R. Shukla, F. Lavore, S. Maity, M. G. N. Derks, C. R. Jones, B. J. A. Vermeulen, A. Melcrová, M. A. Morris, L. M. Becker, X. Wang, R. Kumar, J. Medeiros-Silva, R. A. M. van Beekveld, A. M. J. J. Bonvin, J. H. Lorent, M. Lelli, J. S. Nowick, H. D. MacGillavry, A. J. Peoples, A. L. Spoering, L. L. Ling, D. E. Hughes, W. H. Roos, E. Breukink, K. Lewis and M. Weingarth, *Nature*, 2022, **608**, 390;
47 J. A. Karas, F. Chen, E. K. Schneider-Futschik, Z. Kang, M. Hussein, J. Swarbrick, D. Hoyer, A. M. Giltrap, R. J. Payne, J. Li and T. Velkov, *Annals of the New York Academy of Sciences*, 2020, **1459**, 86.
48 E. J. Ramchuran, A. M. Somboro, S. A. H. Abdel Monaim, D. G. Amoako, R. Parboosing, H. M. Kumalo, N. Agrawal, F. Albericio, B. G. d. La Torre and L. A. Bester, *Frontiers in microbiology*, 2018, **9**, 1535.
49 L. L. Ling, T. Schneider, A. J. Peoples, A. L. Spoering, I. Engels, B. P. Conlon, A. Mueller, T. F. Schäberle, D. E. Hughes, S. Epstein, M. Jones, L. Lazarides, V. A. Steadman, D. R. Cohen, C. R. Felix, K. A. Fetterman, W. P. Millett, A. G. Nitti, A. M. Zullo, C. Chen and K. Lewis, *Nature*, 2015, **517**, 455.
50 L. Pantel, T. Florin, M. Dobosz-Bartoszek, E. Racine, M. Sarciaux, M. Serri, J. Houard, J.-M. Campagne, R. M. de Figueiredo, C. Midrier, S. Gaudriault, A. Givaudan, A. Lanois, S. Forst, A.

Aumelas, C. Cotteaux-Lautard, J.-M. Bolla, C. Vingsbo Lundberg, D. L. Huseby, D. Hughes, P. Villain-Guillot, A. S. Mankin, Y. S. Polikanov and M. Gualtieri, *Mol. Cell*, 2018, **70**, 83.
51 E. Racine, P. Nordmann, L. Pantel, M. Sarciaux, M. Serri, J. Houard, P. Villain-Guillot, A. Demords, C. Vingsbo Lundberg and M. Gualtieri, *Antimicrob. Agents Chemother.*, 2018, **62**, e01016.
52 M. Sarciaux, L. Pantel, C. Midrier, M. Serri, C. Gerber, R. Marcia de Figueiredo, J.-M. Campagne, P. Villain-Guillot, M. Gualtieri and E. Racine, *J Med Pharm Chem*, 2018, **61**, 7814.
53 Z. Wang, B. Koirala, Y. Hernandez, M. Zimmerman, S. Park, D. S. Perlin and S. F. Brady, *Nature*, 2022, **601**, 606.
54 a) H. Spapen, R. Jacobs, V. van Gorp, J. Troubleyn and P. M. Honoré, *Annals of intensive care*, 2011, **1**, 14; b) E. M. Westerman, P. P. H. Le Brun, D. J. Touw, H. W. Frijlink and H. G. M. Heijerman, *Journal of Cystic Fibrosis*, 2004, **3**, 23; c) F. Shahbazi and S. Dashti-Khavidaki, *Expert Review of Clinical Pharmacology*, 2015, **8**, 423;
55 C. E. Seyfert, A. V. Müller, D. J. Walsh, J. Birkelbach, A. M. Kany, C. Porten, B. Yuan, D. Krug, J. Herrmann, T. C. Marlovits, A. K. H. Hirsch and R. Müller, *New Genetically Engineered Derivatives of Antibacterial Darobac-tins Underpin their Potential for Antibiotic Development*, 2023.
56 J. Peterson, S. Kaul, M. Khashab, A. Fisher and J. B. Kahn, *Clin Ther*, 2007, **29**, 2215.